THEORETICA CHIMICA ACTA

edenda curat
Hermann Hartmann

adiuvantibus
C. J. Ballhausen, København
R. D. Brown, Clayton
E. Heilbronner, Basel
J. Jortner, Tel-Aviv
M. Kotani, Tokyo
J. Koutecký, Praha
J. W. Linnett, Cambridge
E. E. Nikitin, Moskwa
R. G. Pearson, Evanston
B. Pullman, Paris
K. Ruedenberg, Ames
C. Sandorfy, Montreal
M. Simonetta, Milano
O. Sinanoğlu, New Haven

Vol. 27, 1972

Springer-Verlag · Berlin · Heidelberg · New York

The exclusive copyright for all languages and countries, including the right for photomechanical and any other reproductions, also in microform, is transferred to the publisher.

The use of registered names, trademarks, etc. in this publication does not imply, even in the absence of a specific statement, that such names are exempt from the relevant protective laws and regulations and therefore free for general use.

Alle Rechte, einschließlich das der Übersetzung in fremde Sprachen und das der fotomechanischen Wiedergabe oder einer sonstigen Vervielfältigung, auch in Mikroform, vorbehalten. Jedoch wird gewerblichen Unternehmen für den innerbetrieblichen Gebrauch nach Maßgabe des zwischen dem Börsenverein des Deutschen Buchhandels e. V. und dem Bundesverband der Deutschen Industrie abgeschlossenen Rahmenabkommens die Anfertigung einer fotomechanischen Vervielfältigung gestattet. Wenn für diese Zeitschrift kein Pauschalabkommen mit dem Verlag vereinbart worden ist, ist eine Wertmarke im Betrage von DM 0,40 pro Seite zu verwenden. *Der Verlag läßt diese Beträge den Autorenverbänden zufließen.*

Die Wiedergabe von Gebrauchsnamen, Handelsnamen, Warenbezeichnungen usw. in dieser Zeitschrift berechtigt auch ohne besondere Kennzeichnung nicht zu der Annahme, daß solche Namen im Sinne der Warenzeichen- und Markenschutz-Gesetzgebung als frei betrachtet wären und daher von jedermann benutzt werden dürften.

Springer-Verlag Berlin Heidelberg New York
Printed in Germany by Brühlsche Universitätsdruckerei, Gießen
© by Springer-Verlag Berlin Heidelberg 1972

[illegible] Number 702
38965
Date 24.4.82

Index

Commentationes et Relationes

Baerends, E.J., Ellis, D.E., Ros, P.: A Theoretical Study of the Interaction of Ethylene with Transition Metal Complexes 339

Barthelat, J.C., Durand, Ph.: Orbitales moléculaires localisées: structure électronique de la molécule de méthane 109

Bendazzoli, G.L., Bernardi, F., Geremia, A., Palmieri, P.: A.M.O. Calculations for Some First Row Diatomic Molecules 63

Bernardi, F., S. Bendazzoli, G.L., *et al.* 63

Buenker R.J., s. Peyerimhoff, S.D. 243

Burden, F.R., Wilson, R.M.: Least-Squares Gaussian Expansions of Atomic Orbitals . . 151

Čársky, P., s. Zahradník, R. 121

Chang, S., s. Loew, G.H. 273

Colpa, J.P., Islip, M.F.J.: Analysis of Correlation Effects in HeI, LiI and BeI Iso-electronic Sequences by Z-expansion Methods 25

Cook, D.B.: A Note on General Core-Valence Orthogonality 161

Copeland, D.A.: Approximate Radial Functions
I. First-Row Transition-Metal 4s and 3d Atomic Orbitals 367

Coutière, M.-M., Demuynck, J., Veillard, A.: Ionization Potentials of Ferrocene and Koopmans' Theorem. An *ab-initio* LCAO-MO-SCF Calculation 281

Demuynck, J., s. Coutière, M.-M., *et al.* 281

Dewar, M.J.S., Weiner, P.: Ground States of Molecules
XXIII. MINDO/2 Calculations for Naphthalene 373

Diercksen, G.H.F., s. Kraemer, W.P. 265

Durand, Ph., s. Barthelat, J.C. 109

Edwards, T.G.: Assignments in Photoelectron Spectroscopy Using the CNDO/2 Method 1

Ellis, D.E., s. Baerends, E.J., *et al.* 339

Ellison, F.O., Larcom, L.L.: Atoms-in-Molecules Treatment of Li_2^+ and Li_2 Using Optimum Gaussian Approximations of Li^+ and Li Eigenstates 81

Fischer-Hjalmars, I., Kowalewski, J.: Simplified Non-Empirical Excited State Calculations
Part I. The Rydberg ns and $np\sigma$ Series of Ethylene 197

Gelius, U., Roos, B., Siegbahn, P.: MO-SCF-LCAO Studies of Sulphur Compounds . . . 171

Geremia, A., s. Bendazzoli, G.L., *et al.* 63

Gliemann, G., Plath, P.: Spin-Bahn-Wechselwirkung räumlich beschränkter Elektronensysteme 153

Goldstein, J.H., s. Long, K.R. 75

Guidotti, C., Lamanna, U., Maestro, M., Moccia, R.: Barriers to the Internal Rotation and Observables of the Ground State for Hydrogen Peroxyde 55

Hartmann, H.: Über die Hartreesche Methode 147

Henriksson, A., Sundbom, M.: Semiempirical Molecular Orbital Studies of Phthalocyanines
I. The Electronic Structure and Excited States of Phthalocyanine, H_2Pc 213

Henriksson, A., Roos, B., Sundbom, M.: Semiempirical Molecular Orbital Studies of Phthalocyanines
II. The Electronic Structure and Excited States of Copper Phthalocyanine, CuPc . 303

Higuchi, J.: Effect of Atomic Dipole in Semi-Empirical Calculation of π-Electron Energy Levels 315

Islip,M.F.J., s. Colpa,J.P. 25

Jansen,H.B., Ros,P.: On the Use of Small Atomic Basis Sets in Non-Empirical Molecular Calculations 95

Jaszuński,M., Sadlej,A.J.: Proton Magnetic Shielding in the Water Molecule 135

Jungen,M.: Spin-Bahn-Kopplungseffekte verschiedener Ordnung bei Jod und Dijodazetylen 33

Kahn,O., Kettle,S.F.A.: Influence du couplage vibronique sur le paramagnétisme d'un complexe cubique dans l'état électronique $^2T_2$ 187

Kettle,S.F.A., s. Kahn,O. 187

Kowalewski,J., s. Fischer-Hjalmars,J. 197

Kraemer,W.P., Diercksen,G.H.F.: SCF LCAO MO Studies on the Hydration of Ions: The System $F^- \cdot 2H_2O$ 265

Lamanna,U., s. Guidotti,C., *et al.* 55

Langlet,J.: PCILO Method for Excited States I. Construction of the Zeroth Order Wave- Function for Planar Conjugated Systems . 223

Larcom,L.L., s. Ellison,F.O. 81

Loew,G.H., Chang,S.: Energy-Conformation Studies of Hydrogen Cyanide Tetramer: A Prebiotic Precursor 273

Long,K.R., Goldstein,J.H.: EHT Conformational Study of Nicotinamide and Related Amides 75

Maestro,M., s. Guidotti,C., *et al.* 55

Moccia,R., s. Guidotti,C., *et al.* 55

Morita,H., Nagakura,S.: CNDO/2 Calculations and Configuration Analyses for Some Hydrogen-Bonded Systems 325

Nagakura,S., s. Morita,H. 325

Niessen,W. v.: Density Localization of Atomic and Molecular Orbitals II. Homonuclear Diatomic Molecules 9

Palmieri,P., s. Bendazzoli,G.L., *et al.* 63

Pamuk,H.Ö., s. Sinanoğlu,O. 289

Peyerimhoff,S.D., Buenker,R.J.: Vibrational Analysis of the Electronic Spectrum of Ethylene Based on *ab initio* SCF-CI Calculations 243

Plath,P., s. Gliemann,G.. 153

Roche,M., Simon,J.-C.: De la possibilité d'utiliser une base de Slater uniquement *s* dans les calculs relatifs aux atomes et aux molécules 165

Rosenfeld,Yu.R., s. Vekhter,B.G., *et al.* 49

Roos,B, s. Gelius,U., *et al.* 171

Roos,B., s. Henriksson,A., *et al.* 303

Ros,P., s. Baerends,E.J., *et al.* 339

Ros,P., s. Jansen,H.B. 95

Sabin,J.R.: A Model Study of the Interaction of a Hydrogen Bond with a π-Electron System 69

Sadlej,A.J., s. Jaszuński,M. 135

Siegbahn,P., s. Gelius,U., *et al.* 171

Simon,J.-C., s. Roche,M. 165

Sinanoğlu,O., Pamuk,H.Ö.: A Semi-Empirical MO-Electron Correlation Method for Molecules and the Correlation Energies of π-System Linear and Polycyclic Hydrocarbons 289

Stewart, R. F., s. Webster, B. C. 355

Sundbom, M., s. Henriksson, A., *et al.* 213, 303

Tsukerblat, B. S., s. Vekhter, B. G., *et al.* 49

Veillard, A., s. Coutière, M.-M., *et al.*. 281

Vekhter, B. G., Tsukerblat, B. S., Rosenfeld, Yu. R.: Optical Manifestation of Jahn-Teller Effect in Square-Planar Complexes 49

Webster, B. C., Stewart, R. F.: First Order Pair Functions for the Beryllium Isoelectronic Sequence 355

Weiner, P., s. Dewar, M. J. S., ... 373

Wilson, R. M., s. Burden, F. R. 151

Zahradník, R., Čársky, P.: Open Shell CNDO Treatments on Small Alipathic Radicals. Electronic Spectra and Some Ground State Properties 121

Indexed in Current Contents

heoret. chim. Acta (Berl.) 27, 1--8 (1972)
) by Springer-Verlag 1972

Assignments in Photoelectron Spectroscopy Using the CNDO/2 Method

T. G. Edwards*

Department of Chemistry, The University, Highfield, Southampton S09 5NH, England

Received March 18, 1972

In the photoelectron spectra of molecules vibrational fine structure often accompanies the observed nization potentials (IPs). For non-diatomic molecules it is difficult to make vibrational assignments because the frequencies of the ion often differ greatly from those of the neutral molecule. In order to make both the vibrational assignments and the assignments of the IPs to molecular orbitals (MOs) using Koopmans' theorem CNDO/2 MO calculations have been carried out. Within the framework of this method a quantity ΔE_{AB} has been calculated which is the change in potential energy between an atom-pair A B for a particular MO on ionization. Application to some diatomic molecules has shown that this quantity reflects the changes in vibrational frequencies on ionization. The IP–MO assignments are made such that removal of an electron from a particular MO is in accord with the observed vibrational fine-structure; attempting to make these assignments on the basis of the calculated MO ordering alone has been shown to be very unsatisfactory.

Photoelektronenspektren von Molekülen zeigen neben den Ionisierungspotentialen oft noch eine Schwingungsfeinstruktur, deren Zuordnung bei nicht-zweiatomigen Molekülen wegen der starken Frequenzverschiebungen vom Molekül zum Ion Schwierigkeiten macht. Um sowohl Schwingungs- als auch Ionisierungs-Zuordnungen vornehmen zu können, wurden Rechnungen mit dem CNDO/2-Verfahren durchgeführt. Dabei stützt man sich auf die Änderung der potentiellen Energie zwischen dem Atompaar AB in bezug auf ein bestimmtes MO bei Ionisierung (ΔE_{AB}). Die Anwendung auf zweiatomige Moleküle zeigt, daß diese Größe tatsächlich die Änderung der Schwingungsfrequenzen wiedergibt, und die Zuweisungen des IP werden so vorgenommen, daß die Entfernung eines Elektrons aus einem MO im Einklang mit der Schwingungsfeinstruktur ist. Dagegen erweist sich die einfache Zuweisung auf Grund der MO-Reihenfolge als schlechter.

1. Introduction

A proper approach to the calculation of IPs of molecules (and atoms, for that matter) involves the calculation of the total electronic energies of the ground state and of the ionized states. Such calculations, which should also include a realistic account of electron-correlation and possibly a relativistic correction [1], are generally impracticable. Consequently, a less rigorous approach must be sought. Koopmans' theorem [2] is a convenient and often used approximation. This theorem results in a direct equality between the observed IP and $-\varepsilon_i$, where ε_i is the energy of the ith MO. Various correction terms have been used in application of the theorem [3]. In this work such correction terms have not been applied since it has been demonstrated [4] that their neglect may be approximately compensated for in the application of semi-empirical MO theory (as used in this work) in the choice of the semi-empirical parameter-values.

---

* Present address: The Royal Liberty School, Upper Brentwood Road, Romford, Essex, RM2 6HJ, England.

The advent of photoelectron spectroscopy (pes) [5] meant that IPs could be determined unambiguously. Apart from the direct observation of ionization high-resolution vacuum ultra-violet pes has a real strength in that the vibrational structure of the ions is also observed. Thus, assignment would be aided substantially if comparison could be made between the vibrations accompanying the IP and those predicted to be excited when an electron is removed from a particular MO. The problem is simply stated: How can one predict which vibrations are excited? The postulate of Koopmans' theorem is that the MOs remain unchanged on ionization. This is equivalent to assuming that the bonding between any pair of atoms in the ion is the same as that before ionization *minus* the contribution from the removed electron. Since the result of Koopmans' theorem is to be assumed it is only fair to assume the postulate. So, when an electron is removed from a MO which is bonding between atoms A and B then *if* the vibration ν_{AB} is observed it should occur at a lower frequency than in the neutral molecule, and *vice versa*; the magnitude of the change in bonding should reflect the change in the frequency of ν_{AB}. This is a severe approximation for a non-diatomic molecule the validity of its adoption is discussed at the end of this paper. But, even yet, the question of whether or not a particular vibration *will* be observed has not been answered. The information on the vibrational states in the ion is carried by the departing electrons, but the ion is not properly formed until the electron is outside the influence of the ion. The manner in which the departing electron acquires this information is not clear. Is it possible for there to be a change in bonding between an atom-pair on ionization, giving rise to a change in vibrational frequency, without the departing electrons relaying the information? Are there selection rules, and, if there are, what are they? In the present work attempts have not been made to answer these questions. The present calculations are meant to be used not in predicting spectra but as an aid to their interpretation. For example, in a molecule A-B C let us suppose that removal of an electron from a particular MO gives a decrease in bonding between A and B and an increase in that between B and C. If a single vibrational series is observed with frequency lower than ν_{AB} or ν_{BC} in the neutral molecule then ν_{AB} is taken as the observed vibration. Of course, it is too much to expect that all assignments may be made in this clear-cut fashion.

It only remains now to obtain a theoretical measure of the change in bonding between all atom-pairs on ionization from each MO. This will be discussed in the next section together with an outline of the MO method adopted. From symmetry it is clear that anti-symmetric vibrations are not considered in the present approach, in keeping with experiment where only symmetric vibrations are observed.

2. Theory

The MO *Method*

The MO Method used was that devised by Pople *et al.* [6] and is known as CNDO/2 (Complete Neglect of Differential Overlap-version 2). An earlier method CNDO/1 is also relevant here [7]. Some familiarity with the symbols used in this now standard method will be assumed.

The integral-values evaluated by Sichel and Whitehead [8] (hereinafter S–W) resulted in far better agreement with experimental IPs [9] and binding energies than those used in the original work. The evaluation procedure adopted in the present work differs only for the average of the electron-interaction terms on atom A, γ_{AA} – the present approach is simpler. While 1st and 2nd row elements were included in the re-parameterization only the former will be discussed since only these atoms occur in the molecules under consideration.

It can be readily shown for Slater orbitals [13] that $\gamma_{AA} = \gamma_{ss} - 12F^2/700$, where F^2 is 8.6 eV for fluorine and is less for the other 1st row elements. γ_{ss} may be calculated from $\gamma_{ss} = I_s - A_s$, where I_s and A_s are the IP and electron affinity, respectively, of the 2s orbital, the experimental values being taken from the valence state data of Hinze and Jaffé [12]. The approximation is made that $\gamma_{AA} = I_s - A_s$. For the 2-centre Coulomb-integral γ_{AB} the Mataga [14] expression has been adopted, where $\gamma_{AB} = 1/(R_{AB} + 2/(\gamma_{AA} + \gamma_{BB}))$.

The U_μ parameters were evaluated in exactly the same manner as that adopted by Pople and Segal [7], except that the more recent data of Hinze and Jaffé were used.

S–W obtained values for β^0_A by adjusting to give agreement with the experimental binding energies [15] for the binary hydrides AH_n, and such a procedure was used in the present work. They used the approximation that $1/R_{AB}$ be replaced by γ_{AB} in evaluating the core-core repulsion. The rationale for this step was that by this means the electrostatic interaction in a homopolar molecule is zero. But this is not a necessary requisite. Further, this means that for the $^3\Sigma_u^+$ state of H_2 the binding energy is zero, but it was in order to make this state repulsive (in agreement with more sophisticated calculations) that the CNDO/2 approximation of replacing V_{AB} by $Z_B \gamma_{AB}$ was adopted (V_{AB} is the interaction between the core of B and a valence electron on A). However, there is no doubting the truth of their observation that such an approximation was necessary to obtain sensible values for β^0_A. Thus, resignedly, this approximation was adopted in the present work. The formulae required for calculation of the atomic energies and the binding energies are given in the work by S–W and so will not be reproduced here.

The β^0_A values for the 1st row atoms are given in Table 1. The experimental and calculated values of the binding energies of C_2H_4, N_2 and F_2 are given in Table 2.

Table 1. Values of the β^0_A parameters (eV)

A	H	Li	Be	B	C	N	O	F
$-\beta^0_A$	5.4	0.9	4.3	6.1	8.8	8.9	13.9	15.5

Table 2. Experimental and calculated binding energies of C_2H_4, N_2 and F_2 (eV)

Binding energies	C_2H_4	N_2	F_2
Calculated	24.32	8.66	1.89
Experimental	24.36	9.90	1.65

Interatomic Bonding

In the literature there are numerous concepts for use in discussing the extent of bonding between atom-pairs in a molecule. More specifically, what is required is the contribution from each MO to the interatomic bonding. The concept of overlap populations in the population analysis theory of Mulliken [17] is appealing. Mulliken's theory and the CNDO/2 theory give rise to the same expression for covalent bond strength (momentarily neglecting electrostatic interaction) although the concept of overlap populations has no meaning in the latter method. In Mulliken's theory overlap integrals occur in the expression for covalent bond strength from lack of orthogonality between the basis functions, whereas in the CNDO/2 theory they occur only because of the approximation adopted for $\beta_{\mu\nu}$. Attempting to use the population analysis formulae in CNDO/2 theory would give, among other discrepancies, a non-integer number of electrons in the molecule! It is not known how clear is the relation between covalent bond strength and overlap population when Coulombic interaction is explicitly included in the expression for ε_i. Such inclusion need not necessarily invalidate the concept of overlap populations, but in the absence of this knowledge, and because CNDO/2 theory neglects overlap in the evaluation of the MOs, another, and very simple, approach has been adopted. In the CNDO/2 method the electronic energy may be partitioned into one- and two-centre contributions [6], the latter being given below.

$$E_{AB} = \sum_{\mu}^{A} \sum_{\nu}^{B} \left(P_{\mu\nu}(\beta_A^0 + \beta_B^0) S_{\mu\nu} + \left| (P_{AA} - Z_A)(P_{BB} - Z_B) - \frac{1}{2} P_{\mu\nu}^2 \right| \gamma_{AB} \right).$$

On removing an electron from the *i*th MO we have

$$\begin{aligned} \Delta E_{AB} = E_{AB} - E^{+}_{AB} = \sum_{\mu}^{A} \sum_{\nu}^{B} & (p^i_{\mu\nu}(\beta_A^0 + \beta_B^0) S_{\mu\nu} \\ & + [(P_{AA} - Z_A) p^i_{\nu\nu} + (P_{BB} - Z_B) p^i_{\mu\mu} - P_{\mu\nu} p^i_{\mu\nu}] \gamma_{AB}) \end{aligned}$$

where $p^i_{\mu\nu}$ is the Coulson partial bond-order [16, 18]. This represents the change in potential energy, and hence the change in bonding, between atoms A and B when an electron is removed from the *i*th MO.

The correlation between ΔE_{AB} and ν_{AB} is not direct since the same value of ΔE_{AB} for two unlike bonds, C–H and C–C say, is unlikely to result in the same changes, fractional or absolute, in ν_{CH} and ν_{CC}. However, as will be demonstrated, ΔE_{AB} may be used successfully, and this is helped by some assignments made by other means e.g. isotopic substitution [19].

It is worth noting that in an investigation of bond length changes on ionization of tetrachloroethylene Coulson and Luz [20] considered in detail, although in a different manner to that adopted here, changes in both bond orders and Coulombic electrostatic forces. They also considered repulsive exchange forces, but concluded that the necessary more complete MOs would destroy the simple picture being sought.

The values calculated for ΔE_{AB} for H_2, N_2, HF, H_2O and C_2H_4 are given in Table 3, together with the pes results and the proposed assignments.

ble 3. Experimental and calculated IPs (eV), and the proposed assignments for H_2, N_2, HF, H_2O and C_2H_4

mpound	IP (calc.)	IP (expt.) (vertical)	$-\Delta E_{AB}$			ν_{AB}				Assignment (orbital symmetry)
$(D_{\infty h})$	14.68	15.98 [23]	7.5			0.27 [23]				$\sigma_g(^2\Sigma_g^+)$
						(0.53)				
$(D_{\infty h})$	14.34	15.59 [23]	4.0			0.27 [24]				$\sigma_g(^2\Sigma_g^+)$
	14.22	16.96	5.7			0.23				$\pi_u(^2\Pi_u)$
	24.19	18.78	−1.6			0.30				$\sigma_u(^2\Sigma_u^+)$
	31.16					(0.29)				
$F(C_{\infty v})$	16.43	16.04 [25]	2.9			0.37 [25]				$\pi\ (^2\Pi_i)$
	16.78	19.90	6.6			0.17				$\sigma\ (^2\Sigma^+)$
	36.29					(0.50)				
			OH	HH		OH	HH			
$O(C_{2v})$	15.86	12.61 [19]	1.5	0.0		0.40	0.17 [19]			b_1
	14.70	14.73	2.8	1.0			0.12			a_1
	15.36	18.55	4.1	−0.2		0.37	0.20			b_2
	33.59					(0.45)	(0.20)			
			CH	CC	HH	CH	CC	HH	$2\nu_4$	
$H_4(D_{2h})$	10.64	10.51 [26]	0.1	4.9	0.0		0.15	0.17	0.05 [26]	b_{1u}
	11.85	12.74	0.9	3.5	0.1	0.36	0.16		0.10	a_g
	11.18	14.6	1.6	−1.0	−0.1	0.21	0.21			b_{1g}
	15.03	15.7	1.8	1.4	−0.1	0.15				b_{2u}
	19.60	~19								b_{3u}
	26.29					(0.37)	(0.20)	(0.17)	(0.10)	

3. Results

All energies are given in electron volts (eV). The vibrational energies of both the neutral molecules (in parentheses in Table 3) and the ions are of the 0→1 transitions for the diatomics and are an average over the bands for H_2O and C_2H_4.

4. Discussion

H_2 Obviously, the 1st IP arises from a strongly bonding orbital.

N_2 The assignments for N_2 have been very well established previously. The agreement between the vibrational spacings in the pe spectrum and those in the electronic spectra of the ions [24] is excellent, as is that between the calculated and observed Franck-Condon factors for the 3rd band [23]. The numerical agreement between the calculated and observed IPs is almost non-existent, a not uncommon feature in calculations on N_2 [1, 8]. Since the calculated IP at 24.19 eV is quite definitely the 3rd, the assignment of the observed 18.78 eV IP to $^2\Sigma_u^+$ is reasonable. Excellent confirmation is given by the slightly anti-bonding nature of the σ_u orbital. For the 1st and 2nd IPs we have from experiment that the 2nd arises from a strongly bonding MO and the 1st from a less strongly bonding one. This suggests the assignments shown, where the ordering of the two IPs has been inverted, in agreement with those proposed in the work cited above.

In an *ab-initio* calculation Scherr [27] correctly predicted the ordering of the IPs, but in an overlap population analysis he predicted the ordering to be weakly anti-bonding, strongly bonding and strongly anti-bonding. This poor agreement with experiment is possibly due to neglect of Coulombic forces in the derivation of the expression for the overlap populations. As pointed out by Mulliken [17], "... the major contributions even for homopolar bond energies may come from Coulomb-energy terms". In the present calculations the Coulombic term constistutes approximately one half of ΔE_{NN} for the 1st MO.

HF In view of the closeness of the predicted IPs it is impossible to attempt assignment on the basis of the ordering alone. Inspection of the ΔE_{HF} values makes it quite clear that the ordering of states is $^2\Pi_i$, $^2\Sigma^+$, the 1st being associated with the fluorine lone pairs and the 2nd with the strongly bonding σ orbital. This is the accepted assignment [25].

H_2O There is little doubt as to the assignment of the 1st IP to the weakly bonding b_1 MO. For the 2nd IP the presence of the scissors vibration, denoted ν_{HH}, at a greatly reduced frequency is strikingly confirmed; the value of $\Delta E_{OH} = -2.8$ eV is not bothersome because, as emphasised previously, a large value of ΔE_{AB} need not be indicative of a strongly allowed vibration. The assignment of the third IP to b_2 seems reasonable because of the strongly bonding OH and essentially non-bonding HH character.

C_2H_4 For the 1st IP the occurence of ν_{CC} at a lower frequency than in the neutral molecule is consistent with the present calculations. The associated MO is the C–C π-orbital. On removing an electron the planar constraint of the molecule is largely lifted, and it might be expected that the CH_2 twist (ν_4) be excited – the $2\nu_4$ sequence is well known in the Rydberg spectrum [28]. And, indeed, a vibrational spacing of 430 cm^{-1} is observed which is in excellent agreement with $2\nu_4(0 \to 1) = 472$ cm^{-1} obtained from the Rydberg spectrum. Excitation of the scissors vibration, denoted ν_{HH}, at a virtually unchanged frequency is also possible, in agreement with the suggestion of Baker *et al.* [26]. For the 2nd IP it is expected that if ν_{CC} and ν_{CH} are excited the former will have a frequency just a little above the value observed in the 1st IP and the latter a frequency lower than that of the neutral molecule. This is in agreement with the proposed assignment. So far, the assignments for the 1st and 2nd IPs are in agreement with those proposed by Baker *et al.* However, they have assigned the observed spacing of 0.10 eV to the ν_{HH} vibration. It is not felt that $\Delta E_{HH} = -0.1$ eV is likely to give a decrease in ν_{HH} of 0.07 eV. For lack of any other evidence it is tentatively suggested that the 0.10 eV spacing arises from $2\nu_4$. For the 3rd IP we might have a substantial decrease in ν_{CH}, and an increase in ν_{CC}, and a very small increase in ν_{HH}. The required change in ν_{HH} is far too large to be associated with $\Delta E_{HH} = 0.1$ eV (compare with the 2nd IP). However, the possibility is not discounted of ν_{CC} and ν_{CH} both being excited at approximately the same frequency; this would certainly account for the observed broadness of the bands. For 4th IP Baker *et al.* have suggested assignments to ν_{CH} or ν_{HH}, whereas Branton *et al.* [29] have suggested assignments to ν_{CC} and ν_{HH}. On the basis of the present calculations ν_{CH} seems to be the most reasonable assignment. It is interesting that there is a good linearity between ΔE_{CH} and ν_{CH} for the 2nd, 3rd and 4th bands, but hardly significant since the appropriate plot fails to go through the origin, unlike the equally good linear plot between ΔE_{CC} and ν_{CC}. For the 5th IP the resolution is insufficient for vibrational analysis. The only comment is that the value of ~ 19 eV is very close to the calculated value of 19.60 eV for the b_{3u} MO.

For all 5 IPs the predicted ordering is only incorrect in the reversal of the a_g and b_{1g} MOs, and in view of the closeness of the calculated values this is not regarded as a serious discrepancy. In a survey of MO calculations Baker *et al.* [26] showed this reversal to be generally the case, with the exception of the results of Berthod [30].

5. Conclusion

It is believed that the general usefulness of the parameter ΔE_{AB} has been demonstrated, and that its application to other molecules will be informative. However, there are weaknesses in the approach, and it will be just as well to point them out here.

It would be more systematic to calculate the changes in vibrational frequency on ionization via a properly constructed force-field. This would circumvent the difficulty in the present work of there being no explicit relationship between the calculated ΔE_{AB} and the experimental ν_{AB}. But a compromise has to be reached between the intrinsic accuracy of the MO theory and the subsequent rigorousness used in the treatment of the results. It is strongly felt that the simplistic concept of ΔE_{AB} as a parameter for pes is consistent with the inherent inaccuracy of the CNDO/2 theory. The procedure of retaining invariancy *via* a series of extremely crude approximations is completely contrary to the proper means of approaching invariancy by including greater numbers of integrals. Cook *et al.* [31] carried out *ab initio* calculations on H_2O and CH_4 and then repeated them neglecting those integrals not included in the CNDO/2 theory. The basis functions were Löwdin orthogonalized orbitals [32], and it would be anticipated that if CNDO/2 type approximations were to work they would work best with such basis functions. The agreement between the two sets of calculations was poor. This does not look promising for the normal CNDO/2 application where Slater orbitals are assumed orthogonal. And yet, applications of the CNDO/2 method have been anything but completely unsuccessful. Like all semi-empirical MO methods the success of the CNDO/2 method lies in the manner of evaluating the integrals. Provided that the demands made of the method are not too great it can be used meaningfully, and it is hoped that this has been done in the present work.

Acknowledgements. The author would like to express his appreciation of the cordiality shown by the photoelectron group of Southampton University, and of the many useful discussions held with Dr. N. B. H. Jonathan.

References

1. Richards, W. G.: Int. J. Mass Spectrometry Ion Physics **2**, 419 (1969).
2. Koopmans, T.: Physica **1**, 104 (1934).
3. Hoyland, J. R., Goodman, L.: J. chem. Physics **36**, 12 (1962).
4. Edwards, T. G., Grinter, R.: Molecular Physics **15**, 349 (1968).
5. Al-Joboury, M. I., Turner, D. W.: J. chem. Physics **37**, 3007 (1962); J. chem. Soc. 4434 (1964).

In Section 2 we give a description of the density localization method, and in Section 3 a short outline of the three other localization methods applied. Some computational aspects will be considered in Section 4 and the calculations are discussed in Section 5.

2. Outline of the Density Localization Method

We are restricting our considerations to the case of a one-determinantal approximation to a wavefunction with doubly filled orthonormal orbitals as for example determined by a SCF calculation. For a $2n$ electron system the wavefunction $|\Psi\rangle$ may be written as (for the notation see I)

$$|\Psi\rangle = (2n!)^{1/2}\,\mathscr{A}\{|1+\rangle|1-\rangle\ldots|n+\rangle|n-\rangle\}\,, \tag{1}$$

where $\mathscr{A}$ is the antisymmetric projection operator with $\mathscr{A}^2 = \mathscr{A}$. The row matrix of molecular orbitals (MO's):

$$\underline{|\Phi\rangle} := (|1\rangle, \ldots, |i\rangle, \ldots, |n\rangle)\,, \tag{2}$$

can be subjected to a unitary transformation without changing the wavefunction $|\Psi\rangle$ itself. The density localized atomic and molecular orbitals are defined as those orbitals resulting from the unitary transformation which minimizes the sum of all density overlap integrals between the orbitals:

$$D = \sum_{i<j} [i^2 j^2] = \min\,, \tag{3}$$

where the density overlap between orbitals $|i\rangle$ and $|j\rangle$ is defined by

$$[i^2 j^2] := \int |\langle \boldsymbol{r}|i\rangle|^2\, |\langle \boldsymbol{r}|j\rangle|^2\, d^3\boldsymbol{r}$$

and the charge density of some orbital $|i\rangle$ is given by $|\langle \boldsymbol{r}|i\rangle|^2$. It is to be noted that the quantity $\sum_{i,j}[i^2 j^2]$ is invariant under unitary transformations, whereas the terms $\sum_i [i^4]$ and $\sum_{i\neq j}[i^2 j^2]$, into which it can be decomposed, are not invariant. Minimization of D is equivalent to maximization of $\sum_i [i^4]$, which is the sum of the self-overlaps of the charge densities.

The localization is done via a sequence of pairwise rotations of the orbitals in the vector space spanned by them which are chosen such that the maximum decrease in D is obtained. Convergence to the DLMO's is reached if for all pairs of orbitals $|i\rangle$, $|j\rangle$ the following conditions hold:

$$[i^3 j] - [i j^3] = 0 \tag{5}$$

with

$$[ijkl] := \int \langle i|\boldsymbol{r}\rangle\langle \boldsymbol{r}|j\rangle\langle k|\boldsymbol{r}\rangle\langle \boldsymbol{r}|l\rangle\, d^3\boldsymbol{r}\,. \tag{6}$$

Numerically it may be more convenient to test the decrease in D directly. Convergence is reached, if any further decrease in D is smaller than a given threshold.

3. Energy, Boys, and Magnasco-Perico Localization Methods

Because the results of the density localization method will be compared to those of the energy localization method, the Boys, and the Magnasco-Perico localization method, the bases of these methods are briefly described in this section. For a more detailed discussion we refer to the original literature. In the energy localization method of Edmiston and Ruedenberg [2, 4], which is based on an earlier suggestion of Lennard-Jones and Pople [8], the sum of the orbital self-interaction energies is maximized and thus the sum of the exchange and Coulomb energies between the orbitals minimized. The electron interaction energy

$$E = 2\sum_{i,j}[i^2|j^2] - \sum_{i,j}[ij|ij] \tag{7}$$

consists of two terms, the Coulomb and exchange energy, which are separately invariant under unitary transformations. This is not the case for the term $D = \sum_i [i^2|i^2]$ occurring in both energy terms. Maximization of D, which is the orbital self-interaction energy, defines the ELMO's. Maximization of D implies the minimization of the terms

$$2\sum_{i\neq j}[i^2|j^2] \quad \text{and} \quad \sum_{i\neq j}[ij|ij] \tag{8}$$

which are the Coulomb and exchange energies between the orbitals. This fact is important for the physical interpretation.

The method of Boys [5, 6] consists in maximizing the sum of the squares of the distances between the charge centroids of the orbitals

$$D = \sum_{i,j}[\langle i|\mathbf{r}|i\rangle - \langle j|\mathbf{r}|j\rangle]^2 . \tag{9}$$

This has been shown by Boys to be equivalent to the minimization of

$$I = \sum_i \langle ii|r_{12}^2|ii\rangle \tag{10}$$

which Boys calls the sum of the quadratic repulsions of the orbitals with themselves [6]. The first formula is more convenient for computations because then only the $3n^2$ dipole moment matrix elements are required.

In the procedure of Magnasco and Perico [7] one starts with the definition of local electron populations for each MO. They have to be localized around atoms or between pairs of atoms, forming inner shells and lone pairs of electrons and bonds. This makes necessary a concept of the orbital structure prior to localization. For each orbital a local electron population is defined

$$P_i := \sum_{p,q\in\Gamma_i} c_{pi}c_{qi}\langle p|q\rangle , \tag{11}$$

where Γ_i denotes the set of functions contributing to this population. By maximizing the expression

$$P = \sum_i P_i \tag{12}$$

the uniformly localized orbitals of Magnasco and Perico (MPLMO's) are obtained. The arbitrariness of the method is contained in the definition of the sets Γ_i. It is an external method.

4. Computational Aspects

In I we have commented qualitatively on the computational aspects of the energy and the density localization method. We would like to come back to this point and compare the computational expense of all four localization methods under investigation. The two-electron integrals required for the energy localization procedure are in general available from the SCF calculation, but they have to be transformed to the basis of the occupied molecular orbitals. For the density localization method the basic density overlap integrals have to be computed and then transformed to the basis of the molecular orbitals. The calculation of these basic integrals as well as their transformation is significantly simplified by the high degeneracy of these integrals compared to the two-electron energy integrals. They are invariant with respect to any permutation of the four indices. It turned out that for the energy localization method the basis transformation of the integrals is computationally dominant in the cases considered. For the density localization procedure the dominant part is the calculation of the basic integrals. Comparing the calculation times of the energy, density, Boys, and Magnasco-Perico localization methods we find that the first two use large amounts of computer time, because the computation time is proportional to at least the fifth power of the number of basis functions. Which of the two methods, the energy or the density localization method, is faster cannot be stated in general. For small systems the energy localization method seems to be faster while for larger systems the density localization method becomes more and more favourable. The computation time of the Boys and the Magnasco-Perico localization method is proportional to the second power of the number of basis functions. The two methods are thus very fast and require few seconds of computer time on an IBM 360/91 computer for the largest molecules examined. For basis sets of 9*s*-type and 5*p*-type Gaussian lobe functions contracted to 5*s*-type and 3*p*-type functions for the second row atoms and of 4*s*-type functions for the H atom (contracted to 2*s*-type functions) some typical computation times are given in Table 1.

To investigate the sensitivity of the LMO's to a change in the wavefunction and to a different choice of starting point in the numerical process of localization the C_2 and N_2 molecules were examined in more detail. For C_2 $(1\sigma_g^2\, 1\sigma_u^2\, 2\sigma_g^2\, 2\sigma_u^2\, 1\pi_u^4, {}^1\Sigma_g^+)$ Edmiston and Ruedenberg [9] analyzing the wavefunction of Ransil [10] did not find equivalent orbitals as LMO's. We have calculated a fair

Table 1. Typical computation times in minutes for the energy and the density localization method[a]

Molecule	Energy localization method	Density localization method
C_2	1.4	3.7
N_2	2.2	3.8
F_2	5.2	4.4
HF	0.13	0.5
H_2O	0.4	0.7
NH_3	1.05	1.1
CH_4	1.9	1.5

[a] The numbers refer to an IBM 360/91 computer.

number of wavefunctions for this molecule with basis sets of type (5/1), (5/2), (7/3), and (9/5) with different contractions [11–14]. From our results we can draw the following conclusions. For a given wavefunction and a given localization method only one set of LMO's is obtained as solution, but if different wavefunctions are examined by the same localization method sets of LMO's differing qualitatively can be obtained. This was found for the density and the Boys localization method; for the Edmiston-Ruedenberg localization method on the other hand the solutions were always of the same type.

For the N_2 molecule a number of wavefunctions were calculated using the same basis sets as described for C_2. In all cases the methods of Edmiston and Ruedenberg and of Boys gave the same results, but we had some difficulties when applying the density localization method. For internuclear separations larger than 2.3 a.u. the answer was unique: trigonally equivalent banana bond orbitals resulted. But at the experimental distance of 2.0693 a.u. some wavefunctions gave distorted bond orbitals as solutions. The reason for this sensitivity of the density localization method might be the tight bonding structure of N_2 and the short range character of the δ-function potential which is the basis of this method. Aside from these two cases no indications for different sets of LMO's as solutions were found with other molecules. However, a further example will be discussed in another context [15].

To examine the existence of multiple extrema, we took different starting points for the localization. In all cases investigated convergence to the same solution was achieved. This does not disprove the existence of multiple extrema, we only did not find any.

5. The Calculations

Programs have been written to calculate SCF wavefunctions and from these the energy, density, Boys, and Magnasco-Perico localized molecular orbitals. We present here the results for the homonuclear diatomic molecules Li_2, Be_2, B_2, C_2, N_2, and F_2. The basis functions used are the Gaussian lobe functions. For all atoms except the H atom 9 functions of s-type are used, the 5 with the largest exponents being contracted into one group. For the H atom 4 functions of s-type are used, the two with the largest exponents contracted into one group. The exponents and contraction coefficients are taken from Huzinaga's paper [13]. For the Li and Be atom 2 functions of p-type are used. The exponents η and the distance R from the center are for Li: $\eta_1 = 0.5$, $R_1 = \pm 0.075$ a.u., $\eta_2 = 2.0$, $R_2 = \pm 0.065$ a.u. and for Be: $\eta_1 = 0.6$, $R_1 = \pm 0.07$ a.u., $\eta_2 = 2.4$, $R_2 = \pm 0.06$ a.u. For the atoms from B to F 5 functions of p-type are used, the three with the largest exponents contracted to one group with exponents and contraction coefficients as given by Whitten [14].

The results we obtained for the LMO's of these molecules agree qualitatively with the results given by Edmiston and Ruedenberg [4, 9] except for the C_2 molecule. We are going to discuss this case in detail below. The following conclusions can be drawn from a comparison of the different localized orbitals: The numerical agreement is very satisfactory in general among the results of the intrinsic methods. The best agreement is found between the LMO's of the energy and the Boys localization methods. The agreement between the ELMO's and DLMO's is nearly as good. The more "important" coefficients ($c \geqq 0.1$) in the expansion of the LMO's often agree to two and sometimes three significant figures, which is quite satisfactory in view of the fact that different separation functions are used in these three methods. The results of the Magnasco-Perico procedure show greater deviations, although there is good agreement with the results of the other methods in some cases. It is difficult to understand why the agreement is good in some cases and only fair in others. The *s*-type Gaussian functions with small exponents give the largest contribution to the inner shell LMO's of the heavy atoms in the case of the MPLMO's and smaller contributions in the case of the DLMO's, ELMO's, and the LMO's of Boys (BLMO's). If equivalent orbitals are found for a molecule the equivalence is in general numerically best fulfilled for the BLMO's and the MPLMO's and is not so good for the DLMO's and the ELMO's. The reason might be the insensitivity (to a variation in the LMO's) of the potential used as the separation function and the amount of numerical processes involved.

It has been stated in the literature [7, 16] that for molecules containing lone pairs of electrons the MPLMO's have a larger 2*p*-contribution in the lone pair orbitals than do the ELMO's and that the reverse is true for the bond orbitals. We have examined a fairly large number of molecules, some of which have not been analyzed from this point of view so far, and our results are not in complete agreement with this statement. In Table 2 we give the local 2*p*-type populations for several atoms for the lone pair and bond orbitals obtained by the energy, density, Boys, and Magnasco-Perico localization method. We have added the results for a number of other molecules which we shall discuss in more detail in a subsequent paper [15]. In most cases the BLMO's have about the same 2*p*-contribution as the ELMO's. But apparently no general statement can be made about the 2*p*-contribution to the MPLMO's compared to the ELMO's. For the atoms F in F_2, F in LiF, B in BF, N in NH_3, and O in H_2O the MPLMO's exhibit a larger 2*p*-contribution in the lone pair orbital (and a smaller 2*p*-contribution in the bond orbital) than do the ELMO's in agreement with previous work. The

Table 2. 2*p*-type populations of unnormalized hybrids on different atoms in bond and lone pair LMO's

	Bond orbital				Lone pair orbital			
Atom	ELMO	DLMO	BLMO	MPLMO	ELMO	DLMO	BLMO	MPLMO
B in B_2	0.1973	0.2045	0.1904	0.2492	0.2067	0.2006	0.2122	0.1673
N in N_2	0.3046	0.3119	0.2997	0.3362	0.2618	0.2417	0.2735	0.1883
F in F_2	0.3768	0.3909	0.3452	0.3695	0.6888	0.6847	0.6956	0.6904
F in LiF	0.7039	0.7000	0.7008	0.5701	0.7413	0.7407	0.7426	0.7842
B in BF	0.0525	0.0600	0.0477	0.0457	0.1118	0.1039	0.1170	0.1188
F in BF	0.5735	0.5753	0.5828	0.6074	0.6756	0.6768	0.6714	0.6571
N in BN	0.3863	0.3359	0.4087	0.4328	0.2245	0.3533	0.1601	0.0619
C in CO	0.1259	0.1371	0.1223	0.1387	0.1765	0.1615	0.1928	0.1722
O in CO	0.5091	0.3912	0.5130	0.5834	0.4007	0.5142	0.3823	0.1749
N in NH_3	0.3303	0.3316	0.3280	0.2999	0.7026	0.6982	0.7095	0.7912
O in H_2O	0.3929	0.3954	0.3884	0.3497	0.7005	0.6979	0.7051	0.7423
F in HF	0.4799	0.4803	0.4712	0.4973	0.7162	0.7162	0.7197	0.7109

Table 3. Bond distances (R) and total SCF energies (E)

Molecule	R [a.u.]	E [a.u.]
Li_2	5.0504	− 14.8626115
Be_2	3.78	− 29.0862513
B_2	3.0028	− 49.0324955
C_2	*2.4788*	− *75.3576030*
N_2	2.0693	− 108.8862996
F_2	2.6791	− 198.7058343

reverse is true for B in B_2, N in N_2, N in BN, F in BF, C in CO, O in CO, and F in HF. It seems also that there is a dependence on the wavefunction.

The results for the individual molecules are discussed in more detail in the following. Table 3 contains information about the geometry and the total energies obtained. Because of the length of the Gaussian function expansions of the orbitals we do not give them here. Instead only the transformation matrices from the canonical MO's (CMO's) to the LMO's are given. This seems to be the most useful information, because, as Edmiston and Ruedenberg [4] stated, the transformation matrices are approximately independent of the size of the basis set used to approximate the wavefunction. The signs of the CMO's are chosen in the following way: The largest coefficient of an s-type function in the expansion of a particular CMO or of a $2p\pi$-type function is given the positive sign. If there are two coefficients of equal magnitude and opposite sign, the first one carries the positive sign. In cases of degeneracy or of wavefunctions differing considerably in the basis set size this might not be sufficient, but this choice of the signs should eliminate the major uncertainties [17]. The transformation matrices for the four localization methods are given in Tables 4–10 for the different molecules.

Table 4. Transformation matrices for Li_2

ENERGY LOCALIZATION

	1Li	1Li'	bσLiLi'
$1\sigma_g$	0.70373	0.70373	0.09763
$1\sigma_u$	0.70711	-0.70711	0.00000
$2\sigma_g$	-0.06903	-0.06903	0.99522

DENSITY LOCALIZATION

	1Li	1Li'	bσLiLi'
$1\sigma_g$	0.69921	0.69921	0.14908
$1\sigma_u$	0.70711	-0.70711	0.0
$2\sigma_g$	-0.10541	-0.10541	0.98883

BOYS LOCALIZATION

	1Li	1Li'	bσLiLi'
$1\sigma_g$	0.70705	0.70705	0.01264
$1\sigma_u$	0.70711	-0.70711	0.0
$2\sigma_g$	-0.00893	-0.00893	0.99992

MAGNASCO-PERICO LOCALIZATION

	1Li	1Li'	bσLiLi'
$1\sigma_g$	0.68976	0.68976	0.22013
$1\sigma_u$	0.70711	-0.70711	0.0
$2\sigma_g$	-0.15565	-0.15565	0.97547

The LMO's resulting from the Magnasco-Perico localization method cannot be directly compared to the other LMO's, because orbitals of σ- and π-type symmetry are not mixed. Therefore a unitary transformation [7] has been applied after the localization.

Li_2 (Table 4)

Localization yields an inner shell on each Li atom and a bond orbital connecting the two atoms (Table 4). As mentioned previously the most important change in the localization functions results from the combination of the $1\sigma_g$ and $1\sigma_u$ orbitals. The exchange integrals change by about a factor of 200 and the density overlap integrals by about a factor of 400. Similar figures apply to all homonuclear diatomic molecules. The transformation matrices are nearly an identity with respect to the bond orbital.

Be_2 (Table 5)

Be_2 is a "nonbonded molecule". Consequently we obtain by localization an inner and an outer shell on each Be atom. The localization consists essentially in a left-right combination of $1\sigma_g$ and $1\sigma_u$ on the one hand and of $2\sigma_g$ and $2\sigma_u$ on the other hand, as indicated by the transformation matrices (Table 5). Because of the arbitrariness in the choice of the local electron populations in the Magnasco-Perico method a starting point can be selected that gives rise to two bonds as LMO's. This is perhaps the simplest example of forcing an unreasonable result. But it should be mentioned that in other cases (LiF e.g.) this method is fairly independent of the initial choice of the local electron populations.

Table 5 Transformation matrices for Be_2

ENERGY LOCALIZATION

	1Be	1Be'	2Be	2Be'
$1\sigma_g$	0.70160	0.70160	0.08809	0.08809
$1\sigma_u$	0.70332	-0.70332	0.07314	-0.07312
$2\sigma_g$	-0.08810	-0.08808	0.70160	0.70160
$2\sigma_u$	-0.07313	0.07312	0.70331	-0.70332

DENSITY LOCALIZATION

	1Be	1Be'	2Be	2Be'
$1\sigma_g$	0.69564	0.69564	0.12685	0.12685
$1\sigma_u$	0.69900	-0.69900	0.10679	-0.10679
$2\sigma_g$	-0.12685	-0.12685	0.69564	0.69564
$2\sigma_u$	-0.10679	0.10679	0.69900	-0.69900

BOYS LOCALIZATION

	1Be	1Be'	2Be	2Be'
$1\sigma_g$	0.70708	0.70708	-0.00668	-0.00668
$1\sigma_u$	0.70680	-0.70680	-0.02090	0.02090
$2\sigma_g$	0.00668	0.00668	0.70708	0.70708
$2\sigma_u$	0.02090	-0.02090	0.70680	-0.70680

MAGNASCO-PERICO LOCALIZATION

	1Be	1Be'	2Be	2Be'
$1\sigma_g$	0.68188	0.68188	0.18719	0.18719
$1\sigma_u$	0.69619	-0.69619	0.12377	-0.12377
$2\sigma_g$	-0.18719	-0.18719	0.68188	0.68188
$2\sigma_u$	-0.12377	0.12377	0.69619	-0.69619

Table 6. Transformation matrices for B_2

ENERGY LOCALIZATION

	1B	1B'	bσBB'	ℓσB	ℓσB'
$1\sigma_g$	0.70099	0.70099	0.10140	0.05893	0.05893
$1\sigma_u$	0.70299	-0.70299	-0.00000	0.07616	-0.07616
$2\sigma_g$	-0.08852	-0.08853	0.92124	0.26043	0.26043
$2\sigma_u$	-0.07616	0.07616	0.00000	0.70299	-0.70300
$3\sigma_g$	-0.02788	-0.02788	-0.37555	0.65476	0.65475

DENSITY LOCALIZATION

	1B	1B'	bσBB'	ℓσB	ℓσB'
$1\sigma_g$	0.69481	0.69481	0.14307	0.08370	0.08370
$1\sigma_u$	0.69803	-0.69803	0.0	0.11292	-0.11292
$2\sigma_g$	-0.12586	-0.12586	0.90735	0.26929	0.26929
$2\sigma_u$	-0.11292	0.11292	0.0	0.69803	-0.69803
$3\sigma_g$	-0.03742	-0.03742	-0.39528	0.64844	0.64844

BOYS LOCALIZATION

	1B	1B'	bσBB'	ℓσB	ℓσB'
$1\sigma_g$	0.70511	0.70511	0.05860	0.03312	0.03312
$1\sigma_u$	0.70611	-0.70611	0.0	0.03744	-0.03744
$2\sigma_g$	-0.05053	-0.05053	0.93204	0.25120	0.25120
$2\sigma_u$	-0.03744	0.03744	0.0	0.70611	-0.70611
$3\sigma_g$	-0.01615	-0.01615	-0.35760	0.66015	0.66015

MAGNASCO-PERICO LOCALIZATION

	1B	1B'	bσBB'	ℓσB	ℓσB'
$1\sigma_g$	0.68728	0.68728	0.14354	0.13171	0.13171
$1\sigma_u$	0.69347	-0.69347	0.0	0.13821	-0.13821
$2\sigma_g$	-0.15317	-0.15317	0.85477	0.33350	0.33350
$2\sigma_u$	-0.13821	0.13821	0.0	0.69347	-0.69347
$3\sigma_g$	-0.06471	-0.06471	-0.49877	0.60945	0.60945

B_2 (Table 6)

For the B_2 molecule the electronic configuration $1\sigma_g^2\, 1\sigma_u^2\, 2\sigma_g^2\, 2\sigma_u^2\, 3\sigma_g^2,\ {}^1\Sigma_g^+$ was analyzed. After localization we find an inner shell and a lone pair orbital on each B atom and a bond orbital linking the two atoms (Table 6). This lone pair orbital has a marked *s*-type contribution, which is largest for the Magnasco-Perico LMO's and decreases for the energy, the Boys and the density localized orbitals in the given order.

C_2 (Tables 7, 8)

According to the literature [9] the MO's of C_2 wavefunctions are difficult to localize. The conclusions reached here are the following: The energy localization method gave rise to effectively no problems, only one set of LMO's resulted. The density localization method gave two different solutions depending on the wavefunction examined. The method of Boys yielded two different solutions in most cases too, but sometimes did not converge and gave non-equivalent orbitals as intermediate solution. The method of Magnasco and Perico lead to easy convergence. A number of wavefunctions was examined for the C_2 molecule in the electronic configuration $1\sigma_g^2\, 1\sigma_u^2\, 2\sigma_g^2\, 2\sigma_u^2\, 1\pi_u^4,\ {}^1\Sigma_g^+$ using basis sets of type (5/1), (5/2), (7/3), and (9/5) with different contraction coefficients and different parameters for the *p*-type functions [11–14]. We give representative results of our investigations without specifying the wavefunctions in detail [17]. For all wave-

Table 7. Transformation matrices for C_2

ENERGY LOCALIZATION

	1C	1C'	b1CC'	b2CC'	b3CC'	b4CC'
$1\sigma_g$	0.70074	0.70090	0.06650	0.06650	0.06655	0.06649
$1\sigma_u$	0.70223	-0.70207	0.05908	0.05910	-0.05901	-0.05914
$2\sigma_g$	-0.09405	-0.09407	0.49558	0.49545	0.49583	0.49537
$2\sigma_u$	-0.08356	0.08355	0.49643	0.49665	-0.49587	-0.49704
$1\pi_u$	-0.00001	-0.00001	-0.70675	0.70664	0.02423	-0.02398
	0.00001	0.00000	0.02353	-0.02469	0.70694	-0.70645

DENSITY LOCALIZATION A

	1C	1C'	b1CC'	b2CC'	b3CC'	b4CC'
$1\sigma_g$	0.69267	0.69267	0.10051	0.10052	0.10048	0.10050
$1\sigma_u$	0.69383	-0.69383	0.09646	0.09642	-0.09649	-0.09644
$2\sigma_g$	-0.14214	-0.14214	0.48982	0.48989	0.48970	0.48977
$2\sigma_u$	-0.13640	0.13640	0.49067	0.49042	-0.49079	-0.49055
$1\pi_u$	0.0	0.00000	-0.51834	0.51829	-0.48103	0.48094
	0.0	0.0	0.48086	-0.48111	-0.51820	0.51844

DENSITY LOCALIZATION B

	1C	1C'	b1CC'	b2CC'	b3CC'	b4CC'
$1\sigma_g$	0.69398	0.69414	0.01992	0.02005	0.13376	0.13368
$1\sigma_u$	0.69635	-0.69620	0.17332	-0.12328	0.00010	0.00002
$2\sigma_g$	-0.13570	-0.13520	0.10223	0.10276	0.68665	0.68626
$2\sigma_u$	-0.12330	0.12330	0.69635	-0.69620	0.00047	0.00004
$1\pi_u$	-0.00002	-0.00002	0.69920	0.69928	-0.09168	-0.11714
	0.00000	0.00000	-0.01784	-0.01741	0.70868	-0.70531

BOYS LOCALIZATION A

	1C	1C'	b1CC'	b2CC'	b3CC'	b4CC'
$1\sigma_g$	0.70621	0.70532	0.01773	0.03476	0.03476	0.03473
$1\sigma_u$	0.70737	-0.70648	0.00553	-0.01273	-0.01271	-0.01263
$2\sigma_g$	-0.02964	-0.05113	0.55539	0.47904	0.47899	0.47869
$2\sigma_u$	0.00428	0.02806	0.83147	-0.32156	-0.32109	-0.31834
$1\pi_u$	0.00005	0.00001	0.00188	0.58761	0.19496	-0.78530
	-0.00001	-0.00000	-0.00028	0.56609	-0.79752	0.22683

BOYS LOCALIZATION B

	1C	1C'	b1CC'	b2CC'	b3CC'	b4CC'
$1\sigma_g$	0.70445	0.70452	0.04623	0.04621	0.03953	0.03953
$1\sigma_u$	0.70622	-0.70616	0.03595	-0.03594	0.00003	0.00003
$2\sigma_g$	-0.06071	-0.06068	0.56349	0.56357	0.42279	0.42279
$2\sigma_u$	-0.03596	0.03593	0.70597	-0.70642	0.00037	0.00037
$1\pi_u$	0.00315	0.00316	0.34683	0.34612	-0.87013	-0.05258
	0.00223	0.00224	0.24572	0.24522	0.25012	-0.90384

functions examined the energy localization method gave one set of LMO's as solution (the transformation matrix for the wavefunction calculated with the (9/5) basis set is listed in Table 7). These ELMO's are equivalent orbitals. The analysis of the C_2 wavefunction of Ransil [10] by Edmiston and Ruedenberg [9] did on the other hand not give equivalent orbitals of any kind. To describe the bonding orbitals which we have obtained (b1CC', b2CC', b3CC', and b4CC') their charge centroids are given in Table 8. These orbitals have the symmetry property expected of equivalent orbitals. Bond orbitals 1 and 2 are transformed into each other by a rotation through 180° about the CC' axis, so are orbitals 3 and 4. A rotation through 90° plus a reflection in the plane perpendicular to and bisecting the internuclear axis transforms 1 into 3 and 2 into 4 and vice versa. From the transformation matrix in Table 7 it follows that these orbitals arise roughly in the following way: left-right combination of $2\sigma_g$ and $2\sigma_u$ gives a 2s-type atomic orbital on atoms C and C'. combination of the 2s orbital on atom C with the π_x-canonical orbital gives orbitals 1 and 2 lying in the $x-z$-plane in the neighbourhood of one C atom. A similar combination of the 2s orbital on atom C' with the π_y canon-

Table 8. Charge centroids of the bonding orbitals in C_2[a]

Orbital	Method	x	y	z
b1CC′	Energy	0.588	0.008	0.749
b2CC′		−0.588	−0.007	0.749
b3CC′		0.008	−0.589	1.730
b4CC′		−0.008	0.588	1.730
b1CC′	Density A	−0.003	0.574	0.679
b2CC′		0.003	−0.574	0.679
b3CC′		0.574	0.003	1.799
b4CC′		−0.574	−0.003	1.799
b1CC′	Density B	−0.121	−0.004	1.094
b2CC′		−0.121	−0.004	1.385
b3CC′		0.145	−0.816	1.239
b4CC′		0.097	0.823	1.239
b1CC′	Boys A	0.000	−0.002	0.356
b2CC′		−0.507	−0.418	1.535
b3CC′		0.616	−0.229	1.535
b4CC′		−0.109	0.648	1.532
b1CC′	Boys B	−0.373	−0.121	0.426
b2CC′		−0.372	−0.121	2.053
b3CC′		0.523	−0.345	1.239
b4CC′		0.222	0.586	1.239

[a] The molecule lies along the z-axis with one C atom in the origin the other at a z-value of 2.4788 a.u.

ical orbital gives orbitals 3 and 4 lying in the $y-z$-plane in the neighbourhood of the other C atom.

The same type of orbital is obtained by the density localization method for a wavefunction calculated with a (5/1) basis set. The transformation matrix is given as "Density Localization A" in Table 7 and the charge centroids of the bonding orbitals are given in Table 8. An analysis of the wavefunction resulting from the (9/5) basis set gave a different type of orbital which is presented as "Density Localization B" in Table 7 and 8. These orbitals form two sets of equivalent orbitals. Orbitals b1CC′ and b2CC′ lie quite close to the middle of the bond, one to the left, one to the right. Orbitals b3CC′ and b4CC′ have their charge centroids in the $x-y$-plane defined by the middle of the bond. Result B was found most frequently in the analysis of the different wavefunctions.

Applying the Boys localization method to a wavefunction calculated with a (7/3) basis set gave orbitals similar to type B described above. The results are given as "Boys Localization B" in Tables 7 and 8. Compared to the corresponding DLMO's the charge centroids of the orbitals b1CC′ and b2CC′ lie much closer to the C atoms. They appear to be mixtures of bond and lone pair orbitals. Localization of the MO's of a similar (7/3) wavefunction using slightly different parameters for the p-functions by the Boys method gave still a new set of LMO's, which are unsymmetric with respect to the two C atoms. All four orbitals are mixtures of lone pair and bonding orbitals. A single orbital is placed at one C atom and three trigonally equivalent orbitals are placed at the other C atom. There are two degenerate solutions of this type with the C atoms interchanged. We list one solution in Tables 7 and 8 ("Boys Localization A"). These two types of

Table 9. Transformation matrices for N_2

ENERGY LOCALIZATION

	1N	1N'	ℓσN	ℓσN'	bt1NN'	bt2NN'	bt3NN'
$1\sigma_g$	0.69991	0.69991	0.05983	0.05984	0.06615	0.06608	0.06596
$1\sigma_u$	0.70195	-0.70196	0.08523	-0.08523	-0.00001	0.00001	-0.00000
$2\sigma_g$	-0.09417	-0.09417	0.18904	0.18905	0.55172	0.55125	0.55002
$2\sigma_u$	-0.08522	0.08523	0.70194	-0.70196	0.00000	0.00000	-0.00001
$3\sigma_g$	-0.03547	-0.03548	0.67875	0.67873	-0.15976	-0.15942	-0.15866
$1\pi_u$	0.00001	0.00002	-0.00005	-0.00007	-0.67895	0.73228	-0.05281
	0.00000	0.00000	-0.00028	-0.00029	-0.45247	-0.36070	0.81558

DENSITY LOCALIZATION

	1N	1N'	ℓσN	ℓσN'	bt1NN'	bt2NN'	bt3NN'
$1\sigma_g$	0.69276	0.69276	0.07955	0.07956	0.09726	0.09679	0.09323
$1\sigma_u$	0.69650	-0.69650	0.12200	-0.12200	0.00000	-0.00000	0.00000
$2\sigma_g$	-0.13724	-0.13724	0.23031	0.23032	0.54423	0.54102	0.51706
$2\sigma_u$	-0.12200	0.12200	0.69650	-0.69650	0.00001	-0.00001	0.00001
$3\sigma_g$	-0.03541	-0.03541	0.66375	0.66374	-0.20646	-0.20323	-0.18015
$1\pi_u$	0.00000	0.00000	0.00070	0.00068	-0.61421	0.77229	-0.16221
	-0.00001	-0.00001	-0.00836	-0.00836	-0.52390	-0.24535	0.81559

BOYS LOCALIZATION

	1N	1N'	ℓσN	ℓσN'	bt1NN'	bt2NN'	bt3NN'
$1\sigma_g$	0.70440	0.70440	0.03408	0.03408	0.04207	0.04207	0.04207
$1\sigma_u$	0.70565	-0.70565	0.04531	-0.04531	0.0	0.0	-0.00000
$2\sigma_g$	-0.05810	-0.05810	0.16508	0.16508	0.55939	0.55939	0.55939
$2\sigma_u$	-0.04531	0.04531	0.70565	-0.70565	0.0	0.00000	0.0
$3\sigma_g$	-0.02099	-0.02099	0.68672	0.68672	-0.13655	-0.13655	-0.13655
$1\pi_u$	0.00000	0.0	0.0	0.0	-0.45401	-0.36071	0.81472
	0.0	0.0	0.0	0.00000	-0.67863	0.73250	-0.05387

MAGNASCO-PERICO LOCALIZATION

	1N	1N'	ℓσN	ℓσN'	bt1NN'	bt2NN'	bt3NN'
$1\sigma_g$	0.69123	0.69123	0.10911	0.10911	0.08283	0.08283	0.08283
$1\sigma_u$	0.69697	-0.69697	0.11929	-0.11929	0.0	0.0	0.0
$2\sigma_g$	-0.14224	-0.14224	0.34004	0.34004	0.49271	0.49271	0.49271
$2\sigma_u$	-0.11929	0.11929	0.69697	-0.69697	0.0	0.0	0.0
$3\sigma_g$	-0.04432	-0.04432	0.61030	0.61030	-0.28933	-0.28933	-0.28933
$1\pi_u$	0.0	0.0	0.0	0.0	-0.81650	0.40825	0.40825
	0.0	0.0	0.0	0.0	0.0	-0.70711	0.70711

orbitals are typical results of the Boys localization method, but other solutions are obtained too: orbitals of the type as described above but considerably distorted and nonequivalent orbitals. These were generally found if no satisfactory convergence in the localization process could be achieved. These results indicate that the hypersurface involved in the localization process is very flat in the neighbourhood of the extremum. (See also the discussion in Ref. [9].)

The orbitals resulting from the Magnasco-Perico localization are two inner shells, two 2*s* orbitals and two π-bonds. A mixing of the 2*s*- with the π-orbital is expected to give better localized orbitals (see above). However, it is not obvious which transformation has to be applied to give this result. The external character of the Magnasco-Perico method gives too great an arbitrariness in this case (see Section 3).

Finally two things should be noted. All types of LMO's which we have found for the C_2 molecule do not conform with the classical chemical concepts of electron pairs. Secondly different wavefunctions can give different sets of LMO's as solutions, but there is little indication of multiple extrema in the localization process, because in no case two different solutions have been obtained for a given wavefunction.

N_2 (Table 9)

All localization procedures yield an inner shell and a lone pair orbital on each atom and three trigonally equivalent banana bond orbitals linking the two atoms. (Table 9; the transformation matrix for the density localization method was obtained from a wavefunction calculated with a (7/3) basis set because the (9/5) wavefunction lead to somewhat distorted bond orbitals (we would like to note that N_2 wavefunctions calculated with Cartesian Gaussian functions as basis functions do not seem to show this distortion)). The lone pair orbitals have a large *s*-type contribution, although it is smaller than in the case of the B_2 molecule. If one compares the structure of these orbitals with the lone pair orbital in NH_3, which will be discussed in a subsequent paper, we find that for NH_3 the 2*p*-contribution is more than doubled. This gives rise to a much larger extension of the lone pair orbital away from the molecule. This can explain why NH_3 will easily accept a proton to form NH_4^+ whereas N_2 will not. The lone pair orbitals of N_2

Table 10. Transformation matrices for F_2

ENERGY LOCALIZATION

	1F	1F'	t1F	t2F	t3F	t1F'	t2F'	t3F'	bσFF'
$1\sigma_g$	0.69962	0.69963	0.05762	0.05762	0.05756	0.05763	0.05759	0.05757	0.03387
$1\sigma_u$	0.69917	-0.69917	0.06102	0.06101	0.06095	-0.06104	-0.06099	-0.06096	-0.00000
$2\sigma_g$	-0.09896	-0.09897	0.35389	0.35384	0.35350	0.35396	0.35368	0.35356	0.47919
$2\sigma_u$	-0.10565	0.10565	0.40385	0.40379	0.40335	-0.40398	-0.40360	-0.40343	-0.00001
$1\pi_u$	-0.00000	-0.00000	0.19395	0.37357	-0.56818	-0.45296	-0.08300	0.53660	-0.00001
	-0.00000	-0.00001	-0.54366	0.44008	0.10376	-0.35765	0.57140	-0.21352	-0.00003
$3\sigma_g$	-0.02705	-0.02705	0.19561	0.19559	0.19528	0.19571	0.19545	0.19532	-0.87706
$1\pi_g$	0.00001	0.00000	0.28921	0.28769	-0.57757	0.38069	0.18512	-0.56640	0.00012
	0.00000	0.00000	-0.49954	0.50046	-0.00085	0.43377	-0.54692	0.11279	0.00004

DENSITY LOCALIZATION

	1F	1F'	t1F	t2F	t3F	t1F'	t2F'	t3F'	bσFF'
$1\sigma_g$	0.69307	0.69308	0.07935	0.07915	0.07905	0.07933	0.07921	0.07902	0.04095
$1\sigma_u$	0.69172	-0.69171	0.08490	0.08468	0.08456	-0.08487	-0.08474	-0.08453	0.00000
$2\sigma_g$	-0.13612	-0.13612	0.36071	0.35988	0.35945	0.36059	0.36013	0.35933	0.43045
$2\sigma_u$	-0.14673	0.14673	0.40025	0.39919	0.39864	-0.40010	-0.39950	-0.39848	-0.00000
$1\pi_u$	0.00000	0.00000	0.50507	-0.49474	-0.01171	0.52641	-0.46841	-0.05897	0.00031
	0.00000	0.00000	0.27835	0.29784	-0.57777	0.23578	0.33735	-0.57499	0.00045
$3\sigma_g$	-0.02350	-0.02350	0.17613	0.17533	0.17492	0.17602	0.17556	0.17480	-0.90169
$1\pi_g$	0.00000	-0.00000	0.44630	-0.54050	0.09313	-0.47501	0.52176	-0.04616	0.00006
	0.00000	-0.00000	0.36525	0.20332	-0.57032	-0.32723	-0.24694	0.57614	-0.00003

BOYS LOCALIZATION

	1F	1F'	t1F	t2F	t3F	t1F'	t2F'	t3F'	bσFF'
$1\sigma_g$	0.70392	0.70393	0.03718	0.03718	0.03718	0.03718	0.03718	0.03718	0.02613
$1\sigma_u$	0.70388	-0.70387	0.03901	0.03901	0.03901	-0.03901	-0.03901	-0.03901	0.00000
$2\sigma_g$	-0.06350	-0.06350	0.33444	0.33444	0.33444	0.33444	0.33444	0.33444	0.56641
$2\sigma_u$	-0.06757	0.06757	0.40638	0.40638	0.40638	-0.40638	-0.40638	-0.40638	0.0
$1\pi_u$	0.00000	-0.00000	-0.39192	0.56311	-0.17119	-0.10676	0.54476	-0.43800	0.0
	0.0	0.00000	0.42395	0.12744	-0.55139	-0.56739	0.19124	0.37616	0.00000
$3\sigma_g$	-0.02134	-0.02134	0.23116	0.23116	0.23116	0.23116	0.23116	0.23116	-0.82371
$1\pi_g$	0.00000	0.0	-0.46223	0.53071	-0.06849	0.00223	-0.50111	0.49888	0.00000
	0.0	0.0	0.34595	0.22732	-0.57327	0.57735	-0.28674	-0.29060	0.0

MAGNASCO-PERICO LOCALIZATION

	1F	1F'	t1F	t2F	t3F	t1F'	t2F'	t3F'	bσFF'
$1\sigma_g$	0.68277	0.68278	0.10343	0.10343	0.10343	0.10343	0.10343	0.10343	0.05866
$1\sigma_u$	0.68263	-0.68262	0.10650	0.10650	0.10650	-0.10650	-0.10650	-0.10650	0.00000
$2\sigma_g$	-0.17553	-0.17553	0.33913	0.33913	0.33913	0.33913	0.33913	0.33913	0.49833
$2\sigma_u$	-0.18447	0.18447	0.39411	0.39411	0.39411	-0.39411	-0.39411	-0.39411	0.00000
$1\pi_u$	0.0	0.0	0.40765	0.15025	-0.55790	-0.47496	-0.04680	0.52175	0.0
	0.0	0.0	-0.40885	0.55746	-0.14861	-0.32825	0.57545	-0.24720	0.0
$3\sigma_g$	-0.05482	-0.05482	0.20239	0.20239	0.20239	0.20239	0.20239	0.20239	-0.86500
$1\pi_g$	0.0	0.0	0.47496	0.04680	-0.52175	0.40765	0.15025	-0.55790	0.0
	0.0	0.0	-0.32825	0.57545	-0.24720	0.40885	-0.55746	0.14861	0.0

are close to 2s-atomic orbitals. Hall and Lennard-Jones [8] have discussed this in detail. The banana bonds show a fairly small contribution of the s- and 2pσ-type functions, the 2pπ-contribution is dominating.

F_2 (Table 10)

Localization gives an inner shell orbital, three trigonally equivalent lone pair orbitals on each F atom and a bond orbital which is mostly formed by the 2pσ-functions (Table 10). No preferential orientation of the two sets of trigonal lone pair orbitals with respect to each other exist, which agrees with earlier studies [4, 9]. For a group-theoretical explanation see the recent article of England [18].

6. Conclusions

In this paper we have presented the applications of the density localization method to a number of homonuclear diatomic molecules. A good agreement between the ELMO's and DLMO's was found, as expected. For most of the atoms and molecules investigated so far the LMO's calculated by the four localization methods agree qualitatively and frequently quantitatively with the exception of the C_2 molecule, which seems to present a particular case. The best quantitative agreement is found in general between the ELMO's and the BLMO's. The agreement between the ELMO's and DLMO's is about as satisfactory, whereas the MPLMO's show sometimes a more marked difference.

All four methods have their justification and it depends on the problem under investigation (and on the preference of the user) which method is to be applied.

The Edmiston-Ruedenberg method is completely general and works reliably in all cases examined so far. It is the only method which uses the energy criterion for the localization. Unfortunately the computation time needed to determine the ELMO's is considerable. The density localization method stresses the charge density aspect of the electronic structure of atoms and molecules. This method is completely general as well, but appears to be more sensitive against the choice of the wavefunction at least in a few cases (C_2, N_2). From the physical point of view it is complementary to the energy localization method. Examining the calculations we can establish this method as a new localization method which adds information to our knowledge about the concept of localization and of localized orbitals. The procedures of Boys and of Magnasco and Perico have the advantage of requiring very little computation time. The method of Boys is intrinsic in character and simple in its structure. Therefore we tend to prefer it over the localization procedure of Magnasco and Perico. The restrictions to the applicability of this method seem to be of minor importance. As discussed before the Magnasco-Perico localization method is external in character, the MPLMO's thus depend on our choice of the orbital structure. This is in some respect a disadvantage limiting the applicability of the method, but for some purposes this may give an added flexibility which can be of use.

Acknowledgement. The author would like to thank Professor Ruedenberg very much for a valuable discussion. A number of points were also discussed with Dr. J. Schäfer and Dr. W. Meyer. We thank Dr. G. Diercksen for reading the manuscript. The calculations have in part been performed at the IBM Research Laboratory in San José, California and in part at the Max-Planck-Institut für Physik und Astrophysik, München, Germany. Financial support of IBM Germany and IBM World Trade while the author was a guest in San José and of the Deutsche Forschungsgemeinschaft is gratefully acknowledged.

References

1. von Niessen, W.: Density localization of atomic and molecular orbitals I. J. chem. Physics **55**, 4290 (1972).
2. Edmiston, C., Ruedenberg, K.: Rev. mod. Physics **35**, 457 (1963).
3. Ruedenberg, K.: Modern quantum chemistry, Vol. I. Sinanoğlu, O. (Ed.), p. 85. New York: Academic Press 1965.
4. Edmiston, C., Ruedenberg, K.: J. chem. Physics **43**, S97 (1965).
5. Foster, J. M., Boys, S. F.: Rev. mod. Physics **32**, 300 (1960).
6. Boys, S. F.: Quantum theory of atoms, molecules, and the solid state. Löwdin, P. O. (Ed.), p. 253. New York: Academic Press 1966.
7. Magnasco, V., Perico, A.: J. chem. Physics **47**, 971 (1967); **48**, 800 (1968).
8. Lennard-Jones, J.: Proc. Roy. Soc. (London) A **198**, 1, 14 (1949). - Hall, G. G., Lennard-Jones, J.: Proc. Roy. Soc. (London) A **202**, 155 (1950). Lennard-Jones, J., Pople, J. A.: Proc. Roy. Soc. (London) A **202**, 166 (1950). – Hall, G. G.: Proc. Roy. Soc. (London) A **202**, 336 (1950). Pople, J. A.: Proc. Roy. Soc. (London) A **202**, 323 (1950). – Hall, G. G., Lennard-Jones, J.: Proc. Roy. Soc. (London) A **205**, 357 (1951).
9. Edmiston, C., Ruedenberg, K.: Quantum theory of atoms, molecules, and the solid state. Löwdin, P. O. (Ed.), p. 263. New York: Academic Press 1966.
10. Ransil, B. J.: Rev. mod. Physics **32**, 239 (1960).
11. Preuss, H.: Z. Naturforschg. **20**a, 1290 (1965).
12. Clementi, E.: J. chem. Physics **46**, 4737 (1967).
13. Huzinaga, S.: J. chem. Physics **42**, 1293 (1965).
14. Whitten, J. L.: J. chem. Physics **44**, 359 (1966).
15. von Niessen, W.: Density localization of atomic and molecular orbitals III, to be submitted.
16. Trindle, C., Sinanoğlu, O.: J. chem. Physics **49**, 65 (1968).
17. The detailed results (basis set, expansion coefficients for the canonical MO's and LMO's and transformation matrices) can be obtained upon request from the author.
18. England, W.: Int. J. quant. Chemistry **5**, 683 (1971).

Dr. W. von Niessen
Max-Planck-Institut für Physik und Astrophysik
D-8000 München 23, Föhringer Ring 6
Germany

Theoret. chim. Acta (Berl.) 27, 25—32 (1972)
© by Springer-Verlag 1972

Analysis of Correlation Effects in HeI, LiI and BeI Iso-electronic Sequences by Z-expansion Methods

J. P. Colpa and M. F. J. Islip

Department of Chemistry, Queen's University, Kingston, Ontario, Canada

Received June 2, 1972

Correlation effects for the energy and the expectation values of the electron-nuclear attraction and the inter-electronic repulsion in atomic states are discussed in terms of Z expansions for these quantities. Numerical examples are given for the HeI, LiI and BeI iso-electronic sequences.

It is shown that a series expansion of the type $\langle V_{en}\rangle = 2\varepsilon_0 Z^2 + \varepsilon_1 Z$ (a.u.) gives very accurate results for the expectation value of the electron-nuclear attraction.

Der Korrelationsanteil an der Energie und an den Erwartungswerten der Elektron-Kernanziehung sowie der Elektronenabstoßung für atomare Zustände wird mit Hilfe der Z-Entwicklung dieser Größen diskutiert. Für die isoelektronischen Reihen HeI, LiI und BeI werden numerische Beispiele angegeben. Es wird gezeigt, daß eine Reihenentwicklung vom Typ $\langle V_{en}\rangle = 2\varepsilon_0 Z^2 + \varepsilon_1 Z$ (a.E.) sehr genaue Ergebnisse für den Erwartungswert der Elektron-Kernanziehung liefert.

1. Introduction

Recently, an interpretation of the correlation energy in atoms in terms of the expectation values of the various terms in the Hamiltonian has been suggested by Gruninger, Öhrn and Löwdin [1], hereafter referred to for the sake of brevity, as G.O.L. These authors quote as examples some numerical results for the ground states of the HeI and LiI iso-electronic sequences.

In the present paper, we indicate a method of an analysis of the correlation energy in atoms and ions of iso-electronic sequences based on Z-expansions for the energy and expectation values for the electron-nuclear attraction and electron-electron repulsion energies. Such an analysis was suggested by Löwdin [2] several years ago, but seems to have received little attention. We have presented elsewhere [3], an analysis of some anomalies surrounding the interpretation of Hund's Rule based on similar series expansions.

We shall here briefly review the necessary formalism. Consider the non-relativistic Hamiltonian $H = T + V_{en} + V_{ee}$, where T is the kinetic energy operator, and V_{en} and V_{ee} the electron-nuclear attraction and electron-electron repulsion operators, respectively. Applying the Hellmann-Feynman theorem, we have,

$$\frac{\partial E}{\partial Z} = \left\langle \frac{\partial H}{\partial Z} \right\rangle = \frac{\partial}{\partial Z}\langle V_{en}\rangle = Z^{-1}\langle V_{en}\rangle . \tag{1}$$

The Virial theorem states, $2E = \langle V_{en} \rangle + \langle V_{ee} \rangle$, hence, from (1) we obtain

$$\langle V_{ee} \rangle = 2E - Z \frac{\partial E}{\partial Z} \tag{2}$$

E as a function of Z is given by the well-known Hylleraas expansion [2, 4]

$$E = \varepsilon_0 Z^2 + \varepsilon_1 Z + \varepsilon_2 + \frac{\varepsilon_3}{Z} + \frac{\varepsilon_4}{Z^2} + \cdots \tag{3}$$

which, when substituted into (1) and (2) leads to

$$\langle V_{en} \rangle = 2\varepsilon_0 Z^2 + \varepsilon_1 Z - \frac{\varepsilon_3}{Z} - \frac{2\varepsilon_4}{Z^2} - \cdots \tag{4}$$

and

$$\langle V_{ee} \rangle = \varepsilon_1 Z + 2\varepsilon_2 + \frac{3\varepsilon_3}{Z} + \frac{4\varepsilon_4}{Z^2} + \cdots; \tag{5}$$

The coefficients ε_n are the n^{th} order perturbation energy corrections obtained by taking V_{ee} as the perturbation [2, 4]. Hence in zeroth order, the wavefunction is a Slater determinant constructed from hydrogenic orbitals.

Eqs. (1), (2), and (3), and hence (4) and (5) are satisfied by exact wavefunctions. That the Hellmann-Feynman theorem and the Virial theorem are satisfied by solutions to the full Hartree-Fock equations has been shown by Coulson [5] and Löwdin [2] respectively. The validity of Eq. (3) for exact Hartree-Fock energies has been demonstrated by Linderberg and Shull [6]. Consequently, (3), (4), and (5) are valid in both exact and Hartree-Fock cases. In what follows, primed symbols will refer to Hartree-Fock, and unprimed symbols to exact cases, respectively. It has been shown [6] that $\varepsilon_0 = \varepsilon_0'$, and moreover, that when no zeroth order degeneracy exists between states with the same spectroscopic designation, $\varepsilon_1 = \varepsilon_1'$. Such is the case for the ground states of the He*I* and Li*I* sequences, but for the Be*I* sequence, where the $2s^2$ and $2p^2\,{}^1S$ states are degenerate in zeroth order, $\varepsilon_1 \neq \varepsilon_1'$, and ε_1 is calculated from degenerate perturbation theory. The coefficients ε_1 and ε_1' have been calculated for first row atoms and ions [6].

Defining the correlation energy E_c, by $E_c = E_{\text{exact}} - E_{\text{HF}}$, we obtain

$$E_c = (\varepsilon_1 - \varepsilon_1') Z + (\varepsilon_2 - \varepsilon_2') + \frac{(\varepsilon_3 - \varepsilon_3')}{Z} + \frac{(\varepsilon_4 - \varepsilon_4')}{Z^2} + \cdots \tag{6}$$

where the zeroth order term has vanished. Similarly the effect of correlation on electron-nuclear attraction, and electron-electron repulsion is given by

$$\langle V_{en} \rangle_c = (\varepsilon_1 - \varepsilon_1') Z - \frac{(\varepsilon_3 - \varepsilon_3')}{Z} - \frac{2(\varepsilon_4 - \varepsilon_4')}{Z^2} - \cdots \tag{7}$$

and

$$\langle V_{ee} \rangle_c = (\varepsilon_1 - \varepsilon_1') Z + 2(\varepsilon_2 - \varepsilon_2') + \frac{3(\varepsilon_3 - \varepsilon_3')}{Z} + \frac{4(\varepsilon_4 - \varepsilon_4')}{Z^2} + \cdots. \tag{8}$$

The first order terms in (6), (7), and (8) will vanish for the He*I* and Li*I* sequences, but not for the Be*I* sequence, and so we shall discuss the two separately.

2. Helium I and Lithium I Sequences

Hartree-Fock, configuration interaction and exact non-relativistic energies of atoms and ions of the He*I* and Li*I* sequences for Z up to 8, are reported in several places in the literature [1, 7–9].

We have carried out least-square fits of the available data, to Eq. (3) correct up to the term in ε_4, where we have made use of the exact theoretical values for ε_0 and $\varepsilon_1(\varepsilon_1')$ given by Linderberg and Shull [6], and have fitted the remaining parameters. We found that the expression fitted the reported values of the energy extremely accurately. In all cases, the relative error was found to be of the order of $10^{-4}\%$. The perturbation energy coefficients to fourth order, for the various types of wavefunction are displayed in Tables 1 and 2.

Table 1. Summary of perturbation energy coefficients ε_n for the He*I* sequence (in a.u.)

n	HF	CI		Exact	
	Weiss [8]	G.O.L. [1]	Weiss [8]	H.M. [14]	S.K. [13]
0	−1.0	−1.0	−1.0	−1.0	−1.0
1	0.625	0.625	0.625	0.625	0.625
2	−0.11116	−0.15551	−0.15674	−0.15766	−0.15766
3	0.00011	0.00690	0.00842	0.00854	0.00869
4	−0.00239	−0.00218	−0.00266	−0.00034	−0.00089

Table 2. Summary of perturbation energy coefficients ε_n, for the Li*I* sequence (in a.u.)

n	HF	CI		Exact	
	G.O.L. [1]	G.O.L. [1]	Weiss [8]	S.S.M. [9]	Weiss [8]
0	−1.125	−1.125	−1.125	−1.125	−1.125
1	1.0228	1.0228	1.0228	1.0228	1.0228
2	−0.35577	−0.40280	−0.40679	−0.41054	−0.41175
3	−0.02379	−0.01854	−0.00432	0.00918	0.01987
4	−0.11138	−0.08515	−0.11027	−0.12588	−0.14737

It is not completely obvious that (4) and (5) should apply to configuration interaction wavefunctions, which although very good, are still nevertheless not exact. If the wavefunctions are suitably scaled, however, the Virial theorem is certainly satisfied [2].

Moreover, calculations of $\langle V_{en}\rangle$ and $\langle V_{ee}\rangle$ according to (4) and (5) based on the perturbation coefficients corresponding to CI (G.O.L.) in Tables 1 and 2 reproduce rather pleasingly the results calculated directly from the wavefunctions. We also notice that, in accordance with (5), the calculated values for $\langle V_{ee}\rangle$ of those authors is approximately linear in Z, with slope near to ε_1.

In Table 3, $\varepsilon_n - \varepsilon_n'$ have been displayed for $n = 2, 3, 4$, describing the correlation effects up to fourth order, for the helium and lithium sequences. In Table 4, we summarize for the lithium sequence, the values of E_c, $\langle V_{ee}\rangle_c$ and $\langle V_{en}\rangle_c$ as given by (6)–(8) and the coefficients from Table 3, together with the corresponding values reported by G.O.L. [1]. One notices that E_c is reproduced by the series expansion with almost perfect accuracy, but that the agreement for $\langle V_{ee}\rangle_c$ is less good especially for $Z = 3, 4$. On the other hand, the discrepancy is only about 4%. For $\langle V_{en}\rangle_c$, however, the agreement between the results of our series expansion (7), and the results of the above authors direct calculation is peculiarly unsatisfactory.

Table 3. Summary of expansion coefficients $\varepsilon_n - \varepsilon'_n$ for the correlation energy, for various wavefunctions in the He*I* and Li*I* sequences (in a.u.)

	Wavefunction		*n* 2	3	4
Helium					
	CI	G.O.L [1]	-0.04435	0.00679	0.00021
		Weiss [8]	-0.04558	0.00831	0.00027
	Exact	H.M [14]	-0.04650	0.00843	0.00205
		S.K [13]	-0.04650	0.00858	0.00150
Lithium					
	CI	G.O.L. [1]	-0.04703	0.00525	0.02623
		Weiss [8]	-0.05102	0.01947	0.00111
	Exact	S.S.M [9]	-0.05477	0.03297	-0.01450
		Weiss [8]	-0.05598	0.04366	-0.03599

Table 4. Comparison of E_c, $\langle V_{ee}\rangle_c$ and $\langle V_{en}\rangle_c$ for the Li*I* sequence (in a.u.)

Z	G.O.L. [1]			Z Exp.		
	E_c	$\langle V_{ee}\rangle_c$	$\langle V_{en}\rangle_c$	E_c	$\langle V_{ee}\rangle_c$	$\langle V_{en}\rangle_c$
3	-0.0424	-0.0804	-0.0044	-0.0424	-0.0772	-0.0076
4	-0.0440	-0.0852	-0.0028	-0.0441	-0.0836	-0.0046
5	-0.0448	-0.878	-0.0018	-0.0449	-0.0867	-0.0032
6	-0.0456	-0.0902	-0.0011	-0.0454	-0.0885	-0.0018
7	-0.0460	-0.0465	-0.0016	-0.0458	-0.0897	-0.0014
8	-0.0457	-0.0901	-0.0014	-0.0459	-0.0905	-0.0014

One is dealing here with small numbers and might expect a somewhat larger relative error. It appears, however, that $\langle V_{en}\rangle_c + \langle V_{ee}\rangle_c = 2E_c$ for all values of Z reported by G.O.L.; that is, the Virial theorem is satisfied for the correlation energy. The splitting of the correlation effect for the total potential energy into a repulsive and attractive part requires the Hellmann-Feynman theorem to be valid for the Hartree-Fock and configuration-interaction energies, and hence for their differences. So, we have

$$\langle V_{en}\rangle_c = Z\,\frac{\partial E_c}{\partial Z}\,. \tag{9}$$

This expression, however, does not seem to be obeyed by the reported values of $\langle V_{en}\rangle_c$ and E_c of G.O.L. Noticing the trend of these authors' values of E_c,

$\partial E_c/\partial Z$ clearly changes sign between $Z=6$ and $Z=8$, and hence one should expect this to be reflected by a change in sign of the corresponding $\langle V_{en}\rangle_c$. Since this is not the case, one may conclude that these wavefunctions, whilst satisfying the Virial theorem do not satisfy the Hellmann-Feynman theorem completely exactly. The deviation from the Hellmann-Feynman theorem is of course a minor one, but we should like to point out that this theorem furnishes a sensitive test of the internal consistency of the accuracy of wavefunctions in an isoelectronic sequence.

By virtue of the development of our formalism, the Virial theorem and Hellmann-Feynman theorem are automatically satisfied. However, we do not wish to convey the impression that we consider our values of $\langle V_{en}\rangle_c$ as very accurate. Our values and those of G.O.L. are small and the same order of magnitude, and this is probably the best one can say. We note in this context that higher order terms may have a relatively greater effect on $\langle V_{en}\rangle_c$ than on either of the quantities E_c and $\langle V_{ee}\rangle_c$ (see (6), (7) and (8) for $\varepsilon_1-\varepsilon_1'=0$). In the limit of infinite Z we see that $\langle V_{ee}\rangle_c=2E_c=2(\varepsilon_2-\varepsilon_2')$. G.O.L. have made a similar observation from their numerical results [1]. Reference to (6), (7), and (8) with $\varepsilon_1-\varepsilon_1'=0$, and Table 3, shows that E_c and $\langle V_{ee}\rangle_c$ are dominated by the second order terms, whereas $\langle V_{en}\rangle_c$ depends only on higher order terms whose contributions diminish for increasing Z.

It is customary [1] to define a quantity $\Delta E_c=E_{\text{exact}}-E_{\text{CI}}$, where E_{exact} is the non-relativistic exact eigenvalue usually obtained from experimental data and corrected for relativistic effects. A Z-expansion for ΔE_c can be obtained by subtracting the appropriate component expressions. For E_{exact} as reported by Matsen [9], and the E_{CI} reported by G.O.L. [1] (see Table 3) we find for the lithium sequence

$$\Delta E_c=-0.0077+\frac{0.0277}{Z}-\frac{0.0407}{Z^2}+\cdots. \qquad (10)$$

This expression gives very accurately the ΔE_c reported by G.O.L. We note that this formula contains only corrections in second and higher order. It is interesting that the third and fourth order coefficients are larger than the second order term. With reference to Table 3, it is apparent that whilst the second order coefficients obtained from configuration interaction approximate fairly closely the exact coefficients, the third and fourth order coefficients are to a noticeably lesser degree consistent with each other. We remark also that the exact second order coefficients calculated from energy values published by different authors are not precisely the same. This variance can probably be largely attributed to the difference in ways of correcting for relativistiv effects.

We have confined ourselves above to a discussion of the lithium sequence, although the data tabulated for the helium sequence may be similarly analysed. We only remark that application of (9) to the E_c and $\langle V_{en}\rangle_c$ of G.O.L. leads to no obvious discrepancy so that the Hellmann-Feynman theorem for the correlation energy is more exactly obeyed by the wavefunctions of G.O.L. for the helium sequence than for the lithium sequence.

3. Beryllium I Sequence

For the Beryllium I sequence, $\varepsilon_1 \neq \varepsilon_1'$ as we have noted before. Hartree-Fock, configuration interaction and exact energies are available in the literature [7–9], for $Z = 3$ to 8. We have made a least-squares fit for these energies using the theoretical values of ε_0, ε_1 and ε_1' [6]. The results are summarized in Table 5. In this case, (6), (7), and (8) show a much stronger Z-dependence than occurs in the Li*I* sequence. In particular, $\langle V_{en} \rangle_c$, which is almost negligible for the He*I* and Li*I* sequences, and which vanishes for high Z values, is clearly non-vanishing for the Be*I* sequence, and becomes linear in Z for high Z values. For He*I* and Li*I* sequences, the ratio of $\langle V_{ee} \rangle_c$ to E_c is 2 : 1 for high Z, but in the case of the Be*I* sequence, this ratio approaches 1 : 1 for high Z. As $(\varepsilon_1 - \varepsilon_1')$ is smaller than $(\varepsilon_2 - \varepsilon_2')$, one has to go to fairly high Z values in order to approach the limit 1 (unity). For the helium and lithium sequences however, the limiting value of 2 is already approximately obeyed for the neutral atoms. Finally, we notice that ε_2 according to the CI wavefunction is closer to the ε_2 for the exact energies in the He*I* and Li*I* sequences than in the case of the Be*I* sequence.

Table 5. Summary of perturbation energy coefficients ε_n for Be*I* sequence (in a.u.)

n	Wavefunction		
	HF (R.S.W.) [7]	CI (Weiss) [8]	Exact (Weiss) [8]
0	−1.125	−1.125	−1.125
1	1.57100	1.55927	1.55927
2	−0.80972	−0.85678	−0.88973
3	−0.06712	−0.12142	0.09419
4	−0.48768	−0.17439	−0.61549

4. Two-Term Expansion for $\langle V_{en} \rangle$

We see in (4) in the Z expansion for $\langle V_{en} \rangle$, a constant term ε_2 is not present. One may expect contributions from terms in $1/Z$ and higher, to be very small compared to terms in Z^2 and Z. Hence, the simple two-term expansion,

$$\langle V_{en} \rangle = 2\varepsilon_0 Z^2 + \varepsilon_1 Z \tag{11}$$

should be a relatively accurate approximation for $\langle V_{en} \rangle$ and approach the exact values in the limit for high Z. Moreover, ε_0 and ε_1 have been tabulated for many cases and are otherwise reasonably easy to calculate on the basis of hydrogenic orbitals [10, 11].

For the He*I* sequence, one gets

$$\langle V_{en} \rangle = -2Z^2 + 0.625Z \tag{12}$$

and for the Li*I* sequence,

$$\langle V_{en} \rangle = -2.25Z^2 + 1.0228Z\,. \tag{13}$$

Table 6 lists our calculations for the He*I* and Li*I* sequences, with those calculated by G.O.L. from their CI wavefunctions. The above two-term expansions reproduce the calculated values with 99.97 % accuracy for the lower Z values, and rather better for the higher Z values. For the ground state of the Boron atom,

$$\langle V_{en}\rangle_{\mathrm{HF}} = -2.75Z^2 + 2.3345Z\,,$$

whereas in the CI approximation we obtain for the same,

$$\langle V_{en}\rangle_{\mathrm{CI}} = -2.75Z^2 + 2.3275Z\,.$$

This leads to $\langle V_{en}\rangle_{\mathrm{HF}} = -57.0778$ a.u. and $\langle V_{en}\rangle_{\mathrm{CI}} = -57.1124$ a.u. Direct calculations give $\langle V_{en}\rangle_{\mathrm{HF}} = -56.8972$ a.u. and $\langle V_{en}\rangle_{\mathrm{CI}} = -56.9462$ a.u. [12]. The accuracy with which we reproduce this value is less good than for the He*I* and Li*I* sequences, but is still about 99.7% accurate. Hence, the two-term expansion provides a simple and relatively accurate way of calculating $\langle V_{en}\rangle$.

Table 6. Electron-nuclear attraction energies calculated from two-term expansion for He*I* and Li*I* sequences (in a.u.)

Z	Helium		Lithium	
	Eq. (12)	CI (G.O.L.) [1]	Eq. (13)	CI (G.O.L.) [1]
2	− 6.7500	− 6.7523		
3	− 16.1250	− 16.1268	− 17.1816	− 17.1508
4	− 29.5000	− 29.5015	− 31.9088	− 31.8920
5	− 46.8750	− 48.8762	− 51.1360	− 51.1244
6	− 68.2500	− 68.2510	− 74.8632	− 74.8540
7	− 93.6250	− 93.5295	−103.0904	−103.0837
8	−123.0000	−123.0008	−135.8176	−135.8119

Acknowledgements. This research was made possible through a grant from the National Research Council of Canada. We also would like to thank Dr. R. E. Brown for making available results of unpublished calculations. We thank both Drs. R. E. Brown and D. A. Hutchinson for fruitful discussions.

References

1. Gruninger, J., Öhrn, Y., Löwdin, P.-O.: J. chem. Physics **52**, 5551 (1970).
2. Löwdin, P.-O.: J. molecular Spectroscopy **3**, 46 (1959).
3. Colpa, J. P., Islip, M. F. J.: Submitted for publication.
4. Hylleraas, E. A.: Z. Physik **65**, 209 (1930). Bethe, H. A., Salpeter, E. E.: Quantum mechanics of one- and two-electron atoms and ions. Berlin: Springer-Verlag 1957.
5. Coulson, C. A.: Molecular Physics **20**, 687 (1971).
6. Linderberg, J., Shull, H.: J. molecular Spectroscopy **5**, 1 (1960).
7. Roothaan, C. C. J., Sachs, L. M., Weiss, A. W.: Rev. mod. Physics **32**, 186 (1960).
8. Weiss, A. W.: Physic. Rev. **122**, 1826 (1961).
9. Scherr, C. W., Silverman, J. N., Matsen, F. A.: Physic. Rev. **127**, 830 (1962).
10. Crossley, R. J. S., Coulson, C. A.: Proc. physic. Soc. **81**, 211 (1963).
11. – Proc. physic. Soc. **83**, 375 (1964).

12. Brown, R. E.: Private communication.
13. Scherr, C. W., Knight, R. E.: Rev. mod. Physics **35**, 436 (1963).
14. Hylleraas, E. A., Midtal, J.: Physic. Rev. **103**, 829 (1956).

Dr. J. P. Colpa
Department of Chemistry
Queen's University
Kingston, Ontario
Canada

Theoret. chim. Acta (Berl.) 27, 33--47 (1972)
© by Springer-Verlag 1972

Spin-Bahn-Kopplungseffekte verschiedener Ordnung bei Jod und Dijodazetylen

MARTIN JUNGEN

Physikalisch-Chemisches Institut der Universität Basel, Schweiz

Eingegangen am 29. Mai 1972

Spin-Orbit-Coupling Effects of Different Order from J_2 and C_2J_2

Two investigations were performed to understand the anomalous spin-orbit splitting of the $^2\Pi_u$-doublet in the photoelectron-spectrum of J_2. Model calculations on H_2^+ show the dependence of the spin-orbit coupling constants on internuclear distance. The validity of the theory of Ishiguro and Kobori [13] is discussed. By comparison of the level diagrams of J_2^+ and $C_2J_2^+$ the $^2\Pi_u$-states of J_2^+ are proposed to be perturbed by spin-orbit induced configuration interaction. In the PE-spectrum of J_2 we found lines which can be interpreted as transitions to non-Koopmans states of the cation.

Um die anomale Spin-Bahn-Aufspaltung des $^2\Pi_u$-Dubletts im Photoelektron-Spektrum von J_2 zu verstehen, wurden zwei Untersuchungen durchgeführt. Modellrechnungen über H_2^+ zeigen die Abhängigkeit der Spin-Bahn-Kopplungskonstanten vom Kernabstand. Wir diskutieren die Gültigkeit der Theorie von Ishiguro und Kobori [13]. Durch Vergleich des Termschemas von J_2^+ mit $C_2J_2^+$ kann man die Aufspaltung der $^2\Pi_u$-Zustände von J_2^+ als einen Effekt von Spin-Bahn-induzierter Konfigurationswechselwirkung deuten. Wir fanden im PE-Spektrum von J_2 Linien, welche sich als Übergänge zu nicht-Koopmans-Zuständen interpretieren lassen.

Pour comprendre la séparation anomale du doublet $^2\Pi_u$ dans le spectre photoélectronique de J_2 deux recherches ont été effectuées. Des calculs sur le modèle H_2^+ montrent la dépendence des constantes de couplage spin-orbite de la séparation internucléaire. La validité de la théorie d'Ishiguro et Kobori [13] est discutée. En comparant les diagrammes de niveaux de J_2^+ et $C_2J_2^+$ nous concluons que les états $^2\Pi_u$ de J_2^+ sont perturbés par couplage spin-orbite d'ordre supérieur. Dans le spectre photoélectronique de J_2 on trouve des lignes que nous interprétons comme transitions à des états non-Koopmans de l'ion.

1. Einleitung

a) Der Operator der Spin-Bahn-Wechselwirkung

Spin-Bahn-Kopplung nennt man die Wechselwirkung eines bewegten (Elektronen)-Spins im Feld von Kernen und anderen Elektronen. Anschaulich: Ein π_+-Elektron in einem linearen Molekül hat verschiedene Energie, je nachdem, ob es α- oder β-Spin trägt, weil die Wechselwirkungsenergie des Spins mit dem elektrischen Feld sich einmal zu der elektronischen Energie addiert, im anderen Fall jedoch subtrahiert. Die Spin-Bahn-Kopplung in einem Mehrelektronensystem theoretisch zu behandeln, ist schwierig, wenn man exakt vorgeht, jedoch recht einfach, wenn man den in $\mathscr{H}$ zusätzlich auftretenden Spin-Bahn-Kopplungsoperator vereinfacht. Dies sei mit den folgenden Ansätzen für $\mathscr{H}_{SO}$ (1)–(3) illustriert (alle in diesem Abschnitt verwendeten Symbole haben die konventionelle Bedeutung):

$$\mathscr{H}_{\mathrm{SO}} = h\left(\frac{e}{mc}\right)^2 \left\{\sum_K \sum_i \frac{Z_K}{r_{iK}^3} [(\boldsymbol{r}_i - \boldsymbol{r}_K) \times (\tfrac{1}{2}\boldsymbol{p}_i - \boldsymbol{p}_K)]\, \boldsymbol{s}_i \right.$$
$$\left. - \sum_{i>j} \frac{1}{r_{ij}^3} [(\boldsymbol{r}_i - \boldsymbol{r}_j) \times (\tfrac{1}{2}\boldsymbol{p}_i - \boldsymbol{p}_j)] \cdot \boldsymbol{s}_i \right\}, \tag{1}$$

$$\mathscr{H}_{\mathrm{SO}} = \sum_i \frac{2h}{(2mc)^2} (\operatorname{grad} U \times \boldsymbol{p}_i) \cdot \boldsymbol{s}_i\,, \tag{2}$$

$$\mathscr{H}_{\mathrm{SO}} = A \cdot \boldsymbol{L} \cdot \boldsymbol{S}\,. \tag{3}$$

Der „mikroskopische" Kopplungsoperator (1) (Van Vleck [1]) besteht aus einer Summe von kernladungsabhängigen Ein-Elektronen-Operatoren und aus Zwei-Elektronen-Operatoren, welche den Namen „Spin-andere Bahn-Kopplung" ("spin-other orbit") tragen. Diese Spin-Bahn-Wechselwirkung von Elektronen untereinander bewirkt hauptsächlich eine Abschirmung des Kernfeldes (K indiziert Kerne, i, j Elektronen). Der „phänomenologische" Operator (3) andererseits nimmt von den einzelnen Elektronen nicht Kenntnis, sondern benützt nur den Gesamtdrall $\boldsymbol{L}$ und den Gesamtspin $\boldsymbol{S}$; die Spin-Bahn-Kopplungskonstante A wird aus dem Experiment bestimmt (zur besseren Unterscheidung seien die Kopplungskonstanten von Atomen ζ, von Molekülen A genannt). Dazwischen steht der Operator (2), ein effektiver Ein-Elektronen-Operator, welchen man aus (1) herleiten kann, indem man gemäß einer SCF-Näherung die Kerne festhält ($\boldsymbol{p}_K = 0$) und das elektrische Feld durch ein effektives Potential von Kernen und unbewegt gedachter Elektronenladung ($\boldsymbol{p}_j = 0$) ersetzt[1]. Operator (2) hat dieselbe Gestalt wie der Spin-Bahn-Operator in der Diracgleichung. Ist ein Orbital von zwei Elektronen entgegengesetzten Spins besetzt, so heben sich deren Beiträge zur Spin-Bahn-Kopplung auf.

Die Spin-Bahn-Kopplung wird meist in Atomen und linearen Molekülen studiert, weil sie dort entartete Niveaus aufspaltet, also meßbar ist.

Man kann zeigen, daß der Operator (2), umgeschrieben

$$\mathscr{H}_{\mathrm{SO}} = \sum_i \zeta(r_i)(\boldsymbol{l}_i \cdot \boldsymbol{s}_i)$$

für Atome mit höchstens einem ungepaarten Elektron korrekt ist [2], falls man die Kopplungs„konstante" ζ durch eine Funktion $\zeta(r_i)$ ersetzt. Für lineare Moleküle stellt (2) immerhin eine Verfeinerung des phänomenologischen Ansatzes (3) dar.

Durch Vergleich der Erwartungswerte von (2) und (3) läßt sich die Spin-Bahn-Kopplungskonstante A linearer Moleküle berechnen. Für weitere Einzelheiten verweisen wir auf die Literatur und die Lehrbücher [3–8, 21].

Für die folgende Untersuchung ist wichtig zu wissen:

Für ein Elektron im Zylinderfeld nackter Kerne gilt (in atomaren Einheiten)

$$\mathscr{H}_{\mathrm{SO}} = \frac{\alpha^2}{2} \sum_K \frac{1}{r_K^3} (\boldsymbol{l} \cdot \boldsymbol{s})$$

---

[1] Arbeitet man mit dem effektiven Ein-Elektronen-Operator (2), so genügt eine SCF-Wellenfunktion mit formal unabhängigen Orbitalen im effektiven Potential zur Beschreibung des Moleküls.

(α = Feinstrukturkonstante), die Kopplungskonstante ist gleich dem Erwartungswert (r_K = Abstand zum K-ten Kern)

$$A = \frac{\alpha^2}{2}\left\langle \sum_K \frac{1}{r_K^3} \right\rangle . \tag{4}$$

In der Basis von Eigenfunktionen von L_z und S_z hat $\mathscr{H}_{SO}$ nichtverschwindende Matrixelemente zwischen Zuständen mit gleichem $\Omega = \Lambda + \Sigma$, wobei $\Delta\Lambda$ resp. $\Delta\Sigma = 0, \pm 1$ betragen darf. Die $g-u$-Symmetrie bleibt erhalten, $\Sigma^{\pm}$ wird mit $\Sigma^{\mp}$ vermischt. Man beachte, daß wegen der kurzen Reichweite der Spin-Bahn-Wechselwirkung die lokale Symmetrie der Wellenfunktion bei den Kernen von großer Bedeutung sein kann.

Da die Spin-Bahn-Energien in der Regel vergleichsweise klein sind, pflegt man den Effekt störungstheoretisch zu behandeln. In 1. Ordnung korrigiert man die ungestörten Terme mit den Diagonalelementen von $\mathscr{H}_{SO}$, in 2. Ordnung (oder mit Konfigurationswechselwirkung) berücksichtigt man die außerdiagonalen Glieder (Mischen der Zustände). Wechselwirkung von Konfigurationen, welche sich in zwei Orbitalen unterscheiden, ist wegen der geringen Bedeutung des 2-Elektronen-Teils von $\mathscr{H}_{SO}$ viel schwächer als Wechselwirkung von nur in einem Orbital differierenden Konfigurationen. Nach [21] betragen die 2-Elektronen-Wechselwirkungsenergien einige Prozent der 1-Elektronen-Wechselwirkungen.

Bei linearen Molekülen sind die Spin-Bahn-Effekte 2. Ordnung meist nicht von Bedeutung. Man erhält aus dem Operator (3) in 1. Ordnung die äquidistante Aufspaltung eines Niveaus: $\Delta E = 2A\Lambda\Sigma$ (das ungestörte Niveau liegt in der Mitte).

In Atomen darf man wegen der Entartungen die außerdiagonalen Glieder von $\mathscr{H}_{SO}$ nicht vernachlässigen. Mit dem Operator (3) erhält man die Landésche Intervallregel [8]: $\Delta E_{J,J-1} = \zeta J$. Sie besagt, daß z. B. ein atomarer P-Zustand in einen $P_{\frac{1}{2}}$ und einen $P_{\frac{3}{2}}$ aufspaltet, welche wegen der Wechselwirkung mit der dritten P-Komponente um $\frac{3}{2}\zeta$ voneinander entfernt sind. Analog wird ein D-Zustand in einen $D_{\frac{3}{2}}$ und einen um $\frac{5}{2}\zeta$ entfernten $D_{\frac{5}{2}}$-Zustand aufgespalten. Das ungestörte Niveau liegt in diesen Fällen nicht in der Mitte zwischen den gestörten.

In Fig. 1 ist für den Fall eines (entarteten) π-Elektrons die Korrelation zwischen äquidistanter Aufspaltung im zylindersymmetrischen Feld und Landé-Aufspaltung im kugelsymmetrischen Feld schematisch dargestellt.

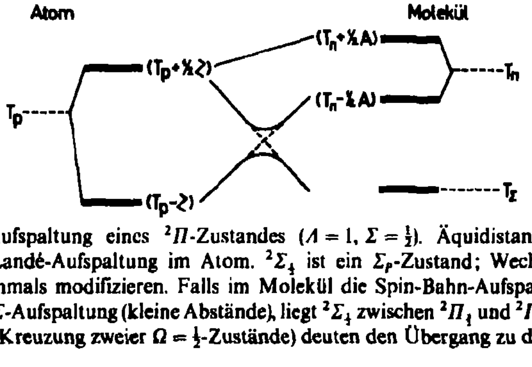

Fig. 1. Spin-Bahn-Aufspaltung eines $^2\Pi$-Zustandes ($\Lambda = 1$, $\Sigma = \frac{1}{2}$). Äquidistante Aufspaltung im linearen Molekül, Landé-Aufspaltung im Atom. $^2\Sigma_{\frac{1}{2}}$ ist ein Σ_p-Zustand; Wechselwirkung mit Σ_S würde das Bild nochmals modifizieren. Falls im Molekül die Spin-Bahn-Aufspaltung groß ist, verglichen mit der $\Pi - \Sigma$-Aufspaltung (kleine Abstände), liegt $^2\Sigma_{\frac{1}{2}}$ zwischen $^2\Pi_{\frac{3}{2}}$ und $^2\Pi_{\frac{1}{2}}$. Die gestrichelten Linien (verbotene Kreuzung zweier $\Omega = \frac{1}{2}$-Zustände) deuten den Übergang zu dieser Situation an

b) Experimente

Dieser Untersuchung sind die folgenden Experimente zugrunde gelegt: Die von Heilbronner u. Mitarb. vermessenen Photoelektronen-(PE)-Spektren der Halogenazetylene X—C≡C—Y (X, Y = H, Cl, Br, J) [9, 10] sowie die PE-Spektren der Halogenmoleküle von Frost u. Mitarb. [11, 12]. In den Elektronenspektren der Halogenazetylene treten - entsprechend den drei im Molekül mit je 4 Elektronen besetzten π-Orbitalen – drei offenbar durch Spin-Bahn-Kopplung aufgespaltene Dublette auf. Die Differenz ΔI der beiden Ionisierungsenergien eines Dubletts läßt sich als Energiedifferenz der $\Pi_{\frac{3}{2}}$- und $\Pi_{\frac{1}{2}}$-Ionenzustände deuten. Heilbronner erklärte das Maß dieser Aufspaltungen auf Grund der Knotenverteilung der verschiedenen π-Orbitale. Er bemerkte auch, daß die Summe der drei Aufspaltungen in allen Fällen, wo das Experiment eine Prüfung erlaubt, gleich der Summe der Spin-Bahn-Kopplungskonstanten der beteiligten Halogenatome ist: $\Delta I(1\Pi)+\Delta I(2\Pi)+\Delta I(3\Pi)\sim\zeta(\mathrm{X})+\zeta(\mathrm{Y})$. Wir wollen dieses Verhalten „Summenregel“ nennen. Bei den Halogenen Br_2 und J_2 – je ein π_u- und ein π_g-Orbital sind besetzt - läßt sich die Summenregel nicht bestätigen. Im Br_2-Spektrum ist das π_u-Dublett nicht aufgelöst, bei J_2 wird die Regel verletzt: $\Delta I(\Pi_g)=0{,}63$ eV, $\Delta I(\Pi_u)=0{,}79$ eV, $2\zeta(\mathrm{J})=1{,}26$ eV [22, 23]. Es sei hier bemerkt, daß die PE-Spektroskopie die Energiedifferenz von Molekül und einer Anzahl von Zuständen des Kations mißt (wir schlagen vor, die mit PE-Spektroskopie erreichbaren Konfigurationen des Ions „Koopmans-Konfigurationen“ zu nennen), wobei die Geometrie des Moleküls (im Rahmen der Born-Oppenheimer-Näherung) beibehalten bleibt („vertikale“ Ionisation).

c) Semiempirische Ansätze

Die Spin-Bahn-Kopplung hängt stark von der Kernladung der beteiligten Atome ab. Sie ist deshalb, außer man kann hochauflösende Spektroskopie betreiben, nur bei Molekülen zu beobachten, welche schwere Atome enthalten. Für die Theorie bedeutet das: Exakte Berechnungen der Spin-Bahn-Kopplungseffekte sind im allgemeinen ausgeschlossen; man muß sich semiempirischer Methoden bedienen, welche von den bekannten Spin-Bahn-Kopplungskonstanten der freien Atome ausgehen.

Dafür zwei Beispiele: Heilbronner konnte mit einem Hückel-Verfahren (ZDO-Näherung) die Spektren der Halogenazetylene interpretieren, indem er die Aufenthaltswahrscheinlichkeit der Elektronen jedes π-Orbitals bei den Halogenatomen berechnete und mit den freien Atomen (Aufenthaltswahrscheinlichkeit = 1) verglich [9, 10].

Ishiguro u. Kobori [13] studierten die Abhängigkeit der Kopplungskonstanten eines bindenden und eines antibindenden π-Orbitals von der Überlappung S der Atomorbitale (LCAO-Näherung). Für ein homonukleares zweiatomiges Molekül erhalten sie mit $\varphi_{\substack{u\\g}}=\dfrac{\chi_a\pm\chi_b}{(2(1\pm S))^{\frac{1}{2}}}$ die „Konstanten“

$$A_{\substack{u\\g}}=\frac{\zeta}{1\pm S}\,, \tag{5}$$

wo ζ die Kopplungskonstante im freien Atom bedeutet. Bei der Herleitung der Formel (5) wurden alle Mehrzentrenintegrale vernachlässigt. Die Aufspaltung eines antibindenden π_g-Orbitals durch Spin-Bahn-Kopplung sollte gemäß (5) größer sein als jene des zugehörigen bindenden π_u-Orbitals, entsprechend der Tatsache, daß sich bei der antibindenden Wellenfunktion weniger Ladung zwischen den Kernen befindet und mehr in Kernnähe als bei der bindenden Funktion. Diesem Resultat widerspricht das PE-Spektrum von J_2 (s. Abschn. 1b).

Wir wollen in den folgenden Abschnitten untersuchen, weshalb im PE-Spektrum von J_2 die Summenregel und die Ishiguro-Regel (5) verletzt sind. Nach einer Bemerkung über die Summenregel in Abschn. 2 werden wir in Abschn. 3 eine modellmäßige Studie über das Verhalten der Spin-Bahn-Kopplung 1. Ordnung von π_u- und π_g-Orbitalen als Funktion des Kernabstandes durchführen. In Abschn. 4 präsentieren wir einen semiquantitativen Vergleich der Zustände der Kationen J_2^+ und $C_2J_2^+$ und deren Kopplungen 2. Ordnung.

2. Die Summenregel

Im Rahmen eines LCAO-Ansatzes mit Vernachlässigung der differentiellen Überlappung (ZDO) ist die Summenregel wegen der Orthogonalität der LCAO-Koeffizienten-Matrix erfüllt, wenn alle Orbitale, welche zur Spin-Bahn-Kopplung beitragen können, voll besetzt sind[2]. Hierbei wird angenommen, daß sich die Orbitale bei Ionisation nicht ändern, so daß jede Koopmans-Konfiguration (s. Abschn. 1b) die Spin-Bahn-Aufspaltung des ionisierten Orbitals erleidet.

Da die Überlappung der AO's nach (5) in die Berechnung der Kopplungskonstanten eingeht, wollen wir hier die Summenregel für einen LCAO-Ansatz ohne Vernachlässigung der differentiellen Überlappung begründen. Wir betrachten ein heteronukleares Zweizentrenproblem mit AO's χ_a und χ_b und setzen für das bindende resp. antibindende Orbital

$$\left.\begin{aligned}\varphi_+ &= \left(\frac{1-\lambda^2}{2(1+S)}\right)^{\frac{1}{2}}(\chi_a+\chi_b)+\left(\frac{\lambda^2}{2(1-S)}\right)^{\frac{1}{2}}(\chi_a-\chi_b)=c_{1a}\chi_a+c_{1b}\chi_b\\ \varphi_- &= \left(\frac{1-\lambda^2}{2(1-S)}\right)^{\frac{1}{2}}(\chi_a-\chi_b)-\left(\frac{\lambda^2}{2(1+S)}\right)^{\frac{1}{2}}(\chi_a+\chi_b)=c_{2a}\chi_a+c_{2b}\chi_b\end{aligned}\right.\qquad(\lambda^2\leqq 1)$$

an. Diese Orbitale sind orthonormal. Aus der Beziehung

$$c_{1a}^2+c_{2a}^2=c_{1b}^2+c_{2b}^2=\frac{1}{1-S^2}$$

schließen wir, daß im Rahmen unseres Ansatzes die Summenregel bis auf Fehler proportional zu S^2 erfüllt ist. Überdies wird klar, daß die Regel versagt, wenn die einfache LCAO-Näherung schlecht ist, sei es wegen Orbitalkontraktion (veränderte effektive Kernladung im Molekül) oder Orbitalpolarisation (z. B. Beimischen von d-Orbitalen) oder aus anderen Gründen. In Abschn. 3 werden wir die Probleme von Orbitalpolarisation und -kontraktion behandeln.

---

[2] Bei den Mono- und Dihalogenazetylenen trifft diese Voraussetzung nur dann zu, wenn man von einem 3-Zentren-LCMO-Ansatz ausgeht.

3. π-Zustände von H_2^+. Abhängigkeit der Kopplungskonstanten vom Kernabstand

Im Grenzfall der getrennten Atome gehen die $n\pi_u$- und $n\pi_g$-Orbitale von H_2^+ für $n = 1$ oder 2 in die $(n+1)p$-Orbitale des H-Atoms über. Im Grenzfall des vereinigten Atoms (He$^+$-Ion) korrelieren $n\pi_u$ mit $(n+1)p$, $n\pi_g$ mit $(n+2)d$. Fig. 2 zeigt das Korrelationsdiagramm der Spin-Bahn-Aufspaltungen dieser vier Orbitale (vgl. Formel (4)). Für $n > 2$ ist die Situation komplizierter [24].

Wegen

$$\zeta(n, l) = \frac{\alpha^2}{2} \cdot \frac{Z^4}{n^3 l(l+\frac{1}{2})(l+1)}$$

[3] gilt

$$\tfrac{3}{2}\,\zeta(n+1, p) : \tfrac{5}{2}\,\zeta(n+2, d) = 3 \cdot \left(\frac{n+2}{n+1}\right)^3 .$$

Die Spin-Bahn-Wechselwirkungsenergie des $n\pi_u$-Orbitals im vereinigten Atom beträgt deshalb trotz der größeren Aufspaltung des Landé-Intervalls bei den antibindenden Orbitalen (Faktor $\frac{5}{2}$ statt $\frac{3}{2}$) mindestens das dreifache des $n\pi_g$-Orbitals (Fig. 2). Dies bedeutet: Für kurze Bindungslängen ist die Regel von Ishiguro (5), welche besagt, daß bei festem Kernabstand $A(n\pi_g) > A(n\pi_u)$, sicher falsch.

Um das Verhalten der Spin-Bahn-Kopplungskonstanten von H_2^+ besser kennenzulernen, haben wir mit einer mittelguten Gauß-Basis (8 p-GO pro Atom) einige π-Orbitale bei Kernabständen von bis zu 50 a.u. bestimmt sowie deren

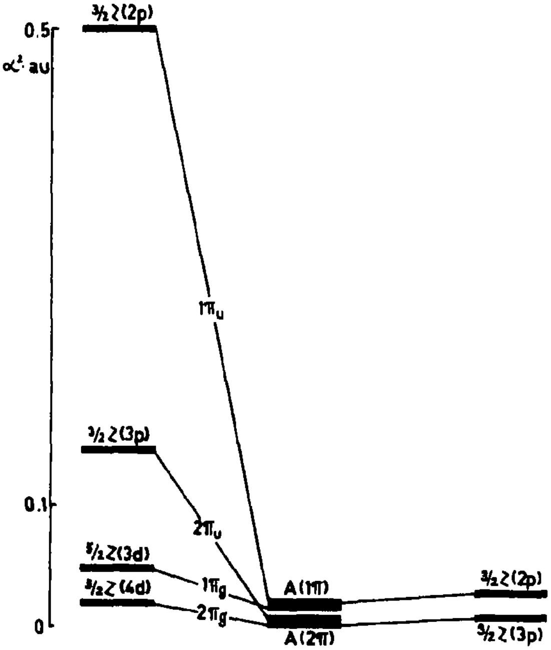

Fig. 2. Spin-Bahn-Aufspaltung der 1π- und 2π-Orbitale von H_2^+. Korrelation des linearen Moleküls mit dem vereinigten Atom und mit den getrennten Atomen. Einheiten: $\alpha^2 \cdot$ a.u. (α = Feinstrukturkonstante)

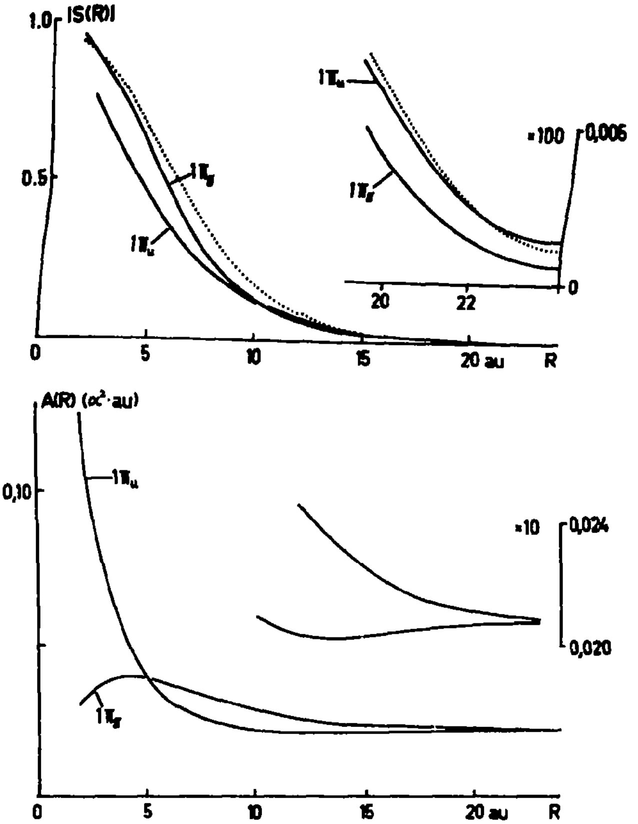

Fig. 3. H_2^+: Unten: Spin-Bahn-Kopplungskonstante der 1π-MO's. Oben: Überlappungen der rekonstruierten AO's (---) und Überlappungsintegral von atomaren $2p_\pi$-AO's (-----) (s. Text)

Spin-Bahn-Kopplungskonstanten 1. Ordnung, d. h. den Erwartungswert $\langle r_a^{-3} + r_b^{-3} \rangle$ berechnet. Fig. 3 (unterer Teil) zeigt das Ergebnis für $1\pi_u$ und $1\pi_g$. Bei Kernabständen von über 18 a.u. gilt die Regel von Ishiguro und die Summenregel, bei kürzeren Abständen sind sie immer stärker verletzt. Die Kurven kreuzen sich bei ca. 5 a.u.

Eine LCAO-Interpretation der Wellenfunktionen erlaubt, unsere Resultate besser zu verstehen. Im oberen Teil von Fig. 3 ist die Überlappung S der rekonstruierten Atomorbitale aufgetragen als Funktion des Kernabstandes. Die gestrichelte Linie beschreibt den Gang der Überlappung von zwei unveränderten atomaren $2p$-Orbitalen. Eine geringere Überlappung ist zurückzuführen auf Kontraktion der Orbitale, größere Überlappung bedeutet Dilatation. Orbitalkontraktion resp. -dilatation heißt: Die effektive Kernladung der Atome, welche in die Orbitalexponenten der AO's eingeht, ist größer resp. kleiner als im freien Atom.

Bei sehr großen Kernabständen dilatiert das bindende π_u-Orbital leicht, während π_g sich leicht kontrahiert. Zwischen 22a.u. und 2 a.u. sind beide Orbitale kontrahiert, π_g bei großen Abständen stärker, bei kurzen schwächer als π_u. Die

Kreuzung der Kurven (8 a.u.) tritt bei einem etwas größeren Kernabstand auf als die Kreuzung der Kopplungskonstanten. Wir wollen zeigen, daß die Kreuzung der Kopplungskonstanten durch die Lage des Kreuzungspunktes der Überlappungsintegrale bestimmt ist.

In der Ishiguro-Formel (5) muß man genau genommen für π_u- und π_g-Orbitale zwei verschiedene Überlappungsintegrale S_u und S_g sowie zwei verschiedene atomare Kopplungskonstanten ζ_u und ζ_g verwenden. Beides rührt davon her, daß die mit einer flexiblen Basis ausgeführten Rechnungen – im LCAO-Bild interpretiert verschiedene effektive Kernladungen und damit verschiedene AO-Orbitalexponenten voraussagen für π_g- und π_u-Molekülorbitale[3].

$$\begin{aligned} A(\pi_u) &\sim \frac{\breve{\zeta}_u}{1+S_u} \\ A(\pi_g) &\sim \frac{\breve{\zeta}_g}{1-S_g}\,. \end{aligned} \tag{6}$$

Zweizentren-Integrale sind auch hier vernachlässigt worden. Bei Kernabstand $R \to \infty$ (getrennte Atome) und bei $R \sim 8$ a.u. stimmen die effektiven Kernladungen im π_u- und π_g-Orbital und damit die Überlappungsintegrale S_u, S_g und die atomaren Kopplungskonstanten ζ_u, ζ_g – überein. Formel (5) ist anwendbar, solange $S_u \sim S_g$ und $\zeta_u \sim \zeta_g \sim \zeta\,(\mathrm{H};(n+1)p)$, bei großen Kernabständen also.

Ebenso ist beim Kreuzungspunkt der Überlappungsintegrale $A(\pi_g) > A(\pi_u)$; bei kürzeren Bindungslängen jedoch vertauscht sich die Reihenfolge der Kopplungskonstanten wegen der starken Kontraktion resp. Dilatation des bindenden resp. antibindenden Orbitals.

Ruedenberg u. Mitarb. [14] haben für das bindende und antibindende $1\sigma_g$- und $1\sigma_u$-MO von H_2^+ ähnliche Untersuchungen durchgeführt; sie fanden qualitativ dieselbe Abhängigkeit der effektiven Kernladungen vom Kernabstand. Diese Autoren gingen noch einen Schritt weiter als wir, indem sie auch Polarisation der $1s$-AO's zuließen. Ihre Resultate wurden dadurch freilich kaum verändert, denn $1s$-Atomorbitale lassen sich – wie auch $2p_\pi$-AO's in unserem Fall – nur schwer polarisieren.

Gehen wir nun zur Diskussion der aus $3p_\pi$-AO's aufgebauten $2\pi_u$-, $2\pi_g$-Molekülorbitale von H_2^+ über, so ändert sich das Bild, weil hier Polarisation durch $3d_\pi$-Orbitale auftritt. In Fig. 4 sind die Kurven der Spin-Bahn-Kopplungskonstanten $A(2\pi_u)$, $A(2\pi_g)$ gezeichnet, einmal ohne die Orbitalpolarisation zu berücksichtigen (gestrichelt) and berechnet mit einer Basis, welche auch $3d_\pi$-AO's enthielt (ausgezogene Kurven).

Wir bemerken, daß bei einer Separation von 50 a.u. die gestrichelten Kurven bereits den asymptotischen Wert für getrennte Atome erreichen ($\breve{\zeta}\,(\mathrm{H};3p) \sim 0{,}006 17\,\alpha^2 \cdot$ a.u.), während die ausgezogenen Linien bei ca. 75% dieses Wertes verlaufen[4]. Durch Polarisation wird der Erwartungswert $\langle r^{-3} \rangle$ und damit die

---

[3] Man könnte die effektiven Kernladungen aus dem rekonstruierten Überlappungsintegral, d. h. aus dem Verhalten der AO's im Gebiet zwischen den Kernen bestimmen oder aus den atomaren Spin-Bahn-Kopplungskonstanten, d. h. aus dem Verhalten der AO's nahe bei den Kernen. Die beiden Methoden brauchen nicht übereinzustimmen.

[4] Mit $\breve{\zeta}\,(\mathrm{H};3d) \sim 0{,}00123\,\alpha^2 \cdot$ a.u. läßt sich aus diesen Zahlen ein Polarisationsgrad des $3p$-AO's von ca. 31 % berechnen.

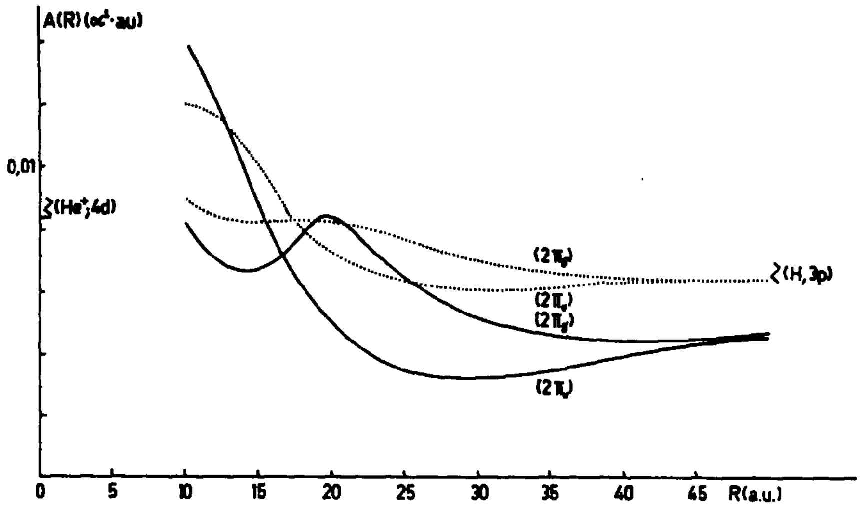

Fig. 4. H_2^+: Spin-Bahn-Kopplungskonstanten der 2π-MO's, berechnet mit (—— --) und ohne (--- ·—) Polarisation der AO's

Spin-Bahn-Kopplungskonstante stark erniedrigt (das Elektron ist im Mittel weiter von den Kernen entfernt). Um weitere Eigenheiten der Kurven in Fig. 4 deuten zu können, zeigen wir in Fig. 5 Bilder der $2\pi_u$-, $2\pi_g$-Orbitale bei verschiedenen Kernabständen. Bei großen Abständen sind die AO's beider Orbitale gleich polarisiert. Verkürzen der Bindungslänge läßt den Polarisationssinn bei $2\pi_u$ unverändert; die AO's werden kontrahiert, was sich in einem Ladungsanstieg in Kernnähe ausdrückt und die Ladungsdichte zwischen den Kernen nimmt zu. Bei $2\pi_g$ jedoch wechselt der Polarisationssinn: Die Ladung fließt aus dem Raum zwischen den Kernen ins Gebiet jenseits der Kerne. Hierbei machen die $2p$-Vorläufer der $3p$-AO's die entgegengesetzte Bewegung von außen nach innen. Bei einem Kernabstand von ca. 20 a.u. sind sie den Kernen am nächsten; die Kurve der $2\pi_g$-Kopplungskonstanten hat ein Maximum (Fig. 4).

Versuchen wir nun, mit unserem Modell H_2^+ die Spektren von J_2 und von C_2J_2 (vgl. Abschn. 1 b) zu deuten. Hierbei ist natürlich Vorsicht geboten, schon weil wir bisher nur Spin-Bahn-Effekte 1. Ordnung untersuchten.

Die Summenregel könnte verletzt werden wegen Orbitalpolarisation durch die vielen nicht besetzten Orbitale der N- und O-Schale im Jodatom. Man müßte freilich erwarten, daß dadurch die Summe der Spin-Bahn-Aufspaltungen erniedrigt würde und nicht vergrößert wie im PE-Spektrum von J_2. Auch sollte man begründen, weshalb die Jod-AO's in C_2J_2 nicht im selben Maß polarisiert sind.

Eine vergleichsweise kurze Bindungslänge in J_2 und damit ein π_u-Orbital, welches eher als kontrahiertes Einzentren-Orbital eines vereinigten Atoms aufzufassen wäre, denn als LCAO-MO, könnte erklären, weshalb J_2^+ die Summenregel und Regel (5) verletzt. Ohne genaue Rechnungen über die verschiedenen Ionenzustände von J_2^+ und $C_2J_2^+$ können wir diese Vermutung nicht beweisen – und solche Rechnungen durchzuführen ist praktisch unmöglich.

accession number
38965

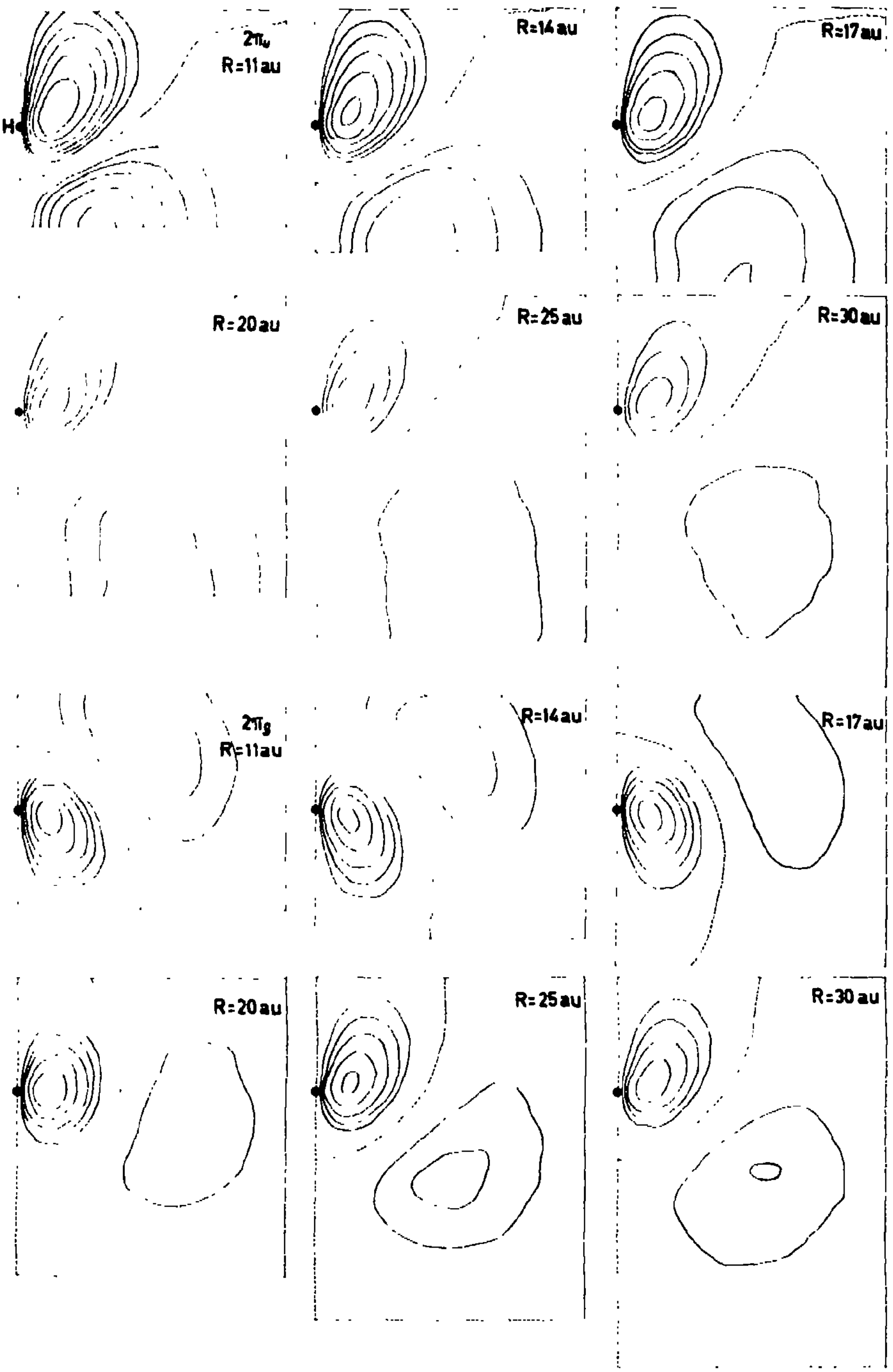

Fig. 5. 2π-Orbitale von H$_2^+$ bei verschiedenen Kernabständen. Der Mittelpunkt der H H-Verbindung befindet sich jeweils in der linken unteren Ecke der Bilder. Knotenlinien sind gestrichelt; die ausgezogenen Linien entsprechen Wellenfunktionswerten von ±0.010, 0.013, 0.017, 0.022, 0.027, 0.034

Falls wirklich Orbitalkontraktion Ursache der großen Spin-Bahn-Aufspaltung des $^2\Pi_u$-Zustands von J_2^+ ist, so haben wir eine experimentelle Bestätigung der Theorie von Ruedenberg [14] gefunden. Wir müßten freilich annehmen, daß bei Molekülbildung die 5*p*-AO's von Jod nicht nur außen modifiziert würden, sondern sich bis zuinnerst beim J-Kern veränderten, denn von dort her rührt der größte Teil bei Spin-Bahn-Energie[5]. Eine solche Modifikation aller Teile der AO's müßten wir auch wegen der Orthogonalität der AO's erwarten. Das Modell H_2^+ lehrt uns, daß es Spin-Bahn-Effekte 1. Ordnung gibt, mit welchen man das PE-Spektrum von J_2 erkären könnte. In Abschn. 4 werden wir die Rolle der Effekte 2. und höherer Ordnung untersuchen.

4. Spin-Bahn-Kopplung höherer Ordnung bei J_2^+ und $C_2J_2^+$

Wir wollen in diesem Abschnitt die Kationen J_2^+ und $C_2J_2^+$ miteinander vergleichen und untersuchen, inwiefern man mit Spin-Bahn-Kopplung höherer Ordnung, d. h. Wechselwirkung verschiedener Konfigurationen mit demselben Gesamtdrall Ω, die Spektren von Jod und Dijodazetylen (vgl. Abschn. 1b) und die Widersprüche zu einfachen theoretischen Ansätzen (Abschn. 1c) erklären kann.

Für die Moleküle J_2 und C_2J_2 stand je eine SCF-Rechnung von Straub und McLean [16] zur Verfügung, deren Orbitalenergien man laut Koopmans' Theorem in guter Näherung für die vertikalen Anregungsenergien des Moleküls zu den Koopmans-Konfigurationen des Kations verwenden darf. (Wir benützten für J_2 eine mit erweitertem Basissatz durchgeführte Rechnung, welche in [16] nicht publiziert ist).

Der – in den SCF-Rechnungen nicht berücksichtigte – Operator der Spin-Bahn-Wechselwirkung mischt, wie oben (Abschn. 1a) erläutert, Zustände vom selben Gesamtdrall (Quantenzahl Ω), wobei die $g-u$-Symmetrie erhalten bleibt. Wir müssen ferner Wechselwirkung mit nicht-Koopmans-Konfigurationen beachten.

In Fig. 6 ist ein semiquantitatives Termschema von J_2^+ und $C_2J_2^+$ skizziert. Für die Lage der Koopmans-Konfigurationen (ausgezogene Linien) wurden die Orbitalenergien ε_i der SCF-Rechnungen verwendet; die Spin-Bahn-Aufspaltungen der Π-Zustände entstammen den PE-Spektren [9, 11]. Mit Pfeilen sind einige mögliche Wechselwirkungen angedeutet, welche wegen der kleinen Energiedifferenz der Konfigurationen von Bedeutung sind.

Weil die Lage der nicht-Koopmans-Zustände in beiden Kationen unsicher ist, sind wir auf Vermutungen angewiesen. In Fig. 6 sind für J_2^+ und $C_2J_2^+$ einige nicht-Koopmans-Konfigurationen gestrichelt eingezeichnet.

Der $(n\rightarrow\sigma^*)$- und der $(\pi_u\rightarrow\pi_g^*)$-Zustand von $C_2J_2^+$ sind so festgelegt, daß ihre Energiedifferenz zum Grundzustand des Kations gleich den im UV-Spektrum von Dijodazetylen [17] beobachteten Übergangsenergien (4,5 eV resp. 6,5 eV) ist. Die 4,5 eV-Bande ist im UV-Spektrum vieler Jod-Verbindungen zu sehen; sie entspricht wahrscheinlich einem $n\rightarrow\sigma^*$-Übergang am Jod [17]. Für unsere Zwecke ist wichtig zu wissen, daß im Bereich der ersten PE-Banden kein nicht-Koopmans-

---

[5] Bei einem 2*p*-AO stammen 50% der Spin-Bahn-Wechselwirkung aus einem Raum dicht beim Kern, welcher 5% der Elektronenladung enthält.

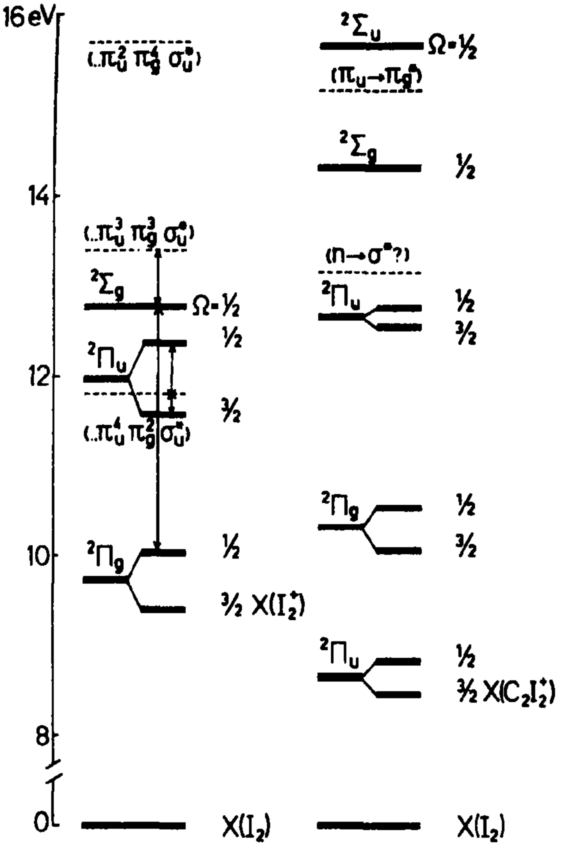

Fig. 6. Semiquantitatives Termschema von J_2^+ und $C_2J_2^+$. Koopmans-Konfigurationen sind durch , nicht-Koopmans-Konfigurationen durch markiert. Pfeile deuten verhältnismäßig starke Konfigurationswechselwirkung an

Zustand zu erwarten ist und daß wegen der verhältnismäßig großen Energiedifferenzen Spin-Bahn-Wechselwirkung höherer Ordnung nicht von Bedeutung sein dürfte (die dritte $^2\Pi_u$-Bande im PE-Spektrum könnte durch den $n\rightarrow\sigma^*$-Zustand gestört werden, falls dieser u-Symmetrie hat).

Komplizierter ist die Situation bei J_2^+. Mulliken [18] hat die mittleren vertikalen Anregungsenergien zu den Konfigurationen $(\sigma_g)^2(\pi_u)^4(\pi_g)^3(\sigma_u^*)$ und $(\sigma_g)^2(\pi_u)^3(\pi_g)^4(\sigma_u^*)$ von J_2 zu 2,1 eV resp. 3,7 eV abgeschätzt. Wir nehmen deshalb an (Fig. 6), daß sich der Schwerpunkt der Zustände, welche der $(\sigma_g)^2(\pi_u)^4(\pi_g)^2(\sigma_u^*)$-Konfiguration von J_2^+ entspringen, 2,1 eV über dem Grundzustand von J_2^+ (9,72 eV, Mittel von $\frac{1}{2}$- und $\frac{3}{2}$-Komponente) befindet. Bei 13,4 eV resp. 15,7 eV – 3,7 eV über $^2\Pi_g$ resp. $^2\Pi_u$ – wären die Schwerpunkte der Konfigurationen $(\sigma_g)^2(\pi_u)^3(\pi_g)^3(\sigma_u^*)$ resp. $(\sigma_g)^2(\pi_u)^2(\pi_g)^4(\sigma_u^*)$ zu suchen.

Aus der $(\pi_u)^4(\pi_g)^2(\sigma_u^*)$-Konfiguration von J_2^+ leiten sich die folgenden Elektronenzustände ab: Ein $^2\Delta_u$-Zustand, durch Spin-Bahn-Kopplung in zwei Komponenten mit $\Omega=\frac{5}{2}$ und $\Omega=\frac{3}{2}$ getrennt, ein $^4\Sigma_u$ mit einer $\Omega=\frac{3}{2}$- und einer $\Omega=\frac{1}{2}$-

Komponente und zwei Σ-Zustände (Σ_u^+ und Σ_u^-) mit $\Omega = \frac{1}{2}$. Mit der gestrichelten Linie schätzen wir den Schwerpunkt dieser Zustände ab, deren gegenseitige Lage wir nicht kennen. Mit Ausnahme von $^2\Delta_{u\frac{5}{2}}$ können alle Zustände mit der einen Komponente des $^2\Pi_u$-Dubletts kombinieren.

Analog leiten sich auch von den anderen nicht-Koopmans-Konfigurationen mehrere Elektronenzustände ab.

Starke Spin-Bahn-Kopplung höherer Ordnung ist zu erwarten, wenn die wechselwirkenden Konfigurationen einen geringen Energie-Abstand haben oder weil der ein-Elektronen-Teil von $\mathscr{H}_{SO}$ den zwei-Elektronen-Teil dominiert (vgl. Abschn. 1a) – wenn sie mit einem ein-Elektronen-Sprung ineinander überführt werden können.

Ein Gasspektrum von J_2^+ scheint nicht bekannt zu sein; das UV-Spektrum des gelösten Ions wurde von Gillespie u. Milne vermessen [19]. Diese Autoren fanden Übergangsenergien von 1,94 eV, 2,53 eV und 3,02 eV, welche sie nicht definitiv zuordnen konnten. Unsere Energieabschätzung scheint zu stimmen, was schon daraus hervorgeht, daß gelöstes J_2^+ dieselbe Farbe hat wie J_2 [19].

Venkateswarlu [20] hat im UV-Spektrum von J_2 Zustände gefunden, welche er als niedrig liegende Glieder von Rydbergserien deutet, die zu den verschiedenen Zuständen der $(\pi_u)^4\,(\pi_g)^2\,(\sigma_u^*)$-Konfiguration des Kations führen. Die Seriengrenzen hat er freilich nicht entdeckt. Immerhin entnehmen wir dieser Arbeit, daß die fraglichen Ionenzustände zwischen 11 eV und 12 eV über dem Grundzustand des J_2-Moleküls liegen, also genau beim $^2\Pi_u$-Dublett von J_2^+.

Der $^2\Pi_u$-Zustand $(\sigma_g)^2\,(\pi_u)^3\,(\pi_g)^4$ unterscheidet sich in der Anordnung von zwei Elektronen von der fast entarteten Konfiguration $(\sigma_g)^2\,(\pi_u)^4\,(\pi_g)^2\,(\sigma_u^*)$. Die um ca. 3,7 eV entfernte Konfiguration $(\sigma_g)^2\,(\pi_u)^2\,(\pi_g)^4\,(\sigma_u^*)$ kann mit einem ein-Elektronen-Sprung erreicht werden.

Nehmen wir überdies an, daß die Zustände der beiden nicht-Koopmans-Konfigurationen durch („gewöhnliche") Konfigurationswechselwirkung miteinander vermischt sind, so darf eine anomale Spin-Bahn-Aufspaltung der $^2\Pi_u$-Bande im PE-Spektrum nicht verwundern. Es ist sogar denkbar, daß einer der $\pi_g \rightarrow \sigma_u^*$-Zustände mit dem einen Zustand von $^2\Pi_u$ so stark mischt, daß im PE-Spektrum der Übergang zu beiden resultierenden Zuständen mindestens schwach erlaubt ist. Wir schlagen deshalb vor, die im PE-Spektrum von J_2 bei 11,3 eV auftretende schwache Bande als Übergang zu einem Zustand von $\pi_g \rightarrow \sigma_u^*$-(nicht-Koopmans)-Konfiguration zu deuten, welcher durch Spin-Bahn-Kopplung Intensität gewonnen hat (vgl. Fig. 7).

Wenn diese Deutung richtig ist, müßte man im J_2-Spektrum Übergänge zu weiteren nicht-Koopmans-Zuständen beobachten, z. B. bei 13,4 eV oder 15,7 eV. Zwischen 13,5 eV und 16,5 eV erscheint im Spektrum nur Rauschen. Vergleichen wir jedoch Fig. 7 mit dem in [12] publizierten J_2-Spektrum, so finden wir übereinstimmende Strukturen um 14 eV und 16 eV. Vielleicht kann man durch statistisches Wegmitteln des Rauschens die Lage einiger nicht-Koopmans-Zustände von J_2^+ bestimmen, welche wegen experimenteller Schwierigkeiten im UV-Spektrum nicht beobachtet werden.

Nur eine sehr ausgedehnte SCF-CI-Rechnung für viele Zustände des J_2^+-Kations könnte unsere Vermutungen bestätigen. Eine derartige Rechnung ist

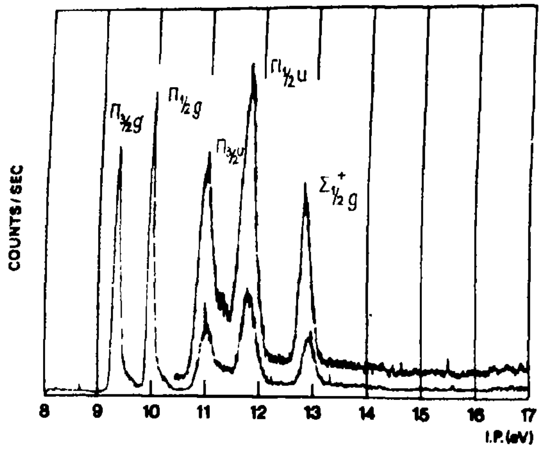

Fig. 7 Photoelektron-Spektrum von J_2 (F. Brogli/Dr. V. Hornung, Universität Basel)

heute nicht möglich. Wir verzichten deshalb auf eine quantitative Kontrolle der Aussagen dieses Abschnitts.

Wittel [25] hat das Orbitaldiagramm von J_2 benützt, um die anomale Spin-Bahn-Aufspaltung von $^2\Pi_u$ zu erklären. Obwohl sein Wechselwirkungsschema anders aussieht als das Zustandsdiagramm in Fig. 6, konnte er die Aufspaltung richtig berechnen.

Versuchen wir, diese Überlegungen auf die anderen Halogene und Halogenazetylene zu erweitern, deren PE-Spektrum bekannt ist [9–11]. Die nicht aufgelöste $^2\Pi_u$-Bande im Br_2-Spektrum könnte ihre Gestalt ebenfalls einer Spin-Bahn-induzierten Konfigurationswechselwirkung verdanken. Aus der Tatsache, daß die dritte PE-Bande (Π_u) der Dihalogen-Azetylene in zwei Komponenten aufgelöst ist bei den „reinen“ X–C≡C–X-Verbindungen, nicht aufgelöst bei den „gemischten“ X–C≡C–Y, vermuten wir, daß bei den symmetrischen Verbindungen die Erhaltung der $g-u$-Symmetrie eine CI mit der $n-\sigma^*$-Konfiguration (vgl. Fig. 6) verhindert, im Gegensatz zu den unsymmetrischen Molekülen.

Ähnliche Effekte im PE-Spektrum könnten auch bei Σ-Banden der Halogene und Halogenazetylene auftreten. Es wird sich jedenfalls lohnen, PE- und UV-Spektren dieser Verbindungen nach weiteren Hinweisen auf Spin-Bahn-Kopplung höherer Ordnung zu durchsuchen.

Dank. Für Ratschläge und Diskussionen danke ich den Herren Prof. Dr. E. Miescher, Dr. Ch. Jungen, Dr. R. Gleiter, H. J. Haink und Dr. H. Christen. Unveröffentlichte Spektren wurden mir freundlicherweise zur Verfügung gestellt von Dr. V. Hornung, Dr. R. Boschi und F. Brogli. Herrn Dr. P. A. Straub danke ich dafür, daß er mir seine Rechnungen und Manuskripte vor der Veröffentlichung zur Verfügung gestellt hat. Ich danke der Firma Sandoz AG, Basel und dem Personal ihrer EDV-Abteilung für Rechenzeit und für sorgfältige Durchführung der Rechenarbeiten.

Diese Arbeit ist Teil des Projekts Nr. SR 2.477.71 des Schweizerischen Nationalfonds.

Literatur

1. Van Vleck, J.H.: Rev. mod. Physics **23**, 213 (1951).
2. Horie, H.: Progr. theoret. Physics **10**, 296 (1953).
3. Bethe, H.A., Salpeter, E.E.: Quantum mechanics of one- and two-electron atoms. Berlin: Springer-Verlag 1957.
4. Herzberg, G.: Molecular spectra and molecular structure, I. Spectra of diatomic molecules. New York: D. Van Nostrand Comp. Inc. 1950.
5. Mizushima, M., Koide, S.: J. chem. Physics **20**, 765 (1952).
6. Kayama, K., Baird, J.C.: J. chem. Physics **46**, 2604 (1967).
7. Hellmann, J., Ballhausen, C.J.: Theoret chim. Acta (Berl.) **3**, 159 (1965).
8. Condon, E.U., Shortley, G.H.: The theory of atomic spectra. Cambridge: Cambridge University Press 1951.
9. Heilbronner, E., Hornung, V., Kloster-Jensen, E.: Helv. chim. Acta **53**, 331 (1970).
10. Haink, H.J., Heilbronner, E., Hornung, V., Kloster-Jensen, E.: Helv. chim. Acta **53**, 1073 (1970).
11. Frost, D.C., McDowell, C.A., Vroom, D.A.: J. chem. Physics **46**, 4255 (1967).
12. Cornford, A.B., Frost, D.C., McDowell, C.A., Ragle, J.L., Stenhouse, I.A.: J. chem. Physics **54**, 2651 (1971).
13. Ishiguro, E., Kobori, M.: J. physic. Soc. Japan **22**, 263 (1967).
14. Feinberg, M.J., Ruedenberg, K., Mehler, E.L.: Advances in quant. Chemistry **5**, 28 (1970), New York: Academic Press 1970.
15. Chiu, L.I.C.: J. chem. Physics **37**, A 384 (1964).
16. Straub, P.A., McLean, A.D.: In Vorbereitung.
17. Boschi, R.: Dissertation (Basel 1972) und unveröffentlichte Resultate.
18. Mulliken, R.S.: J. chem. Physics **55**, 288 (1971).
19. Gillespie, R.J., Milne, J.B.: Inorg. Chemistry **5**, 1577 (1966). – Gillespie, R.J., Milne, J.B., Morton, M.J.: Inorg. Chemistry **7**, 2221 (1968).
20. Venkateswarlu, P.: Canad. J. Physics **48**, 1055 (1970).
21. Lefebvre-Brion, H., Bessis, N.: Canad. J. Physics **47**, 2727 (1969).
22. Evans, S., Orchard, A.F.: Inorg. chim. Acta **5**, 81 (1971).
23. Potts, A.W., Price, W.C.: Trans. Faraday Soc. **67**, 1242 (1971).
24. Bates, D.R., Ledsham, K., Stewart, A.L.: Philos. Trans. Roy. Soc. (London) **1954**, A 246, 215.
25. Wittel, K.: Chem. Physics Letters (1972), in Vorbereitung.

Dr. Martin Jungen
Physikalisch-Chemisches Institut der Universität
CH-4056 Basel
Klingelbergstraße 80
Schweiz

Theoret. chim. Acta (Berl.) 27, 49—54 (1972)
© by Springer-Verlag 1972

Optical Manifestation of Jahn-Teller Effect in Square-Planar Complexes

B. G. VEKHTER, B. S. TSUKERBLAT, and YU. B. ROSENFELD
Department of Quantum Chemistry, Academy of Sciences, Moldavian SSR, Kishinev, USSR

Received February 22, 1972

The optical band shape singlet-doublet transition in the square-planar complexes has been investigated in the framework of the quasiclassical approach, the spin-orbit coupling has been included. The optical band shape has been examined in the cases of static and dynamic Jahn-Teller effect.

In den Grenzen der quasi-klassischen Näherung werden die optischen Singulett-Dublett-Übergänge für quadratische Komplexe untersucht. Dabei wird auch der Einfluß der Spin-Bahn-Kopplung auf die Form der Banden untersucht. Das Verhalten der optischen Bande wird für den statischen und dynamischen Jahn-Teller-Effekt untersucht.

La forme de la bande de transition singlet-doublet a été étudiée dans les complexes quadratiques-planes, en utilisant l'approximation quasiclassique. On tient compte des effets de l'intéraction spine-orbitale. La forme de la bande a été étudiée dans les cas des effets statique et dynamique de Jahn-Teller.

Introduction

At present there is considerable interest in Jahn-Teller effect (JTE) and related problems (see [1, 2]). The JTE in two-fold degenerate electronic level is qualitatively different for the cubic and trigonal systems on the one hand and for the tetragonal systems from the other hand. In the first case the two-fold degenerate e-mode is active in the JTE and the matrix Hamiltonian of vibronic interaction with such mode

$$\hat{H} = c(\sigma_z q_1 + \sigma_x q_2)$$

contains only one constant c (q_1, q_2 and σ_x, σ_z are the normal coordinates and the Pauli matrixes respectively). By contrast in the second case nondegenerate modes b_{1g} and b_{2g} are active in the JTE, so that in the case of square-planar complex the vibronic Hamiltonian

$$\hat{H} = c_1 \sigma_z q_1(b_{1g}) + c_2 \sigma_x q_2(b_{2g})$$

contains two independent constants c_1 and c_2. This last circumstance gives the opportunity to examine so the dynamic JTE ($c_1 \neq 0$ and $c_2 \neq 0$) as the static JTE (c_1 or c_2 is equal zero) varying the values of constants c_1 and c_2.

The case of static JTE was investigated by Hougen in his important paper [3]. The general case of dynamical JTE in square-planar complexes was examined in details by Ballhausen [4]. On the basis of numerical methods he obtained the optical spectra for ${}^2A \rightarrow {}^2E$ transition in the case of intermediate coupling ($\Delta E_{JT} \sim 3\hbar\omega$) and at $T = 0° K$ when the quantum effects in the optical band structure may be observed. The envelope curve of optical band may be received by quasiclassical approximation in the another limit case of the high temperature and strong coupling $\Delta E_{JT} \gg \hbar\omega$. Such investigation we give in this note for $A \to E$ *transition in square-planar complexes.*

General Expressions

As it is mentioned above for doublet ^2E *term in square-planar complexes two nondegenerate mode* b_{1g} *and* b_{2g} *are JT active. The secular equation including spin-orbit coupling has the form [4]:*

$$\begin{array}{c|cccc|}
\varphi_x\alpha & -c_1q_1-\varepsilon & 0 & c_2q_2+\frac{1}{2}i\lambda & 0 \\
\varphi_x\beta & 0 & -c_1q_1-\varepsilon & 0 & c_2q_2-\frac{1}{2}i\lambda \\
\varphi_y\alpha & c_2q_2-\frac{1}{2}i\lambda & 0 & c_1q_1-\varepsilon & 0 \\
\varphi_y\beta & 0 & c_2q_2+\frac{1}{2}i\lambda & 0 & c_1q_1-\varepsilon
\end{array} = 0\,. \tag{1}$$

The solutions are

$$\varepsilon = \pm\sqrt{c_1^2q_1^2 + c_2^2q_2^2 + \frac{\lambda^2}{4}} \equiv \pm\varepsilon_0\,. \tag{2}$$

the eigenfunctions can be written as

$$\left.\begin{aligned}
\Psi_+(r,q,\sigma) &= N\left|\left(c_2q_2 + i\,\frac{\lambda}{2}\right)\varphi_x + (c_1q_1+\varepsilon_0)\varphi_y\right|\chi(\sigma) \\
\Psi\ \ (r,q,\sigma) &= N\left|-(c_1q_1+\varepsilon_0)\varphi_x + \left(c_2q_2 - i\,\frac{\lambda}{2}\right)\varphi_y\right|\chi(\sigma) \\
N &= \left[2\left(c_1^2q_1^2 + c_2^2q_2^2 + \frac{\lambda^2}{4} + c_1q_1\varepsilon_0\right)\right]^{1/2}
\end{aligned}\right\} \tag{3}$$

where $\sigma = \pm\frac{1}{2}$, $\chi(\frac{1}{2}) = \alpha$, $\chi(-\frac{1}{2}) = \beta$.

Within the semiclassical approximation the line shape function of the optical absorption is given by

$$\begin{aligned}
K(x) = \frac{1}{\pi\hbar}\left(\frac{k_1k_2\vartheta_1\vartheta_2}{\omega_1\omega_2}\right)^{1/2} \sum_{\pm} \iint dq_1\,dq_2\,|\langle\Psi_0|\hat{d}|\Psi_\pm\rangle|^2 \\
\cdot\exp\left(-\frac{k_1\vartheta_1}{\hbar\omega_1}\cdot q_1^2 - \frac{k_2\vartheta_2}{\hbar\omega_2}\,q_2^2\right)\delta(\hbar x \pm \varepsilon_0)\,,
\end{aligned} \tag{4}$$

$$\vartheta_i = \tanh\frac{\hbar\omega_i}{2k_B\mathrm{T}}\,,\qquad x = \Omega - \Omega_0$$

where d is the dipole moment operator, Ψ_0 is the orbital singlet ground state wavefunction, Ω is the light frequency, $\hbar\Omega_0$ is the energy gap between the electronic terms when the nuclear configuration is fixed in the high symmetry point $q_1 = q_2 = 0$. Introducing ϱ and φ coordinates by the relations

$$c_1q_1 = \varrho\cos\varphi\,,\qquad c_2\,q_2 = \varrho\sin\varphi \tag{5}$$

one can obtain for K_+ following expression

$$K_+(x)=\frac{1}{2\pi\hbar c_1 c_2}\left(\frac{k_1 k_2 \vartheta_1 \vartheta_2}{\omega_1\omega_2}\right)^{1/2}\int_0^{2\pi} d\varphi\int_0^{\infty}\varrho\, d\varrho$$
$$\cdot\frac{\exp\left[\left(-\frac{k_1\vartheta_1}{\hbar\omega_1 c_1^2}\cos^2\varphi-\frac{k_2\vartheta_2}{\hbar\omega_2 c_2^2}\sin^2\varphi\right)\varrho^2\right]}{\varrho^2+\frac{\lambda^2}{4}+\varrho\cos\varphi\sqrt{\varrho^2+\frac{\lambda^2}{4}}} \tag{6}$$
$$\cdot\left[d_{0x}^2\left(\varrho^2\sin^2\varphi+\frac{\lambda^2}{4}\right)+d_{0y}^2\left(\varrho^2\cos^2\varphi+\varrho^2+\frac{\lambda^2}{4}+2\varrho\cos\varphi\sqrt{\varrho^2+\frac{\lambda^2}{4}}\right)\right]$$
$$\cdot\delta\left(\hbar x\pm\sqrt{\varrho^2+\frac{\lambda^2}{4}}\right).$$

The expression for K_- looks similarly. For nonpolarised light $d_{0x}^2=d_{0y}^2\equiv d^2$ and the expression (6) becomes more simply

$$K_{\pm}(x)=\frac{d^2}{\pi\hbar c_1 c_2}\left(\frac{k_1 k_2 \vartheta_1 \vartheta_2}{\omega_1\omega_2}\right)^{1/2}\int_0^{2\pi} d\varphi\int_0^{\infty}\varrho\, d\varrho$$
$$\cdot\exp\left[\left(-\frac{k_1\vartheta_1}{\hbar\omega_1 c_1^2}\cos^2\varphi-\frac{k_2\vartheta_2}{\hbar\omega_2 c_2^2}\sin^2\varphi\right)\varrho^2\right]\delta\left(\hbar x\pm\sqrt{\varrho^2+\frac{\lambda^2}{4}}\right). \tag{7}$$

Performing the integration we get

$$K(x)=\frac{2d^2}{c_1 c_2}\left(\frac{k_1 k_2 \vartheta_1 \vartheta_2}{\omega_1\omega_2}\right)^{1/2}$$
$$\cdot|x|\exp\left[-\frac{1}{2}\left(\frac{k_1\vartheta_1}{\hbar\omega_1 c_1^2}+\frac{k_2\vartheta_2}{\hbar\omega_2 c_2^2}\right)\left(\hbar^2x^2-\frac{\lambda^2}{4}\right)\right] \tag{8}$$
$$\cdot I_0\left[-\frac{1}{2}\left(\frac{k_1\vartheta_1}{\hbar\omega_1 c_1^2}-\frac{k_2\vartheta_2}{\hbar\omega_2 c_2^2}\right)\left(\hbar^2x^2-\frac{\lambda^2}{4}\right)\right]\left[\Theta\left(x-\frac{|\lambda|}{2\hbar}\right)+\Theta\left(-x-\frac{|\lambda|}{2\hbar}\right)\right].$$

In Eq. (8) I_0 and Θ are the Bessel function of image argument and the step function respectively.

Discussion

If $\lambda=0$ the optical band is splitted into two components with zero intensity at $x=0$. (Fig. 1a.) This line shape resembles that of $A\to E$ transitions in cubic and trigonal cases [5] and coincides with the last when $\frac{k_1\vartheta_1}{\hbar\omega_1 c_1^2}=\frac{k_2\vartheta_2}{\hbar\omega_2 c_2^2}$. Note, that at the high temperature ($k_BT\gg\hbar\omega_1,\hbar\omega_2$) the condition $\frac{k_1\vartheta_1}{\hbar\omega_1 c_1^2}=\frac{k_2\vartheta_2}{\hbar\omega_2 c_2^2}$ transforms into the condition $\frac{k_1}{c_1^2}=\frac{k_2}{c_2^2}$ when the lowest potential sheet surface possesses the continuum of minima, i.e. the complex can "rotate" freely between an "elongate" and "rhombic" configuration [4].

The interaction with one of the active mode becoming weaker the splitting is decreasing, when $c_2 = 0$ the dip of the optical curve at $x = 0$ disappears, and the optical band becomes the Gaussian one with the maximum at the Franck-Condon frequency $x = 0$.

$$K(x) = \frac{d^2 \hbar \sqrt{\vartheta_1}}{c_1 \sqrt{2\pi}} \exp\left(- \frac{\vartheta_1 \hbar^2 x^2}{2c_1^2} \right). \tag{9}$$

The appearance of the Gaussian curve in this case may be easily understood. Indeed in $q_2 = 0$ section the potential surfaces are two intersecting parabolas; so the dynamic JTE becomes the static one. Then point $q_1 = 0$ turns out to be the turning point for the nuclear motion, so the absorption intensity has maximum at $x = 0$.

The account of the spin-orbit interaction gives the following expression for the absorption coefficient in the case $c_2 = 0$:

$$K(x) = \frac{2d^2}{c_1} \left(\frac{\hbar k_1 \vartheta_1}{\pi \omega_1} \right)^{1/2} \frac{|x|}{\left(\hbar^2 x^2 - \frac{\lambda^2}{4} \right)^{1/2}} \tag{10}$$
$$\cdot \exp\left[- \frac{k_1 \vartheta_1}{\hbar \omega_1 c_1^2} \left(\hbar^2 x^2 - \frac{\lambda^2}{4} \right) \right] \left[\Theta\left(x - \frac{|\lambda|}{2\hbar} \right) + \Theta\left(-x - \frac{|\lambda|}{2\hbar} \right) \right].$$

Eq. (10) describes the optical band with two sharp peaks at $x = \pm \frac{\lambda}{2\hbar}$, separated by the zero absorption range (Fig. 1 b). Absence of the absorption in the range $|x| < \frac{|\lambda|}{2\hbar}$ takes place in the case of dynamic JTE ($c_2 \neq 0$) too. In this case, however, the optical band shape is more smoothed and its two peaks may be placed at $x \neq \frac{\lambda}{2\hbar}$. So, in the case $\frac{k_1 \vartheta_1}{\omega_1 c_1^2} = \frac{k_2 \vartheta_2}{\omega_2 c_2^2} \equiv \frac{k \vartheta}{\omega c^2}$ we get

$$K(x) = \frac{2d^2 \hbar \vartheta}{c^2} |x| \exp\left[- \frac{\vartheta}{c^2} \left(\hbar^2 x^2 - \frac{\lambda^2}{4} \right) \right] \left[\Theta\left(x - \frac{|\lambda|}{2\hbar} \right) + \Theta\left(-x - \frac{|\lambda|}{2\hbar} \right) \right]. \tag{11}$$

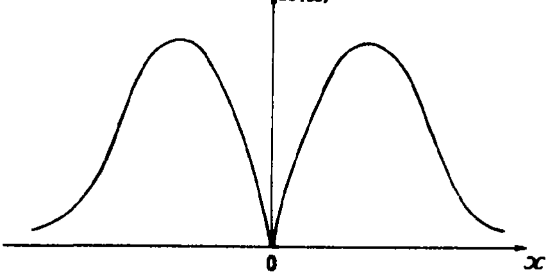

Fig. 1a

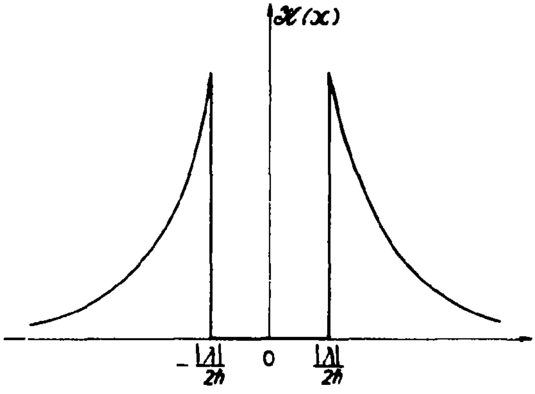

Fig. 1b

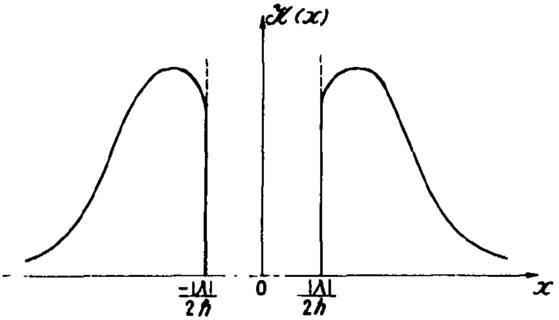

Fig. 1c

Fig. 1. The optical absorption band shape of $^2A \to {}^2E$ transition: a $\lambda = 0$, $c_1 \neq 0$, $c_2 \neq 0$; b $\lambda \neq 0$, $c_1 \neq 0$, $c_2 = 0$; c $\lambda \neq 0$, $\frac{k_1 \vartheta_1}{\omega_1 c_1^2} = \frac{k_2 \vartheta_2}{\omega_2 c_2^2} \equiv \frac{k \vartheta}{c \omega}$

The maxima of curve (11) are either at

$$x_{\max} = \pm \sqrt{\frac{c^2}{2\hbar^2 \vartheta}}, \quad \text{if} \quad \sqrt{\frac{c^2}{2\hbar^2 \vartheta}} > \frac{|\lambda|}{2\hbar},$$

or at (12)

$$x_{\max} = \pm \frac{|\lambda|}{2\hbar}, \quad \text{if} \quad \sqrt{\frac{c^2}{2\hbar^2 \vartheta}} < \frac{|\lambda|}{2\hbar}.$$

In the first case (12) (Fig. 1c) when the vibronic interaction exceeds the spin-orbit one maxima positions are temperature dependent, and the splitting of two peaks is proportional to $\sqrt{T}$ (at high temperature). This temperature dependence of the splitting takes place only in the temperature range $\vartheta < \vartheta_0 \equiv \frac{2c^2}{\hbar^2 \lambda^2}$. In this connection it is interesting to note the difference in the shapes of optical bands splitted by spin-orbit interaction in two cases: 1) the active modes forming the band shape are total symmetrical, 2) the JT b_{1g} and b_{2g} – modes are active. In

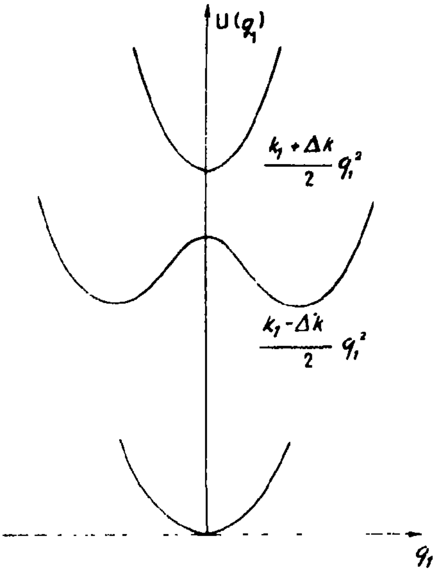

$U(q_1)$
$\frac{k_1+\Delta k}{2} q_1^2$
$\frac{k_1-\Delta k}{2} q_1^2$
q_1

Fig. 2. Adiabatic potentials in the case $c_2 = 0$, $\lambda \neq 0$

the case 1) the spin-orbit interaction manifests itself as a "rigid" shift of Gaussian bands, and the structure of whole band may be not observe if λ is small enough. In contrary, in the case 2) the zero intensity range is appeared and two peaks are easily resolved. This result may be easily understood in the case $c_2 = 0$. Such form of the optical band results from the frequency shift of square-complex vibrations due to the simultaneous action of spin-orbit interaction and vibronic coupling (Fig. 2). Optical Franck-Condon transitions on the upper surface occurs at the $x > \frac{|\lambda|}{2h}$, whereas the transitions on the lower surface leads to the absorption at $x < -\frac{|\lambda|}{2h}$, so in the region $|x| < \frac{|\lambda|}{2h}$ the absorption is absent.

References

1. Sturge, M. D.. Solid State Physics **20**, New York-London (1968).
2. Bersuker, I. B.: Stroenie i Svoistva Koordinatsionih Soedinenii. Leningrad: Himia 1971.
3. Hougen, J. T.: J. molecular Spectroscopy **13**, 149 (1964).
4. Ballhausen, C. J.. Theoret. chim. Acta (Berl.) **3**, 368 (1965).
5. Toyozawa, Y., Inoue, M.: J. physic. Soc. Japan **21**, 1663 (1966).

Dr. B. G Vekhter
Department of Quantum Chemistry
Academy of Sciences
Moldavian SSR
Kishinev, USSR

Theoret. chim. Acta (Berl.) 27, 55—62 (1972)
© by Springer-Verlag 1972

Barriers to the Internal Rotation and Observables of the Ground State for Hydrogen Peroxyde

C. GUIDOTTI, U. LAMANNA*, M. MAESTRO, and R. MOCCIA

Centro di Chimica Teorica del CNR, Istituto di Chimica Fisica dell'Università di Pisa,
56100 Pisa, Italy

Received February 21, 1972

SCF energy and one electron properties of the H_2O_2 molecule have been calculated by using a basis of 52 STO's. The minimum total energy reached is -150.83188 a.u. By carrying out the calculation for three different geometrical configurations a reasonable agreement with experimental values of the barriers to the internal rotation is obtained.

Die SCF-Energie und die Einelektroneneigenschaften des H_2O_2-Moleküls werden mit einer Basis von 52 Slaterorbitalen berechnet. Als minimale Gesamtenergie werden der Wert von $-150{,}83188$ a.E. erreicht. Die Ergebnisse für 3 verschiedene Geometrien liefern eine befriedigende Übereinstimmung mit dem experimentellen Wert der Barriere für die innere Rotation.

L'énergie SCF et les propriétés monoélectroniques de la molécule H_2O_2 ont été calculées en utilisant une base de 52 orbitales de Slater. L'énergie minimum totale atteinte est -150.83188 u.a. Un accord raisonnable avec les valeurs expérimentales des barrières de rotation est obtenu en effectuant les calculs pour trois configurations géométriques différentes.

1. Introduction

In the recent years, it has become possible to achieve accurate "*ab initio*" calculations, at least for the simpler cases of polyatomic molecules, and the problem of the evaluation of the barriers to the internal rotation has drawn increased attention. Among the cases that have been considered, the H_2O_2 molecule presents a particular interest for two reasons. On the one hand, it is probably the most simple stable system (lowest number of electrons and nuclei) which shows such a type of barriers, and on the other hand, the smallness of the lower of the two barriers (1.10 kcal/mole) renders a prediction of this observable a very critical test for the calculation methods that one may utilize.

The Hartree-Fock (H.F.) scheme is still the most largely used one for *ab initio* calculations of the ground state of molecular systems, and the question as to whether this approximation is able to yield correct predictions for the barriers to the internal rotation, is still open. Many recent works [1–4] seem to give a positive answer to this question, at least in most cases. The trans barrier of the H_2O_2 molecule has, however, furnished contrasting results [1, 4, 5]. In any case one must face two difficulties. Firstly it is not easy to guess a plausible limit for the H.F. energy of a molecule in a given geometry, and sometimes the execution of calculations on more and more extended basis sets has entailed the lowering of the presumed H.F. limit. The previsions that one may guess for this limit frequently present errors that are at least of the same order of magnitude as the barriers that one wishes to calculate, so that it is difficult to decide whether the result obtained as a difference between two SCF energies of two different molecular geometries, represents effectively the result of the H.F. approximation. One must rather acknowledge that the majority of the calculations carried out even now, still utilizes too limited basis sets. It is evident that the only rigorous way to overcome the obstacle (and that has indeed been followed in the case of atoms and of the simplest molecules), i.e. the increasing and improvement of the basis up the attainement of the stability in the energy to the required limits, is, at present, too expensive for molecules that present barriers to the internal rotation.

---

* Istituto di Chimica Analitica dell'Università di Bari, Bari, Italy.

In the second place, one must take into account the effect of the nuclear relaxation, i.e. the variation of the molecular geometry (distance and bond angles) together with the rotation angle of the barrier. The verifying as to whether the H.F. approximation is able to describe this effect correctly, involves the calculation of the H.F. energy for an adequate number of geometrical configurations and this is out of the actual concrete possibilities. When one has experimental indications for the geometries at the maximum and minimum of the barriers, it seems therefore preferable to evaluate the best SCF energy for these geometries. Usually, however, the geometrical data are known for the equilibrium configuration only, in addition, the same deduction of the values for the barriers from the spectroscopic experimental data, is often based on the hypothesis of the rigidity of the molecule during the rotation (this is, for instance, the case of the most reliable data for the H_2O_2 barriers [6]). The minimization of the SCF energy with respect to the geometrical parameters, produces a relaxation effect, but it is not certain that it correctly represents the physical situation.

In any case, this type of calculations implies a further increase in the cost.

In the H_2O_2 molecule, Veillard [4], on the basis of the optimization of the geometrical parameters in an SCF calculation, has emphasized the critical role of the relaxation effect.

This paper presents a SCF calculation on H_2O_2 molecule, that is carried out by employing a STO basis set, more extended than any other considered until now, and that attains an energy correspondingly lower. The results that one obtains for the two barriers by using such a basis for evaluating the energy in the *cis*- and *trans*-configurations, are near to the experimental ones. In this calculation, the relaxation effect is not considered, and it is not necessary to invoke it to attain the relative agreement with the experiment. For the equilibrium configuration, some one electron properties are also calculated and compared with experiment where possible.

2. Results and Discussion

In Fig. 1, the geometrical parameters and the position of the axes are defined. The reported parameters are assumed constant for all the values of the rotation angle; they correspond to the most plausible value in the equilibrium configuration [6]. For the angle β the values 0°, 120° and 180° were considered. The largest considered basis set is reported in Table 1; the criteria for this particular choice are essentially empirical in their origin, and it is rather useless to try to justify

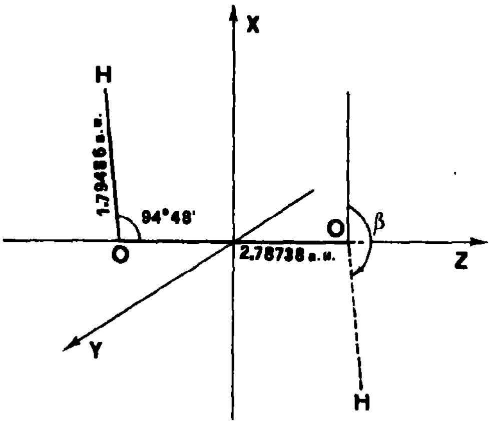

Fig. 1. Geometrical parameters

Table 1. STO's on the oxygen and hydrogen atoms

Atom	Type	Zeta
O	1*s*	12.39
	1*s*′	7.02
	2*s*	2.86
	2*s*′	1.72
	3*s*	8.65
	4*s*	1.00
	2*p*	3.76
	2*p*′	2.12
	2*p*″	1.28
	3*d*	2.00
H	1*s*	1.31
	1*s*′	2.44
	2*s*	2.30
	2*p*	2.00

Table 2. Total energy and barriers to internal rotation

	Energy (a.u.)			Barriers			
	0°	120°	180°	*cis*		*trans*	
				(a.u.)	(kcal/mole)	(a.u.)	(kcal/mole)
A[a]	−150.81459	−150.83188	−150.83073	0.01729	10.9	0.00115	0.72
B[b]	−150.81168	−150.82853	−150.82754	0.01685	10.6	0.00099	0.62
C[c]		−150.83165	−150.83043			0.00122	0.76
$(-V/2T)$[a]	1.00056	1.00069	1.00067				
Expt.[d]					7.04		1.10

[a] With the complete basis.

[b] Without the 1*s*′ functions on the hydrogen atoms.

[c] Without the 4*s* functions on the oxygen atoms.

[d] Hunt, R. H., Leacock, R. A., Peters, C. W., Hecht, K. T.: J. chem. Physics **42**, 1931 (1965).

Table 3. Different estimates of the H.F. limit for H_2O_2[a]

$2E_O{}^{b} + 2E_H$	-151.2130	$2E_O^{H.F.\ h}$	-149.6295	$2E_{OH}^{H.F.\ i}$	-150.8425	$E^{tot}_{H_2O}$	-76.458	$E^{tot}_{H_2O_2}$	-151.6389
$1/2\sum_i h\nu_i{}^{c}$	$-\ 0.0252$	$2E_H$	$-\ 1.0$	$E_{OO}^{bound\ j}$	$-\ 0.0776$	$-E^{H.F.\ h}_{H_2O}$	$+76.089$	$-2E^{corr}_{H_2O}$	$+\ 0.640$
$H_2 + O_2 = H_2O_2{}^{c}$	$-\ 0.0495$	$E^{bound}_{H_2O_2}$	$-\ 0.4259$	$-(1/2\sum h\nu_i)^{k}$	$-\ 0.0170$	$-E_O^{rel}$	$+\ 0.049$	$-2E_O^{rel}$	$+\ 0.099$
$H_2 = H + H^{d}$	$-\ 0.1645$	$-3E^{extracorr}$	$+\ 0.12$	$-E^{extracorr}$	$+\ 0.04$	$E^{corr}_{H_2O}$	$-\ 0.320$	$E^{extracorr}$	$-\ 0.04$
$O_2 = O + O^{d}$	$-\ 0.1867$								
$E^{tot}_{H_2O_2}$	-151.6389	$E^{H.F.}_{H_2O}$	-150.94	$E^{H.F.}_{H_2O_2}$	-150.90			$E^{H.F.}_{H_2O_2}$	-150.94
$-2E_O^{corr.\ e}$	$+\ 0.4930$								
$-2E_O^{rel.\ f}$	$+\ 0.098$			$E^{H.F.}_{H_2O} = -150.92 \pm 0.02$					
$-3E^{extracorr\ g}$	$+\ 0.12$								
$E^{H.F.}_{H_2O_2}$	~ -150.93								

[a] Values used for physical constants: 1 a.u. = 27.211644 eV, 1 eV = 8065.465 cm^{-1} From Taylor, B. N., Park, W. H., Langenberg, D. N.: Rev. mod. Physics **41**, 375 (1969).

[b] Moore, C. E.: Atomic energy levels III. Washington: The National Bureau of Standards 1958.

[c] Giguère, P. A., Liu, I. D.: J. Amer. chem. Soc. **77**, 6477 (1955).

[d] Herzberg, G.: Molecular spectra and molecular structure, Vol. I. Spectra of diatomic molecules. New York: Van Nostrand 1955.

[e] Obtained as $E^{expt} - (E^{H.F.} + E^{rel})$.

[f] Clementi, E., McLean, A. D.: Physic. Rev. **133**, A 419 (1964).

[g] Assumed as ~0.04 for bound in analogy with the first row hydride molecules.

[h] Neuman, D., Moskowitz, J. W.: J. chem. Physics **49**, 2056 (1968).

[i] Cade, P. E., Huo, W. M.: J. chem. Physics **47**, 614 (1967).

[j] Foner, S. N., Hudson, R. L.: J. chem. Physics **36**, 2676 (1962).

[k] Difference of zero point energies for $2OH \rightarrow H_2O_2$ from Ref. [c].

[l] Eisenberg, D., Kauzmann, W.: The structure and properties of water. Oxford: Clarendon Press 1969

them in a systematic manner. A previous experience with calculation on hydrogen peroxyde with limited basis sets has suggested to us the introduction of the *d* functions on the oxygen nuclei; the 4*s* functions with low orbital exponent have been added chiefly in view of the evaluation of some second order observables such as the electric polarizability.

Due to the largeness of the basis used, each attempt to optimize it or to minimize the energy, with respect to the geometry, would result to be prohibitively expensive.

In the Table 2 are reported the calculated values for the total energy in the different configurations and the related values for the barriers, in the hypothesis that the minimum is near to the configuration at 120°.

In the Table 3, we report some guesses for the H.F. limit for hydrogen peroxyde that one can obtain in different ways. One of these consists in subtracting the extimated correlation contributions from the total energy obtained from the experimental data on H_2O_2, while the others utilize also calculated H.F. energies for simple molecules (such as OH and H_2O) that may be considered as fragments of the whole molecule H_2O_2. From the reported data it may be seen that: 1) the difference between the obtained values for the H.F. limit is almost four times the experimental value of the greatest barrier (0.011 a.u.); 2) even in the most favourable hypothesis, the limit is still at 0.066 a.u. from our best result. From this point of view, it is clear that also the previsions that we obtained in this paper, are not free from the fundamental criticism already considered in the introduction. This criticism is *a fortiori* valid for other results (some of which are reported for the sake of comparison in Table 4), that are more distant than ours from the plausible

Table 4. Some previous results for energies and barriers to internal rotation

	Energy (a.u.)			Barriers (kcal/mole)	
	0°	120°	180°	*cis*	*trans*
A[a]	−150.6860	−150.7074[f]	−150.7078	13.7	
B[b]	−150.7017	−150.7228[f]	−150.7224	13.2	0.32
C[c]	−150.2024	−150.2213	−150.2232	13.1	
D[d]	−150.2201	−150.2353[l]	−150.2353	9.4	--
E[e,g]	−150.7819	−150.7992	−150.7983	10.9	0.6
F[h]	−150.7689	−150.7910[l]	−150.7906	13.9	0.24
G[i]	−150.8146	−150.8319	−150.8307	10.9	0.72
H[j]			−150.82016[k]	8.34	1.09

[a] Fink, W. H., Allen, L. C.: J. chem. Physics **46**, 2261 (1967).

[b] Fink, W. H., Allen, L. C.: J. chem. Physics **46**, 2276 (1967).

[c] Palke, W. E., Pitzer, R. M.: J. chem. Physics **46**, 3948 (1967).

[d] Stevens, R. M.: J. chem. Physics **52**, 1397 (1970).

[e] Veillard, A.: Theoret. chim. Acta (Berl.) **18**, 21 (1970).

[f] Value at 150°.

[g] Optimized geometry.

[h] Davidson, R. B., Allen, L. C.: J. chem. Physics **55**, 519 (1971).

[i] This work.

[j] Dunning, T. H., Winter, N. W.: Chem. Physics Letters **11**, 194 (1971).

[k] Value at 113.7°.

[l] Value at 132°.

H.F. limit. Nevertheless, it is presumable that if a result remains more or less stable when the basis is allowed to grow, it will rest so even at the H.F. limit. As a further check of these considerations, we have carried out two other SCF calculations with partial cancellation of the basis; the results are also reported in Table 2. Even though the incompleteness of these attempts does not allow us to carry out a detailed analysis of the effectiveness of some particular function of the basis in describing the barriers, (an analysis that, in our opinion, has a rather doubtful physical meaning), it is, at any rate, comforting that one could verify a sensible persistence of the results. From our results, together with those previously obtained by several authors (see Table 4), one may reasonably infer that the H.F. calculation for the largest barrier is substantially correct. The remaining difference of 3.86 kcal/mole can by no means, however, be considered negligible; the consideration of the nuclear relaxation should, presumably, permit an improvement of these results. For the lowest one, our results, even though encouraging, do not seem to give a sufficient basis of credibility.

Indeed, one must take into account that, among the previous results for this last quantity, that of Veillard is the only one (as far we know) that shows a discrete agreement with experiments, and this is true only for the version in which the nuclear relaxation is considered.

In a recent paper [8] Davidson and Allen have found for the lowest barrier an improvement of 0.001 a.u. due to the nuclear relaxation and this value is in a good agreement with that of Veillard (0.0009). Presumably the relaxing of the constraint of geometrical rigidity would bring a similar change in our result displacing it to 1.2 kcal/mole, still in a good agreement with experiment. A similar situation seems also to be valid for the main barrier. In conclusion, the nuclear relaxation seems to be crucial for a quantitative agreement to be reached, but not necessary for a qualitative answer on the existence of the barriers and the approximate values for the potential minima.

In Table 5 are reported the forces on the H nuclei in the three configurations examined. These forces are evaluated on the hypothesis that the calculated wave function is a sufficiently good approximation of the H.F. solution, so that for it the Hellmann-Feynman theorem is valid. Due to noticeably complexity of the neglected terms [7] (that are zero only for the true H.F. orbitals), it is not easy to appreciate how such an approximation is suitable. Very plausibly, the error in the case of the oxygen atoms is greater (for the more severe conditions that the SCF orbitals must fulfil near these nuclei), and for that, we do not consider the forces on the oxygen nuclei. If at least the sign of the forces on the protons is exact, from the reported values it may be seen that the effect of the forces is such that the OH bonds tend to be spread apart. This fact shows a qualitative agreement with Veillard

Table 5. Components of the forces at the H nuclei (a.u.)

	x	y	z
0°	−0.00777	0.0	−0.02654
120°	−0.00199	0.00009	−0.01490
180°	−0.00145	0.0	−0.01347

Table 6. Calculated quantities for H_2O_2 molecule

Total energy (Hartree)	-150.83188	-151.6389^{a}
$\langle x \rangle^{b}$ (a.u.)	0.5530	
μ (debye)	1.7356	2.26^{c}
θ^{d}_{xx} (10^{-26} esu.cm^2)	$-$ 1.353	
θ_{zz} (10^{-26} esu.cm^2)	5.476	
Θ^{e}	122° 30′	
φ	$-$ 30	
$\langle r^2 \rangle^{f}$ (10^{-16} cm^2)	18.656	
$(e^2qQ^D/h)^{g,h}_{x'x'}$ (MHz)	$-$ 0.138	
$(e^2qQ^D/h)_{z'z'}$ (MHz)	0.3377	
η^D	0.186	
Θ	83° 32′	
$(e^2qQ^{O^{17}}/h)^{i}_{x'x'}$ (MHz)	0.100	
$(e^2qQ^{O^{17}}/h)_{z'z'}$ (MHz)	$-$ 2.849	
$\eta^{O^{17}}$	0.930	
Θ	12° 20′	
φ	$-$ 1° 12′	
χ	1° 54′	
$\Omega^{j}_{3,0}$ (10^{-34} esu.cm^3)	0.074	
$\Omega_{3,1}$ (10^{-34} esu.cm^3)	2.374	
$\Omega_{3,\bar{1}}$ (10^{-34} esu.cm^3)	$-$ 0.732	
$\Omega_{3,2}$ (10^{-34} esu.cm^3)	$-$ 4.496	
$\Omega_{3,\bar{2}}$ (10^{-34} esu.cm^3)	$-$ 0.685	
$\Omega_{3,3}$ (10^{-34} esu.cm^3)	4.980	
$\Omega_{3,\bar{3}}$ (10^{-34} esu.cm^3)	2.108	

[a] See Table 3.

[b] Electronic part.

[c] Landolt-Börnstein: Num. data etc., new series Vol. 4.

[d] Components of the total molecular quadrupole tensor.

[e] Eulerian angles between a system oriented as in Fig. 1, and the principal axes of the tensor. The angles are defined as in Wilson, E. B., Jr., Decius, J. C., Cross, P. C.: Molecular vibrations. McGraw Hill 1955. Only the significant angles are reported.

[f] Electron mean quadratic distance from the center of mass.

[g] The D nucleus is placed in the plane of the Fig. 1.

[h] $Q^D = 0.00277 \cdot 10^{-24}$ e cm^2. Emsley, J. W., Sutcliffe, L. H.: High resolution nuclear magnetic resonance spectroscopy. Oxford: Pergamon Press 1965.

[i] $Q^{O^{17}} = -0.004 \cdot 10^{-24}$ e cm^2. Emsley, J. W., Sutcliffe, L. H.: High resolution nuclear magnetic resonance spectroscopy. Oxford: Pergamon Press 1965.

[j] Spherical components of the total molecular octupole tensor referred to the center of mass as origin.

results [4]; indeed, this author has found that for all the considered values of the rotation angle between 0° and 180°, the value of the total energy is lowered for values of the HOO angle greater than the experimental one. In Table 6, some one electron quantities calculated for the equilibrium configuration of H_2O_2 are reported. The only experimental datum that we found for comparison is the molecular dipole moment, for which the agreement is decidely not good.

The same quantity calculated for the configuration with $\beta = 0°$ is 3.293 D. If the approximation of rigidity of the electronic charge distribution would be valid, one would expect a result of 1.647 D at 120°, a value that is not far from that effectively found.

Insofar as it concerns the electric field gradient, it may be seen that the main direction of the tensor on the proton is practically coincident with the OH bond, while on the oxygen atom it is slightly shifted from the OO bond.

Note. When this paper was completed, we have received the work of Dunning and Winter. Their main results are quoted in Table 4. The agreement of the result for the trans barrier is very good. As in the case of Ref. [4] and [8] the geometry optimization contributes heavily (75% of the total value) to the result for the trans barrier

References

1. Fink, W. H., Allen, L. C.: J. chem. Physics **46**, 2261 (1967).
2. Pedersen, L., Morokuma, K.: J. chem. Physics **46**, 3941 (1967).
3. Stevens, R. M.: J. chem. Physics **52**, 1397 (1970).
4. Veillard, A.: Theoret. chim. Acta (Berl.) **18**, 21 (1970).
5. Palke, W. E., Pitzer, R. M.: J. chem. Physics **46**, 3948 (1967).
6. Hunt, R. H., Leacock, R. A., Peters, C. W., Hecht, K. T.: J. chem. Physics **42**, 1931 (1965).
7. Moccia, R.: Chem. Physics Lett. **5**, 260 (1970).
8. Davidson, R. B., Allen, L. C.: J. chem. Physics **55**, 519 (1971).
9. Dunning, T. H., Winter, N. W.: Chem. Physics Letters **11**, 194 (1971).

Dr. M. Maestro
Centro di Chimica Teorica del CNR
Istituto di Chimica Fisica dell'Università di Pisa
I-56100 Pisa, Italy

Theoret. chim. Acta (Berl.) 27, 63—68 (1972)
© by Springer-Verlag 1972

Relationes

A.M.O. Calculations for Some First Row Diatomic Molecules

G. L. BENDAZZOLI, F. BERNARDI, and A. GEREMIA
Istituto di Chimica Fisica e Spettroscopia, 40136 Bologna, Italy

P. PALMIERI
Istituto Chimico "G. Ciamician", 40126 Bologna, Italy

Received March 23, 1972

AMO wavefunctions for LiH, Li_2, HF, F_2 are presented.

An explicit formula for computing the energy of a closed shell system composed by doubly occupied MO's and singly filled AMO's is given.

The AMO-method provides a simple tool to construct partially correlated wavefunctions for molecules and crystals [1–2]. It is a version of the Different Orbitals for different spin method particularly suited for molecular systems and can be considered as a particular case of the general EHF scheme. Because of the relatively small amount of computations involved it is convenient for studying large size molecules and there is no doubt that its most useful applications are concerned with systems too large to be treated with more accurate procedures.

Nevertheless the AMO technique found interesting applications also in the field of small molecular systems [3-7]. In this case an essential advantage of the AMO w.f. over the one-determinant approximation is a correct asymptotic behaviour for large internuclear distances. Thanks to this property AMO is one of the simplest theoretical tools to compute potential energy curves or surfaces. Moreover *ab initio* AMO calculations on small systems are useful tests of the accuracy of the method. An exaustive discussion on this point would involve the optimization of the molecular orbitals to be paired to build the AMO w.f. and lies outside the aim of the present work. In this paper we simply derive AMO w.f. using SCF orbitals for the following 1st row diatomics: LiH, Li_2, HF, F_2. In all cases the splitting of doubly occupied MO's was restricted to valence shell orbitals. This involved a straightforward extension of the energy formulae given in Ref. [2] as detailed in the next section.

Construction of the AMO Wave Function

The AMO wavefunctions, we consider here, are of the form:

$$\psi = A\hat{O}_{S,M}[\psi_{\text{core}}\psi_{\text{val}}] \tag{1}$$

where A is the antisymmetrizer, $\hat{O}_{S,M}$ a spin projection operator and ψ_{core}, ψ_{val} are Slater determinants representing respectively a core of $2n$ electrons in n doubly occupied orbitals and a valence shell of $2m$ electrons in $2m$ singly occupied alternant molecular orbitals. Both ψ_{core} and ψ_{val} are built from a set of orthonormal orbitals $\Phi = \{\varphi_i\}$, here taken to be the SCF orbitals. As far as ψ_{val} is concerned, an occupied MO φ_i is paired to a virtual orbital $\varphi_{\bar{\imath}}$ to give a couple of alternant molecular orbitals u_i, v_i according to the following equation [8]

$$u_i = \cos\theta_i \varphi_i + \sin\theta_i \varphi_{\bar{\imath}}; \qquad v_i = \cos\theta_i \varphi_i - \sin\theta_i \varphi_{\bar{\imath}}. \tag{2}$$

The energy corresponding to function (1) is given by:

$$E(\psi) = E(\psi_{\text{core}}) + E(\psi_{\text{val}}) + E_{\text{int}} \tag{3}$$

where $E(\psi_{\text{core}})$, $E(\psi_{\text{val}})$ are the usual expressions for the energy of a closed shell MO and AMO wave functions respectively, and:

$$E_{\text{int}} = \sum_{i=1}^{n} \sum_{j=n+1}^{n+m} \{n_j[2(ii/jj) - (ij/ij)] + n_{\bar{j}}[2(ii/\bar{j}\bar{j}) - (i\bar{j}/i\bar{j})]\}. \tag{4}$$

In Eq. (4) n_j and $n_{\bar{j}}$ are the fractional occupation numbers of orbitals φ_j and $\varphi_{\bar{j}}$ as defined in Ref. [2]. Eqs. (3) and (4) are easily obtained by the following considerations: i) the operator $\hat{O}_{S,M}$ for $2n + 2m$ electrons appearing in Eq. (1) can be replaced by an $\hat{O}'_{S,M}$ for $2m$ electrons acting on ψ_{val} only. This property is easily proved if one remembers that the spin projection can be obtained by a suitable averaging of rotations in spin space [9] and ψ_{core} is obviously invariant under such operation; ii) ψ_{core} and ψ_{val} are strongly orthogonal because of the orthogonality of the basis Φ, and then the formulae given by McWeeny [10] for strongly orthogonal group functions can be used; iii) the density matrices of ψ_{core} and ψ_{val} are both diagonal in the basis Φ.

The last stage of the computation involves optimization of the variational parameters $\lambda_i = \cos 2\theta_i$.

Numerical Applications

SCF molecular orbitals were expressed as a linear combination of contracted gaussians centered on each atom, according to Table 1.

Orbital exponents and contraction coefficients were chosen according to Veillard [11]. A SCF procedure was performed and the resulting molecular orbitals used to build the AMO function.

The process was repeated for a number of internuclear distances for each molecule. Energies and symmetries of occupied and virtual canonical orbitals of interest are reported in Table 2. Several pairing schemes between molecular orbitals were tried; they follow the criterion of mixing orbitals having not too different energies, under the constraint that the correct spatial symmetry of the molecular wavefunction is preserved.

Energies and optimum values of variational parameters for various AMO functions are reported in Table 3. It is well known that AMO wavefunctions are equivalent to a limited C.I., where the mixing coefficients of configurations are functions of the non linear variational parameters λ_i [2]. A large number of CI-type wavefunctions have been reported in the literature for the molecules here investigated; for some of them see Ref. [13–20].

Table 1. Atomic basis set

Atom	Number of uncontracted GTO's		Number of contracted GTO's	
	s	*p*	*s*	*p*
H	6	0	2	0
Li	11	0	5	0
F	11	7	5	3

Table 2. Orbital symmetries for canonical MO SCF

Molecule and state, int. distance (a.u.)	LiH($^1\Sigma^+$) 3.02		Li$_2$($^1\Sigma_g^+$) 5.25		HF($^1\Sigma^+$) 1.7328		F$_2$($^1\Sigma_g^+$) 2.680	
	Symmetry	Energy	Symmetry	Energy	Symmetry	Energy	Symmetry	Energy
	1σ	−2.4726	$1\sigma_g$	−2.4744	1σ	−26.2963	$1\sigma_g$	−26.4364
	2σ	−0.2990	$1\sigma_u$	−2.4742	2σ	− 1.6002	$1\sigma_u$	−26.4362
	3σ	0.0109	$2\sigma_g$	−0.1845	3σ	− 0.7618	$2\sigma_g$	− 1.7745
	4σ	0.0779	$2\sigma_u$	0.0021	1π	− 0.6538	$2\sigma_u$	− 1.5020
	5σ	0.3638	$3\sigma_g$	0.0479	4σ	0.0899	$1\pi_u$	− 0.8175
			$3\sigma_u$	0.0844	5σ	0.2714	$3\sigma_g$	− 0.7463
					2π	0.2769	$1\pi_g$	− 0.6789
					6σ	0.4711	$3\sigma_u$	0.0640
					7σ	0.9954	$4\sigma_g$	0.5048
					8σ	1.6192	$4\sigma_u$	0.6207
							$2\pi_u$	0.6370
							$2\pi_g$	0.7830

Table 3. Total energies and optimum values of variational parameters λ_i (all quantities in atomic units)

Molecule and state	Int. distance	SCF Energy	AMO 2σ—3σ		AMO 2σ—4σ	
			Energy	λ	Energy	λ
LiH	2.52	— 7.9548	— 7.9553	0.949	- 7.9551	0.960
	3.02	- 7.9706	- 7.9712	0.937	— 7.9710	0.952
	3.52	-- 7.9672	— 7.9682	0.920	— 7.9678	0.948
			AMO $2\sigma_g$—$2\sigma_u$		AMO $2\sigma_g$- $3\sigma_g$	
Li$_2$	4.50	- 14.8543	- 14.8573	0.808	- -14.8545	0.894
	5.25	-- 14.8614	-- 14.8656	0.753	- 14.8616	0.978
	6.00	14.8597	— 14.8660	0.678	—14.8600	0.976
			AMO 3σ-—4σ			
HF	1.3328	— 99.9205	-- 99.9205	1.000		
	1.7328	--100.0079	—-100.0081	0.975		
	2.1328	99.9720	— 99.9736	0.965		
			AMO $3\sigma_g$—$3\sigma_u$			
F$_2$	2.267702	—198.6845	—198.7020	0.818		
	2.679718	-- 198.7256	—198.7814	0.600		
	3.023600	—198.6964	-- 198.7895	0.471		

Results

a) Li_2 *and* F_2

In both cases the most effective pairing scheme is the ($2\sigma_g - 2\sigma_u$) which leads to a Coulson-Fischer type wave function. This splitting insures the correct limiting behaviour as the internuclear distance R approaches infinity and introduces a fraction of "left-right" correlation in the bond. For Li_2 the improvements ΔE in energy from SCF range from 0.003-0.006 a.u., which is about one half of the improvement obtained by the ODC technique [14]. Rai and Calais [4], obtained for this molecule an AMO wavefunction built from orthogonalized symmetry orbitals expressed as a linear combination of STO's of s symmetry. The improvement of the AMO energy with respect to the single determinant energy, reported by these authors is 0.017 a.u. at 6 a.u. The difference between Rai-Calais' and our results is related to the fact that they did not use SCF orbitals. In fact, by expanding each of the STO's of Rai-Calais in 4 GTO's according to the criterion of McWeeny and Huzinaga [21], we obtained the following values at $R = 6$ a.u.: -14.8504 a.u. for the $1\sigma_g^2\, 1\sigma_u^2\, 2\sigma_g^2$ MO wavefunction; and -14.8625 for the AMO ($2\sigma_g - 2\sigma_u$) wavefunctions; i.e., a lowering of 0.0121 a.u. A comparison with the more refined calculations by Shukla [7] gives the same results. Similar conclusions were reached previously, on the basis of semiempirical calculations on conjugated systems [2].

The pairing scheme $2\sigma_g - 3\sigma_g$ was also tried for Li_2, as it is suggested by CI treatments [13, 16]. In this case very little improvement is obtained on the SCF function; our excited $3\sigma_g$ orbital cannot account for an effective in-out correlation in the bond. Other important mixing of orbitals would require the inclusion of π orbitals in the basis in order to allow for angular correlation.

As far as F_2 is concerned, the $3\sigma_g - 3\sigma_u$ AMO wavefunction gives satisfactorily values of ΔE: they range from 0.018 to 0.093 a.u. and compare favourably with those obtained from much more sophisticated calculations [14]. More complicate pairing schemes can be used for this molecule because of the presence of π orbitals. The following ones were tried: i) ($3\sigma_g - 3\sigma_u$, $1\pi_g - 2\pi_u$, $1\pi_u - 2\pi_g$) and ii) ($3\sigma_g - 3\sigma_u$, $1\pi_g - 2\pi_g$, $1\pi_u - 2\pi_u$).

In both cases mixing parameters of π orbitals were given a common value λ_π in order to ensure the correct total symmetry of the molecule. One can easily show that previous pairings lead to many determinant wavefunctions, containing configurations which have non negligible weight in some CI type wavefunctions [14] like e.g. the double excitations $1\sigma_u - 2\sigma_g$, $3\sigma_g - 3\sigma_u$ and $1\pi_g - 2\pi_u$, $3\pi_g - 3\pi_u$. The minimum was found for $\lambda_\pi = 1$, corresponding to a non-split π-orbitals.

b) LiH, HF

Results for these molecules are worse than in homonuclear cases. The only reasonable pairing scheme which introduces correlation in the bond are of the type $n\sigma - m\sigma$; they give results comparable with the $2\sigma_g - 3\sigma_g$ in homonuclear case; i.e. optimum values of λ close to 1 and small energy improvements from SCF. Numerical value of ΔE are in essential agreement with those found in an earlier split-shell calculation by Harris and Pohl [22] and smaller than those obtained by Lindner [6].

An attempt was made to improve the function by constructing the AMO's molecular orbitals from localized rather than from canonical MO's. Following the scheme of Boys and Foster [23], 2σ, 3σ and 1π were transformed in 3 equivalent lone pairs localized on F atoms and one bonding orbital l with σ-symmetry about internuclear axis. Oscillatory orbitals were than obtained from 4σ, 5σ and 2π. The AMO wavefunction was then built by pairing l with the corresponding oscillatory orbital. At the internuclear distance of 1.7328 a.u. the optimum λ is 0.980 and the energy -100.0081 a.u. Surprisingly enough no improvement in respect of the conventional AMO w.f. is obtained.

Negligible effects of this localization procedure on the AMO energy were found also in case of H_2O [24].

The computed values of the energy were used to estimate the internuclear equilibrium distances by simple parabolic interpolation. The AMO values are always larger than SCF and experimental ones, especially in the cases of Li_2 and F_2 (0.1 Å). This seems to be an indesirable consequence of the fact that the energy lowering ΔE of our calculations increases with the internuclear distance, as one can also see from Table 3. Similar behaviours have been observed in limited CI calculations [25].

As a general comment the improvement over the SCF does not seem to be very significant. AMO w.f.s comparable or even better in accuracy than the present ones were obtained using non SCF orbitals but containing adjustable parameters [4 -7]. This probably means that the best orbitals for an AMO w.f. are not derivable in a simple way from the SCF ones. Analogous situations were observed in the application of the DODS scheme to atomic systems, like He [26].

Acknowledgements. The authors thank Doc. J. L. Calais and Prof. C. Zauli for stimulating discussions and critical reading of the manuscript. Financial support from CNR of Italy is gratefully acknowledged. The calculations were carried on the CDC 6600 of the Computing Centre of Bologna University.

References

1. Löwdin, P. O.: Symp. Mol. Phys. Nikko Japan, Maruzen **13**, 1953 (1954).
2. Paunc,z R.: Alternant molecular orbital method. Philadelphia and London: W. B. Saunders Co. 1967.
3. Coulson, C. A., Fischer, I.: Phil. **40**, 386 (1949).
4. Rai, D. K., Calais, J. L.: J. chem. Physics **47**, 906 (1967).
5. Brändas, E.: Int. J. quant. Chemistry **1**, 847 (1967); **2**, 37, 391, 793 (1968).
6. Lindner, P.: Theoret. chim. Acta (Berl.) **5**, 336 (1966).
7. Shukla, G. C.: Acta physica polon., in press. We thank Dr. Shukla for sending his results before publication.
8. Paunc,z R.: Alternant molecular orbital method, chap. 3, page 47. Philadelphia and London: W. B. Saunders Co. 1967.
9. Percus, J. K., Rotenberg, A.: J. math. Physics **3**, 928 (1962).
10. McWeeny, R.: Rev. mod. Physics **32**, 360 (1960).
11. Paunc,z R.: Alternant molecular orbital method, chap. 6, page 128. Philadelphia and London: W. B. Saunders Co. 1967.
12. Veillard, A.: IBMOL Version IV, IBM Research Laboratory, St. José, California.

13. Ebbing, D. E.: J. chem. Physics **36**, 1361 (1962).
14. Das, G., Wahl, A. C.: J. chem. Physics **44**, 87 (1966).
15. Bender, C. F., Davidson, E. R.: J. physic. Chem. **70**, 2675 (1966).
16. — —: Physic. Rev. **183**, 23 (1969).
17. Das, G.: J. chem. Physics **46**, 1568 (1967).
18. Wahl, A. C.: Physic. Rev. Letters **24**, 440 (1970).
19. Harris, F. E., Michels, H.: Int. J. quant. Chemistry S **3**, (1967).
20. Bender, C. F., Davidson, E. R.: J. chem. Physics **47**, 360 (1967).
21. Huzinaga, S.: J. chem. Physics **42**, 1293 (1965).
22. Harris, F. H., Pohl, H. A.: J. chem. Physics **42**, 3648 (1965).
23. Foster, J. M., Boys, S. F.: Rev. mod. Physics **32**, 300 (1960).
24. Bendazzoli, G. L., Geremia, A., Palmieri, P.: unpublished results.
25. Schafer II, H.: J. chem. Physics **54**, 2207 (1971). See also Ref. [20].
26. Shull, H., Löwdin, P. O.: J. chem. Physics **30**, 617 (1959).

Dr. G. L. Bendazzoli
Istituto di Chimica Fisica e Spectroscopia
Viale Risorgimento 4
I-40136 Bologna, Italy

Theoret. chim. Acta (Berl.) 27, 69—74 (1972)
© by Springer-Verlag 1972

A Model Study of the Interaction of a Hydrogen Bond with a π-Electron System

JOHN R. SABIN

Quantum Theory Project, Department of Physics and Astronomy, University of Florida,
Gainesville, Florida 32601, USA

Received March 10, 1972

A semi-empirical CNDO/2 calculation of the structure of the diimide-hydrogen fluoride hydrogen bonded complex is reported. The results are compared to calculations on a similar saturated system in an attempt to elucidate the effect of a neighboring π-system on a hydrogen bond, and to uncomplexed diimide to study the effect of the hydrogen bond on the π-system.

Introduction

The question of the interaction of π-electron systems with hydrogen bonds has long been of theoretical interest, as entities of this type are not uncommon. In the past few years, there has been a variety of semi-empirical calculations reported on systems of biological importance, such as the base pairs of DNA [1–6], which contain just such π-bond/hydrogen bond units. One problem encountered in such work is that the methods which have been used are of the Pariser-Parr-Pople or Hückel type, and have not taken the coupling of π and hydrogen bond electrons properly into account [5, 7].

With the recent availability of large, very fast computers, problems of this type, such as the DNA base pairs, can now be handled in an *ab initio* fashion [8]. The extreme expense of such calculations makes it desirable to take a middle course, however, and attempt to treat such problems with a semi-empirical, but all valence electron treatment. In this way, it is hoped that the important qualitative features of such valence electron interactions as the π-bond/hydrogen bond interaction can be profitably investigated.

To this end, a CNDO/2 calculation has been carried out on a very simple system containing both a π-bond and a hydrogen bond; namely the diimide-hydrogen fluoride complex. The results of this calculation are compared to calculations on the separated species and on similar non-π-bonded complexes, in order to draw conclusions concerning the effect of a π-bond on a neighboring hydrogen bond and vice versa.

Calculational Method

Recent studies [9] have shown that the all-valence-electron semi-empirical CNDO/2 method works quite well in a semiquantitative sense for describing the properties of hydrogen bonds among first row hydrides. As this method has the two qualities desired for this calculation, namely speed and consideration of all of the valence electrons, and has been shown to give reasonable results, it was used. As the method is well known [10], it will not be described here other than to say it is a semi-empirical, all-valence-electron, SCF-MO method. The program used is a modified version of Dobosh's CNDO/INDO program [11] and employs the CNDO/2 parametrization scheme [10].

Results and Discussion

One of the simplest molecules containing a π-bond which will participate in hydrogen bonding is diimide (HN=NH). Consequently, the diimide-hydrogen fluoride hydrogen bonded complex was chosen as a model system for this study.

Calculations were initially carried out on the HF and N_2H_2 fragments in order to determine their minimum energy geometries and properties. The results obtained for HF are presented in Table 1. It should be noted that the calculated results agree exactly with those previously published [9, 10] except for the stretching force constant, which is reported to be 19.2 mdyn/Å by Pople and Beveridge [10].

For diimide, the N–H and N–N distance, as well as the H–N–N angle (θ) and the internal rotation angle (φ) about the N–N bonds were varied. The minimum energy geometry was found to be the *cis* configuration ($\varphi = 0°$) with $R_{NH} = 1.07$ Å, $R_{NN} = 1.22$ Å, and $\theta = 115.5°$. The molecular parameters calculated at this geometry are given in Table 2.

Table 1 Calculated and experimental properties of HF

	Calculated	Experimental [10]
r_e	1.00 Å	0.917 Å
μ	1.861 D	1.819 D
B.E.	6.771 eV	6.11 eV
I.P.	21.14 eV	15.77 eV
k_{st}	18.92 mdyn/Å	9.6 mdyn/Å
$\left\lvert \frac{\partial\mu}{\partial r} \right\rvert_{av}$	0.0136	—
E_{tot}	−28.436693 a.u.	—

Table 2. Calculated and experimental molecular properties of diimide

	Calculated	Experimental
R_{NH}	1.07 Å	—
R_{NN}	1.22 Å	—
θ	115.5°	—
μ	3.066 D	—
I.P.	13.548 eV	9.85 eV[a]
E_{tot}	− 24.710500 a.u.	—

[a] See Ref. [12].

When the barrier to internal rotation was calculated, the *cis* configuration was found to be more stable than the *trans* configuration by 3.44 kcal/mole, with a maximum in the potential at $\varphi = 90°$ which was 67.62 kcal/mole above this *cis* configuration. This result is in agreement with previous semi-empirical calculations [13], but not with more recent *ab initio* results [14], which show the *trans* form to be the most stable. Although it would be nice to agree with more elaborate calculations, agreement is not necessary in this case, since changes in the properties of diimide when it undergoes hydrogen bonding are what are of interest here.

There are two possible structures for the hydrogen-bonded N_2H_2–HF complex, $H_2N_2 \cdot HF$(I) and HNNH · FH(II).

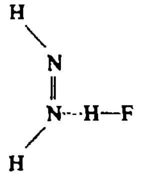

(I)

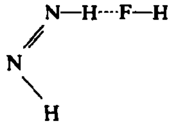

(II)

A geometry search, holding the N_2H_2 and HF fragments at their previously determined geometries, showed both structures to be stable with respect to the separated fragments, but that structure I was much more stable than structure II. The minimum energy was obtained when the H–F bond bisected the N–N–H angle, and the N–F distance was 2.48 Å. In this configuration (see Fig. 1), the total energy of the complex was found to be −53.172282 a.u., corresponding to a hydrogen bond energy of 15.73 kcal/mole. Small variations of the placement of HF, such that the NHF line deviated from the Z-axis by 10–15°, led to energy changes of considerably less than 1 kcal/mole as long as the N–F distance was kept at 2.48 Å. It thus appears that the HF molecule is only weakly held in place in an angular sense, and considerable thermal wagging may be expected in the complex.

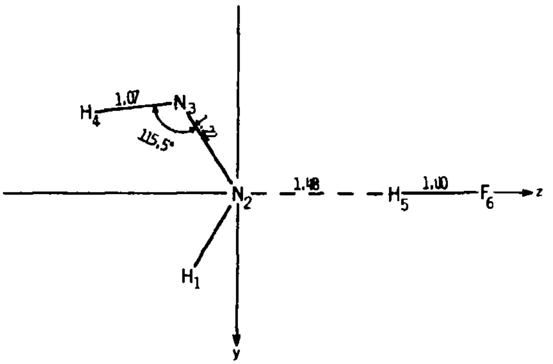

Fig. 1. The minimum energy geometry and coordinate system for N_2H_2–HF

Keeping all other atoms fixed, the hydrogen atom in the bond was moved along the N−F line of centers to obtain the protonic potential curve. This was found to be an asymmetric single well, with an energy minimum at $R_{NH} = 1.48$ Å, which corresponds to $R_{HF} = 1.00$ Å. From the curvature of the potential at the minimum, the quadratic force constant was found to be 17.39 mdyn/Å, and $\left|\frac{\partial \mu}{\partial r}\right|$ to be 2.998. Thus the H−F stretching force constant decreases on hydrogen bond formation, which is the expected result.

Table 3. Density matrix elements between orbitals involved in the N−N π-bond

	N_2H_2	HF	$H_2N_2 \cdot HF$
(N2X, N2X)	1.0000		1.0427
(N3X, N3X)	1.0000		0.9573
(N2X, N3X)	1.0000		0.9991
H_1	0.9615		0.9359
N_2	5.0385		5.0443
N_3	5.0385		5.0079
H_4	0.9615		0.9426
H_5		0.7737	0.7557
F_6		7.2263	7.3136

There are two questions which we now wish to consider. Namely, what is the influence of the hydrogen bond on the π-system of N_2H_2 and what is the influence of the π-system of N_2H_2 on the N−H−F hydrogen bond. Some light can be shed on the first question by consideration of the results presented above. A summary of the density matrix elements for the orbitals involved in the N−N π-bond are presented in Table 3, along with the atomic populations for the various atoms involved. Consideration of the Table shows that hydrogen bonding causes a buildup of charge in the $2p_x$ π-bonding AO of N_2 at the expense of the $2p_x$ orbital charge at N_3 and the bond population. This charge shift is also reflected in the decrease in gross atomic charge on N_3 and increase in net atomic charge on N_2 on hydrogen bond formation. The orbital energy of the N−N π-bonding orbital is −0.6604 a.u. in N_2H_2, but combines in a bonding and antibonding way with the $2p_x$ orbital on F_6 to give a pair of π-orbitals of energies −0.7119 and −0.7009 a.u. in the complex. Thus, the effect of the hydrogen bond on the π-system seems to be to polarize the orbital significantly, and to stabilize it via combination with the $2p_x$ orbital of fluorine. This is just what might be expected from intuitive reasoning.

The question of the effect of the π-system on the hydrogen bond is a much more difficult one to treat. In order to prepare a non-π-bonded system with which the results on $H_2N_2 \cdot HF$ could be compared, a hydrazine-type molecule was considered. Here, hydrogen atoms were added 1.07 Å above and below N_2 and N_3 respectively (see Fig. 1), but all other distances and angles were maintained as in $H_2N_2 \cdot HF$. Thus a complex, $H_4N_2 \cdot HF$ was considered which is as like $H_2N_2 \cdot HF$ as possible, but without the double bond. Because of the desire to maintain similarity with $H_2N_2 \cdot HF$, the N_2H_4 fragment in this complex does not have the hydrazine minimum energy geometry [15].

The energy of the N_2H_4 fragment in the configuration described above was found to be -26.301064 a.u., while that of the $H_4N_2 \cdot HF$ complex was -54.760843 a.u., giving the complex an hydrogen bond energy of 14.49 kcal/mole. Table 4 presents some of the density matrix elements and gross atomic populations of interest.

Table 4. Density matrix elements and atomic populations involved in the N---H—F bond

	$H_4N_2 \cdot HF$	$H_2N_2 \cdot HF$
(H5S, F6X)	0.3660	0.3661
(H5S, F6Z)	−0.8448	−0.8447
(H5S, N2S)	0.1691	0.1781
(H5S, N2Z)	0.2447	0.2448
(N2X, N2X)	1.1670	1.0427
(N3X, N3X)	1.1579	0.9573
(N2X, N3X)	0.2051	0.9991
(F6S, N2S)	−0.0615	−0.0642
(F6Z, N2Z)	0.1126	0.1148
(N2S, N2S)	1.4569	1.5447
(N2Z, N2Z)	1.3801	1.3949
N2	5.0681	5.0443
H5	0.7544	0.7557
F6	7.3140	7.3136
ΔE (kcal/mole)	−14.49	−15.73

The most striking feature of Table 4 seems to be the excellent agreement between the two cases. That is, it seems that the breaking of the π-bond between N_2 and N_3 has remarkably little effect on the hydrogen bond, except for the 2*s* orbital population on N_2 which decreases by ~0.1 electron. Thus the 1sH-2sN interaction becomes less bonding, as reflected in the lower (H5S, N2S) density matrix element. This destabilization is slight, however, and the hydrogen bond energy is decreased by only 1.24 kcal/mole. The remarkable lack of influence of the π-bond on the hydrogen bond is most probably due to the nearly constant gross charge distribution in the two cases, and consequent nearly equivalent electrostatic contribution to the hydrogen bond. For example, the HF fragment has a gross population of 8.0685 in $H_4N_2 \cdot HF$, and of 8.0693 in $H_2N_2 \cdot HF$.

It appears then that the effect of a π-bond on an adjacent hydrogen bond is small, and consists primarily of a destabilization with respect to an equivalent non-π-bonded case. The opposite effect, that of the hydrogen bond on the π-system, seems to be much more pronounced, and consists primarily of polarization and stabilization of the delocalized bond.

Acknowledgement. Acknowledgement is made to the Donors of the Petroleum Research Fund, administered by the American Chemical Society, and to the National Science Foundation for support of this work. The Computer Center, University of Florida, is acknowledged for a grant of computer time.

References

1. Pullman, A., Pullman, B.: Biochim. biophysica Acta **36**, 343 (1959).
2. Hoffman, T. A., Ladik, J.: Advances chem. Physics **7**, 84 (1964).
3. Ladik, J., Appel, K.: Theoret. chim. Acta (Berl.) **4**, 132 (1966).
4. Rein, R., Ladik, J.: J. chem. Physics **40**, 2466 (1964).
5. Harris, F. E.: J. chem. Physics **42**, 2144 (1965).
6. Lunnell, S., Sperber, G.: J. chem. Physics **46**, 2119 (1967).
7. Sabin, J. R.: Int. J. quant. Chemistry **2**, 23 (1968).
8. Clementi, E., Mehl, J., Niessen, W von: J. chem. Physics **54**, 508 (1971).
9. Kollman, P. A., Allen, L. C.: J. Amer. chem. Soc **92**, 753 (1970).
10. For a full description of the method and reference to the original literature, see Pople, J. A., Beveridge, D. L.: Approximate molecular orbital theory. New York: McGraw-Hill 1970.
11. Dobosh, P. A.: Program CNINDO, No. 141 from the Quantum Chemistry Program Exchange, Bloomington, Indiana.
12. Foner, S. N., Hudson, R. L.: Advan. chem. Ser. **36**, 34 (1962).
13. Gordon, M. S., Fischer, H.: J. Amer. chem. Soc. **90**, 2471 (1968).
14. Wong, D. P., Fink, W. H., Allen, L. C.: J. chem. Physics **52**, 6291 (1970). See this paper for a bibliography of recent calculations on N_2H_2.
15. For an *ab initio* determination of the structure of hydrazine see: Fink, W. H., Pan, D. C., Allen, L. C.: J. chem. Physics **47**, 895 (1967), and references contained therein.

Dr. J. R. Sabin
Quantum Theory Project
Department of Physics and Astronomy
University of Florida
Gainesville, Florida 32601
USA

Theoret. chim. Acta (Berl.) 27, 75—79 (1972)
© by Springer-Verlag 1972

EHT Conformational Study of Nicotinamide and Related Amides

KATHRYN R. LONG* and J. H. GOLDSTEIN
Chemistry Department, Emory University, Atlanta, Georgia, 30322, USA

Received April 10, 1972

EHT rotational energy curves are presented for various nicotinamides and benzamide. The conformations calculated for nicotinamide and benzamide are comparable to those determined by X-ray methods. Protonation, N-methyl substitution and the introduction of a ring nitrogen meta to the amide group are discussed in terms of the corresponding calculated effect on the rotational energy curves. Some implications for the conformation of NAD⊕ are presented.

1. Introduction

Attention has recently been drawn by Sarma *et al.* to the relationship between side chain conformation and the folding mechanism in NAD⊕ [1, 2]. However, efforts by these workers to determine preferred conformations by *pmr* proved unsuccessful. Following this Coubeils and coworkers carried out a series of PCILO calculations in an effort to theoretically determine conformation preferences in nicotinamide, 1-methyl-4-hydronicotinamide and the reduced nicotinamide mononucleoside [3]. Calculations were carried out in 30° rotations around the ring-amide linkage.

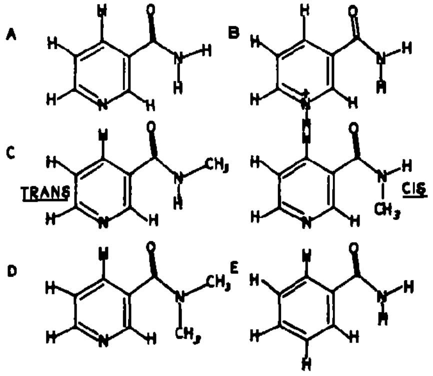

Fig. 1. Molecular formula of *a* nicotinamide, *b* nicotinamide cation, *c trans* and *cis* N-methyl nicotinamide, *d* N,N-dimethyl nicotinamide and *e* benzamide

---

* NSF Fellow 1971–1972.

This paper reports the results of a series of Extended Hückel molecular orbital (EHT) calculations carried out on nicotinamide, nicotinamide cation, N-methylnicotinamide, N,N-dimethylnicotinamide, and benzamide, the molecular formulas of which are given in Fig. 1. The purpose of this work was to determine, within the limits of the EHT method, the preferred conformations, if any, for this series of compounds. It will be noticed that only nicotinamide is common to this study and that of Ref. [3]. The results are presented in the form of plots of energy, taken relative to that of the least stable conformation, *vs.* angle of rotation. Although not one of the nicotinamides, benzamide is included to ascertain the effect of a ring nitrogen on the energy curves. Some implications of these results for the conformational situation in the biologically important system NAD⊕ are also presented.

2. Method of Calculation

The basic method employed in this study has been described previously in the literature [4] and will not be repeated here. The diagonal elements of the Hamiltonian matrix were approximated by the valence state ionization potentials of the appropriate orbitals [5, 6]. The off-diagonal elements, H_{ij}, were estimated by the Wolfsberg-Helmholtz-Mulliken geometrical-mean formula

$$H_{ij} = KS_{ij}(H_{ii}H_{jj})^{1/2}$$

with K taken as -1.50.

Structural parameters used for nicotinamide [7] are identical to those of Coubeil *et al.* [3]. X-ray values were employed for benzamide [8] and average literature values [9] were used to specify the structure of N-alkyl substituents. The amide N–H bond distance was taken as that found in urea [10]. The $\overset{+}{\mathrm{N}}$–H bond distance was the average of a number of tabulated values [10]. For the purposes of this study, the amide group is assumed to be planar. The orientation of the amide group relative to the ring was specified by the dihedral angle, θ, between the two planes, measured from the planar *trans* arrangement of the ring $C_\alpha - C_\beta$ bond and the carbonyl group. The two stable N-methylnicotinamide rotamers will be referred to as *cis* and *trans*, with the understanding that in the *trans* form the N-methyl group is *cis* to the carbonyl oxygen.

Energy calculations were made for every 5° rotation of the amide group relative to the ring, except near the minima, in which case the interval was decreased to 1°. All calculations were performed on a Digital Equipment Corporation PDP-10 computer.

3. Results and Discussion

The energy dependence on amide conformation in nicotinamide systems and in benzamide is shown in Figs. 2 and 3. Fig. 2a is representative of the energy curves obtained for nicotinamide, nicotinamide cation and *trans* N-methylnicotinamide. The calculated minimum falls at 16°, 15° and 18°, respectively, for the above three molecules. Thus, within the approximations employed, the cal-

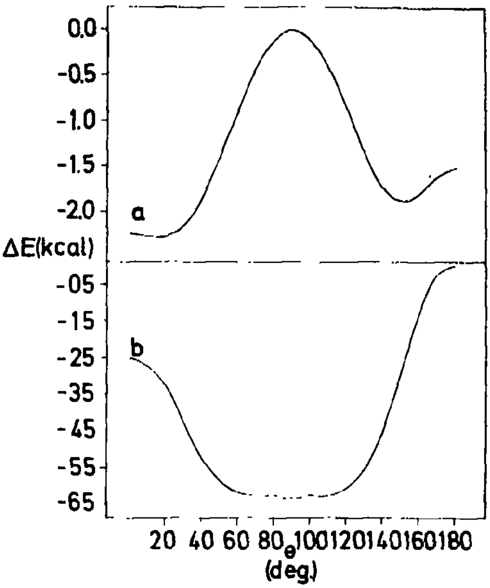

Fig. 2. Angular dependence of energy, measured relative to least stable conformer, in nicotinamide systems. *a* represents the ΔE curve for nicotinamide, nicotinamide cation and *trans*-N-methylnicotinamide. *b* represents the ΔE curve in *cis*-N-methylnicotinamide and N,N-dimethylnicotinamide

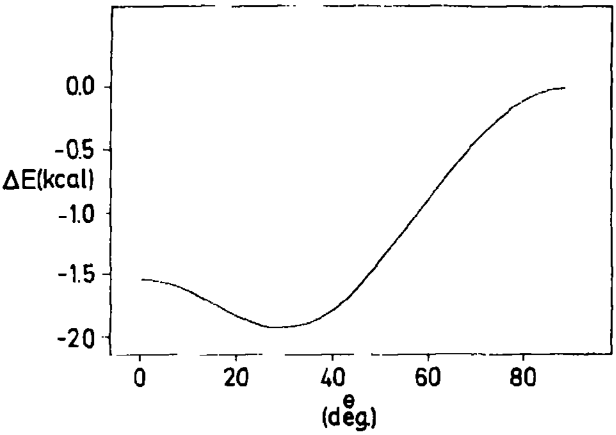

Fig. 3. Angular dependence of energy, measured relative to the least stable conformer, in benzamide

culated energy curves are largely unaffected by either protonation of the ring nitrogen or by N-alkyl substitution in the *trans* position of the amide group. The orientation calculated here for nicotinamide is not greatly different from the value of 24° obtained from an analysis of the X-ray data [7]. The corresponding calculated minimum reported by Coubeils *et al.*, using PCILO falls at 30° [3]. Hence, both calculated minima are within approximately 6° of the experimental value.

Moreover, the energy difference between orientations of 16° and 30°, as calculated in this study, is not very large due to the rather shallow nature of the minimum. It is interesting that the energy difference between the planar conformer and the most stable conformer is 0.042 kcal, which is much smaller than 0.62 kcal, the value of kT at body temperature. Thus the amide group is able to oscillate rather easily over an angle of about 40° on either side of the molecular plane without significantly exceeding kT in energy. A second stable conformation lies in a somewhat shallower minimum at an orientation of 150°, also reported by Ref. [3]. The barrier between the two stable conformers, ~2.7 kcal, is considerably larger than kT.

In the case of benzamide, Fig. 3, a calculated energy minimum occurs at 30°, compared with a value of 26° in the experimental case [8]. The calculated energy curve for benzamide, however, differs from that of nicotinamide in several respects. The height of the barrier between conformers is considerably smaller in benzamide, ~1.53 kcal. The minimum is also shallower, permitting facile rotation through an angle of about 65° on either side of the molecular plane. It appears, then, that the presence of a ring nitrogen atom *meta* to the amide increases the relative stability of the preferred conformation in nicotinamide as compared to that of benzamide. It also substantially restricts the extent of oscillation of the amide group.

Fig. 2b is representative of the rotational energy curves in N,N-dimethylnicotinamide and the *cis* isomer of N-methylnicotinamide. In these molecules the calculated energy minima occur at 89°, with a torsional energy barrier of 63.40 kcal. While this value may to some extent reflect the tendency of EHT to overestimate torsional barriers [4], it nevertheless suggests that the true barrier is quite sizeable compared to kT. Structural models also indicate qualitatively the existence of very sizeable barriers. The dihedral angle predicted from such models, 90°, is in surprisingly good agreement with those determined here. In addition, the amide group seems to be able to oscillate without significant interference in the range $80° \leqq \theta \leqq 100°$.

Some approximation of the steric interaction between the N-methyl group and the pyridine ring can be obtained from a comparison of the total energy of the two N-methylnicotinamide rotamers in the planar conformation −21406.77 kcal and −21448.13 kcal for the *cis* and *trans* rotamers, respectively. The energy of steric interaction, ~41.36 kcal, is decreased to ~1.0 kcal by rotation into the perpendicular conformation, i.e., $\theta = 90°$, where the total energy of the two rotamers is −21444.86 kcal and −21445.50 kcal for the *cis* and *trans* rotamers, respectively. Thus, the *trans* rotamer is, for all conformations, the more sterically favored rotamer. Simple calculations give more than 99% of N-methylnicotinamide molecules present as the *trans* isomer at body temperature, as calculated from the most stable conformations.

Sarma *et al.* have reported that, whereas the folding mechanism in NAD⊕ is unaffected by N-alkyl substitution, N,N-dialkyl substitution results in the dissociation of the nicotinamide and adenine base pairs. Sarma and coworkers then postulated that an alkyl substituent *trans* to the carbonyl oxygen is responsible for the changes in folding [1]. The results obtained here substantiate this hypothesis, insomuch as the only change in the calculated energy curve occurs upon formation of *cis* N-methylnicotinamide or upon N,N-dimethyl substitution. The shape of the curve is thus essentially dependent upon the presence or absence of a *cis* N-alkyl substituent, as is the spatial relationship of the amide group with the pyridine ring. With the introduction of a *cis* N-alkyl substituent, steric interference with the adenine base should become prominent, the result being a change in the folding mechanism observed in NAD⊕.

Acknowledgment. The authors wish to thank S. Y. Randall for her assistance in program size reduction. This work was supported in part by a grant from the National Institutes of Health.

References

1. Sarma, R. H., Ross, V., Kaplan, N. O.: Biochemistry 7, 3052 (1968).
2. — Moore, M., Kaplan, N. O.: Biochemistry 9, 549 (1970).
3. Coubeils, J. L., Pullman, B., Courriere, Ph.: Biochem. biophysic. Res. Commun. **44**, 1131 (1971).
4. Hoffman, R.: J. chem. Physics **39**, 1397 (1963).
5. Skinner, H. A., Pritchard, H. O.: Trans. Faraday Soc. **49**, 1254 (1953).
6. Pritchard, H. O., Skinner, H. A.: Chem. Rev. **55**, 745 (1955).
7. Wright, E. B., King, G. S. D.: Acta crystallogr. 7, 283 (1954).
8. Penfold, B. R., White, J. C. B.: Acta crystallogr. **12**, 130 (1959).
9. Momany, F. A., McQuire, R. F., Yan, J. F., Scheraga, H. A.: J. physic. Chem. **75**, 2286 (1971).
10. Tables of interatomic distances and configuration in molecules and ions. L. E. Sutton, ed. Margent, Kent: Thanet Press 1965.

Prof. Dr. J. H. Goldstein
Chemistry Department
Emory University
Atlanta, Georgia 30322
USA

Theoret. chim. Acta (Berl.) 27, 81—93 (1972)
© by Springer-Verlag 1972

Commentationes

Atoms-in-Molecules Treatment of Li_2^+ and Li_2 Using Optimum Gaussian Approximations of Li^+ and Li Eigenstates*

Frank O. Ellison and Lyndon L. Larcom

Department of Chemistry, University of Pittsburgh, Pittsburgh, Pennsylvania 15213, USA

Received November 4, 1971/July 4, 1972

Expectation energies for the Li^+, Li and Li ground states and for the $1s^2 2p$ Li excited state are individually minimized with respect to variation of parameters in Gaussian lobe expansions of the $1s$, $2s$ and $2p$ AO's. A new technique is used to control $1s-2s$ orthonormality. The resulting approximate many-electron atomic eigen-functions are utilized for determining interatomic matrix elements in atoms-in-molecules (AIM) calculations on the two lowest energy ${}^1\Sigma_g^+$ states of Li_2 and on the lowest energy ${}^2\Sigma_g^+$ and ${}^2\Sigma_u^+$ states of Li_2^+. For R greater than 4 a.u., convergence to exact theoretical AIM limits, within about 0.001 h.u., is obtained by using three-term expansions. Three-structure Li_2 and two-structure Li_2^+ AIM energies are above experimental by 0.005 and 0.007 h.u., respectively. It is conjectured that an AIM model extended to permit scaling of valence electrons independently of inner-shell electrons would reduce significantly these energy differences.

Die Energieerwartungswerte für die Grundzustände von Li^+, Li und Li^- sowie für den angeregten Zustand $1s^2 2p$ von Li werden einzeln bezüglich der Variationsparameter einer Entwicklung der $1s$-, $2s$- und $2p$-Atomorbitale nach Gaußfunktionen minimisiert. Zur Kontrolle der Orthonormalität der $1s$- und der $2s$-Funktion wird eine neue Technik angewandt. Die resultierenden angenäherten Atomeigenfunktionen werden bei Atom-in-Molekül (AIM)-Rechnungen für die zwei niedrigsten ${}^1\Sigma_g^+$-Zustände von Li_2 und die niedrigsten Zustände der Symmetrie ${}^2\Sigma_g^+$ und ${}^2\Sigma_u^+$ von Li_2^+ verwendet. Für einen Atomabstand R größer als 4 A.E. wird mit einer Entwicklung mit drei Termen eine Annäherung bis zu 0,001 A.E. an den exakten theoretischen AIM-Grenzwert erreicht. Die AIM-Energiewerte, die mit drei Resonanzstrukturen von Li_2 bzw. zwei Resonanzstrukturen von Li_2^+ erhalten werden, liegen 0,005 A.E. bzw. 0,007 A.E. über den experimentellen Werten. Es wird angenommen, daß eine Erweiterung des AIM-Modells, bei der eine Skalierung der Valenzelektronenfunktionen unabhängig von den inneren Elektronen möglich ist, diese Energiedifferenz stark herabsetzen würde.

Les énergies de l'état fondamental de Li^+, Li et Li^-, et de l'état excité $1s^2 2p$ de Li sont individuellement minimisées par rapport à la variation des paramètres dans le développement gaussien des orbitales atomiques $1s$, $2s$ et $2p$. Une technique nouvelle est utilisée pour contrôler l'orthonormalité $1s-2s$. Les fonctions d'onde polyélectroniques approchées résultantes sont utilisées pour des calculs du type atomes dans les molécules (ADM) pour les deux états ${}^1\Sigma_g^+$ de plus basse énergie de Li_2 et sur les états ${}^2\Sigma_g^+$ et ${}^2\Sigma_u^+$ de plus basse énergie de Li_2^+. Pour R supérieur à 4 u.a., la convergence vers les limites théoriques exactes ADM est obtenue avec un développement à trois termes, à 0,001 u.a. près. Les énergies ADM à trois structures pour Li_2 et à deux structures pour Li_2^+ sont respectivement à 0,005 et 0,007 a.u. au dessus des énergies expérimentales. On émet l'hypothèse qu'un modèle ADM étendu pour permettre le calibrage des électrons de valence indépendamment des électrons des couches internes réduirait d'une manière significative ces différences d'énergie.

1. Introduction

Atoms-in-molecules (AIM) theory was formally developed by Moffitt for the purpose of eliminating atomic correlation energy errors from molecular calcu-

---

* Supported in part by National Science Foundation Grant GP 25415.

lations [1]. Practical modifications have been devised by Arai [2], by Hurley [3], and by Balint-Kurti and Karplus [4]. The basic approach has been reviewed and discussed by Parr [5].

The wave function basis in AIM theory consists, in the first place, of linear combinations of antisymmetrized products of atomic substate eigenfunctions. As the number of basis functions Ψ_n is increased, one would expect predicted molecular eigenvalues to converge toward experiment in accordance with the variational principle. In AIM methods, *exact* equations are used for determining, by reference to experimental atomic energies, all *intraatomic* contributions to the energy matrix elements. All other parts of these elements, as well as all overlap matrix elements, are *interatomic* in nature, and these parts are computed using previously determined *approximate* atomic eigenfunctions. Because of this dichotomy, common to all AIM methods, the variational principle is not necessarily followed; predicted molecular energies may lie above or below experiment[1]. However, as the approximate atomic functions are successively refined, a predicted molecular energy should converge toward an exact theoretical AIM limit which will satisfy the variational principle; as the number of basis functions Ψ_n is increased, results should converge to experiment.

Sometime ago, a new AIM approach called *scaled atoms-in-molecules* (SAIM) theory for predicting potential energy curves of diatomic molecules was developed [6]. In this method, each basis function Ψ_n is modified by introducing factors s_n^A and s_n^B into its component A- and B-atom eigenfunctions. Exact equations were developed for determining, again by reference to experimental atomic energies, all intraatomic contributions to the energy matrix elements. Total molecular expectation energies could be minimized with respect to the several scale factors. Thus, a principal objection to pure AIM theory is overcome: namely, that the scale factors (i.e., effective nuclear charges) appropriate to free atoms and ions simply are not favorable for fast convergence of the AIM series [2, 3, 5].

We have reported initial calculations on various electronic states of H_2, He_2^{++}, He_2^+, H_2 and He_2 [6-8]. For the ground X $^1\Sigma_g^+$ and excited E $^1\Sigma_g^+$ states of H_2, five basis functions were considered, corresponding to the following interacting states: (1) $1s$ H + 1s H; (2) ^{1}S $H^- + H^+$; (3) $1s$ H + $2s$ H; (4) $1s$ H + $2p_0$ H; and (5) $2p_+$ H + $2p_-$ H [8]. Use of $1s^2$ approximation for ^1S H^-, where $1s$ is the STO (Slater-type orbital) appropriate to H^-, leads to SAIM H_2 energies lower than experimental. Use of the Hylleraas-Eckart $1s\,1s'$ function [9] or the Silverman-Platas-Matsen $1s\,1s' + \lambda 2p^2$ [10] for H^- leads to SAIM H_2 energies approaching the exact limit within 0.001 h.u. (1 Hartree unit = 27.21 eV).

It seems clear from all work done so far that the optimized STO minimal basis set is not sufficiently accurate for SAIM calculations. If this theory is to be useful for prediction and explanation of ground and excited electronic state potential energy curves (and surfaces), it is essential that approximate ground and excited state atomic eigenfunctions be developed that are both adequate to achieve the exact theoretical SAIM limit and practical from the computational viewpoint.

---

[1] Our experience has shown that use of defective approximate atomic eigenfunctions usually *depress* calculated AIM molecular energies. For infinite internuclear separations, AIM predicted energies will, of course, be identical to experiment.

In this paper, we report AIM calculations on electronic states of Li_2^+ and Li_2 in which approximate Li^+, Li and Li^- substate wave functions (used to determine molecular interaction and overlap matrix elements) are constructed from orbitals varied so as to minimize the total energy of each individual many-electron atomic substate function. The orbitals are expressed as linear combinations of simple Gaussian functions. A technique slightly different from that used before is outlined for controlling $1s-2s$ orthonormality; the new method leads to shorter series for the orthogonalized $2s$ orbital. Finally, we find that three-term energy-optimized Gaussian orbitals are sufficient to obtain convergence to exact theoretical AIM limits for Li_2^+ and Li_2.

2. Least Energy Minimal Atomic Orbitals: Gaussian Lobe Functions (LEMAO-NGL's)

A) General

In this paper, we report pure atoms-in-molecules (AIM) calculations in which the approximate many-electron atomic substate wave functions (used to determine the interaction and overlap elements) are constructed from orbitals varied so as to minimize the total energy of the given many-electron atomic substate functions. These orbitals are expressed as linear combinations of simple Gaussian functions. For $1s$ and $2s$ orbitals, the Gaussians have their origin at the given nucleus. For $2p$ orbitals, we have elected to utilize "lobe" functions [11][2]; a $2pz$ orbital, for example, is represented as the difference between two identical linear combinations of Gaussian functions, one with origin located at $z = P$ and the other with origin located at $z = -P$[3]. Thus,

$$\begin{aligned} 1s &= \sum_i^N b_{1i} \exp(-a_{1i} r_0^2), \\ 2s &= \sum_i^M b_{2i} \exp(-a_{2i} r_0^2), \\ 2pz &= \sum_i^L b_{3i} [\exp(-a_{3i} r_1^2) - \exp(-a_{3i} r_2^2)], \end{aligned} \tag{1}$$

in which r_0, r_1, and r_2 are radial coordinates from the nucleus, from $z = P$, and from $z = -P$, respectively.

For a given electron configuration $1s^q 2s^r 2p^s$, where $n_1 = q$, $n_2 = r$, and $n_3 = s$ are the orbital occupation numbers, a manifold of atomic substates are obtained. For any one of these substates, a proper wave function, in the restricted orbital approximation, may be expressed as a linear combination of Slater determinants. If the atomic orbitals are kept orthonormal, the total electronic energy may be expressed in the form

$$E = \sum_i n_i H_i + \tfrac{1}{2} \sum_i \sum_j [n_i(n_j - \delta_{ij}) J_{ij} - A_{ij} K_{ij}]. \tag{2}$$

---

[2] It has been shown that the "lobe" Gaussian function basis is essentially equivalent to the Cartesian Gaussian basis [12, 13].

[3] P is equivalent to R_0 in Ref. [12].

The indices 1, 2, and 3 refer to 1s, 2s, and 2p, respectively; H_i is the diagonal element of the one-electron core hamiltonian; J_{ij} and K_{ij} are the usual coulomb and exchange integrals, except that

$$\begin{aligned} J_{33} &= (J_{2pz,2pz} + 2J_{2pz,2px})/3, \\ K_{33} &= K_{2pz,2px}. \end{aligned} \tag{3}$$

The coefficients $A_{ij} = A_{ji}$ are characteristic of each atomic substate: $A_{ij} = \frac{1}{2} n_i n_j \delta_{ij}$ if $i < 3$ and $j < 3$; numerical values of A_{23} and A_{33} are listed in Ref. [14], but not needed in this work.

Eqs. (1) are used to express the integrals appearing in Eq. (2) in terms of integrals over simple Gaussian functions, all of which are easily evaluated [15]. The total electronic energy E is thus obtained as a function of the parameters a_{ni}, b_{ni}, and P of Eq. (1). The so-called *least energy minimal atomic orbitals* [16] (which we shall refer to as LEMAO-NGL orbitals, N being the number of terms in the expansion, GL standing for Gaussian lobe) will be determined if the parameters are chosen so as to minimize the total energy E of a given atomic substate.

This has been accomplished, for example, for a selection of atomic ground states using Gaussian lobe functions by Grimmelmann and Chesick [17] and using Cartesian Gaussians by Pople and coworkers [16].

In AIM theory, we have need for such LEMAO's appropriate not only to atomic ground states, but also to excited states, to positive ion states, and to negative ion states. We do not expect to require that these approximate eigenfunctions yield extremely accurate *intra-atomic* energies; they are not used for that purpose in AIM calculations. It is the principal purpose of this research to determine the expansion lengths in Eq. (1) necessary to provide acceptably accurate interatomic contributions to the AIM matrix elements.

Let us rewrite the Eqs. (1) generally as follows:

$$\psi_n = \sum_i^N b_{ni} \varphi_i . \tag{4}$$

For the special case $\psi_3 = 2pz$, φ_i represents a difference between two Gaussians located at $z = \pm P$. Since Eq. (2) requires that the ψ_n be orthonormal, the b_{ni} and a_{ni} are not all independent. We may take the first coefficient in each orbital to be determined by normalization:

$$\begin{aligned} \psi_n &= b_{n1} \sum_i c_{ni} \varphi_i , \\ c_{ni} &= b_{ni}/b_{n1} , \\ b_{n1} &= \left| \sum_i \sum_j c_{ni} c_{nj} S_{ij} \right|^{1/2} , \\ S_{ij} &= \int \varphi_i \varphi_j dv . \end{aligned} \tag{5}$$

We now take the c_{ni} $(i > 1)$ to be independent, c_{n1} being set equal to one.

Now, if one is minimizing E with respect to the exponents a_{1i} $(i = 1, 2, \ldots)$ or the coefficients c_{1i} $(i = 2, 3, \ldots)$ (i.e., with respect to variations in the 1s AO), and if $n_2 \neq 0$ (i.e., if the 2s AO is occupied), then the parameters c_{1i} $(i = 2, 3, \ldots)$ are not all independent; orthogonality between 1s and 2s must be preserved. We have elected to choose c_{12} so as to constrain this orthogonality:

$$c_{12} = -\left[\sum_{i\neq 2}\sum_{j} c_{1i}c_{2j}S_{ij}\right]\Big/\sum_{j} c_{2j}S_{2j}\,. \tag{6}$$

Thus, the true independent variables are c_{1i}, $i > 2$; a_{1i}, $i \geqq 1$. In like manner,

$$c_{22} = -\left[\sum_{i}\sum_{j\neq 2} c_{1i}c_{2j}S_{ij}\right]\Big/\sum_{i} c_{1i}S_{i2} \tag{7}$$

if one is minimizing with respect to variations in the 2*s* AO and $n_1 \neq 0$ (which will always be the case in this work); the true independent variables are c_{2i}, $i > 2$, and a_{2i}, $i \geqq 1$.

This approach for handling 1*s* – 2*s* orthogonality differs from that most often used. Usually, a 2*s* Gaussian expansion is Schmidt orthonormalized with respect to a predetermined 1*s* Gaussian expansion to yield the orthogonalized 2*s* AO, now expressed in terms of two Gaussian expansions. Our approach generally leads to a shorter series for the orthogonalized 2*s* AO.

B) LEMAO-NGL's *for* Li^+ *and* Li

In Table 1, we list parameters for Gaussian expansions of the 1*s* AO chosen so as to minimize the total electronic energy of $1s^2\,{}^1S$ Li^+; the energies are listed in Table 2. For comparison, we list also in Table 2 Li^+ energies calculated with an

Table 1. Orbital exponents and expansion coefficients for $1s^2\,{}^1S$ Li^+

N	a_{1i}	b_{1i}	N	a_{1i}	b_{1i}
2	1.388532	0.7513883	5	0.6818738	0.2156861
	10.11372	1.130360		2.318487	0.6496735
				8.464990	0.7436694
3	1.015169	0.4701795		37.17722	0.5505841
	4.993060	0.9747399		248.8885	0.3114376
	33.64526	0.7669813			
			6	0.5323748	0.1161647
4	0.8190934	0.3184732		1.586883	0.4959026
	3.254383	0.8049811		5.161091	0.7114812
	14.83208	0.7783552		18.93839	0.6067729
	98.15334	0.4812371		85.20426	0.3834520
				547.6970	0.2069751

Table 2. Energies (h.u.) for $1s^2\,{}^1S$ Li^+

N		1s-STO-NG	1s-LEMAO-NG
2			−6.9804
3		−7.1673	−7.1797
4		−7.2092	−7.2224
5		−7.2191	−7.2326
6			−7.2353
STO	−7.2227		
Hartree-Fock	−7.2364		
Experimental	−7.2799		

Table 3 Orbital exponents and expansion coefficients for 2*s* orbital in $1s^2 2s\ {}^2S$ Li

$N(1s)$	$M(2s)$	a_{2i}	b_{2i}	$N(1s)$	$M(2s)$	a_{2i}	b_{2i}
2	3	0.015819661	0.005736902	3	4	0.02776284	0.02312028
		0.04855379	0.06446754			0.06563349	0.05461865
		1.240164	-0.1628947			0.9753701	−0.1378904
						7.421443	−0.1628015
2	4	0.01700869	0.007848712				
		0.05755439	0.07048959	4	3	0.008535179	0.001434313
		1.031532	0.1346667			0.04155497	0.06373754
		8.040977	-0.1420034			1.322863	−0.1819831
2	5	0.02705561	0.02075375	4	4	0.01358333	0.004907548
		0.06614091	0.05877351			0.05168967	0.06906989
		1.027527	0.1363496			1.104849	−0.1521092
		8.052362	-0.1423947			8.545282	−0.1708829
		25.00000	0.0008272647				
3	3	0.02232988	0.01140161				
		0.04800623	0.05601393				
		1.267782	-0.1739216				

Table 4 Energies (h.u.) for $1s^2 2s\ {}^2S$ Li

$N(1s)$	$M(2s)$	E	$N(1s)$	$M(2s)$	E	$N(1s)$	$M(2s)$	E
2	3	7.1693	3	3	−7.3641	4	3	−7.4046
2	4	7.1782	3	4	7.3742	4	4	−7.4159
2	5	7.1783						
STO		7.4179						
Hartree-Fock		7.4327						
Experimental		7.4779						

appropriately scaled ($Z_{\text{eff}} = 2.6875$) 1*s*-STO-NG. Our work here overlaps to some extent that presented by Chesick and coworkers [18]. Gaussian expansions of the STO's 1*s* and 2*s* used in this research were obtained from Huzinaga [19]; Gaussian lobe expansions of the STO 2*p* were obtained from Sambe [20].

In Tables 3 and 4, we list results for Gaussian expansions of the 2*s* AO in $1s^2 2s\ {}^2S$ Li. We first appropriated a 1*s*-LEMAO-NG determined previously for $1s^2\ {}^1S$ Li^+; independent parameters for the 2*s*-LEMAO-MG ($a_{2i}, i = 1, 2, 3, \ldots, M$, and $c_{2i}, i = 3, 4, \ldots, M$) were determined by minimizing the total electronic energy of $1s^2 2s\ {}^2S$ Li. Then, the independent parameters for the 1*s*-LEMAO-NG (a_{1i}, $i = 1, 2, 3, \ldots, N$ and c_{1i}, $i = 3, 4, \ldots, N$) were revaried to seek a still lower energy for Li. Never were we able to gain as much as 0.001 h.u. by this revariation of the inner-shell. Consequently, the 1*s*-LEMAO-NG parameters listed in Table 1 are used not only in Li^+ but also in $1s^2 2s\ {}^2S$ Li.

In Tables 5 and 6, we list results for excited $1s^2 2p\ {}^2P$ Li. Again, it was found that revariation of the inner 1s-shell made little difference in the final total energy. Furthermore, we found that an optimized 2*p*-LEMAO-NGL function with given N can be used arbitrarily in conjunction with 1s-LEMAO-MG functions with

Table 5. Orbital exponents and expansion coefficients for $2p$ orbital in $1s^2 2p\ ^2P$ Li[a]

N	a_{3i}	b_{3i}
2	0.0332337	0.2015516
	0.1535016	0.1251251
3	0.03081741	0.1756399
	0.1167678	0.1365198
	0.688099	0.03659062
4	0.02265422	0.1090897
	0.06546205	0.1517314
	0.2240412	0.07309883
	1.702588	0.02239308

[a] $P = 0.6$ for $N = 2, 3, 4$.

Table 6. Energies (h.u.) for $1s^2 2p\ ^2P$ Li

$N(1s)$	$M(2p)$	STO-GL	LEMAO-GL
2	2		−7.1051
2	3		−7.1073
2	4		−7.1078
3	2		−7.3046
3	3	−7.2942	−7.3071
3	4	−7.2946	
STO	−7.3504		
Experimental	−7.4100		

Table 7. Orbital exponents, expansion coefficients, and energies (h.u.) for $1s^2 2s^2\ ^1S$ Li^-

$N(1s)$	$M(2s)$	a_{2i}	b_{2i}	$-E$
	3	0.008381412	0.01056586	
		0.04016744	0.03681205	7.1664
		1.257558	−0.1110685	
	3	0.008047178	0.01013226	
		0.03700817	0.03462523	7.3602
		1.290961	−0.1187769	
Hartree-Fock			$E = -7.4282$	
Experimental			$E = -7.5054$	

various different M. That is, suppose we are initially given two different $2p$-LEMAO-2GL functions: the first yields an optimum energy $E = -7.1051$ h.u. or $1s^2 2p\ ^2P$ Li using $1s$-LEMAO-2G; the second yields an optimum energy $E = -7.3046$ h.u. for $1s^2 2p\ ^2P$ Li using $1s$-LEMAO-3G. It turns out that both of hese $2p$-LEMAO-2GL functions will give the same energy $E = -7.1051$ h.u. if hey are used with $1s$-LEMAO-2G or $E = -7.3046$ h.u. if they are used with s-LEMAO-3G. Thus in Tables 5 and 6, only one $2p$-LEMAO-NGL for each N s needed. Such transferability of $2s$-LEMAO's with different $1s$-LEMAO's was not possible because of the orthogonality requirement.

In Table 7, results are given for the ground electronic state $1s^2 2s^2\ ^1S$ Li^-. Again, it was found that revariation of the inner $1s$-shell made no significant difference in the final total energy. Consequently, the 1s-LEMAO-NG parameters listed in Table 1 are used in $1s^2\,{}^1S$ Li$^+$, $1s^2 2s\,{}^2S$ Li, $1s^2 2p\,{}^2P$ Li, as well as in $1s^2 2s^2\,{}^1S$ Li .

3. AIM Calculations on Li_2^+ and Li_2

A) General

The following correlation of lower states of Li$^+$, Li, and Li$^-$ with states of Li_2 and Li_2^+ can be obtained:

$$1s^2 2s\ \mathrm{Li} + 1s^2 2s\ \mathrm{Li} \rightarrow {}^1\Sigma_g^+ + {}^3\Sigma_u^+\ \mathrm{Li}_2\,, \tag{8}$$

$$1s^2 2s\ \mathrm{Li} + 1s^2 2p\ \mathrm{Li} \rightarrow {}^1\Sigma_g^+ + {}^3\Sigma_u^+ + {}^1\Pi_g + {}^3\Pi_u\ \mathrm{Li}_2\,, \tag{9}$$

$$1s^2\ \mathrm{Li}^+ + 1s^2 2s^2\ \mathrm{Li} \rightarrow {}^1\Sigma_g^+ + {}^1\Sigma_u^+\ \mathrm{Li}_2\,, \tag{10}$$

$$1s^2\ \mathrm{Li}^+ + 1s^2 2s\ \mathrm{Li} \rightarrow {}^2\Sigma_g^+ + {}^2\Sigma_u^+\ \mathrm{Li}_2^+\,, \tag{11}$$

$$1s^2\ \mathrm{Li}^+ + 1s^2 2p\ \mathrm{Li} \rightarrow {}^2\Sigma_g^+ + {}^2\Sigma_u^+ + {}^2\Pi_g + {}^2\Pi_u\ \mathrm{Li}_2^+\,. \tag{12}$$

The total energies (relative to a state of all electrons and nuclei infinitely separated), in h.u., of the reactants are -14.956, -14.888, -14.785, -14.758, and -14.690 for reactions (8)–(12), respectively. Actually, there are a number of separated atom states, $1s^2 2s$ Li + $1s^2$ nl Li, $n = 3$ and 4, the energies of which lie between levels (9) and (10); i.e., between -14.888 h.u. and -14.785 h.u. If we were interested, for example, in the second excited ${}^1\Sigma_g^+$ state of Li_2 (i.e., the third lowest energy ${}^1\Sigma_g^+$ state), then at least some of these omitted separated-atom states would be extremely important. In the present study of the lowest two singlet states, it is asserted that the ionic interaction (10) should be included at the expense of these lower energy neutral atom interactions.

Corresponding to a given component of any molecular state shown on the right of Eqs. (8)–(12), an AIM basis function may be written as a known linear combination of antisymmetrized products of atomic substate functions from the left of Eqs. (8)–(12). For example, the AIM basis function corresponding to ${}^1\Sigma_g^+$ Li_2 in Eq. (9) can be written as follows:

$$\Omega_1 = \Psi_1 - \Psi_2 \tag{13}$$

where

$$\Psi_1 = a'(\Phi_1^A \Phi_4^B - \Phi_2^A \Phi_3^B), \quad \Psi_2 = a'(\Phi_3^A \Phi_2^B - \Phi_4^A \Phi_1^B)\,; \tag{14}$$

here, Φ_1^X to Φ_4^X represent Li atom eigenfunctions corresponding to lowest energy states ${}^2S\,(M_S = 0.5)$, ${}^2S\,(M_S = -0.5)$, ${}^2P\,(M_L = 0, M_S = 0.5)$, and ${}^2P\,(M_L = 0, M_S = -0.5)$, respectively ($z$-axes on the two atoms A and B are taken to lie along the internuclear axis, and both have the same positive directions). Electrons 1–3 are initially assigned to the Φ_i^A eigenfunction and electrons 4–6 to the Φ_i^B eigenfunctions; a' is a partial antisymmetrization operator which causes Ψ_1 and Ψ_2 to obey the Pauli principle.

Calculations on ${}^1\Sigma_g^+$ Li_2 were done with: (1) the one function from Eq. (8); (2) the resonance of two functions from Eqs. (8)–(9); and (3) the resonance of three functions from Eqs. (8)–(10). Calculations on ${}^2\Sigma_g^+$ and ${}^2\Sigma_u^+$ Li_2^+ were done with: (1) the one function from Eq. (11); and (2) the resonance of two functions from Eqs. (11)–(12).

B) Results

In all cases, we carried out AIM calculations using Gaussian expansions of appropriately scaled Slater-type orbitals (i.e., 1*s*-STO-NG, 2*s*-STO-NG, and 2*p*-STO-NGL) [19, 20] in addition to our own newly developed LEMAO-NGL's. AIM predicted energies for $^2\Sigma_g^+$ Li_2^+, $R = 6.0$ a.u., and $^1\Sigma_g^+$ Li_2, $R = 5.05$ a.u., are listed in Table 8.

Table 8. AIM ground state energies (h.u.) for Li_2^+ and Li_2 using 1*s*, 2*s*, and 2*p* Gaussian expansions of lengths (*N*, *M*, *L*)

N	*M*	*L*	Li_2^+ ($R = 6$ a.u.) STO	Li_2^+ ($R = 6$ a.u.) LEMAO	Li_2 ($R = 5.05$ a.u.) STO	Li_2 ($R = 5.05$ a.u.) LEMAO
One-structure calculations						
2	3			−14.776		−14.976
3	3		−14.774	−14.773	−14.987	−14.973
3	4		−14.774	−14.774	−14.986	−14.972
4	3		−14.773		−14.986	
4	4		−14.773			
5	3		−14.772		−14.986	
Two-structure calculations						
2	3	2		−14.798		−14.985
2	3	3		−14.799		−14.985
3	3	2		−14.795		−14.980
3	3	3	−14.796	−14.796	−15.021	−14.980
3	3	4	−14.796		−15.020	
4	3	3	−14.795			
4	4	3	−14.795			
Three-structure calculations						
2	3	2				−14.993
3	3	2				−14.989
Expt'l			−14.803[a]		−14.994	

[a] Based upon estimated $D_e = 1.24$ eV.

Results for a given number of structures should converge toward an exact theoretical AIM limit as the Gaussian expansion lengths (*N*, *M*, *L* denote lengths of the 1*s*, 2*s* and 2*p* expansions, respectively) are increased; it appears that $(N, M, L) = (3, 3, 2)$ is nearly sufficient to give results within 0.001–0.002 h.u. from this limit. As the number of structures is increased, we expect the exact theoretical AIM limit to approach experiment.

Initial investigations made use of STO-NGL expansions. Results for the two-structure calculation on ground state Li_2 at $R = 5.05$ were below experiment; this was consistent with our previous experience with the STO-basis as described in Sect. 1 above. It was for this reason, of course, that we began developing the LEMAO-NGL expansions. In Table 8, we see that AIM energies using these new functions are not depressed below experimental. The three-structure Li_2 energy appears to be about 0.005 h.u. above the experimental result. For Li_2^+, our com-

Table 9. AIM energies (h.u.) and projection numbers for Li_2^+ using LEMAO-(3, 3, 3)

R	$^2\Sigma_g^+$				$^2\Sigma_u^+$			
	w_1	w_2	$-E_{AIM}$	$-E_{PP}$[a]	w_1	w_2	$-E_{AIM}$	$-E_{PP}$[a]
4	0.650	0.350	14.757		0.201	0.799	14.617	
5	0.661	0.339	14.786	14.799	0.515	0.485	14.657	14.670
5.7	0.680	0.320	14.794		0.702	0.298	14.678	
6	0.688	0.312	14.796	14.803	0.768	0.232	14.685	14.696
7	0.714	0.286	14.796	14.799	0.934	0.066	14.706	14.716
8	0.738	0.262	14.791		1.015	−0.015	14.723	
Inf	1.000	0.000	14.758	14.758	1.000	0.000	14.758	14.758

[a] We have added the experimental energy of $2Li^+$ to the valence-electron energies for Li_2^+ calculated by a pseudopotential model in Ref. [21]

puted two-structure energy appears 0.007 h.u. above the estimated experimental value.

The present *scaled* atoms-in-molecules (SAIM) theory provides for scaling of each individual many-electron atom in a molecule [6]; such scaling does not discriminate between inner- and outer-shell electrons. Most of the electronic energy of a molecule is inner-shell energy, and this is primarily affected by the scaling process. On the other hand, the interatomic binding energy in a molecule is largely outer-shell energy, and this is affected least by scaling. Therefore, the scaling feature of present SAIM theory is most important only for molecules containing one- and two-electron atoms, for which inner-shell-outer-shell discrimination is usually not significant. We are presently working upon an extension of the SAIM model which will allow for this discrimination; that is, it will permit scaling of valence electrons independently of inner-shell electrons. It is our opinion that the gap between present AIM results and experiment, for Li_2^+ and Li_2, may be nearly closed in an extended SAIM model which allows for such valence-electron scaling.

In Table 9, we list AIM results for $^2\Sigma_g^+$ and $^2\Sigma_u^+$ Li_2^+ as a function of R. We include, for comparison, energies computed by Bardsley using the pseudopotential model [21]; his values should be very close to experimental. A Rydberg series of three Li_2 states leads to predicted ionization potential of 4.99 eV [22], which gives $D_e(Li_2^+) \simeq 1.45$ eV, or $E = -14.811$ h.u. relative to all electrons and nuclei infinitely separated. Most theoretical calculations indicate $D_e(Li_2^+) \simeq 1.24$ eV [23-26], $E = -14.803$ h.u. The ground state potential energy curve is very broad and quite shallow.

Given a wave function

$$\Omega_0 = \sum_i C_i \Psi_i \tag{15}$$

like Eq. (13), the projection numbers

$$w_i = C_i \sum_j C_j \int \bar{\Psi}_i \Psi_j dv \tag{16}$$

may be defined. For Li_2^+, w_1 and w_2 correspond to structures derived from separated atom states indicated in Eqs. (11) and (12), respectively. We see that ground state Li_2^+ contains a significant fraction of the structure $1s_A^2 1s_B^2(2pz_A + 2pz_B)$;

Table 10. Comparison of Li_2^+ results

Method	R	$-E_R$	$-E_{\inf}$	$E_{\inf} - E_R$		R_{eq}
	a.u.	h.u.	h.u.	h.u.	eV	a.u.
$1s_A^2\,1s_B^2(2s_A + 2s_B)$	5.6	14.6517	14.6405	0.0112	0.30	5.96
LCAO-MO-SCF	6.5	14.6692	14.6405	0.0287	0.78	6.5
$1s_A^2\,1s_B^2(\varphi_A + \varphi_B)$	5.6	14.6874	14.6418	0.0456	1.24	5.96
SCF	6.0	14.7139	14.6691	0.0448	1.22	5.7
AIM-1[a]	6.0	14.772	14.758	0.014	0.38	~6.5
AIM-2	6.0	14.795	14.758	0.037	1.01	~6.5
Pseudopot.	6.0	14.803	14.758	0.045	1.23	5.9

[a] AIM-n = Atoms-inMolecules calculation including *n* structures.

that is, the Li^+ ion induces considerable polarization in the oncoming Li atom[4].

In Table 10, results for ground state Li_2^+ are compared with those of other calculations. The first and third lines refer to work done by James [23]; the LCAO-MO-SCF calculation was done by Fraga and Ransil [24] using the AO basis $(1s_{Li}, 2s_{Li}, 2p_{Li})$ with optimized orbital exponents; the SCF result is by Fischer and Kemmy using a basis of Gaussian orbitals [25]; and, the pseudopotential result is by Bardsley [21].

In Table 11, we list AIM results for the ground and first excited ${}^1\Sigma_g^+$ states of Li_2 as a function of R. Experimental results are taken from a tabulation in Ref. [31]. We see that results based upon the less accurate LEMAO-(2, 3, 2) expansions are depressed below results based upon the more accurate LEMAO-(3, 3, 2) expansions by 0.001, 0.004, and 0.006 h.u. at $R = 7.0$, 5.05 and 3 a.u., respectively. At $R = 4.0$ a.u., one finds $E_1 = -14.982$ h.u. using LEMAO-(3, 3, 2), by interpolation; experimental is $E = -14.981$ h.u. Thus results for $R \leqq 4.0$ a.u. are depressed below experiment; longer Gaussian expansions would be required to obtain exact AIM results which, in theory, would provide upper bounds to experiment.

Finally, results for ground state Li_2 are compared in Table 12 with results of other calculations. The first line refers to an LCAO-MO-SCF calculation by Ransil [32] using the AO basis $(1s_{Li}, 2s_{Li}, 2p_{Li})$ with optimized orbital exponents. The next two lines refer to calculations performed by James [33]. The SCF and ODC ("optimized double configuration") are given by Das and Wahl [34] and the 7-CI (seven configuration calculation using optimized orbitals) is by Das [31]. The most recent experimental value is by Velasco and coworkers [35].

---

[4] In the first approximation, Pauling long ago argued that the one-electron homopolar bond energy should be about one-half of the two-electron bond energy. However, an additional contribution would be derived from polarization of the atom in the ion field [21]. For H_2^+, the first part is said to account for (4.74 eV)/2 = 2.37 eV of the observed 2.78 eV bond energy, and polarization is said to account for most of the remaining 0.41 eV. The $s - p$ separation energies in H and Li are 10.2 eV and 1.85 eV, respectively. Hence, induced polarization should be more important in Li_2^+ than in H_2^+. A number of years ago, a theoretical approximate predecessor of SAIM theory, called modified atoms-in-molecules theory [28, 29], was used to calculate the potential energy curve for Li_2^+ using but one structure, that one derived from Eq. (11). The result $D_e(Li_2^+) = 0.65$ eV, which is about one-half of $D_e(Li_2) = 1.03$ eV, was considered reasonable (by FOE) at that time for the one-electron bond. The reason was wrong; there is an additional contribution of about 0.6 eV due to ion-atom polarization. Incidentally, the subsequent Diatomics-in-Molecules energy predictions for Li_3^+ and Li_2H^+ were too high because of the incorrect Li_2^+ potential used in those calculations [29, 30].

Table 11 AIM ground state energies E_1 (h.u.), ground state projection numbers w_i, and excited $^1\Sigma_g^+$ state energies E_2 for Li_2 [a]

R	$-E_{exp}$	$-E_1$	w_1	w_2	w_3	$-E_2$
2.5		14.914	0.051	0.387	0.562	
3.0		14.954	0.182	0.330	0.489	14.778
		(14.948)	(0.120)	(0.354)	(0.525)	(14.790)
3.5		14.976	0.301	0.280	0.419	
4.0	14.981	14.987	0.402	0.240	0.358	
4.5		14.992	0.483	0.208	0.309	
5.05	14.994	14.993	0.552	0.179	0.269	14.868
		(14.989)	(0.542)	(0.175)	(0.283)	(14.871)
5.5	14.993	14.990	0.597	0.157	0.247	
6.0	14.989	14.987	0.637	0.133	0.231	
7.0	14.979	14.977	0.707	0.084	0.209	14.894
		(14.976)	(0.719)	(0.081)	(0.199)	(14.895)
8.0	14.971	14.969	0.784	0.040	0.175	

[a] Results in parentheses calculated with the more accurate LEMAO-(3, 3, 2); all other results calculated with LEMAO-(2, 3, 2)

Table 12 Comparison of Li_2 results

Method	R a.u.	E_R h.u.	$-E_{inf}$ h.u.	$E_{inf} - E_R$ h.u.	eV	R_{eq} a.u.
$1s_A^2 1s_B^2(2s_A 2s_B)$	5.05	14.845	2(7.4179)	0.009	0.24	~6.0
LCAO-MO-SCF	5.34	14.8422	2(7.4179)	0.006	0.17	5.34
$1s_A^2 1s_B^2(\varphi_A \varphi_B)$	5.63	14.866	2(7.4192)	0.028	0.76	
SCF	5.07	14.8716	2(7.4327)	0.006	0.16	5.26
ODC	5.0	14.8796	2(7.4327)	0.014	0.38	5.43
7-CI	5.07	14.9026	2(7.4327)	0.037	1.01	5.09
AIM-1 [a]	5.05	14.972	2(7.4779)	0.016	0.43	~5.2
AIM-2	5.05	14.980	2(7.4779)	0.024	0.65	~5.2
AIM-3	5.05	14.989	2(7.4779)	0.033	0.90	~5.0
Pseudopot.	5.0	14.989	2(7.4779)	0.033	0.90	~5.0
Expt'l	5.05	14.994	2(7.4779)	0.038	1.03	5.05

[a] AIM-n = Atoms-in-Molecules calculation including *n* structures.

4. Conclusions

There are two important characteristics of Atoms-in-Molecules (AIM) theory which make it an especially attractive model in quantum chemistry. First, the basis set need not be as large as in an *ab initio* calculation of comparable accuracy; much of the configuration interaction required in the latter is accounted for by exact determination of intra-atomic energy in AIM theory. Second, the AIM method is conceptually satisfying since explanation of molecular properties is couched directly in terms of interacting exact atomic eigenfunctions.

In AIM theory, interatomic contributions to matrix elements are calculated with approximate many-electron atomic eigenfunctions. We have shown in this paper that if these approximate eigenfunctions are built from Gaussian lobe functions, parameters of which are chosen by individually minimizing the given atomic substate expectation energies, practical AIM results can be achieved. For

i_2^+ and Li$_2$, convergence to exact theoretical AIM limits within about 0.001 h.u., s achieved by using three-term expansions for $R > 4$ a.u.; longer expansions vould be required for smaller internuclear distances.

References

1. Moffitt, W.: Proc. Roy. Soc. (London) A **210**, 245 (1951).
2. Arai, T.: Rev. mod. Physics **32**, 370 (1960).
3. Hurley, A. C.: Rev. mod. Physics **35**, 448 (1963).
4. Balint-Kurti, G. G., Karplus, M.: J. chem. Physics **50**, 478 (1969).
5. Parr, R. G.: Quantum theory of molecular electronic structure, pp. 101–108. New York: W. A. Benjamin, Inc. 1963.
6. Ellison, F. O., Wu, A. A.: J. chem. Physics **47**, 4408 (1967).
7. Wu, A. A., Ellison, F. O.: J. chem. Physics **48**, 1103 (1968).
8. Ellison, F. O., Slezak, J. A.: J. chem. Physics **50**, 3942 (1969).
9. Hylleraas, E. A.: Z. Physik **54**, 347 (1929).

0. Silverman, J. N., Platas, O., Matsen, F. A.: J. chem. Physics **32**, 1402 (1960).
1. Preuss, H.: Z. Naturforsch. **11**, 823 (1956); Whitten, J. L.: J. chem. Physics **39**, 349 (1963).
2. Shih, S., Buenker, R. J., Peyerimhoff, S. D., Wirsam, B.: Theoret. chim. Acta (Berl.) **18**, 277 (1970).
3. Brown, R. D., Burden, F. R., Hart, B. T.: Theoret. chim. Acta (Berl.) **25**, 49 (1972).
14. See, for example, Roothaan, C. C. J.: Technical Report, 1955, p. 24. Laboratory of Molecular Structure and Spectra, Department of Physics· University of Chicago.
5. Shavitt, I.: Methods in computational physics, vol. 2, edited by Alder, B. *et al.* New York: Academic Press.
6. Hehre, W. J., Ditchfield, R., Pople, J. A.: J. chem. Physics **53**, 932 (1970).
7. Grimmelmann, E. K., Chesick, J. P.: J. chem. Physics **55**, 1690 (1971).
8. Chesick, J. P., Fraser, S. J., Linnett, J. W.: Trans. Faraday Soc. **64**, 257 (1968).
9. Huzinaga, S.: J. chem. Physics **42**, 1293 (1965).

0. Sambe, H.: J. chem. Physics **42**, 1732 (1965).
1. Bardsley, J. N.: Chem. Physics Letters **7**, 517 (1970).
2. Barrow, R. F., Travis, N., Wright, C. V.: Nature **4732**, 141 (1960); Robinson, E. W., Barrow, R. F.: Proc. chem. Soc. 329 (1961); Mercier, J. L., Rico, F. R., Velasco, R.: Optica Pura y Aplicada **2**, 96 (1969).
3. James, H. M.: J. chem. Physics **3**, 9 (1935).
4. Fraga, A., Ransil, B. J.: J. chem. Physics **35**, 669 (1961).
5. Fischer, C. R., Kemmey, P. J.: Physic. Rev. **186**, 272 (1969).
6. Dalgarno, A., Bottcher, C., Victor, G. A.: Chem. Physics Letters **7**, 265 (1970).
7. Pauling, L.: The nature of the chemical bond, p. 15, 340. Ithaca N.Y.: Cornell Univ. Press.
8. Ellison, F. O.: J. chem. Physics **43**, 3654 (1965).
9. Pfeiffer, G. V., Ellison, F. O.: J. chem. Physics **43**, 3405 (1965).

0. Wu, A. A., Ellison, F. O.: J. chem. Physics **47**, 1458 (1967).
1. Das, G.: J. chem. Physics **46**, 1568 (1967).
2. Ransil, B. J.: Rev. mod. Physics **32**, 239 (1960).
3. James, H. M.: J. chem. Physics **2**, 794 (1934).
4. Das, G., Wahl, A. C.: J. chem. Physics **44**, 87 (1966).
5. Velasco, R., Ottinger, C., Zare, R. N.: J. chem. Physics **51**, 5522 (1969).

rof. Frank O. Ellison
epartment of Chemistry
niversity of Pittsburgh
ittsburgh, Pa. 15213
SA

Dr. Lyndon L. Larcom
Department of Chemistry
University of Pittsburgh
Pittsburgh, Pa. 15213
USA

Theoret. chim. Acta (Berl.) 27, 95—107 (1972)
© by Springer-Verlag 1972

On the Use of Small Atomic Basis Sets in Non-Empirical Molecular Calculations

H. B. Jansen and P. Ros

Chemistry Laboratory, Free University, Amsterdam

Received April 24, 1972

The quality of an atomic basis set in molecular calculations can be characterized by the deviation of the valence-shell orbital energies from their values in a Hartree-Fock limit calculation. For atoms of a certain row of the periodic system, this quality appears to depend not only on the number of basis functions used in the calculations, as is usually accepted, but also on the number of valence shell electrons of the various atoms.

As a consequence of this result, rules can be formulated for the combination of small atomic basis sets to a basis set for a molecular calculation. In fact, the best results are obtained with basis sets in which the deviations of all atomic valence shell orbital-energies from their Hartree-Fock limit values are of the same order of magnitude.

Die Qualität eines Atombasissatzes zur Rechnung an Molekülen kann durch die Abweichung der Energien der Orbitale der Valenzschalen von den Werten einer Hartree-Fock-Grenzrechnung charakterisiert werden. Im Falle der Atome einer bestimmten Periode im Periodensystem scheint diese Qualität nicht nur von der Zahl der bei der Rechnung benutzten Basisfunktionen abzuhängen, wie allgemein akzeptiert ist, sondern auch von der Anzahl der Elektronen der Valenzschale der verschiedenen Atome.

Aufgrund dieses Resultats können Regeln zur Kombination kleiner Atombasissätze zu einem Basissatz für Rechnungen an Molekülen formuliert werden. In der Tat werden die besten Resultate mit Basissätzen erhalten, bei denen die Abweichungen aller Orbitalenergien der Atomvalenzschalen von ihrem Hartree-Fock-Grenzwert in der gleichen Größenordnung sind.

Introduction

In general non-empirical molecular calculations are performed with a set of basis function built up from atomic basis sets. The last few years a large number of atomic basis sets have been published, both with Gaussian Type Orbitals (GTO's) [1–6], and with Slater Type Orbitals (STO's) [7–9]. It is dangerous, however, to use just some arbitrary combination of atomic basis sets in a molecular calculation, since there is a possibility that the resulting basis set is "unbalanced" as indicated by Mulliken [10]. Unbalanced basis sets may lead to an incorrect prediction of various quantities like dipole moments or charge distributions obtained from a population analysis.

In molecular calculations, usually little attention is paid to the question which combination of atomic basis sets on the various atoms in the molecule can be used to result in a balanced basis.

Since at this moment a large number of atomic basis sets is available, we want to be able to compare the quality of these basis sets and to decide which basis sets can be combined.

Usually the quality of an optimized atomic basis set is assumed to be determined by the number of functions of the various symmetry types in the set, e.g.

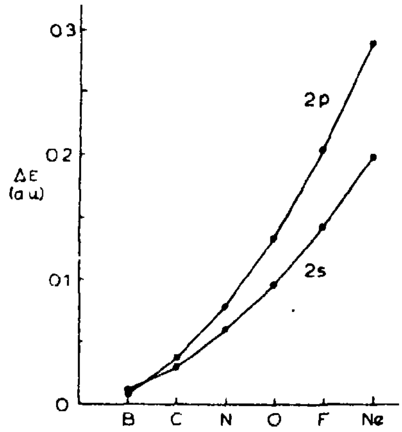

Fig. 1. $\Delta\varepsilon_{2s}$ and $\Delta\varepsilon_{2p}$ obtained with a minimum STO basis for the averaged configuration s^2p^n of the atoms B to Ne

for a certain atom a set consisting of three *s*-type functions and two *p*-type functions, a (3, 2) set, is better than a set consisting of two *s*-type functions and one *p*-type function, a (2, 1) set.

There is, however, another parameter that affects the quality of the basis set. Even when an atomic basis set is completely optimized, the deviations of the orbital energies calculated with this basis set from the values obtained in the Hartree-Fock limit, are a function of the number of electrons in the different shells of the atom. This effect especially shows up when an atomic shell is being filled. For example, in a set of calculations for the first-row atoms with a fixed number of *s*- and *p*-type basis functions the difference between ε_{2p} in these calculations and ε_{2p} in the Hartree-Fock limit,

$$\Delta\varepsilon_{2p} = \varepsilon_{2p}(\mathrm{calc}) - \varepsilon_{2p}(\mathrm{H.F.}), \qquad (1)$$

becomes rapidly larger going from B to Ne. The value of $\Delta\varepsilon_{2s}$, similarly defined as

$$\Delta\varepsilon_{2s} = \varepsilon_{2s}(\mathrm{calc}) - \varepsilon_{2s}(\mathrm{H.F.}), \qquad (2)$$

also becomes larger, but less than the value of $\Delta\varepsilon_{2p}$.

As an illustration the values of $\Delta\varepsilon_{2s}$ and $\Delta\varepsilon_{2p}$ for a minimal STO calculation are shown in Fig. 1 for the averaged configurations s^2p^n of the atoms B through Ne. Likewise, the same dependence of the quality of the basis set on the number of electrons can be found for other basis sets, GTO sets and STO sets of any size. However, for larger basis sets the effect rapidly becomes much less pronounced. This effect is not restricted either to atoms with *s*- and *p*-type functions. A similar effect occurs with the *d*-electrons of transition metal atoms.

Theory

If we want to discuss the origin of the deviations of the orbital energies, we first have to analyse the effect somewhat more in detail. The values of $\Delta\varepsilon_i$ for a series of atoms in which one shell is being filled, obtained with basis sets of the same size, may be expanded in a limited power series in n, the number of electrons in that particular shell.

The coefficients of the different powers of n are shown in Table 1 for the $\Delta\varepsilon_{2p}$ values of some STO basis sets for the first row atoms [11]. Terms that do not make a significant contribution to the fit of the expansion are omitted. In this table we see that if the values of $\Delta\varepsilon$ are relatively small, there is a linear correlation between $\Delta\varepsilon$ and n. If, however, the deviations are larger, a quadratic term appears.

In the same way we can analyse the mean deviation of the function calculated in a certain basis from the corresponding function in the Hartree-Fock limit, defined as

$$\langle \Delta\Psi_{2p} \rangle = [\int \{\Psi_{2p}(\text{H.F.}) - \Psi_{2p}(\text{calc})\}^2 \, d\tau]^{\frac{1}{2}} \tag{3}$$

for the same STO-basis sets. The results of these calculations are shown in Table 2. From these results we may conclude that the linear dependance of $\langle \Delta\Psi \rangle$ of n is small compared with the constant term. We therefore may introduce as a perturbation in our Hartree-Fock equations some $\Delta\Psi$ that is independent of n.

Suppose we want to solve the Hartree-Fock equations

$$F(1)\,\Psi_i(1) = \varepsilon_i \Psi_i(1) \tag{4}$$

by expanding Ψ_i in a limited basis set. The resulting solution $\tilde{\Psi}_i$ in general will deviate from the correct solution Ψ_i (Hartree-Fock limit). This in turn affects the Hartree-Fock operator F, defined by

$$F(1) = h(1) + \sum_k \int \Psi_k(2) \frac{(1-P_{12})}{r_{12}} \Psi_k(2)\, d\tau_2 \tag{5}$$

yielding

$$\tilde{F}(1) = h(1) + \sum_k \int \tilde{\Psi}_k(2) \frac{(1-P_{12})}{r_{12}} \tilde{\Psi}_k(2)\, d\tau_2 \,. \tag{6}$$

Introducing $\Delta\Psi_i = \tilde{\Psi}_i - \Psi_i$ the deviation in the Hartree-Fock operator will be

$$\Delta F(1) = \sum_k \int \Delta\Psi_k(2) \frac{(1-P_{12})}{r_{12}} \Psi_k(2)\, d\tau_2 + \sum_k \int \Psi_k(2) \frac{(1-P_{12})}{r_{12}} \Delta\Psi_k(2)\, d\tau_2 \,. \tag{7}$$

We now can calculate the deviation in the one-electron energies according to

$$\Delta\varepsilon_i = 2\langle \Delta\Psi_i | F | \Psi_i \rangle + \langle \Psi_i | \Delta F | \Psi_i \rangle \,. \tag{8}$$

The result is

$$\begin{aligned} \Delta\varepsilon_i = {} & 2\langle \Delta\Psi_i | h | \Psi_i \rangle + 2\sum_k [(\Delta\Psi_i \Psi_i | \Psi_k \Psi_k) \\ & - (\Delta\Psi_i \Psi_k | \Psi_i \Psi_k) + (\Psi_i \Psi_i | \Delta\Psi_k \Psi_k) - (\Psi_i \Delta\Psi_k | \Psi_i \Psi_k)] \,. \end{aligned} \tag{9}$$

The summation over k in the Eqs. (5) to (9) is in principle over all electrons. This summation can be seperated into a summation over electrons in inner shells and a summation over electrons in the valence shell. The first sum contributes to the constant term in Table 1, the second sum leads to a term that is proportional to the number of electrons in the valence shell (since in that case all integrals $\langle \Delta\Psi_i \Psi_i | \Psi_k \Psi_k \rangle$ etc. will approximately have the same value). As a consequence of this, $\Delta\varepsilon_i$ will to a first-order approximation be proportional to n.

Table 1. Coefficients in the power series expansion of $\Delta\varepsilon_{2p}$ in n for a number of STO basis sets for the first row atoms [11]. $10^4\,\Delta\varepsilon_{2p} = a + bn + cn^2 + \cdots$ (non-significant entries are omitted)

	a	b	c
minimal (2, 1)	− 316	547	718
marginal (3, 2)	114	170	20
nominal (4, 3)	− 29	15	

If the deviations in the molecular orbitals are small, we only have to take into account these first-order terms. However, when the deviations are larger, we also have to consider higher-order terms, as can be seen in Table 1 for the minimal basis set.

Atomic Calculations

In Figs. 2 through 5 some examples are given of the change of $\Delta\varepsilon$ with the number of electrons in the open shell. In these examples calculations from literature are used on a special state of a configuration (in general the ground state). Therefore the electronic interaction does not change as smoothly along a series of atoms as for the averaged configuration. Especially nitrogen (^4S) and manganese

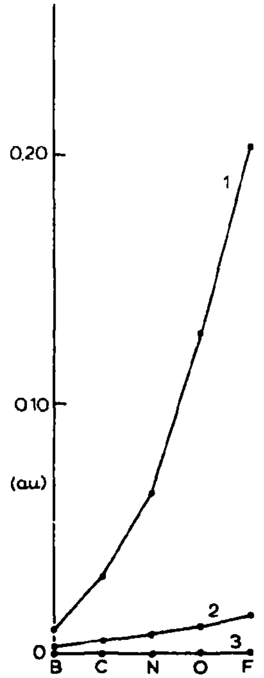

Fig. 2. $\Delta\varepsilon_{2p}$ for a series of STO basis sets. For each line the number of p-type functions is indicated

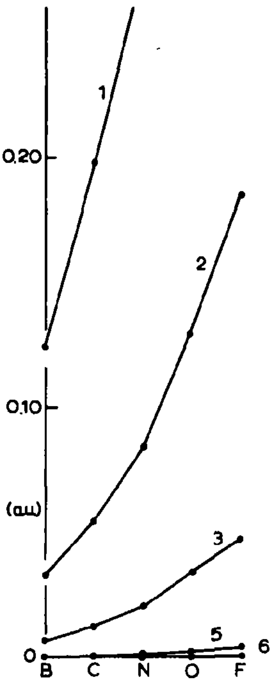

Fig. 3. $\Delta\varepsilon_{2p}$ for a series of GTO basis sets. For each line the number of p-type functions is indicated

(^6S), with one electron in each orbital of the open shell, have large exchange contributions that cancel part of the Coulombic repulsion terms and therefore the values of $\Delta\varepsilon$ for these atoms are relatively small.

Fig. 2 shows the values of $\Delta\varepsilon_{2p}$ for a series of STO basis sets with an increasing number of p-type functions and a comparable number of s-type functions [11]. In Fig. 3 the same is done for a series of GTO basis sets [12]. Figs. 4 and 5 illustrate the situation for transition metals. Here, too, all calculations are for the lowest state of the $(3d)^n(4s)^2$ configuration. As reference calculations we used the large basis STO calculations of Clementi [8]. In Fig. 4 the results are given for the calculations of Roos *et al.* [4], who used a basis of nine s-type, five p-type and three d-type GTO's. In Fig. 5 similar results are shown for the basis sets published by Wachters [5], who used a (14, 9, 5) set.

We obtain another illustration, when we consider Van Duyneveldt's [6] large series of optimized atomic GTO basis sets. We can calculate the $\Delta\varepsilon$-values for all calculations of this series, a selection of which is given in Table 3. From this table we see for example that the $\Delta\varepsilon$-values of a boron (5, 3) set are almost equal to the $\Delta\varepsilon$-values of a fluorine (7, 4) set.

All the basis sets discussed so far in this chapter are not contracted. With contracted basis sets the atomic orbitals are disturbed by the contraction and are no longer fully optimized. Now the general trend will be the same, but the position of the curve is contraction-dependent. As an example Table 4 gives $\Delta\varepsilon$-values for the contracted GTO basis sets of Basch *et al.* [13], (15 s-type, 8 p-type and 5 d-

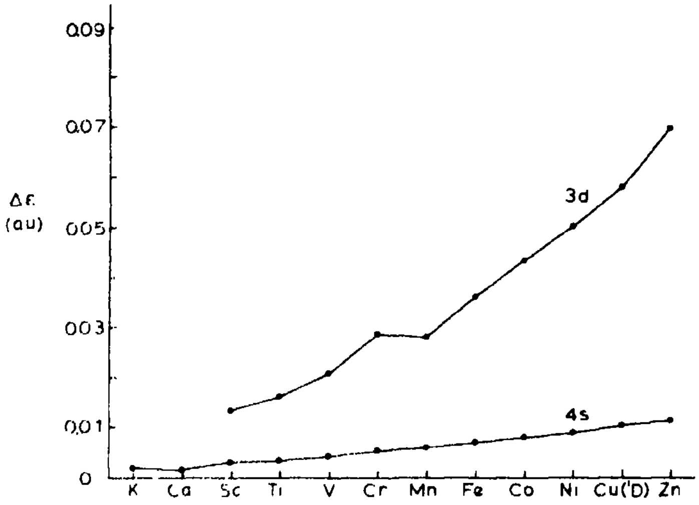

Fig. 4. $\Delta\varepsilon_{3d}$ and $\Delta\varepsilon_{4s}$ for the basis sets of Roos *et al.* [4]

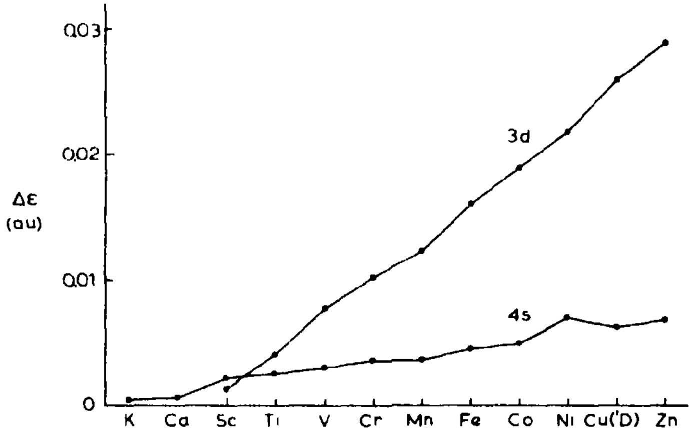

Fig. 5. $\Delta\varepsilon_{3d}$ and $\Delta\varepsilon_{4s}$ for the basis sets of Wachters [5]

Table 2. Coefficients in the power series expansion of $\langle \Delta\Psi_{2p} \rangle$ in *n* for a number of STO basis sets for th first row atoms. $10^3 \langle \Delta\Psi_{2p} \rangle = a + bn + \cdots$ (non-significant entries are omitted)

	a	b
minimal (2, 1)	97	14
marginal (3, 2)	14	2
nominal (4, 3)	0.01	-

Table 3. E, ε_{1s}, ε_{2s} and ε_{2p} for B to Ne with large accurate basis ΔE, $\Delta\varepsilon_{1s}$, $\Delta\varepsilon_{2s}$ and $\Delta\varepsilon_{2p}$ for a number of basis sets from van Duyneveldt [6]

		B	C	N	O	F	Ne
Large accurate basis	E	−24.529	−37.689	−54.401	−74.809	−99.409	−128.547
	ε_{1s}	− 7.695	−11.326	−15.629	−20.669	−26.383	− 32.773
	ε_{2s}	− 0.495	− 0.706	− 0.945	− 1.244	− 1.573	− 1.930
	ε_{2p}	− 0.310	− 0.433	− 0.568	− 0.632	− 0.730	− 0.850
(4, 2)	$10^3\Delta E$	193	333	583	834	1228	1731
	$10^3\Delta\varepsilon_{1s}$	63	80	101	124	153	186
	$10^3\Delta\varepsilon_{2s}$	17	29	47	72	102	138
	$10^3\Delta\varepsilon_{2p}$	53	59	89	135	188	249
(5, 2)	$10^3\Delta E$	82	173	321	551	869	1288
	$10^3\Delta\varepsilon_{1s}$	5	− 3	− 11	− 19	− 28	− 36
	$10^3\Delta\varepsilon_{2s}$	16	28	12	69	99	133
	$10^3\Delta\varepsilon_{2p}$	34	57	75	132	185	244
(5, 3)	$10^3\Delta E$	63	107	170	256	368	508
	$10^3\Delta\varepsilon_{1s}$	18	25	34	45	59	75
	$10^3\Delta\varepsilon_{2s}$	17	28	42	61	84	109
	$10^3\Delta\varepsilon_{sp}$	15	23	33	48	66	85
(6, 3)	$10^3\Delta E$	38	66	106	167	248	353
	$10^3\Delta\varepsilon_{1s}$	16	21	28	37	45	61
	$10^3\Delta\varepsilon_{2s}$	2	5	9	15	23	33
	$10^3\Delta\varepsilon_{2p}$	7	13	20	33	48	65
(7, 4)	$10^3\Delta E$	10	17	28	43	63	89
	$10^3\Delta\varepsilon_{1s}$	4	7	9	13	17	23
	$10^3\Delta\varepsilon_{2s}$	2	2	4	6	3	13
	$10^3\Delta\varepsilon_{2p}$	1	4	6	10	14	19
(8, 4)	$10^3\Delta E$	4	9	16	28	44	65
	$10^3\Delta\varepsilon_{1s}$	1	2	3	5	8	10
	$10^3\Delta\varepsilon_{2s}$	1	2	3	6	9	12
	$10^3\Delta\varepsilon_{2p}$	2	3	5	9	14	19
(9, 5)	$10^3\Delta E$	2	3	5	8	13	19
	$10^3\Delta\varepsilon_{1s}$	1	1	2	2	3	5
	$10^3\Delta\varepsilon_{2s}$	1	1	2	3	3	5
	$10^3\Delta\varepsilon_{2p}$	1	1	2	3	4	6

Table 4. ΔE, $\Delta\varepsilon_{3p}$, $\Delta\varepsilon_{3d}$ and $\Delta\varepsilon_{4s}$ for the contracted GTO basis sets of Basch *et al.* [13]

	ΔE	$\Delta\varepsilon_{3p}$	$\Delta\varepsilon_{3d}$	$\Delta\varepsilon_{4s}$
Sc	0.8203	−0.0115	−0.0121	0.0023
Ti	0.9165	−0.0055	−0.0067	0.0032
V	1.0204	−0.0029	−0.0055	0.0042
Cr	1.1244	−0.0024	−0.0060	0.0047
Mn	1.2462	0.0181	0.0077	0.0062
Fe	1.3573	−0.0042	0.0158	0.0048
Co	1.4881	0.0064	0.0037	0.0058
Ni	1.6419	0.0481	0.0371	0.0090
Cu	1.7882	0.0044	0.0049	0.0075

type GTO's, contracted to 4 *s*-type, 2 *p*-type and 1 *d*-type function, i.e. a (15, 8, 5) set contracted to [4, 2, 1]). The data in this table show that the contraction may result in additional deviations, as can be seen in the case of nickel, where the $\Delta\varepsilon$-values are much larger than for the other atoms. Furthermore the 3*p* and 3*d* orbital energies for Sc through Cr are about 0.005 a.u. below Clementi's values [8], although the total energy is about 1 a.u. above the value from Clementi's calculation. Mostly this effect arises from the frozen core orbitals. Furthermore the incorrect description of the inner orbitals may cause a deformation of the outer orbitals, but this will not be the case when the contracted combinations are carefully chosen as is discussed by Dunning [14].

Molecular Calculations

The results of the previous section show that the deviation in the orbital energies from the Hartree-Fock limit situation depends both upon the number of basis functions and the number of electrons within a shell. This may have its consequences for molecular calculations. It was shown that for a balanced calculation the number of basis functions on different atoms may have to be different, especially when a small basis set is used, as is the case e.g. in calculations on large molecules.

To study the influence in molecular calculations we have performed a set of calculations on the BF molecule using GTO basis sets of different size. We have compared these results with a calculation in which the large basis set of Huzinaga and Arnau [15] was used. This basis set can be characterized as (11, 6) contracted to a [4, 2] set for each of the atoms B and F. In this reference calculation we have deliberately not used polarization functions (*d*-type orbitals and higher), because we wanted to keep the calculations with small and large basis sets comparable. The reference calculation can be considered to approach the *s*, *p*-limit. The basis sets we used in this test are those of Whitman and Hornback [12]. Their quality in atomic calculations is shown in Table 5, which gives the energy differences between the atomic limited basis set calculations and the Hartree-Fock calculation.

Since not all the basis sets that we derive from the results of Whitman and Hornback are optimized, the separate values of $\Delta\varepsilon$ given in Table 5 are not very reliable as a test for the quality of the basis set, since in these cases one or more ε-values may by accident be quite correct, *e.g.* a poor description of the 1*s* orbital may result in an incorrect ε_{1s} but an almost correct ε_{2s}. As a matter of fact, the

Table 5. B and F atomic basis sets. Values of ΔE, $\Delta\varepsilon_{1s}$, $\Delta\varepsilon_{2s}$ and $\Delta\varepsilon_{2p}$ for a number of basis sets from Whitman and Hornback [12]

Basis	B				F			
set	ΔE	$\Delta\varepsilon_{1s}$	$\Delta\varepsilon_{2s}$	$\Delta\varepsilon_{2p}$	ΔE	$\Delta\varepsilon_{1s}$	$\Delta\varepsilon_{2s}$	$\Delta\varepsilon_{2p}$
(3, 1)	0.816	0.253	0.004	0.125	5.267	0.275	0.004	0.595
(3, 2)	0.735	0.351	0.030	0.045	2.992	1.073	0.156	0.218
(3, 3)	0.718	0.359	0.029	0.027	2.495	1.143	0.135	0.094
(4, 2)	0.193	0.071	0.018	0.038	1.230	0.189	0.110	0.201
(4, 3)	0.175	0.081	0.018	0.021	0.731	0.268	0.092	0.080

Table 6. Experimental dipole moment of BF and computed values of the dipole moment from calculations with various basis set. The dipole moments are given in Debye and have a positive sign for (B^-F^+)

Basis	μ_{BF}
Huzinaga	0.51
B(3, 1) F(3, 1)	4.41
B(3, 1) F(3, 2)	0.93
B(3, 2) F(3, 2)	1.59
B(3, 2) F(3, 3)	0.53
B(3, 2) F(4, 2)	1.48
B(3, 2) F(4, 3)	0.43
Experimental [22]	0.5 ± 0.2

combination of ΔE, $\Delta\varepsilon_{1s}$, $\Delta\varepsilon_{2s}$ and $\Delta\varepsilon_{2p}$ gives a more reliable picture. The influence of further optimalization on molecular calculations, however, is small.

The quality of these molecular calculations can be investigated by comparing the calculated dipolemoments with the experimental value [22] or by analysing the wave function using standard methods, like a Mulliken population analysis [16] and density difference maps, in which the difference in electron density along a line or in a plane in the molecule is visualized [17–21].

The calculated dipole moments, given in Table 6, indicate, that the charge distribution found in the calculation with the basis of Huzinaga and Arnau is correct, but that especially in calculations with small basis sets large deformations of the charge distribution may occur.

Table 7. Gross atomic populations and overlap populations in BF from calculations with various basis sets

Basis	Symmetry	N_B	N_F	P_{BF}
Huzinaga	σ	4.24	5.76	0.025
	π	0.13	1.87	0.153
	total	4.50	9.50	0.331
B(3, 1) F(3, 1)	σ	4.40	5.60	0.162
	π	0.52	1.48	0.271
	total	5.44	8.56	0.704
B(3, 1) F(3, 2)	σ	4.34	5.66	0.285
	π	0.25	1.75	0.211
	total	4.84	9.16	0.707
B(3, 2) F(3, 2)	σ	4.45	5.55	0.435
	π	0.24	1.76	0.197
	total	4.93	9.07	0.829
B(3, 2) F(3, 3)	σ	4.45	5.55	0.387
	π	0.15	1.85	0.163
	total	4.75	9.25	0.713
B(3, 2) F(4, 2)	σ	4.40	5.60	0.388
	π	0.24	1.76	0.195
	total	4.88	9.12	0.778
B(3, 2) F(4, 3)	σ	4.40	5.60	0.342
	π	0.15	1.85	0.162
	total	4.70	9.30	0.666

Table 8. Net population per set of orbitals in BF from calculations with various basis sets

Basis	s(B)	$p\sigma$(B)	$p\pi$(B) (each)	s(F)	$p\sigma$(F)	$p\pi$(F) (each)
Huzinaga	3.82	0.41	0.05	3.98	1.77	1.79
B(3, 1) F(3, 1)	3.86	0.46	0.38	3.94	1.58	1.35
B(3, 1) F(3, 2)	3.85	0.35	0.14	3.67	1.85	1.65
B(3, 2) F(3, 2)	3.78	0.45	0.28	3.66	1.68	1.66
B(3, 2) F(3, 3)	3.82	0.43	0.07	3.58	1.66	1.77
B(3, 2) F(4, 2)	3.78	0.43	0.14	3.73	1.67	1.67
B(3, 2) F(4, 3)	3.83	0.40	0.07	3.66	1.77	1.77

A more directly calculated charge distribution is given in Table 7, in which the results of a population analysis for the various computations are shown.

The charge density shift from B to F of 0.5 electron in the calculation using Huzinaga's basis set is rather large in comparison with the experimental dipole moment but this has to be ascribed to the division of the overlap population in two equal parts in a Mulliken population analysis.

In Table 8 the net populations are shown for sets of orbitals of the same type, e.g. the set of the s-orbitals on B. In this table it is especially interesting to see how the p_σ and the p_π populations on F increase and the s population decreases when the basis on this atom, or on both atoms, becomes larger. For larger basis sets these values approach the values from the calculation with the large set from Huzinaga, but using a small number of p-functions on F, the electrons shift to other, energetically more favourable orbitals.

In the electron density difference map, shown in Fig. 6 for the difference between the small basis (B(3, 1) and F(3, 1)) and the large basis calculation, this

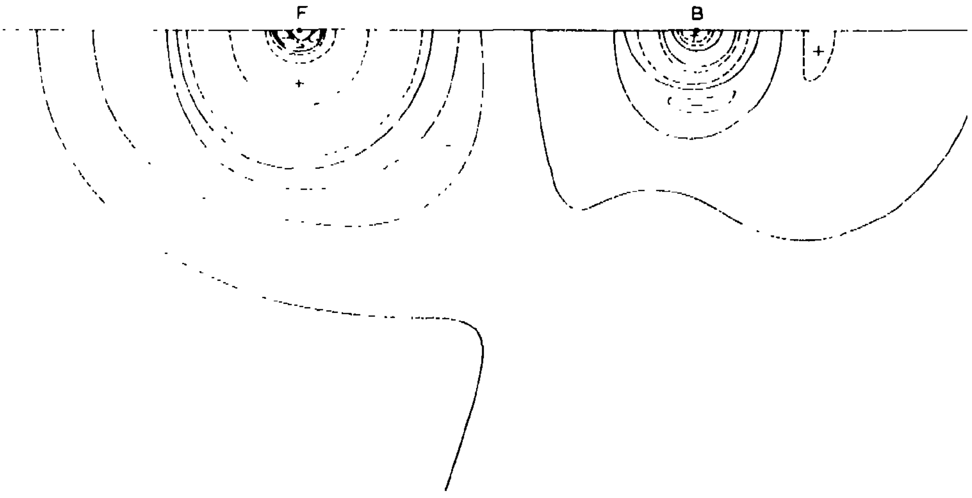

Fig. 6. Density difference map for BF between the small and the large basis calculation. ——— lines of zero density difference. · — - lines of positive density difference, · - lines of negative density difference. Starting from the zero lines, the positive and negative lines represent successively ± 0.003, ± 0.01, ± 0.03, ± 0.1

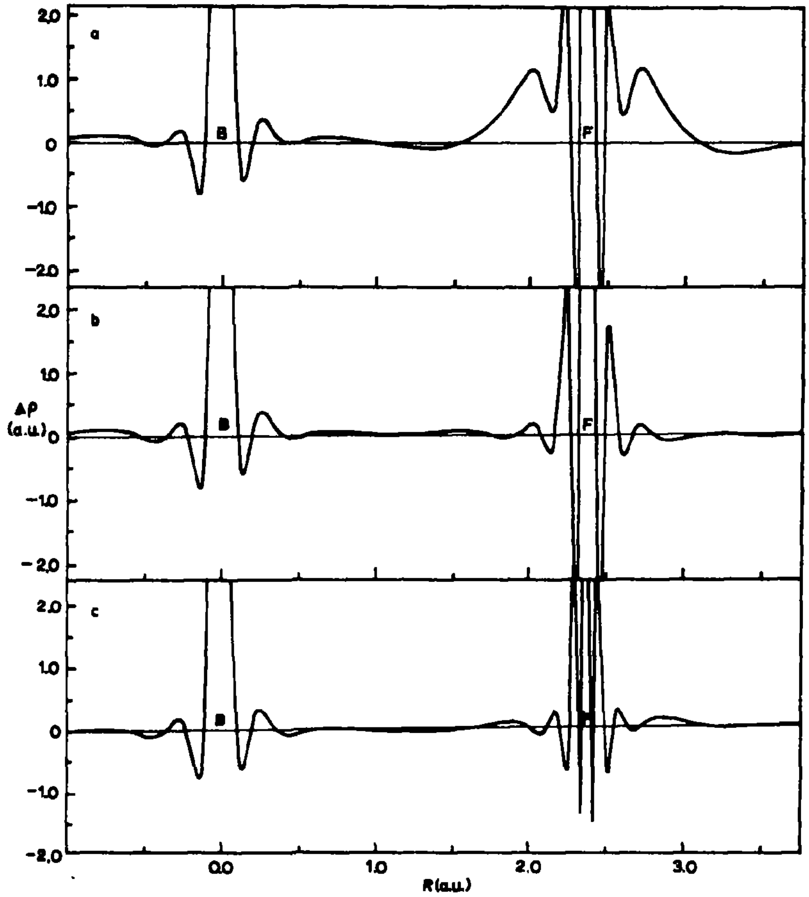

ig. 7. Density difference along the molecular axis of BF between a number of small-basis calculations and the large-basis calculation. (a) B(3, 1) F(3, 1), (b) B(3, 1) F(3, 2), (c) B(3, 2) F(4, 3)

ame effect of a shift from the F $2p$ orbitals to other orbitals shows up. The effect or the π-orbitals is the same as for the p_σ-orbitals, although perhaps somewhat veaker. We therefore may as well concentrate on the σ-situation and give for a election from these calculations the density difference along the molecular xis (Fig. 7). In this figure, going from (a) to (b), we see that mainly the description f the valence electron distribution at fluorine is improved, while from (b) to (c) nost of the improvement is found in the description of the core electron distribution of fluorine.

Both from the calculated dipole moment and from the population analysis, t is clear that the best description is not that using an equally small number of unctions for B and F, but that a description with more functions on F than on B ives a better charge distribution. In fact, the best description is obtained if the alues of $\Delta\varepsilon$ for all (valence) orbitals are of the same order of magnitude.

This conclusion will have consequences for the choice of the atomic basis sets in other molecular calculations. To reach a certain level of accuracy in a molecular calculation we now seek those basis sets on the different atoms that have the same order of magnitude for $\Delta\varepsilon$. From Van Duyneveldt's [6] series of atomic basis sets (compare Table 3) we therefore may combine a boron (5, 3) set with a fluorine (7, 4) set, and so on. The same procedure can be followed for molecules with transition metals. Wheras to reach a certain degree of accuracy for vanadium the basis set from Roos *et al.* [4], can be used, we shall have to use in the same situation Wachters' set [5] for nickel (compare Figs. 4 and 5).

In this connection one remark has to be made. Nearly all atomic basis set calculations are on the lowest state of a certain configuration. In molecular calculations we are not interested in that specific state, but in a situation that in general will be much closer to the averaged configuration. Therefore it would be preferable to publish atomic basis set calculations for averaged configurations. Even closer to the situation in a molecule is the valence state configuration instead of the ground state configurations. It would therefore be most profitable for use in molecular calculations if these atomic calculations to obtain optimal basis sets, would also be performed for the valence state configuration. However, the influence of these changes on the results of molecular calculations will not be as large as the influence of an unbalanced basis set.

Conclusions

From the previous sections we may summarize the following conclusions:

The quality of optimized atomic basis sets depends, for atoms in the same row of the periodic system, not only on the number of basis functions, but also on the number of valence electrons.

Basis sets built up from small atomic basis sets of the same size for atoms at the beginning and at the end of atoms of the periodic system are unbalanced and usually lead to a severe deformation in the calculated charge distribution.

In order to obtain a balanced basis set in molecular calculations more basis functions have to be used for an atom at the end of a row of the periodic system than for an atom at the beginning of the row.

A simple method to find a balanced basis set is to select the atomic basis sets in such a way that the $\Delta\varepsilon$-values for all (valence) orbitals are of the same order of magnitude.

Acknowledgement. For this study use has been made of facilities at the following computers: CDC 3200, Zeeman Laboratory, University of Amsterdam; IBM 360/65, Technical University, Delft; IBM 1130, Department of Electrochemistry, Free University. These facilities are gratefully acknowledged.

References

1. Huzinaga, S.: J. chem. Physics **42**, 1293 (1965).
2. Claxton, T. A., Smith, N. A.: Theoret. chim. Acta (Berl.) **22**, 378 (1971).
3. Stewart, R. F.: J. chem. Physics **50**, 2485 (1969).
4. Roos, B., Veillard, A., Vinot, G.: Theoret. chim. Acta (Berl.) **20**, 1 (1971).
5. Wachters, A. J. H.: J. chem. Physics **52**, 1033 (1970).

6. van Duyneveldt, F. B.: I.B.M. Technical Report RJ 945 (1971).
7. Clementi, E., Raimondi, D. L.: J. chem. Physics **38**, 2628 (1963).
8. — Tables of atomic functions, Suppl. to I.B.M. J. of Research and Developm. **9**, (2), (1965).
9. — Matcha, R., Veillard, A.: J. chem. Physics **47**, 1865 (1967).
10. Mulliken, R. S.: J. chem. Physics **36**, 3428 (1962).
11. Gilbert, T. L., Bagus, P.: Private communication (1965).
12. Whitman, D. R., Hornback, C. J.: J. chem. Physics **51**, 398 (1969).
13. Basch, H., Hornback, C. J., Moskowitz, J. W.: J. chem. Physics **51**, 1311 (1969).
14. Dunning, T. H. Jr.: J. chem. Physics **53**, 2823 (1970).
15. Huzinaga, S., Arnau, C.: J. chem. Physics **52**, 2224 (1970).
16. Mulliken, R. S.: J. chem. Physics **23**, 1833, 1841, 2338, 2343 (1955).
17. Roux, M., Besnainou, S., Daudel, R.: J. Chim. physique **54**, 218 (1956).
18. — Cornille, M., Burnelle, L.: J. chem. Physics **37**, 933 (1962).
19. Kern, C. W., Karplus, M.: J. chem. Physics **40**, 205 (1964).
20. Bader, R. F. W., Beddal, P. M., Cade, P. E.: J. Amer. chem. Soc. **93**, 3095 (1971).
21. — Henneker, W. H., Cade, P. E.: J. chem. Physics **46**, 3341 (1967).
22. Lovas, F. J., Johnson, D. R.: J. chem. Physics **55**, 41 (1971).

Dr. H. B. Jansen
Chemistry Laboratory
Free University
De Lairessestraat 174
Amsterdam-Z. The Netherlands

Theoret. chim. Acta (Berl.) 27, 109--119 (1972)
© by Springer-Verlag 1972

Orbitales moléculaires localisées: structure électronique de la molécule de méthane

J. C. Barthelat et Ph. Durand

Laboratoire de Physique Quantique, Université Paul Sabatier, 118, route de Narbonne
31-Toulouse, France

Reçu le 1 mars 1972

Localized Molecular Orbitals: Electronic Structure of the Methane Molecule

Molecular orbitals localized on the C H bonds of the methane molecule are constructed by using one or two optimized spherical gaussian orbitals. If two gaussian orbitals are used, a problem of pseudodependence appears; consequently, we examine the introduction of constraints into the variational process. For the two bases we consider, the computed values of bond-length and force constant for the "breathing" vibrational mode are in good agreement with the experimental results; electronic isodensity curves are also presented.

Les orbitales moléculaires localisées sur les liaisons C-H de la molécule de méthane sont construites avec une ou deux orbitales gaussiennes sphériques optimisées en position et en grandeur. Lorsque deux orbitales gaussiennes sont utilisées, un problème de pseudodépendance des paramètres optimisés apparaît; l'introduction de contraintes dans le processus variationnel est alors étudiée. Pour les deux bases envisagées, les valeurs calculées de la longueur de la liaison C-H et de la constante de force pour le mode de vibration totalement symétrique de la molécule sont en bon accord avec l'expérience; des courbes d'isodensité électronique sont également présentées.

Mittels ein oder zwei optimalisierten Kugelgaußfunktionen werden lokalisierte MOs für die C-H-Bindungen des Methans konstruiert. Weil im Falle zweier Gaußfunktionen Pseudoabhängigkeit auftritt, wird die Einführung von Zusatzbedingungen in den Variationsprozeß untersucht. Bei beiden Basen sind die berechneten Werte für Bindungslänge und symmetrische Streckschwingung in guter Übereinstimmung mit dem Experiment.

1. Introduction

Bien des molécules peuvent être décrites en termes de liaisons localisées possédant leurs propriétés spécifiques. Ainsi la liaison C-H apparaît-elle identique à l'expérimentateur, quel que soit l'alcane considéré. Les méthodes d'orbitales moléculaires localisées ont l'avantage de donner une image des molécules en accord avec cette description: les électrons sont localisés dans le coeur des atomes, les liaisons et éventuellement les paires libres.

De nombreux modèles d'orbitales localisées ont déjà été présentés: méthode de liaison de valence, fonctions de loges [1], orbitales de liaisons localisées [2], orbitales obtenues par application d'un critère de localisation aux orbitales moléculaires délocalisées fournies par la méthode du champ autocohérent de Hartree et de Fock (H.F.) [3]. Les fonctions de base utilisées dans de tels calculs sont le plus souvent des orbitales *s*, *p*, *d*, ... de type Slater centrées sur les différents atomes de la molécule. Il en résulte que les densités électroniques associées aux différents types de liaisons ou aux paires libres sont approximativement égales à la somme des densités électroniques des atomes constituants [4].

L'emploi de bases de type Slater ne permet donc pas de mettre facilement en évidence la spécificité de la structure électronique d'une liaison chimique. Nous pensons qu'une bonne description des liaisons et des paires libres devraient s'appuyer sur des fonctions de base centrées dans les régions de grande densité électronique. En accord avec cette idée, Frost dans une série d'articles [5], a décrit un modèle localisé dans laquel chaque orbitale est représentée par une fonction gaussienne sphérique «flottante», c'est-à-dire optimisée en grandeur et en position. Il faut aussi signaler l'emploi de telles bases flottantes par Ford, Hall et Packer [6] dans la méthode du champ auto-cohérent. Les résultats satisfaisants obtenus dans les deux cas et la simplicité du calcul due à l'utilisation de fonctions gaussiennes sphériques justifient une étude plus approfondie du comportement de ce type de bases.

Dans la présente publication, les bases utilisées sont volontairement d'étendue très réduite, car il n'est pas nécessaire d'atteindre la valeur de l'énergie calculée par la résolution exacte des équations de Hartree et de Fock, pour que le modèle rende compte de façon satisfaisante des observables qui relèvent de l'état fondamental. En effet, les bases importantes introduites dans les calculs *ab initio* très élaborés améliorent pendant le processus itératif aussi bien l'état des électrons de valence que celui des électrons de coeur, bien que ceux-ci correspondent à des énergies très différentes. Les gains en énergie totale ne s'accompagnent pas forcément d'un meilleur accord avec l'expérience pour les grandeurs observables qui sont sous la dépendance des seuls électrons de valence. Aussi nous sommes-nous placés dans le cadre de l'approximation du «coeur bloqué» en associant des orbitales fixes aux électrons internes des atomes de la molécule.

2. La méthode des orbitales moléculaires localisées (Déterminant de Slater)

Soit une molécule à $N=2n$ électrons. Les orbitales moléculaires localisées sont réparties en orbitales de coeurs, orbitales de liaisons et orbitales de paires libres, chaque paire d'électrons occupant une de ces orbitales. La fonction d'onde totale qui décrit l'état fondamental du système est le déterminant de Slater:

$$\psi = \det[\phi_1(1)\,\overline{\phi_1}(2)\,\ldots\,\phi_n(N-1)\,\overline{\phi_n}(N)]\,.$$

Chaque orbitale moléculaire ϕ_p est une combinaison linéaire de fonctions gaussiennes sphériques normées χ_μ:

$$\phi_p = \sum_\mu C_{\mu p}\chi_\mu\,,$$

$$\chi_\mu = (2\alpha_\mu/\pi)^{3/4}\exp[-\alpha_\mu|\boldsymbol{r}-\boldsymbol{R}_\mu|^2]\,.$$

L'orbitale gaussienne sphérique χ_μ est caractérisée par deux paramètres son exposant α_μ et les coordonnées cartésiennes de son centre g_μ, définies par le vecteur $\boldsymbol{R}_\mu$. L'expression de l'énergie électronique dans le cas d'orbitales non orthogonales a été donnée par Löwdin [7]:

$$E_{\mathrm{el}} = 2\sum_{p,q}^{n}(p|q)\,T_{pq} + \sum_{p,q,r,s}^{n}(pq|rs)\,[2T_{pq}T_{rs}-T_{ps}T_{qr}]$$

avec

$$(p|q) = \int \phi_p(1) \left[-\frac{1}{2}\Delta_1 - \sum_{a=1}^{m} \frac{Z_a}{r_{a1}} \right] \phi_q(1)\, dv_1 ,$$

$$(pq|rs) = \int \phi_p(1)\, \phi_q(1) \frac{1}{r_{12}} \phi_r(2)\, \phi_s(2)\, dv_1\, dv_2 ,$$

m étant le nombre d'atomes de la molécule et Z_a le numéro atomique de l'atome a.

$$T_{pq} = (S^{-1})_{pq} ,$$

S est la matrice de recouvrement entre les orbitales moléculaires localisées dont l'élément pq est:

$$S_{pq} = \int \phi_p(1)\, \phi_q(1)\, dv_1 .$$

Après avoir ajouté l'énergie de répulsion nucléaire, l'énergie totale a pour expression:

$$E = E_{el} + \sum_{a>b}^{m} \frac{Z_a Z_b}{R_{ab}} .$$

Les orbitales moléculaires les mieux adaptées à la description du système sont déterminées en appliquant le principe variationnel. L'énergie totale n'est minimisée que par rapport aux paramètres des orbitales de liaison, les paramètres des orbitales de coeur étant invariants. Ceci revient à laisser les nuages électroniques associés aux liaisons se mettre en place dans le «potentiel» défini par les électrons des coeurs. La recherche du minimum d'une fonction dépendant de plusieurs paramètres est faite selon l'algorithme de Powell [8].

Les résultats que nous allons présenter concernent la molécule de méthane dans son état fondamental. Le but de cette étude détaillée de la liaison covalente C–H est de pouvoir dégager des conclusions générales valables pour d'autres liaisons de même type.

3. Calculs sur la molécule de méthane

La géométrie de la molécule est celle fournie par l'expérience [9]; la longueur de la liaison C–H est de 1,093 Å.

L'orbitale de coeur est placée sur le noyau de l'atome de carbone; nous étudierons successivement le cas où elle est décrite par 1, 2, 3 ou 4 fonctions gaussiennes. Les paramètres utilisés sont ceux du développement d'une orbitale de Slater 1*s* en gaussiennes sphériques donnés par Huzinaga [10]. La valeur de l'exposant ζ_s de l'orbitale de Slater de référence est celle donnée par Clementi et Raimondi [11] pour l'atome libre. Nous supposons ainsi que la formation des 4 liaisons C–H n'affecte pratiquement pas les électrons internes de l'atome de carbone.

A. Une orbitale gaussienne sphérique sur la liaison C–H

L'orbitale de liaison est d'abord décrite par une seule gaussienne sphérique ($N_l = 1$); son centre g est maintenu sur l'axe de la liaison C–H. L'énergie totale est minimisée par rapport à 2 paramètres: l'exposant α de l'orbitale gaussienne

Tableau 1. Cas d'une gaussienne par liaison CH ($N_l = 1$). Valeurs optimisées des paramètres et énergies en fonction du nombre de gaussiennes du coeur

N_c	α	$\frac{Cg}{CH}$	E_{min} (u.a.)	Gains en énergie (u.a.)
1[a]	0,3564	0,5980	−33,99035	0
2	0,3566	0,5975	−38,23784	4,24749
3	0,3553	0,5961	−39,01785	5,02750
4	0,3567	0,5974	−39,17902	5,18867

[a] La valeur de l'exposant α_c de la gaussienne de coeur est celle donnée par Frost [5].

et la position de son centre g. Le Tableau 1 donne les valeurs optimisées des paramètres α et $\frac{Cg}{CH}$ de l'orbitale de liaison en fonction du nombre N_c d'orbitales gaussiennes utilisées dans la description du coeur. Les valeurs optimisées des paramètres ne varient pas de façon sensible d'un cas à l'autre. Il faut en conclure que les paramètres de l'orbitale de liaison sont indépendants du plus ou moins grand degré de perfection de la description de l'orbitale de coeur.

Par contre, l'énergie totale est fortement améliorée quand on passe de 1 à 2 gaussiennes sphérique pour décrire le coeur. Dans le cas $N_c = 1$, notre calcul ne donne que 84,5% de l'énergie SCF égale à −40,20452 u.a. calculée par Arrighini *et al.* [12]. Une seule gaussienne est donc une représentation trop pauvre du coeur, et dans la suite des calculs nous ne considérerons plus ce cas. Le cas $N_c = 4$ donne déjà 97,4% de l'énergie SCF, et augmenter la base de l'orbitale de coeur au delà de $N_c = 4$ ne ferait que faire tendre insensiblement l'énergie vers la valeur de l'énergie SCF, au détriment du temps de calcul et de la simplicité du modèle, sans rien gagner sur la description des orbitales de liaisons.

B. Deux orbitales gaussiennes sphériques sur la liaison C–H

Cherchant alors à améliorer la description des orbitales de liaison, nous avons représenté chacune de ces orbitales par une combinaison linéaire de 2 gaussiennes sphériques:

$$\phi_l = C_1\chi_1(\alpha_1, g_1) + C_2\chi_2(\alpha_2, g_2).$$

L'énergie est minimisée par rapport à 5 paramètres: l'exposant α_1 de la gaussienne χ_1 et la position de son centre g_1, l'exposant α_2 de la gaussienne χ_2 et la position de son centre g_2, le rapport des coefficients C_2/C_1.

Le Tableau 2 rassemble les valeurs optimisées de ces cinq paramètres dans les différents cas où l'orbitale de coeur est décrite par 2, 3 ou 4 gaussiennes. Tous les paramètres, et en particulier C_2/C_1, accusent de fortes variations lorsqu'on tente d'améliorer la description du coeur. De plus, le processus itératif converge très lentement lors de la minimisation de l'énergie. Le problème variationnel semble donc mal défini. Les gains en énergie par rapport au cas $N_c = 2$, $N_l = 1$ sont consignés dans le Tableau 3; ils sont d'environ 0,25 u.a. lorsque N_l passe de 1 à 2, quel que soit le nombre de gaussiennes utilisées dans la description du coeur.

Tableau 2. Cas de deux gaussiennes par liaison CH ($N_l = 2$). Valeurs optimisées des paramètres et énergies en fonction du nombre de gaussiennes du coeur

N_c	α_1	$\frac{Cg_1}{CH}$	α_2	$\frac{Cg_2}{CH}$	C_2/C_1	E_{min} (u.a.)	Gains en énergie (u.a.)
2	0,6289	0,4503	0,2038	0,7544	1,3466	−38,49349	0
3	0,8422	0,3741	0,2420	0,6825	2,3963	−39,28532	0,79183
4	1,1717	0,2902	0,2783	0,6325	4,0893	−39,45699	0,96350

Tableau 3. Gains en énergie (u.a.)

N_c \ N_l	1	2
2	0	0,25565
3	0,78001	1,04748
4	0,94118	1,21915

Pour remédier à l'instabilité des paramètres optimisés vis-à-vis de la description du coeur, instabilité qui constitue pour notre modèle un grave défaut, nous avons introduit une contrainte dans le problème variationnel: l'énergie n'est donc plus minimisée que par rapport à quatre paramètres. Trois types de contrainte on été successivement étudiés:

1. les deux gaussiennes χ_1 et χ_2 interviennent avec des poids égaux, soit $C_2/C_1 = 1$
2. leurs exposants α_1 et α_2 sont égaux
3. leurs centres g_1 et g_2 sont confondus.

Les résultats sont donnés dans le Tableau 4. Pour chacune des trois contraintes considérées, on obtient un jeu de valeurs optimisées des paramètres de l'orbitale de liaison; l'écart entre deux valeurs d'un même paramètre obtenues l'une pour $N_c = 2$, l'autre pour $N_c = 4$, est au maximum de l'ordre de 1%. Ces paramètres ne dépendent donc pas de l'état plus ou moins parfait de la description de l'orbitale de coeur. La pseudodépendance qui existait entre les paramètres

Tableau 4. Deux gaussiennes par liaison CH ($N_l = 2$). Stabilité des paramètres optimisés et énergies en fonction du nombre de gaussiennes du coeur

Contrainte	N_c	α_1	$\frac{Cg_1}{CH}$	α_2	$\frac{Cg_2}{CH}$	C_2/C_1	E_{min} (u.a.)	Δ (u.a.)
$C_2/C_1 = 1$	2	0,5817	0,4691	0,1955	0,8381	1	−38,48715	0,00634
	4	0,5830	0,4661	0,1954	0,8348	1	−39,43258	0,02441
$\alpha_1 = \alpha_2$	2	0,4019	0,4160	0,4019	1,2802	0,2640	−38,37120	0,12229
	4	0,4033	0,4118	0,4033	1,2754	0,2673	−39,31411	0,14288
$Cg_1 = Cg_2$	2	0,2016	0,5047	0,7001	0,5047	0,4225	−38,46695	0,02654
	4	0,2008	0,5004	0,7031	0,5004	0,4184	−39,41172	0,04527

Δ perte en énergie par rapport au cas correspondant sans contrainte (cf. Tableau 2).

dans le cas général a disparu après introduction de l'une des contraintes précédentes, sans pour cela modifier de façon sensible l'énergie totale. Les pertes en énergie sont en effet inférieures à 0,1% pour la contrainte 1, à 0,4% pour la contrainte 2 et à 0,15% pour la contrainte 3.

Pour une liaison covalente de type CH, il semble, si l'on ne considère que l'énergie, qu'il soit préférable de maintenir le rapport C_2/C_1 égal à 1; les quatre autres paramètres varient alors de façon à compenser la perte en énergie qu'entraine l'introduction d'une contrainte dans le processus variationnel.

C. Grandeurs déduites de la fonction d'onde

Il est ensuite fondamental de voir dans quelle mesure la fonction d'onde totale construite à partir de telles bases, permet d'atteindre les diverses observables qui caractérisent la molécule de méthane: densité électronique, longueur de la liaison C–H et constante de force pour le mode de vibration totalement symétrique. La comparaison a porté sur les deux bases précédemment étudiées qui nous ont paru les plus significatives:

Base I: orbitale de coeur décrite par deux fonctions gaussiennes sphériques fixes; une orbitale gaussienne sphérique sur la liaison C–H.

Base II: même description de l'orbitale de coeur; une combinaison linéaire à coefficients égaux de deux orbitales gaussiennes sphériques sur la liaison C–H.

Les Figs. 1 et 2 donnent l'allure des courbes d'isodensité électronique dans un plan contenant deux liaisons C–H. L'emploi de la base plus élaborée II ne modifie pas l'aspect général de ces courbes; une légère différence apparaît cependant dans la position du nuage électronique de liaison: l'utilisation de la base II entraine un déplacement de ce nuage d'environ 0,2 u.a. vers l'atome de carbone. Il est intéressant de remarquer par ailleurs que Walter et Cohen [13] ont obtenu à partir d'une base d'ondes planes, une image analogue pour la liaison covalente $G_e - G_e$ dans un cristal de germanium.

Pour chacune des bases envisagées, l'énergie totale a été minimisée en fonction des différents paramètres définis ci-dessus pour quatre valeurs de la longueur de liaison R_{CH} entourant la valeur expérimentale. Les mêmes calculs ont été repris sans aucune optimisation, les paramètres ayant alors les valeurs correspondant au calcul optimisé pour la distance CH expérimentale. Les résultats sont consignés dans les Tableaux 5, 6 et 7. La Fig. 3 représente les courbes correspondantes. Le calcul du rapport $(-E/T)$ où T désigne l'énergie cinétique et E l'énergie totale, a permis de constater que le théorème du viriel est quasiment satisfait au voisinage de l'équilibre. Le léger écart qui subsiste est dû au fait que le processus variationnel n'englobe pas l'orbitale de coeur.

Les résultats présentés entraînent deux remarques:

a) les paramètres optimisés varient en fonction de la distance internucléaire. Dans le cas simple de la base I, cette variation est susceptible d'une interprétation qualitative: lorsque R_{CH} augmente, pour un rapport $\frac{Cg}{\mathrm{CH}}$ sensiblement constant,

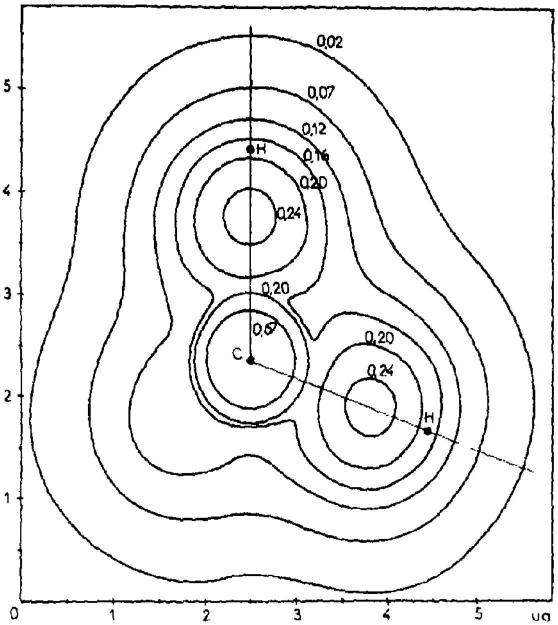

ig. 1. Base I. Densité électronique dans un plan contenant deux liaisons C–H. Toutes les grandeurs sont exprimées en u.a.

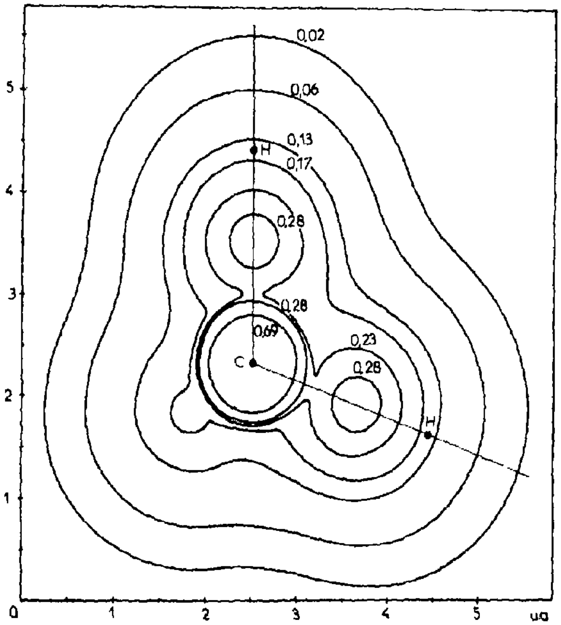

ig. 2. Base II. Densité électronique dans un plan contenant deux liaisons C–H. Toutes les grandeurs sont exprimées en u.a.

l'exposant α de la gaussienne qui constitue l'orbitale de liaison diminue. Ceci correspond à une diminution de l'énergie cinétique des électrons de liaison.

b) Les écarts en énergie entre les cas optimisés et non optimisés sont petits. Ceci laisse supposer que dans le cas de grosses molécules, il sera possible d'atteindre certaines grandeurs géométriques sans recourir à une optimisation de la base au cours du processus variationnel, donc au bout d'un temps de calcul beaucoup plus court.

Dans chacun des cas précédents, on a déterminé un polynôme du 4ème degré passant par les 5 points calculés. On en a déduit la longueur de liaison R_e et la valeur de l'énergie à l'équilibre, ainsi que la constante de force k pour la vibration totalement symétrique. Les différentes valeurs de ces observables sont comparées à un jeu de valeurs H.F. obtenu à partir d'une base minimale de Slater [14] et aux valeurs expérimentales [15, 16] dans le Tableau 8.

La valeur de R_e obtenue dans le cas de calculs optimisés est de 2,1% supérieure à la valeur expérimentale pour la base I, alors que pour la base II, elle lui est inférieure de 2,3%. Par contre, l'emploi de la base II apporte une nette amélioration dans l'évaluation de la constante de force.

Les calculs non optimisés conduisent à des courbes situées au-dessus des courbes optimisées correspondantes; les valeurs fixes choisies pour les paramètres étant celles qui correspondent à la valeur expérimentale 1,093 Å, les courbes optimisées et non optimisées sont tangentes au point $R_{CH} = 1{,}093$. Pour

Tableau 5. Base I. Variation de l'énergie en fonction de la longueur de liaison R_{CH} avec optimisation des paramètres de l'orbitale de liaison

R_{CH} (Å)	α_{opt}	$\left(\frac{Cg}{CH}\right)_{opt}$	E_{min} (u.a.)	Viriel $\left(-\frac{E}{T}\right)$
1,00	0,3921	0,6042	−38,18292	0,9852
1,05	0,3725	0,6014	−38,22285	0,9981
1,093	0,3566	0,5975	−38,23784	1,0079
1,15	0,3367	0,5933	−38,23560	1,0197
1,20	0,3202	0,5871	−38,21698	1,0287

Tableau 6. Base II. Variation de l'énergie en fonction de la longueur de liaison R_{CH} avec optimisation des paramètres de l'orbitale de liaison

R_{CH} (Å)	$\alpha_{1\,opt}$	$\left(\frac{Cg_1}{CH}\right)_{opt}$	$\alpha_{2\,opt}$	$\left(\frac{Cg_2}{CH}\right)_{opt}$	E_{min} (u.a.)	Viriel $\left(-\frac{E}{T}\right)$
1,00	0,6387	0,5155	0,1957	0,7940	−38,47260	0,9977
1,05	0,6067	0,4942	0,1948	0,8167	−38,48794	1,0081
1,093	0,5817	0,4691	0,1955	0,8381	−38,48715	1,0153
1,15	0,5485	0,4260	0,2009	0,8667	−38,47249	1,0227
1,20	0,5264	0,3758	0,2129	0,8982	−38,45246	1,0259

Tableau 7. Variation de l'énergie en fonction de la longueur de liaison R_{CH} sans optimisation des paramètres

R_{CH} (Å)	Base I		Base II	
	E (u.a.)	Ecart avec le cas optimisé	E (u.a.)	Ecart avec le cas optimisé
1,00	−38,15806	0,02486	−38,44509	0,02751
1,05	−38,21789	0,00496	−38,48226	0,00568
1,093	−38,23784	0	−38,48715	0
1,15	−38,22740	0,00820	−38,46269	0,00980
1,20	−38,18972	0,02726	−38,41791	0,03455

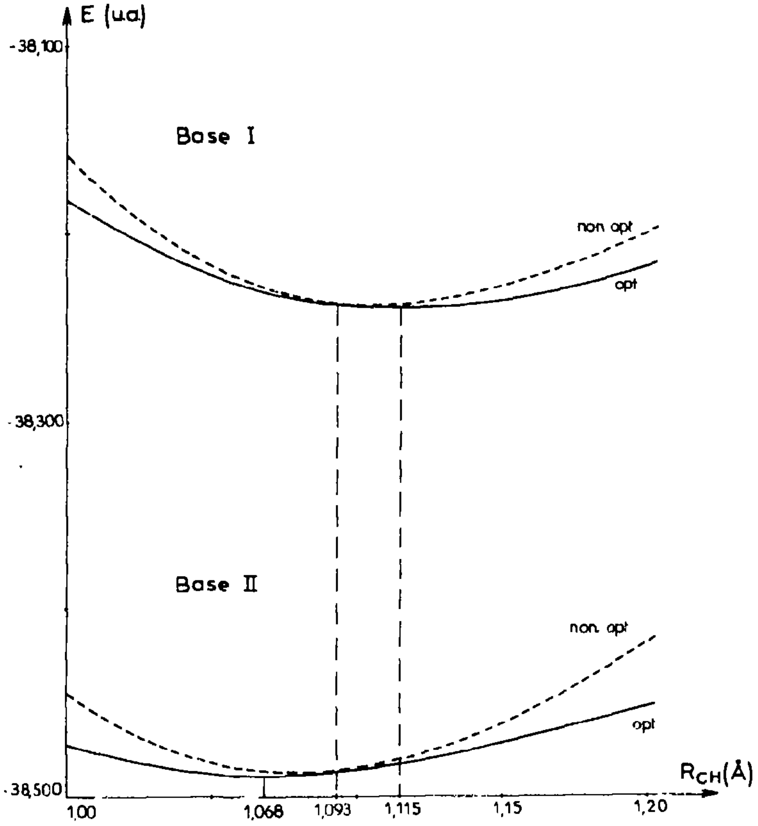

Fig. 3. Variation de l'energie totale en fonction de la distance interatomique R_{CH}

les deux bases étudiées, la valeur de R_e donnée par la courbe non optimisée est plus proche de la valeur expérimentale que la valeur de R_e obtenue après optimisation. Ceci ne signifie pas que de meilleurs résultats seront obtenus avec

Tableau 8. Distance d'équilibre, constante de force et énergie totale

		R_e (Å)	k(mdyn/Å)	E (u.a.)
Base I	opt	1,115	31,2	−38,23968
	non opt	1,106		−38,23888
Base II	opt	1,068	26,5	−38,48895
	non opt	1,081	--	−38,48801
Valeurs H.F.		1,089	23,5	−40,12827
Valeurs expérimentales		1,093	23,47	−40,525

une base non optimisée. En effet, les valeurs $(R_e)_{\text{non opt}}$ dépendent de la position du point initial optimisé et se rapprochent d'autant plus de $(R_e)_{\text{opt}}$ que ce point est voisin du point d'équilibre optimisé. Néanmoins un calcul non optimisé peut constituer une première approche lorsque la valeur de la longueur de liaison n'est que très imparfaitement connue. En ce qui concerne la constante de force, seul un calcul optimisé a un sens, et nous n'avons pas calculé sa valeur dans les cas non optimisés.

4. Conclusion

Les résultats précédents montrent clairement l'intérêt de l'emploi de bases très réduites d'orbitales gaussiennes sphériques. L'optimisation des seuls paramètres de l'orbitale de liaison permet de compenser la pauvreté de la base, aussi bien pour l'énergie totale que pour la qualité de la fonction d'onde. Que l'orbitale de liaison CH soit décrite par une ou par deux fonctions gaussiennes sphériques, l'accord du calcul avec l'expérience est satisfaisant pour les différentes observables examinées: en particulier la longueur de la liaison C–H est obtenue à 2% près. Les courbes d'isodensité électronique ont la même allure dans les deux cas, et donnent une image de la liaison covalente C–H en accord avec l'intuition chimique.

Sur le plan technique, nous avons remarqué que sur les cinq paramètres associés aux deux fonctions gaussiennes sphériques décrivant l'orbitale de liaison CH, quatre seulement peuvent être considérés comme indépendants. L'utilisation de contraintes est nécessaire pour assurer la stabilité du processus variationnel. Nous espérons pouvoir étendre l'expérience numérique acquise sur la molécule de méthane à d'autres molécules possédant des paires libres ou des électrons π.

Lorsque l'orbitale de liaison CH est représentée par une combinaison linéaire de deux fonctions gaussiennes sphériques, la base ainsi construite pourrait aussi trouver son utilité dans les deux cas suivants:

- au-delà du modèle à un électron, il serait intéressant de voir dans quelle mesure elle permet de rendre compte de l'essentiel des corrélations entre les électrons;
- peut-être également serait-elle bien adaptée à un calcul variationnel de la susceptibilité diamagnétique de la liaison C–H.

Remerciements. Les calculs ont été effectués sur l'ordinateur IBM 7044 de l'Institut de Calcul Numérique de l'Université Paul Sabatier. Nous tenons à remercier Monsieur R. Devilliers pour sa participation au travail de programmation.

Références

1. Aslangul, C., Constanciel, R., Daudel, R., Kottis, Ph.: Advances in quantum chemistry, ed. P. O. Löwdin. New York: Academic Press (sous presse).
2. Hoyland, J. R.: J. Amer. chem. Soc. **90**, 2227 (1968).
3. Gilbert, T. L.: Molecular orbitals in Chemistry, Physics, and Biology, p. 405, ed. P. O. Löwdin et B. Pullman. New York: Academic Press 1964.
4. Berthier, G.: Aspects de la chimie quantique contemporaine, p. 64. Colloques internationaux du C.N.R.S., n° 195, Editions du C.N.R.S. Paris (1971).
5. Frost, A. A.: J. chem. Physics **47**, 3707 (1967); J. chem. Physics **47**, 3714 (1967); J. physic Chem. **72**, 1289 (1968).
6. Ford, B., Hall, G. G., Packer, J. C.: Int. J. quant. Chemistry **4**, 533 (1970).
7. Löwdin, P. O.: J. chem. Physics **18**, 365 (1950).
8. Powell, M. J. D.: The computer journal **7**, 155 (1964).
9. Interatomic Distances, spec. publ. **18**, the Chemical Society, London. L. E. Sutton (1965).
10. Huzinaga, S.: J. chem. Physics **42**, 1293 (1965).
11. Clementi, E., Raimondi, D. L.: J. chem. Physics **38**, 2686 (1963).
12. Arrighini, G. P., Guidotti, C., Maestro, M., Moccia, R., Salvetti, O.: J. chem. Physics **49**, 2224 (1968).
13. Walter, J. P., Cohen, M. L.: Physic. Rev. Letters **26**, 17 (1971).
14. Pitzer, R. M.: J. chem. Physics **46**, 4871 (1967).
15. Jones, L. H., McDowell, R. S.: J. molecular Spectroscopy **3**, 632 (1959).
16. Ritchie, C. D., King, H. F.: J. chem. Physics **47**, 564 (1967).

Dr. J. C. Barthelat
Laboratoire de Physique Quantique
Université Paul Sabatier
118, route de Narbonne
F-31 Toulouse
France

Theoret. chim. Acta (Berl.) 27, 121—134 (1972)
© by Springer-Verlag 1972

Open Shell CNDO Treatments on Small and Aliphatic Radicals. Electronic Spectra and Some Ground State Properties

R. Zahradník and P. Čársky
Institute of Physical Chemistry, Czechoslovak Academy of Sciences, Prague

Received April 10, 1972

Electronic spectra, ionization potentials and ground state geometries of nine radicals containing 3 or 4 atoms were studied by configuration interaction treatment based on SCF MO's (standard CNDO/2 and the version of Del Bene and Jaffé). SCF open shell procedures used were those developed by Roothaan and Longuet-Higgins, Pople (LHP). It appears that the LHP procedure is satisfactory; if based on the SCF MO's of Del Bene and Jaffé it gives results which agree fairly well with observed electronic spectra and first ionization potentials.

Elektronenspektren, Ionisierungspotentiale und Grundzustandsgeometrien von neun drei- und vieratomigen Radikalen wurden mit Hilfe der Konfigurationswechselwirkungsmethode mit SCF MO (CNDO/2 und Version nach Del Bene and Jaffé) untersucht. Es wurden die SCF "open-shell"-Verfahren nach Roothaan, Longuet-Higgins und Pople (LHP) benutzt. Es scheint daß das LHP-Verfahren zu zufriedenstellenden Ergebnissen führt; zusammen mit SCF-MO nach Del Bene und Jaffé ergibt sich bei Elektronenspektren und Ionisierungspotentialen befriedigende Übereinstimmung mit dem Experiment.

On a étudié les spectres électroniques, les potentiels d'ionisation et la géometrie de l'état fondamental de 9 radicaux contenant 3 ou 4 atomes par la méthode de l'interaction des configurations fondée sur les orbites moléculaires autocohérentes (standard CNDO/2 et la version de Del Bene et Jaffé). Les procédés autocohérents pour les couches ouvertes utilisés étaient ceux de Roothaan et de Longuet-Higgins, Pople (LHP). On voit que le procédé LHP est satisfaisant; dans le cas où il est basé sur les MO autocohérents de Del Bene et Jaffé, il donne des résultats qui sont en assez bon accord avec les spectres électroniques et les premiers potentiels d'ionisation observés.

In recent years the number of quantum chemical studies on conjugated radicals appears to be increasing [1], similarly as the number of *ab initio* studies on larger than biatomic radicals. The majority of semiempirical all-valence-electron open shell treatments has concerned calculations on spin densities, using the unrestricted INDO method; this topic will be disregarded in the present paper. The number of semiempirical studies devoted to other properties of radicals is still limited. The restricted open shell CNDO/2 treatment combined with configuration interaction was used to interpret the electronic spectrum of H_2NO [2]. Unrestricted methods were applied to determine the geometries of small radicals [3–12], ionization potentials [13–15], and the electronic spectrum of SO_3F [16]. Geometries and heats of formation were also studied by the recently developed "half-electron" method [17–20]. Several attempts were reported to estimate the structure of excited states by means of the open shell version of the CNDO/2 method [21–23].

The extended Hückel MO treatment of reactivity of small and aliphatic radicals and biradicals was reported by Hoffmann and co-workers [24].

The subject of this paper is the application of restricted open shell procedures (developed by Roothaan (R) [25] and Longuet-Higgins and Pople (LHP) [26]) in the frame of all-valence-electron methods. In the actual calculations, either the standard CNDO/2 parameter set [3, 27] or the one modified by Del Bene and Jaffé (DBJ) [28] will be adopted. For the NO_2 radical the INDO [29] and MINDO/2 [30] methods will also be employed. All these methods will be used to interpret the properties of radicals I-IX (Fig. 1) containing three or four atoms.

Electronic spectra of radicals I-IX represent the main field of our interest. Until now, semiempirical theoretical studies of the electronic spectra of radicals where rather rare [2, 16]. This is, of course, a very unsatisfactory state of affairs from the view-point of free radical chemistry, because the electronic spectroscopy gains its true importance [32] only if effectively combined with quantum chemical calculations.

Just as with π-electron semiempirical calculations, we think that here also one should investigate the range of properties and structural types amenable to the treatment based on a given parameter set and, more specifically, whether this parameter set gives fair agreement with both ground and excited state properties. Therefore we shall also consider heats of formation (in a later paper), molecular geometries, dipole moments, and ionization potentials.

Description of Calculations

If the procedure of Longuet-Higgins and Pople [26] is used, the F matrix elements are exactly the same as those given in the CNDO scheme for closed-shell systems [3]. The only differences concern the density matrix, which is now defined as

$$P_{\mu\nu} = \sum_{i=1}^{m-1} 2c_{i\mu}c_{i\nu} + c_{m\mu}c_{m\nu} \tag{1}$$

where m is an index of the singly occupied nondegenerate molecular orbital (SOMO), and a slightly modified expression for the total SCF energy (without core-core repulsions)

$$E = \sum_{i=1}^{m-1} \varepsilon_i + \frac{1}{2}\varepsilon_m + \frac{1}{2}\sum_{\mu}\sum_{\nu} P_{\mu\nu}H^c_{\mu\nu} - \frac{1}{4}J_{mm}, \tag{2}$$

where ε_i and $H^c_{\mu\nu}$ are orbital energies and core matrix elements, respectively, and J_{mm} is the Coulomb repulsion integral for the SOMO:

$$J_{mm} = \iint \varphi_m(1)\,\varphi_m(2)\,\frac{e^2}{r_{12}}\,\varphi_m(1)\,\varphi_m(2)\,d\tau_1\,d\tau_2\,. \tag{3}$$

Further, if

$$\varphi_m = \sum_{\varrho} c_{m\varrho}\chi_{\varrho}\,,$$

we obtain

$$J_{mm} = \sum_{\mu}\sum_{\nu} c^2_{m\mu}c^2_{m\nu}\gamma_{\mu\nu}\,, \tag{4}$$

where $\gamma_{\mu\nu}$ is the electronic repulsion integral in terms of AO.

In the Roothaan method the F matrix is expressed in the form

$$F_{\mu\nu} = H^c_{\mu\nu} + 2J_{C,\mu\nu} - K_{C,\mu\nu} + 2J_{0,\mu\nu} - K_{0,\mu\nu} + (D_T B)_{\mu\nu} + (BD_T)_{\mu\nu} - B_{\mu\nu} . \quad (5)$$

Elements of the matrices contributing to the F matrix in the CNDO approach are easily derived from those given by Adams and Lykos [33] for a π-electronic case:

$$J_{C,\mu\mu} = \sum_A D_{C,AA}\gamma_{AB} , \qquad \mu \in B , \quad (6)$$

$$K_{C,\mu\nu} = D_{C,\mu\nu}\gamma_{AB} , \qquad \mu \in A, \nu \in B , \quad (7)$$

$$J_{0,\mu\mu} = \sum_A D_{0,AA}\gamma_{AB} , \qquad \mu \in B , \quad (8)$$

$$K_{0,\mu\nu} = D_{0,\mu\nu}\gamma_{AB} , \qquad \mu \in A, \nu \in B , \quad (9)$$

$$J_{C,\mu\nu} = J_{0,\mu\nu} = 0 , \qquad \mu \neq \nu , \quad (10)$$

$$B_{\mu\nu} = 2\alpha J_{0,\mu\nu} - \beta K_{0,\mu\nu} , \quad (11)$$

$$D_{C,AA} = \sum_\mu^A D_{C,\mu\mu} , \quad (12)$$

$$D_{0,AA} = \sum_\mu^A D_{0,\mu\mu} , \quad (13)$$

$$D_{C,\mu\nu} = \sum_k c_{k\mu} c_{k\nu} , \quad (14)$$

$$D_{0,\mu\nu} = f \sum_m c_{m\mu} c_{m\nu} , \quad (15)$$

$$D_{T,\mu\nu} = D_{C,\mu\nu} + D_{0,\mu\nu} . \quad (16)$$

Here $k, m, \mu\nu, AB$ are indices which run over closed-shell and open-shell molecular orbitals, atomic orbitals, and atoms, respectively. The definitions of the various terms in Eqs. (5)–(16) are the same as those given in the original papers [3, 25, 33]. All approximations involved and semiempirical parameters adopted are either the CNDO/2 ones [3, 27] or those due to Del Bene and Jaffé [28]. In the latter we employed the following modification: we use the Mataga-Nishimoto approximation for two center repulsion integrals rather than that of Pariser and Parr. From the trends in CNDO/2 parameters we tentatively chose for boron and fluorine the following parameters in the computational scheme of Del Bene and Jaffé: $\gamma_{BB} = 10.2$ eV; $\beta^0_B = -15$; $\gamma_{FF} = 13.9$ eV; $\beta^0_F = -55$. INDO and MINDO/2 calculations closely follow the original papers [29, 30]. The geometries assumed are given in Fig. 1.

Assuming the same molecular geometry and the same MO's for both the parent ($R^{(n-1)+}$) and ionized (R^{n+}) systems, the first ionization potential can in the SCF approach (Longuet-Higgins and Pople or Roothaan) be expressed [34] as

$$-I_m = E(R^{(n-1)+}) - E(R^{n+}) = \varepsilon_m - \tfrac{1}{2} J_{mm} \quad (17)$$

where m is the index for the singly occupied MO in a radical; ε_m and J_{mm} were defined before (cf. Eqs. (2) and (3)). Eq. (17) can be called an extension of the Koopmans' theorem to radicals.

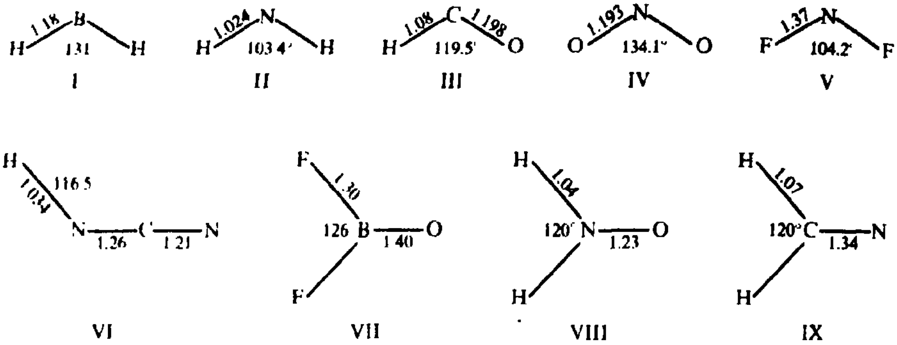

Fig. 1. Small radicals under study and geometries assumed
For radicals I–V, VI (in part), and VII experimental geometries were considered [31, 46]

For an electron removal from lower MO's the situation is more complicated because either an α-spin electron or a β-spin electron can be removed. Hence the ionized system formed can be in a singlet or a triplet state. Within the framework of the Longuet-Higgins and Pople method, the following expressions for higher ionization potentials were derived:

$$-I_i^S = \varepsilon_i - \tfrac{3}{2} K_{im}, \tag{18}$$

$$-I_i^T = \varepsilon_i + \tfrac{1}{2} K_{im}, \tag{19}$$

where

$$K_{im} = \iint \varphi_i(1)\,\varphi_m(2)\,\frac{e^2}{r_{12}}\,\varphi_m(1)\,\varphi_i(2)\,d\tau_1\,d\tau_2\,. \tag{20}$$

Assuming a singlet ionized system, the relation (18) holds, while for a triplet system Eq. (19) is valid. In the frame of the Roothaan method the following expressions hold

$$-I_i^S = \varepsilon_i - \tfrac{5}{2} K_{im}, \tag{21}$$

$$-I_i^T = \varepsilon_i - \tfrac{1}{2} K_{im}\,. \tag{22}$$

It is noteworthy that the difference in the ionization potentials I_i^S and I_i^T of the radical is equal, in the SCF approach, to the difference in transition energies, ${}^1\Delta\varepsilon_{i\to m}$ and ${}^3\Delta\varepsilon_{i\to m}$, in the ionized system

$$I_i^S - I_i^T = {}^1\Delta\varepsilon_{i\to m} - {}^3\Delta\varepsilon_{i\to m} = 2K_{im}\,. \tag{23}$$

The expression for the electron affinity for an uptake of one electron into the singly occupied molecular orbital (SOMO), φ_m, is given in the two open-shell methods as follows:

$$-A_m = \varepsilon_m + \tfrac{1}{2} J_{mm}\,. \tag{24}$$

Configuration interaction (CI) was incorporated into the computational scheme in the same way as in the procedure within a π-electron approach [35] and therefore its description need not be repeated here. With all radicals under study, the CI basis consists of configurations arising formally from one-electron transitions between several highest doubly occupied MO, the SOMO and several lowest vacant orbitals. The transition moments were calculated by means of the following formula (the x-component is considered):

$$\langle\varphi_i|\vec{x}|\varphi_j\rangle=\sum_A\left[\sum_\mu^A c_{i\mu}c_{j\mu}x_A+(c^A_{i,2s}c^A_{j,2p_x}+c^A_{j,2s}c^A_{i,2p_x})\langle\chi^A_{2s}|\vec{x}|\chi^A_{2p_x}\rangle\right] \quad (25)$$

where the second term accounts for the local transitions owing to the *sp* polarization [27, 36].

Equations (1), (2), (17)–(20), (23), (24) also apply in the INDO and MINDO/2 scheme based on the open shell procedure of Longuet-Higgins and Pople.

Calculations were performed on an IBM 7040 computer by programs written by the authors.

Results

The entries in Table 1 are the SCF characteristics of radicals I-V[1] for the five lowest ionization potentials, for the first electron affinity, and for the dipole moment.

Table 2 also presents the results for radicals I-V[1]. Here the entries are results of the limited configuration interaction calculations, viz. the energy depression of the ground state (i.e. the energy difference between the LCI and SCF ground states), number of configurations, wavenumbers of maxima, logarithms of oscillator strengths, and the data on the experimentally observed positions of absorption bands [31]. On the basis of theoretical and experimental study of electronic spectra of small closed-shell systems [31, 40] and analysis of spectral data on radicals [31], it can be anticipated the Rydberg transitions in the radicals under study are irrelevant to the understanding of the nature of absorption bands located in the near infra-red, visible, and near ultra-violet regions. Therefore, we did not think it necessary to extend the ordinary AO basis set employed in all-valence-electron methods.

Discussion

First we give the results concerning the possibility of estimating molecular geometry and ionization potentials. Then the individual systems will be discussed.

Molecular geometry. We calculated the equilibrium bond lengths and valence angles for radicals I-V by the CNDO/2-LHP method. The results are compared, in Table 3, with the experimental data on the one hand, and with calculated values obtained by the unrestricted CNDO/2 method on the other hand. With systems under study the difference between the calculated and observed bond lengths amounts to about 0.02 Å. The calculated N–F bond length is about 0.1 Å too short when compared to the assumed value. This possible discrepancy is not due to deficiencies in the open shell approach, since too short N–F bond

---

[1] Theoretical characteristics for the remaining radicals VI-IX are available from the authors on request.

Table 1. Ground state characteristics for radicals I–V: Ionization potentials (IP, eV), electron affinities (EA, eV), dipole moments (μ, D), and atomic charges

System		IP[a]					EA[b]	μ	Charges[c]		
		1	2	3	4	5			1	2	3
BH_2	CNDO/2-R	11.52(S)	19.39(T)	19.74(S)	24.55(T)	24.75(S)	−1.14	0.46	−0.047	−0.047	0.093
	CNDO/2-LHP	10.24(S)	19.38(T)	19.79(S)	24.55(T)	24.81(S)	0.14	0.52	−0.048	−0.048	0.096
	DBJ-LHP	10.16(S)	17.27(T)	17.55(S)	22.77(T)	23.17(S)	0.46	0.61	−0.040	−0.040	0.080
	Obs.[d]	9.8 ± 0.2	—	—	—	—	—		—	—	—
NH_2	CNDO/2-R	15.87(S)	17.69(T)	17.69(S)	20.33(T)	20.33(S)	−3.41	2.19	0.080	0.080	−0.160
	CNDO/2-LHP	15.87(S)	17.69(T)	17.69(S)	20.33(T)	20.33(S)	−3.41	2.19	0.080	0.080	−0.160
	DBJ-LHP	12.38(S)	14.56(T)	14.56(S)	18.07(T)	18.07(S)	0.37	2.27	0.083	0.083	−0.166
	Obs.[d]	11.4	—	—	—	—	—	—		—	—
HCO	CNDO/2-R	12.16(S)	18.26(T)	19.58(T)	19.58(S)	20.75(T)	−1.84	1.41	0.029	0.071	−0.100
	CNDO/2-LHP	11.98(S)	18.46(T)	19.47(T)	19.47(S)	20.75(T)	−1.64	1.28	0.019	0.092	−0.112
	DBJ-LHP	10.01(S)	14.27(T)	14.96(T)	14.96(S)	17.34(T)	1.70	1.83	0.066	0.101	−0.167
	Obs.[d]	9.88	—	—	—	—	—	—	—	—	—
NO_2	CNDO/2-R	13.82(S)	15.02(T)	15.62(T)	15.62(S)	21.82(S)	−0.12	0.92	0.413	−0.207	−0.207
	CNDO/2-LHP	13.55(S)	14.91(T)	15.67(S)	15.67(S)	20.67(S)	0.15	0.84	0.406	−0.203	−0.203
	DBJ-LHP	11.11 (S)	11.52 (T)	12.40 (S)	12.40(T)	15.88(S)	3.15	0.80	0.417	−0.208	−0.208
	Obs.[e]	11.23	13.01	13.60	14.06	14.51	2.30 ± 0.15[f]	0.29–0.58[g]	—	—	—
NF_2	CNDO/2-R	16.66(S)	19.12(T)	19.12(S)	20.67(T)	20.67(S)	−0.89	0.10	0.229	−0.114	−0.114
	CNDO/2-LHP	16.16(S)	19.14(T)	19.14(S)	20.80(T)	20.80(S)	−0.38	0.03	0.208	−0.104	−0.104
	DBJ-LHP	12.40(S)	15.75(T)	15.75(S)	16.53(T)	16.53(S)	2.24	0.21	0.158	−0.079	−0.079
	Obs.[h]	12.10	14.60		16.38		—	—	—	—	—

[a] Calculated through (17)–(22), symbols in parentheses stand for spin multiplicity of the ionized systems.

[b] Calculated through (24).

[c] Numbering of positions corresponds to the order of atomic numbers.

[d] Ref. [31]. – [e] Ref. [37]. – [f] Ref. [38]. – [g] Ref. [39]. – [h] Ref. [13].

Table 2. Electronic spectra of radicals I–V

System	Method	Depr.[a]	CI-basis[b]	Wavenumbers (10^{-3} cm^{-1}) and logarithms of oscillator strengths					
				$\tilde{\nu}_1$	$\log f_1$	$\tilde{\nu}_2$	$\log f_2$	$\tilde{\nu}_3$	$\log f_3$
BH_2	CNDO/2-R	−0.003	18	8.01	−2.23	58.67	−2.08	70.55	−1.33
	CNDO/2-LHP	−0.009	18	8.01	−2.23	58.60	−2.08	70.45	−1.32
	DBJ-LHP	−0.026	18	7.96	−2.24	61.22	−1.94	72.76	−1.83
	Obs.[c]	—	—	11.6–15.6	—	—	—	—	—
NH_2	CNDO/2-R	0	18	21.95	−2.14	60.04	forbidden	70.75	−1.68
	CNDO/2-LHP	0	18	21.95	−2.14	60.04	forbidden	70.75	−1.68
	DBJ-LHP	0	18	22.60	−2.09	65.09	forbidden	79.13	−1.59
	Obs.[c]	—	—	11.1–23.3	—	—	—	—	—
HCO	CNDO/2-R	−0.122	39	20.44	−2.23	49.02	−1.50	52.64	−2.41
	CNDO/2-LHP	−0.153	39	20.66	−2.23	49.85	−1.48	53.21	−2.37
	DBJ-LHP	−0.047	39	15.08	−2.42	35.98	−2.70	36.70	−1.49
	Obs.[c]	—	—	11.6–21.7	—	24.4–38.5	—	—	—
NO_2	CNDO/2-R	−0.241	39	16.61	−3.88	17.90	forbidden	19.16	−2.39
	CNDO/2-LHP	−0.231	39	16.83	−2.92	17.52	forbidden	17.87	−2.32
	DBJ-LHP	−0.034	39	11.41	−2.11	12.08	forbidden	13.00	−3.21
	Obs.[c]	—	—	—		10.0–31.2			
				$\tilde{\nu}_4$	$\log f_4$	$\tilde{\nu}_5$	$\log f_5$	$\tilde{\nu}_6$	$\log f_6$
				37.58	forbidden	42.87	forbidden	64.51	−1.31
				36.55	forbidden	43.58	forbidden	63.46	−1.21
				23.16	forbidden	30.51	forbidden	55.14	forbidden
				$\tilde{\nu}_1$	$\log f_1$	$\tilde{\nu}_2$	$\log f_2$	$\tilde{\nu}_3$	$\log f_3$
NF_2	CNDO/2-R	0.000	33	42.85	−2.10	54.03	−1.82	57.51	forbidden
	CNDO/2-LHP	−0.115	33	41.07	−2.10	55.48	−1.80	58.92	forbidden
	DBJ-LHP	−0.075	33	38.48	−1.98	63.81	forbidden	69.97	−1.27
	Obs.[c]	—	—	35.7–42.5		—	—	—	—

[a] Doublet ground state energy depression (eV).

[b] Number of configurations (A, B, C_α, C_β) taken into account; one-electron promotions between the highest occupied, singly occupied, and the lowest unoccupied MO's were considered.

[c] Ref. [31].

Table 3. Calculated and experimental bond lengths and angles

System	l θ	CNDO/2-LHP	CNDO/2-UHF[a]	Exp.[b]
BH_2	Å	1.179	—	1.18
	[°]	136.3	136.6	131
NH_2	Å	1.064	—	1.024
	[°]	106.1	107.3	103.4
NO_2	Å	1.189		1.1934
	[°]	138.7	137.7	134.1
NF_2	Å	1.227		1.37[c]
	[°]	105.8	102.5	104.2
HCO	C–H	1.109		1.08
	C–O	1.220		1.198
	[°]	131.7		119.5

[a] Ref. [3]. [b] Ref. [31]. [c] Assumed.

lengths are also predicted[2] for closed-shell systems [41]. Estimated valence angles are in all five cases higher than the observed values; the average deviation is 5°. Unfortunately, this deviation is systematic. The later experimental data [42] on the valence angle of III are in better agreement with the theory. A recent ab initio calculation yielded the value 130° [43].

Ionization potentials. Table 1 summarizes the calculated and observed first ionization potentials of radicals I-V. The DBJ-LHP values are in a fair agreement with the experimental data (the average error amounts to about 0.4 eV). As with closed shell systems, the estimated ionization potentials are too high if the repulsion integrals are calculated analytically (CNDO/2-LHP, CNDO/2-R, cf. Table 1). It is noteworthy that, with the systems under study, the extended Hückel energies of SOMO, being near (deviations lesser than 1 eV) to the $\varepsilon_m^{\mathrm{SCF}} - \frac{1}{2}J_{mm}$ terms (DBJ-LHP procedure), give fair estimates of the observed first ionization potentials. Since the extended Hückel theory entirely disregards electron spin, it is inherently incapable of giving even qualitative estimates of higher ionization potentials of radicals.

Boron dihydride (I). Boron represents a positive pole in the B–H bonds. Table 4 presents, for the sake of illustration, the CNDO/2-R values for the dipole

Table 4. Calculated (CNDO/2-R) dipole moments (D) and electronic repulsion integrals (eV) for BH_2 as a function of the H–B–H valence angle (θ in degrees)

θ	μ	J_{33}	K_{13}	K_{23}
160	0.493	12.785	0.034	0.060
140	0.541	12.691	0.088	0.147
120	0.316	12.645	0.125	0.184
100	0.054	12.637	0.146	0.177
90	0.036	12.641	0.155	0.162

---

[2] The calculations mentioned are of the INDO type, however the CNDO and INDO methods give practically the same estimations of molecular geometry, as expected on theoretical grounds (the interatomic contribution to the total energy is the same in both methods).

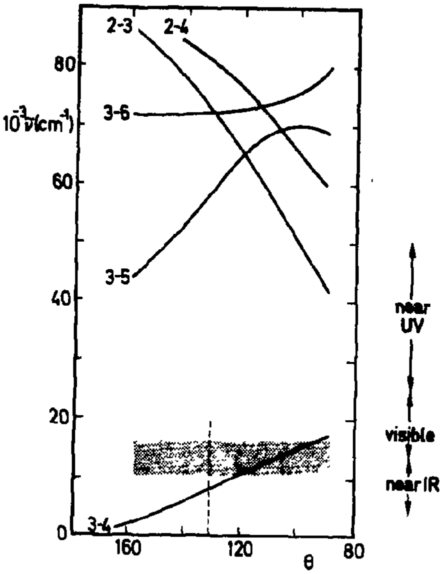

Fig. 2. Calculated CNDO/2-R transition energies in BH_2 as a function of the valence angle θ. Main configurations (weights above 90% except 2 4) are indicated. The dotted area corresponds to the observed absorption [31]. The experimental valence angle [31] is indicated by a dashed line

moment and for the repulsion integrals J_{33}, K_{13}, and K_{23} as functions of the valence angle. The experimental dipole moment can be expected to have the value of about 0.4 *D*. On the basis of values of DBJ-LHP orbital energies and of repulsion ntegrals one can expect (Table 1) in the photoelectron spectrum three peaks in he region up to 21 eV (at 10.2, 17.3(*T*), 17.6(*S*) eV).

In the electronic spectrum only one band ($^2B_1 \leftarrow {}^2A_1$) was recorded [31], which occupies the great part of the visible region up to the near infra-red region. In spite of the great effort [31], no other band was found in the near ultraviolet. Fig. 2 presents the five lowest transition energies as a function of the valence angle. With the first four transitions the configurational mixing is insignificant. The calculation successfully interprets the first observed band as a $^2B_1 \leftarrow {}^2A_1$ transition from a singly occupied lone *sp* orbital to the empty $2p_z$ boron orbital, and explains why no other band was detected in the UV region.

Nitrogen dihydride (II). As is known, the SOMO is localized in the $2p_z$ AO of nitrogen [44], and therefore the value of the J_{44} integral is high. Because the coefficients in MO's φ_1, φ_2, and φ_3 standing at that AO are zero, all K_{i4} integrals in the CNDO approach vanish. Thus theoretical values for all higher ionization potentials equal the orbital energies ε_1, ε_2, and ε_3. The increase in the ionization potential on passing from BH_2 to NH_2 is understandable: in the SCF approach this increase is connected not only with the increase in J_{mm} (localized MO) but also with the decrease in the energy of SOMO.

As with the radical I, here also only one absorption band ($^2A_1 \leftarrow {}^2B_1$) was observed, its location expanding over the visible region up to the near infra-red:

The LCI calculations accord with this experimental finding (Table 2). The electronic transition is of the same type as in I, but here the lone *sp* orbital is doubly occupied and the $2p_z$ nitrogen orbital singly occupied in the ground state. The second band is predicted to lie in the vacuum ultra-violet.

Formyl radical (III). In the electronic spectrum two bands were observed [31], one in the visible ($\tilde{A} \leftarrow \tilde{X}$) and one in the ultra-violet. Herzberg pointed out [31] that it is uncertain that the lower state of the UV band is the ground state of III. However, the LCI calculations (DBJ-LHP) support the idea that both are due to excitation from the doublet ground state; in the region of the UV band (24,400–38,500 cm^{-1}) there occur two theoretical transitions (Table 2). The lowest three transitions can be characterized as follows: the first one is a 6–7 transition from a singly occupied "non-bonding" orbital to a π^* orbital, the second and third transitions are of the $\pi \to$ "n" (5–6) and "σ" $\to$ "n" (4–6) types.

Nitrogen dioxide (IV). The DBJ-LHP calculation interprets well the first ionization potential (Table 1). As none of the CNDO computational schemes employed gives reasonable results for higher ionization potentials determined by photoelectron spectroscopy [37], we also performed open shell INDO-LHP and MINDO/2-LHP calculations. Experimental [37] and MINDO/2-LHP ionization potentials are summaried in Fig. 3. The overall correspondence between

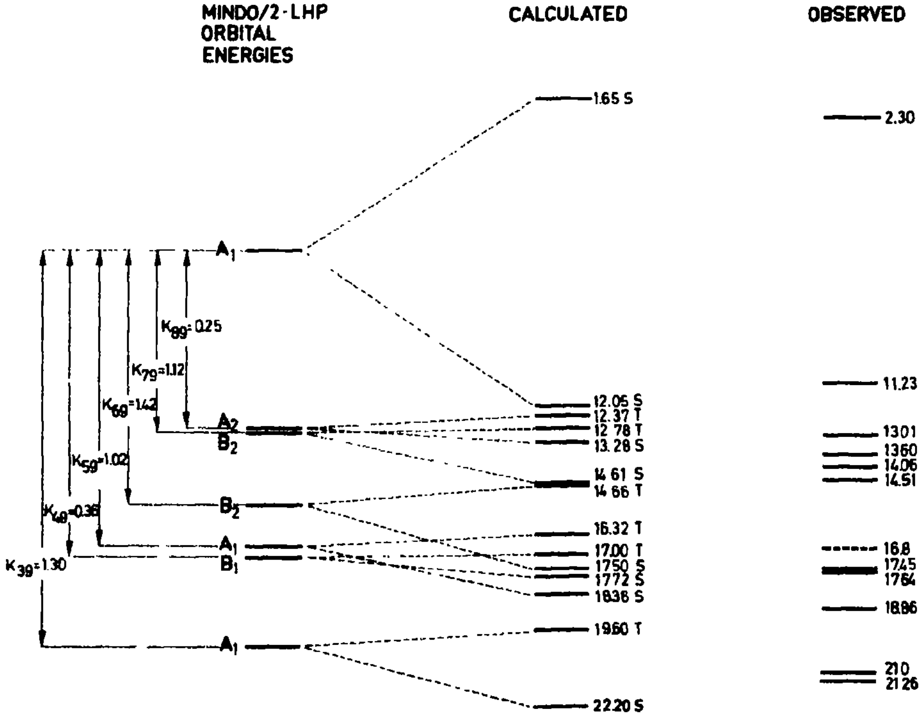

Fig. 3. Ionization potentials [37] and electron affinity [38] for NO_2. The theoretical values were calculated through Eqs. (21), (22), and (24). Values of K_{i9} exchange integrals, MO symmetries (C_{2v}), and multiplicity of states after electron removal or addition (S singlet, T triplet) are indicated

the calculated and observed potentials is fairly good, as well as that for the first electron affinity. As expected by analogy with closed shell systems, the INDO-LHP treatment gives too high values even though the agreement for the four lowest ionization potentials is reasonable.

The very nature of the absorption band of IV in the region of 10,000–31,200 cm^{-1}, its breadth and complexity, makes an analysis on this level prohibitive. It seems that this band consists of about five electronic transitions.

Nitrogen difluoride (V). From Table 1 it is apparent that a rather low dipole moment, 0.1–0.2 D, can be expected. Of the twelve MO's available, nine are doubly occupied, the tenth being the SOMO localized considerably in the nitrogen $2p_z$ AO (CNDO/2-R)

$$\varphi_{10} = 0.945\,\chi(2p_z N) - 0.230[\chi(2p_z F^1) + \chi(2p_z F^2)]\,. \tag{26}$$

Accordingly, the value of the $J_{10,10}$ integral is very high (16.53 eV; CNDO/2-LHP). For in most of the occupied MO's the coefficient standing at the nitrogen $2p_2$ AO is zero; the exchange K_{i10} integrals accordingly mostly vanish. The DBJ-LHP values (Table 1) interpret well the photoelectron spectrum [13].

The LCI calculations lead to only one electronic transition in the UV region, in agreement with experiment [31]. The transition energy afforded by the DBJ parameter set is in quantitative agreement with the experimental value.

The observed band is interpreted as a $^2A_1 \leftarrow {}^2B_1$ transition from a σ molecular orbital (φ_9) to antibonding π molecular orbital (φ_{10}), the latter being SOMO in the ground state.

HNCN radical (VI). The calculated (DBJ-LHP and CNDO/2-LHP) dipole moment amounts to 2.5 D; the estimated value (DBJ-LHP) of the first ionization potential is 10.3 eV. Self-consistency in the CNDO/2-LHP or DBJ-LHP calculations is reached after 30 iterations; the Roothaan procedure here does not converge.

The LCI-DBJ-LHP calculation predicts a weak band ($\log f = -3.0$) in the region between the visible and infrared (11,500 cm^{-1}). The second, third, and forth transitions (31,500–33,100 cm^{-1}) can be assigned to the observed band [31] at 29,100 cm^{-1}. In the four lowest excited states the following configurations predominate (in %): 7–8 (90), 8–10 (70), 8–9 (92), and 5–8 (80). The respective molecular orbitals can be characterized as follows: φ_5 as a σ orbital, φ_7 as an orbital resembling a nonbonding π-orbital in allyl but constructed from the p_y AO's (y axis lying in the molecular plane and being perpendicular to the N–C–N direction), φ_8 as a nonbonding π-orbital (SOMO), φ_9 as an antibonding π-orbital (contructed from the p_y AO's) localized in the CN bond with the N atom being terminal, and φ_{10} as an antibonding π orbital. This implies that all these four transitions should be very weakly allowed.

BOF_2 radical (VII). The work of Mathews [45, 46] strongly suggests that F_2BO arises in the BF_3–O_2 discharge. The electronic emission spectrum exhibits two bands at 17,200 and 22,400 cm^{-1}, the second being polarized in the molecular plane perpendicularly to the molecular axis. The experimental data, however, do not exclude the possible presence of the F_2BO cation and do not afford positive evidence that both bands can be assigned to transitions from the same electronic state. The LCI calculations on the electronic spectra of VII and VII^+

were performed within the DBJ computational scheme, for VII using the LHP method. Given the uncertainties in the tentative parametrization for boron and fluorine, it is possible to characterize the results of calculations in a qualitative manner as follows. Probably both observed bands cannot be assigned to the F_2BO emission, because the calculation gives only one (forbidden) $^2B_1 \leftarrow {}^2B_2$ electronic transition (17,800 cm^{-1}) in the visible region, the next calculated one being at 36,400 cm^{-1} ($\log f = -2.05$). The closed shell calculation on $F_2BO^{\oplus}$ gives the first transition, $^1A_2 \leftarrow {}^1A_1$, at 8,700 cm^{-1} (forbidden), the second one, $^1B_2 \leftarrow {}^1A_1$, at 14,000 cm^{-1} ($\log f = -2.60$) polarized in the same manner as the short-wave observed band, and the next energy lowest transition at 31,600 cm^{-1}. These values suggest that the 22,400 cm^{-1} band observed by Mathews is due to the $F_2BO^{\oplus}$ emission and the longest-wavelength band is due to $F_2BO^{\oplus}$ and/or F_2BO first calculated transition.

It is noteworthy that the SOMO resembles a $2p$ lone pair orbital in carbonyl compounds. The calculated (CNDO/2-LHP) dipole moment amounts to 0.3 D.

Nitroxide (VIII). Besides the parent radical we also took into consideration the dimethyl derivative as the simplest dialkyl derivative. CNDO/2-LHP procedures give for the dipole moment of VIII and its dimethyl derivative the values of 3.06 and 3.48 D. These values are reasonable because the dipole moments of the N—O bonds [47] in both di-*t*-butyl- and diphenylnitroxides amount to 2.4 D, and the hydrogen atoms (methyl groups) possess a positive charge.

CI-DBJ-LHP calculations underestimate the transition energy of the band in the visible and overestimate it for the band in the ultraviolet region (Table 5). In agreement with the experimental finding [47], the theory characterizes the first transition as $n \rightarrow \pi^*$. The assignment for the second band made on experimental grounds admits, besides the $\pi \rightarrow \pi^*$ transition, the $n \rightarrow \sigma^*$ transition; according to the calculations this band is due to a $\pi^* \rightarrow \sigma^*$ transition. The calculated $\pi - \pi^*$ transition energies are 60,800 and 55,000 cm^{-1}, respectively, for VIII and its dimethyl derivative. We also employed a nonplanar geometry of H_2NO predicted by the ab initio calculation [48] ($r_{NH} = 0.99$ Å, $r_{NO} = 1.34$ Å, $\sphericalangle$ HNH $= 116°$, out-of-plane angle 26°); the results, however, mean no improvement, the calculated first transition energy being 6,250 cm^{-1} and the second one 45,600 cm^{-1}.

Methyleneimino radical (IX). This radical arises as an intermediate in the photolysis of formalazine [49]

$$CH_2{=}N{-}N{=}CH_2 \xrightarrow{h\nu} 2\,CH_2{=}N^{\cdot} \rightarrow CH_2NH + HCN \qquad (27)$$

and its presence was proved by analyzing the ESR spectrum.

Table 5. Spectral data for nitroxides

	$\tilde{\nu}$(cm^{-1})	$\log f$	assignment	$\tilde{\nu}$(cm^{-1})	$\log f$	assignment
H_2NO (calcd.)	10,800	forbidden	$n \rightarrow \pi^*$	50,360	-1.79	$\pi^* \rightarrow \sigma^*$
$(CH_3)_2NO$ (calcd.)	12,750	forbidden	$n \rightarrow \pi^*$	52,750	-2.14	$\pi^* \rightarrow \sigma^*$
$(t\text{-}C_4H_9)_2NO$ (obs.[a])	22,000 24,500	0.9[b]	$n \rightarrow \pi^*$	~43,500	~3.5[b]	$\pi \rightarrow \pi^*$ or $n \rightarrow \sigma^*$

[a] Ref. [47]. [b] $\log \varepsilon$.

Since there is real hope of measuring the electronic spectrum and other properties of this radical, we offer here some predictions. The dipole moment was estimated (CNDO/2-LHP) at $2.4\,D$ and the first ionization potential (DBJ-LHP) at 10.8 eV, the ionization being from the singly occupied MO. In agreement with a previous suggestion [50], the singly occupied orbital is approximately a nonbonding orbital localized in the $2p_y$ AO of nitrogen (the x direction along the C–N bond). The LCI-DBJ-LHP calculation gives the theoretical electronic spectrum consisting of four transitions in the visible and UV regions (17,700, 20,500, 21,200, and 37,500 cm^{-1}) which are due to almost pure 6–7, 5–7, 5–6, and 4–6 electron promotions. Only the fourth transition is allowed ($\log f = -1.91$). The first transition is of the $n \rightarrow \pi^*$ type; the next ones are of the $\pi \rightarrow \pi^*$, $\pi \rightarrow n$, and $\sigma \rightarrow n$ types.

Concluding Remark

The results obtained permit the following conclusions about the utility of various open shell treatments considered in this paper. As with conjugated radicals [51] the method of Longuet-Higgins and Pople and the Roothaan method yield similar results, the differences mostly being unimportant from the practical point of view. It appears that computational methods appropriate for interpretation of individual properties of radicals can be chosen on the basis of experience accumulated with closed shell systems [52, 53]. Thus for estimates of molecular geometry and dipole moments the standard CNDO/2 procedure is suitable, while for ionization potentials and electronic spectra the CNDO version of Del Bene and Jaffé is to be preferred.

Acknowledgements. Several FORTRAN subroutines incorporated in our program were written by Dr. P. Rosmus and Dr. J. Vojtík. Their assistance is gratefully acknowledged.

References

1. For references see Zahradník, R., Čársky, P.: In: Progr. physic. org. Chem. (A. Streitwieser, Jr., R. W. Taft), submitted for publication.
2. Kikuchi, O.: Bull. chem. Soc. Japan **42**, 47 (1969).
3. Pople, J. A., Segal, G. A.: J. chem. Physics **44**, 3289 (1966).
4. Andrews, P. R.: J. molecular Structure **6**, 85 (1970).
5. Grimm, F. A., Godoy, J.: Chem. Physics Letters **6**, 336 (1970).
6. Underwood, G. R., Vogel, V. L.: Molecular Physics **19**, 621 (1970).
7. Benson, H. G., Bowles, A. J., Hudson, A., Jackson, R. A.: Molecular Physics **20**, 713 (1971).
8. Wood, D. E., Lloyd, R. V., Lathan, W. A.: J. Amer. chem. Soc. **93**, 4145 (1971).
9. Beveridge, D. L., Guth, E.: J. chem. Physics **55**, 458 (1971).
10. Kelkar, V. K., Balla, K. C., Khubchandani, P. G.: J. molecular Structure **9**, 383 (1971).
11. Boyd, R. J., Whitehead, M. A.: J. C. S. Dalton **1972**, 78.
12. Boyd, R. J., Whitehead, M. A.: J. C. S. Dalton **1972**, 81.
13. Cornford, A. B., Frost, D. C., Herring, F. G., McDowell, C. A.: J. chem. Physics **54**, 1872 (1971).
14. Cornford, A. B., Frost, D. C., Herring, F. G., McDowell, C. A.: Chem. Physics Letters **10**, 345 (1971).
15. Boyd, R. J., Whitehead, M. A.: J. chem. Soc. (A) Inorg. Phys. Theor. **1971**, 3579.
16. King, G. W., Santry, D. P., Warren, C. H.: J. chem. Physics **50**, 4565 (1969).
17. Baird, N. C., Dewar, M. J. S.: J. chem. Physics **50**, 1262 (1969).
18. Dewar, M. J. S., Haselbach, E.: J. Amer. chem. Soc. **92**, 590 (1970).
19. Haselbach, E.: Chem. Physics Letters **7**, 428 (1970).

20. Kollmar, H.: Chem. Physics Letters **8**, 533 (1971).
21. Nixon, R. N.: Molecular Physics **12**, 83 (1967).
22. Kroto, H. W., Santry, D. P.: J. chem. Physics **47**, 2736 (1967).
23. Kirby, G. H., Miller, K.: Chem. Physics Letters **3**, 643 (1969).
24. Hoffmann, R., Swaminathan, S., Odell, B. G., Gleiter, R.: J. Amer. chem. Soc. **92**, 7091 (1970).
25. Roothaan, C. C. J.: Rev. mod. Physics **32**, 179 (1960).
26. Longuet-Higgins, H. C., Pople, J. A.: Proc. physic. Soc. **68 A**, 591 (1955).
27. Pople, J. A., Segal, G. A.: J. chem. Physics **43**, S 136 (1965).
28. Del Bene, J., Jaffé, H. H.: J. chem. Physics **48**, 1807 (1968).
29. Pople, J. A., Beveridge, D. L., Dobosh, P. A.: J. chem. Physics **47**, 2026 (1967).
30. Bodor, N., Dewar, M. J. S., Harget, A., Haselbach, E.: J. Amer. chem. Soc. **92**, 3854 (1970).
31. Herzberg, G.: Molecular spectra and molecular structure. III. Electronic spectra and electronic structure of polyatomic molecules. New York: Nostrand Reinhold Comp. 1966.
32. Atkins, P. W., Symons, M. C. R.: The structure of inorganic radicals. Amsterdam: Elsevier Publ. Comp. 1967.
33. Adams, G. W., Lykos, P. G.: J. chem. Physics **34**, 1444 (1961).
34. Hush, N. S., Pople, J. A.: Trans. Faraday Soc. **51**, 600 (1955).
35. Zahradník, R., Čársky, P.: J. physic. Chem. **74**, 1235 (1970).
36. Giessner-Prettre, C., Pullman, A.: Theoret. chim. Acta (Berl.) **13**, 265 (1969).
37. Brundle, C. R., Neumann, D., Price, W. C., Evans, D., Potts, A. W., Streets, D. G.: J. chem. Physics **53**, 705 (1970).
38. Lifshitz, C., Hughes, B. M., Tiernan, T. O.: Chem. Physics Letters **7**, 469 (1970).
39. McClellan, A. L.: Tables of experimental dipole moments. San Francisco and London: W. H. Freeman and Comp. 1963.
40. Salahub, D. R., Sandorfy, C.: Theoret. chim. Acta (Berl.) **20**, 227 (1971).
41. Gordon, M. S., Pople, J. A.: J. chem. Physics **49**, 4643 (1968).
42. Ogilvie, J. S.: Spectrochim. Acta **23 A**, 737 (1967).
43. Claxton, T. A.: Trans. Faraday Soc. **67**, 897 (1971).
44. Walsh, A. D.: J. chem. Soc. **1953**, 2266 and the following papers.
45. Mathews, C. W., Innes, K. K.: J. molecular Spectr. **15**, 199 (1965).
46. Mathews, C. W., Innes, K. K.: J. molecular Spectr. **19**, 203 (1966).
47. Forrester, A. R., Hay, J. M., Thompson, R. H.: Organic chemistry of stable free radicals. London: Academic Press 1968.
48. Salotto, A. W., Burnelle, L.: J. chem. Physics **53**, 333 (1970).
49. Kamachi, M., Kuwata, K., Murahashi, S.: J. physic. Chem. **75**, 164 (1971).
50. Brivati, J. A., Root, K. D. J., Symons, M. C. R., Tinling, D. J. A.: J. chem. Soc. (A) **1969**, 1942.
51. Čársky, P., Zahradník, R.: Collect. czechoslov. chem. Commun. **36**, 961 (1971).
52. Jaffé, H. H.: Accounts chem. Res. **2**, 136 (1969).
53. Klopman, G., O'Leary, B.: Fort. chem. Forsch. **15**, 445 (1970).

Notes Added in Proof: 1. We found in the literature further experimental data: the electron affinity 1.21 eV for NH_2 (Buchelnikova, N. S.: Usp. fiz. nauk **65**, 351 (1958)) and the first ionization potential 10.87 eV for H_2CN (Pottie, R. F., Lossing, F. P.: J. Amer. chem. Soc. **83**, 4737 (1961)).

2. The name of our Institute was changed to The J. Heyrovský Institute of Physical Chemistry and Electrochemistry.

Dr. R. Zahradník
Dr. P. Čársky
Institute of Physical Chemistry
Czechoslovak Academy of Sciences
7 Máchova
Prague 2 – Vinohrady
Czechoslovakia

Theoret. chim. Acta (Berl.) 27, 135—145 (1972)
© by Springer-Verlag 1972

Proton Magnetic Shielding in the Water Molecule

Michał Jaszuński and Andrzej J. Sadlej
Institute of Organic Chemistry, Polish Academy of Sciences, Warsaw 42, Poland

Received March 21, 1972

The variation-perturbation uncoupled Hartree-Fock procedure of Karplus and Kolker is employed for the calculation of the second-order properties of the water molecule. The SCF MO LCGO ground state wave function was chosen and the first-order perturbed orbitals were approximated in the multiplicative form. The convergence of the method as well as the violation of the gauge independence are studied. For the preferred gauge origin at the electronic centroid the calculated proton shielding constant is 28.30 ppm and compares favourably with the experimental data (30.20, 30.03 ± 0.60 ppm). The results for the magnetic susceptibility of the water molecule are also in reasonable agreement with experimental values.

Die ungekoppelte Hartree-Fock Variationsstörungsrechnung von Karplus u. Kolker wird für die Berechnung von Eigenschaften 2. Ordnung des Wassermoleküls verwendet. Für die Berechnung wird die SCF MO SCGO-Wellenfunktion des Grundzustandes gewählt, und die gestörten Orbitale 1. Ordnung werden in der multiplikativen Form approximiert. Die Konvergenz der Methode und die Frage, ob die Eichinvarianz verletzt wird, werden untersucht. Für den gewählten Potential-Nullpunkt im Zentrum der negativen Ladungsverteilung beträgt die errechnete Protonenabschirmungskonstante 28,30 ppm in guter Übereinstimmung mit den experimentellen Werten (30.20, 30.03 ± 0.60 ppm). Die Ergebnisse für die magnetische Suszeptibilität des Wassermoleküls sind gleichfalls in vernünftiger Übereinstimmung mit dem Experiment.

Introduction

The idea of the LCGO (Linear Combination of Gaussian Orbitals) approximation [1, 2] in the Hartree-Fock-Roothaan SCF procedure stimulated a rapid progress in large scale molecular calculations and a number of reliable, near-Hartree-Fock SCF MO LCGO wave functions for polyatomic molecules is now available [3–6]. In spite of very encouraging results for the molecular energies and several one-electron first-order properties [4, 7], the SCF MO LCGO wave functions were only seldom utilized for the calculation of the second-order properties related to external field perturbations [8–11]. To get more information about the usefulness of the LCGO molecular wave functions in the perturbation calculations we have undertaken a systematic study of the second-order magnetic properties of polyatomic molecules. Also the corresponding methods in the Hartree-Fock perturbation theory have recently been analysed [12–14].

The present paper is concerned with the calculation of the magnetic second-order properties of the water molecule from the SCF MO LCGO wave functions obtained recently by Diercksen [15]. A particular attention has been paid to the problem of the proton magnetic shielding in the water molecule. The results obtained are in remarkably good agreement with experimental data and indicate the usefulness of accurate SCF MO LCGO functions for the calculation of molecular magnetic properties. They also confirm our previous conclusions about the validity of the simplified variation-perturbation method [16] in the case of pure imaginary perturbing operators [12, 13].

Method

In the Hartree-Fock approximation the accurate procedure for the calculation of the second-order energies is known as the coupled Hartree-Fock (CHF) method [17 19]. Applying this method one can circumvent almost all the sum-over-states and related problems but one has to calculate a number of two-electron integrals. Usually the corresponding solutions for the first-order perturbed orbitals u_i^1 are expressed in terms of the unperturbed virtual orbitals u_k^0 [18, 20]. However, the convergence of this expansion is rather slow [21, 22]. This can be improved by using a more general variation formulation of the CHF scheme [23] but even in this case the CHF procedure can hardly be applied to the calculation of the second-order properties of polyatomic molecules.

To avoid the computational difficulties of the CHF method several simpler, so-called uncoupled Hartree-Fock (UCHF) perturbation schemes were proposed [24 26, 12, 13]. The simplest one is due to Karplus and Kolker [16] and is based on the functional which contains only one-electron integrals. It was shown [13] that the validity of this approximate UCHF approach can be reasonably justified when the perturbation corresponds to a pure imaginary operator.

Both, the paramagnetic part of the magnetic susceptibility tensor $\chi_{\mu\nu}^p$ and the paramagnetic part of the nuclear magnetic shielding tensor $\sigma_{\mu\nu}^p(N)$ of the N-th nucleus are related to one-electron pure imaginary operators

$$H_\mu^{(1,0)}(\mathscr{H}_\mu) = \sum_{i=1}^{2n} h_\mu^{(1,0)}(i) = \sum_{i=1}^{2n} M_\mu^A(i)\,, \tag{1}$$

and

$$H_\mu^{(0,1)}(I_\mu^N) = \sum_{i=1}^{2n} h_\mu^{(0,1)}(i) = \sum_{i=1}^{2n} \frac{1}{r_{Ni}^3} M_\mu^N(i)\,, \tag{2}$$

respectively [27]. Thus, to calculate the magnetic susceptibility and the proton magnetic shielding constant for the water molecule we applied the Karplus-Kolker method. In Eqs. (1) and (2) the superscripts (n, m) refer to the order with respect to the external magnetic field $\mathscr{H}_\mu$ and nuclear magnetic moment I_μ^N of the N-th nucleus, respectively. The symbol M_μ^B $(B = A, N)$ denotes the μ-th component of the angular momentum operator with the origin at $\boldsymbol{R}_B$ and $2n$ corresponds to the number of electrons.

The tensors $\chi_{\mu\nu}^p$ and $\sigma_{\mu\nu}^p$ can be expressed in terms of the second-order energies $E_{\mu\nu}^{(2,0)}$ and $E_{\mu\nu}^{(1,1)}$

$$\chi_{\mu\nu}^p = -2E_{\mu\nu}^{(2,0)}\,, \tag{3}$$

$$\sigma_{\mu\nu}^p = E_{\mu\nu}^{(1,1)} \tag{4}$$

where (in atomic units)

$$\begin{aligned} E_{\mu\nu}^{(2,0)} &= \tfrac{1}{4}\alpha^2\, \mathscr{Re} \langle \Psi_\mu^{(1,0)} | H_\nu^{(1,0)} | \Psi^{(0)} \rangle \\ &= \tfrac{1}{2}\alpha^2\, \mathscr{Re} \sum_{i=1}^{n} \langle u_{i\mu}^{(1,0)} | h_\nu^{(1,0)} | u_i^{(0)} \rangle \end{aligned} \tag{5}$$

and

$$E_{\mu\nu}^{(1,1)} = \alpha^2 \mathcal{R}e \langle \Psi_\mu^{(1,0)} | H_\nu^{(0,1)} | \Psi^{(0)} \rangle$$
$$= 2\alpha^2 \mathcal{R}e \sum_{i=1}^{n} \langle u_{i\mu}^{(1,0)} | h_\nu^{(0,1)} | u_i^{(0)} \rangle \tag{6}$$

$\Psi_\mu^{(1,0)}$ and $\Psi_\mu^{(0,1)}$ denote the first-order perturbed $2n$-electron wave functions while $u_{i\mu}^{(1,0)}$ and $u_{i\nu}^{(0,1)}$ correspond to the first-order perturbed orbitals resulting from the perturbations (1) and (2), respectively. Greek subscripts refer to a given cartesian component of the perturbing operator. An expression similar to (5) can also be written down for the second-order energy $E_{\mu\nu}^{(0,2)}$. Although $E_{\mu\nu}^{(0,2)}$ has no direct physical meaning, its numerical values can be useful in the study of the convergence of the variation procedure.

According to Karplus and Kolker [16, 28] we shall approximate the first-order perturbed orbitals in the multiplicative form (product-form approximation)

$$u_{i\mu}^{(1,0)} = f_{i\mu}^{(1,0)} u_i^{(0)} - \sum_{k=1}^{n} \langle u_k^{(0)} | f_{i\mu}^{(1,0)} u_i^{(0)} \rangle u_k^{(0)}, \tag{7}$$

$$u_{i\mu}^{(0,1)} = f_{i\mu}^{(0,1)} u_i^{(0)} - \sum_{k=1}^{n} \langle u_k^{(0)} | f_{i\mu}^{(0,1)} u_i^{(0)} \rangle u_k^{(0)} \tag{8}$$

where $f_{i\mu}^{(1,0)}$ and $f_{i\mu}^{(0,1)}$ are the variation functions to be determined by extremizing an appropriate functional [16, 28]. It should be pointed out that both $E_{\mu\mu}^{(2,0)}$ and $E_{\mu\mu}^{(0,2)}$ are given by an extremum of the corresponding functionals and allow for an independent determination of the first-order perturbed orbitals $u_{i\mu}^{(1,0)}$ and $u_{i\mu}^{(0,1)}$. On the other hand, $E_{\mu\mu}^{(1,1)}$ is neither maximum nor minimum of an appropriate functional [28] which involves simultaneously both $u_{i\mu}^{(1,0)}$ and $u_{i\mu}^{(0,1)}$. Although Kolker and Karplus [28] in their calculations of the nuclear magnetic shielding determined these first-order perturbed orbitals by extremizing the functional for $E_{\mu\mu}^{(1,1)}$ we prefer to use the method which leads to $u_{i\mu}^{(1,0)}$ and $u_{i\mu}^{(0,1)}$ by an independent extremization of $E_{\mu\mu}^{(2,0)}$ and $E_{\mu\mu}^{(0,2)}$ respectively. Then, the energy $E_{\mu\nu}^{(1,1)}$ can be calculated from (6), or alternatively from

$$E_{\mu\nu}^{(1,1)} = \alpha^2 \mathcal{R}e \langle \Psi_\mu^{(0,1)} | H_\nu^{(1,0)} | \Psi^{(0)} \rangle . \tag{9}$$

In general Eqs. (6) and (9) become completely equivalent in the limit of the exact solution for the first-order perturbed wave functions. This equivalence will also be obtained when the same analytical form of $f_{i\mu}^{(1,0)}$ and $f_{i\mu}^{(0,1)}$ is used.

A usual procedure for the determination of the variation functions $f_{i\mu}^{(1,0)}$ and $f_{i\mu}^{(0,1)}$ is to express them in a polynomial form [16, 28, 29], e.g.,

$$f_{i\mu}^{(1,0)} = \sum_{p=1}^{L} A_{p,i\mu} g_{p\mu} \tag{10}$$

where $g_{p\mu}$ are the products of the cartesian coordinates with appropriate symmetry properties. This approximation does not shift the nodes of the unperturbed orbitals and can lead to several difficulties [28, 30]. However, this should not be very important in the calculations of the paramagnetic susceptibility and proton magnetic shielding [16, 28]. The node shift problems can be avoided by using a generalized form of the multiplicative approximation (7) [31], but for the present purposes a simple product form of $u_{i\mu}^{(1,0)}$ seems to be sufficiently accurate [28].

Having determined the linear variation coefficients $A_{p,i\mu}$ by the extremization of the Karplus-Kolker functional [16] for $E_{\mu\mu}^{(2,0)}$ we can calculate the paramagnetic parts of the magnetic susceptibility and nuclear magnetic shielding tensor. The total magnetic susceptibility and nuclear magnetic shielding tensors are given by a sum of the corresponding diamagnetic ($\chi_{\mu\nu}^{d}$ and $\sigma_{\mu\nu}^{d}$) and paramagnetic components [32]

$$\chi_{\mu\nu} = \chi_{\mu\nu}^{d} + \chi_{\mu\nu}^{p}, \qquad \sigma_{\mu\nu} = \sigma_{\mu\nu}^{d} + \sigma_{\mu\nu}^{p} \tag{11}$$

where

$$\chi_{\mu\nu}^{d} = -\tfrac{1}{2}\alpha^2 \sum_{i=1}^{n} \langle u_i^{(0)} | \boldsymbol{r}_A \cdot \boldsymbol{r}_A \delta_{\mu\nu} - r_{A\mu} r_{A\nu} | u_i^{(0)} \rangle \tag{12}$$

and

$$\sigma_{\mu\nu}^{d} = \alpha^2 \sum_{i=1}^{n} \langle u_i^{(0)} | \frac{\boldsymbol{r}_N \cdot \boldsymbol{r}_A \delta_{\mu\nu} - r_{A\mu} r_{N\nu}}{r_N^3} | u_i^{(0)} \rangle \tag{13}$$

do not involve a knowledge of the perturbed orbitals. Their accuracy is only limited by the accuracy of the unperturbed SCF functions.

For the exact theory the total magnetic susceptibility as well as the total nuclear magnetic shielding tensors should not depend on the choice of the origin $\boldsymbol{R}_A$ for the vector potential of the external magnetic field [33]. However, when an approximate theory is used this so-called gauge-invariance [32] of the final result can be violated and, in general, the results are origin-dependent. Thus, the study of the origin-dependence of $\chi_{\mu\nu}$ and $\sigma_{\mu\nu}$ provides an additional test of the accuracy of the calculated properties. Moreover, Chan and Das pointed out that there are some gauge origins which are better than others [33]. For the magnetic susceptibility the gauge origin at the electronic centroid [33], which maximizes the absolute value of the diamagnetic contribution, appears to be the best one. The same point is considered as a good one for the calculation of the nuclear magnetic shielding, though it does not lead to the extremum of the corresponding diamagnetic contribution. Sometimes the gauge origin which gives vanishing paramagnetic contribution to the nuclear magnetic shielding is considered as the best one [34, 35] but, in general, its determination requires a previous knowledge of $\sigma_{\mu\nu}$.

In the present calculations we have chosen two different origins for the vector potential of the external magnetic field and we studied the violation of the gauge invariance for both the magnetic susceptibility and nuclear magnetic shielding tensor. As it was mentioned, the paramagnetic contribution to $\sigma_{\mu\nu}$ was determined by using Eq. (6) or Eq. (9) with the first-order perturbed orbitals obtained by the extremization of the functionals corresponding to $E_{\mu\mu}^{(2,0)}$ [16] or $E_{\mu\mu}^{(0,2)}$. Some further details of the present approach are described in the next Section.

Calculations

All the results presented in this paper were obtained with the SCF MO LCGO wave function computed recently by Diercksen [15] and we refer to his paper for its complete description and discussion. It should be pointed out that this wave function corresponds to the experimental geometry of the water molecule and the atomic coordinates (in a.u.) are given by: O(0, 0, 0), H1(−1.10717, 0, 1.43045), H2(−1.10717, 0, −1.43045) (see also Fig. 1 of Ref. [15]).

The variation functions $f_{i\mu}^{(1,0)}$ and $f_{i\mu}^{(0,1)}$ were expressed in the form (10) with the same set of $g_{p\mu}$ functions in both cases. For the x-component the following g_{px} functions have been employed:

$$g_{px}: y, z, yz;\ yx^2, y^3, yz^2;\ zx^2, zy^2, z^3;\ yzx^2, y^3z, yz^3; \tag{14}$$

and the functions g_{py} and g_{pz} can be obtained from (14) by a cyclic permutation of the coordinates. The origin of the coordinate system in (14) has been chosen at the oxygen atom. Within the present form of $g_{p\mu}$ its particular choice does not have any influence on the final results. It also follows from the molecular symmetry that some of the terms included in the basis set (14) do not contribute to the second-order energies $E_{\mu\mu}^{(2,0)}$ and $E_{\mu\mu}^{(0,2)}$ depending on the component under consideration.

The form of the basis set (14) is different from that originally employed by Kolker and Karplus [16, 28]. For the sake of the computational convenience we have omitted all the terms involving the distance between an electron and a given center. The present approximation of the variation functions is similar to that recently employed by Chang [29] in the variation-perturbation study of the Faraday effect.

The integrals which appear in the Karplus-Kolker functionals [16] for $E_{\mu\mu}^{(2,0)}$ and $E_{\mu\mu}^{(0,2)}$ were calculated according to well known formulae [36, 37] with $F_m(t)$ functions [37] evaluated from the analytical approximations of Schaad and Morrell [38].

The calculations were performed for two different origins for the vector potential of the external magnetic field. The first origin has been chosen at the electronic centroid (e.c.) and the second one at the hydrogen atom which shielding constant is determined. The first choice corresponds to the prescription of Chan and Das [33] and is considered as a more justified and better than the second one. To study the convergence of the Karplus-Kolker scheme we performed the calculations of the second-order energies with first 3, 6 and 9 and with all the members of the basis set (14). The corresponding results are presented in Table 1.

According to the data of Table 1 both $E_{\mu\mu}^{(2,0)}$ and $E_{\mu\mu}^{(0,2)}$ exhibit a monotonous behaviour with respect to the number of variation parameters. Apparently, we did not reach a complete convergence for all the components of these second-order energies and the poorest result is expected for $E_{xx}^{(2,0)}$. In this latter case the molecular

Table 1. The study of the convergence of the calculated second-order energies[a]

L[b]	$-E^{(2,0)}$			$-E^{(0,2)}$			$E^{(1,1)}$		
	xx	yy	zz	xx	yy	zz	xx	yy	zz
3	0.170	0.745	0.165	0.263	0.403	0.138	3.360	4.573	0.824
6	0.170	0.913	0.165	0.277	0.416	0.138	3.360	5.838	0.824
9	0.170	0.913	0.194	0.277	0.434	0.148	3.360	5.838	0.576
12	0.189	0.938	0.198	0.287	0.440	0.151	3.656	6.261	0.647

[a] The gauge origin is taken at e.c. Both $E^{(2,0)}$ and $E^{(0,2)}$ are expressed in a.u.

$$\chi_{\mu\mu}^{p}(\text{erg/mole}\cdot\text{gauss}^2) = -2.375964\, E_{\mu\mu}^{(2,0)}$$

$E^{(1,1)}$ is given in ppm.

[b] The number of the first terms of the basis set (14) employed in the calculation.

symmetry eliminates eight terms of the largest 12-term set (14) employed in the present study. However, we believe that, in general, the calculated second-order energies should not appreciably change upon addition of higher terms in (10). It should be also pointed out that for all the components of $E^{(0,2)}$ the convergence is remarkably good.

The oscillatory behaviour of $E_{\mu\mu}^{(1,1)}$ can easily be understood if we recall that in contrary to $E_{\mu\mu}^{(2,0)}$ and $E_{\mu\mu}^{(0,2)}$ this second-order energy is neither maximum nor minimum of an appropriate functional [28]. In this paper the energy $E_{\mu\mu}^{(1,1)}$ has been calculated from Eq. (6) (or, equivalently from Eq. (9)) and, thus, depends on the accuracy of previously determined first-order perturbed orbitals. For the variation method the best first-order perturbed-orbitals are those which extremize $E_{\mu\mu}^{(2,0)}$ (or $E_{\mu\mu}^{(0,2)}$), and therefore, we treat the energies $E_{\mu\mu}^{(1,1)}$ calculated with 12-term representation of $f_{i\mu}^{(1,0)}$ ($f_{i\mu}^{(0,1)}$) as the best ones.

The data of Table 1 refer to the gauge origin at the electronic centroid. Quite similar behaviour of the gauge-dependent second-order energies is also observed for the origin taken at the hydrogen atom which shielding constant is considered. However, the convergence of $E_{\mu\mu}^{(2,0)}$ and $E_{\mu\mu}^{(1,1)}$ appears to be somewhat better when the origin of the vector potential is taken at the electronic centroid.

All the calculations reported in this paper were programed in Algol and performed on the ODRA 1204 computer. Almost all the final results obtained for the magnetic susceptibility and proton magnetic shielding in the water molecule refer to 12-term basis set (14). The corresponding paramagnetic contributions for shorter variation functions can easily be calculated from the data of Table 1.

Results and Discussion

a) *Magnetic Susceptibility*

The components of the paramagnetic contribution to the magnetic susceptibility tensor were calculated according to Eq. (3). The corresponding numerical values for the gauge origin at the electronic centroid (e.c.) are shown in Table 2. They are compared with recent results of Arrighini *et al.* [39] obtained by using the CHF approach and also with the experimental data of Taft and Dailey [40].

Table 2. The paramagnetic contribution to the magnetic susceptibility of the water molecule (in erg/mole · gauss²)

	This work[a]	CHF [39]	Exp.[b] [40]
χ_{xx}^{p}	0.45	1.03	1.40
χ_{yy}^{p}	2.23	2.06	2.33
χ_{zz}^{p}	0.47	0.54	0.79
χ_{Av}^{p}	1.05	1.21	1.51

[a] These results correspond to the gauge origin at e.c. while the CHF and the experimental data refer to the gauge origin at the nuclear center of mass. The difference can be estimated as $-\Delta\chi^{d}$ and does not exceed 0.02 erg/mole · gauss².

[b] There are also several other experimental data [45, 46] but the differences are unimportant from the point of view of the present comparison.

Table 3. Total magnetic susceptibility of the water molecule (in erg/mole gauss^2)

	This work		Reference theoretical results				Exp.[g]
	I[a]	II[b]	CHF[c]	VP[d]	GIAO[e]	DG[f]	
χ_{xx}	−14.88	−14.48	−14.55	−14.56	−13.70	−12.10	−13.5 ± 2.0
χ_{yy}	−14.21	−11.85	−14.35	−14.41	−12.67	−13.27	−13.7 ± 1.8
χ_{zz}	−13.99	−13.81	−14.22	−13.68	−12.15	−11.68	−12.1 ± 1.6
χ_{Av}	−14.36	−13.38	−14.37	−14.22	−12.84	−12.38	−13.1 ± 1.8

[a] Gauge origin at e.c.

[b] Gauge origin at the hydrogen.

[c] CHF results of Arrighini *et al.* [39] calculated using an extended STO basis set function. The gauge origin is at the nuclear center of mass.

[d] Variation-perturbation results for the LCGO wavefunction of Neumann and Moskowitz [4] with first three terms of (14) [49]. The gauge origin is at the oxygen.

[e] Calculated using the gauge invariant approach [47] with the SCF function of Ellison and Shull [48].

[f] Variation-perturbation results of Das and Ghose [43] obtained with approximate localized orbitals. The gauge origin is at the electronic centroid.

[g] The experimental data from Ref. [40] for the gauge origin at the nuclear center of mass. See also Footnote b to Table 2.

From the point of view of the theory involved in the present approach a comparison with the CHF results seems to be especially important. According to [12] and [13] the Karplus-Kolker scheme has a reliable justification for pure imaginary perturbations and the calculated paramagnetic contributions to the magnetic susceptibility should not differ remarkably from the corresponding CHF values. This is observed for the y- and z-component. A worse result for χ^p_{xx} can be explained by the fact, that $f_{ix}^{(1,0)}$ has, by symmetry, only four non-zero variation parameters while for e.g. $f_{iz}^{(1,0)}$ almost all the terms (14) do contribute to the second-order energy. It should be also pointed out that the CHF value of χ^p_{xx} agrees much better with the experimental value. In spite of some differences between the present and CHF components of the paramagnetic contribution, the rotational average χ^p_{Av} is almost the same as calculated by Arrighini *et al.* and compares favourably with the experimental value.

In Table 3 we presented a comparison of the calculated and experimental results for the total magnetic susceptibility tensor of the water molecule. Due to significant inaccuracies in the corresponding experimental data for the diamagnetic contribution one can hardly ascribe a definite priority to any theoretical result. However, it is worth attention that the results obtained with very poor wave functions are in general closer to the mean experimental value. It should be also pointed out that our variation-perturbation result for the total magnetic susceptibility tensor (with gauge origin at e.c.) is practically the same as that obtained by Arrighini *et al.* within the CHF approach with extended basis set of the Slater-type orbitals [39]. This indicates the usefulness of the SCF MO LCGO wavefunctions as well as the applicability of the simplified variation-perturbation UCHF approach to the calculation of molecular magnetic properties.

In Table 3 we have also reported our previous variation-perturbation results obtained with the SCF MO LCGO wave function of Neumann and Moskowitz [4]. Concerning the total molecular energy they obtained slightly better result than that reported by Diercksen [15] and their wave function should be closer to that corresponding to the Hartree-Fock limit. However, the components of the magnetic susceptibility tensor calculated with these two SCF MO LCGO wave functions do not differ significantly.

The gauge dependence of our results can be seen by a comparison of the calculated components of the total magnetic susceptibility for the origin at e.c. with those obtained for the origin at H atom. According to Moccia [41], when the results are gauge dependent, the maximum of the total magnetic susceptibility gives the best approximation to the Hartree-Fock limit. Thus, following the results of Arrighini *et al.* [39], the magnetic susceptibility obtained using the electronic centroid for the gauge origin is probably more reliable.

b) Proton Magnetic Shielding

The proton magnetic shielding is undoubtedly one of the most important molecular magnetic properties of the water molecule but there were only few attempts to calculate it non-empirically. The only reliable result is that obtained recently by Arrighini *et al.* [39, 42] by using the CHF method. The variation-perturbation scheme, similar to that applied in the present study, has also been employed by Das and Ghose [43]. However, they used rather poor ground state wave function and their results were rather disappointing. The best result of Das and Ghose does not exceed even 60 percent of the experimental value.

The present variation-perturbation results obtained with 12-term expansion for $f_i^{(1,0)}$ are shown in Table 4. The convergence of the calculated components of the proton shielding constant for the gauge origin at e.c. has been analysed in Table 1. The gauge dependence as well as the convergence for the rotational average of the shielding tensor has been presented in Table 5.

Table 4. Results for the proton magnetic shielding in the water molecule (in ppm)

	Gauge origin	Component			Rotation average
		xx	yy	zz	
σ^p	e.c.	3.66	6.26	0.65	3.52
σ^d	e.c.	23.21	14.04	37.08	24.78
σ	e.c.	26.87	20.30	37.73	28.30
σ^p	H	− 76.65	−118.44	−39.01	− 78.03
σ^d	H	100.96	130.37	75.67	102.33
σ	H	24.31	11.93	36.66	24.30

Table 5. The convergence of the proton shielding constant (in ppm)

	Gauge origin	$L^a = 3$	6	9	12
σ^p_{Av}	e.c.	2.92	3.34	3.26	3.52
σ_{Av}	e.c.	27.70	28.12	28.04	28.30
σ^p_{Av}	H	−79.00	−78.37	−78.31	−78.03
σ_{Av}	H	23.33	23.96	24.02	24.30

[a] See footnote b to Table 1.

The experimental rotation average of the proton shielding constant in the water molecule is estimated as 30.20 ppm [4] or 30.03 ± 0.60 ppm [44]. Hence, according to the data of Table 5, the results obtained for each gauge origin improve upon the addition of new variation parameters. The best result, 28.30 ppm, is apparently for the gauge origin chosen at the electronic centroid. This conclusion agrees with our previous remarks concerning the best gauge origin for the calculation of the magnetic susceptibility. It should be also pointed out that the best value obtained by Arrighini *et al.* [44] for a particular choice of the gauge origin as suggested by Moccia [41], is 28.94 ppm.

It follows from the data of Table 4 that shifting the gauge origin from e.c. to the shielded H atom we induce the gauge dependence of 4 ppm and according to Table 5 this gauge dependence is reduced with increasing number of terms in the variation function. It is worth attention that σ_{xx} and σ_{zz} are almost gauge-invariant, and therefore, these values appear to be more reliable than the results for σ_{yy}. This is also illustrated by the numerical data presented in Table 6. It follows from a comparison with the experimental data for the gauge origin at H atom, that the worst result is obtained for σ^p_{yy}.

In Table 6 we included also the CHF results of Arrighini *et al.* [44]. Evidently, they do not agree with the corresponding experimental values, though for the gauge origin at the central atom the agreement was relatively good [44]. This indicates a much stronger gauge-dependence of the incomplete basis set CHF calculations, than that found in the present approach.

A comparison of the total components of the shielding tensor calculated in the present paper with those obtained by Arrighini *et al.* [44] for several gauge origins is shown in Table 7. It can be seen that our values are in general better

Table 6. Paramagnetic contribution to the proton magnetic shielding for the gauge origin at the hydrogen atom (in ppm)

	This work	CHF[a]	Exp.[b]
σ^p_{xx}	− 76.65	−52.63	− 71.79
σ^p_{yy}	− 118.44	−79.18	− 107.04
σ^p_{zz}	− 39.01	−25.76	− 36.57
σ^p_{Av}	− 78.03	−52.52	− 71.80

[a] The CHF results of Arrighini *et al.* [44].

[b] The experimental data of Bluyssen *et al.* [50] taken from Ref. [44].

Table 7. A comparison of the results for the proton magnetic shielding in the water molecule (in ppm)

	Gauge origin	σ_{xx}	σ_{yy}	σ_{zz}	σ_{Av}
This work	e.c.	26.87	20.30	37.73	28.30
This work	H	24.31	11.93	36.66	24.30
CHF[a]	O	27.57	20.60	36.52	28.23
CHF[a]	H	50.21	50.98	49.52	50.24
Exp.[b]	--	—	—	--	30.20

[a] Results of Arrighini *et al.* [44].

[b] Taken from Ref. [4].

than those calculated within the CHF scheme. It follows that when the gauge origin is chosen at e.c., both the CHF method and the Karplus-Kolker variation-perturbation scheme lead to remarkably good results. However, comparing the calculations for the gauge origin at H atom we find that the Karplus-Kolker scheme gives much better estimate of the proton shielding constant. Undoubtedly, extending the basis set of virtual orbitals one would obtain better results within the CHF approach. This, however, increases enormously the computational effort involved in this scheme. On the other hand, using the variation-perturbation method of Karplus and Kolker we can greatly simplify the computations without a considerable loss of accuracy of final results. The present calculations indicate also the usefulness of the SCF MO LCGO wave functions which allow for a very simple evaluation of all the one-electron integrals appearing in the treatment.

The results of the calculations described in this paper confirm our previous conclusions [12, 13] that for pure imaginary perturbing operators the corrections to the Karplus-Kolker scheme derived from the CHF functional should not be very important. However, one has also to point out some intrinsic limitations of the Karplus-Kolker method which do not arise in the CHF approach. The derivation of the Karplus-Kolker functional is based on the multiplicative approximation (7) for the first-order perturbed orbitals [16, 13]. A rigid form of the perturbed wave functions cannot account for the necessary node shifts, and thus, some properties, e.g., the magnetic shielding constants of heavy nuclei, cannot be accurately calculated within the Karplus-Kolker scheme [28]. Apparently, these difficulties do not arise when the first-order perturbed orbitals are expanded into a set of virtual Hartree-Fock orbitals [51] and from this point of view the method applied by Arrighini *et al.* [22, 39, 44, 51] seems to be more successful. However, in the case of the magnetic susceptibility and proton shielding, the rigidity of the multiplicative approximation appears to be less important [16, 28].

To summarize our discussion we conclude that the Karplus-Kolker scheme can be considered as a simple, practical and probably sufficiently accurate method for the calculation of molecular magnetic susceptibilities and proton shielding constants. To support this conclusion the corresponding calculations for other molecules are in progress. Also the problem of the proton magnetic shielding in the hydrogen-bonded systems will be considered in a subsequent paper.

Acknowledgements. We wish to acknowledge the kindness of Dr. G. H. F. Diercksen who sent us the original computer outputs of his SCF MO LCGO wavefunctions for the water molecule and also the computer outputs of some one-electron properties.

References

1. Boys, S. F.: Proc. Roy. Soc. (London) A **200**, 542 (1950).
2. Nesbet, R. K.: J. chem. Physics **32**, 1114 (1960).
3. Kollman, P. A., Allen, L. C.: J. chem. Physics **52**, 5085 (1970).
4. Neumann, D., Moskowitz, J. W.: J. chem. Physics **49**, 2056 (1968).
5. Neumann, D., Moskowitz, J. W.: J. chem. Physics **50**, 2216 (1969).
6. Hankins, D., Moskowitz, J. W., Stillinger, F. H.: J. chem. Physics **53**, 4544 (1970).
7. Dunning, Jr., T. H.: J. chem. Physics **55**, 3958 (1971).
8. Lim, T.-K., Linder, B.: Theoret. chim. Acta (Berl.) **19**, 38 (1970).
9. Liebmann, S. P., Moskowitz, J. W.: J. chem. Physics **54**, 3622 (1971).

10. Jaszuński, M., Okniński, A., Sadlej, A. J.: Acta physica polon.
11. Kowalewski, J., Vestin, R., Roos, B.: Chem. Physics Letters **12**, 25 (1971).
12. Sadlej, A. J.: Chem. Physics Letters **8**, 100 (1971).
13. Sadlej, A. J.: Molecular Physics **21**, 145 (1971); **21**, 959 (1971).
14. Sadlej, A. J., Jaszuński, M.: Molecular Physics **22**, 761 (1971).
15. Diercksen, G. H. F.: Theoret. chim. Acta (Berl.) **21**, 335 (1971).
16. Karplus, M., Kolker, H. J.: J. chem. Physics **38**, 1263 (1963).
17. Peng, H. W.: Proc. Roy. Soc. (London) A **178**, 499 (1941); Allen, L. C.: Physic. Rev. **118**, 167 (1960).
18. Stevens, R. M., Pitzer, R. M., Lipscomb, W. N.: J. chem. Physics **38**, 550 (1963).
19. Diercksen, G. H. F., McWeeny, R.: J. chem. Physics **44**, 3554 (1966).
20. Moccia, R.: Theoret. chim. Acta (Berl.) **8**, 192 (1967).
21. Stevens, R. M., Karplus, M.: J. chem. Physics **49**, 1094 (1968).
22. Arrighini, G. P., Maestro, M., Moccia, R.: J. chem. Physics **49**, 882 (1968).
23. Lahiri, J., Mukherji, A.: J. physic. Soc. Japan **21**, 1178 (1966).
24. Dalgarno, A.: Proc. Roy. Soc. (London) A **251**, 282 (1959).
25. Tuan, D. F.-T., Davidz, A.: J. chem. Physics **55**, 1286 (1971).
26. Langhoff, P. W., Karplus, M., Hurst, R. P.: J. chem. Physics **44**, 505 (1966).
27. Davies, D. W.: The theory of the electric and magnetic properties of molecules. J. Wiley 1967.
28. Kolker, H. J., Karplus, M.: J. chem. Physics **41**, 1259 (1964).
29. Chang, T. Y.: J. chem. Physics **54**, 1433 (1971).
30. Langhoff, P. W., Hurst, R. P.: Physic. Rev. A **139**, 1415 (1965).
31. Okniński, A., Sadlej, A. J.: Acta physica polon., submitted for publication.
32. O'Reilly, D. E.: Progr. N. M. R. Spectroscopy **2**, 1 (1967).
33. Chan, S. I., Das, T. P.: J. chem. Physics **37**, 1527 (1962).
34. Kern, C. W., Lipscomb, W. N.: J. chem. Physics **37**, 260 (1962).
35. Sadlej, A. J.: Molecular Physics **19**, 749 (1970).
36. Taketa, H., Huzinaga, S., O-ohata, K.: J. physic. Soc. Japan **21**, 2314 (1966).
37. Kern, C. W., Karplus, M.: J. chem. Physics **43**, 415 (1965).
38. Schaad, L. J., Morrell, G. O.: J. chem. Physics **54**, 1965 (1971).
39. Arrighini, G. P., Guidotti, C., Salvetti, O.: J. chem. Physics **52**, 1037 (1970).
40. Taft, H., Dailey, B. P.: J. chem. Physics **51**, 1002 (1969).
41. Moccia, R.: Chem. Physics Letters **5**, 265 (1970).
42. Arrighini, G. P., Guidotti, C.: Chem. Physics Letters **6**, 435 (1970).
43. Das, T. P., Ghose, T.: J. chem. Physics **31**, 42 (1959).
44. Arrighini, G. P., Maestro, M., Moccia, R.: J. chem. Physics **52**, 6411 (1970).
45. Kukolich, S. G.: J. chem. Physics **50**, 3751 (1969).
46. Verhoeven, J., Dymanus, A.: J. chem. Physics **52**, 3222 (1970).
47. Pan, Y., Hameka, H. F.: J. chem. Physics **53**, 1265 (1970).
48. Ellison, F. O., Shull, H.: J. chem. Physics **21**, 1420 (1953); **23**, 2348 (1955).
49. Jaszuński, M., Okniński, A., Sadlej, A. J.: unpublished results.
50. Bluyssen, H., Dymanus, A., Reuss, J., Verhoeven, J.: Physics Letters A **25**, 584 (1967).
51. Arrighini, G. P., Maestro, M., Moccia, R.: Chem. Physics Letters **7**, 351 (1970).

Mr. Michał Jaszuński
Dr. Andrzej J. Sadlej
Institute of Organic Chemistry
Polish Academy of Sciences
Warsaw 42, Kasprzaka 44
Poland

Theoret. chim. Acta (Berl.) 27, 147—149 (1972)
© by Springer-Verlag 1972

Relationes

Über die Hartreesche Methode

HERMANN HARTMANN

Institut für Physikalische Chemie der Johann Wolfgang Goethe-Universität in Frankfurt am Main

Eingegangen am 10. Juni 1972

On the Hartree Method

A certain exactly soluble two-particle problem is treated in which also the corresponding Hartree equation can be solved exactly. A comparison of the two solutions allows a judgement on the usefulness of the Hartree method.

Für die Beurteilung der Leistungsfähigkeit von Näherungsmethoden ist es nützlich, Probleme zu studieren, die sich erstens exakt lösen lassen und auf die zweitens die in Rede stehende Näherungsmethode ohne zusätzliche Vernachlässigungen angewandt werden kann. Wir zeigen hier, daß für ein bestimmtes exakt lösbares Problem auch das System der Hartreeschen Gleichungen exakt gelöst werden kann. Anschließend vergleichen wir die auf beiden Wegen für die Energie des Grundzustandes erhaltenen Ergebnisse.

Es handelt sich um zwei gleiche lineare harmonische Oszillatoren, die durch ein zusätzliches Glied im Ausdruck für die potentielle Energie V gekoppelt sind. Es soll

$$V=\frac{c}{2}(x_1^2+x_2^2)+K x_1 x_2, \quad 0<c,\ 0\leqq|K|<c \tag{1}$$

sein, wobei x_1 und x_2 die Koordinaten der beiden Körper sind. Die Lösung der entsprechenden Schrödingergleichung

$$-\frac{\hbar^2}{2m}\left(\frac{\partial^2\psi}{\partial x_1^2}+\frac{\partial^2\psi}{\partial x_2^2}\right)+\left[\frac{c}{2}(x_1^2+x_2^2)+K x_1 x_2\right]\psi=E\psi \tag{2}$$

ist trivial. Ihr niedrigster Eigenwert ist

$$E=h\nu f\left(\frac{K}{c}\right), \quad \nu=\frac{1}{2\pi}\sqrt{\frac{c}{m}}, \tag{3}$$

$$f\left(\frac{K}{c}\right)=\frac{1}{2}\left[\sqrt{1+\frac{K}{c}}+\sqrt{1-\frac{K}{c}}\right].$$

Da für

$$0<|K|<c, \quad 1>f\left(\frac{K}{c}\right)>1/\sqrt{2} \tag{4}$$

gilt, ist E dann kleiner als $h\nu$, also kleiner als die Summe der Nullpunktsenergien zweier ungekoppelter Oszillatoren, deren Schrödingergleichung aus Gl. (2) dadurch hergestellt werden kann, daß man $K=0$ setzt. Mit der durch

$$\psi(x_1, x_2) = u_1(x_1)\, u_2(x_2) \tag{5}$$

eingeführten Bezeichnungsweise lauten die Hartreeschen Gleichungen für das untersuchte Problem

$$\begin{aligned}
-\frac{\hbar^2}{2m}\frac{d^2u_1}{dx_1^2} + \left[\frac{c}{2}x_1^2 + K x_1 \int u_2(x_2)\, x_2\, u_2(x_2)\, d x_2\right] u_1 &= \varepsilon_1 u_1\\
-\frac{\hbar^2}{2m}\frac{d^2u_2}{dx_2^2} + \left[\frac{c}{2}x_2^2 + K x_2 \int u_1(x_1)\, x_1\, u_1(x_1)\, d x_1\right] u_2 &= \varepsilon_2 u_2 .
\end{aligned} \tag{6}$$

Für die Werte der beiden bestimmten Integrale setzen wir

$$\begin{aligned}
a_1 &= \int u_2(x_2)\, x_2\, u_2(x_2)\, d x_2\\
a_2 &= \int u_1(x_1)\, x_1\, u_1(x_1)\, d x_1 .
\end{aligned} \tag{7}$$

Damit nehmen die Gln. (6) folgende Form an:

$$\begin{aligned}
-\frac{\hbar^2}{2m}\frac{d^2u_1}{dx_1^2} + \left[\frac{c}{2}x_1^2 + K a_1 x_1\right] u_1 &= \varepsilon_1 u_1\\
-\frac{\hbar^2}{2m}\frac{d^2u_2}{dx_2^2} + \left[\frac{c}{2}x_2^2 + K a_2 x_2\right] u_2 &= \varepsilon_2 u_2 .
\end{aligned} \tag{8}$$

Die Koordinatentransformationen

$$\eta_1 = x_1 + \frac{K a_1}{c}, \qquad \eta_2 = x_2 + \frac{K a_2}{c} \tag{9}$$

führen diese Gleichungen schließlich in

$$\begin{aligned}
-\frac{\hbar^2}{2m}\frac{d^2u_1}{d\eta_1^2} + \frac{c}{2}\eta_1^2 u_1 &= \left[\varepsilon_1 + \frac{K^2 a_1^2}{2c}\right] u_1\\
-\frac{\hbar^2}{2m}\frac{d^2u_2}{d\eta_2^2} + \frac{c}{2}\eta_2^2 u_2 &= \left[\varepsilon_2 + \frac{K^2 a_2^2}{2c}\right] u_2
\end{aligned} \tag{10}$$

über. Das sind gewöhnliche Oszillatorgleichungen. Ihre niedrigsten Eigenwerte sind

$$\begin{aligned}
\varepsilon_1 + \frac{K^2 a_1^2}{2c} &= \frac{1}{2} h\nu\\
\varepsilon_2 + \frac{K^2 a_2^2}{2c} &= \frac{1}{2} h\nu
\end{aligned} \tag{11}$$

und daraus folgt für die Energie des Grundzustandes in der Hartreeschen Näherung

$$E_{\text{Hartree}} = \varepsilon_1 + \varepsilon_2 = h\nu - \frac{K^2}{2c}(a_1^2 + a_2^2). \tag{12}$$

Die zu den Eigenwerten (11) der Gln. (10) gehörenden Eigenfunktionen sind

$$\begin{aligned} u_1 &= u_1(\eta_1) = u_1\left(x_1 + \frac{K a_1}{c}\right) = \varphi(\eta_1) \\ u_2 &= u_2(\eta_2) = u_2\left(x_2 + \frac{K a_2}{c}\right) = \varphi(\eta_2). \end{aligned} \tag{13}$$

Dabei ist φ eine Gaussfunktion mit den Eigenschaften

$$\varphi(-z) = \varphi(z), \qquad \int_{-\infty}^{\infty} \varphi^2(z)\, dz = 1. \tag{14}$$

Da u_1 vom Parameter a_1 und u_2 vom Parameter a_2 abhängen, sind die Definitionsgleichungen (7) Beziehungen zwischen a_1 und a_2. Mit Gl. (13) folgen unter Berücksichtigung der Beziehungen (14) aus (7) die notwendig gültigen Gleichungen

$$\begin{aligned} a_1 &= \int_{-\infty}^{\infty} u_2(x_2)\, x_2 u_2(x_2)\, dx_2 = \int_{-\infty}^{\infty} \varphi(\eta_2)\left(\eta_2 - \frac{K a_2}{c}\right)\varphi(\eta_2)\, d\eta_2 = -\frac{K a_2}{c} \\ a_2 &= \int_{-\infty}^{\infty} u_1(x_1)\, x_2 u_1(x_1)\, dx_1 = \int_{-\infty}^{\infty} \varphi(\eta_1)\left(\eta_1 - \frac{K a_1}{c}\right)\varphi(\eta_1)\, d\eta_1 = -\frac{K a_1}{c}. \end{aligned} \tag{15}$$

Diese Gleichungen werden aber nur durch das Wertepaar

$$a_1 = 0, \qquad a_2 = 0 \tag{16}$$

erfüllt. Damit folgt aus (12)

$$E_{\text{Hartree}} = h\nu. \tag{17}$$

Die Anwendung der Hartree-Methode auf das Problem (2) hat also zu einem Resultat geführt, das mit demjenigen übereinstimmt, welches man erhalten hätte, wenn man das Kopplungsglied in der potentiellen Energie $K x_1 x_2$ von vorneherein weggelassen haben würde. Der mit den Funktionen (13) berechnete Erwartungswert der Energie ist gleich der Hartreeenergie (17). Im hier behandelten Fall ist die Hartreesche Näherung eine sehr schlechte Näherung. Sie vermag gerade die Kopplungseffekte nicht zu erfassen.

Prof. Dr. Hermann Hartmann
Institut für Physikalische Chemie
der Johann Wolfgang Goethe-Universität
D-6000 Frankfurt am Main
Robert-Mayer-Straße 11
Bundesrepublik Deutschland

Theoret. chim. Acta (Berl.) 27, 151—152 (1972)
© by Springer-Verlag 1972

Least-Squares Gaussian Expansions of Atomic Orbitals

F. R. BURDEN and R. M. WILSON

Department of Chemistry, Monash University, Clayton, Victoria, Australia 3168

Received March 29, 1972

New Gaussian basis sets, which are derived from the method of least-squares, are presented for the first row atoms.

The Least-Squares Procedure

One of the simplest ways of obtaining Gaussian expansions of atomic orbitals is the method of a least-squares fit to Slater-type functions or Hartree-Fock functions. This method has been employed by Boys and Shavitt [1] in a non-simultaneous adjustment of coefficient and exponential parameters in blocks. Other workers [2] have determined the coefficients and exponents independently and Stewart [3] has recently reported small Gaussian expansions by a full matrix method for 1*s* orbitals through to 5*g* orbitals. Our basis sets for the first row atoms were obtained by simultaneously fitting both the coefficients and exponential parameters to Slater-type functions and Hartree-Fock functions by using a least-squares criterion and the Fletcher-Powell [4] minimization procedure. This allows additional flexibility to the functional form of the orbital. The exponents for the Slater functions were taken as those obtained from molecular optimizations.

The Size of the Basis Set

Various workers [5] have considered the question of determining the relative number of *s*- and *p*- Gaussian type functions needed to give minimal Slater basis accuracy in molecular calculations. It has been found that 5 or 6*s*-functions and 4 or 5*p*-functions are required for this desired accuracy. With this in mind, we have determined the atomic orbitals of the first row atoms in terms of 5-*s* Gaussian and 5-*p* Gaussian functions, except hydrogen where a 4*s* expansion is included.

The Gaussian Function Employed

In both atomic and molecular calculations Gaussian lobe functions give results of equivalent accuracy [6] as the Cartesian Gaussian functions provided the exponents (α) of the lobe function and the distance the lobe is placed from the nucleus (R) are related by the expression [7]

$$R = \gamma \alpha^{-\frac{1}{2}} \tag{1}$$

where γ is a constant, taken as 0.030.

The Tables

The tabulations include the orbital expansion vectors, the exponential parameters, the lobe distances (where appropriate) and the mean-square error. The contents are shown in the following Table 1.

Table 1 Least-squares Gaussian expansions of Slater-type functions

Atom	Range of ζ_{1s}	Range of ζ_{2s}	Range of ζ_{2p}
H	1.00–1.50		
He	1.6875		
Li	2.6865	0.6372	
Be	3.6847	0.9562	
B	4.6794–4.7194	1.33825–1.37825	1.21055–1.25055
C	5.6726–5.7126	1.6028–1.6428	1.63805–1.79805
N	6.6652–6.7052	1.9236–1.9639	1.9170–2.1370
O	7.6680–7.6580	2.2461–2.2861	2.22625–2.35625
F	8.6501–8.6901	2.5639–2.6039	2.54985–2.66985
Ne	9.6421	2.8792	2.8792

Table 2 Least-squares Gaussian expansions of Hartree-Fock functions

Atom	*State*
C, O	^3P, ^1D, ^1S
N	^4S, ^2D, ^2P
F	^2P

The present tabulation is available upon request to the authors.

Acknowledgements. The authors wish to thank the Australian Research Grants Commitee for a computing grant and the Computer Centres at Monash and Adelaide Universities where the calculations were performed.

References

1. Boys, S. F., Shavitt, I.: Proc. Roy. Soc. (London) A **254**, 487 (1960).
2. Reeves, C. M., Fletcher, R.: J. chem. Physics **42**, 4073 (1965).
   O-Ōhata, K., Taketa, H., Huzinaga, S.: J. physic. Soc. Japan **21**, 2306 (1966).
3. Stewart, R. F.: J. chem. Physics **52**, 431 (1970).
4. Fletcher, R., Powell, M. J. D.: Compt. J. **6**, 163 (1963).
5. See for example, Hornback, C. J.: Ph. D. Thesis Case Institute of Technology (1967).
6. Shih, S. *et al.*: Theoret. chim. Acta (Berl.) **18**, 277 (1970).
   Brown, R. D., Burden, F. R., Hart, B. T.: Theoret. chim. Acta (Berl.) **25**, 49 (1972).
7. Petke, J. D., Whitten, J. L., Douglas, A. W.: J. chem. Physics **51**, 256 (1969).

Dr. F. R. Burden
Department of Chemistry
Monash University
Clayton, Victoria
Australia 3168

Theoret. chim. Acta (Berl.) 27, 153—159 (1972)
© by Springer-Verlag 1972

Spin-Bahn-Wechselwirkung räumlich beschränkter Elektronensysteme*

G. Gliemann

Lehrstuhl für Theoretische Chemie der Universität Regensburg

P. Plath

Lehrstuhl für Spezielle Physikalische Chemie der Technischen Universität Berlin

Eingegangen am 6. Juli 1972

Spin-Orbit Interaction of Electron Systems Constrained to a Fixed Region of Space

The spin-orbit interaction of electronic states constrained to a fixed region of space is treated in the case of the hydrogen atom.

1. Einleitung

Das Maß für die Spin-Bahn-Wechselwirkung eines Elektrons in einem freien Atom ist wesentlich bestimmt durch den Wert des Integrals [1]

$$\overline{r^{-3}} = \int_0^\infty r^{-3} R^2(r) r^2 dr \tag{1}$$

Bei der ligandenfeldtheoretischen Behandlung von Übergangsmetallkomplexen tritt im Zusammenhang mit dem sog. „relativistischen nephelauxetischen Effekt“ die Frage auf, welchen Einfluß eine räumliche Beschränkung eines atomaren Elektronensystems auf dessen Spin-Bahn-Wechselwirkung hat. Zur Behandlung dieser Beschränkung kann man entsprechend dem Modell von Michels, de Boer u. Bijl [2] die Randbedingung des Systems ändern.

Im Fall des freien Atoms ist die natürliche Randbedingung, daß die Wellenfunktion im Unendlichen verschwindet:

$$\left.\begin{aligned} \psi(r,\theta,\phi) &\to 0 \\ R(r) &\to 0 \end{aligned}\right\} \quad \text{für} \quad r \to \infty . \tag{2}$$

Eine Beschränkung des Elektronensystems läßt sich dadurch erreichen, daß konzentrisch um das Atom (bei Übergangsmetallkomplexen wäre es das Zentralion) ein kugelsymmetrischer, extrem steiler, undurchdringlicher Potentialwall mit dem Radius r_0 gelegt wird [3]. Dadurch wird die Wellenfunktion der folgenden „künstlichen“ Randbedingung unterworfen:

$$\left.\begin{aligned} \psi(r,\theta,\phi) &= 0 \\ R(r) &= 0 \end{aligned}\right\} \quad \text{für} \quad r = r_0 . \tag{3}$$

---

* Über die grundlegenden Probleme dieser Arbeit hat einer von uns (P. P.) im Februar 1970 im Theoretisch-Chemischen Seminar an der Universität Stuttgart in einem Vortrag „Die Druckabhängigkeit atomarer Energie-Niveaus“ berichtet.

Das heißt, die Wellenfunktion muß für einen vorgegebenen endlichen Wert $r = r_0$ verschwinden. Die Forderung nach Regularität der Wellenfunktion im Ursprung bleibt davon unberührt. Für das Einelektronensystem des Wasserstoffatoms wird so aus dem atomaren Keplerproblem ein beschränktes Keplerproblem. In dieser Arbeit soll die Spin-Bahn-Wechselwirkung für ein derart beschränktes Keplerproblem behandelt werden.

Für das atomare (unbeschränkte) Keplerproblem läßt sich der Landé-Parameter [4, 5]

$$\zeta_{n,l} = \frac{Ze^2\hbar^2}{2m^2c^2a_0^3}\cdot\int_0^{\infty} r^{-3}R_{n,l}^2(r)r^2\,dr \tag{4}$$

mit dem Mittelwert [6]

$$\overline{r^{-3}} = \int_0^{\infty} r^{-3}R_{n,l}^2(r)r^2\,dr = \frac{Z^3}{n^3(l+1)(l+\frac{1}{2})l} \tag{1a}$$

in die folgende Form bringen

$$\zeta_{n,l} = \frac{e^2\hbar^2}{2m^2c^2a_0^3}\cdot\frac{Z^4}{n^3(l+1)(l+\frac{1}{2})l}\,. \tag{5}$$

Beim beschränkten Keplerproblem lautet demgegenüber die Einelektronen-Spin-Bahn-Kopplungskonstante

$$\zeta_{\mu} = \frac{Ze^2\hbar^2}{2m^2c^2a_0^3}\int_0^{r_0} r^{-3}R_{\mu}^2(r)r^2\,dr\,. \tag{6}$$

Hierin ist μ ein Parametersatz, der die Lösungsfunktionen des Radialteiles der Schrödingergleichung kennzeichnet.

2. Die Radialfunktionen beim beschränkten Keplerproblem

Für „gebundene“ Zustände, d. h., $E < 0$, hat der Radialteil der zeitunabhängigen Schrödingergleichung des Keplerproblems die allgemeinen Lösungen

$$R_{n,l}(r) = N_{n,l}\left(\frac{2r}{n}Z\right)^{l}\cdot e^{-\frac{Zr}{n}}\cdot{}_1F_1\left(-n+l+1,\,2l+2,\,\frac{2r}{n}Z\right). \tag{7}$$

${}_1F_1(a, c, br)$ mit $a = -n+l+1$ und $c = 2l+2$ ist die konfluente hypergeometrische Funktion, $N_{n,l}$ eine Normierungskonstante. Die Hauptquantenzahl n unterliegt der Beschränkung $n \geqq l+1$.

Die Nullstellen der Radialfunktionen sind identisch mit den Nullstellen der entsprechenden konfluenten hypergeometrischen Funktionen ${}_1F_1(a, c, br)$. Die *Anzahl* p der im Endlichen liegenden *positiven* Nullstellen dieser Funktionen sind durch den Wert von a bestimmt: $p \leqq -a < p+1$. Bei fester Bahndrehimpulszahl l ist p mithin durch die Größe der Hauptquantenzahl n festgelegt.

Für d-Zustände ($l = 2$) beispielsweise hat die Radialfunktion *eine* positive Nullstelle im Endlichen, wenn n Werte zwischen 3 und 4 annimmt. Für Werte von n zwischen 4 und 5 existieren *zwei* im Endlichen liegende positive Nullstellen usf., vgl. Tab. 1. Bei vorgegebenem l ist auch die *Lage* der Nullstellen vom Wert der Hauptquantenzahl n abhängig. Bei wachsendem n verschieben sich die Nullstellen

Tabelle. Positive Nullstellen der Radialfunktion $R_{n,l}(r)$ für d-Zustände

Hauptquantenzahl n	Anzahl der Nullstellen	Lage der Nullstellen
3	1	$r_1 = \infty$
$3 < n < 4$	1	$r_1 \neq \infty$
4	2	$r_1 \neq \infty, r_2 = \infty$
$4 < n < 5$	2	$r_1 \neq \infty, r_2 \neq \infty$
5	3	$r_1 \neq \infty, r_2 \neq \infty, r_3 = \infty$
...	...	...

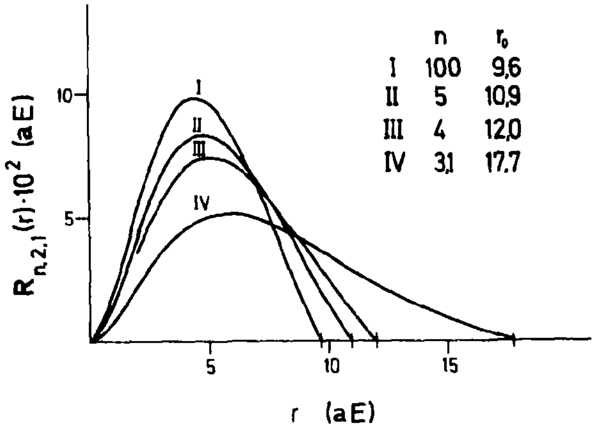

Fig. 1. Funktionsverlauf der Radialfunktion $R_{n,l,p}(r)$ für verschiedene Quantenzahlen n (mit $l = 2$, $Z_{\text{eff}} = 1$) bei Normierung auf die erste positive Nullstelle ($p = l$)

in Richtung des Ursprungs. Fig. 1 zeigt als Beispiel das Verhalten der Funktion $R_{n,2}(r)$ für einige n-Werte. (Der Funktionsverlauf ist nur bis zur ersten positiven Nullstelle aufgezeichnet.) – Mit $n \to \infty$, entsprechend $E \to 0$, nähern sich die Nullstellen asymptotisch jeweils Grenzwerten[1], die durch das zugehörige l charakterisiert sind. Zur Illustration sind in Fig. 2 die erste, zweite und dritte Nullstelle der Funktion $R_{n,l=2}(r)$ in Abhängigkeit von n dargestellt.

Für „natürliche" Randbedingungen ist die Hauptquantenzahl n ganzzahlig positiv; die konfluente hypergeometrische Funktion reduziert sich dann auf das entsprechende Laguerresche Polynom

$$ {}_1F_1\left(-n+l+1, 2l+2, \frac{2r}{n} Z\right) = L_{n+l}^{2l+1}\left(\frac{2r}{n} Z\right) \tag{8}$$

und die Normierungskonstante hat die Form [7, 8]

$$N_{n,l} = \frac{2}{n^2(2l+1)!} \sqrt{\frac{(n+l)!}{(n-l-1)!}}. \tag{9}$$

---

[1] Beim Unterschreiten dieser Grenzwerte wird $E > 0$; die zugehörigen n sind imaginär.

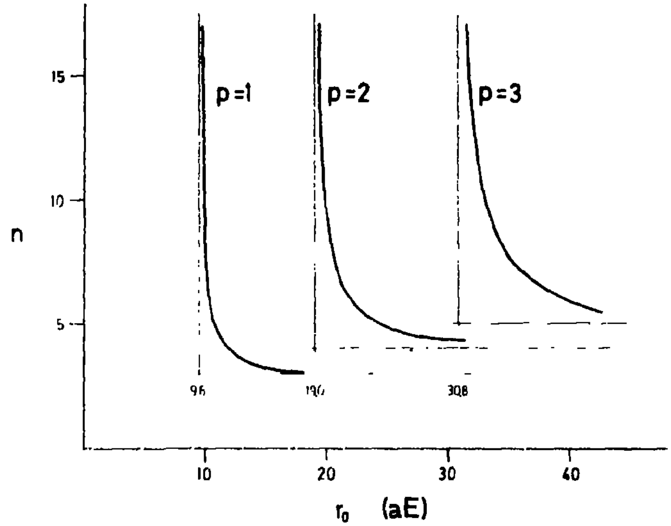

Fig. 2. Anstieg der Hauptquantenzahl n ($l = 2$, $Z_{\mathrm{eff}} = 1$) bei Beschränkung des dem Elektron zur Verfügung stehenden Bewegungsraumes für die Zustände mit $p = 1, 2, 3$

Beim beschränkten Keplerproblem sind nur solche $R(r)$ Lösungsfunktionen, die am Rand ($r = r_0$) des Potentialtopfes eine Nullstelle haben. Der oben geschilderte Zusammenhang zwischen Hauptquantenzahl n und Anzahl sowie Lage der Nullstellen der Radialfunktionen erlaubt es, die $R_{n,l}(r)$ auszuwählen, die für gegebenes r_0 die künstliche Randbedingung erfüllen: Man läßt n so lange anwachsen, bis die erste positive Nullstelle von $R_{n,l}(r)$ mit r_0 zusammenfällt[2]. Die resultierende Radialfunktion ist im Bereich $0 < r < r_0$ knotenfrei und gehört zum energetisch niedrigsten Zustand für den jeweiligen l-Wert. Bei weiter zunehmendem Wert von n rückt die zweite, dann die dritte, ..., p-te positive Nullstelle an die Stelle $r = r_0$. Dabei handelt es sich um den ersten, zweiten, ..., $(p-1)$-ten angeregten Zustand für den jeweiligen l-Wert. – Es empfiehlt sich, die $R_{n,l}(r)$ durch einen weiteren Index p zu kennzeichnen, der angibt, welche der positiven Nullstellen mit dem Rand des Potentialtopfes zusammenfällt: $R_{n,l,p}(r)$. Bei vorgegebenen l und p ist die Hauptquantenzahl n eine Funktion von r_0.[3]

Es ist rechentechnisch sehr aufwendig, zu einem vorgegebenen r_0 die zugehörige Hauptquantenzahl n zu berechnen. Vorteilhafter ist der umgekehrte Weg, die Hauptquantenzahl n vorzugeben und das zugehörige r_0 zu bestimmen. Um einen guten Ausgangswert für die Berechnung der Nullstellen nach dem Newtonschen Verfahren zu erhalten, kann die Verwandtschaft zwischen den konfluenten hypergeometrischen Funktionen und den Besselschen Funktionen ausgenützt werden [9]:

$$
\begin{aligned}
{}_1F_1(a, c, z) = {} & \Gamma(c) \cdot e^{z/2} \cdot (\tfrac{1}{2} cz - az)^{\frac{1}{2} - \frac{1}{2} c} \\
& \cdot \sum_{n=0}^{\infty} A_n \cdot (\tfrac{1}{2} z)^{\frac{1}{2} n} \cdot (c - 2a)^{-\frac{1}{2} n} J_{c-1+n}(\sqrt{2cz - 4az})
\end{aligned}
\tag{10}
$$

---

[2] Gebundene Zustände resultieren dabei nur dann, wenn r_0 größer als die oben genannten Grenzwerte ist.

[3] Wird die Radialfunktion für den Bereich $0 \leqq r \leqq r_0$ normiert, dann ist auch die Normierungskonstante $N_{n,l,p}$ eine Funktion von r_0.

mit

$$A_0 = 1, \quad A_1 = 0, \quad A_2 = -\frac{c}{2}$$

und

$$(n+1)A_{n+1} = (n+c-1)\,A_{n-1} + (2a-c)A_{n-2}; \qquad a = \text{reell}.$$

Danach lassen sich die Nullstellen der konfluenten hypergeometrischen Funktion ${}_1F_1(a, c, z)$ in grober Näherung durch die Nullstellen $j_{c-1,p}$ der Besselfunktionen $J_{c-1}(\sqrt{2cz-4az})$ approximieren.

Die Besselfunktionen können mit Hilfe ihrer Nullstellen als Produktfunktionen dargestellt werden [10]

$$J_\nu(u) = \frac{(\frac{1}{2}u)^\nu}{\sqrt{(\nu+1)}} \prod_{p=1}^{\infty} \left(1 - \frac{u^2}{j^2_{\nu,p}}\right). \tag{11}$$

Daraus ergibt sich die p-te Nullstelle der Besselfunktion $J_{c-1}(\sqrt{2cz-4az})$ zu

$$z_0 = j^2_{c-1,p} \cdot \frac{1}{2c-4a}. \tag{12}$$

Bei Verwendung der McMahon-Näherung [10] reduziert sich (12) auf

$$z_0 \simeq \frac{\pi^2(p+\frac{1}{2}c-\frac{3}{4})^2}{2c-4a}. \tag{13}$$

Übertragen auf die vorliegende spezielle Form der konfluenten hypergeometrischen Funktion erhält man schließlich für die Nullstellen den folgenden Näherungsausdruck:

$$r_0 \simeq \frac{\pi^2}{128 \cdot Z}(4p+4l+1)^2. \tag{14}$$

Die nach (14) berechneten Werte eignen sich als Ausgangswerte für eine iterative Bestimmung der r_0.

3. Die Spin-Bahn-Wechselwirkung beim beschränkten Keplerproblem

In den Fig. 3 und 4 wird gezeigt, wie sich der nach (6) berechnete Landé-Parameter in Abhängigkeit vom Radius des Potentialtopfes bzw. von der (mit der Verkleinerung des Bewegungsgebietes wachsenden) Hauptquantenzahl ändert. Es sind darin nur die Ergebnisse für die „gebundenen“ Zustände ($E \leqq 0$) dargestellt.

In Fig. 3 ist als typisches Beispiel die Spin-Bahn-Kopplungskonstante $\zeta_{n,l=2,p}$ für $p = 1, 2, 3$ als Funktion von r_0 aufgetragen. Für festes p wächst danach ζ mit abnehmenden r_0 an. Während im unbeschränkten System beim Übergang $p \to p+1$ ζ stets *abnimmt*, existieren im beschränkten System r_0-Bereiche, für die dieser Übergang (bei festem r_0) zu einer *Zunahme* der Spin-Bahn-Kopplungskonstante führt. [Vgl. z. B. den Bereich um $r_0 = 20$aE für den Übergang $(p = 1) \to (p = 2)$.]

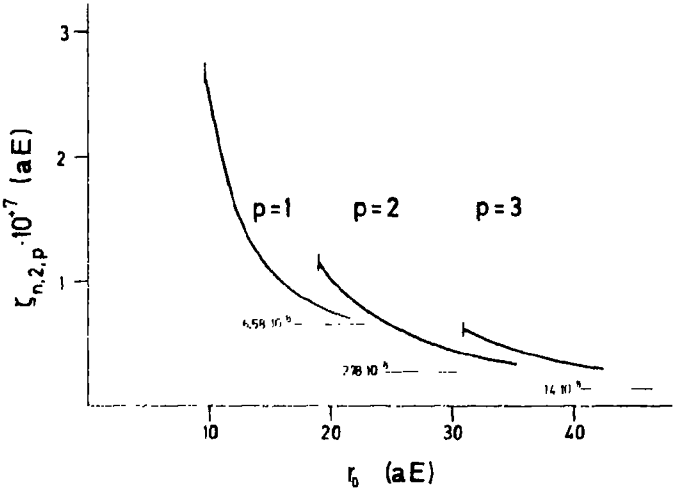

Fig. 3 Anstieg des Landé-Parameters $\zeta_{n,l,p}$ (mit $l = 2$, $Z_{eff} = 1$) bei Beschränkung des dem Elektron zur Verfügung stehenden Bewegungsraumes für die Zustände mit $p = 1, 2, 3$

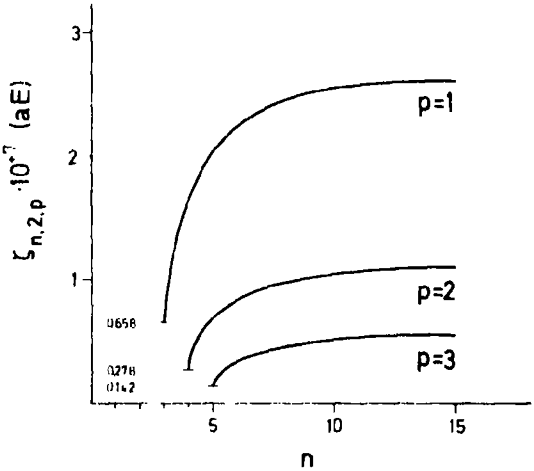

Fig. 4 Anstieg des Landé-Parameters $\zeta_{n,l,p}$ (mit $l = 2$, $Z_{eff} = 1$) bei wachsender Hauptquantenzahl n für die Zustände mit $p = 1, 2, 3$

Fig. 4 zeigt $\zeta_{n,l=2,p}$ (für $p = 1, 2, 3$) als Funktion der Hauptquantenzahl n. Danach wächst ζ (bei festem p) mit zunehmenden n an. Beginnend mit dem ζ-Wert des freien Ions (z.B. $\zeta_{3,2,1} = 0{,}658 \cdot 10^{-7}$ aE) wächst ζ und nähert sich asymptotisch dem Grenzwert für $n \to \infty$.

References

1. Landau, L. D., Lifschitz, E. M.: Lehrbuch der theoretischen Physik, IVa, S. 133. Berlin: Akademie-Verlag 1970.
2. Michels, A., de Boer, J., Bijl, A.: Physica 4, 991 (1938) (van-der-Waals-Festschrift).

3. Sommerfeld, A., Welker, H.: Ann. Physik, 5. Folge, Bd. 32, 56 (1928).
4. Schläfer, H. L., Gliemann, G.: Einführung in die Ligandenfeldtheorie, S. 447. Frankfurt: Akad. Verlagsges. 1967.
5. Jørgensen, C. K.: Modern aspects of ligand field theory, p. 471ff. North Holland Publ. Comp. 1971.
6. Bethe, H.: Handbuch der Physik, Bd. 35 (Atome I), S. 103. Berlin: Springer 1957.
7. Landau, L. D., Lifschitz, E. M.: Lehrbuch der theoretischen Physik III, S. 125. Berlin: Akademie-Verlag 1967.
8. Schläfer, H. L., Gliemann, G.: Einführung in die Ligandenfeldtheorie, S. 219. Frankfurt: Akad. Verlagsges. 1967.
9. Abramowitz, M., Stegun, I. A.: Handbook of mathematical functions, p. 506ff. New York: Dover Publications Inc. 1965.
10. Abramowitz, M., Stegun, I. A.: Handbook of mathematical functions, p. 370ff. New York: Dover Publications Inc. 1965.

Prof. Dr. G. Gliemann
Fachbereich Chemie der Universität Regensburg
D-8400 Regensburg
Universitätsstr. 31
Bundesrepublik Deutschland

Theoret. chim. Acta (Berl.) 27, 161—163 (1972)
© by Springer-Verlag 1972

A Note on General Core-Valence Orthogonality

D. B. Cook

Department of Chemistry, The University, Sheffield S3 7HF, U.K.

Received June 2, 1972

A method of generating a set of basis functions, which satisfy the condition of "strong orthogonality", is developed.

Introduction

It is well-known that the results of an "orbital basis Hartree-Fock" calculation (SCFMO) are invariant against linear transformations of the basis orbitals which preserve normalization and linear independence [1] and that any method going beyond the independent particle model does not have this convenient invariance property [2]. Thus the choice of basis for a calculation of the CI/VB type is a non trivial factor to be considered [3]. The CI/VB analysis is considerably simplified by the use of an orthonormal basis [2] and for practical, computational, reasons most many electron calculations use such a basis set.

The most commonly used orthogonalization procedures, due to Schmidt [4] and Löwdin [5] do not produce an orbital basis which is entirely satisfactory for CI/VB calculations for different reasons. McWeeny and others [6] have shown that a VB type calculation is adversely affected by using an orthogonalization procedure in which the low-lying "core" orbitals contain admixture of "valence" orbitals after orthogonalization. Thus the Löwdin orthogonalization method (which has the physically appealing property of disturbing the orbital basis least consistent with orthogonality [7]) cannot be used directly. The well-known Schmidt orthogonalization method generates an orthonormal basis in which only one orbital is left unchanged and the whole process is highly unsymmetrical, producing an orthonormal set which is dependent on the ordering of the basis. The members of the Schmidt orthogonal basis do not have the symmetry properties of the original basis.

A compromise has been used in Ref. [6] in which a "local" Schmidt orthogonalization is performed on each "heavy" atom and the resulting set being symmetrically orthogonalized by the Löwdin procedure (with possibly a unitary transformation-hybridization). This compromise procedure works well for molecules containing one atom with core orbitals. For more complex molecules the interatomic core-valence overlap causes undesirable core-valence mixture. The interatomic core-valence overlap terms are typically about 0.1 for adjacent first row atoms.

In this note a method is presented for the generation of an orbital basis which leaves any number of core orbitals uncontaminated by valence orbitals on orthogonalization.

Method

We refer to a basis consisting of a set $\{\phi_{i_c}\}$ of n_c "core" orbitals and a set $\{\phi_{i_v}\}$ of n_v "valence" orbitals which are not orthogonal, i.e.

$$\left.\begin{array}{l}\langle\phi_{i_c}|\phi_{j_c}\rangle\neq 0\\ \langle\phi_{i_c}|\phi_{j_v}\rangle\neq 0\\ \langle\phi_{i_v}|\phi_{j_v}\rangle\neq 0\end{array}\right\}\quad\begin{array}{l}i_c, j_c = 1,\ldots,n_c\\ i_v, j_v = 1,\ldots,n_v\end{array}\qquad(1)$$

we require a linear transformation to produce a new set of valence orbitals $\{\bar{\phi}_{i_v}\}$ such that

$$\langle\phi_{i_c}|\bar{\phi}_{j_v}\rangle = 0\left|\begin{array}{l}i_c = 1,\ldots,n_c\\ j_v = 1,\ldots,n_v\end{array}\right.\qquad(2)$$

we write

$$\bar{\phi}_{j_v} = \phi_{j_v} + \sum_{i_c=1}^{n_c} W_{i_c j_v}\phi_{i_c}\qquad(3)$$

and insist that (2) shall hold:

$$\text{i.e.}\quad 0 = \langle\phi_{k_c}|\bar{\phi}_{j_v}\rangle = \langle\phi_{k_c}|\phi_{j_v}\rangle + \sum_{i_c=1}^{n_c}\langle\phi_{k_c}|\phi_{i_c}\rangle W_{i_c j_v}\qquad(k_c = 1,\ldots,n_c)$$

Collecting these equations we have

$$\boldsymbol{S}_c\boldsymbol{W} + \boldsymbol{S}_{cv} = \boldsymbol{0}$$

where

$$(\boldsymbol{S}_c)_{i_c j_c} = \langle\phi_{i_c}|\phi_{j_c}\rangle$$

$$(\boldsymbol{S}_{cv})_{i_c j_v} = \langle\phi_{i_c}|\phi_{j_v}\rangle$$

$$\text{i.e.}\quad \boldsymbol{W} = -\boldsymbol{S}_c^{-1}\boldsymbol{S}_{cv}$$

giving the matrix $\boldsymbol{W}$ which contains the required transformation coefficients since $\boldsymbol{S}_c$ is always non-singular. The remaining non-orthogonalities are now all core-core and valence-valence and can be treated by the Löwdin method still leaving the core orbitals unmixed with valence components.

General Applications

The argument has been developed within the physical idea of a multi-core/valence separation but the derivation is of general applicability to the strong orthogonality condition. Löwdin [8] has shown that the condition that the wave functions of two separate groups of electrons $\Phi_A(1,\ldots,N)$ and $\Phi_B(1,\ldots,N)$ are "strongly" orthogonal:

$$\int dV_i\,\Phi_A(1,\ldots,i,\ldots,N)\,\Phi_B(1,\ldots,i,\ldots,N) = 0\qquad(i = 1,\ldots,N)$$

if all the orbitals used in the construction of Φ_A are orthogonal to all those used in Φ_B. Clearly the matrix W achieves "strong" orthogonality between the set $\{\phi_{i_c}\}$ and $\{\phi_{i_v}\}$ without insisting on orthogonality *within* $\{\phi_{i_c}\}$ or $\{\phi_{i_v}\}$ which is the current general practice.

Acknowledgement. The author wishes to thank Professor R. McWeeny for useful comments on the draft manuscript.

References

1. Lennard-Jones, J. E.: Proc. Roy. Soc. (London) A **198**, 1 (1949).
2. Slater, J. C.: J. chem. Physics **19**, 220 (1951).
3. McWeeny, R.: Proc. Roy. Soc. (London) A **223**, 63 (1954).
4. See, for example, Hall, G. G.: Matrices and tensors, p. 51. Pergamon Press 1963.
5. Löwdin, P.-O.: J. chem. Physics **18**, 365 (1950).
6. McWeeny, R., Ohno, K.: Proc. Roy. Soc. (London) A **255**, 367 (1960).
   McWeeny, R., Klessinger, M.: J. chem. Physics **42**, 3343 (1965).
7. Carlson, B. C., Keller, J. M.: Physic. Rev. **105**, 102 (1950).
8. Löwdin, P.-O.: J. chem. Physics **35**, 78 (1961).

Dr. D. B. Cook
Department of Chemistry
The University
Sheffield S3 7HF
U.K.

Theoret. chim. Acta (Berl.) 27, 165—170 (1972)
© by Springer-Verlag 1972

De la possibilité d'utiliser une base de Slater uniquement *s* dans les calculs relatifs aux atomes et aux molécules

MICHEL ROCHE et JACQUES-CLAUDE SIMON
Laboratoire de Chimie Théorique, Faculté des Sciences, Place Victor Hugo,
F-13 Marseille (3e), France

Reçu le 23 juin 1972

On the Possibility of Using a Basis of s-Slater Type Orbitals alone in Atomic and Molecular Calculations

A $2p$ STO may be replaced by a linear combination of 1s and 2s orbitals, $\Phi = \alpha(1s_A - 1s_f) + \beta(2s_A - 2s_B)$. Such a Φ should improve LCAO-MO-SCF calculations in minimal STO basis set with simpler programs.

1. Introduction

Deux types d'orbitales atomiques (OA) sont généralement utilisés comme base dans la détermination des orbitales moléculaires: d'une part les orbitales hydrogénoïdes et de Slater, d'autre part les orbitales gaussiennes. Dans les deux cas le nombre d'intégrales polycentriques à calculer est multiplié par la présence d'OA qui ne sont pas de symétrie sphérique, en raison des projections nécessaires: aussi est-il tentant de ne considérer que des orbitales s. Cette possibilité, étudiée et utilisée avec succès pour les gaussiennes [1–4], a été également signalée, mais semble-t-il non exploitée, par Parr pour les OA hydrogénoïdes [5].

Soient $2s$ et $2p_z$ deux OA hydrogénoïdes de charge nucléaire effective Z centrées en O. Parr remplace $2p_z$ par $\phi_{2p} = \alpha(1s_A - 1s_B)$, et $2s$ par $\phi_{2s} = \alpha\, 1s_O + \beta\, 1s'_O$

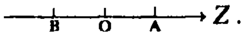

O, A, B désignent les centres des OA's (O est évidemment le milieu de BA), $1s_O$ et $1s'_O$ diffèrent par leur exposant. Les paramètres qui interviennent dans ϕ_{2s} et ϕ_{2p} sont déterminés en minimisant $E(\phi) = \langle\phi|H|\phi\rangle$, où H est l'hamiltonien hydrogénoïde: $H = 1/2\,\nabla^2 - Z/z$. Parr trouve que $E(\phi_{2p})$ est trop grande de 5% par rapport à l'énergie exacte $E(2p_z)$, alors que $E(\phi_{2s})$ est pratiquement égale à $E(2s)$ (trop grande de 0,01%).

Nous nous bornerons dans ce travail à la couche 2 et nous envisagerons *a priori* une base constitutée d'OA $1s$ et $2s$ de Slater et non pas exclusivement $1s$ comme Parr. Le remplacement de $2s$ par ϕ_{2s} nous semble en effet peu intéressant, car il multiplie le nombre d'intégrales polycentriques à calculer, sans en contrepartie supprimer des projections. Il parait plus avantageux de chercher à améliorer la représentation de $2p_z$ en lui substituant:

$$\Phi = \alpha(ns_A - ns_B) + \beta(n's_A - n's_B),$$

où α et β sont des coefficients à déterminer, et où n et n' sont les nombres quantiques principaux qui pourront prendre les valeurs 1 et 2.

Supposons qu'une telle orbitale Φ simule $2p_z$ avec précision. En introduisant Φ dans un calcul LCAO-MO-SCF et en considérant les coefficients de ns_A, ns_B, $n's_A$, $n's_B$ (qui peuvent alors être tous différents) comme des paramètres variationnels, on obtiendra, sans augmentation excessive des dimensions de la matrice de Hartree-Fock, une énergie plus basse que dans la base minimale de Slater, puisque la minimisation se fera par rapport à un plus grand nombre de paramètres; autrement dit, l'orbitale Φ plus souple que $2p_z$ pourra être mieux adaptée au système particulier considéré.

2. Representation de $2p_z$ par une combinaison linéaire Φ d'OA's

Plutôt que de minimiser $E(\Phi)$ comme Parr, il nous a paru plus simple de reproduire directement une $2p$ à l'aide de Φ, en minimisant $\int |2p_z - \Phi|^2 \, dV$, ou, ce qui revient au même, en maximisant le recouvrement:

$$S = \int 2p_z \Phi \, dV.$$

On doit déterminer les valeurs optimales de:

- La distance $R = \mathrm{OA} = \mathrm{OB}$.
- Les charges nucléaires effectives $Z_{ns_A} = Z_{ns_B}$ et $Z_{n's_A} = Z_{n's_B}$.
- Les coefficients α et β, liés par la condition de normation $\int \Phi^2 \, dV = 1$.

Remarquons qu'on peut se contenter d'étudier le comportement de S pour une valeur donnée de la charge nucléaire effective Z de $2p_z$. En effet, $S = \alpha(S_{2pns_A} - S_{2pns_B}) + \beta(S_{2pn's_A} - S_{2pn's_B})$; or S_{2pns_A} par exemple ne dépend que de $\tau = (z - z_{ns_A})/(Z + Z_{ns_A})$ et de $\varrho = (Z + Z_{ns_A})R/2$. Les deux jeux de paramètres suivants: Z, R, Z_{ns_A}, Z_{ns_B}, α, β, d'une part, et λ^Z, R/λ, $\lambda^{Z_{ns_A}}$, $\lambda^{Z_{ns_B}}$, α, β d'autre part, donnent donc la même valeur de S. Il en résulte que si Φ_1 simule une orbitale $2p(Z_1)$ de charge nucléaire effective Z_1, l'orbitale Φ_2 simulant $2p(Z_2)$ sera obtenue en multipliant les Z_{ns} par Z_2/Z_1 et en divisant R par ce même rapport, les valeurs de α et β restant constantes.

Nous supposerons dans ce paragraphe $Z = 3{,}25$.

Pratiquement nous avons opéré ainsi: nous avons considéré diverses valeurs de R: pour chacune d'elles nous avons déterminé Z_{ns_A} et $Z_{n's_A}$ en les faisant varier directement par pas de 0,01 (ce procédé brutal s'est avéré nécessaire par suite de la platitude du maximum de S), α et β étant chaque fois calculés algébriquement. Nous avons envisagé les cinq possibilités différentes correspondant à n (et n') ≤ 2 (avec la possibilité $\beta = 0$).

Les meilleurs résultats sont obtenus pour $n = 1$, $n' = 2$ et $n = 1$, $n' = 1$. Dans ces deux cas S ne montre pas de maximum en fonction de R mais décroit régulièrement quand R augmente. Les valeurs de S pour quelques distances sont données dans les Tableaux 1 et 2. Nous y avons noté également les paramètres Z_{ns}, α, β

Tableau 1. $\Phi = \alpha(1s_A - 1s_B) + \beta(2s_A - 2s_B)$

R(Å)	0,001	0,01	0,05	0,1	0,15	0,2
S	1,000000	1,000000	0,999999	0,999979	0,999886	0,999610
Z_{1s}	1,62 (5)	1,62	1,64	1,77	1,84	1,72
Z_{2s}	3,25	3,25	3,25	3,26	3,27	3,25
α	162,8620	16,3663	3,2357	1,4749	0,9627	0,8399
β	282,0842	28,1187	5,6801	3,0251	2,0633	1,4378
$\langle z^2 \rangle$ u.a.[a]	1,7041	1,7042	1,7062	1,7124	1,7232	1,7402
$\langle x^2 \rangle$ u.a.[a]	0,5680	0,5680	0,5670	0,5640	0,5589	0,5521
θ_0[a]	62,1873	61,8001	59,9304	57,4218	54,6610	51,5869
r_{max}(Å)	$<10^{-4}$	$3 \cdot 10^{-3}$	$2 \cdot 10^{-2}$	$4 \cdot 10^{-2}$	$7 \cdot 10^{-2}$	10^{-1}

[a] Pour $2p_z$: $\langle z^2 \rangle = 1,7041$, $\langle x^2 \rangle = 0,5680$, $\theta_0 = 62,2308$.

Tableau 2. $\Phi' = \alpha(1s_A - 1s_B) + \beta(1s'_A - 1s'_B)$

R(Å)	0,001	0,01	0,05	0,1	0,15	0,2
S	1,000001[b]	1,000000	0,999999	0,999979	0,999885	0,999610
Z_{1s}	1,62	1,62	1,62	1,60	1,59	1,57
$Z_{1s'}$	1,63	1,63	1,63	1,65	1,66	1,68
α	26669,3043	2666,6561	532,1163	54,4742	26,0183	12,5896
β	−26262,1446	−2625,9380	−523,9617	−50,3786	−23,2678	−10,5042
$\langle z^2 \rangle$ u.a.[a]	1,7042[b]	1,7042	1,7062	1,7126	1,7232	1,7401
$\langle x^2 \rangle$ u.a.[a]	0,5681[b]	0,5680	0,5670	0,5640	0,5589	0,5521
θ_0[a]	62,2291	61,8073	59,9173	57,3810	54,5783	51,5578
r_{max}(Å)	$<10^{-4}$	$3 \cdot 10^{-3}$	$2 \cdot 10^{-2}$	$4 \cdot 10^{-2}$	$7 \cdot 10^{-2}$	10^{-1}

[a] Pour $2p_z$: $\langle z^2 \rangle = 1,7041$, $\langle x^2 \rangle = 0,5680$, $\theta_0 = 62,2308$.

[b] Le dernier chiffre est très probablement faux.

correspondants, les valeurs des composantes $\langle z^2 \rangle$ et $\langle x^2 \rangle$ du moment quadrupolaire, l'angle θ_0 en degrés de la tangente à l'origine le long de $0Z$ et la valeur maximale r_{max} de $|\Phi_\theta/\Phi_0 - \cos\theta|$ – qui vaut 0 pour $2p_z$ – pour $\theta = \pi/4$.

On voit qu' a la précision des calculs[1], $S \simeq 1$ pour $R \leqq 0,01$ Å, S, $\langle z^2 \rangle$, $\langle x^2 \rangle$, θ_0, r_{max}, sont très sensiblement les mêmes, à R fixé, pour Φ et pour Φ'. On notera que α et β croissent quand R diminue, et qu'en outre ils sont beaucoup plus grands dans le cas de Φ' que dans le cas de Φ.

La Fig. 1 donne le long de $0Z$ la forme dé Φ pour $R = 0,1$ Å et $R = 0,2$ Å, ainsi que celle de $2p_z$ comme référence.

Les courbes correspondant à Φ' sont pratiquement identiques aux précédentes et n'ont pas été reportées.

On peut dire en conclusion de cette étude que l'on peut reproduire une $2p$ de Slater de façon quasiment parfaite à l'aide de Φ (ou de Φ'), à condition de prendre R suffisamment petit.

---

[1] Tous les calculs ont été effectués sur I B M 360-44 en double précision. S, $\langle z^2 \rangle$, $\langle x^2 \rangle$ ont été évalués à l'aide des fonctions auxilliaires A_n et B_n [6].

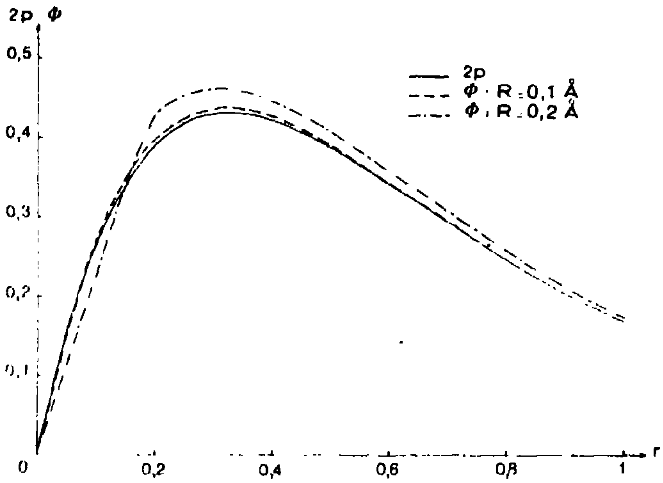

Fig. 1

3. Sur l'utilisation pratique de Φ dans les atomes et les molécules

La précision avec laquelle on peut calculer les intégrales polycentriques (pq, rs) n'est pas illimitée mais dépend des programmes et de l'ordinateur mis à la disposition de l'utilisateur. Cela sera déterminant dans le choix pratique de l'orbitale Φ à employer. En effet il ne suffit pas que Φ simule au mieux $2p_z$: nous avons vu que α et β augmentaient avec S lorsque R diminuait. En introduisant Φ dans un calcul LCAO-MO-SCF on trouvera en particulier des intégrales telles que $J = \int \Phi_A(1)\Phi_B(1)(1/r_{12})\Phi_C(2)\Phi_D(2)\, dV_1\, dV_2$, qui, développées feront apparaître des (pq, rs) entre OA's pondérées par $\alpha^m\beta^n$ avec $m + n = 4$. La précision sur (pq, rs) étant donnée, celle sur J sera d'autant plus faible que α et β seront grands. On constate d'autre part que la précision des programmes disponibles[2], qui permet de calculer les intégrales à environ 10^{-6} u.a. près aux distances usuelles des liaisons chimiques diminue rapidement pour les faibles distances, de quelques dixièmes d'angströms.

Il s'agit donc dans chaque cas particulier de trouver le meilleur compromis entre les trois faits suivants:

a) S est d'autant plus grand que R est petit.

b) α et β sont d'autant plus grands que R est petit.

c) La précision sur les intégrales et notamment (pq, rs) est d'autant plus faible que R est petit; on peut certes l'augmenter[3] mais au détriment des temps de calcul.

---

[2] Programmes standards du QCPE.
QCPE 43 (Corbato-Switendick) pour les intégrales mono et dicentriques.
QCPE 86, 87, 24 (Wright-Pitzer) pour: $(1/r_A, bc)$ et (a^2, bc), (ab, ac), (ab, cd), respectivement.

[3] Afin d'obtenir aux petites distances une précision suffisante et sensiblement la même pour les différents types d'intégrales (quelques unités sur le sixième chiffre en général) nous avons dû prendre un plus grand nombre de points dans les intégrations numériques relatives aux intégrales tri et tétracentriques. Les résultats du Tableau 3 ont été obtenus avec 36 points (Gauss-Legendre) pour (a^2, bc) et $(1/r_A, bc)$, 24 points (Gauss-Legendre et Gauss-Laguerre) pour (ab, ac) et (ab, cd).

Tableau 3. Intégrales pour C(^3P) en u.a. $\Phi = \alpha(1s_A - 1s_B) + \beta(2s_A - 2s_B)$

R (Å)	0,05	0,1	0,15	0,2	$2p_z$
T*	1,2727	1,3198	1,3180	1,3135	1,3203
U*	−4,8898	−4,8732	−4,8665	−4,8492	−4,8750
$J_{1s\Phi}$	0,8099	0,8073	0,8064	0,8040	0,8075
$J_{2s\Phi}$	0,5835	0,5820	0,5819	0,5817	0,5820
$J_{\Phi x \Phi y}$	0,4474	0,5670	0,5660	0,5644	0,5675
$K_{1s\Phi}$	0,0173	0,0172	0,0169	0,0161	0,0173
$K_{2s\Phi}$	0,1222	0,1257	0,1257	0,1259	0,1257
$K_{\Phi x \Phi y}$	−0,0193	0,0337	0,0330	0,0320	0,0343
$J_{\Phi x \Phi x}$	0,2455	0,6372	0,6386	0,6405	0,6360
E_T	−37,7882	−37,6167	−37,6101	−37,5946	−37,6186

* $T = -1/2\langle\Phi|\nabla^2|\Phi\rangle$, $U = -\langle\Phi|N/r|\Phi\rangle$ $(N = 6)$.

Ce sont *a priori* les intégrales intraatomiques telles que $J_{\Phi x \Phi y}$, $K_{\Phi x \Phi y}$, $J_{\Phi x \Phi x}$ qui risquent d'être entachées de la plus grande erreur absolue. C'est pourquoi à titre d'exemple nous avons traité le cas de l'atome de carbone dans son état fondamental ^3P. Les diverses intégrales entrant dans le calcul de l'énergie totale E_T et faisant intervenir $\Phi = \alpha(1s_A - 1s_B) + \beta(2s_A - 2s_B)$, ou $2p$, ainsi que $J_{\Phi x \Phi x}$, sont données dans le Tableau 3 pour plusieurs valeurs de R. $\Phi' = \alpha(1s_A - 1s_B) + \beta(1s'_A - 1s'_B)$ donne des résultats moins satisfaisants que Φ: cela est du au fait que, toutes choses étant égales par ailleurs, α et β sont beaucoup plus grands pour Φ'.

Comme on devait s'y attendre les valeurs de T, U, $J_{1s\Phi}$, $J_{2s\Phi}$, $K_{1s\Phi}$, $K_{2s\Phi}$ où se rencontrent les coefficients $\alpha^m\beta^n$ avec $m + n = 2$, sont moins affectées par la diminution de R (b) et c)), que les valeurs de $J_{\Phi x \Phi y}$, $K_{\Phi x \Phi y}$, $J_{\Phi x \Phi x}$ où les coefficients sont $\alpha^m\beta^n$ avec $m + n = 4$.

La solution la plus satisfaisante correspond à $R = 0{,}1$ Å; soit Φ_0 l'orbitale Φ correspondante; Φ_0 est encore très proche de $2p_z$ (Tableau 1). L'énergie totale E_T est la même que celle calculée en base de Slater ordinaire à $2 \cdot 10^{-3}$ u.a. près. Si $E(\Phi_0) = \langle\Phi_0| -1/2\nabla^2 - z/r|\Phi_0\rangle$ nous avons obtenu $E(\Phi_0) = -1{,}3198_5$ u.a. En comparant cette valeur à $E(2p_z) = -1/8\,Z^2 = -1{,}3203$ u.a., nous constatons un écart de 0,03 % donc très inférieur aux 5 % de Parr. Ce gain appréciable justifie *a posteriori* la plus grande complexité de Φ_0.

Φ_0 pourra être utilisée telle quelle dans un calcul LCAO-MO-SCF. Si dans les molécules interviennent des charges nucléaires effectives Z' différentes de 3,25, on pourra prendre Φ'_0 avec les mêmes coefficients α, β que Φ_0, $Z'_{1s} = Z_{1s} \times Z'/3{,}25$, $Z'_{2s} = Z_{2s} \times Z'/3{,}25$ et $R' = R \times 3{,}25/Z$, ce qui donnera le même S que Φ_0, comme nous l'avons remarqué au 2. Cependant si Z' est nettement plus grand que 3,25, par exemple $Z' = 5{,}20$ (pour le fluor d'après les règles de Slater), $R' = 0{,}0625$, mais le meilleur compromis entre les influences de a), b), c) pourra être obtenu pour une distance légèrement supérieure à R'.

L'OA $2p$ de Slater n'est pas la meilleure dans le cas des atomes (non hydrogénoïdes) et des molécules. Pour les atomes, par suite de leur symétrie sphérique, un seul coefficient α ou β peut être considéré comme paramètre variationnel. En minimisant l'énergie totale E_T de C(^3P) par rapport à α de Φ_0 on obtient: $E_T = -37{,}6262$ u.a. pour $\alpha = 1{,}5706$ $(\beta = 2{,}8523)$; cette énergie est très proche de celle obtenue en optimisant tous les exposants de la base de Slater ordinaire: $E_T = -37{,}6285$ u.a. [7]. Cela laisse espérer une amélioration significative des calculs LCAO-MO-SCF, dans lesquels, la symétrie étant abaissée, le nombre de paramètres variationnels introduits par la substitution d'orbitales Φ aux OA $2p$ sera plus important.

4. Conclusion

Une OA $2p$ de Slater centrée en O peut être représentée aussi bien que l'on veut par une combinaison linéaire Φ d'OA's centrées en deux points A et B seulement. Le choix précis de l'orbitale Φ à utiliser dépend des moyens dont on dispose pour calculer les intégrales polycentriques. $\Phi_0 = \alpha(1s_A - 1s_B) + \beta(2s_A - 2s_B)$ avec $R = OA = OB = 0{,}1$ Å donne des résultats très satisfaisants pour le carbone.

Malgré le plus grand nombre de centres ainsi introduits, l'intérêt d'utiliser une base uniquement s dans les molécules se résume dans les deux points suivants:

Programmes plus simples: OA d'un seul type, et ne nécessitant pas de projections préalables suivant des directions privilégiées.

Abaissement de l'énergie grâce à la flexibilité plus grande de Φ par rapport à la $2p$ classique: le gain est déjà de 10^{-2} u.a. environ pour l'état fondamental ^3P du carbone malgré la symétrie sphérique.

Bibliographie

1. Whitten, J. L.: J. chem. Physics **39**, 349 (1963).
2. — J. chem. Physics **44**, 359 (1966).
3. Harrison, J. F.: J. chem. Physics **46**, 1115 (1967).
4. Tinland, B.: Chem. Physics Letters **2**, 433 (1968).
5. Parr, R. G.: J. chem. Physics **26**, 428 (1957).
6. Mulliken, R. S., Rieke, C. A., Orloff, D., Orloff, H.: J. chem. Physics **17**, 1248 (1949).
7. Tubis, A.: Physic Rev. **102**, 1049 (1956).

Dr. M. Roche
Laboratoire de Chimie Théorique
Faculté des Sciences
Place Victor Hugo
F-13 Marseille (3e)
France

Theoret. chim. Acta (Berl.) 27, 171–185 (1972)
© by Springer-Verlag 1972

Commentationes

MO-SCF-LCAO Studies of Sulphur Compounds

III. Thiophene

U. Gelius

Institute of Physics, University of Uppsala, Sweden

B. Roos and P. Siegbahn

Institute of Theoretical Physics, University of Stockholm, S-113 46 Stockholm, Sweden

Received May 12, 1972

Results from an *ab initio* MO-SCF-LCAO study of the thiophene molecule, using an extended set of contracted Gaussian basis functions, are presented. The ordering of the molecular orbitals and the ionization energies are discussed in relation to experimental data from electron spectroscopy. A number of molecular properties have been computed in good agreement with available experimental information. The effect of 3*d* functions on sulphur for the description of the chemical bond and for the physical and chemical properties of thiophene is elucidated. Molecular potential energy maps are used in a discussion of the mechanism for electrophilic substitution reactions.

Es werden Resultate von *ab initio*-MO-SCF-LCAO-Studien des Thiophenmoleküls mit Hilfe eines erweiterten Satzes von kontrahierten Gauß-Basisfunktionen dargestellt. Die Reihenfolge der Molekülorbitale und die Ionisationsenergien werden diskutiert und mit experimentellen Daten aus elektronenspektroskopischen Messungen verglichen. Eine Anzahl molekularer Daten konnte in guter Übereinstimmung mit verfügbaren experimentellen Werten berechnet werden. Die Bedeutung der 3*d* Funktionen des Schwefels bei der Beschreibung der chemischen Bindungen und der physikalischen und chemischen Eigenschaften des Thiophens wird aufgezeigt. Zur Diskussion des Mechanismus elektrophiler Substitutionsreaktionen werden Diagramme der molekularen potentiellen Energie herangezogen.

Résultats d'un calcul *ab-initio* MO SCF LCAO de la molécule de thiophène, où l'on utilise une base étendue de fonctions gaussiennes contractées. L'ordre des orbitales moléculaires et les énergies d'ionisation sont discutés en fonction de données expérimentales de spectroscopie électronique. Un certain nombre de propriétés moléculaires calculées sont en bon accord avec les données expérimentales. On élucide l'effet des fonctions 3*d* du soufre sur la description de la liaison chimique et sur les propriétés physicochimiques du tiophène. Des cartes d'énergie potentielle moléculaire sont utilisées pour une discussion du mécanisme des réactions de substitution électrophile.

Introduction

Thiophene is one of the simplest conjugated cyclic systems which contain sulphur. The thienyl ring is an important building stone for many larger organic compounds. A detailed understanding of the sulphur-carbon bond in thiophene is therefore of great importance for the discussion of the chemistry of a large class of organic molecules. The electronic structure of thiophene has also interested theoretical chemists for many years. The early work was restricted to studies of the π-electron system. The first attempt to extend the Hückel molecular orbital method to heterocyclics was made by Wheland and Pauling [1] in a study of the thiophene molecule. Only the $3p_\pi$ orbital on sulphur was assumed to contribute to the π-electron wave function. The first suggestion that $3d$-orbitals might participate in the sulphur-carbon bond was made by Schomaker and Pauling a few years later [2]. A number of authors have later presented results from Hückel type calculations on thiophene and related sulphur containing systems using a $3p-3d$ hybrid atomic π-orbital on the sulphur atom.

Bielefeld and Fitts made a Pariser-Parr-Pople type calculation, where the basis set was enlarged with $3d_\pi$ and $4p_\pi$ functions on sulphur [3]. Their results showed that $3d_\pi$ atomic orbitals participate only to a small extent in the ground state. The electronic spectrum was, however, markedly influenced. The $3d_\pi$ orbitals also had a noticeable effect on the dipole moment.

Only the π-electrons were considered in these studies. The first attempt to give a description of the electronic structure of thiophene including all valence electrons was made by Clark [4]. He used the CNDO/2 method of Pople, Santry and Segal, modified in order to include $3d$, $4s$ and $4p$ atomic orbitals for sulphur in the basis set. The results showed a rather large participation of the $3d$-orbitals in the sulphur-carbon bond. The calculated population was 0.24 and 0.14 for $3d_\sigma$ and $3d_\pi$, respectively. Calculation of the dipole moment made it clear that the effect of the $3d$-orbitals was overestimated by the CNDO/2 method.

Clark and Armstrong have recently published results from an *ab initio* calculation on thiophene using contracted Gaussian basis functions [5]. A basis of 127 primitive Gaussians was reduced to 50 contracted functions; four s, two p and two d functions for sulphur, three s and one p functions for carbon and three s functions for hydrogen. The energy lowering due to the inclusion of the $3d$ functions was found to be 0.12 a.u. with a population of 0.72 electrons in S $3d$ orbitals. A large fraction of this population should, however, be attributed to S $3s$, since six d-type functions were used instead of five.

We report in this paper results from an *ab initio* calculation similar to the work of Clark and Armstrong. It is the third paper in a series discussing the electronic structure and molecular properties of sulphur compounds. Preceding papers have given results for the molecules H_2S and SO_2 [6] and the sulphate ion [7].

The basis set used here consists of 126 primitive Gaussians: ten s-type, six p-type and one d-type (exponent 0.5) functions for sulphur, seven s-type and three p-type functions for carbon and four s-type and one p-type Gaussian for hydrogen. This set was contracted to "double zeta", that is, two basis functions per atomic shell. The contracted set, thus obtained, consists of 76 contracted functions. Details of the choice of basis functions have been given previously and will not be further discussed here [6-8].

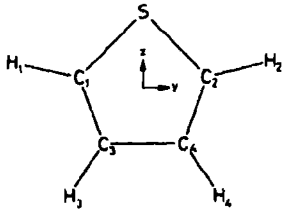

Fig. 1. Numbering of the atoms and the coordinate system for the thiophene molecule

All calculations were made at the experimental equilibrium geometry [9], using the IBMOL IV program system [10] and an IBM 360/91 computer. The coordinate system and the numbering of the atoms is shown in Fig. 1.

Results and Discussion

A. Total and Orbital Energies

Total energies are given in Table 1, where a comparison is made to the results obtained by Clark and Armstrong [5]. A lower total energy is obtained in the present work, since a larger set of contracted Gaussians has been used. The effect of adding polarization functions is, as expected, less pronounced with the larger basis set. The energy decrease due to the addition of $2p$ functions on hydrogen was found to be 0.023 a.u., while the addition of $3d$ functions on sulphur gives a further lowering of 0.030 a.u. The two effects are found to be completely independent of each other.

Orbital energies are reported in Table 2 together with experimental data for ionization energies. Lindholm *et al.* have recently presented an UV excited electron spectrum for thiophene measured up to 25 eV [11]. Their results together with the assignments made in [11] are given in the sixth column of Table 2. However, their assignment for three of the outer orbitals has been questioned by Gelius *et al.* on the basis of an intensity analysis of their ESCA results for thiophene [12]. This intensity analysis rather supported the present *ab initio* orbital assignment. The last column of Table 2 contains the ionization energies and the orbital assignments given in [12].

The structure of the outer molecular orbitals with respect to the distribution of charge and the bonding character is presented in Table 3. Mulliken's population analysis method has been used and the bonding properties have been obtained from the overlap populations.

The molecular orbitals corresponding to ionization energies below 27 eV can be divided into five well separated groups (Fig. 2). The same grouping of the levels is found experimentally as the results of Lindholm *et al.* show. The assignments made in their paper [11] is partly based on the present investigation, partly on experimental information and extended Hückel calculations including comparisons with spectra of related compounds. Both calculations and experiment predict the two outermost orbitals to be of π-type and give them in the

Table 1. Total energies for thiophene (in atomic units)

	T. E.	$-V/T$
Without pol. functions	−550.923	1.997
with H $2p$	−550.946	1.997
with S $3d$	−550.976	1.998
with H $2p$ and S $3d$	−550.999	1.998
Clark and Armstrong [5]:		
s, p basis on S	−550.417	—
s, p, d basis on S	−550.535	

Table 2. Orbital energies and ionization energies for thiophene (in atomic units)

Orbital	no pol.	H $2p$	S $3d$	H $2p$ and S $3d$	Ionization energies[a]	Ionization energies[b]
$1a_1$	-91.981	-91.980	-91.975	-91.974		
$1b_2$	-11.278	-11.279	-11.268	-11.269		10.68 (C $1s$)
$2a_1$	-11.278	-11.279	-11.268	-11.269		
$3a_1$	-11.253	-11.253	-11.247	-11.248		10.67 (C $1s$)
$2b_2$	-11.252	-11.252	-11.247	-11.247		
$4a_1$	- 8.988	- 8.987	- 8.977	- 8.976		
$3b_2$	- 6.680	- 6.679	- 6.669	- 6.669		6.29 (S $2p$)
$5a_1$	- 6.679	- 6.678	- 6.668	- 6.668		6.24 (S $2p$)
$1b_1$	- 6.675	- 6.674	- 6.666	- 6.665		
$6a_1$	- 1.198	- 1.199	- 1.183	- 1.185		0.959 ($6a_1$)
$4b_2$	- 1.001	- 1.001	- 0.995	- 0.995	0.820 ($7a_1$)	0.820 ($4b_2$)
$7a_1$	0.997	- 0.997	- 0.986	- 0.986	0.812 ($4b_2$)	0.812 ($7a_1$)
$8a_1$	- 0.767	- 0.766	- 0.764	- 0.762	0.673 ($8a_1$)	0.691 ($8a_1$)
$5b_2$	- 0.755	- 0.754	- 0.752	- 0.750	0.647 ($5b_2$)	0.654 ($5b_2$)
$9a_1$	- 0.709	- 0.707	- 0.703	- 0.702	0.610 ($9a_1$)	0.610 ($9a_1$)
$6b_2$	- 0.590	- 0.590	- 0.583	- 0.583	0.526 ($6b_2$)	0.526 ($6b_2$)
$10a_1$	- 0.546	- 0.544	- 0.541	- 0.540	0.511 ($10a_1$)	0.511 ($10a_1$)
$2b_1(\pi)$	- 0.531	- 0.530	- 0.524	- 0.524	0.489 ($7b_2$)	0.489 ($2b_1$)
$7b_2$	0.523	- 0.522	- 0.524	- 0.523	0.467 ($11a_1$)	0.467 ($7b_2$)
$11a_1$	- 0.471	- 0.471	- 0.476	- 0.475	0.445 ($2b_1$)	0.445 ($11a_1$)
$3b_1(\pi)$	- 0.350	- 0.350	- 0.342	- 0.342	0.349 ($3b_1$)	0.349 ($3b_1$)
$1a_2(\pi)$	0.339	- 0.338	- 0.333	- 0.332	0.327 ($1a_2$)	0.327 ($1a_2$)

[a] From Ref [11]. - [b] From Ref. [12].

Table 3. Bonding character and populations for the outer molecular orbitals in thiophene[a]

Orb.	Gross atomic populations					Bonding character[b]				
	S	C_1	C_3	H_1	H_3	S C_1	C_1 C_3	C_3-C_4	C_1-H_1	C_3-H_3
$6a_1$	0.50	0.36	0.35	0.02	0.02	b	b	b	nb	nb
$4b_2$	0.11	0.49	0.34	0.08	0.03	wb	sb	wab	wb	wb
$7a_1$	0.84	0.15	0.37	0.00	0.06	b	wb	sb	nb	nb
$8a_1$	0.30	0.36	0.28	0.20	0.02	ab	wb	b	sb	wb
$5b_2$	0.26	0.33	0.28	0.10	0.17	b	nb	wab	b	b
$9a_1$	0.18	0.24	0.40	0.08	0.19	nb	wb	wb	wb	b
$6b_2$	0.01	0.36	0.31	0.16	0.18	nb	b	ab	b	b
$10a_1$	0.06	0.21	0.57	0.12	0.07	nb	nb	sb	b	wb
$2b_1$	0.62	0.37	0.32	—		b	b	wb		--
$7b_2$	0.63	0.38	0.10	0.12	0.09	b	wab	wab	b	wb
$11a_1$	1.35	0.16	0.10	0.00	0.06	wb	wab	b	nb	nb
$3b_1$	1.12	0.00	0.43	–	- -	wab	wb	sb	—	—
$1a_2$	0.03	0.70	0.28		—	nb	b	ab	-	

[a] From the calculation including polarization functions.

[b] Nomenclature: b = bonding, a = anti, w = weakly, s = strongly and n = non.

same order. The next group consists of five orbitals. The present calculation gives them in the order: $11a_1 < 7b_2 < 2b_1 < 10a_1 < 6b_2$, where $2b_1$ is the third π-orbital. Lindholm *et al.*, on the other hand, predict the order to be: $2b_1 < 11a_1 < 7b_2 < 10a_1 < 6b_2$. This assignment is based on a comparison with

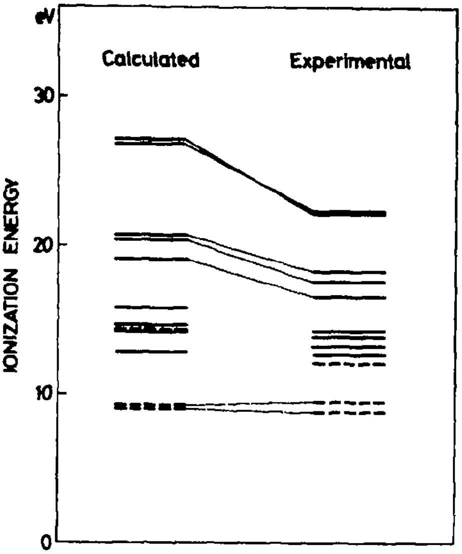

Fig. 2. A comparison between calculated and experimental ionization potentials for the outer molecular orbitals in thiophene. Experimental values and assignments are from the work of Lindholm *et al.* [11]. Dotted lines correspond to π-orbitals

benzene. The inner π-orbital ($1a_{2u}$) in this molecule has a vertical ionization energy of 12.3 eV [18]. Extended Hückel calculations give the values -15.0 and -14.8 eV for the orbital energies of the orbitals $1a_{2u}$ in benzene and $2b_1$ in thiophene [11]. Thus it is suggested that the ionization energy corresponding to $2b_1$ should be around 12.1 eV and the peak found at this energy is assigned to this orbital. A comparison with the results obtained by P. Siegbahn from an *ab initio* calculation on furan [15] is also made.

A series of *ab initio* calculations on azines with a basis set similar to the one used here has recently been performed by Roos *et al.* [16]. This study also includes benzene. It is therefore now possible to make a consistent comparison between experimental ionization energies and calculated orbital energies for the three molecules benzene, thiophene and furan. Ionization energies for the three π-orbitals in these molecules are given in Table 4. There is a good agreement between experimental and calculated shifts for the two outer π-orbitals. The calculations predict, in contrast to the extended Hückel calculations of Lindholm *et al.*, an increase in energy of around one eV for the inner π-orbital in thiophene compared to the corresponding orbital in benzene. If we use this shift to assign the photoelectron spectrum, we would expect to find the experimental value for the vertical ionization energy of $2b_1$ around 13 eV. This corresponds closely to the experimental ionization energy found at 13.3 eV, which has been assigned to $7b_2$ by Lindholm *et al.* Thus, following the same interpretation procedure as Lindholm but using *ab initio* instead of extended Hückel calculations in order to correlate the ionization energies of benzene and thiophene leads to an assignment for the fifth molecular orbital level in thiophene in agreement with the theoretical predictions made in this paper.

Table 4. Calculated and experimental ionization energies for the π-orbitals in C_6H_6, C_4H_4S and C_4H_4O (in eV)[a]

	C_6H_6	C_4H_4S	C_4H_4O
calc	9.08	9.04	9.06
exp.	9.3	8.9	8.9
calc	9.08	9.30	11.03
exp	9.3	9.5	10.3
calc	13.62	14.25	17.28
exp.	12.3	12.1 (13.3)	14.4 (15.6)

[a] Calculated values from [15, 16] and the present study. Experimental values were taken from the work of Lindholm *et al.* [11, 17, 18]. Values within parenthesis have been obtained with the assignments predicted by the calculations.

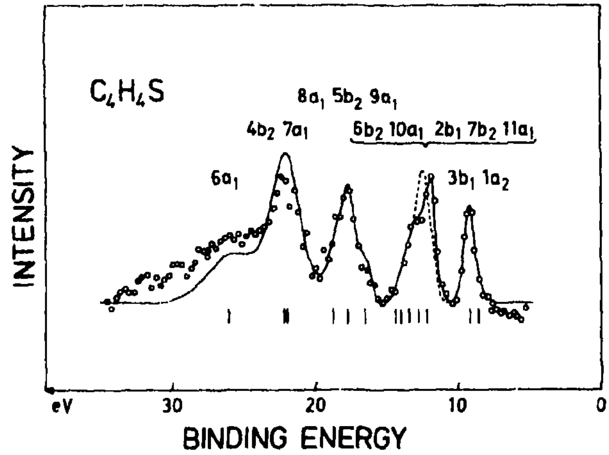

Fig. 3. The electron spectrum of the molecular orbital region in thiophene excited by Mg Kα. The solid and dotted lines are theoretically calculated intensities using different orbital assignments as discussed in the text. The positions of the orbitals are indicated by the vertical lines under the spectrum

It is assumed in the paper by Lindholm *et al.*, that the orbital $11a_1$ is non-bonding (lone-pair on the sulphur atom). It should therefore become impossible to explain the vibrational structure of the band at 12.1 eV with the assignments suggested here. The present results show, however, that $11a_1$ is delocalized with 67% of its charge on sulphur (cf. Table 3). It is found to be S–C_1 and C_3–C_4 bonding and C_1–C_3 antibonding. One should therefore expect to find "ring distorting" and "ring breathing" vibrational structure in the band due to the removal of an electron from $11a_1$.

Recently Gelius *et al.* have proposed a model, involving atomic subshell photoionization cross sections and gross atomic charges, for interpreting the molecular orbital intensities in electron spectra excited by soft X-rays [12]. The theoretical justification for this intensity model is discussed in [14]. The model has been applied to several molecules and the agreement with experimental intensities is generally good. Fig. 3 shows the electron spectrum of the valence electrons of thiophene excited by Mg $K\alpha$ together with the calculated intensity spectrum using the intensity model. The experimental spectrum has been corrected for a linear background and for the contribution from the Mg $K\alpha_{3,4}$ satellite lines. The gross atomic populations used in the intensity model were taken from the present calculation.Two different orbital assignments were examined, the *ab initio* assignment (solid line in Fig. 2) and the assignment proposed by Lindholm *et al.* (dotted line). From Fig. 3 it is obvious that the intensity analysis supports the present *ab initio* orbital assignment.

The ionization energy of the core electrons have also been studied by ESCA [12, 13, 19]. Particular attention has been paid to the chemical shift between the two different C 1*s* levels. Clark and Lilley reported an experimental value of 0.1 eV for this chemical shift [13]. Previously, however, Clark reported a broadening of 0.1 eV of the thiophene C 1*s* line relative to the corresponding line of benzene. Gelius *et al.* performed their ESCA measurements on gaseous thiophene, thereby achieving a somewhat better resolution. From an observed C 1*s* broadening of 0.13 eV relative to benzene they arrived at a C 1*s* chemical shift in thiophene of 0.34 ± 0.12 eV. This experimental shift is somewhat smaller than the 0.58 eV, which is the C 1*s* orbital energy difference in our best *ab initio* calculation. This is consistent with the general trend in MO-LCAO calculations of "double zeta" accuracy to give somewhat too large chemical shifts when Koopmans' theorem is used to estimate the ionization energies [15, 22–25].

B. Population Analysis

The result from a population analysis, using the method of Mulliken, is presented in Table 5. The population in the S 3*d* orbitals is found to be 0.18. Of this only 0.04 electrons is attributed to the $3d\pi$-orbitals. The effect of back-bonding in the π-orbital $1a_2$ is thus found to be small (the 3*d*-population in this orbital is 0.01). It is interesting to compare these populations with the variation of the gross atomic charge on sulphur. The calculation without S 3*d* basis functions gives a charge of $+0.49$. With these functions the charge is reduced to $+0.00$. This decrease is much larger than the corresponding 3*d*-population. The effect of the 3*d* functions is to increase the populations in the S 3*s*- and S 3*p*-orbitals. Thus they act as *polarization functions* rather than as independent valence orbitals. An entirely different situation was found in SO_2 and SO_4^{-2} [6, 7]. The positively charged sulphur atom here stabilized the 3*d*-orbitals, so that they could act as additional valence orbitals. A large 3*d*-population was found with the S 3*s*- and S 3*p*-populations unaffected. Obviously there is a difference between systems like H_2S and C_4H_4S, where sulphur is the most electronegative atom, and systems where sulphur forms bonds with electronegative ligands like oxygen and fluorine. In the former case the 3*d*-functions will behave as polarization functions just as they do when they are added to the basis set for a first row atom. In the second case, however, the 3*d*-level is stabilized and is available for additional bonding as in SO_4^{-2}, SOF_2, SF_6, etc.

The large decrease in charge on the sulphur atom gives a corresponding decrease for the carbon atoms C_1 and C_2. In agreement with semi-empirical

Table 5. Gross atomic populations and charges for thiophene

	no pol.	H 2*p*	S 3*d*	H 2*p* and S 3*d*
S (*s*-orb.)	5.790	5.787	5.804	5.806
S (*pσ*-orb.)	6.003	5.995	6.278	6.284
S (*pπ*-orb.)	3.725	3.727	3.723	3.727
S (*dσ*-orb.)			0.143	0.143
S (*dπ*-orb.)			0.038	0.037
q(S)	+0.482	+0.491	+0.016	+0.001
C_1 (*s*-orb.)	3.324	3.263	3.184	3.134
C_1 (*pσ*-orb.)	2.135	2.076	1.976	1.894
C_1 (*pπ*-orb.)	1.109	1.105	1.085	1.080
$q(C_1)$	−0.568	−0.444	−0.245	−0.108
C_3 (*s*-orb.)	3.166	3.124	3.187	3.146
C_3 (*pσ*-orb.)	1.983	1.907	2.021	1.941
C_3 (*pπ*-orb.)	1.028	1.025	1.035	1.032
$q(C_3)$	0.177	−0.056	−0.243	−0.119
H_1 (*s*-orb.)	0.733	0.826	0.751	0.847
H_1 (*p*-orb.)		0.027		0.030
$q(H_1)$	+0.267	+0.147	+0.249	+0.123
H_3 (*s*-orb.)	0.764	0.864	0.768	0.869
H_3 (*p*-orb.)		0.028		0.028
$q(H_3)$	+0.236	+0.108	+0.232	+0.103

π-electron studies, these calculations also predict a somewhat larger π-electron density on the carbon atom C_1 than on C_3. This is, however, more than counterbalanced by the greater accumulation of σ-electrons on C_3. This is explained by the fact that the sulphur atom acts as an equally strong σ-electron acceptor as it is a π-electron donor. Thus the total negative charge is greater on C_3 than on C_1. *The implications of this charge distribution in the double bond on the molecular potential in this region will be discussed below.*

C. Molecular Properties

A number of molecular properties of the thiophene molecule have been computed. The results are presented in Table 6 together with available experimental data.

The inclusion of the 3*d*S functions has a marked effect on the results. Thus the dipole moment decreases from 0.96 to 0.62 Debye. This change is caused by the reduction of the atomic charges, which results in almost non-polar bonds. The quadrupole moments exhibits a similar, but less pronounced effect. The expectation value $\langle z^2 \rangle_{CM}$ is decreased, due to the increased electron density around the sulphur atom. This in turn leads to the changes of the quadrupole moment components shown in Table 6. These results can be compared with the experimental values given by Sutter and Flygare [21]. Thus, the results for θ_{xx}, θ_{yy} and θ_{zz}, computed without 3*d*S functions are, respectively, 91%, 103% and 48% of the experimental values. With 3*d*S functions in the basis set these figures become 95%, 100% and 73%. The improvement is, as expected, greatest for θ_{zz}.

Table 6. Molecular properties of thiophene[a]

	no pol.	H 2*p*	S 3*d*	H 2*p* and S 3*d*	exp.
Dipole moment (Debye)					
	0.959	0.973	0.606	0.619	0.54[b]
Quadrupole moment (10^{-26} esu · cm^2)					
Q_{xx}	−7.593	−7.597	−7.839	−7.847	−8.3 ± 2.2[c]
Q_{yy}	6.784	6.850	6.536	6.608	6.6 ± 1.5
Q_{zz}	0.809	0.747	1.303	1.239	1.7 ± 1.6
Diamagnetic susceptibility tensor (10^{-6} erg/G^2 mole)					
χ^d_{xx}	−440.64	−440.51	−439.78	−439.70	−438.1 ± 3.0[c]
χ^d_{yy}	−286.64	−286.58	−285.81	−285.78	−284.8 ± 3.0
χ^d_{zz}	−226.90	−226.75	−226.50	−226.38	−225.7 ± 3.0
χ^d_{av}	−318.06	−317.95	−317.36	−317.28	−316.2 ± 3.0
Potential at the sulphur nucleus (a.u.)					
$\Phi(S)$	−59.21	−59.21	−59.22	−59.22	
Electric field gradient at the sulphur nucleus (a.u.)					
$q_{xx}(S)$	1.606	1.601	1.520	1.514	
$q_{yy}(S)$	−1.930	−1.916	−1.929	−1.919	
$q_{zz}(S)$	0.324	0.315	0.410	0.404	
Quadrupole coupling constants for S^{33}, assuming $Q(S^{33}) = -0.062$ barns (MHz)					
$eq_{xx}Q(S^{33})$	−23.40	−23.32	−22.14	−22.06	
$eq_{yy}Q(S^{33})$	28.12	27.91	28.10	27.96	
$eq_{zz}Q(S^{33})$	−4.72	−4.59	−5.97	−5.89	
Other expectation values (a.u.)					
$\langle x^2\rangle_{CM}$	30.68	30.65	30.53	30.50	30.4 ± 4.3[c]
$\langle y^2\rangle_{CM}$	160.31	160.22	160.13	160.06	159.3 ± 4.3
$\langle z^2\rangle_{CM}$	210.60	210.58	210.06	210.06	209.3 ± 4.6
$\langle 1/r_S\rangle$	66.11	66.11	66.12	66.12	
$\langle 1/r_{C_2}\rangle$	25.66	25.66	25.67	25.67	
$\langle 1/r_{C_3}\rangle$	25.04	25.04	25.05	25.05	
$\langle 1/r_{H_2}\rangle$	11.19	11.20	11.19	11.20	
$\langle 1/r_{H_3}\rangle$	10.76	10.77	10.76	10.78	

[a] The *y* and *z* axes are in the molecular plane and the *z* axis bisects the CSC angle.
[b] Ref. [20]. – [c] Ref. [21].

With a bulk magnetic susceptibility of -57.40×10^{-6} erg/G^2 mole, Sutter and Flygare obtain the elements of the diamagnetic susceptibility tensor. As can be seen in Table 6 the agreement with our calculated values is excellent. The effect of the 3*d*S functions on this property is negligible.

There is, to our knowledge, no experimental determination of the quadrupole coupling constants for S^{33} in thiophene. The values given in Table 6 have been obtained with a value of −0.062 barns for the nuclear quadrupole moment of S^{33} [6]. In a previous work we have calculated the quadrupole coupling constants for S^{33} in SO_2 [6]. The results were in good agreement with experiment. We therefore believe that the results obtained in the present study are also close to the true values.

D. Molecular Potentials and Electrophilic Substitution

The five-membered rings pyrrole, furan and thiophene undergo electrophilic substitution preferentially at the α-position (C_1 in Fig. 1):

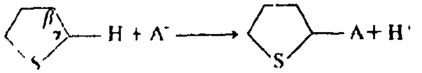

(1)

The orientation to the α-position seems to be more pronounced in furan and thiophene than in pyrrole [26]. It is generally assumed that the mechanism for aromatic electrophilic substitution proceeds via an intermediate addition complex [27]:

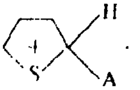

(2)

It is, however, also possible that complexes of π-type are involved in some reactions of this type. This possibility will be discussed below for the thiophene molecule.

The theoretical interpretation of the preferential position for electrophilic attack has traditionally been made by means of π-electron theory. Discussions based on frontier electron densities and localization energies have in many cases been able to give results in good agreement with experiments, while the orientation role of the total π-electron distribution seems to be less well established. Actually these three concepts refer to different steps in the reaction. The π-electron distribution is assumed to be related to the electrostatic potential in the C–C double bond. Therefore it should give information about the orientation of the electrophilic reagent in an intermediate π-complex. The frontier electron density and the localization energy give, on the other hand, information about the formation of the addition complex (2) where the double bond has been broken and a bond is established between the aromatic compound and the electrophile. Interpretations by means of frontier electron densities are quite straight forward for the five-membered heterocycles pyrrole, furan and thiophene. Semi-empirical π-electron calculations on these molecules show that the frontier orbital is of symmetry $1a_2$ (symmetric with respect to rotation about the symmetry axis) and with most of the charge located at the α-position. The present study also gives this (cf. Table 3) and a similar result was obtained for furan in a previous study [15].

Scrocco *et al.* have suggested that useful information about the reactivity of molecules can be obtained from a study of molecular potentials [28]. The electrostatic interaction energy between the molecule and a positive test charge was mapped. These maps showed well defined nucleophilic regions around the molecules and the results could be used to discuss the protonation of a series of three-membered ring systems [29]. Recently the same method has been used in a discussion of the protonation of formamide [30].

One might expect to gain some insight into the mechanism for electrophilic substitution reactions from a study of such molecular potential maps. The possibility for a π-complex intermediate, where the electrostatic interaction will be dominant, can be discussed. Preferential directions for electrophilic attack might also be elucidated from a study of such maps.

Such a study has been performed for the thiophene molecule. A computer program, constructed by Almlöf [31], was used. For computational reasons the calculations were made with the 3*d*S functions excluded from the basis set. This is, however, not a serious drawback since the influence of these functions on the wave function is small. Further, the potential energy, being a quantity which is optimized in a calculation based on the variational principle, is insensitive to small changes in the basis set. The potential energy at the sulphur nucleus has been computed with and without the 3*d*S functions and was found to change less than 0.02% (cf. Table 6).

The first map was made in the plane of the molecule. The potential was found to be positive everywhere except in the sulphur lone-pair region, where a minimum was found at a distance of 1.90 Å from the sulphur nucleus and with a depth of −9.4 kcal/mole. Next the potential was mapped in a plane through the C–C double bond and perpendicular to the molecular plane. The energy was found to be positive up to a height of 1.25 Å. A minimum of −14.0 kcal/mole occurred at a distance of 1.74 Å from the molecular plane. In order to investigate this region closer, a map was made in a plane parallel to the molecule at this distance. This potential energy map is shown in Fig. 4. The potential is negative

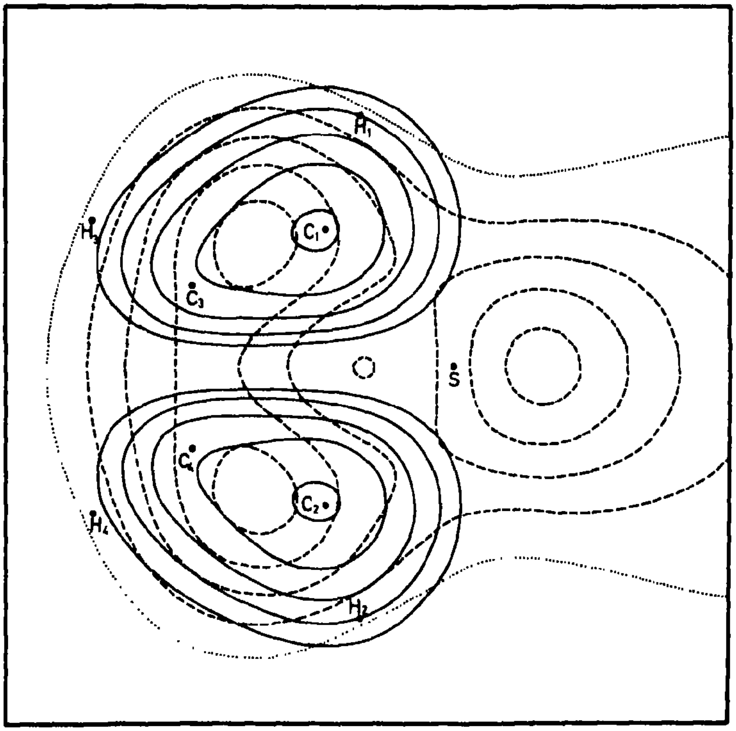

Fig. 4. Molecular potential surface in a plane parallel to the molecule at a distance of 1.74 Å (dotted lines). The following lines are plotted: 0, −0.005, −0.010, −0.015 and −0.020 a.u. Superimposed on this figure is an electron density map for the frontier orbital $1a_2$. The density lines are: 0.001, 0.002, 0.004, 0.008 and 0.016

everywhere, which illustrates the nucleophilic character of the π-electron system. Three distinct minima are found, one over each of the double bonds (-14.0 kcal/mole) and one in the sulphur lone-pair region, with the same energy. This region was investigated in more detail by means of a map in a plane through the symmetry axis and perpendicular to the plane of the molecule. The result is shown in Fig. 5. The energy minimum occurs at a distance of 1.95 Å from the sulphur nucleus and at a height above the plane of 1.59 Å.

These results indicate two possible pathways for an electrophilic attack on thiophene. If a π-complex intermediate is formed, a position of the reagent at the sulphur atom seems equally probable as a position above one of the double bonds. It is noteworthy that the energy minima occur at such large distances from the molecule that the overlap between the frontier orbitals and the electron accepting orbital of the electrophile can be assumed to be small. The electrostatic interaction is therefore dominant, and the minima found in the potential energy maps should correspond rather closely to minima in the true interaction energy. Thus, the results give some confidence to the idea that the reaction can proceed via weak intermediate addition complexes of π-type.

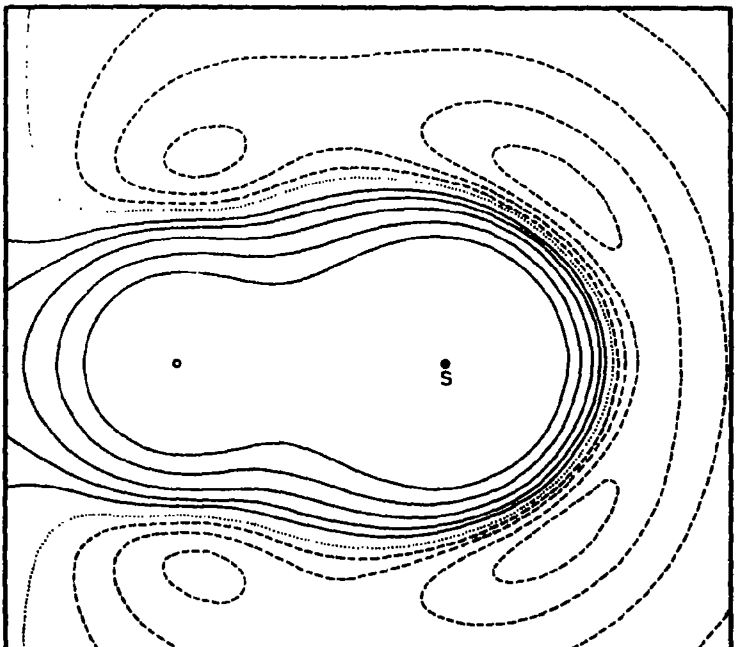

Fig. 5. Molecular potential surface in a plane perpendicular to the molecule and through the two-fold symmetry axis. The following lines are plotted: -0.020, -0.015, -0.010, -0.005, 0.0 (dotted line), 0.01, 0.02, 0.04, 0.08 and 0.16 a.u.

It is interesting to note that the distances from the energy minimum at the double bond to the two carbon nuclei are almost exactly equal. The population analysis data show that the α-carbon has a somewhat larger π-electron population than the β-carbon (cf. Table 5). This is consistent with results obtained from semi-empirical calculations [32]. It might therefore be dangerous to use only π-electron populations, which is often done, to draw conclusions about the orientation role of the electrostatic interaction between the π-electron system and the electrophile.

The results from the present study suggest another explanation for the orientation of the substitution to the α-carbon. The reaction coordinate would most probably go through regions of negative potential energy. Thus one can assume that the attack occurs either through the double bond or through the sulphur lone-pair. The results suggest the existence of outer complexes of π-type, but this is not necessary for the determination of the reaction path. An attack through the sulphur atom would most likely lead to substitution at the C_α-position. The intermediate (2) is formed by a charge transfer mainly from the frontier orbital $1a_2$, which has most of its electrons at C_α but also some population at sulphur due to $3d\pi - 2p\pi$ conjugation. Attack through the double bond could lead to substitution at both positions. The uneven charge distribution in the orbital $1a_2$ also in this case favours substitution at the C_α-position. The electron density distribution in this molecular orbital is illustrated in Fig. 4.

A quantitative estimate of the orientation, taking into account the pathway through the lone-pair region and the uneven charge distribution in $1a_2$, gives 85–90% C_α-substitution. Nitration of thiophene is known to give 70% α-substitution and only 5% β-substitution [26].

It should be remembered, however, that the discussion made above does only take into account first order interactions between the aromatic system and the electrophile. The results might be modified by polarization and solution effects. In a future work these effects will be studied by means of a comparison of potential energy maps and detailed computations of the reaction surfaces for protonation reactions.

Conclusions

The sulphur atom in thiophene forms almost non-polar bonds, with a gross atomic charge of zero on the sulphur atom and +0.02 on the adjacent CH group. The $3d$S functions have been found to behave as polarization functions rather than as an extra valence orbital. This is shown by the fact that the population of these functions in small. Instead, their introduction into the basis set causes considerable changes in the $3s$ and $3p$ population.

The orbital energy ordering has been found to be in agreement with the ordering obtained from an intensity analysis of the ESCA results, but to deviate slightly from the molecular level order suggested by Lindholm *et al.* from an analysis of the UV excited electron spectrum.

A number of molecular properties have been calculated and found to be in good agreement with available experimental data. The $3d$S functions gave a considerable improvement on the results for the dipole and quadrupole moments.

Molecular potential energy maps have been used to discuss the mechanism for electrophilic substitution reactions. The existence of weak intermediate complexes of π-type is suggested together with two possible explanations for the preferentiality of C_α-substitution. The molecular energy maps show a possible pathway for the reaction which goes through an energy minimum above the sulphur atom and leads to substitution at the C_α-positions. The other pathway, through the C_α-C_β double bond, might give substitution at both positions. However, also in this case C_α-substitution will probably dominate, due to the uneven charge distribution in the frontier orbital $1a_2$.

Acknowledgements. We are indebted to IBM World Trade Corporation and to the Swedish IBM Corporation for granting a fellowship for one of us (U. G.) that made it possible to perform the larger part of the calculation at IBM Research Laboratory in San Jose. Part of this work has been supported by a grant from the Swedish Board for Technical Development and the Swedisch Natural Science Research Council.

We wish to thank fil. lic. Jan Almlöf for help with the use of his program for the construction of the molecular potential energy maps.

References

1 Wheland, G. W., Pauling, L.: J. Amer. chem. Soc. **57**, 2086 (1935).
2 Shomaker, V., Pauling, L.: J. Amer. chem. Soc. **61**, 1769 (1939).
3 Bielefeld, M. J., Fitts, D. D.: J. Amer. chem. Soc. **88**, 4804 (1966).
4 Clark, D. T.: Tetrahedron **24**, 2663 (1968).
5 Clark, D. T., Armstrong, D. R.: Chem. Comm. **1970**, 319.
6 Roos, B., Siegbahn, P.: Theoret. chim. Acta (Berl.) **21**, 368 (1971).
7 Gelius, U., Roos, B., Siegbahn, P.: Theoret. chim. Acta (Berl.) **23**, 590 (1971).
8 Roos, B., Siegbahn, P.: Theoret. chim. Acta (Berl.) **17**, 209 (1970).
9 Bak, B., Christensen, D., Hansen-Nygaard, L., Rastrup-Anderson, J.: J. molecular Spectroscopy **7**, 58 (1961).
10 Veillard, A.: IBMOL version IV, IBM manual.
11 Derrick, P. J., Åsbrink, L., Edqvist, O., Jonsson, B.-Ö., Lindholm, E.: Int. J. Mass. Spectrom. Ion Phys. **6**, 177 (1971).
12 Gelius, U., Allan, C. J., Johansson, G., Siegbahn, H., Allison, D. A., Siegbahn, K.: Physica Scripta **3**, 237 (1971).
13 Clark, D. T., Lilley, D. M. J.: Chem. Physics Letters **9**, 234 (1971).
14 Gelius, U.: Electron spectroscopy. Proceedings of an international conference on electron spectroscopy at Asilomar, 1971. Editor: D. A. Shirley, p. 311. Amsterdam: North-Holland Publ. Co. 1972.
15 Siegbahn, P.: Chem. Physics Letters **8**, 245 (1971).
16 Almlöf, J., Johansen, H., Roos, B., Wahlgren, U.: To be published.
17 Derrick, P. J., Åsbrink, L., Edqvist, O., Jonsson, B.-Ö., Lindholm, E.: Int. J. Mass Spectrom. Ion Phys. **6**, 161 (1971).
18. Jonsson, B.-Ö., Lindholm, E.: Ark. Fysik **39**, 65 (1969).
19. Clark, D. T.: Chem. Comm. **1971**, 230.
20. Harris, B., Le Fevre, R. J. W., Sullivan, E. P. A.: J. chem. Soc. **1953**, 1622.
21. Sutter, D. H., Flygare, W. H.: J. Amer. chem. Soc. **91**, 4063 (1969).
22. Basch, H., Snyder, L.: Chem. Physics Letters **3**, 333 (1969).
23. Gelius, U., Roos, B., Siegbahn, P.: Chem. Physics Letters **4**, 471 (1970).
24. Gelius, U., Allan, C. J., Allison, D. A., Siegbahn, H., Siegbahn, K.: Chem. Physics Letters **11**, 224 (1971).
25. Gelius, U., Hedén, P. F., Hedman, J., Lindberg, B. J., Manne, R., Nordberg, R., Nordling, C., Siegbahn, K.: Physica Scripta **2**, 70 (1970).
26. Ridd, J.: Heteroatomic reactivity. In: Physical methods in heterocyclic chemistry. Editor: A. R. Katritzky. New York: Academic Press 1963.

27. Liberles, A.: Introduction to theoretical chemistry. New York: The Macmillan Company 1968.
28. Bonaccorsi, R., Petrolongo, C., Scrocco, E., Tomasi, J.: Quantum aspects of heterocyclic compounds, in chemistry and biochemistry, Vol. 2, p. 181. Editors: E. D. Bergmann and B. Pullman. New York: Academic Press 1970.
29. Bonaccorsi, R., Scrocco, E., Tomasi, J.: J. chem. Physics **52**, 5270 (1970).
30. Bonaccorsi, R., Pullman, A., Scrocco, E., Tomasi, J.: Chem. Physics Letters **12**, 622 (1972).
31. Almlöf, J.: Private communication.
32. Skancke, A., Skancke, P. N.: Acta chem. scand. **24**, 23 (1970).

Dr. B. Roos
Institute of Theoretical Physics
University of Stockholm
S-11346 Stockholm
Sweden

Theoret. chim. Acta (Berl.) 27, 187—196 (1972)
© by Springer-Verlag 1972

Influence du couplage vibronique sur le paramagnétisme d'un complexe cubique dans l'état électronique $^2T_2$

O. Kahn

Ecole Nationale Supérieure de Chimie de Paris, 11, rue Pierre et Marie Curie, 75 Paris 5ème, France

S. F. A. Kettle

School of Chemical Sciences, University of East Anglia, Norwich, England

Reçu le 4 mai, 1972

The Influence of Vibronic Coupling on the Paramagnetism of a Cubic Complex in a $^2T_2$ Electronic State

A study of temperature dependence of the paramagnetism of cubic complexes in a $^2T_2$ electronic state is reported. It is necessary to introduce four parameters: the spin-orbit coupling coefficient λ, the vibronic coupling parameter x, the frequency $\hbar\omega_\varepsilon$ of the twofold degenerate modes of vibration and the covalence parameter k. The perturbations due to the spin-orbit coupling and the vibronic coupling are both diagonalized using the vibronic functions in the Born-Oppenheimer approximation as basis set; the Zeeman perturbation is then diagonalized using the new vibronic functions as basis set.

It is shown that the smaller the absolute value of the parameter $\varrho = \frac{3}{2\hbar\omega_\varepsilon}$, the greater the influence of the vibronic coupling on the temperature dependence of the paramagnetism. This influence is similar to that of the covalence but is not identical.

On étudie l'influence du couplage vibronique sur la variation du paramagnétisme en fonction de la température des complexes cubiques dont l'état électronique est $^2T_2$. Pour cela il est nécessaire d'introduire les quatre paramètres suivants: le coefficient de couplage spin-orbite λ, le paramètre de couplage vibronique x, la fréquence $\hbar\omega_\varepsilon$ des modes de vibration E et le paramètre de covalence k. Sur la base des fonctions vibroniques dans l'approximation de Born-Oppenheimer on diagonalise dans un premier temps les perturbations dues au couplage spin-orbite et au couplage vibronique et dans un second temps sur la nouvelle base des fonctions vibroniques on diagonalise la perturbation Zeeman.

On montre que l'influence du couplage vibronique sur la variation du paramagnétisme en fonction de la température est d'autant plus forte que le paramètre $\varrho = \frac{3}{2\hbar\omega_\varepsilon}$ est en valeur absolue plus faible et que cette influence est proche de celle de la covalence mais non identique.

Es wird über die Temperaturabhängigkeit des Paramagnetismus von kubischen Komplexen im $^2T_2$ Zustand berichtet. Dazu ist es notwendig vier Parameter einzuführen: einen Spin-Bahn-Kopplungskoeffizienten λ, einen Parameter für die Kopplung zwischen Elektron- und Schwingungszustand x, eine Frequenz $\hbar\omega_\varepsilon$ der zweifach degenerierten Schwingungen und einen Kovalenzparameter k. Die Störungen aufgrund der Kopplungen zwischen Spin- und Bahn- und zwischen Elektronen- und Schwingungszuständen werden beide mit Hilfe der Elektronen-Schwingungsfunktionen diagonalisiert, wobei die Born-Oppenheimer Näherung als Basis benutzt wird. Danach wird die Zeeman Störung mit Hilfe der neuen Elektronen-Schwingungsfunktionen als Basis diagonalisiert.

Es wird gezeigt, daß der Einfluß der Kopplung der Elektronen- und Schwingungszustände auf die Temperaturabhängigkeit des Paramagnetismus sich umgekehrt wie der absolute Betrag des Faktors $\varrho = \frac{3}{2\hbar\omega_\varepsilon}$ verhält. Dieser Einfluß ähnelt dem der Kovalenz.

Introduction

Dans deux précédents articles [1, 2], nous avons étudié comment le couplage vibronique influait sur les propriétés magnétiques des complexes cubiques, en particulier de ceux dont l'état fondamental est un triplet orbital. Plus précisément nous avons développé le résultat de Ham [3] qui, le premier, a montré que le couplage vibronique entraîne une réduction des éléments matriciels hors diagonale associés à un opérateur électronique. Cela est par exemple le cas des opérateurs $\hat{L}_x$, $\hat{L}_y$ et $\hat{L}_z$, composantes du moment orbital $\hat{L}$.

Nous nous proposons dans cet article d'introduire le couplage vibronique dans la théorie de paramagnétisme des complexes des métaux de transition telle qu'elle a été exposée par Van Vleck [4] et développée par de nombreux auteurs [5–8]. En effet la théorie du paramagnétisme de Van Vleck suppose implicitement que l'on se place dans l'approximation de Born-Oppenheimer, c'est-à-dire que l'on étudie le mouvement électronique en supposant les noyaux fixes dans leur position d'équilibre. Ainsi les sommations qui interviennent dans la formule de Van Vleck donnant la susceptibilité paramagnétique molaire χ en fonction de la température

$$\chi = \frac{N \sum_n [(E_n^{(1)})^2/kT - 2E_n^{(2)}] \exp(-E_n^{(0)}/kT)}{\sum_n \exp(-E_n^{(0)}/kT)} \qquad (1)$$

sont faites sur les seuls niveaux électroniques. Au contraire, nous cherchons à tenir compte de l'influence des vibrations non totalement symétriques sur les fonctions électroniques de sorte que les sommations dans la formule ci-dessus seront faites sur les différents niveaux vibroniques pour lesquels il intervient un couplage entre fonction électronique et fonction de vibration.

Cette étude concerne les complexes dont l'état électronique est ${}^2T_2$, c'est-à-dire les ions d^1 dans un environnement octaédrique, d^9 dans un environnement tétraédrique et d^5 dans un environnement octaédrique ou tétraédrique dans la limite du champ fort.

Les variations du paramagnétisme en fonction de la température obtenue expérimentalement coïncident généralement bien avec les courbes données par la formule (1) à condition d'introduire un paramètre k de réduction du moment orbital. Ce paramètre, introduit pour la première fois par Steven [9], a été interprété comme une conséquence de la covalence, c'est-à-dire de la délocalisation partielle des électrons du métal de transition vers les ligands. Gerloch et Miller [10] ont récemment calculé ce facteur de réduction k en fonction des coefficients des orbitales moléculaires du complexe et des intégrales de recouvrement métal-ligands et ligands-ligands. Le couplage vibronique provoque également, avons-nous vu, une réduction du moment orbital, ainsi serons-nous conduits à comparer les effets respectifs du paramètre de covalence k et du paramètre de couplage vibronique x que nous avons défini dans un précédent article [1].

En d'autres termes nous calculons les courbes de variation du paramagnétisme en fonction de la température d'un complexe cubique dont l'état électronique est ${}^2T_2$ en ajoutant aux paramètres généralement utilisés, à savoir λ le coefficient de couplage spin-orbite et k le paramètre de covalence, des paramètres introduits dans l'étude du couplage vibronique, à savoir x et la fréquence des modes de vibration engendrant un couplage vibronique. De fait, afin de simplifier le problème, nous supposerons que le couplage vibronique engendré par les modes de vibration T_2 peut être négligé et nous ne tiendrons compte que des modes de vibration E.

Méthode de calcul

Appelons $\mathscr{H}$ l'hamiltonien vibronique du complexe cubique étudié. Nous avons:

$$\mathscr{H} = H_E + H_N + H_{SO} \tag{2}$$

où H_E, H_N et H_{SO} sont respectivement les hamiltoniens électronique, nucléaire et de couplage spin-orbite. H_E peut être développé en série taylorienne selon:

$$H_E = H_E^0 + \sum_{k=1}^{n} \left(\frac{\partial H_E}{\partial Q_k} \right)_0 Q_k . \tag{3}$$

H_E^0 est l'hamiltonien électronique pour la configuration d'équilibre de la molécule et les $n\,Q_k$ sont les coordonnées normales de vibration.

$\mathscr{H}$ s'écrit:

$$\mathscr{H} = H_E^0 + H_N + H_{SO} + \sum_{k=1}^{n} \left(\frac{\partial H_E}{\partial Q_k} \right)_0 Q_k \tag{4}$$

avec dans l'approximation harmonique

$$H_N = \sum_{k=1}^{n} \frac{1}{2} \left(\frac{P_k^2}{\mu_k} + \mu_k \omega_k^2 Q_k^2 \right) \tag{5}$$

où ω_k est la fréquence angulaire de la vibration normale associée à Q_k, μ_k la masse réduite et P_k le moment conjugué, et

$$H_{SO} = \lambda \hat{L} \cdot \hat{S} . \tag{6}$$

$\hat{L}$ et $\hat{S}$ sont respectivement les opérateurs moment orbital et moment de spin. λ est le coefficient de couplage spin-orbite qui est positif dans le cas d'une couche électronique moins que demi remplie et négatif dans le cas d'une couche électronique plus que demi remplie.

La recherche des valeurs propres et vecteurs propres de l'hamiltonien vibronique dans (4) se fera selon une méthode variationnelle analogue à celle déjà utilisée par Ballhausen [11]. Les fonctions de base sont les fonctions de Born-Oppenheimer qui diagonalisent $H_E^0 + H_N$. Les termes de couplage spin-orbite $\lambda \hat{L} \cdot \hat{S}$ et de couplage vibronique $\sum_{k=1}^{n} \left(\frac{\partial H_E}{\partial Q_k} \right)_0 Q_k$ sont considérés comme des perturbations du même ordre de grandeur qui seront diagonalisées en même temps.

Appelons ψ_i^0 les fonctions propres de H_E^0 formant une base pour la représentation T_2 du groupe cubique; E_E^0 est la valeur propre correspondante. $\left\langle \psi_i^0 \middle| \frac{\partial H_E}{\partial Q_k} \middle| \psi_j^0 \right\rangle$ n'est différent de zéro que pour les seules coordonnées normales Q_1 se transformant comme A_1, Q_2 et Q_3 se transformant comme E, Q_4, Q_5 et Q_6 se transformant comme T_2 (on considère soit un complexe tétraédrique ML_4, soit un complexe octaédrique ML_6; dans ce dernier cas les coordonnées normales $Q_1, Q_2 \ldots Q_6$ sont symétriques par rapport à l'inversion et se transforment comme A_{1g}, E_g et T_{2g}). La coordonnée normale totalement symétrique Q_1 n'entraîne pas de distorsion dynamique du complexe cubique de sorte qu'il est possible, sans perte de généralité, de n'en pas tenir compte à condition de considérer que H_E^0

est l'hamiltonien électronique non plus pour la configuration d'équilibre du complexe mais pour toute configuration où la symétrie cubique est conservée. De la sorte H_E^0, ψ_i^0 et E_E^0 dépendent paramétriquement de Q_1. D'autre part, nous admettons avec Sturge [12] que les modes de vibration E se couplent beaucoup plus fortement avec l'état électronique que les modes de vibration T_2 et nous nous plaçons dans le cas limite où le couplage vibronique engendré par les modes de vibration T_2 est négligeable.

Les fonctions de la base sont $\psi_i^0 s_u \varphi^{m,n}$. Les s_u sont les fonctions du doublet de spin ($s_1 = \alpha$ et $s_2 = \beta$) et $\varphi^{m,n}$ est la fonction de vibration où m et n réfèrent aux nombres quantiques de vibration correspondant à Q_2 et Q_3. La qualité du résultat dépend de l'étendue de la base; nous avons limité celle-ci à $m+n=4$.

Les différents termes intervenant dans le calcul de la matrice associée à $\mathscr{H}$ sont:

$$\langle \psi_i^0 s_u \varphi^{m,n} | H_E^0 | \psi_j^0 s_v \varphi^{m',n'} \rangle = E_E^0 \delta_{ij} \delta_{uv} \delta_{mm'} \delta_{nn'} \tag{7}$$

$$\langle \psi_i^0 s_u \varphi^{m,n} | H_N | \psi_j^0 s_v \varphi^{m',n'} \rangle = \hbar\omega_r (m + n + \tfrac{1}{2}) \delta_{ij} \delta_{uv} \delta_{mm'} \delta_{nn'} \tag{8}$$

avec

$$\omega_r = \omega_2 = \omega_3 \,, \tag{9}$$

$$\langle \psi_i^0 s_u \varphi^{m,n} | H_{SO} | \psi_j^0 s_v \varphi^{m',n'} \rangle = H_{SO_{iu,jv}} \delta_{mm'} \delta_{nn'} \,. \tag{10}$$

$H_{SO_{iu,jv}}$ est un élément de la matrice carrée d'ordre 6:

$$\begin{array}{cccccc}
\psi_1^0 s_1 & \psi_1^0 s_2 & \psi_2^0 s_1 & \psi_2^0 s_2 & \psi_3^0 s_1 & \psi_3^0 s_2 \\
\hline
0 & 0 & 0 & \frac{k\lambda}{2} & 0 & -\frac{ik\lambda}{2} \\
0 & 0 & -\frac{k\lambda}{2} & 0 & -\frac{ik\lambda}{2} & 0 \\
0 & -\frac{k\lambda}{2} & 0 & 0 & \frac{ik\lambda}{2} & 0 \\
\frac{k\lambda}{2} & 0 & 0 & 0 & 0 & -\frac{ik\lambda}{2} \\
0 & \frac{ik\lambda}{2} & -\frac{ik\lambda}{2} & 0 & 0 & 0 \\
\frac{ik\lambda}{2} & 0 & 0 & \frac{ik\lambda}{2} & 0 & 0
\end{array} \tag{11}$$

où ψ_1^0, ψ_2^0 et ψ_3^0 se transforment respectivement comme les orbitales d_{xy}, d_{yz} et d_{zx} et où k est le paramètre de covalence qui peut être défini par [9, 10]:

$$k = \frac{\langle \psi_2^0 | \hat{L}_z | \psi_3^0 \rangle}{\langle d_{yz} | \hat{L}_z | d_{zx} \rangle} \,. \tag{12}$$

Enfin:

$$\begin{aligned}
&\left\langle \psi_i^0 s_u \varphi^{m,n} \left| \frac{\partial H_E}{\partial Q_2} Q_2 + \frac{\partial H_E}{\partial Q_3} Q_3 \right| \psi_j^0 s_v \varphi^{m'n'} \right\rangle \\
&\qquad = \frac{\sqrt{6(m+1)x}}{3} \hbar\omega_r \delta_{uv} \cdot [\varepsilon_{ij}(2) \delta_{nn'} \delta_{m,m'-1} + \varepsilon_{ij}(3) \delta_{mm'} \delta_{n,n'-1}]
\end{aligned} \tag{13}$$

Cette relation (13) est valable pour $m' \geqq m$ et $n' \geqq n$. Dans le cas contraire, m et m' ou n et n' devront être échangés pour que cette condition soit remplie.

$\varepsilon_{ij}(2)$ et $\varepsilon_{ij}(3)$ sont les éléments des matrices $\varepsilon(2)$ et $\varepsilon(3)$ qui sur la base des ψ_i^0 sont:

$$\varepsilon(2) = \begin{vmatrix} -1 & 0 & 0 \\ 0 & \frac{1}{2} & 0 \\ 0 & 0 & \frac{1}{2} \end{vmatrix} ; \quad \varepsilon(3) = \begin{vmatrix} 0 & 0 & 0 \\ 0 & -\frac{\sqrt{3}}{2} & 0 \\ 0 & 0 & \frac{\sqrt{3}}{2} \end{vmatrix}$$

x est le paramètre de couplage vibronique défini précédemment [1]:

$$x = \frac{4K_\varepsilon^2}{3\hbar\mu_\varepsilon\omega_\varepsilon^3} \tag{15}$$

avec

$$\mu_\varepsilon = \mu_2 = \mu_3 \tag{16}$$

et

$$K_\varepsilon = -\left\langle \psi_1^0 \middle| \frac{\partial H_E}{\partial Q_2} \middle| \psi_1^0 \right\rangle . \tag{17}$$

Nous rappelons qu'en absence de couplage spin-orbite, le couplage vibronique réduit le moment orbital d'un facteur γ qui, si on ne considère que le niveau fondamental de vibration, c'est-à-dire à 0° K, est:

$$\gamma = e^{-x} . \tag{18}$$

Une fois obtenues par diagonalisation de $\mathscr{H}$ les énergies et fonctions vibroniques dérivant de l'état électronique $^2T_2$, on applique la perturbation Zeeman $H_{ZE} = \hat{\mu} \cdot H$ où H est le champ magnétique externe et $\hat{\mu}$ l'opérateur moment magnétique défini par:

$$\hat{\mu} = \beta(\hat{L} + 2\hat{S}) \tag{19}$$

où β est le magnéton de Bohr.

Les complexes étudiés étant cubique, on peut, sans perte de généralité, orienter le champ magnétique suivant l'axe des z. Les éléments matriciels de $\hat{\mu}_z$ composante de $\hat{\mu}$ suivant l'axe des z sur la base des fonctions électroniques $^2T_2$ sont en unités atomiques:

$$\begin{array}{cccccc} \psi_1^0 s_1 & \psi_1^0 s_2 & \psi_2^0 s_1 & \psi_2^0 s_2 & \psi_3^0 s_1 & \psi_3^0 s_2 \\ \hline 1 & 0 & 0 & 0 & 0 & 0 \\ 0 & -1 & 0 & 0 & 0 & 0 \\ 0 & 0 & 1 & 0 & ik & 0 \\ 0 & 0 & 0 & -1 & 0 & ik \\ 0 & 0 & -ik & 0 & 1 & 0 \\ 0 & 0 & 0 & -ik & 0 & -1 \end{array} \tag{20}$$

Cette perturbation Zeeman est beaucoup plus faible (moins de 1 cm^{-1}) que les perturbations dues au couplage spin-orbite et au couplage vibronique (plus de 100 cm^{-1}); il est donc légitime de diagonaliser d'abord sur la base des fonctions de Born-Oppenheimer les deux plus fortes perturbations et en un second temps de diagonaliser sur la nouvelle base des fonctions vibroniques la perturbation Zeeman.

Les valeurs propres E_n de la matrice $\mathscr{H} + H_{ZE}$ peuvent être développées en série taylorienne selon

$$E_n = E_n^{(0)} + E_n^{(1)}H + E_n^{(2)}H^2 \tag{21}$$

où $E_n^{(0)}$ est le niveau d'énergie vibronique en absence de champ magnétique, $E_n^{(1)}$ et $E_n^{(2)}$ les coefficients Zeeman du premier et second ordre. Ces coefficients peuvent être calculés en appliquant les relations:

$$E_n^{(1)} = \langle n|\hat{\mu}_z|n\rangle\,, \tag{22}$$

$$E_n^{(2)} = \sum_m{}' \frac{\langle n|\hat{\mu}_z|m\rangle^2}{E_n - E_m}\,. \tag{23}$$

Les $|n\rangle$ sont les fonctions vibroniques qui diagonalisent $\mathscr{H} + H_{ZE}$ pour un champ magnétique infiniment faible. La sommation dans (23) porte sur toutes les fonctions $|m\rangle$ non dégénérées avec $|n\rangle$ en absence de champ magnétique.

Le calcul se termine par l'application de la formule (1) donnant la susceptibilité paramagnétique molaire en fonction de la température T. Le moment magnétique μ_{eff} se déduit de χ selon

$$\mu_{\text{eff}} = 2{,}828(\chi T)^{\frac{1}{2}}\,. \tag{24}$$

Compte tenu de la limitation de la base à $m + n = 4$ (m et n étant ici les nombres quantiques de vibration), le calcul des susceptibilités magnétiques requiert en principe des diagonalisations de matrices hermitiques d'ordre 90. En fait une transformation unitaire sur la base de départ permet à chaque étape de travailler sur deux matrices disjointes réelles d'ordre 45.

Résultats et discussions

Les paramètres de cette étude sont les suivants:

λ le coefficient de couplage spin-orbite,
x le paramètre de couplage vibronique,
$h\omega_E$ la fréquence des modes de vibration E,
k le paramètre de covalence.

Deux cas sont à considérer: celui où λ est positif, c'est le cas des ions d^1 en environnement octaédrique et d^5 en environnement tétraédrique; celui où λ est négatif, c'est le cas des ions d^5 en environnement octaédrique et d^9 en environnement tétraédrique.

La courbe de variation de μ_{eff} en fonction de $\frac{kT}{|\lambda|}$ (où k est la constante de Boltzmann) pour $x \neq 0$ dépend d'un paramètre ϱ que nous avions déjà introduit précédemment [2].

$$\varrho = \frac{3\lambda}{2h\omega_E}\,. \tag{25}$$

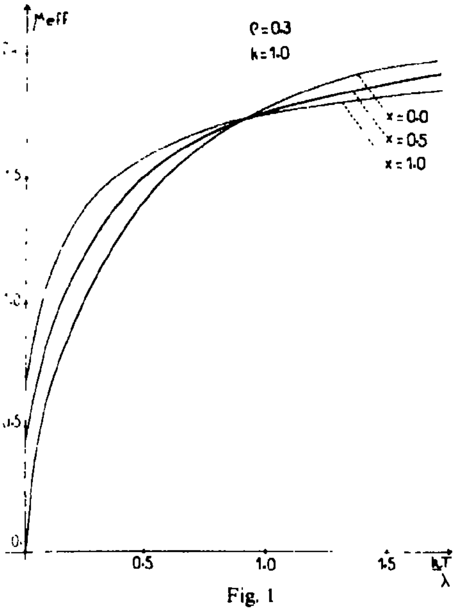

Fig. 1

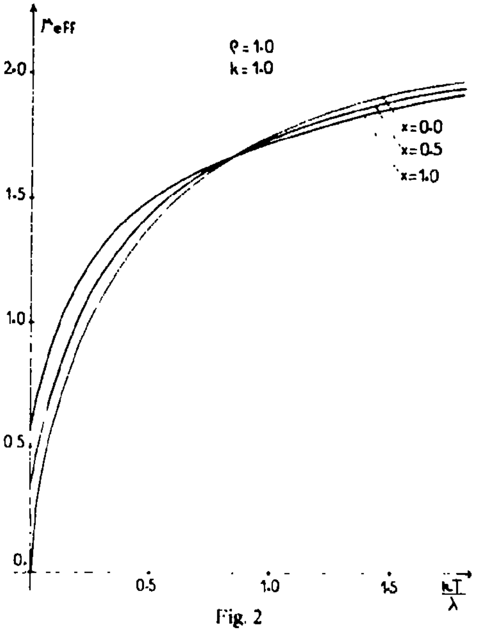

Fig. 2

Ce paramètre est le rapport du splitting du niveau $^2T_2$ du au couplage spin-orbite en absence de couplage vibronique par la fréquence des modes de vibration E. Plus ϱ devient important en valeur absolue et plus l'influence du couplage vibronique devient faible.

Dans la Fig. 1, nous avons représenté les variations de μ_{eff} en fonction de $\frac{kT}{\lambda}$ pour $x = 0$, c'est-à-dire en absence de couplage vibronique, $x = 0.5$ et $x = 1$ en donnant à ϱ la valeur 0.3 (par exemple $\lambda = 100\,\text{cm}^{-1}$ et $h\omega_\varepsilon = 500\,\text{cm}^{-1}$). Dans la Fig. 2, les mêmes courbes ont été tracées avec $\varrho = 1$. On voit que l'influence du couplage vibronique dans ce dernier cas est effectivement très réduite par rapport à ce qu'elle est avec $\varrho = 0.3$. Dès que ϱ atteint 2, le couplage vibronique apparaît à peu près sans influence sur le paramagnétisme.

Les Figs. 1 et 2 ont été tracées avec $k = 1$, c'est-à-dire en négligeant la covalence. A titre de comparaison, sur la Fig. 3 nous représentons la variation de μ_{eff} pour $k = 1$, $k = 0.8$ et $k = 0.6$ en négligeant cette fois le couplage vibronique. Une étude attentive montre que pour une valeur donnée de ϱ, à une courbe de variation de μ_{eff} en fonction de $\frac{kT}{\lambda}$ définie par $x = 0$ et $k = k_0\,(\neq 1)$, il n'est jamais possible de superposer une courbe définie par $k = 1$ et $x = x_0\,(\neq 0)$. En d'autres termes le couplage vibronique et la covalence ont des effets voisins mais non identiques sur la variation du paramagnétisme en fonction de la température.

Les Figs. 4, 5 et 6 concernent le cas où λ et ϱ sont négatifs. A nouveau on peut remarquer d'une part que l'influence du couplage vibronique est d'autant plus faible que $|\varrho|$ est plus grand, d'autre part que les influences respectives du couplage vibronique et de la covalence ne sont pas identiques.

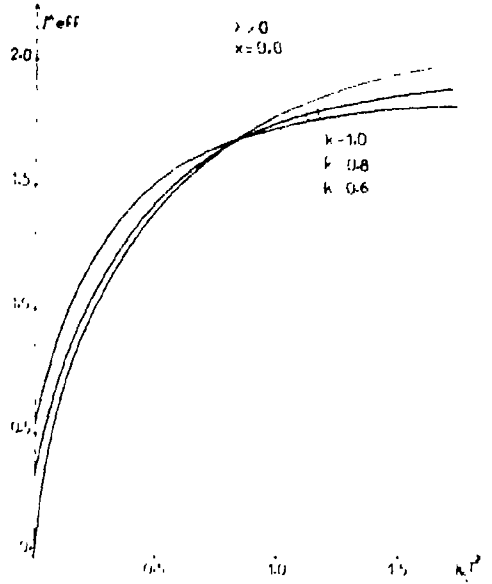

Fig 3

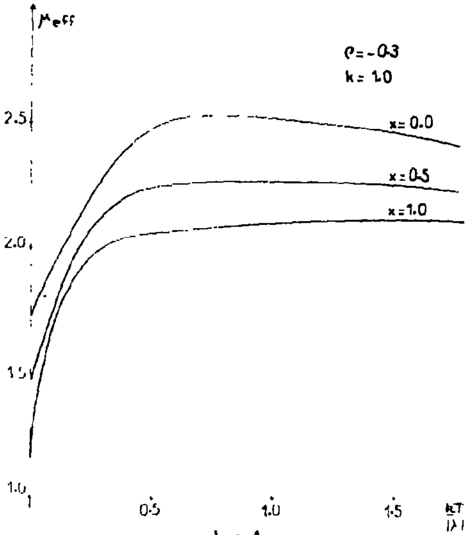

Fig 4

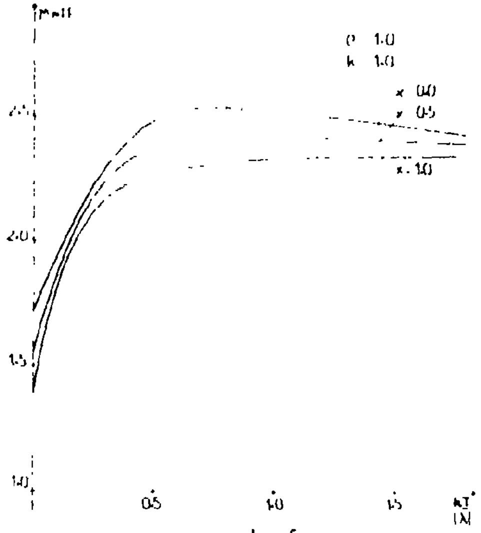

Fig 5

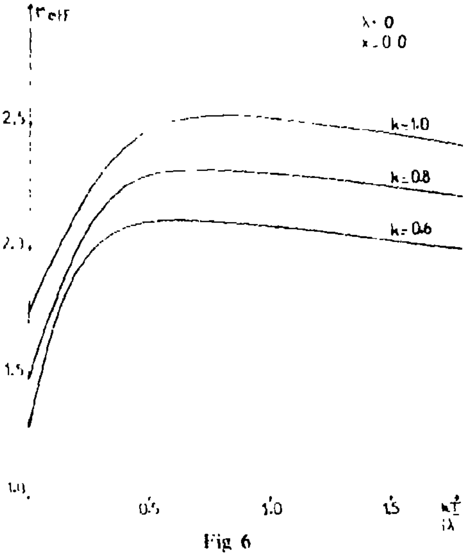

Fig 6

On notera que les courbes des Figs. 3 et 6 diffèrent de celles que l'on peut tracer à partir des valeurs de μ_{eff} en fonction de $\frac{kT}{\lambda}$ données par Figgis [6] en ce que celui-ci considère que seul le moment orbital intervenant dans l'opérateur Zeeman est réduit et que, par contre, le moment orbital dans l'hamiltonien de couplage spin-orbite n'est pas réduit. En fait, en remplaçant dans les valeurs de Figgis λ par $k\lambda$, on retrouve les résultats des Figs. 3 et 6.

Conclusion

Nous avons étudié l'influence du couplage vibronique sur le paramagnétisme des complexes cubiques dont l'état électronique est ${}^2T_2$. Pour ce faire, nous avons étendu la théorie de Van Vleck au cas où les modes de vibration doublement dégénérés se couplent avec l'état électronique de sorte que l'approximation de Born-Oppenheimer ne peut plus être utilisée. L'importance de l'écart à l'approximation de Born-Oppenheimer est déterminée par un paramètre de couplage vibronique x.

Deux résultats principaux doivent être retenus de cette étude: d'une part les courbes donnant la variation du paramagnétisme en fonction de $\frac{kT}{|\lambda|}$ sont d'autant plus modifiées par introduction du couplage vibronique que le paramètre $\varrho = \frac{3}{2h\omega_r}$ est en valeur absolue plus faible. Dans la limite $\varrho = 0$, l'influence du couplage vibronique s'interprète comme une réduction du moment orbital d'un facteur γ qui décroît avec la température ainsi qu'il a été montré dans le premier article de cette série [1]. A l'opposé, un très fort couplage spin-orbite rend le couplage vibronique sans effet sur le paramagnétisme. D'autre part l'influence du couplage vibronique sur la variation du paramagnétisme en fonction de la température est voisine de celle de la covalence mais non identique. La différence provient de ce que la réduction du moment orbital produite par le couplage vibronique dépend de la température alors qu'on admet que le paramètre de covalence k est indépendant de la temperature. De la sorte il est en principe possible à partir d'une courbe expérimentale de variation de μ_{eff} en fonction de la température et si on connaît le coefficient de couplage spin-orbite λ et la fréquence $h\omega_\varepsilon$ de déterminer de façon univoque k et x. Cela suppose évidemment que l'on soit sûr qu'aucun champ axial ne se superpose au champ cubique. De plus, il faut noter que dans le calcul de la susceptibilité magnétique nous avons admis que les composés étaient magnétiquement dilués et que nous pouvions ignorer toute interaction d'échange; cette approximation n'est certainement plus valable aux très basses températures. Ainsi lorsque T tend vers zéro, la variation expérimentale de la susceptibilité magnétique peut-elle devenir très différente de la variation théorique telle qu'elle est représentée sur une des Figs. 1 6.

Il faut enfin ne pas perdre de vue que les quatre paramètres utilisés dans cette étude, à savoir λ, x, $h\omega_\varepsilon$ et k, ne sont pas rigoureusement indépendants. Ainsi peut-on voir en (15) que x dépend de la fréquence angulaire ω_r et de l'élément matriciel $\left\langle \psi_1^0 \middle| \frac{\partial H_E}{\partial Q_2} \middle| \psi_1^0 \right\rangle$; cet élément est lié à la forme des fonctions ψ_1^0 donc d'une certaine façon à la covalence. Cette difficulté conceptuelle n'est pas particulière au problème étudié ici; elle se rencontre entre autres à toutes les étapes de la théorie du champ de ligands. La possibilité que nous avons d'ajuster indépendamment les uns des autres certains paramètres qui en fait sont plus ou moins liés entre eux donne à la théorie une flexibilité qui facilite indûment l'accord entre courbes théoriques et courbes expérimentales.

Références

1. Kahn, O., Kettle, S.F.A : Molecular Physics, à paraître.
2. . Molecular Physics, à paraître.
3. Ham, F.S Physic. Rev. A **138**, 1727 (1965)
4. Van Vleck, J. H. The theory of electric and magnetic susceptibilities. Oxford University Press 1932.
5. Kotani, M : J physic Soc. Japan **4**, 293 (1949).
6. Figgis, B N : Trans Faraday Soc. **57**, 198 (1961).
7. Figgis, B N : Trans. Faraday Soc. **57**, 204 (1961).
8. Gerloch, M . J chem Soc **1968**, 2023.
9. Stevens, K W.H : Proc Roy Soc (London) A **219**, 542 (1953).
10. Gerloch, M., Miller, J.R : Progr. inorg. Chem. **10**, 1 (1968).
11. Ballhausen, C J Theoret chim Acta (Berl) 3, 368 (1965).
12. Sturge, M D . Solid State Physics, **1967**, 91.

Dr. O. Kahn
Ecole Nationale Supérieure de Chimie de Paris
11, rue Pierre et Marie Curie
F-75 Paris 5ème, France

Theoret. chim. Acta (Berl.) 27, 197–212 (1972)
© by Springer-Verlag 1972

Simplified Non-Empirical Excited State Calculations

Part I. The Rydberg *ns* and *npσ* Series of Ethylene

I. Fischer-Hjalmars and J. Kowalewski

Institute of Theoretical Physics and Institute of Inorganic and Physical Chemistry
University of Stockholm, Stockholm, Sweden

Received May 12, 1972

A simple non-empirical method for calculating electronic molecular states based on the description of excited states by mixing singly-excited configurations is presented. The complexity of the multiconfigurational wavefunctions is overcome by using the frozen-core approximation combined with natural orbital transformation. The method is tested on some low-lying excited states of the hydrogen molecule and is applied on Rydberg *ns* and *npσ* series of ethylene for $n = 3, 4, 5$, and 6. Transition energies, oscillator strengths and some other properties are computed. Internal consistency of the results and their agreement with available experimental data are good.

Ein einfaches nicht-empirisches Verfahren für die Berechnung angeregter molekularer Zustände, das auf der Darstellung durch Linearkombinationen einfach angeregter Zustände beruht, wird vorgeschlagen. Die Komplexität des Mehrfach-Determinanten-Ansatzes wird durch Verzicht auf die Änderung der Rumpfzustände und Transformation auf natürliche Orbitale gemeistert. Testrechnungen für einige tiefliegende H_2-Zustände und Rydbergzustände von Äthylen werden ausgeführt und Übergangsenergien, Oszillatorstärken und anderes mehr berechnet. Konsistenz untereinander und Übereinstimmung mit dem Experiment sind gut.

Presentation d'une méthode non empirique simple pour le calcul des états électroniques moléculaires fondée sur la description des états excités par interaction de configurations monoexcitées. La complexité des fonctions d'onde multiconfigurationelles est évitée en utilisant l'approximation du coeur fixe combinée avec l'emploi des orbitales naturelles. La méthode est éprouvée sur certains états excités inférieurs de la molécule d'hydrogène et appliquée aux séries de Rydberg *ns* et *npσ* de l'éthylène pour $n = 3, 4, 5$ et 6. Calculs des énergies de transition, des forces oscillatrices et de quelques autres propriétés. La cohérence interne des résultats et l'accord avec les données expérimentales disponibles sont bons.

1. Introduction

During the last decade non-empirical calculations on electronic states of molecules have steadily become more frequent and the quality of results from such calculations has considerably improved. Recently also excited electronic states have been successfully treated by such methods. One goal towards which various attempts have already been made is to develop methods yielding reliable results without requiring excessive computational effort or computer time. This goal forms one of the two aims of the present study. The other aim is to investigate the molecular Rydberg states of ethylene by applying our method to perform calculations on them. This kind of close investigation of the Rydberg states is one of many necessary steps to a better interpretation of the electronic spectra of various molecules. In particular, the calculation of both the excited state energies and the transition probabilities is required since both these quantities are used in making spectral assignments.

Sects. 2 and 3 are a brief outline of the theory, stressing a few points the principles of which are well understood although their applications on performing calculations of this kind seems to have been somewhat neglected. In Sect. 4 our method of computation is presented in detail. In Sect. 5 an application to the hydrogen molecule is carried out in order to illuminate certain features of our method. Sect. 6 describes the application to the Rydberg states of ethylene. The results of the calculations are presented in Sect. 7. Finally we conclude in Sect. 8 with a commentary and evaluations of the present study and its relationship to similar work being done elsewheres.

2. Theory

As is well-known, the Hartree-Fock equations for a closed-shell system can be written

$$F\varphi_r = \varepsilon_r \varphi_r , \tag{1}$$

$$F = H + \sum_{j=1}^{N} (2J_j - K_j) . \tag{2}$$

As usual, H is the bare-nuclei one-electron operator, and J_j and K_j are the Coulomb and exchange operators. Since F is Hermitian, the eigenfunctions $\{\varphi_r\}$ will form a complete orthonormal set. As discussed in detail e.g. by Huzinaga and Arnau [1] this set can be divided into two subsets $\{\varphi_0\}$ and $\{\varphi_v\}$, representing the occupied and the virtual orbitals. $\{\varphi_0\}$ and $\{\varphi_v\}$ will span orthogonal subspaces of the complete Hilbert space spanned by $\{\varphi_r\}$. As is well-known, the finite set $\{\varphi_0\}$ is adequate for construction of a Slater determinant Ψ_0 representing the ground state wavefunction

$$\Psi_0 = \mathscr{A}(\varphi_1 \bar{\varphi}_1 \varphi_2, \ldots, \bar{\varphi}_N) . \tag{3}$$

In principle $\{\varphi_v\}$ will be an infinite set. However, in practice the Eqs. (1) are solved by setting

$$\varphi_r = \Sigma\, \chi_\mu c_{\mu r} \tag{4}$$

where $\{\chi_\mu\}$ is ome suitably chosen finite basis set, $\mu = 1, 2, \ldots, M$. Consequently, the subsets $\{\varphi_v\}$ will now be reduced to $(M - N)$ members.

The simplest way of constructing an excited state wavefunction is to replace one of the ground state orbitals φ_i, $i \subset 0$, by a virtual orbital φ_m, $m \subset v$. The resulting wavefunction of the correct multiplicity may be denoted $\Psi(\varphi_i \to \varphi_m)$. Usually this wavefunction is not entirely adequate for the description of an excited state, not even when the φ_r's have emerged from a large basis SCF calculation.

Various suggestions have been made to remedy this deficiency. One way is to keep to the method of replacement of a single orbital of Ψ_0 but to search for other virtual orbitals than those of Eq. (1), i.e. to make a transformation of the subspace $\{\varphi_v\}$ without changing the subspace $\{\varphi_0\}$.

To this end, various procedures have been suggested, e.g. by Hunt and Goddard [2] and by Huzinaga and Arnau [1]. However, these treatments imply orthogonality problems or rather lengthy and somewhat arbitrary projection techniques. Another possibility is to carry out separate SCF calculations for each excited state, see e.g. Buenker and Peyerimhoff [3]. These authors have combined the SCF procedures with extensive CI treatments. Their method may be the most adequate for special cases, but becomes very cumbersome when several excited states of the same symmetry are of interest and/or large molecules are considered.

In the present study a rather simple method is presented, though obviously reasonably adequate for certain purposes. The method is a CI method which in the general case means that an excited state is described by combination of several configurations:

$$\Phi^\alpha = \Sigma\, \Psi(\psi_i \psi_j \ldots \to \psi_l \psi_m \ldots)\, C^\alpha_{ij\ldots lm\ldots} \tag{5}$$

where the sum is extended over all possible combinations of occupied orbitals with virtual orbitals. However, in our method the frozen-core approximation has been adopted, i.e. only singly excited configurations are included and the sum is restricted to excitations from a specific occupied orbital ψ_i:

$$\Phi^\alpha = \sum_m \Psi(\psi_i \to \psi_m)\, C^\alpha_{im}\,. \tag{6}$$

The ψ_i's, $i \subset 0$, are eigenfunctions of the ground state Hartree-Fock operator F. Furthermore, all the ψ_m's, $m \subset v$, also belong to this same set $\{\psi_r\}$.

The coefficients C^α_{im} are to be determined by a variational procedure. With the present choice of $\{\psi_r\}$ the matrix elements of the Hamiltonian are composed of ε_r's and two-electron integrals. There is no orthogonality problem and the calculation of transition probabilities is straightforward. However, an attempt to treat several kinds of excited states by use of the same expansion (4) will give rise to either poorly convergent series (6) or unwieldy calculations.

A way out of this dilemma is to limit the interest to a certain class of excited states, e.g. the *ns* series of Rydberg states. The choice of $\{\chi_\mu\}$ has to be made *with particular reference to this class*. Consequently, it may be possible to extend the basis sufficiently for a good description of this particular class, yet keeping the number $(M - N)$ within reasonable limits. Thus, the clue is to choose the set $\{\chi_\mu\}$ to give a good representation of only a special subset $\{\psi_w\}$ of the whole set of virtual orbitals $\{\psi_v\}$. Then, the diagonalisation of the Hamiltonian matrix may provide adequate description of several excited states of the same symmetry.

The adoption of a frozen core implies that the ionization potential can be obtained from Koopmans' theorem within an approximation similar to that of the excitation energies. This expectation is reasonable since both reorganization and correlation are likely to be roughly the same in a Rydberg state as in the corresponding ionized state.

Although the multiconfigurational wavefunctions (6) are not easily surveyable, a simplified interpretation of the excitation process can easily be regained by a transformation to natural orbitals (NO's) ϕ_l [4, 5]. This can be achieved by diagonalization of the first-order density matrix in the ψ-space representation. Then, Eq. (6) can be written

$$\Phi^\alpha = \Sigma\, \Phi(\phi_i \to \phi_m)\, B^\alpha_{im}\,. \tag{7}$$

Since the frozen-core approximation is used this diagonalization leads to $N-1$ doubly occupied NO's identical with the ground state occupied molecular orbitals φ_j, $j \neq i$, and two singly occupied NO's one being identical with φ_i, the other one being the orbital occupied in the excited state under consideration but not in the ground state. The values of the diagonal elements of the first order density matrix representation in the NO space satisfy the sufficient condition for Φ^a to be a single-configuration wavefunction, i.e. the sum in (7) is reduced to a single term.

3. Rydberg States

Molecular Rydberg states are commonly defined from the orbital point of view [6–8]. Using this model, a Rydberg state can be described by replacing one of the ground state orbitals by a molecular orbital, called Rydberg orbital, so large in size compared with the molecular core that it can be well described by the united atom (UA) model. Rydberg states fall into series such that the excitation energies, E_n, fit the formula

$$E_n = E(IP) - R/(n-\delta)^2 \tag{8}$$

where R is the Rydberg constant and δ the quantum defect (a positive quantity that varies rather strongly with the azimuthal quantum number l of the UA orbital, but only slightly with the principal quantum number n). In (8), a singly-charged core has been assumed. $E(IP)$ is the energy of ionisation (ionization potential).

4. Computational Details

In the present study the basis set (χ_μ) has been chosen as Gaussian Type Functions (GTF). From the primitive set a smaller set of Contracted Gaussian Type Functions (CGTF) has been obtained as described below. The SCF-MO wavefunctions and the electron repulsion integrals over the CGTF's have been computed with the IBMOL program version 4 [9] using the method described by Clementi and Davis [10]. The CI procedure involves the transformation of the two-electron integrals to the MO basis and construction and diagonalization of the Hamiltonian matrix. The symmetry of the system has been used extensively to bring down the number of integrals to be computed and the size of the matrices to be diagonalized. The computations have been carried out for both singlet and triplet excited states. Dipole matrix elements have been computed by the method of Browne and Poshusta [11].

5. Applications to Hydrogen

A test of the present method has been made by applying it to some lowlying excited states of the hydrogen molecule. The basis chosen in this case included ten GTF's of s-type with exponents optimized by Huzinaga [12], three GTF's of p-type and one of each of the types d_{xx}, d_{yy} and d_{zz} on each atom. No contraction was applied.

Table 1. Energy data for some of the lower states of the H_2 molecule with ground state equilibrium distance, $R = 1.40$ a.u.

State	Total energy, a.u.			Vertical transition energy from the ground state, e.V.			
	CI	SCF	Accurate	Single configuration	CI	SCF	Accurate
$X\,^1\Sigma_g^+$ (ground)	-1.133595	-1.133595	-1.174442^a				
$B\,^1\Sigma_u^+$	-0.665456	-0.699693	-0.703744^a	13.43	12.73	11.81	12.81^a
$E\,^1\Sigma_g^+$	-0.622893		-0.681254^a	13.27	13.08		13.42^a
$b\,^3\Sigma_u^+$	-0.767200		-0.783150^a	13.21	9.97		10.65^a
$a\,^3\Sigma_g^+$	-0.691346		-0.71294^b	12.93	12.03		12.56^b
$H_2^+\,^2\Sigma_g^+$		-0.569979	-0.569979^c		16.18^d	15.34	16.45^c

[a] Ref. [13]. - [b] Ref. [14]. [c] Ref. [15]. - [d] Koopmans' theorem value.

To compare the present CI method with the above-mentioned method including SCF calculations for excited states the Hartree-Fock equations were solved both for the ground state $X\,^1\Sigma_g^+$ and for the lowest excited singlet $B\,^1\Sigma_u^+$. The total energy of the ground state was found to be -1.133595 a.u., cf. Table 1. According to Kolos and Roothaan [13] the Hartree-Fock limit is -1.133630 a.u., 0.040812 a.u. (1.11 eV) above the accurate energy value [13], the difference being the correlation energy. For the $B\,^1\Sigma_u^+$ state we obtained an SCF energy of -0.699693 a.u. only 0.00405 a.u. (0.11 eV) above the accurate value. Our basis set was not particularly well adapted to describe this state which is a Rydberg state [16], since our lowest orbital exponent was 0.0285649 and more diffuse basis functions may be required for a good description. The correlation energy of this state is therefore surely smaller than 0.1 eV. This result is in strong support of the above-mentioned conjecture about equality of the correlation energy of a Rydberg state and the corresponding ionized state.

Our CI method with fifteen singly excited configurations produced an energy value of -0.665456 a.u., cf. Table 1. The transformation to NO's showed that the state can be described as built from a ground state $1s\sigma_g$ orbital and a $2p\sigma_u$ NO. The latter orbital was found to be rather similar to the $2p\sigma_u$ orbital, obtained from our SCF calculation. Since we have used the frozen-core approximation, the total energy difference between the results of the SCF and the CI calculations, 0.034237 a.u. (0.9 eV), can be interpreted as reorganization energy.

This value may be compared with the reorganisation energy of the H_2^+ ion. Using Koopmans' theorem, the orbital energy of the ground state, $\varepsilon = -0.594485$, the correlation energy of this state and the accurate energy of the H_2^+ ground state, the ionic reorganisation energy is found to be 0.030834 a.u. (0.84 eV). Thus, it is borne out that also the conjecture about the reorganisation energies is correct in this case. Moreover, it is noticeable that the change in correlation energy between the ground state and the excited state has almost the same value as the reorganisation energy so that these two quantities almost cancel. This cancellation is also obvious from the vertical transition energies, listed in Table 1, showing that the CI-values are very close to the accurate values, in particular for the first excited singlet. A similar cancellation has been found also in other calculations of ionization potentials using Koopmans' theorem.

Finally, vertical transition energies found from the single configuration description using ground state optimized MO's should be compared with the CI result, cf. Table 1. Obviously, this kind of single configuration is not entirely adequate for the description of excited states. As discussed by previous authors [2, 3] some kind of improvement is called for. The present scheme for CI calculations seems to show one possibility for the desired improvement.

6. Applications to Ethylene

The electronic spectrum of ethylene is of great interest and has been studied both experimentally and theoretically by many authors. A comprehensive review of the literature until 1968 has been given by Merer and Mulliken [17]. Several new theoretical [18 21] and experimental [22, 23] investigations have been reported in recent years. Most interest has been devoted to the valence excited *T* and *V* states and the lowest Rydberg states, while studies of higher Rydberg states have been more infrequent. The present investigation concerns two different Rydberg series, viz. the well-known *ns* series and a *npσ* series, including states with $n = 3, 4, 5$, and 6.

6.1. Basis Set

The choice of suitable GTF's for the description of molecular Rydberg states is a rather complicated matter. Preliminary computations on ethylene with some different basis sets indicated that the basis functions actually can be separated into two subsets:

1. Ground state (Normal state) basis functions, NGTF's, with exponents and contraction coefficients optimized in the usual way;
2. Rydberg state basis functions, RGTF's.

These two sets seem to be rather independent. Inclusion of the RGTF's has an insignificant effect both on the total energy of the ground state and on the orbital energies of the occupied orbitals. On the other hand, computations using quite different NGTF's but the same set of RGTF's display very small changes in the orbital energies of the lower virtual orbitals. The influence of the NGTF's on the Rydberg state energies E_n of Eq. (8) appears almost solely in the values of ε_i. Since the same ε_i is responsible for the value of $E(IP)$ the values computed for the quantum defects are effectively independent of the NGTF's. A change of the RGTF's, however, was found to have a drastic effect on the energies of both virtual orbitals and Rydberg states.

As a consequence, the choice of basis set was divided into two separate problems. The set of NGTF's was chosen as the ethylene-optimized basis set of Schulman *et al.* [24], including eight GTF's of *s*-type and four of *p*-type on each carbon atom and four GTF's of *s*-type on each hydrogen. All basis functions composing σ-orbitals were contracted to a minimal basis set as given by Schulman *et al.* [24]. Since we aimed at a rather good description of the occupied π-orbital, only a four-to-two contraction was used for the π-type GTF's.

Table 2. RGTF's for the *ns* and *npσ* Rydberg series in ethylene

Center	Orbital exponent	
	s-functions	*p*-functions
Carbon atoms	0.048708[a]	0.028858[a]
	0.019631[a]	
Molecular midpoint	0.00791	0.01582
	0.00319	0.00638
	0.00129	0.00258
	0.00052	0.00104
Hydrogen atoms	0.0413[a]	

[a] Ref. [25].

The choice of a RGTF set is less straightforward. In a study of Rydberg states of the methyl radical McDiarmid [25] has reported orbital exponents suitable for two 3*s*-type and one 3*p*-type GTF on carbon and for one 2*s*-type GTF on hydrogen. Gaussians with still smaller exponents can hardly be centered on the carbons since this would cause so large overlap integrals that convergence of the SCF calculations might be prohibited. We therefore chose to center the most diffuse GTF's at the midpoint of the C–C bond. Refraining from the complicated procedure of optimizing the exponents of these functions we adopted the method of obtaining the exponents simply by division with a constant factor, starting with the most diffuse of the carbon 3*s* functions and using the ratio of the two 3*s* exponents as our constant. In this way we constructed four *s*-type GTF's. To get GTF's of p_z-type (along the C–C bond) we multiplied the *s*-type exponents by two. The RGTF's thus obtained (eighteen) are listed in Table 2. A calculation of the radial distribution functions of these RGTF's indicated that this basis set should be adequate also for higher members of the Rydberg series.

It should be stressed that the present set of RGTF's is chosen to be a *subset* $\{\chi_w\}$ of the whole set $\{\chi_v\}$ necessary to represent all kinds of virtual orbitals, cf. Sect. 2 above. Using this subset we cannot expect to obtain good results for all kinds of excited states, only for the Rydberg *ns* and *npσ* series we had in mind making our choice of $\{\chi_w\}$. For a study of e.g. the *T* and *V* states or other Rydberg series a different subset $\{\chi_w\}$ must be constructed.

6.2. Ground State SCF Calculation

All the calculations on ethylene have been carried out with the ground state equilibrium geometry as given by Allen and Plyler [26]. With this geometry the ethylene molecule belongs to the point group D_{2h}. The coordinate system was chosen according to the recommendation by Mulliken [27], the molecule lying in the *yz* plane with the CC and *z* axes collinear. The notations B_1, B_2, and B_3 of the symmetry species are referred to this particular choice of axes. Then the ground state electronic configuration is $(1a_g)^2\,(1b_{1u})^2\,(2a_g)^2\,(2b_{1u})^2\,(1b_{2u})^2\,(3a_g)^2\,(1b_{3g})^2\,(1b_{3u})^2$. The first seven orbitals constitute the σ-core while the $1b_{3u}$ orbital is the carbon-carbon bonding π-orbital.

Table 3. Orbital energies for some low-lying virtual orbitals of ethylene

Orbital	Orbital energy, a.u.
$4a_g$	0.00066
$5a_g$	0.00323
$6a_g$	0.01029
$7a_g$	0.02924
$8a_g$	0.08168
$9a_g$	0.09734
$3b_{1u}$	0.00217
$4b_{1u}$	0.00799
$5b_{1u}$	0.02181
$6b_{1u}$	0.05153

With our basis set of 74 GTF's, contracted to 34 CGTF's, the computation of the electron repulsion integrals with IBMOL 4 was by far the most computer-time-consuming part of this study. The total energy obtained from the SCF treatment was −77.91451 a.u. to be compared with the value −77.90830 obtained by Schulman *et al.* [24] with a basis set of NGTF's only and four-to-one contraction of all the *p*-functions. The Hartree-Fock energy of ethylene is close to the best value computed by Siegbahn [28], −78.062 a.u. The present values of the ε_i's of the occupied orbitals are very close to those of Schulman *et al.* [24]. The energy of the π-orbital, −0.3873 a.u. (10.54 eV), is of particular interest since Koopmans' theorem has been used in the discussion of the results for the Rydberg states. The experimental value of the vertical ionization potential reported by Eland [29] is 10.51 eV.

The ε-values found for the virtual orbitals are very low; as many as ten of them lie below 0.1 a.u. Some of the values are listed in Table 3. They are throughout lower than the corresponding values obtained by Buenker *et al.* [20] from their ground state SCF calculation to be used in a subsequent CI treatment. We do not expect these virtual orbitals to have any physical significance individually. Nevertheless, they may constitute an adequate subset $\{\varphi_w\}$ for a CI description of certain excited states, cf. Sect. 2.

6.3. *Choice of Configurations for the* CI *Procedure*

According to the frozen-core approximation the configurations to be included in the CI treatment should be singly-excited and originating from a chosen occupied orbital φ_v, cf. Eq. (6). In case of the present Rydberg series this occupied orbital should be the π-orbital. The computation is extremely fast. It requires less than one minute computer time on an IBM 360/75 computer for both the Rydberg series, singlets and triplets included.

In the special case of ethylene other kinds of CI treatments are also feasible. One possibility would be to include all singly-excited configurations of appropriate symmetry, excluding only excitations from the carbon inner shells. Such an approach would allow for some reorganization, the amount of which being strongly basis set dependent. Also a partly valence character of the excited states may be described in this way. The wavefunctions obtained will, however, be multiconfigurational both in the (MO) ψ-basis of Eq. (5) and in the (NO) ϕ-basis of Eq. (7). Natural orbitals may still be used for computation of one-electron properties, but the clearness of the model will be lost, at least partly. The interpretation of Eq. (8) will become obscured. Ionization potentials cannot be obtained in a consistent manner neither from Koopmans' theorem nor from SCF computations.

For the sake of comparison, some Rydberg state energy calculations have been carried out by the more extended CI method. However, most of the results presented below refer to first method described above being the one we judge suitable for future development and applications.

7. Results

7.1. B_{3u} States – ns Rydberg Series

Excitations from the occupied π-orbital to a virtual σ-orbital and belonging to the B_{3u} species are of the type $1b_{3u}\rightarrow ma_g$, with $m = 4, 5, \ldots, 12$. Excitations from an occupied σ-orbital to a virtual π-orbital belonging to the same species and included in the extended CI treatment are $2a_g\rightarrow 2b_{3u}$, $3a_g\rightarrow 2b_{3u}$, $2b_{1u}\rightarrow 1b_{2g}$ and $2b_{1u}\rightarrow 2b_{2g}$.

The energies obtained for the five lowest Rydberg singlets and triplets and the singlet-triplet splittings are summarized in Table 4, which also displays experimental data for the singlets [30, 31]. Results from the frozen-core approximation (nine configurations) as well as results from an extended CI treatment (thirteen configurations) are given. It is seen that the extension to $\sigma\rightarrow\pi$ excitations has an almost negligible effect on the energy values. The agreement between calculated and experimental values is rather good, which seems to confirm the expectation that correlation and reorganization energies should almost cancel for Rydberg states. The somewhat inferior agreement for the first member of the series may be due to some valence character of this state.

The singlet-triplet splittings are small for all the states and in particular for the higher ones. This may be interpreted as a result of the very small differential overlap between the occupied π-orbital and the very diffuse Rydberg NO's of these states.

Table 4. Some lower B_{3u} states of ethylene

Frozen core CI				Experimental	Extended CI	
Vertical transition energies, eV		Singlet-triplet splitting eV	Oscillator strength of singlet	0-0 transition energies, eV	Vertical transition energies, eV	
Singlet	Triplet				Singlet	Triplet
7.523	7.376	0.157	0.045	7.11[a]	7.522	7.363
9.090	9.025	0.065	0.022	8.90[b]	9.089	9.020
9.404	9.377	0.027	0.003	-	9.403	9.376
9.770	9.758	0.012	0.003	9.62[b]	9.770	9.757
10.049	10.026	0.023	0.004	9.95[a]	10.048	10.021

[a] Ref. [30]. - [b] Ref. [31].

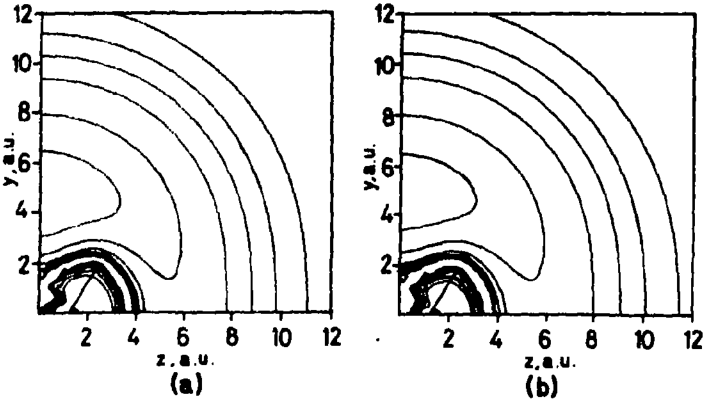

Fig. 1. Charge density contours for (a) 3s natural orbital and (b) corresponding $4a_g$ MO obtained from the open shell SCF calculation

To compare the present method with other possible methods we have carried out a restricted Hartree-Fock open shell calculation for the lowest $^1B_{3u}$ state using the same basis set as described above. The total energy was found to be 6.734 eV above the ground state energy. As could be anticipated, this energy difference is too small since reorganization but not correlation is taken into account by this kind of SCF method. An interesting result of this calculation is that the $4a_g$ orbital obtained by the SCF method is very similar to the Rydberg $4a_g$ orbital obtained by a very different procedure, viz. by the transformation to natural orbitals of the CI result for the lowest $^1B_{3u}$ state. Charge density contours in the molecular plane of these two differently computed $4a_g$ orbitals are presented in Fig. 1.

Table 4 also includes the computed oscillator strengths of the $^1A_g \rightarrow {}^1B_{3u}$ transitions which are fully allowed. No experimental values of the oscillator strengths are available. It is not very helpful to quote the experimental intensity values since the Rydberg transitions are found in the same region as a strong absorption continuum. Nevertheless, the experimental values strongly indicate that the intensity is considerably larger for the first members of the series than for the higher ones in good accord with the calculated values.

The $(n-\delta)^2$ values listed in Table 5 were found for all singlets by use of Eq. (8). The necessary value of the ionization potential, $E(IP)$, was calculated from Koopmans' theorem to be 10.539 eV. As discussed above the use of this theorem is consistent with our method of finding the energy values E_n of the Rydberg states. In order to obtain quantum defects δ which are reasonably constant within the series and of proper magnitude for Rydberg states of *ns* type the third state with $(n-\delta)^2 = 12.0$ must be excluded. Still, the composition of the CI vector of the third state does not immediately call for an exclusion. The motivation is however easily provided by inspection of the natural orbitals. The NO's of this state indicate that it should be interpreted as originating from a $\pi \rightarrow 4d\sigma$ transition. The Rydberg NO is mainly a $3p_z - 3p_z$ orbital. Its charge density contours in the molecular plane are presented in Fig. 2. It is easily seen that the orbital has a

Table 5. Properties of Rydberg natural orbitals found for some of the lower $^1B_{3u}$ states of ethylene

$(n-\delta)^2$	Rydberg natural orbital	Quantum defect	r_{max} of the outermost loop, a.u.	Expectation values of second moment components, a.u.		
				$\langle x^2 \rangle$	$\langle y^2 \rangle$	$\langle z^2 \rangle$
4.51	3*s*	0.88	5.7	18.18	21.29	14.89
9.40	4*s*	0.93	8.3	59.12	59.25	74.07
12.00	(4*dσ*)	(0.54)	—	47.86	47.89	62.47
17.72	5*s*	0.79	25.5	267.2	266.8	264.9
27.8	6*s*	0.7	42	740	740	739

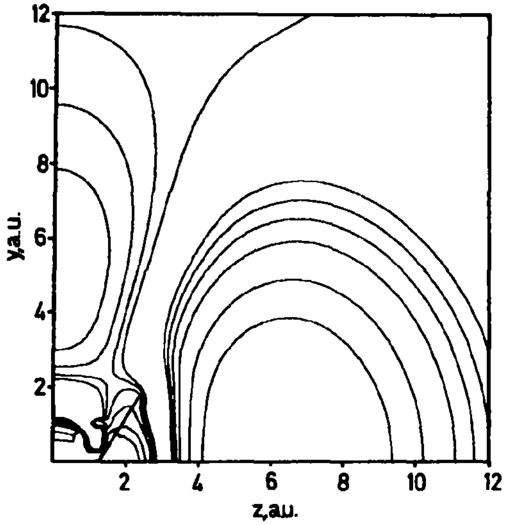

Fig. 2. Charge density contours for the natural Rydberg orbital of the third $^1B_{3u}$ state

clear *d* character. The presence of a transition of this type is by no means surprising and has actually been reported by Buenker *et al.* [20].

The present description of this state is however rather poor since our choice of the subset $\{\chi_w\}$ was made with the *ns* and *npσ* Rydberg orbitals in mind and not *ndσ* orbitals.

The assignments of the Rydberg orbitals and their quantum defects are listed in Table 5. In accord with Merer and Mulliken [17] we assume the lowest Rydberg *ns* orbital to be the 3*s* orbital. This assignment is at variance with the interpretation of Buenker *et al.* [20] who argue that this orbital must be the 4*s* since they assume all the three ground state occupied a_g orbitals to be united-atom *s* orbitals. Merer and Mulliken [17] on the other hand assumed the $3a_g$ orbital to be the united-atom 3*dσ* orbital. This latter assignment is strongly supported by our results. In Fig. 3 the charge density contours for the $3a_g$ orbital are displayed. This picture is very similar to the one for the $5a_g$ MO obtained by Buenker *et al.* [20] and assigned as united-atom *dσ* by themselves.

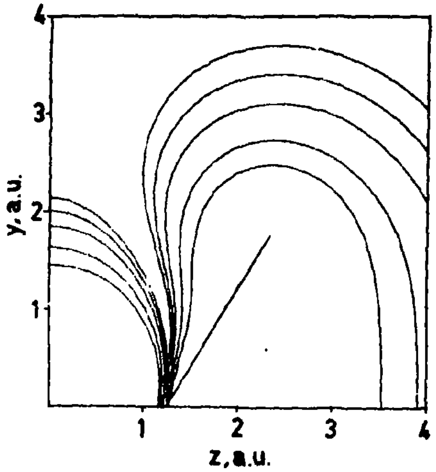

Fig. 3 Charge density contours for the $3a_g$ orbital

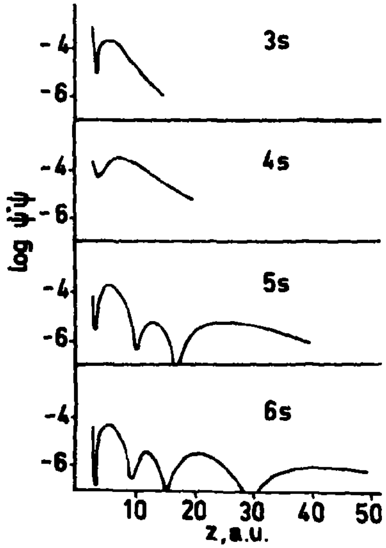

Fig. 4. Logarithm of charge density *vs* distance from the molecular midpoint along the z-axis (C–C axis) for ns natural orbitals

The charge densities of the Rydberg natural orbitals of ns type have been computed along the z-axis and are presented in Fig. 4. We have chosen to plot the logarithm of the density since we wanted to display the whole range of interest including all the loops. It should be mentioned that the curves have been obtained by computing $\psi^*\psi$ at rather arbitrarily chosen points so that neither the maxima nor the minima are very accurate. A rough estimate of the z-value, corresponding to the maximum of the outermost loop and called r_{max}, is given in Table 5. According to Mulliken [6] this r_{max} should be related to the effective quantum number: $r_{max} \approx (n-\delta)^2$. This relation holds moderately well for the first two orbitals but not so well for the highest ones. The outermost loop is found well outside the molecular core even for the 3*s* orbital. The 4*s* NO seems to have one loop missing, but an additional loop was observed on an analogous curve along the *y*-axis. The spherical symmetry of the 3*s* and 4*s* orbitals is somewhat distorted, as could be anticipated. This is clearly shown by the expectation values $\langle x^2 \rangle$, $\langle y^2 \rangle$, and $\langle z^2 \rangle$ listed in Table 5. The 5*s* and 6*s* orbitals are however very closely spherical. They are also very diffuse. It should be noted that all the *ns* NO's were found to be C-H antibonding in agreement with the maintainance of Merer and Mulliken [17].

7.2. B_{2g} States – *npσ* Rydberg Series

Excitations from the occupied π-orbital to a virtual σ-orbital and belonging to the B_{2g} species are of the type $1b_{3u} \rightarrow mb_{1u}$ with $m = 3, 4, \ldots, 12$. Excitations from an occupied σ-orbital to a virtual π-orbital belonging to the same species and included in the extended CI treatment are $2a_g - 1b_{2g}$, $2a_g \rightarrow 2b_{2g}$, $3a_g \rightarrow 1b_{2g}$, $3a_g \rightarrow 2b_{2g}$, and $2b_{1u} \rightarrow 2b_{3u}$. The energies obtained for the four lowest singlets and the corresponding triplets are presented in Table 6 together with the singlet-triplet splittings. Results from the frozen-core approximation (ten configurations) as well as from an extended CI treatment (fifteen configurations) are given. Also for this series the extension to $\sigma \rightarrow \pi$ excitations has a negligible effect. No experimental data are available since the ${}^1A_g \rightarrow {}^1B_{2g}$ transitions are dipole forbidden. Also in this case a restricted SCF open shell calculation was carried out for the lowest state of the series. The total energy was found to be 7.374 eV above the ground state energy. With the same argument as above this energy difference is presumably too small. A comparison of the SCF 3*pσ* orbital with the Rydberg NO orbital again shows large similarity between the two counterparts, cf. Fig. 5. The values of the singlet-triplet splitting, given in Table 6, seem to be reasonable for all the states.

Some properties of the *npσ* natural orbitals are presented in Table 7. The quantum defects are quite constant and of proper magnitude for a Rydberg series of *p*-type. The values of r_{max}, found from the densities displayed in Fig. 6, fit in with Mulliken's relation slightly better than in the *ns* series.

Table 6. Some lower B_{2g} states of ethylene

Frozen core CI Vertical transition energies, eV		Singlet-triplet splitting eV	Extended CI Vertical transition energies, eV	
Singlet	Triplet		Singlet	Triplet
8.224	8.153	0.079	8.222	8.143
9.406	9.381	0.025	9.405	9.375
9.864	9.851	0.013	9.863	9.852
10.098	10.088	0.010	10.096	10.087

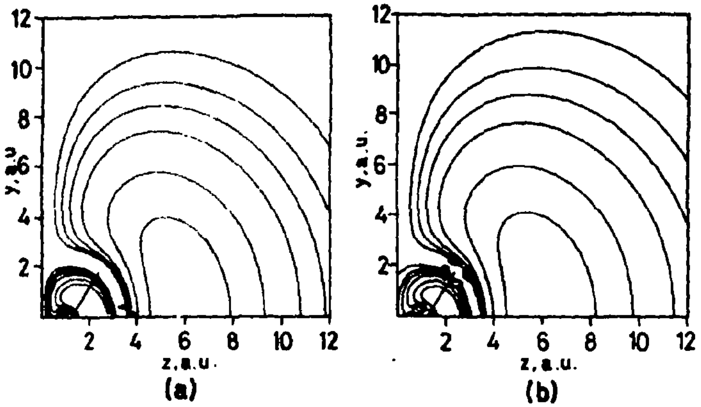

Fig. 5. Charge density contours for (a) $3p\sigma$ natural orbital and (b) corresponding $3b_{1u}$ MO obtained from the open shell SCF calculation

Table 7 Properties of some Rydberg $np\sigma$ natural orbitals in ethylene singlets

$(n - \delta)^2$	Principal quantum number n	Quantum defect δ	r_{max} for outermost loop, a.u.	Expectation values of second moment components, a.u. $\langle x^2 \rangle$	$\langle y^2 \rangle$	$\langle z^2 \rangle$
5.88	3	0.58	5.9	14.56	16.06	46.79
12.01	4	0.53	15.2	67.60	67.65	203.52
20.16	5	0.51	27.5	197.5	197.4	592.7
30.9	6	0.4	43	332	331	995

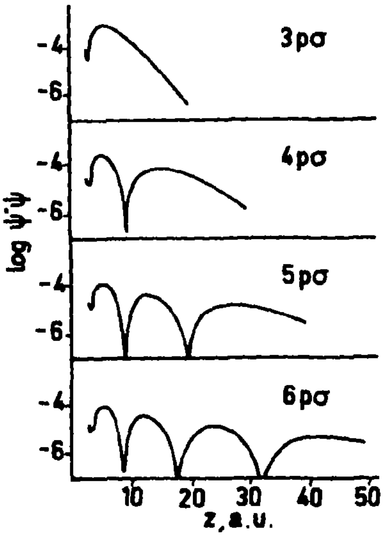

Fig. 6. Logarithm of charge density *vs.* distance from the molecular midpoint along the z-axis (C–C axis) for $np\sigma$ natural orbitals

It should be noted that the number of nodes in this series is in complete agreement with the assignments of principal quantum numbers provided that all the density minima indicated in Fig. 6 do represent nodes. The expectation values $\langle x^2 \rangle$, $\langle y^2 \rangle$, and $\langle z^2 \rangle$ show that the orbitals are very nearly ellipsoids of revolution. Further, it was found that also all the $np\sigma$ orbitals are C–H antibonding.

8. Discussion

The present study has been carried out in search for an excited state treatment, intermediate between very elaborate methods, such as the combined SCF and CI method [3], and drastically simplified methods, such as pseudopotential methods [32]. The drawback of the elaborate methods is that long experience and great care is needed in order to treat all states considered at equal levels of accuracy, including equal amounts of correlation, etc. Further, even if the principles of the treatment have been disentangled, the application to large systems will easily give rise to an unwieldy complexity. Also, liberal access to a large computer is a necessary pre-requisite for using such a method. Moreover, even the most extended (and costly) treatments have hitherto given only limited physical information.

At present, the most interesting results concerning excited Rydberg states seem to have emerged from the opposite kind of approach, viz. from the use of model potentials. As an example, Betts and McKoy [32] have presented calculations including sizable series of term values for both diatomic and polyatomic molecules, apparently in excellent agreement with experiments, using a one-particle model with a drastically simplified potential. Their results are indeed very encouraging. However, even their approach has certain drawbacks. Singlet and triplet states ought to be treated separately. A more serious deficiency is that the handling of the potential from hydrogen atoms seems to be rather casual. In its present form the method is seemingly unable to distinguish between Rydberg states of e.g. ethane and acetylene.

The present method is non-empirical and the application to any system is straightforward. Some consideration must be given to the choice of basis functions, but this part of the procedure can easily be handled after some more experience of various systems. More serious may be the necessity to carry out an SCF calculation for the ground state with the chosen basis set. However, the present rapid development of efficient programs may be helpful in this respect. Since the single necessary SCF calculation is by far the most computer-time-consuming part of the procedure, the whole calculation may hopefully become a rather modest operation, even for comparatively large molecules. In view of the completely non-empirical character of the method, the results obtained so far are rather promising. Both energies, transition probabilities, description of orbitals and other properties seem to come out with very reasonable values. Furthermore, the method is very flexible since it is easy to modify the accuracy in keeping with the actual need by extension or contraction of the basis set.

In conclusion, the present method seems to offer a useful alternative for studies of molecular excited states. Further applications are currently being performed in our Laboratories and will be published in the near future.

Acknowledgments We are indebted to Dr. Björn Roos and Mr. Per Siegbahn for valuable discussions and information about unpublished results and to Mrs. Janina Kowalewska for drawing the figures. One of us (J.K.) gratefully acknowledges support from Professor Ragnar Vestin.

References

1. Huzinaga, S., Arnau, C.: Physic. Rev. A **1**, 1285 (1970); J. chem. Physics **54**, 1948 (1971).
2. Hunt, W. J., Goddard III, W. A.: Chem. Physics Letters **3**, 414 (1969).
3. Buenker, R. J., Peyerimhoff, S. D.: J. chem. Physics **53**, 1368 (1970).
4. Löwdin, P.-O.: Physic. Rev. **97**, 1474 (1955).
5. Fischer-Hjalmars, I.: Trans. International Symp. Mol. Structure and Spectroscopy, B**205** (1962).
6. Mulliken, R. S.: J. Amer. chem. Soc. **86**, 3183 (1964).
7. Mulliken, R. S.: J. Amer. chem. Soc. **88**, 1849 (1966).
8. Mulliken, R. S.: J. Amer. chem. Soc. **91**, 4615 (1969).
9. Veillard, A.: IBMOL Version 4, Special IBM Technical Report, San José (1968).
10. Clementi, E., Davis, D. R.: J. comput. Physics **2**, 223 (1967).
11. Browne, J. C., Poshusta, R. D.: J. chem. Physics **36**, 1933 (1962).
12. Huzinaga, S.: J. chem. Physics **42**, 1293 (1965).
13. Kolos, W., Roothaan, C. C. J.: Rev. mod. Physics **32**, 219 (1960).
14. Wakefield, C. B., Davidson, E. R.: J. chem. Physics **43**, 834 (1965).
15. Bates, D. R., Ledsham, K., Stewart, A. L.: Philos. Trans. Roy. Soc. (London) A**246**, 215 (1953).
16. Herzberg, G.: Molecular spectra and molecular structure, Vol I. Spectra of diatomic molecules, 2nd Ed. Princeton, N. J.: Van Nostrand 1950.
17. Merer, A. J., Mulliken, R. S.: Chem. Reviews **69**, 639 (1969).
18. Dunning Jr., T. H., Hunt, W. J., Goddard III, W. A.: Chem. Physics Letters **4**, 147 (1969).
19. Basch, H., McKoy, W.: J. chem. Physics **53**, 1628 (1970).
20. Buenker, R. J., Peyerimhoff, S. D., Kammer, W. E.: J. chem. Physics **55**, 814 (1971)
21. Buenker, R. J., Peyerimhoff, S. D., Hsu, H. L.: Chem. Physics Letters **11**, 65 (1971).
22. Merer, A. J., Schoonveld, L.: Canad. J. Physics **47**, 1731 (1969).
23. Hubin-Franskin, M. J., Collin, J. E.: Int. J. Mass Spectrom. Ion Physics **5**, 163 (1970).
24. Schulman, J. M., Hornback, C. J., Moskowitz, J. W.: Chem. Physics Letters **8**, 361 (1971).
25. McDiarmid, R.: Theoret. chim. Acta (Berl.) **20**, 282 (1971)
26. Allen, H. C., Plyler, E. K.: J. Amer. chem. Soc. **80**, 2673 (1958)
27. Mulliken, R. S.: J. chem. Physics **23**, 1997 (1955)
28. Siegbahn, P.: Private Communication
29. Eland, J. H. D.: Int. J. Mass Spectrom. Ion Physics **2**, 471 (1969)
30. Price, W. C., Tutte, W. T.: Proc. Roy. Soc. (London) A **174**, 207 (1940).
31. Wilkinson, P. G.: Canad. J. Physics **34**, 643 (1956).
32. Betts, T., McKoy, V.: J. chem. Physics **54**, 113 (1971).

Prof. I. Fischer-Hjalmars
Institute of Theoretical Physics
University of Stockholm
Vanadisvägen 9
S-113 46 Stockholm
Sweden

Theoret. chim. Acta (Berl.) 27, 213–222 (1972)
© by Springer-Verlag 1972

Semiempirical Molecular Orbital Studies of Phthalocyanines

I. The Electronic Structure and Excited States of Phthalocyanine, H_2Pc

A. Henriksson* and M. Sundbom

Institute of Theoretical Physics, University of Stockholm, Vanadisvägen 9, 113 46 Stockholm, Sweden

Received May 23, 1972

The π and σ lone pair electron system of the phthalocyanine molecule has been studied by a semiempirical SCF-MO method. Electronic transitions of both $\pi-\pi^*$ and $n-\pi^*$ types have been considered. The excited states have been calculated by means of the method of superposition of configurations where all singly excited states are included Assignments for the electronic spectrum of phthalocyanine could be made in good agreement with experiment. The position of the lowest electronically allowed $n-\pi^*$ transition is predicted to be found in the region of the strong Soret band.

Das Elektronensystem der einsamen π- und σ-Elektronenpaare des Phthalocyaninmoleküls wurde mit Hilfe einer semiempirischen SCF-MO-Methode untersucht. Dabei wurden Elektronenübergänge vom $\pi-\pi^*$-Typ und vom $n-\pi^*$-Typ behandelt. Die angeregten Zustände wurden nach der CI-Methode unter Einschluß aller einfach angeregten Zustände berechnet. Die Zuordnung der Ergebnisse zum Elektronenspektrum des Phthalocyanins brachte gute Übereinstimmung mit dem Experiment. Die Lage des niedrigsten elektronisch erlaubten $n-\pi^*$-Übergangs wird für das Gebiet der starken Soret-Bande vorhergesagt.

Les électrons π et les paires libres σ de la molécule de phthalocyanine ont été étudiés par une méthode SCF MO semi-empirique. On envisage les transitions du type $\pi-\pi^*$ et $n-\pi^*$. Les états excités ont été calculés par la méthode de superposition des configurations incluant tous les états monoexcités. Les attributions du spectre électronique de la phthalocyanine sont en bon accord avec l'expérience. La position de la plus basse transition permise du type $n-\pi^*$ est prédite dans la région de la forte bande de Soret.

1. Introduction

Phthalocyanines have many important technological applications. They can be used as dyestuffs, catalysts and semiconductors. The literature contains several reviews of the chemistry and physics of these molecules [1–3]. In many respects the phthalocyanines resemble the biologically important porphyrins. It is therefore of great interest to perform a parallel study of phthalocyanines and porphyrins. Porphin and copper porphin have already been investigated by a semiempirical molecular orbital method at this laboratory [4, 5]. The present MO investigation of H_2Pc is the first in a series in progress studying phthalocyanines and metal phthalocyanines. Quite many Hückel calculations of these molecules have been reported in the literature [6–13].

Calculations with the free electron method have also been made [14]. Schaffer and Gouterman [15] used the extended Hückel method for a study of free base and metal phthalocyanines. SCF MO calculations with the Pariser-Parr-Pople (PPP) method were performed by Weiss, Kobayashi, and Gouterman [16]. They assumed D_{4h} symmetry and calculated the electronic spectra using a four orbital model. McHugh, Gouterman, and Weiss recently reported a full CI treatment with D_{4h} symmetry [17].

---

* Permanent address: Department of Physical Chemistry, University of Helsinki, Meritullink. 1, Helsinki 17.

As far as we know the present investigation is the first PPP CI study of H_2Pc assuming D_{2h} symmetry. The calculated spectrum shows a very good agreement with the observed vapour phase spectra. Especially the splitting of the Q band is well reproduced. The positions of the $n-\pi^*$ transitions are predicted. The lowest allowed $n-\pi^*$ transition is found in the region of the strong Soret band. The theoretical model is the same one as used in previous porphin calculations [4, 5].

2. Theoretical Model and Details of the Calculations

Method

The PPP method in the SCF-MO-LCAO form was adopted. A parameter scheme devised at this laboratory [18, 19] was used. These fixed parameters have been tested on a number of conjugated molecules containing nitrogen [4, 18, 19] and the results are in good overall agreement with available experimental data.

Excited states were calculated by means of the method of superposition of configurations, where all singly excited configurations are included.

The oscillator strengths were determined from the standard formula of Mulliken and Rieke [20].

Geometry

It is well known that crystalline H_2Pc exists in at least two polymorphic modifications: the stable β-form and the unstable α-form. The molecular geometry used in the calculations is based on the neutron diffraction data for the β-form [21]. These data show that the molecule can be considered as almost completely planar.

In the first calculation we have assumed D_{4h} symmetry for the carbon-nitrogen skeleton by taking the arithmetic means of the experimental values for equivalent bonds. These bond lengths are given in Table 3 (observed). The numbering of the atoms is shown in Fig. 1 together with the averaged bond angles.

The position of the protons attached to the inner ring atoms in H_2Pc has been the subject of much discussion [10, 11, 15]. According to the neutron diffraction data [21] the two protons are shared by all four nitrogens. UV- [22, 11] and IR-data [23], however, indicate that the symmetry of H_2Pc is D_{2h} and not D_{4h}.

In this study we have assumed that the two protons are located on two opposite nitrogens (2 and 4 in Fig. 1), leading to D_{2h} symmetry.

Schaffer and Gouterman [15] used extended Hückel calculations to study the location of free base protons. They concluded that the bonded structure, with two pyrrole and two *aza* nitrogens, is the most probable in the vapour.

Calculated bond distances were obtained from the calculated bond orders, $p_{\mu\nu}$, by means of the following bond order-bond length relations [18]:

$$R_{\mu\nu}(C, C) = 1.517 - 0.18\, p_{\mu\nu}\,, \tag{1}$$

$$R_{\mu\nu}(C, N) = 1.458 - 0.18\, p_{\mu\nu}\,. \tag{2}$$

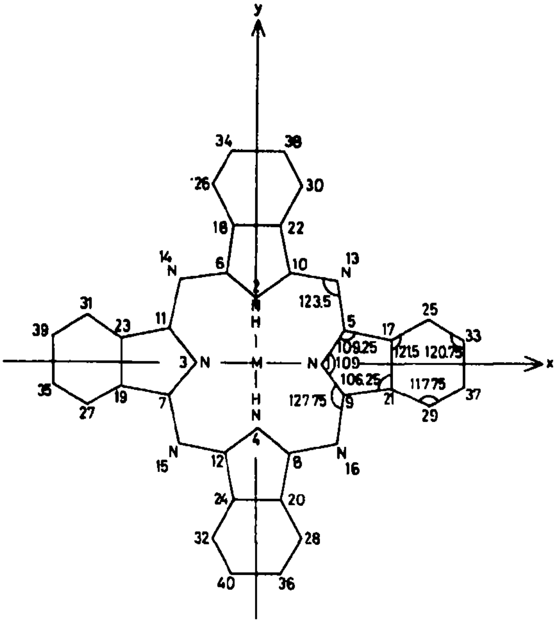

Fig. 1. The numbering system of phthalocyanine used in the present investigation. The bond angles are the averaged values from [21] giving the carbon-nitrogen skeleton D_{4h} symmetry. This geometry was used in the first calculation, cf. text

The calculation was repeated with the obtained values as input for the new geometry. After one iteration the calculated bond lengths deviated by less than ± 0.004 Å from the input value.

Calculations

The number of atomic orbitals that constitute the basis for the calculations is 46: 40π orbitals and $6sp^2$-hybridized nitrogen lone pair orbitals at the pyridine nitrogens. The number of electrons taken into account is 54.

The SCF molecular orbitals have been calculated by means of a computer program SCF-OPSZDO, written by Roos and Sundbom. This program also calculates the energy levels of excited states by mixing configurations obtained from single excitations. An IBM 360/75 computer was used for the present calculations.

3. Molecular Orbitals and Ground State Properties

The SCF molecular orbitals of H_2Pc are presented in Table 1, where the orbital energies, ε_i, and the electronic populations are given.

The vertical ionization potential of H_2Pc, obtained from the energy of the highest filled orbital, is 5.7 eV. As fas as we know there are no observed gasphase ionization potentials for phthalocyanines. For the solid state several measure-

Table 1 Molecular orbitals of H_2Pc. Orbital energies ε_i in a.u. Population analysis. The numbering system as in Fig.

No	MO	ε_i	Population analysis[a]										
	Symmetry		N_1[b]	N_2	C_5	C_6	N_{13}[b]	C_{17}	C_{18}	C_{25}	C_{26}	C_{33}	C_{34}
Occupied													
1	$1b_{1u}$	−0.5074	0.0313	0.0621	0.0357	0.0537	0.0428	0.0131	0.0369	0.0035	0.0115	0.0012	0.0050
2	$1b_{3g}$	−0.4982		0.0893	0.0063	0.0702	0.0319	0.0004	0.0625	0.0001	0.0227	0.0000	0.0113
3	$1b_{2g}$	−0.4887	0.0810		0.0809	0.0137	0.0468	0.0438	0.0013	0.0156	0.0003	0.0070	0.0000
4	$2b_{1u}$	−0.4636	0.0507	0.0198	0.0413	0.0098	0.0035	0.0405	0.0387	0.0207	0.0267	0.0127	0.0209
5	$2b_{3g}$	−0.4368		0.0620	0.0078	0.0156	0.0220	0.0009	0.0199	0.0004	0.0610	0.0001	0.0913
6	$1a_u$	−0.4352			0.0431	0.0692	0.1133	0.0049	0.0122	0.0021	0.0052	0.0003	0.0008
7	$3b_{1u}$	0.4327	0.0006	0.0757	0.0002	0.0158	0.0090	0.0152	0.0091	0.0256	0.0400	0.0313	0.0658
8	$2b_{2g}$	−0.4263	0.0138		0.0070	0.0169	0.0253	0.0274	0.0031	0.0670	0.0017	0.0945	0.0003
9	$4b_{1u}$	0.4108	0.0700	0.0760	0.0294	0.0091	0.0036	0.0027	0.0001	0.0361	0.0055	0.0746	0.0160
10	$1a_g$	0.3818					0.2500*n*						
11	$1b_{3u}$	−0.3818					0.2500*n*						
12	$1b_{2u}$	0.3818					0.2500*n*						
13	$2a_g$	0.3818	0.5000*n*										
14	$1b_{1g}$	0.3818					0.2500*n*						
15	$2b_{3u}$	0.3818	0.5000*n*										
16	$3b_{2g}$	0.3756	0.0668		0.0160	0.0574	0.0164	0.0038	0.0342	0.0030	0.0538	0.0200	0.0121
17	$3b_{3g}$	−0.3715		0.1426	0.0652	0.0015	0.0560	0.0205	0.0009	0.0266	0.0002	0.0055	0.0024
18	$2a_u$	0.3505			0.0160	0.0046	0.0051	0.0120	0.0331	0.0267	0.1159	0.0062	0.0305
19	$5b_{1u}$	−0.3391	0.0020	0.1322	0.0001	0.0004	0.0016	0.0001	0.0963	0.0000	0.0000	0.0002	0.0841
20	$4b_{3g}$	−0.3373		0.0945	0.0008	0.0001	0.0001	0.0022	0.1026	0.0074	0.0000	0.0019	0.0876
21	$3a_u$	−0.3277			0.0002	0.0061	0.0108	0.0265	0.0032	0.1265	0.0333	0.0334	0.0101
22	$4b_{2g}$	−0.3254	0.0168		0.0020	0.0250	0.0344	0.0186	0.0082	0.0000	0.1036	0.0178	0.0321
23	$5b_{3g}$	0.3184		0.0135	0.0075	0.0003	0.0310	0.0178	0.0110	0.1312	0.0001	0.0367	0.0078
24	$6b_{1u}$	−0.3049	0.0429	0.0043	0.0022	0.0001	0.0073	0.1232	0.0012	0.0032	0.0000	0.0885	0.0008
25	$5b_{2g}$	−0.3007	0.1094		0.0056	0.0067	0.0016	0.1008	0.0000	0.0035	0.0059	0.0689	0.0022
26	$7b_{1u}$	−0.2637	0.1308	0.0653	0.0015	0.0120	0.1083	0.0001	0.0180	0.0000	0.0021	0.0000	0.0099
27	$4a_u$	0.2096			0.0940	0.0878	0.0021	0.0052	0.0102	0.0158	0.0154	0.0089	0.0108
Unoccupied													
28	$6b_{3g}$	−0.0391		0.0552	0.0906	0.0420	0.0237	0.0241	0.0026	0.0071	0.0122	0.0133	0.0068
29	$6b_{2g}$	−0.0215	0.0732		0.0058	0.0566	0.0696	0.0003	0.0474	0.0025	0.0059	0.0013	0.0240
30	$5a_u$	0.0415			0.0246	0.0057	0.0559	0.0376	0.0585	0.0013	0.0005	0.0246	0.0413
31	$8b_{1u}$	0.0451	0.0253	0.0193	0.0061	0.0290	0.0094	0.0006	0.0117	0.0101	0.1202	0.0031	0.0376
32	$7b_{3g}$	0.0569		0.0030	0.0042	0.0056	0.0175	0.0135	0.0243	0.0001	0.1341	0.0102	0.0390
33	$9b_{1u}$	0.0714	0.0195	0.0005	0.0077	0.0007	0.0028	0.0299	0.0062	0.1335	0.0190	0.0352	0.0051
34	$7b_{2g}$	0.0718	0.0188		0.0075	0.0003	0.0034	0.0317	0.0098	0.1400	0.0001	0.0368	0.0109
35	$6a_u$	0.1002			0.0038	0.0223	0.0043	0.0386	0.0276	0.0029	0.0079	0.0674	0.0752
36	$8b_{2g}$	0.1029	0.0113		0.0043	0.0395	0.0094	0.0072	0.0378	0.0126	0.0141	0.0028	0.1167
37	$8b_{3g}$	0.1074		0.0116	0.0157	0.0249	0.0008	0.0514	0.0116	0.0083	0.0133	0.1152	0.0029
38	$10b_{1u}$	0.1223	0.0385	0.0389	0.0192	0.0932	0.0130	0.0116	0.0292	0.0131	0.0244	0.0026	0.0049
39	$7a_u$	0.1363			0.0360	0.0199	0.0401	0.0038	0.0000	0.0190	0.0164	0.0731	0.0416
40	$9b_{3g}$	0.1593		0.0272	0.0188	0.0842	0.0558	0.0018	0.0140	0.0183	0.0062	0.0363	0.0010
41	$9b_{2g}$	0.1853	0.0532		0.0517	0.0036	0.0066	0.0082	0.0615	0.0034	0.0465	0.0005	0.0412
42	$8a_u$	0.1975			0.0000	0.0269	0.0062	0.0106	0.0988	0.0085	0.0530	0.0076	0.0384
43	$11b_{1u}$	0.2069	0.0884	0.0058	0.1068	0.0263	0.0487	0.0131	0.0026	0.0041	0.0006	0.0006	0.0001
44	$10b_{2g}$	0.2120	0.0557		0.0691	0.0303	0.0365	0.0081	0.0467	0.0024	0.0181	0.0003	0.0106
45	$10b_{3g}$	0.2220		0.0012	0.0330	0.0056	0.0144	0.1174	0.0005	0.0505	0.0001	0.0308	0.0000
46	$9a_u$	0.2225			0.0323	0.0076	0.0123	0.1110	0.0075	0.0473	0.0023	0.0286	0.0012

[a] Formal population of the virtual orbitals. N_i and C_i denotes π orbitals on nitrogen and carbon.

[b] The letter *n* after the number indicates a nitrogen σ lonepair orbital.

Table 2. The total electron population of the atomic orbitals in H_2Pc. For comparison the population for porphin, H_2P, and pyrrole are also included. The numbering of the atoms is given in Fig. 1

AO[a]	H_2Pc	H_2P[b]	Pyrrole[c]
N_1	1.232	1.217	1.656
N_2	1.675	1.673	
C_5	0.925	0.956	1.072
C_6	0.952	0.968	
N_{13}	1.146	1.057	
C_{17}	0.959	1.029	1.099
C_{18}	1.003	1.051	
C_{25}	1.030		
C_{26}	1.010		
C_{33}	1.019		
C_{34}	1.003		

[a] N_i and C_i denotes π orbitals on nitrogen and carbon.

[b] From previous calc. [4].

[c] From previous calc. [18].

Table 3. Observed and calculated bond lengths of H_2Pc. The numbering of the atoms as in Fig. 1. All values in Å

Bond	Bond lengths		
	H_2Pc		Pyrrole
	Observed[a] [21]	Calculated	Observed [27]
5-1	1.373	1.349	1.374
6-2	1.373	1.379	
13-5	1.315	1.351	
14-6	1.315	1.338	
17-5	1.470	1.463	1.381
18-6	1.470	1.448	
21-17	1.405	1.409	1.417
22-18	1.405	1.412	
25-17	1.388	1.403	
26-18	1.388	1.409	
33-25	1.390	1.394	Benzene:
34-26	1.390	1.389	1.397
37-33	1.425	1.402	
38-34	1.425	1.407	
M[b]-1	1.959	2.040[c]	
M-2	1.959	1.946[c]	

[a] The observed values are the arithmetic means of the values of equivalent bonds, assuming the geometry has D_{4h} symmetry.

[b] *M* denotes the center of the phthalocyanine molecule.

[c] Cf. text.

ments have been performed (see Ref. [3], Table 6.7 for a review). According to Komp and Fitzsimmons [24] the bulk ionization potential of H_2Pc is 6.1 eV, whereas the surface ionization potential is 5.3 eV.

The two highest occupied orbitals have symmetries b_{1u} and a_u and the two lowest empty orbitals are b_{3g} and b_{2g} orbitals.

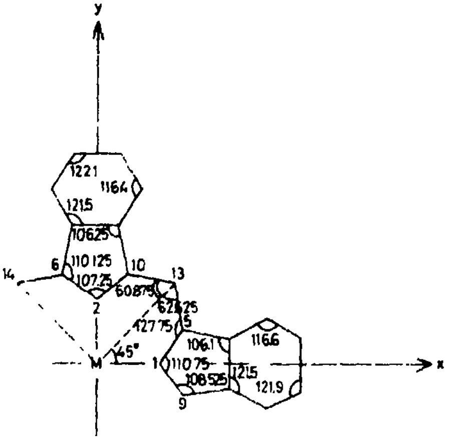

Fig. 2. The finally adopted bond angles, cf. text

The total electron population of the atomic orbitals is given in Table 2. The highest π-electron density is found on atoms N_1 and N_2 closely followed by atom N_{13}, whereas the lowest π-electron density is found for C_5 and C_6. This ordering is in accordance with most of the previous calculations.

The computed bond lengths are collected in Table 3 together with experimental data. For comparison the observed bond distances for pyrrole and benzene are also included. The computed bond distances from the first calculation were used to construct a new geometry in the following way: The angles 1-M-13 and 2-M-14 were assumed unchanged (45°). New structures were then tried using the computed bond distances and with the main angular change in the angles 5-1-9 and 6-2-10. A reasonable structure was obtained for an increase of the 5-1-9 angle by 1.75° and a decrease of the 6-2-10 angle by the same amount. The finally adopted bond angles are shown in Fig. 2. This structure has a somewhat larger hole size than the experimentally determined structure [21]. This is to be expected since the MO calculations describe a free molecule, whereas the neutron diffraction measurements give information about the structure of the molecule in a crystal.

4. Excited States

All singly excited configurations were included in the calculation of the transition energies. The results of the present CI treatment are presented in Tables 4 and 5. In Table 4 the allowed singlets (<55 kK) are given together with the four lowest triplets. A detailed presentation of the configuration mixing for some of the excited states is found in Table 5. Only those configurations which contribute to the wave function with coefficients larger than 0.2 are given in the table. Table 5 shows that the four lowest triplets and the two lowest singlets can almost be completely described by a four orbital model. Most of the singlets are however, characterized by a more extensive configuration mixing. Edwards and Gouterman [25] recently measured vapour absorption spectra of phthalocyanine

Table 4. Calculated electronic transitions in H_2Pc. The four lowest triplets. All allowed transitions below 55 kK. The strongest transitions in the region 55–65 kK[a]. For choice of symmetry axes, see Fig. 1

Calculated				Observed [25] vapour		
Symmetry	pol.	ν (kK)	f	Notation	ν (kK)	range
$^3B_{3u}$		3.2				
$^3B_{2u}$		9.6				
$^3B_{3u}$		14.1				
$^1B_{2u}$	y	14.3	0.11		14.6	14–15
$^3B_{2u}$		14.9		Q		
$^1B_{3u}$	x	15.9	0.53		16.1	15–17
$^1B_{2u}$	y	26.6	1.09			
$^1B_{3u}$	x	32.2	2.38			
$^1B_{2u}$	y	32.8	2.92	B	29.4	26–34
$^1B_{1u}$	z[b]	33.1				
$^1B_{3u}$	x	34.2	0.08			
$^1B_{3u}$	x	35.4	0.42			
$^1B_{1u}$	z[c]	35.7			35.7[d]	
$^1B_{2u}$	y	36.0	0.22	N		34–38
$^1B_{2u}$	y	38.6	0.004			
$^1B_{3u}$	x	38.8	0.01		37.0	
$^1B_{3u}$	x	39.3	0.59			
$^1B_{1u}$	z[b]	41.9				
$^1B_{2u}$	y	42.6	0.23	L	41.7	40–43
$^1B_{3u}$	x	43.0	0.05			
$^1B_{2u}$	y	44.6	0.007			
$^1B_{3u}$	x	45.2	0.02			
^1B	[illegible]	46.3	0.26			
$^1B_{3u}$	x	46.7	0.56		45.5[d]	
$^1B_{2u}$	y	46.7	0.01			
$^1B_{3u}$	x	49.4	0.002	C		43–50
$^1B_{2u}$	y	50.3	0.000			
$^1B_{2u}$	y	51.0	0.71		47.6	
$^1B_{2u}$	y	52.5	0.000			
$^1B_{3u}$	x	52.9	0.31			
$^1B_{3u}$	x	53.6	0.003			
$^1B_{3u}$	x	54.6	0.14			
$^1B_{2u}$	y	55.1	0.13			
$^1B_{3u}$	x	56.3	0.62	X_1	55.6	52–56
$^1B_{2u}$	y	57.3	0.40			
$^1B_{2u}$	y	58.7	0.40			
$^1B_{2u}$	y	59.2	0.89	X_2	62.5	59–64
$^1B_{3u}$	x	61.8	0.67			
$^1B_{2u}$	y	64.6	0.24			

[a] In this region transitions with f-values lower than 0.2 have been omitted.
[b] $n \rightarrow \pi^*$ transition from lone pairs of the bridge nitrogens.
[c] $n \rightarrow \pi^*$ transition from the inner ring nitrogen lone pairs.
[d] Shoulder.

and metallophthalocyanines. They identified five bands, denoted by Q, B, N, L and C. In the far UV two broad bands (X_1 and X_2) were observed.

In free base H_2Pc the Q band splits into two, which can be ascribed to the reduction of symmetry from D_{4h} to D_{2h}. The observed data from Ref. [25] are quoted in Table 4 and Fig. 3 for comparison with the calculated transitions.

Table 5. Configuration mixing for some of the excited states of H_2Pc

ν (kK)	Wave function[a]
3.2	$0.90(4a_u-6b_{3g})^T+0.28(7b_{1u}-6b_{2g})^T+\cdots$
9.6	$0.95(4a_u-6b_{2g})^T+\cdots$
14.1	$0.86(7b_{1u}-6b_{2g})^T+0.37(4a_u-6b_{3g})^T+\cdots$
14.3	$0.75(4a_u-6b_{2g})+0.62(7b_{1u}-6b_{3g})$
14.9	$0.94(7b_{1u}-6b_{3g})^T+\cdots$
15.9	$0.89(4a_u-6b_{3g})-0.42(7b_{1u}-6b_{2g})+\cdots$
26.6	$0.62(6b_{1u}-6b_{3g})+0.51(7b_{1u}-6b_{3g})-0.47(4a_u-6b_{2g})-0.22(5b_{2g}-5a_u)+\cdots$
32.2	$0.79(7b_{1u}-6b_{2g})+0.37(4a_u-6b_{3g})+0.29(3a_u-6b_{3g})+0.21(5b_{1u}-6b_{2g})+\cdots$
32.8	$0.66(6b_{1u}-6b_{3g})+0.50(7b_{1u}-6b_{3g})-0.38(4a_u-6b_{2g})+\cdots$
35.4	$0.66(4a_u-7b_{3g})-0.35(3a_u-6b_{3g})-0.33(5b_{2g}-9b_{1u})-0.32(6b_{1u}-7b_{2g})-0.24(6b_{1u}-6b_{2g})+\cdots$
36.0	$\begin{cases}0.44(5b_{1u}-6b_{3g})-0.37(4b_{3g}-8b_{1u})+0.33(4a_u-7b_{2g})+0.32(2a_u-6b_{2g})-0.29(5b_{1u}-7b_{3g})\\+0.27(7b_{1u}-7b_{3g})+0.23(4b_{2g}-5a_u)+0.22(3a_u-6b_{2g})+0.21(4a_u-8b_{2g})+\cdots\end{cases}$
39.3	$0.71(5b_{1u}-6b_{2g})+0.41(6b_{1u}-6b_{2g})-0.33(3a_u-6b_{3g})-0.29(4b_{3g}-5a_u)+\cdots$
42.6	$0.81(5b_{1u}-6b_{3g})-0.25(2a_u-6b_{2g})-0.24(7b_{1u}-7b_{3g})-0.22(3a_u-6b_{2g})+\cdots$
46.7	$\begin{cases}0.55(4a_u-8b_{3g})+0.38(4a_u-9b_{3g})-0.27(6b_{1u}-7b_{2g})+0.23(3a_u-6b_{3g})-0.21(5b_{2g}-9b_{1u})\\+0.21(2a_u-7b_{3g})-0.21(2a_u-6b_{3g})+\cdots\end{cases}$
51.0	$\begin{cases}0.41(5b_{1u}-7b_{3g})+0.40(4b_{3g}-8b_{1u})+0.39(7b_{1u}-7b_{3g})+0.27(2a_u-6b_{2g})-0.26(4b_{1u}-6b_{3g})\\+0.24(5b_{2g}-5a_u)-0.20(3a_u-7b_{3g})+\cdots\end{cases}$

[a] T stands for triplet. The singlet configurations have no special notation.

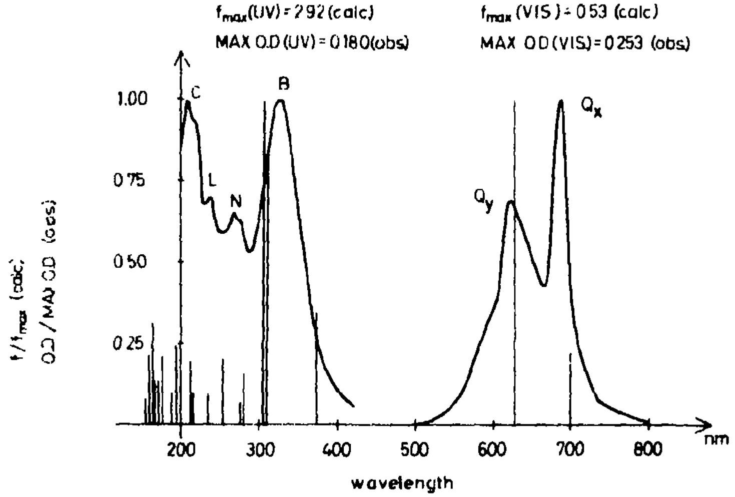

Fig. 3. Observed vapor-phase absorption spectra of H_2Pc from [25]. Calculated $\pi-\pi^*$ singlets with $f>0.2$, cf. Table 4

The Q Band. The calculated position and splitting of the Q band (14.3 and 15.9 kK) are in very good agreement with the experimental findings (14.6 and 16.1 kK). According to our calculations, the lower energy Q band (14.3 kK) is polarized along the NH-NH axis (y axis in Fig. 1), as was also the case for porphin [4].

The B Band. The present calculation gives three allowed $\pi-\pi^*$ transitions in the B band region: at 26.6 kK, 32.2 kK, and 32.8 kK.

The lowest allowed $n-\pi^*$ transition (33.1 kK) might also be found within the B band. This transition arises from the lone pairs of the bridge nitrogens.

The N, L, and C Bands. At higher energies than the B-band, observations show several bands: N, L, and C. On both the N and the C band a shoulder can clearly be distinguished.

According to our calculations, many transitions are expected to occur in the region between 35 and 50 kK. It is consequently difficult to make unambiguous assignments of the bands in this region. We suggest the following assignments: The $\pi-\pi^*$ transitions at 35.4, 36.0, 38.6, and 39.3 are assigned to the N band. An allowed $n-\pi^*$ transition at 35.7 kK is also expected to be found in this band. It is a transition from the inner ring nitrogen lone pairs.

The $\pi-\pi^*$ transitions at 42.6 and 43.0 kK and the $n-\pi^*$ transition (from the lone pairs of the bridge nitrogens) at 41.9 kK are assigned to the L band. As much as twelve allowed $\pi-\pi^*$ transitions are predicted to be found in the C band region, 44–55 kK.

The X_1 and X_2 Bands. In the high energy region, 55–65 kK, the calculation also gives many allowed $\pi-\pi^*$ transitions. Transitions with f-values lower than 0.2 have been omitted in Table 4. The strong transition at 56.3 kK can be attributed to the X_1 band. The two bands at 59.2 and 61.8 kK are assigned to the X_2 band.

Triplets. The parameter values in our parameter scheme are taken so as to give agreement between calculated and observed singlet transitions of a chosen set of small molecules [18, 19]. The parametrization implicitly takes into account part of the correlation. But since correlation effects are different for singlet and triplet states, our parameters will give too low values (around 2–7 kK [19]) for triplets. The calculated triplets at 14.1 and 14.9 kK will probably be above the lowest singlet.

Rieckhoff and Voigt [26] observed a phosphorescence band of H_2Pc in various solvents at 77°. It occured at 11–12 kK. The present calculation indicates the possibility of two triplets below the lowest singlet (Table 4).

Acknowledgements. This investigation has been supported by grants from the Swedish Natural Science Research Council. The authors wish to express their gratitude to Professor Inga Fischer-Hjalmars for her encouraging interest throughout the work. Thanks are also due to Mr. Lars Norén for assistance in the numerical calculations. One of us (A.H.) wish to express her gratitude for grants from "Kulturfonden för Sverige och Finland".

References

1. Moser, F. H., Thomas, A. L.: Phthalocyanine compounds. New York: Reinhold 1963.
2. Lever, A. B. P.: Advances inorg. chem. Radiochem. 7, 115 (1965).
3. Gutmann, F., Lyons, L. E.: Organic semiconductors. New York: Wiley 1967.
4. Sundbom, M.: Acta chem. scand. **22**, 1317 (1968).
5. Roos, B., Sundbom, M.: J. molecular Spectroscopy **36**, 8 (1970).
6. Pullman, A., Berthier, G.: C. R. Acad. Sci. Paris **236**, 1494 (1953).
7. Kobayashi, H.: Nippon Kagaku Zasshi **82**, 272 (1961).
8. Nowakowski, J.: Roczniki Chem. **35**, 257 (1961); **40**, 141 (1966).

9. Gouterman,M., Wagnière,G.H., Snyder,L.C.: J. molecular Spectroscopy **11**, 108 (1963).
10. Berezin,R.D.: Russ. J. physic. Chem. **39**, 165 (1965).
11. Chen,I.: J. molecular Spectroscopy **23**, 131 (1967).
12. Ponomarev,O.A., Kubarev,S.I.: Teor. Eksp. Khim **4**, 492 (1968).
13. Taube,R.: Z. Chem. **6**, 8 (1966).
14. Martin,H., Försterling,H.D., Kuhn,H.: Tetrahedron **19**, Suppl. 2, 243 (1963).
15. Schaffer,A.M., Gouterman,M.: Theoret. chim. Acta (Berl.) **25**, 62 (1972).
16. Weiss,C., Kobayashi,H., Gouterman,M.: J. molecular Spectroscopy **33**, 292 (1970).
17. McHugh,A.J., Gouterman,M., Weiss,C.: In press.
18. Fischer-Hjalmars,I., Sundbom,M.: Acta chem. scand. **22**, 607 (1968).
19. Sundbom,M.: Acta chem. scand. **25**, 487 (1971).
20. Mulliken,R.S., Rieke,C.A.: Rep. Progr. Physics **8**, 231 (1941).
21. Hoskins,B.F., Mason,S.A., White,J.C.B.: J. chem. Soc. D **1969**, 554.
22. Gouterman,M.: J. molecular Spectroscopy **6**, 138 (1961).
23. Kobayashi,T.: Spectrochim. Acta **26** A, 1305, 1313 (1970).
24. Komp,R.J., Fitzsimmons,Th.J.: Photochem. Photobiol. **8**, 419 (1968).
25. Edwards,L., Gouterman,M.: J. molecular Spectroscopy **33**, 292 (1970).
26. Rieckhoff,K.E., Voigt,E.M.: In: Molecular luminescence, Ed. E. C. Lim. New York, Amsterdam: Benjamin 1969
27. Bak,B., Christensen,D., Hansen,L., Rastrup-Andersen,J.: J. chem. Physics **24**, 720 (1956). Bak,B.: Report at Nordisk Strukturkjemikermöte, Oslo 1964.

Dr. M. Sundbom
Institute of Theoretical Physics
University of Stockholm
Vanadisvägen 9
S-113 46 Stockholm, Sweden

Theoret. chim. Acta (Berl.) 27, 223–242 (1972)
© by Springer-Verlag 1972

PCILO Method for Excited States

I. Construction of the Zeroth Order Wave-Function for Planar Conjugated Systems

J. Langlet

Institut de Biologie Physico-Chimique, Laboratoire de Biochimie Théorique, associé au C.N.R.S.
13, rue P. et M. Curie, Paris 5è

Received February 17, 1972/July 14, 1972

In the scope of building a PCILO method for excited states, one builds and tests excitonic zeroth order wave-functions. For $\binom{\pi^*}{\pi}$ transitions, the $(\sigma+\pi)$ excitonic and purely (π) excitonic wave functions are compared, showing that the $\sigma-\pi$ coupling between $\binom{\pi^*}{\pi}$ and $\binom{\sigma^*}{\sigma}$ single excitations may be considered as a perturbation. The excited state wave-functions are analyzed in terms of neutral and ionic structures, and the fluctuation of the charges in the two-electrons loges are studied, showing that the $\sigma-\pi$ coupling favours the neutral structures and diminishes the charge-fluctuations.

Im Rahmen der Aufstellung einer PCILO-Methode für angeregte Zustände werden Wellenfunktionen 0. Ordnung mit delokalisierter Anregung konstruiert und getestet. Für $\binom{\pi^*}{\pi}$-Übergänge werden $(\sigma+\pi)$-angeregte und rein π-angeregte Wellenfunktionen verglichen, wobei gezeigt wird, daß die $\sigma-\pi$-Kopplung zwischen $\binom{\pi^*}{\pi}$- und $\binom{\sigma^*}{\sigma}$-Einfachanregungen als Störung behandelt werden kann. Die Wellenfunktionen der angeregten Zustände werden nach neutralen und ionischen Strukturen analysiert. Die Ladungsverschiebungen in den Zweielektronen-Elektronendichteanteilen werden untersucht, wobei gezeigt wird, daß die $\sigma-\pi$-Kopplung die neutralen Strukturen begünstigt und die Ladungsverschiebungen verringert.

Introduction

A method hereafter named PCILO has been proposed recently [1] for the study of the ground state of closed shell molecules [1] and of localized radicals [2] in the CNDO hypotheses. This method is much more rapid, even to the third order of perturbation, than the classical variational Hartree-Fock method although it includes correlation effects. This method, which has been widely used for the study of conformational properties of large molecules [3], has the following principles:

a) The bonding and antibonding orbitals localized on bond i may be represented with two hybrids i_1 and i_2 by the linear combination.

$$i = \alpha i_1 + \beta i_2 ,$$
$$i^* = \beta' i_1 - \alpha' i_2 .$$

b) The bonding orbitals are used to build a zeroth order wave function as a fully localized determinant.

c) The antibonding orbitals are used to build an excited configurations basis allowing the construction of a CI matrix.

d) The lowest eigenvalue and eigenstate of this matrix are developed according to a Rayleigh-Schrödinger perturbation series.

The use of localized orbitals to represent ground-state wave functions is very successful, because of the existence of a large overlap between the zeroth order fully localized determinant and the SCF one [4]. But even when a satisfactory single determinant representation of an excited state can be found using symmetry (therefore delocalized) Molecular Orbitals, obtained by diagonalization of a symmetrical hamiltonian (Hückel, SCF hamiltonian), one cannot find in general a satisfactory single determinant representation for the excited state using localized MO's.

In fact, when using localized MO's, the singly excited determinants only represent local excitations from the bonding MO φ_i on the bond i towards the antibonding MO φ_{j^*} on the bond j. To get a reasonable representation of the excited state which transforms the excited state according to the symmetry operations of the molecule, one must represent it as a linear combination of several determinants, each of them representing a local excitation. In the excitonic treatment [5], the excited states are represented by localized singly excited determinants

$$\Psi_0^m = \sum_i \sum_{j^*} C^m_{ij^*} \Phi \begin{pmatrix} j^* \\ i \end{pmatrix}.$$

Each bonding MO can be excited towards its antibonding MO; this process leads to a determinant $\Phi \begin{pmatrix} i^* \\ i \end{pmatrix} = a^+_{i^*} a_i \Phi_0$, which will be called a polarization determinant hereafter.

In the same way, each bonding MO φ_i can be excited towards an antibonding MO φ_{j^*}, and we obtain the delocalization (or charge-transfer) determinant $\Phi_{ij^*} = a^+_{j^*} a_i \Phi_0$.

At the beginning of the calculation, all these determinants are (nearly) degenerate. When the total hamiltonian including electron repulsion is considered, these single excited determinants interact. According to the perturbation theory for degenerate states [6], the correct first-order energies are solutions of the Configuration Interaction (CI) problem limited to these states.

All excited states obtained after diagonalization of the matrix are linear combination of locally excited states and therefore represent delocalized excitations ("exciton states"). The good symmetry properties result from the $C^m_{ij^*}$ values obtained as the eigenvector m of the CI matrix.

The excitonic treatment has been applied to the $\begin{pmatrix} \pi^* \\ \pi \end{pmatrix}$ transition of unsaturated molecules by Simpson [5], using $\Phi \begin{pmatrix} \pi^* \\ \pi \end{pmatrix}$ polarization configurations only. Other authors [7, 8] have introduced the $\begin{pmatrix} \pi^* \\ \pi \end{pmatrix}$ delocalization configurations.

Our purpose is to build a PCILO method for excited states, i.e. an all-valence electrons method taking correlation effects into account. The inclusion of localized orbitals implies the multiconfigurational character of a correct zeroth-order wave function Ψ_0^m for the excited state, but it is hoped that the simplifications due to the full localization of the MO's (especially in the molecular integrals calculation) will give the same advantages as what does the PCILO method for the ground-state energy.

In the present work we study the correctness of various zeroth order representations of the $\begin{pmatrix}\pi^*\\ \pi\end{pmatrix}$ excited states. In all-valence electrons methods, one may build an excitonic matrix which involves simultaneously the $\begin{pmatrix}\pi^*\\ \pi\end{pmatrix}$ and $\begin{pmatrix}\sigma^*\\ \sigma\end{pmatrix}$ singly excited determinants i.e. the $(\sigma+\pi)$ excitonic treatment. Another possibility consists in building the (π) excitonic matrix of the $\begin{pmatrix}\pi^*\\ \pi\end{pmatrix}$ singly excited determinants, and in treating the interaction between $\begin{pmatrix}\pi^*\\ \pi\end{pmatrix}$ and $\begin{pmatrix}\sigma^*\\ \sigma\end{pmatrix}$ determinants [9, 10, 11] as a perturbation (π excitonic treatment).

As well as in the PCILO method for energy calculation of the groundstate, we have used the CNDO II parametrization [12]. This preliminary study deals with the linear polyenes series.

1. Structure of the $(\sigma+\pi)$ Excitonic Matrix

As said in the introduction, the CI matrix contains all (σ and π) polarization and delocalization configurations.

a) The *diagonal elements* of the CI matrix, which represent the mean values of the energy for local excitations, are given in Table 1. The order of the energies of these local excitations may be summarized as follows,

$$E\begin{pmatrix}\pi_A^*\\ \pi_A\end{pmatrix}\ \text{polarization} < E\begin{pmatrix}\pi_B^*\\ \pi_A\end{pmatrix}\ \text{delocalization} < E\begin{pmatrix}\sigma_{CHB}^*\\ \sigma_{CHA}\end{pmatrix}\ \text{delocalization}$$
$$< E\begin{pmatrix}\sigma_{CHA}^*\\ \sigma_{CHA}\end{pmatrix}\ \text{polarization} < E\begin{pmatrix}\sigma_{CC}^*\\ \sigma_{CH}\end{pmatrix}\ \text{delocalization} < E\begin{pmatrix}\sigma_{CH}^*\\ \sigma_{CC}\end{pmatrix}\ \text{delocalization}$$
$$< E\begin{pmatrix}\sigma_{CCB}^*\\ \sigma_{CCA}\end{pmatrix}\ \text{delocalization} < E\begin{pmatrix}\sigma_{CCA}^*\\ \sigma_{CCA}\end{pmatrix}\ \text{polarization.}$$

The $\Phi\begin{pmatrix}\sigma^*\\ \pi\end{pmatrix}$ excited configurations are close in energy to the $\Phi\begin{pmatrix}\pi^*\\ \pi\end{pmatrix}$ configurations, especially in the CNDO/2 parametrization; The $\Phi\begin{pmatrix}\sigma^*\\ \pi\end{pmatrix}$ configurations which represent an excitation from a bond to the antibonding adjacent CH MO have a lower energy than the $\Phi\begin{pmatrix}\pi^*\\ \pi\end{pmatrix}$ polarization configuration (13.84 eV against 14.40 eV).

b) *Off Diagonal Elements.* The polarization configurations $\Phi\begin{pmatrix}\pi_A^*\\ \pi_A\end{pmatrix}$ which were supposed to be the most important in the $\begin{pmatrix}\pi^*\\ \pi\end{pmatrix}$ excited states are coupled with

Table 1 Energy (in eV) of the different polarization and delocalization configurations

1) The subscript A means delocalization configuration $\binom{(i+1)^*}{i}$ i.e. from the MO i to the adjacent $i+1$ MO

2) For the $\binom{\pi^*}{\pi}$ delocalization configurations subscript A means delocalization configurations $\binom{j^*}{i}$ where i and j are two π MO's separated by a σ MO. For instance in Butadiene i is the first π bond and j the second one

3) The subscript I mean delocalization configurations $\binom{j^*}{i}$ when the distances between the two MO's i and j is infinite. The energy of these configurations are calculated by: $E_2 = F(j^*, j^*) - F(i, i)$ because when the distance between i and j is infinite, the integral $J_{ij^*} = \langle ii^* | jj^* \rangle = 0$

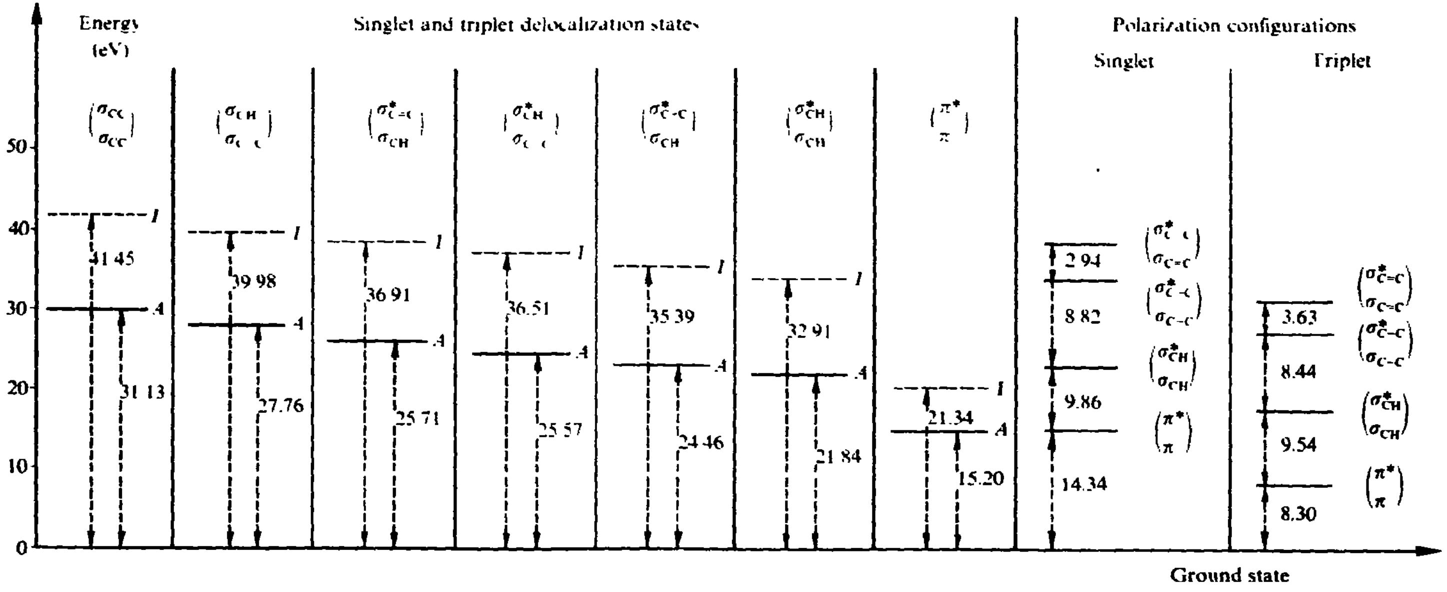
Energy (eV)
Singlet and triplet delocalization states
Polarization configurations
Singlet
Triplet
0
10
20
30
40
50
$\binom{\sigma_{CC}^*}{\sigma_{CC}}$
41.45
31.13
$\binom{\sigma_{CH}^*}{\sigma_{C-C}}$
39.98
27.76
$\binom{\sigma_{C=C}^*}{\sigma_{CH}}$
36.91
25.71
$\binom{\sigma_{CH}^*}{\sigma_{C=C}}$
36.51
25.57
$\binom{\sigma_{C-C}^*}{\sigma_{CH}}$
35.39
24.46
$\binom{\sigma_{CH}^*}{\sigma_{CH}}$
32.91
21.84
$\binom{\pi^*}{\pi}$
21.34
15.20
I
A
2.94
8.82
9.86
14.34
$\binom{\sigma_{C=C}^*}{\sigma_{C=C}}$
$\binom{\sigma_{C-C}^*}{\sigma_{C-C}}$
$\binom{\sigma_{CH}^*}{\sigma_{CH}}$
$\binom{\pi^*}{\pi}$
3.63
8.44
9.54
8.30
Ground state

$\Phi\begin{pmatrix}\pi_B^*\\ \pi_B\end{pmatrix}$ polarization configurations by dipolar type interactions, and with the $\Phi\begin{pmatrix}\pi_B^*\\ \pi_A\end{pmatrix}$ or the $\Phi\begin{pmatrix}\pi_A^*\\ \pi_B\end{pmatrix}$ delocalization configurations which have the same hole (π_A) or the same particle (π_A^*). These $\Phi\begin{pmatrix}\pi_B^*\\ \pi_A\end{pmatrix}$ delocalization configurations are coupled between themselves, according to the same rule. For planar systems, the singlet $\Phi\begin{pmatrix}\sigma_A^*\\ \sigma_A\end{pmatrix}$ polarization configurations are coupled with all the singlet $\Phi\begin{pmatrix}\pi_B^*\\ \pi_B^*\end{pmatrix}$ polarization configurations, and with themselves by dipolar type interaction. The $\Phi\begin{pmatrix}\sigma_B^*\\ \sigma_A\end{pmatrix}$ delocalization configurations are coupled with some of the $\Phi\begin{pmatrix}\sigma_A^*\\ \sigma_A\end{pmatrix}$ polarization configurations but they are not coupled directly with the $\Phi\begin{pmatrix}\pi^*\\ \pi\end{pmatrix}$ configurations in the CNDO hypotheses. Therefore they should have a less important weight than the $\Phi\begin{pmatrix}\sigma_A^*\\ \sigma_A\end{pmatrix}$ polarization configurations in the $\begin{pmatrix}\pi^*\\ \pi\end{pmatrix}$ excited states. The structure of the CI matrix for a planar molecule is given in Fig. 1. The $\Phi\begin{pmatrix}\pi^*\\ \sigma\end{pmatrix}$ and $\Phi\begin{pmatrix}\sigma^*\\ \pi\end{pmatrix}$ configurations only appear in $\begin{pmatrix}\pi^*\\ \pi\end{pmatrix}$ excited states for non-planar molecules. Two $\Phi\begin{pmatrix}\pi^*\\ \pi\end{pmatrix}$ configurations do not interact very strongly and the dipolar type interaction element between two $\Phi\begin{pmatrix}\pi^*\\ \pi\end{pmatrix}$ configurations decreases as r^{-3} with the distance between the two π bonds. So with Hexatriene we obtain the following values:

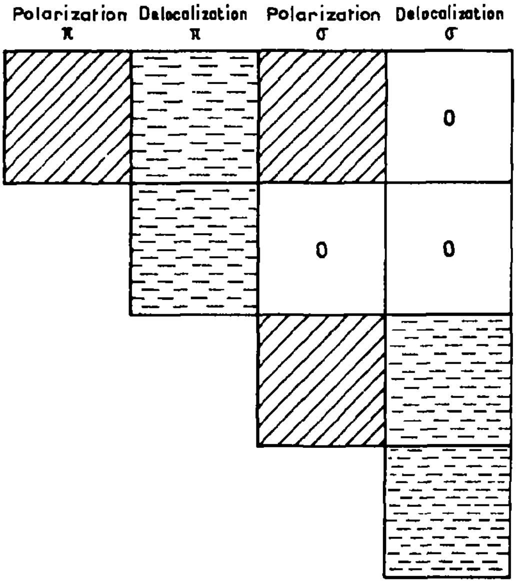

Fig. 1. Structure of the ($\sigma + \pi$) excitonic matrix

0.753 eV when the two π bonds are separated by a single bond, and 0.131 eV when the two π bonds are separated by 2 single bonds and 1 double bond.

The interaction matrix elements between the $\Phi\binom{i^*}{i}$ configurations and the $\Phi\binom{i^*}{j}$ delocalization configurations are stronger than the interaction matrix elements between the $\Phi\binom{i^*}{i}$ polarization configurations and the $\Phi\binom{j^*}{i}$ delocalization configurations. For instance, when two π MO's are separated by a σ MO we obtain 2.93 eV in the former case and 1.56 eV in the latter case. If F is the Fock operator, $F_{ij} > F_{i^*j^*}$. These interaction matrix elements decrease exponentially with the distance between the two different MO's.

There is a very strong interaction matrix element between the $\Phi\binom{\sigma^*_{CC}}{\sigma_{CC}}$ and $\Phi\binom{\pi^*}{\pi}$ polarization configurations: 6.03 eV when the σ and π MO's belong to the same double bond. Then this interaction decreases and becomes 1.28 eV, when the two π and σ MO's are adjacent. This interaction matrix element becomes 0.75 eV, 0.55 eV when the π MO is separated from the σ MO by 1 or 2 other bonds respectively. This agrees with the r^{-3} theoretical decreases. The interaction matrix element between $\Phi\binom{\pi^*}{\pi}$ and $\Phi\binom{\sigma^*_{CH}}{\sigma_{CH}}$ polarization configurations is very weak (0.38 eV) when these two bonds are adjacent.

The coupling between $\Phi\binom{\pi^*}{\pi}$ and $\Phi\binom{\sigma^*_{CC}}{\sigma_{CC}}$ polarization configurations being stronger than the coupling between the $\Phi\binom{\pi^*}{\pi}$ and $\Phi\binom{\sigma^*_{CH}}{\sigma_{CH}}$ polarization configurations, we may expect a more important component of the excited state $\Phi\binom{\pi^*}{\pi}$ on the σ_{C-C} than on the σ_{CH} bonds.

In the triplet excited states, the delocalization configurations have the same mean energies than in the singlet excited states, because in the PCILO method, due to ZDO hypothesis, the exchange integral K_{ij} is zero. But the polarization configurations have lower energies than in the singlet excited states.

For the triplet excited states, in the CNDO hypothesis the transition dipole-transition dipole interactions disappear, and the ${}^3\Phi\binom{\pi A^*}{\pi A}$ configurations no longer interact between themselves nor with ${}^3\Phi\binom{\sigma^*}{\sigma}$ excited configurations. The ${}^3\Phi\binom{\pi^* A}{\pi A}$ configurations only interact with the ${}^3\Phi\binom{\pi B^*}{\pi A}$ delocalization configurations as noticed by several authors [11]. The σ system does not play any role at this stage.

2. Results Obtained with the ($\sigma+\pi$) Excitonic Matrix

The wave function ψ_0^m resulting from the diagonalization of the excitonic matrix will be considered as a zeroth order representation of the excited state m, as does the fully localized determinant Φ_0 for the ground state. Therefore, the zeroth order transition energies are calculated as the difference between the eigenvalue E_m of the excitonic matrix and the energy of the fully localized determinant.

$$\Delta E_m = \langle \Psi_0^m | H | \Psi_0^m \rangle - \langle \Phi_0 | H | \Phi_0 \rangle .$$

We have studied three molecules, ethylene, butadiene and hexatriene.

For ethylene and butadiene, the first excited state is a $\binom{\pi^*}{\sigma}$ state, and the second excited state in these two molecules is a $\binom{\pi^*}{\pi}$ state while for Hexatriene, the first excited state becomes the $\binom{\pi^*}{\pi}$ state. In the same way, comparing the ordering of excited states for butadiene and hexatriene, one may notice that two $\binom{\pi^*}{\sigma}$ states and three $\binom{\sigma^*}{\pi}$ states ary lying between the two first $\binom{\pi^*}{\pi}$ states of butadiene, while three $\binom{\pi^*}{\sigma}$ states and zero $\binom{\sigma^*}{\pi}$ states appear between the first two $\binom{\pi^*}{\pi}$ states of hexatriene. These results are in agreement with the INDO calcula-

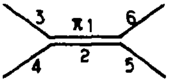

ethylene

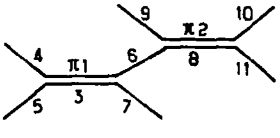

butadiene

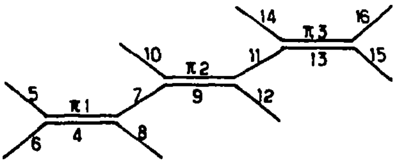

hexatriene

Fig. 2. Ethylene II A, butadiene II B, hexatriene II C with the numbering of the bonds (i.e. the MO's)

tions [13] including the CI between all singly excited determinants. But Clark and Ragle [14] using CNDO SCF CI method with spectrum fitted parameters [15] for a calculation of excited states of butadiene, have predicted many $\begin{pmatrix}\pi^*\\ \sigma\end{pmatrix}$ or $\begin{pmatrix}\sigma^*\\ \pi\end{pmatrix}$ states lying before the first $\begin{pmatrix}\pi^*\\ \pi\end{pmatrix}$ state which is obtained as the 7th state.

The assignment of the first band of Ethylene as a Berry band [16] was also found in Clark and Ragle calculations, by C. Giessner-Prettre and A. Pullman with both CNDO II and INDO method, when including in the CI matrix all the singly-excited configurations built from σ and π delocalized MO's [13], and by Kaldor and Shavitt in their non empirical LCAO-SCF with a minimal basis [17]. But theoretical work by Moskowitz [18] and co-workers [19] on the spectrum of ethylene showed that the $\begin{pmatrix}\pi^*\\ \sigma\end{pmatrix}$ excitations were rather close to the $\begin{pmatrix}\pi^*\\ \pi\end{pmatrix}$ excitation $({}^1A_g \to {}^1B_{1u})$ and might even fall below it in some olefins; Robin and co-workers [20], in their SCF-CI Gaussian orbital calculation on ethylene, claimed that the first band was a $\begin{pmatrix}\sigma^*\\ \pi\end{pmatrix}$ excitation (B_{2u}) where σ^* was interpreted as being composed partly of Rydberg 3s orbitals and partly of σ^*CH sigma valence-shell orbitals. Berthod [21] and Polak [22] had also found this first band as being a $\begin{pmatrix}\sigma^*\\ \pi\end{pmatrix}$ band.

From column 7 in Table 2, we notice that $\begin{pmatrix}\pi^*\\ \sigma\end{pmatrix}$ in these three molecules, the first $\begin{pmatrix}\pi^*\\ \sigma\end{pmatrix}$ excitation is a linear combination of the four $\Phi\begin{pmatrix}\pi^*\\ \sigma_{\mathrm{CH}}\end{pmatrix}$ configurations in Ethylene, and of the $\Phi\begin{pmatrix}\pi^*\\ \sigma_{\mathrm{CC}}\end{pmatrix}$ configuration (where σ_{CC} is the single bond adjacent to the π bonds) and of the $\begin{pmatrix}\pi^*\\ \sigma_{\mathrm{CH}}\end{pmatrix}$ configurations where σ_{CH} is adjacent to the

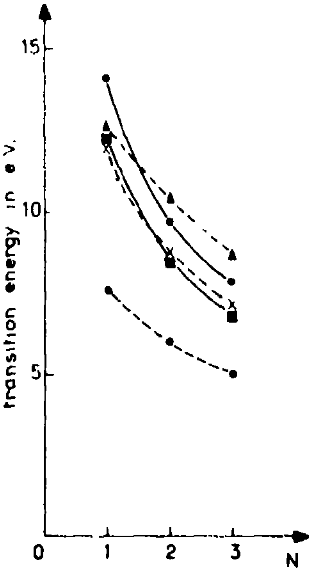

Fig. 3. Transition energy from the ground state to the first $^1\begin{pmatrix}\pi^*\\ \pi\end{pmatrix}$ state. ●- ● experimental values. ■ — ■ values obtained with the (π) excitonic matrix, the σ configurations being introduced by perturbation treatment. × - - - × values obtained with the ($\sigma+\pi$) excitonic matrix, ● —— ● values obtained with the (π) excitonic matrix, ▲ - - - ▲ values obtained with delocalized orbitals using a SCF-CI (with all monoexcited configurations) INDO method by Giessner-Prettre and Pullman [15]

π bond in butadiene and hexatriene. The second $\begin{pmatrix}\pi^*\\ \sigma\end{pmatrix}$ state is predominantly represented by the $\begin{pmatrix}\pi^*\\ \sigma_{CC}\end{pmatrix}$ configurations (where σ_{CC} belongs to the double bond) and the third $\begin{pmatrix}\pi^*\\ \sigma\end{pmatrix}$ state is represented by the $\Phi\begin{pmatrix}\pi^*\\ \sigma_{CH}\end{pmatrix}$ configurations, the three $\begin{pmatrix}\sigma^*\\ \pi\end{pmatrix}$ states are predominantly represented by the $\Phi\begin{pmatrix}\sigma_{CH}^*\\ \pi\end{pmatrix}$ configurations (when σ_{CH} bonds are adjacent to the double bonds).

Analysis of the $\begin{pmatrix}\pi^*\\ \pi\end{pmatrix}$ wave function will be given in paragraph 7.

We have found a ${}^3\begin{pmatrix}\pi^*\\ \pi\end{pmatrix}$ as the first triplet state in the three molecules we have studied so far. In butadiene and hexatriene the second triplet state is another ${}^3\begin{pmatrix}\pi^*\\ \pi\end{pmatrix}$ state which is followed by a ${}^3\begin{pmatrix}\pi^*\\ \sigma\end{pmatrix}$ triplet state (where σ is the single σ bond adjacent to the π bonds).

The calculated transition energies are collected in column 6 of Table 2.

3. $(\sigma-\pi)$ Mixing in the $\begin{pmatrix}\pi^*\\ \pi\end{pmatrix}$ States

Table 2 shows that in the three molecules we have studied for the $\begin{pmatrix}\pi^*\\ \pi\end{pmatrix}$ states, besides the $\begin{pmatrix}\pi^*\\ \pi\end{pmatrix}$ delocalization or polarization configurations, one finds some $\begin{pmatrix}\sigma^*\\ \sigma\end{pmatrix}$ polarization configurations (especially when σ_{CC} belongs to the double bond) with non-negligible weights. *Ab initio* calculations also show that the $\begin{pmatrix}\pi^*\\ \pi\end{pmatrix}$ monoexcited states have important components on $\begin{pmatrix}\sigma^*\\ \sigma\end{pmatrix}$ monoexcited configurations. For instance Dunning and McKoy calculated that in ethylene the $\begin{pmatrix}\sigma^*\\ \sigma\end{pmatrix}$ configuration has a coefficient of 0.206 [10]. Denis and Malrieu on the basis of a second-order perturbation treatment [11] estimated that the effect of $\begin{pmatrix}\sigma_{CC}^*\\ \sigma_{CC}\end{pmatrix}$ configurations is twice larger than the effect of $\begin{pmatrix}\sigma_{CH}^*\\ \sigma_{CH}\end{pmatrix}$ configuration, and demonstrated that both of them decrease as n^{-1}.

We have calculated the $(\sigma-\pi)$ mixing as the difference between 1 and the sum of the square coefficients of all the $\Phi\begin{pmatrix}\pi^*\\ \pi\end{pmatrix}$ configurations. The results obtained for the three molecules we have studied are shown in Table 3: The $(\sigma-\pi)$ mixing in the first $\begin{pmatrix}\pi^*\\ \pi\end{pmatrix}$ decreases rapidly from ethylene (15.50%) to hexatriene (4.63%)

Table 2 Transition energies of singlet and triplet states obtained

1) after diagonalization of the $(\sigma+\pi)$ excitonic matrix, in column 6. $(E'_{(\sigma+\pi)})$.
2) after diagonalization of the (π) excitonic matrix, in column 8 $(E'_{(\pi)})$.
3) after diagonalization of the π excitonic matrix plus correction of the $\Phi\binom{\sigma^*}{\sigma}$ configurations obtained by perturbation in column 9

The values are given in eV, referred to the fully localized zeroth order ground state. In column 7, there are the coefficients (in absolute value) of the most important configurations representing a given excited state. The subscript $C^m_{(\sigma+\pi)}$ represents the coefficients obtained with the $(\sigma+\pi)$ excitonic matrix and the subscript $C^m_{(\pi)}$ represents the coefficient obtained with the (π) excitonic matrix ($C^m_{(\pi)}$ are the values between brackets in column 7)

See Fig. 2 for the numbering of MO's for ethylene, butadiene and hexatriene.

The subscript P_i refers to the polarization configuration $\binom{i^*}{i}$. The subscript D_{ij} refers to the delocalization configuration $\binom{j^*}{i}$ i and j are the numbers of two MO's.

Molecules	States			Experimental transition energies	$E'_{(\sigma+\pi)}$	$C^m_{(\sigma+\pi)}(C^m_{(\pi)})$	$E'_{(\pi)}$	$E''_{(\pi)}$
Ethylene	Singlet	$\binom{\pi^*}{\sigma}$	$^1B_{1g}$		9.99	$D_{3,1}=D_{4,1}=D_{5,1}=D_{6,1}=0.50$		
		$\binom{\pi^*}{\pi}$	$^1B_{1u}$	7.6 [17]	12.05	$P_1=0.91\ (1)$ $P_2=0.31$	14.19	12.38
		$\binom{\pi^*}{\sigma}$	$^1B_{2g}$		12.07	$D_{21}=0.70$ $D_{3,1}=D_{4,1}=D_{5,1}=D_{6,1}=0.35$		
		$\binom{\sigma^*}{\pi}$	$^1B_{2g}$		12.33	$D_{1,3}=D_{1,4}=D_{1,5}=D_{1,6}=0.46$ $D_{1,2}=0.39$		
		$\binom{\sigma^*}{\pi}$	$^1B_{1g}$		12.75	$D_{1,3}=D_{1,4}=D_{1,5}=D_{1,6}=0.50$		
		$\binom{\sigma^*}{\pi}$	$^1B_{3u}$		13.32	$D_{1,3}=D_{1,4}=D_{1,5}=D_{1,6}=0.50$		
	Triplet	$\binom{\pi^*}{\pi}$	$^3B_{1g}$	4.6 [22]	8.11	$P_1=1\ (1)$	8.11	8.11
		$\binom{\pi^*}{\sigma}$			9.99	$D_{3,1}=D_{4,1}=D_{5,1}=D_{6,1}=0.50$		
		$\binom{\pi^*}{\sigma}$			12.07	$D_{21}=0.71$ $D_{3,1}=D_{4,1}=D_{5,1}=D_{6,1}=0.35$		

Table 2b

Molecules	States			Experimental transition energies	$E^t_{(\sigma+\pi)}$	$C^m_{(\sigma+\pi)}(C^m_{(\pi)})$	$E^t_{(\pi)}$	$E^{t1}_{(\pi)}$
Butadiene	Singlet I	$\begin{pmatrix}\pi^*\\ \sigma\end{pmatrix}$	^1B_u		8.67	$D_{6,1}=D_{6,2}=0.41$		
	II	$\begin{pmatrix}\pi^*\\ \pi\end{pmatrix}$	^1B_u	5.92 [23]	8.72	$P_1=P_2=0.55\ (0.54)$ $D_{1,2}=D_{2,1}=0.40\ (0.46)$ $P_3=P_8=0.13$	9.69	8.65
	III	$\begin{pmatrix}\pi^*\\ \sigma\end{pmatrix}$	^1A_u		9.76	$D_{3,1}=D_{8,2}=0.43$ $D_{7,1}=D_{9,2}=0.36$		
	IV	$\begin{pmatrix}\pi^*\\ \sigma\end{pmatrix}$	^1B_g		10.36	$D_{5,1}=D_{10,2}=0.41$		
	V	$\begin{pmatrix}\sigma^*\\ \pi\end{pmatrix}$	^1A_u		10.87	$D_{1,7}=D_{2,9}=0.53$		
	VI	$\begin{pmatrix}\sigma^*\\ \pi\end{pmatrix}$	^1B_g		11.38	$D_{1,4}=D_{2,11}=0.46$ $D_{1,7}=0.37$		
	VII	$\begin{pmatrix}\sigma^*\\ \pi\end{pmatrix}$	^1A_u		11.62	$D_{1,5}=D_{1,10}=0.54$		
	VIII	$\begin{pmatrix}\pi^*\\ \pi\end{pmatrix}$	^1A_g	7.20 [23]	11.78	$P_1=P_2=0.59\ (0.50)$ $D_{1,2}=D_{2,1}=0.25\ (0.50)$ $P_3=P_8=0.22$	13.69	12.34
	Triplet I	$\begin{pmatrix}\pi^*\\ \pi\end{pmatrix}$	^3B_u	3.20 [22]	5.99	$P_1=P_2=0.63\ (0.63)$ $D_{1,2}=D_{2,1}=0.32\ (0.32)$	5.99	5.99
	II	$\begin{pmatrix}\pi^*\\ \pi\end{pmatrix}$	^3A_g	3.90 [22]	8.03	$P_1=P_2=0.69\ (0.69)$ $D_{1,2}=D_{2,1}=0.14\ (0.14)$	8.03	8.03
	III	$\begin{pmatrix}\pi^*\\ \sigma\end{pmatrix}$			8.67	$D_{6,1}=D_{6,2}=0.41$ $D_{7,1}=D_{9,2}=0.34$		

Table 2c

Molecules	States		Experimental transition energies	$E_{\sigma+\pi}$	$C^{*}_{\sigma+\pi}(C^{*}_{\pi})$	$E^{I}_{(\pi)}$	$E^{II}_{(\pi)}$
Hexatriene	**Singlet I**	$\begin{pmatrix}\pi^*\\ \pi\end{pmatrix}$	5 [25]	7 14	$P_2 = 0.60\,(0.57)$ $P_1 = P_3 = 0.31\,(0.31)$ $D_{1,2} = D_{3,2} = 0.32\,(0.34)$ $D_{2,1} = D_{2,3} = 0.29\,(0.32)$ $D_{1,3} = D_{3,1} = 0.12\,(0.15)$ $P_{14} = 0.14$	7.94	6.96
	II	$\begin{pmatrix}\pi^*\\ \sigma\end{pmatrix}$		7.95	D [illegible] $= D_{11,2} = 0.42$		
	III	$\begin{pmatrix}\pi^*\\ \sigma\end{pmatrix}$		8.88	D [illegible] $= 0.46$ $D_{10,2} = D_{12,2} = 0.42$		
	IV	$\begin{pmatrix}\pi^*\\ \sigma\end{pmatrix}$		9.48	D [illegible] $= D_{10,3} = 0.34$ D [illegible] $= D_{11,3} = 0.34$		
	V	$\begin{pmatrix}\pi^*\\ \pi\end{pmatrix}$		9.90	$P_1 = 0.53\,(0.47)$ $P_2 = 0\,(0)$ $D_{1,2} = D_{3,2} = 0.14\,(0.12)$ $D_{1,3} = D_{3,1} = 0.11\,(0.17)$ $D_{2,1} = D_{2,3} = 0.38\,(0.48)$ $P_4 = P_{13} = 0.16$	10.99	9.91
	VI	$\begin{pmatrix}\sigma^*\\ \pi\end{pmatrix}$		10.43	$D_{2,10} = D_{2,12} = 0.55$	4.81	4.81
	Triplet I	$\begin{pmatrix}\pi^*\\ \pi\end{pmatrix}$	2.6 [22]	4.81	$P_1 = P_3 = 0.33\,(0.33)$ $P_2 = 0.72\,(0.72)$ $D_{1,2} = 0.28\,(0.28)$ $D_{1,3} = D_{3,1} = 0.08\,(0.08)$ $D_{2,1} = D_{2,3} = 0.27\,(0.27)$		
	II	$\begin{pmatrix}\pi^*\\ \pi\end{pmatrix}$		6.83	$P_1 = P_3 = 0.65\,(0.65)$ $P_2 = 10^{-4}\,(10^{-4})$ $D_{2,1} = D_{2,3} = 0.26\,(0.26)$ $D_{1,2} = D_{3,2} = 0.12\,(0.12)$ D [illegible] $= D$ [illegible] $= 0.05\,(0.05)$	6.83	6.83

in conformity with the conclusions reached by Denis and Malrieu [11]; in the second $\begin{pmatrix}\pi^*\\ \pi\end{pmatrix}$ excited state, the $(\sigma-\pi)$ mixing decreases also with n, but it is always higher than in the first $\begin{pmatrix}\pi^*\\ \pi\end{pmatrix}$ excited state $\left(2.8 \text{ and } 2.4 \text{ times larger than in the first } \begin{pmatrix}\pi^*\\ \pi\end{pmatrix} \text{ state, for butadiene and hexatriene respectively}\right)$. The $(\sigma-\pi)$ mixing is predominantly due to the $\begin{pmatrix}\sigma^*_{CC}\\ \sigma_{CC}\end{pmatrix}$ polarization configurations (see Table 2) and the $\Phi\begin{pmatrix}\sigma^*_{CH}\\ \sigma_{CH}\end{pmatrix}$ polarization configurations have a light weight.

Table 3. $(\sigma\pi)$ mixing and weight of the $\Phi\begin{pmatrix}\sigma^*\\ \sigma\end{pmatrix}$ polarization configurations which interact directly with $\Phi\begin{pmatrix}\pi^*\\ \pi\end{pmatrix}$ configurations and weight of the $\Phi\begin{pmatrix}\sigma'^*\\ \pi\end{pmatrix}$ delocalization configurations which interact indirectly $\left(\text{through the } \Phi\begin{pmatrix}\sigma^*\\ \pi\end{pmatrix} \text{ polarization configurations}\right)$ with the $\Phi\begin{pmatrix}\pi^*\\ \pi\end{pmatrix}$ configurations

		State	Ethylene %	Butadiene %	Hexatriene %
	$(\sigma-\pi)$ mixing	Singlet I	15.50	6.00	4.63
		II		17.00	8.10
		Triplet I et II	0	0	0
hts of configurations which interact directly with $\begin{pmatrix}\pi^*\\ \pi\end{pmatrix}$ configurations	$\begin{pmatrix}\sigma^*\\ \sigma\end{pmatrix}$ polarization configurations	Singlet I	9.64	4.04	3.18
		II		9.50	5.42
	$\begin{pmatrix}\sigma^*_{CH}\\ \sigma_{CH}\end{pmatrix}$ polarization configurations	Singlet I	0.64	0.46	0.40
		II		1.00	0.39
Weights of configurations which interact indirectly with $\begin{pmatrix}\pi^*\\ \pi\end{pmatrix}$ configurations	$\begin{pmatrix}\sigma^*_{C-H}\\ \sigma_{CH}\end{pmatrix}$ delocalization configurations	Singlet I	3.18	0.76	0.40
		II		1.72	1.14
	$\begin{pmatrix}\sigma^*_{C-C}\\ \sigma_{CH}\end{pmatrix}$ delocalization configurations	Singlet I		0.25	0.18
		II		0	0.09
	$\begin{pmatrix}\sigma^*_{CH}\\ \sigma_{C-C}\end{pmatrix}$ delocalization configurations	Singlet I	0.31	0.05	0.03
		II		0.46	0.09
	$\begin{pmatrix}\sigma^*_{CH}\\ \sigma_{C-C}\end{pmatrix}$ delocalization configurations	Singlet I		0.05	0.03
		II		1.02	0.11
	$\begin{pmatrix}\sigma'^*_{CH}\\ \sigma_{CH}\end{pmatrix}$ delocalization configurations with σ_C and σ'_{CH} gem bond	Singlet I	1.11	0.07	0.01
		II		0.57	0.07
	$\begin{pmatrix}\sigma'^*_{CC}\\ \sigma_{CC}\end{pmatrix}$ delocalization configurations	Singlet I		0.281	0.09
		II		1.57	0.17

So, with the perturbation treatment, the $\Phi\begin{pmatrix}\sigma'^*\\ \sigma\end{pmatrix}$ delocalization configurations would appear in the $\begin{pmatrix}\pi^*\\ \pi\end{pmatrix}$ states at the 2nd order only, and their introduction in the $\begin{pmatrix}\pi^*\\ \pi\end{pmatrix}$ states can be visualized by the following diagrams

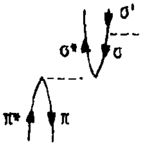

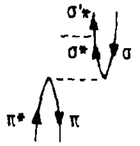

Table 3 shows that the $\Phi\begin{pmatrix}\sigma'^*_{CC}\\ \sigma_{CH}\end{pmatrix}$ delocalization configuration where σ_{CC} belongs to the double bond have a more important weight than the $\Phi\begin{pmatrix}\sigma'^*_{CC}\\ \sigma_{CH}\end{pmatrix}$ where σ_{CC} belongs to a single bond, and than the $\begin{pmatrix}\sigma^*_{CH}\\ \sigma_{CC}\end{pmatrix}$ configurations. This can be easily understood because when σ_{CC} belongs to a double bond, $\begin{pmatrix}\sigma^*_{CH}\\ \sigma_{CC}\end{pmatrix}$ interacts with $\Phi\begin{pmatrix}\pi^*\\ \pi\end{pmatrix}$ configuration through the $\Phi\begin{pmatrix}\sigma^*_{CC}\\ \sigma_{CC}\end{pmatrix}$ polarization configuration (with σ_{CC} belonging to a double bond) which has a very strong interaction matrix element with the $\Phi\begin{pmatrix}\pi^*\\ \pi\end{pmatrix}$ configurations.

4. Possibility of Treatment of the ($\sigma-\pi$) Mixing as a Perturbation

If we consider all the singly excited configurations (σ and π) as degenerate, it becomes impossible to treat the excited states of large molecules because the CI matrix will be too large. For a molecule with N bonds, the matrix involves $N^2 \times N^2$ elements (N polarization configuration $+ (N-1)N$ delocalization configurations). For hexatriene the CI matrix already is a 256×256 matrix (neglecting symmetry considerations).

Generally we are much more concerned by the $\begin{pmatrix}\pi^*\\ \pi\end{pmatrix}$ excited states, so it would be interesting to consider a (π) excitonic matrix with only the $\Phi\begin{pmatrix}\pi^*\\ \pi\end{pmatrix}$ polarization and delocalization configurations. Thus for hexatriene we only have a 9×9 CI matrix. We will now demonstrate that such a thing is possible, and that the interaction of the $\begin{pmatrix}\pi^*\\ \pi\end{pmatrix}$ configurations with the $\begin{pmatrix}\sigma^*\\ \sigma\end{pmatrix}$ configurations may be considered as a perturbation.

Treating by perturbation theory the interaction of a $\Phi\binom{\sigma^*}{\sigma}$ configuration with the $\Phi\binom{\pi^*}{\pi}$ state of ethylene, the coefficient of $\Phi\binom{\sigma^*}{\sigma}$ in the first order perturbed wave function Ψ_1 will be given by

$$\frac{\left\langle \Phi\binom{\sigma^*}{\sigma} |H| \Phi\binom{\pi^*}{\pi} \right\rangle}{E\binom{\pi^*}{\pi^*} - E\binom{\sigma^*}{\sigma}} = 0.28$$

when σ and π bonds belong to the same double bond.

When the σ_{CH} is a single σ bond adjacent to the π bond, the expression is

$$\frac{\left\langle \Phi\binom{\sigma^*_{\mathrm{CH}}}{\sigma_{\mathrm{CH}}} |H| \Phi\binom{\pi^*}{\pi} \right\rangle}{E\binom{\pi^*}{\pi} - E\binom{\sigma^*_{\mathrm{CH}}}{\sigma_{\mathrm{CH}}}} = 0.04 .$$

When the σ and the π bonds set wider apart, these coefficients become negligible.

So with a polyenic planar molecule, it is correct to consider as degenerate the $\Phi\binom{\pi^*}{\pi}$ polarization configurations and the $\Phi\binom{\pi'^*}{\pi}$ delocalization configurations only, and to treat the influence of the $\Phi\binom{\sigma^*}{\sigma}$ configurations as a perturbation.

5. Results of the π Excitonic Calculation

In Table 2, column 8, gives the transition energies obtained after diagonalization of the excitonic matrix containing the $\Phi\binom{\pi^*}{\pi}$ polarization and $\Phi\binom{\pi'^*}{\pi}$ delocalization configurations only.

The excitations energies obtained for the singlet states are higher than those calculated with the excitonic matrix containing σ and π monoexcited states, which shows the importance of the $\Phi\binom{\sigma^*}{\sigma}$ configurations in lowering the excitation energy from the ground state to a $\binom{\pi^*}{\pi}$ state. But the difference between the excitation energies calculated by diagonalization of these two excitonic matrices is more important for the second $\binom{\pi^*}{\pi}$ excited state than for the first $\binom{\pi^*}{\pi}$ one. We expected this result since the $(\sigma-\pi)$ mixing is stronger in the second $\binom{\pi^*}{\pi}$ excited state than in the first $\binom{\pi^*}{\pi}$ one. The difference ΔE between the excitation energies we obtain after the diagonalization of the two excitonic matrices, decreases while n increases. (For the first singlet state $\Delta E = 2.14$ eV for ethylene and 0.80 eV for hexatriene). For the triplet state the transition energy remains of course unchanged, when one goes from the $(\sigma+\pi)$ to the (π) excitonic treatment.

If we introduce the effect of the σ monoexcited configurations by a Rayleigh Schrödinger perturbation [6] on the multideterminantal Ψ_0^m wave functions resulting from the purely π excitonic treatment, we obtain the transitions energies given in Table 2, column 9. We can see that the interaction of $\Phi\begin{pmatrix}\sigma^*\\ \sigma\end{pmatrix}$ singly excited configurations lowers the transition energies, and comparison with the transition energies obtained after diagonalization of the excitonic matrix containing $(\sigma+\pi)$ monoexcited states, shows that for ethylene, the transition energy obtained after perturbation is only a little higher (0.33 eV) that the one obtained with the $(\sigma+\pi)$ excitonic matrix.

Experimentally, the separation between the lowest triplet and singlet states for ethylene, butadiene and hexatriene is respectively 3 eV, 2.8 eV, 2.6 eV [22]. With the (π) excitonic matrix we obtain 6.08 eV, 3.70 eV, and 3.13 eV, and with the $(\sigma+\pi)$ excitonic matrix we obtain 3.94 eV, 2.73 eV, and 2.33 eV: These last results are better than the first ones, because the $(\sigma-\pi)$ mixing only reduces the singlet energies. The results obtained with the $(\sigma+\pi)$ excitonic matrix are not too far from the experimental ones.

7. Analysis of the Wave Function of the $\begin{pmatrix}\pi^*\\ \pi\end{pmatrix}$ Excited States Obtained after Diagonalization of an Excitonic Matrix

A) Ionic Character of the Excited States

With the two types of excitonic matrices we have used, we show that the $\begin{pmatrix}\pi^*\\ \pi\end{pmatrix}$ states are not purely polarization or delocalization configurations, but a mixing of both excitations. This is in agreement with the introduction by Pople and Walmsley [7] of the delocalization configurations in the excitonic model. As was said by Salem [27], some ionic terms which appear in the molecular orbital wave function – those which give a charge separation within double bonds – can be found in the exciton states of Simpson, whereas others – for charge separation across the single bonds – are found in the charge transfer states only.

For hexatriene, in both first singlet and triplet states, the excitation tends to localize on the central bond but with a non negligible coefficient for the terminal bond polarization configurations while in the second singlet and triplet states, the excitation moves towards the two terminal bonds, with a completly negligible coefficient for the central bond polarization configurations. One may analyse from Table 4 the influence of the σ system on the ionic character of the $\pi\pi^*$ excited states.

a) In both singlet and triplet $\begin{pmatrix}\pi^*\\ \pi\end{pmatrix}$ states, the weight of the delocalization configurations (i.e. their ionic character) increases when the number n of double bonds increases. (From 0% in ethylene to 39.79% in hexatriene for the first singlet for instance).

Table 4. Weight of polarization and delocalization configurations in singlet and triplet states obtained with the $(\sigma+\pi)$ excitonic matrix (4A) and with the (π) excitonic matrix (4B)

(4A)

Molecules	State	Ethylene %	Butadiene %	Hexatriene %
Weight of polarization	Singlet I	84.50	61.83	55.58
configuration $\begin{pmatrix}\pi^*\\ \pi\end{pmatrix}$	II		70.50	57.03
	Triplet I	100	79.38	72.52
	II		95.22	83.72
Weight of delocalization	Singlet I	0	32.17	39.79
configuration $\begin{pmatrix}\pi^*\\ \pi\end{pmatrix}$	II		12.50	34.87
	Triplet I	0	20.62	27.48
	II		4.78	16.28

(4B)

Molecules	State	Ethylene %	Butadiene %	Hexatriene %
Weight of polarization	Singlet I	100	58.10	51.37
configuration $\begin{pmatrix}\pi^*\\ \pi\end{pmatrix}$	II		49.80	44.57
	Triplet I	100	73.38	72.52
	II		95.22	83.72
Weight of delocalization	Singlet I	0	41.90	48.63
	II		50.20	55.43
	Triplet I	0	20.62	27.48
	II		4.78	16.28

b) The ionic character is more pronounced for the singlet than for the triplet $\begin{pmatrix}\pi^*\\ \pi\end{pmatrix}$ states. This is due to the fact that the local neutral (polarization) triplet configurations have lower energies than the local polarization singlet configurations (${}^3E_{\text{pol}} = {}^1E_{\text{pol}} - 2K_{ii^*}$) while the local triplet and singlet delocalization configurations have the same energies (K_{ij^*} being zero in the CNDO hypothesis).

c) Except for ethylene, the weight of neutral (polarization) excitations in the $\begin{pmatrix}\pi^*\\ \pi\end{pmatrix}$ excited state is increased by the inclusion of the σ system in the excitonic matrix. This fact may be understood as follows. If the π wave function resulting from the π excitonic matrix diagonalization may be written as follows:

$$\Psi = \alpha\Psi^n + \beta\Psi^i,$$

where Ψ^n and Ψ^i represent neutral and ionic structures, then the $\sigma-\pi$ interaction lowers the transition energy by an amount which increases when α increases. Therefore the best value of α in the $(\sigma+\pi)$ treatment is higher in absolute value than in the purely π treatment. This fact also explains that the $(\sigma-\pi)$ mixing is larger on the second $\begin{pmatrix}\pi^*\\ \pi\end{pmatrix}$ excited states (more strongly neutral) than in the first one.

d) One may notice that the inclusion of the $(\sigma-\pi)$ interaction may reverse the relative ionic character of the two first $\begin{pmatrix}\pi^*\\ \pi\end{pmatrix}$ singlet states; for instance in the butadiene molecule the (π) excitonic treatment gives respectively 58 and 50% of neutral character to the two first $\begin{pmatrix}\pi^*\\ \pi\end{pmatrix}$ singlet excited states of butadiene while the $(\sigma+\pi)$ excitonic treatment gives respectively 62 and 70%.

B) Charges and Charge-Fluctuations in the Double-Bonds Loges

In Table 5 the mean populations of each π double bonds (column 3, 4) show that the relatively high ionic character does not lead to significant net charges; The central loge gains 0.03 electrons in the lowest $^1\begin{pmatrix}\pi^*\\ \pi\end{pmatrix}$ excited state, and lose 0.43 (in the π model) or 0.25 (in the $\sigma+\pi$ model) electron in the second $^1\begin{pmatrix}\pi^*\\ \pi\end{pmatrix}$ excited state.

We have analyzed the fluctuations of the number of electrons in the loge. This statistical concept gives an insight on the delocalization of electrons from one volume to another. In the PCILO method for the ground state, this fluctuation is kept to zero in the zeroth order wave function. For the excited states we must introduce a rather important fluctuation of the bond charge in the zeroth order wave function.

It appears from Table 5 that the $(\sigma-\pi)$ coupling diminishes strongly the charge fluctuation in the excited states.

Table 5. Mean population and charge fluctuation in the double-bonds loges for the two first singlet states obtained with the $(\sigma+\pi)$ or (π) excitonic matrix

Molecules	State	Mean population in the first loge	Fluctuation in the first loge[a]	Mean population in the second loge[a]	Fluctuation in the second loge[a]
Butadiene	*First singlet*				
	$(\sigma+\pi)$ excitonic matrix	2	0.57		
	(π) excitonic matrix	2	0.65		
	Second singlet				
	$(\sigma+\pi)$ excitonic matrix	2	0.35		
	(π) excitonic matrix	2	0.71		
Hexatriene	*First singlet*				
	$(\sigma+\pi)$ excitonic matrix	1.98	0.46	2.04	0.61
	(π) excitonic matrix	1.99	0.51	2.03	0.67
	Second singlet				
	$(\sigma+\pi)$ excitonic matrix	2.13	0.41	1.75	0.51
	(π) excitonic matrix	2.22	0.51	1.57	0.51

[a] The first loge is the external one. The second loge is the central one in hexatriene.

Conclusion

At this stage of calculation, the numerical results suffer from three defects: a) the CI is limited to the single excitations, b) the Rydberg AO's are not included, c) the parameters have been fitted on ground state properties. Therefore we do not discuss in details the agreement between our calculated spectra and the experimental ones.

From a methodological point of view, one must notice the agreement between our results and those obtained from the diagonalization of the singly excited CI matrix built using SCF delocalized MO's [15]. If we used SCF localized MO's, the results would be identical, since the space of singly excited configuration is unvariant under the unitary transformations in the spaces of occupied or virtual MO's. We actually used fully localized MO's, and the similarity of our results with those of Giessner and Pullman shows the unimportance of the tails of localized SCF MO's, i.e. of the delocalization in the ground state.

The main purpose of this paper was to build and test a zero-order wave function using localized MO's. For $\begin{pmatrix}\pi^*\\ \pi\end{pmatrix}$ transitions we had two possibilities; i) a $(\sigma+\pi)$ excitonic wave function, involving a rather large number of determinants; ii) a purely (π) excitonic wave function, which will only consider the $(\pi\rightarrow\pi^*, \sigma\rightarrow\sigma^*)$ coupling as a perturbation. The analysis of the wave functions shows that the $(\sigma-\pi)$ coupling has strong effects on the wave function (especially on the ionic character and charge fluctuations in the π system) but as concerns the energy it may be actually considered as a perturbation. At this stage the transition energies obtained with the CNDO/2 parameters are too high. But this is only a zeroth order model; the interaction of the ground state determinant with singly and doubly excited configurations and the interaction of the multiconfigurational wave function for the excited state with doubly and triply excited determinants will be taken into account through an appropriate second order perturbation treatment. The PCILO method for excited states so constructed will be developped in a further publication.

We thank Dr. J. P. Malrieu for many fruitful discussions and for his interest and very helpful critiscisms.

References

1. Diner, S., Malrieu, J. P., Claverie, P.: Theoret. chim. Acta (Berl.) **13**, 1 (1969); Diner, S., Malrieu, J. P., Jordan, F., Gilbert, M.: Theoret. chim. Acta (Berl.) **15**, 100 (1969); Jordan, F., Gilbert, M., Malrieu, J. P., Pincelli, U.: Theoret. chim. Acta (Berl.) **15**, 211 (1969).
2. Langlet, J., Gilbert, M., Malrieu, J. P.: Theoret. chim. Acta (Berl.) **22**, 60 (1971).
3. Langlet, J., Pullman, B., Berthod, H.: J. chem. Physics **67**, 480 (1970).
   Maigret, B., Pullman, B., Caillet, J.: Biochem. biophysic. Res. Commun. **40**, 808 (1970).
4. McWeeny, R., Ohno, K.: Proc. Roy. Soc. (London) A **255**, 367 (1960); Tsuchida, A., Ohno, K.: J. chem. Physics **39**, 600 (1963); McWeeny, R., Del Re, G.: Theoret. chim. Acta (Berl.) **10**, 13 (1968).
5. Simpson, W. T.: J. Amer. chem. Soc. **73**, 5363 (1951); **77**, 6164 (1955).
6. Messiah, A.: Mécanique quantique, Tome 2, p. 596. Paris: Dunod 1960.
7. Pople, J. A., Walmsey, S. H.: Trans. Faraday Soc. **58**, 441 (1962).
8. Murell, J. N.: J. chem. Physics **37**, 1162 (1962).

9. Kutzelnigg, W., Del Re, G., Berthier, G.: Fortschr. chem. Forsch., Topics in Current Chemistry **22**, 1 (1971).
10. Dunning, T. H., McKoy, V.: J. chem. Physics **47**, 1735 (1965).
11. Denis, A., Malrieu, J. P.: Theoret. chim. Acta (Berl.) **12**, 66 (1968).
12. Pople, J. A., Santry, D. P., Segal, G. A.: J. chem. Physics **43**, S 129 (1965); Pople, J. A., Segal, G. A.: J. chem. Physics **43**, S 136 (1965), Pople, J. A., Segal, G. A.: J. chem. Physics **44**, 3289 (1966).
13. Giessner-Prettre, C., Pullman, A.: Theoret. chim. Acta (Berl.) **13**, 265 (1969).
14. Clark, P. A.: J. chem. Physics **54**, 45 (1971)
15. Clark, P. A., Ragle, J. L.: J. chem. Physics **46**, 4235 (1967); J. chem. Physics **48**, 4795 (1969).
16. Berry, R. S.: J. chem. Physics **38**, 1934 (1963)
17. Kaldor, U., Shavitt, I.: J. chem. Physics **48**, 191 (1968).
18. Moskowitz, J. W., Harrison, M. C.: J. chem. Physics **42**, 1723 (1964).
19. Schulman, J. M., Moskowitz, J. W., Hollister, C.: J. chem. Physics **46**, 2759 (1967).
20. Robin, M. B., Hart, R. R., Kueblen, N. A.: J. chem. Physics **44**, 1803 (1960).
21. Berthod, H.: J. chem. Physics **45**, 1859 (1966).
22. Polak, R., Paldus, J.: Theoret. chim. Acta (Berl.) **5**, 422 (1966).
23. Evans, D. F.: J. chem. Soc. **2**, 1735 (1960)
24. American Petroleum Research Project 44, serial number 39, 65, 91, 32.
25. Schuler, H., Elulz, ., Arnold, G.: Spectrochim Acta **17**, 1043 (1961).
26. Denis, A., Malrieu, J. P.: J. chem. Physics **52**, 6076 (1970).
27. Salem, L.: The molecular orbital theory of conjugated systems, p. 450. New York, Amsterdam: W. A. Benjamin Inc. 1966

Dr. J. Langlet
Institut de Biologie Physico-Chimique
Laboratoire de Biochimie Théorique
associé au C.N.R.S
13, rue P. et M. Curie
F-75 Paris 5è
France

Theoret. chim. Acta (Berl.) 27, 243—264 (1972)
© by Springer-Verlag 1972

Vibrational Analysis of the Electronic Spectrum of Ethylene Based on *ab initio* SCF-CI Calculations

Sigrid D. Peyerimhoff
Institut für physikalische Chemie, Johannes Gutenberg Universität, 65 Mainz, Germany

Robert J. Buenker
Department of Chemistry, University of Nebraska, Lincoln, Nebraska 68508

Received June 22, 1972

Ab initio calculations for CH_2 twisting and CC stretching vibrational wavefunctions and energy levels are reported for various electronic states of ethylene C_2H_4. Electronic transition moments between these states are also obtained to allow a calculation of the oscillator strengths for vibrational transitions involved in various electronic band systems; from this study it is concluded that the *vertical electronic* energy difference ΔE_e may differ significantly from the energy of the absorption maximum $\Delta E_{\max}$ with which it is often equated. In particular it is found in the case of the $\pi \rightarrow \pi^*$ singlet-singlet excitation of ethylene that the ΔE_e value overestimates the most probable vibrational transition energy (7.89 eV) by some 0.4 eV, thereby offering an explanation for the fact that previous attempts to predict the location of the $V-N$ Franck-Condon absorption maximum have consistently obtained substantially higher results than the 7.66 eV value actually observed. Similar calculations for various Rydberg species and for the $N-T$ transition are also found to obtain a quite consistent representation of the electronic spectrum of this system.

Mit Hilfe von *ab initio*-Methoden werden Energieniveaus und Wellenfunktionen für die CH_2-Rotation und CC-Streckschwingung des Äthylens in einer Reihe von Elektronenzuständen berechnet. Aus den elektronischen Übergangsmomenten zwischen diesen Zuständen werden die Oszillatorenstärken der Schwingungsübergänge in den einzelnen Elektronenbanden erhalten. Die Untersuchungen führen zu dem Schluß, daß die Energiedifferenz für *vertikale* Anregung, berechnet als Unterschied der *Elektronenenergie* ΔE_e der entsprechenden Zustände, ganz erheblich von der Energie für maximale Absorption abweichen kann, wenn sie auch dieser oft gleichgesetzt wird. Insbesondere stellt sich heraus, daß bei der Singulett-Singulett $\pi \rightarrow \pi^*$-Anregung im Äthylen der Wert von ΔE_e ungefähr um 0,4 eV über dem entsprechenden Wert für den wahrscheinlichsten Schwingungsübergang (7,89 eV) liegt; dadurch läßt sich wohl die Tatsache erklären, daß frühere Versuche zur Berechnung des $V-N$ Franck-Condon-Absorptionsmaximums immer einen beträchtlich höheren Wert ergaben als wirklich beobachtet worden ist (7,66 eV). Ähnliche Berechnungen für die verschiedenen Rydberg-Banden und den $N-T$-Übergang führen ebenfalls zu einer durchaus konsequenten Beschreibung des Elektronenspektrums des C_2H_4-Moleküls.

1. Introduction

For the past forty years and continuing into the present there have been numerous theoretical calculations which have attempted to obtain agreement with the experimental details of the electronic spectrum of ethylene. Most of this work has centered around the so-called $T \leftarrow N$ and $V \leftarrow N$ transitions, characterized by Mulliken [1, 2] as being *valence* $\pi \rightarrow \pi^*$ excitations. The observed absorption maxima for these two band systems have almost invariably been attributed to *vertical* transitions between the N ground state and the respective excited states in question, in accordance with the Franck-Condon Principle [3].

Nevertheless the results of *ab initio* calculations[1] (through 1970) are not found to be entirely consistent with such an interpretation of the ethylene spectrum, since they indicate that the lowest excited $\pi \rightarrow \pi^*$ singlet state possesses a considerable amount of diffuse character, and yield a *vertical* transition energy for the $V \leftarrow N$ system which exceeds that of the experimental Franck-Condon maximum by a considerable margin.

Given the apparent lack of success on the part of previous calculations on this subject, more recent theoretical treatments have attempted to improve the situation either by enlarging the scope of the earlier calculations (by upgrading the level of CI undertaken [5–7], for example) or by utilizing substantially different methods, such as the RPA approximation [8]. These later calculations have led to some conflicting results concerning the *degree* of diffuse character of the $\pi \rightarrow \pi^*$ singlet and also with respect to the *magnitude* of the vertical transition energy to this state; yet the basic findings that 1) the singlet is calculated to exhibit substantially less valence character than the corresponding triplet and 2) that the vertical transition energy obtained by subtracting the total energies of ground and excited states (for the equilibrium geometry of the ground state) exceeds that of the $V \leftarrow N$ absorption maximum by from 0.3 to 0.6 eV remain unchanged.

The apparently exceptional nature of the transition to the $\pi \rightarrow \pi^*$ singlet is further emphasized by the fact that the calculated results for the corresponding $\pi \rightarrow \pi^*$ triplet seem to be totally consistent with the earlier interpretation of the spectrum; these calculations also find good agreement with the experimental excitation energies to the various low-lying Rydberg states of ethylene [4, 5]. As a result it has been speculated that the measured absorption maximum in the $V \leftarrow N$ bands might actually correspond to a non-vertical transition, whose energy is significantly *lower* than that of the true vertical species. Additional support for this interpretation has been provided by the finding that in the twisted C_2H_4 nuclear arrangement the $\pi \rightarrow \pi^*$ singlet state of planar geometry correlates with the $2\,^1B_1$ rather than the lowest state of this symmetry; at the same time the $\pi \rightarrow \pi^*$ state for the *antiplanar* CH_2 conformation is found to correlate with the $\pi \rightarrow 3p_y$ Rydberg species of the planar molecule. Consequently the calculations indicate that the potential curves for CH_2 twist are significantly different for the $\pi \rightarrow \pi^*$ singlet state than for the corresponding triplet and hence suggest that these two states quite possibly exhibit radically different vibrational characteristics.

Ultimately a complete characterization of the electronic spectrum of ethylene must necessarily involve consideration of the vibrational motion which accompanies the transitions between various electronic states. To this end potential curves for both CC stretch and CH_2 twist in the ground and various excited states of ethylene have been obtained in earlier work [5] in order to effect the necessary vibrational analysis for the electronic transitions of this molecule.

2. Outline of the Theoretical Method

The potential curves for ethylene as a function of the CH_2 twisting angle θ and the CC separation R reported previously [5] have been obtained using the

---

[1] A survey of this work may be found in Ref. [4].

Born-Oppenheimer approximation. Accordingly the total wavefunction of the system is defined as the product of the electronic function ψ_e obtained from the CI treatment and a vibrational function ψ_v, which in this treatment is assumed to depend only on the nuclear coordinates R and θ. In addition the assumption is made that the stretching and twisting vibrations are completely separable[2], leading to the following expression for the total wavefunction:

$$\Psi = \psi_e(\boldsymbol{r}_i; R, \theta) \cdot \psi_v(R) \cdot \psi_v(\theta) \tag{1}$$

where the $\boldsymbol{r}_i$ are the coordinates of the electrons of the system.

The vibrational wavefunctions are obtained by an expansion technique. The expression for the stretching mode is taken to be:

$$\psi_v(R) = \sum_n c_n R^{n-1} \exp(-\alpha R^2) \tag{2}$$

with $\alpha = \frac{1}{2}\sqrt{k\mu}$, the harmonic oscillator value (k being the stretching force constant and μ the associated reduced mass with each CH_2 group treated as a point mass). The twisting vibration, in turn, is described by:

$$\psi_v(\theta) = \sum_n a_n \sin 2n\theta \quad \text{or} \quad \sum_n b_n \cos 2n\theta \,. \tag{3}$$

Standard formulas for the kinetic energy [9] are used in constructing the Hamiltonian operators for the two types of nuclear motion. Corresponding potential energy functions are obtained from Fourier series representations of the aforementioned Born-Oppenheimer potential curves. For CC stretch a polynomial in R is employed, while a linear combination of functions of the form $\cos 2n\theta$ is used to represent the CH_2 twisting potential; the number of terms in a given fitting is always taken to be equal to the number of data points available (i.e. four to six for CC stretch and nine to eleven for CH_2 twist [5]).

For a given Hamiltonian the set of vibrational wavefunctions is obtained by energy minimization with respect to the appropriate expansion coefficients. In the representation of $\psi_v(R)$ a total of 16 terms was normally employed but it was found that increasing the size of this basis and/or varying the exponent α from its harmonic oscillator value by $\pm 20\%$ had no significant effect on the position of at least the first ten calculated energy levels. The highest order terms in $\psi_v(\theta)$ are $\sin 60\theta$ and $\cos 60\theta$ respectively; again it was found that inclusion of higher order terms had essentially no effect on the location of the important low-lying vibrational levels. Because the potentials under consideration are of period π, the solutions obtained are necessarily either pure cosine or pure sine series, as indicated in Eq. (3).

The transition moment $\boldsymbol{R}_{e'v'e''v''}$ between vibrational levels of the ground and excited electronic states respectively is then given by the expression

$$\begin{aligned} \boldsymbol{R}_{e'v'e''v''} = \int \cdots \int \psi_{e'}^{*}(\boldsymbol{r}_i; R, \theta) \\ \cdot \psi_{v'}^{*}(R)\, \psi_{v'}^{*}(\theta) \Big(\sum_i \boldsymbol{r}_i\Big) \psi_{e''}(\boldsymbol{r}_i; R, \theta)\, \psi_{v''}(R)\, \psi_{v''}(\theta) \cdot d\boldsymbol{r}_i \, dR \, d\theta \,. \end{aligned} \tag{4}$$

---

[2] Explicit SCF and CI calculations indicate that these two types of nuclear motion are only slightly dependent on one another so that this assumption seems quite justified.

In this equation and hereafter primed subscripts refer to the electronic excited state, doubly-primed to the electronic ground state. Within the Born-Oppenheimer Approximation this expression reduces to:

$$\boldsymbol{R}_{e'v'e''v''} = \int\int \psi^*_{v'}(R)\,\psi^*_{v'}(\theta)\,\boldsymbol{R}_{e'e''}(R,\theta)\,\psi_{v''}(R)\,\psi_{v''}(\theta)\,dR\,d\theta \tag{5}$$

where the electronic transition moment, defined as

$$\boldsymbol{R}_{e'e''}(R,\theta) = \int\cdots\int \psi^*_{e'}(\boldsymbol{r}_i;R,\theta)\,(\sum_i \boldsymbol{r}_i)\,\psi_{e''}(\boldsymbol{r}_i;R,\theta)\,d\boldsymbol{r}_i\,, \tag{6}$$

depends only parametrically on the nuclear coordinates. Analogous formulas for the transition moments based on the dipole velocity operator ($\boldsymbol{V}_{e'v'e''v''}$) are obtained similarly.

In the usual assumption $\boldsymbol{R}_{e'e''}$ is treated as a constant vector, leading to what is commonly referred to as the Franck-Condon Principle [3]. Explicit calculation of $\boldsymbol{R}_{e'e''}$ for the various states of ethylene show, however, that $\boldsymbol{R}_{e'e''}$ generally depends quite strongly on θ, although only to a much smaller extent on R, and thus in what follows the electronic transition moment is assumed to be a function of θ but to be independent of R. As a result the contribution to the total transition moment due to CC stretch is made strictly in terms of the vibrational overlap of the two corresponding wavefunctions, while the part caused by the twisting vibration is obtained more directly. The final expression used is thus:

$$\boldsymbol{R}_{e'v'e''v''} = \int \psi_{v'}(R)\,\psi_{v''}(R)\,dR \cdot \int \psi_{v'}(\theta)\,\boldsymbol{R}_{e'e''}(\theta)\,\psi_{v''}(\theta)\,d\theta\,. \tag{7}$$

This equation is then evaluated by inserting a Fourier representation of $\boldsymbol{R}_{e'e''}$. Corresponding oscillator strengths for a given vibrational transition have subsequently been obtained as:

$$f_{e'v'e''v''} = \tfrac{2}{3}\,\Delta E\,|\boldsymbol{R}_{e'v'e''v''}|^2 \tag{8}$$

or

$$f_{e'v'e''v''} = \tfrac{2}{3}\,|\boldsymbol{V}_{e'v'e''v''}|^2/\Delta E \tag{9}$$

where ΔE is the transition energy between the vibrational levels involved[3]. The *total* oscillator strength for a given electronic transition is then obtained as the sum of all $f_{e'v'e''v''}$ values between the ground state vibrational level of $\psi_{v''}$ (that is, ignoring the possibility of thermally excited vibrations in the electronic ground state) and *all* the vibrational states of the electronically excited species.

3. Transition Probabilities to the $\pi\rightarrow\pi^*$ States in Ethylene

A) Vibrational Wavefunctions and Energy Levels

The potential curves used in the treatment of the vibrational characteristics of the electronic spectrum of ethylene are those of the CI-1 calculation reported earlier [5, 10]. The ground state CH_2 twisting potential curve is given in Fig. 1 and has been obtained by means of pointwise calculation of the total energy for 11 different values of θ between 0° and 90° inclusively ($R = 1.35$ Å). The vibrational levels calculated for this potential are also shown in Fig. 1; successive

---

[3] All values are in atomic units.

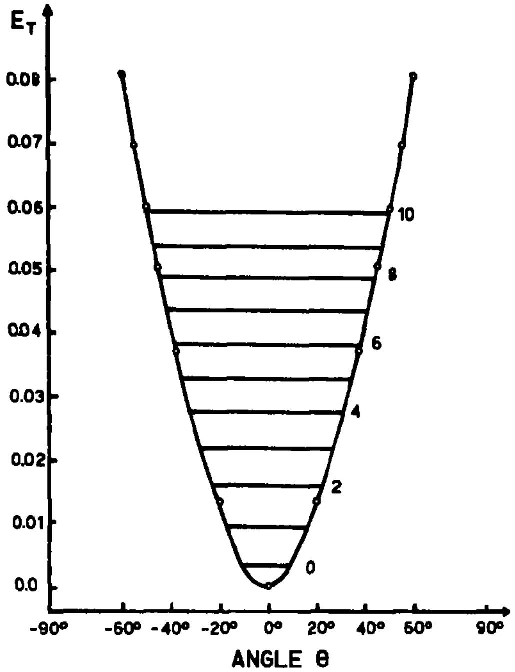

Fig. 1. CH_2 twisting potential curve for the ground state of ethylene obtained from the CI-1 treatment ($R_{CC} = 1.35$ Å). Calculated vibrational levels for $v_4'' = 0$ to $v_4'' = 10$ are also included. In this paper all energy values, unless specified otherwise, are given in hartrees

energy differences between even levels[4] are found to decrease with increasing vibrational quantum number, levelling off to a value of approximately 1100 cm^{-1}, as compared to the experimental [11] result of 1023 cm^{-1}. The corresponding vibrational wavefunctions for the lowest three states of even quantum number are plotted in Fig. 2.

The ground state CC stretch potential curve was obtained for a planar arrangement of CH_2 groups and the resulting optimum value of R (1.35 Å) and the calculated stretching force constant (9.9 mdyn/Å) are in good agreement with the experimental values of 1.338 ± 0.003 Å [11] and 9.305 mdyn/Å [12, 13] respectively. Since the CC stretch normal coordinate is actually a mixture involving some CH stretch and ∢ HCH bending (a_g species), however, the calculated frequency of 1100 cm^{-1} obtained by using the pure CC stretch potential curve considerably underestimates the observed spectral frequency (1623 cm^{-1}) [11]. The three lowest energy vibrational wavefunctions for the pure stretching motion are plotted in Fig. 3.

Previous calculations [5] have shown that in the planar molecule the $\pi \rightarrow 3py(^1B_{1g})$ state possesses a lower energy than the $\pi \rightarrow \pi^*(^1B_{1u})$, a result which is of great interest since both of these states transform according to the same $(^1B_1)$ irreducible representation in the reduced symmetry of the twisted molecule.

---

[4] The selection rules for the (a_u) twisting vibration are such that only the even (cosine) levels of the upper electronic state can combine with the lowest vibrational level of the ground state.

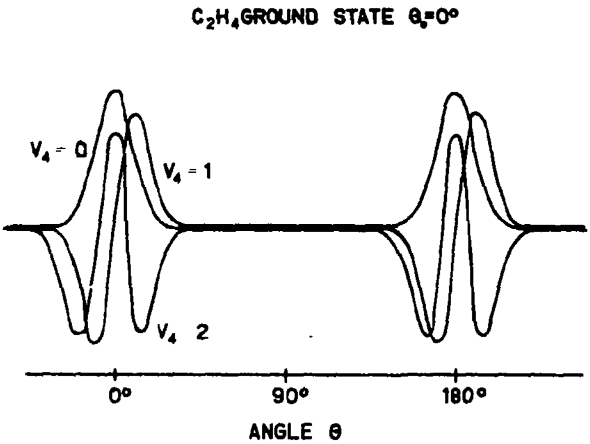

Fig. 2. Calculated vibrational wavefunctions for the CH_2 twisting mode in the C_2H_4 ground state obtained from the potential curve in Fig. 1

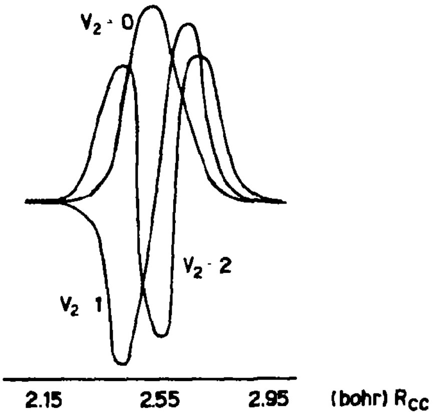

Fig. 3. Calculated vibrational wavefunctions for the CC stretching mode in the ground state of ethylene

Consequently application of the non-crossing rule for these two states leads to a quite sharp avoided crossing, as can be seen from the calculated CH_2 twisting potential curves given in Fig. 4 ($R = 1.35$ Å in both cases). In other words, according to the calculations the valence $\pi \rightarrow \pi^*$ singlet species for $\theta = 90°$ (lowest $^1B_1$ state at this angle) does not correlate with the more diffuse $\pi \rightarrow \pi^*$ singlet found for the planar molecule; such a situation has not been anticipated in the earlier analysis by Mulliken [1, 2, 11] and others. Because there is reason to believe that *both* $^1B_1$ states are responsible for the $V \leftarrow N$ absorption in the ethylene spectrum, the more stable of these species will hereafter be referred to as the V_g, the less stable as the V_u state; the respective subscripts refer to the inversion symmetry characteristics of each species in the planar nuclear arrangement.

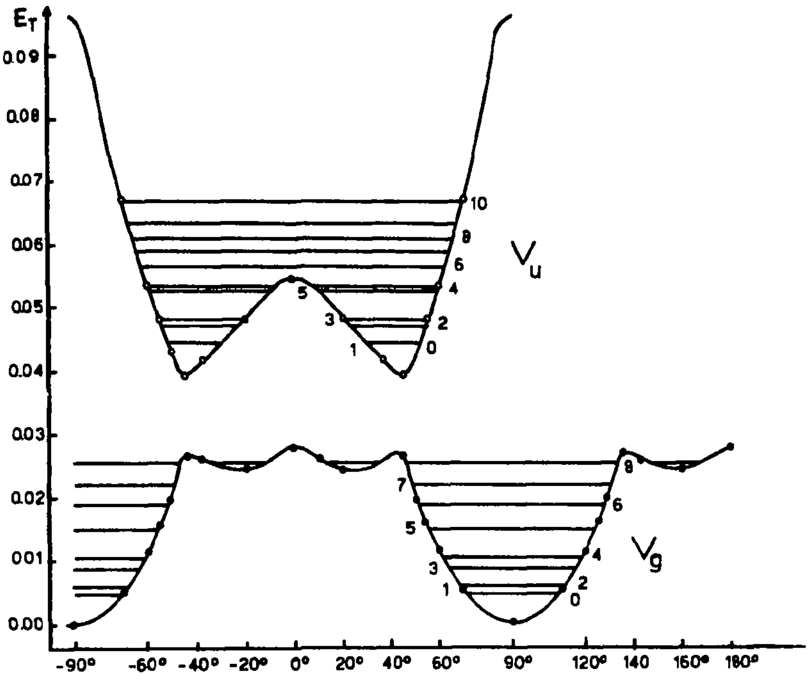

Fig. 4. CH_2 twisting potential curves for the $({}^1B_{1g} - 1\,{}^1B_1 - {}^1B_2)V_g$ and the $({}^1B_{1u} - 2\,{}^1B_1 - {}^1A_2)V_u$ excited states of ethylene obtained from the CI-1 treatment ($R_{CC} = 1.35$ Å). The lowest calculated vibrational levels are also indicated

Vibrational levels calculated for both states are also indicated in Fig. 4. In the upper V_u state one observes a characteristic doubling of levels, which is expected in view of the double-minimum nature of the corresponding twisting potential curve ($\theta_0 = \pm 42.5°$). Vibrational levels for the V_g state are also doubled but to a lesser extent than for the V_u species. The V_g state possesses two types of energy minima, one corresponding to the valence $\pi \rightarrow \pi^*$ region, the other to the more Rydberg-like region of the potential. The optimum bond distances for the V_g and V_u states are calculated to be nearly equal (1.39 Å) and, perhaps more importantly, are found to differ by a relatively small amount from the ground state equilibrium value, in sharp contrast to the behavior predicted for the V state in previous work [11].

B) Electronic Transition Moments

In the present theoretical treatment calculation of the electronic transition moment $R_{e'e''}$ is complicated by the fact that the electronic wavefunctions obtained for ground and excited states are expanded in configurations based on *different* sets of MO's, due to the nature of the CI(PCMO) method employed[5]. In order to take advantage of the computional simplifications arising from the use of the

---

[5] In these calculations the SCF MO's of a given state (parent configuration) are used in its own CI expansion; details of this procedure are given elsewhere [10].

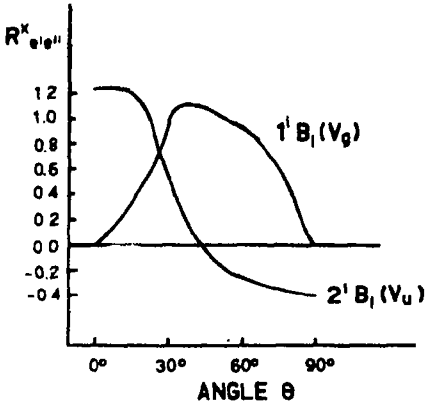

Fig. 5 Variation of the x-component of the electronic transition moment $R_{e'e''}$ between the ground state and the two states of ${}^1B_1$ symmetry [obtained in the CI(GSMO) treatment] as a function of the CH$_2$ twisting angle θ

same set of MO's in the CI expansions for $\psi_{e'}$ and $\psi_{e''}$, additional CI calculations have been carried out which employ the ground state SCF MO's as the basis in the treatment for each excited state [CI(GSMO) method]; in addition the ground state wavefunction has also been obtained by using the SCF MO's of various of the excited states.

The variation with θ of the electronic transition moment $R_{e'e''}$ between the ground state and each of the two ${}^1B_1$ excited states obtained from the CI(GSMO) treatment is shown in Fig. 5. (Only the x-component is non-zero.) Transitions to the V_u state are allowed for the planar geometry and hence $R^x_{e'e''}$ for this species begins with a non-zero value at $\theta = 0°$ but decreases quite rapidly beyond $\theta = 20°$, reaching a negative value for $\theta = 90°$ ($2\,{}^1B_1$ correlates with a ${}^1A_2$ state in D_{2d} symmetry, to which transitions from the ${}^1B_1$ ground state are also allowed). In contrast the corresponding curve for the V_g state is zero[6] at $\theta = 0$ and $\theta = 90°$ and has a maximum around 38°. In both cases the transition moments are far from constant with twisting, contrary to what is often assumed in connection with the application of the Franck-Condon Principle.

From the $R^x_{e'e''}$ curve for the V_u state it is clear that simple changes in the valence character of excited states are not sufficient to explain even the most rudimentary aspects of the transition moment behavior upon CH$_2$ twist since the observed increase in valence character for this state with increasing θ would ordinarily be expected to lead to an *increase* rather than to the decrease actually calculated. A factor of greater importance is the relative orientation of initial and final orbitals in such electronic transitions; thus the fact that these two MO's in the case of the $N - V_u$ transition possess their respective charge density maxima in rapidly diverging coordinate planes as CH$_2$ twist prodeeds is largely responsible for the calculated decrease in transition moment. These observations emphasize quite strongly that the degree of valence character for an excited state is far from the sole determining factor in the probability of its transitions from the ground state and thus that calculations of quantities such as $\langle x^2 \rangle$ and $\langle z^2 \rangle$, which are a measure almost exclusively of the diffuseness of the upper state, can be quite misleading.

---

[6] Transitions from the ${}^1A_g$ to the ${}^1B_{1g}$ in D_{2h} and from ${}^1B_1$ to ${}^1B_2$ in D_{2d} symmetry are forbidden under the dipole selection rules.

C) Transition Probabilities

Oscillator strengths for transitions between the vibrationless ($v_2'' = v_4'' = 0$) ground state and the $2\,{}^1B_1(V_u)$ excited state, as calculated from Eq. (8) using the electronic transition moments discussed above, are contained[7] in Table 1. These results show the most probable vibrational transition to the V_u upper state to correspond to an excitation energy of 7.894 eV, despite the fact that the *vertical* transition energy (calculated as the difference between the electronic energies of ground and excited state for the equilibrium geometry of the former) is considerably larger [5], namely 8.250 eV. The upper vibrational state in question is characterized by $v_2' = 0$ (pure stretching) and $v_4' = 2$ (torsional vibration); the "vertical" transition, on the other hand, corresponds most closely to either $v_4' = 8$ (on the basis of the 8.275 eV ΔE value of Table 1) or to $v_4' = 6$ (based on the results in Fig. 4)[8]. In other words, these calculations find that the most probable transition is markedly non-vertical, as has been speculated earlier [4, 5].

The cause of this non-verticality can be qualitatively understood from the form of the vibrational wavefunctions given in Fig. 6. Since the potential curve

Table 1. Tabulation of transition energies ΔE and oscillator strengths f for the $2\,{}^1B_1(V_u)$ state of C_2H_4. All results are obtained relative to the lowest vibrational level of the (${}^1A_g$) ground state ($v_2'' = v_4'' = 0$). The corresponding calculated electronic vertical transition energy is 8.250 eV

v_4'	f $v_2' = 0$	ΔE (eV)	f $v_2' = 1$	ΔE (eV)	f $v_2' = 2$	ΔE (eV)
0	0.0005	7.813	0.0001	7.925	0.0000	8.036
2	0.1405	7.894	0.0239	8.005	0.0009	8.116
4	0.0109	8.049	0.0019	8.160	0.0001	8.271
6	0.0644	8.154	0.0109	8.265	0.0004	8.376
8	0.0157	8.275	0.0027	8.387	0.0001	8.497
10	0.0081	8.427	0.0014	8.539	0.0001	8.650
12	0.0035	8.580	0.0006	8.692	0.0000	8.803
14	0.0014	8.749	0.0002	8.861	0.0000	8.972
16	0.0006	8.924	0.0001	9.035	0.0000	9.146
18	0.0002	9.093	0.0000	9.205	0.0000	9.316
20	0.0001	9.249	0.0000	9.360	0.0000	9.471
$\sum_{v_4'}$	0.2459	—	0.0418		0.0016	—

$\sum_{v_2'} \sum_{v_4'} f = 0.289$

---

[7] The notation for the vibrational quantum numbers used in this paper is essentially that of Herzberg [14], except that in the present work v_2 refers to a pure CC stretch motion rather than to a normal coordinate (see Sect. 3 A).

[8] The uncertainty as to which of these values for v_4' most closely corresponds to the condition of verticality is a reflection of the rather large difference between the zero point energies of the N and V_u states respectively.

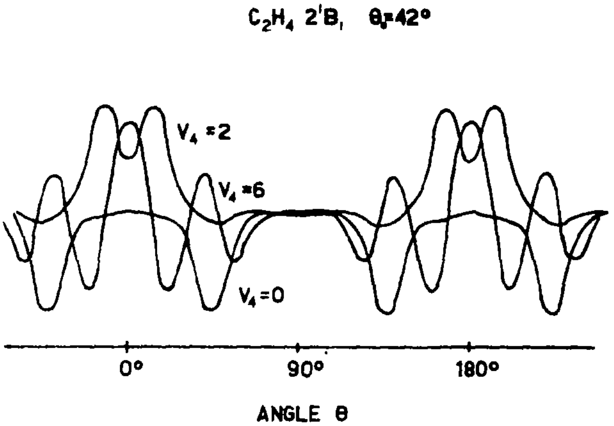

Fig. 6. Calculated important vibrational wavefunctions for the CH_2 twisting mode in the $2\,^1B_1(V_u)$ excited state obtained from the corresponding potential curve in Fig. 4

Table 2. Vibrational overlaps $S(v_4', v_4'')$ and electronic transition moments $R^x_{v_4' v_4''}$ between various $2\,^1B_1(V_u)$ twisting vibrational wavefunctions and that of the lowest vibrational level ($v_4''=0$) of the ground state

v_4'	v_4''	$S(v_4', v_4'')$	$R^x_{v_4' v_4''}$	$R^x_{v_4' v_4''}/S(v_4', v_4'')$
0	0	0.045	0.053	1.164
	2	0.762	0.923	1.211
	4	0.206	0.255	1.238
	6	0.503	0.615	1.223
	8	0.253	0.302	1.194
	10	0.184	0.215	1.168
	12	0.121	0.140	1.157
	14	0.074	0.087	1.183
	16	0.046	0.056	1.219
	18	0.028	0.036	1.254
	20	0.019	0.024	1.279

of the V_u state has its minimum at $\theta = 42°$, there is as expected practically no overlap between the $v_4'=0$ function with its maximum at this angle and the $v_4''=0$ function with its maximum at $\theta = 0°$ (Fig. 2). Nevertheless, the equilibrium angles for the N and V_u states are sufficiently close to one another to enable the vibrational wavefunction for $v_4'=2$ to have the greatest overlap with the $v_4''=0$ function of any of the upper state twisting species (see Table 2), even though its maxima occur for a distinctly non-planar conformation of the CH_2 groups (see Fig. 6). One finds that of the two species to which transitions could be called vertical, the $v_4'=8$ function has only a relatively small overlap with the vibrationless ground state, while that for the $v_4'=6$ function is quite substantial; in the latter case the Franck-Condon factor (S^2) is still only 0.25, however, as compared to the corresponding value of 0.58 for the $v_4'=2$ species. Moreover, the fact that the so-called vertical transitions are not found to be the most probable does not actually constitute a violation of the Franck-Condon Principle, which merely states that the ratio between the transition moment $R_{e'v'e''v''}$ and the corresponding vibrational overlap is very nearly constant (see Table 2).

These results serve to emphasize the need for unequivocal evidence (experimental or theoretical) concerning the relative location of the V_g state, since it is obvious from the present treatment that the presence of this state below the V_u has a dramatic effect upon the description of the absorption bands in the 7.5 to 8.5 eV region of the electronic spectrum of ethylene. In addition, since the validity of the Born-Oppenheimer approximation depends critically upon the magnitude of the energy difference between neighboring states, it is clear that an accurate estimate of the closest approach of the twisting potential curves for the V_g and V_u species is also required (in the present treatment this energy difference is calculated to be 0.3 eV; see Fig. 4). In the absence of the V_g state the V_u potential curve would be very similar to that of the $\pi \rightarrow \pi^*$ triplet state, namely with a minimum occurring for $\theta = 90°$, as has been assumed in earlier interpretations.

In order to determine to what extent the results given in Tables 1 and 2 depend on the specific nature of the calculated potential curves and electronic transition moment data, a number of additional calculations have been carried out. A limited CI(GSMO) calculation has been employed in the treatment of the important ${}^1B_1$ excited states, but this method is clearly not as reliable, primarily because it leads to an excessively diffuse wavefunction [5] for the $\pi \rightarrow \pi^*$ singlet in the planar geometry. As a result not only is the absolute energy of this state ($2\,{}^1B_1$) substantially higher than in the CI(PCMO) treatment but also the curvature of its twisting potential curve is much less pronounced in the neighborhood of $\theta = 0°$ [9]. Consequently the fact that the non-verticality of the most probable transition is not as pronounced in this case (absorption maximum at 8.09 eV after correcting for the difference in vertical electronic transition energy) is not at all surprising; indeed, since more extensive calculations [6, 7] indicate *more* rather than less valence character for the planar $\pi \rightarrow \pi^*$ singlet than has been found in the present CI(PCMO) treatment, it seems likely that the actual non-verticality of the observed $V \leftarrow N$ transition is even *greater* than that indicated by the results of Table 1.

An alternative method has also been used to calculate the electronic transition moment $R_{e'e''}$. If the curves in Fig. 5, which result from the use of the ground state SCF MO's are replaced by those obtained from a CI calculation in which the excited state SCF MO's are used for all species (including the ground state), the essential features of the vibrational structure of the $N - V_u$ transition remain unchanged; in particular, the most probable transition is again found to occur at an energy of 7.894 eV.

Use of the dipole velocity rather than the dipole length operator in the transition moment calculation leads to identical oscillator strengths according to Eqs. (8) and (9) respectively if the exact wavefunctions are employed. For the wavefunctions of the present treatment, however, oscillator strengths obtained using the dipole velocity operator are found to be considerably smaller than the corresponding dipole length values given in Table 1; thus while the total oscillator strength for the $N - V_u$ transition calculated using $R_{e'e''}$ is 0.289, in good agreement with the experimental value [11] of 0.34, the value obtained by employing $V_{e'e''}$ is only one-eighth as large[10]. Nevertheless despite the large disparity in the absolute magnitudes of the two types of oscillator strengths, it is still found that the prediction of the *relative* intensities of the various vibrational transitions in this system is essentially unaffected by the exchange of these two operators, especially in the identification of the most probable transition. In summary, while the uncertainty in the absolute intensity calculated for the $N - V_u$ system underscores the need for more accurate wavefunctions in this study, the observed stability in the relative transition probability results leaves little doubt that this calculated excitation should be identified with the experimental $V \leftarrow N$ absorption bands, at least in the region of the Franck-Condon maximum.

---

[9] The situation is entirely analogous to that found in formaldehyde [10], for which the limited CI(GSMO) predicts a planar geometry for the $n \rightarrow \pi^*$ excited states whereas the analogous CI(PCMO) treatment correctly finds the non-planar structure to be more favored.

D) Importance of the V_g State

The indirect role of the $^1B_1(V_g)$ state in determining the shape of the CH_2 twisting potential curve for the $2\,^1B_1(V_u)$ species has already been discussed. The more direct influence of the V_g state upon the electronic spectrum of ethylene may be considered from the results of Table 3. The O–O transition is calculated to

Table 3. Tabulation of transition energies ΔE and oscillator strengths f for the $1\,^1B_1(V_g)$ state of C_2H_4. All results are obtained relative to the lowest vibrational level of the (^1A_g) ground state ($v''_2 = v''_4 = 0$). The corresponding calculated electronic vertical transition energy is 7.517 eV

v'_4	f	ΔE (eV)	f	ΔE (eV)	f	ΔE (eV)
	$v'_2 = 0$		$v'_2 = 1$		$v'_2 = 2$	
0	0.00000	6.756	0.00000	6.886	0.00000	7.015
2	0.00009	6.786	0.00003	6.917	0.00001	7.046
4	0.00000	6.911	0.00000	7.042	0.00000	7.171
6	0.00000	7.140	0.00000	7.270	0.00000	7.400
8	0.00003	7.326	0.00001	7.456	0.00000	7.586
10	0.00011	7.393	0.00003	7.523	0.00001	7.653
12	0.00005	7.583	0.00002	7.713	0.00000	7.843
14	0.00116	7.728	0.00035	7.858	0.00007	7.988
16	0.00008	7.791	0.00002	7.922	0.00001	8.051
18	0.00026	7.997	0.00008	8.128	0.00002	8.257
20	0.00054	8.233	0.00016	8.364	0.00003	8.493
22	0.00132	8.469	0.00040	8.600	0.00008	8.729
24	0.00212	8.679	0.00064	8.809	0.00013	8.939
26	0.00098	8.886	0.00030	9.016	0.00006	9.145
28	0.00016	9.139	0.00005	9.270	0.00001	9.399
30	0.00000	9.425	0.00000	9.555	0.00000	9.684
$\sum_{v'_4}$	0.00690		0.00209		0.00043	–

$\sum_{v'_2} \sum_{v'_4} f = 0.00945$

---

[10] In previous work fairly large discrepancies between $f(r)$ and $f(V)$ values have been noted in connection with near Hartree-Fock calculations [15, 16] and also for some rather limited CI treatments [17].

occur at an energy of 6.756 eV, and this result coupled with the more qualitative information that the potential minimum for this state corresponds to the $\pi \rightarrow \pi^*$ singlet species for the antiplanar CH_2 conformation leads one to associate this state with the experimental O–O transition of the $V-N$ bands. Such an assignment presupposes that what has heretofore been assumed to be a *single* electronic transition corresponds in realty to two such species, and in fact the rather irregular spacing of the vibrational levels found for both the V_g and V_u states and the near equality of their respective twisting force constants (V_g: $4.05 \cdot 10^{-11}$ erg/rad^2 and V_u: $3.07 \cdot 10^{-11}$ erg/rad^2) indicate that under these circumstances a complete resolution might indeed be difficult. The experimental value for the O–O energy of the $V-N$ bands is obtained from a long extrapolation of the (supposed) CH_2 twisting frequency of the upper state in this system and has been a matter of no little controversy, with values of 4.9 eV and 5.8 eV both having been proposed [11, 18]; at present the higher of these values seems to be the favored result [19]. In any event the calculated value in Table 3 appears to be too high and it thus appears likely that more extended CI treatments will find a lowering in the energy of the $\pi \rightarrow \pi^*$ singlet in the antiplanar CH_2 arrangement relative to that of the planar ground state.

The calculated transition probabilities for the V_g state show one fairly sharp and relatively weak line at 7.728 eV for $v'_4 = 14$ and a second broader maximum of greater intensity between 8.469 and 8.679 eV with $v'_4 = 22$ and 24 respectively ($v'_2 = 0$ is again most probable for the CC stretching vibration)[11]. Since the vertical *electronic* excitation energy to the V_g state is 7.52 eV [5], the first of these maxima can be said to correspond roughly to a vertical transition. From the vibrational wavefunctions plotted in Fig. 7 it can qualitatively be seen that this species has by far the greatest overlap with the vibrationless ground state

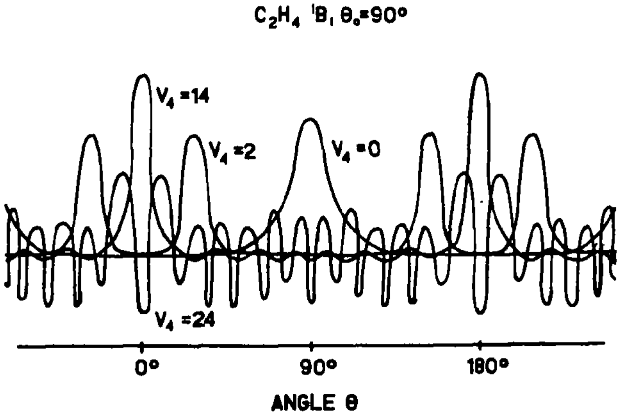

Fig. 7. Calculated important vibrational wavefunctions for the CH_2 twisting mode in the $^1B_1(V_g)$ excited state obtained from the corresponding potential curve in Fig. 4

---

[11] If a deeper potential minimum for the V_g state is assumed for better agreement with the experimental O–O transition energy while the $\theta = 0°$ region of this potential curve is left unaltered, only rather small changes in the location of the probability maxima occur, with a general shift towards larger wavelengths.

Table 4. Vibrational overlaps $S(v_4', v_4'')$ and electronic transition moments $R^x_{e'v'e''v''}$ between various $^1B_1(V_g)$ twisting vibrational wavefunctions and that of the lowest vibrational level ($v_4''=0$) of the ground state

v_4''	v_4'	$S(v_4', v_4'')$	$R^x_{e'v'e''v''}$	$R^x_{e'v'e''v''}/S(v_4', v_4'')$
0	0	0.0000	0.0000	0.496
	2	0.0555	0.0270	0.486
	4	0.0003	0.0001	0.456
	6	0.0024	0.0010	0.419
	8	0.0355	0.0143	0.403
	10	0.0747	0.0295	0.395
	12	0.0587	0.0201	0.342
	14	0.9226	0.0918	0.099
	16	0.0067	0.0243	3.627
	18	0.0704	0.0423	0.600
	20	0.1123	0.0604	0.537
	22	0.1796	0.0932	0.519
	24	0.2308	0.1168	0.506
	26	0.1620	0.0788	0.486
	28	0.0725	0.0314	0.433
	30	0.0242	0.0057	0.235

(Fig. 2) but at the same time it is obvious from Table 4 that the ratio between the electronic transition moment and vibrational overlap is far from constant for this system, reflecting of course the nominal (dipole) forbiddenness of the $N - V_g$ transitions. As a result the upper vibrational state with the greatest transition probability corresponds to $v_4' = 24$, by virtue of the relatively delocalized characteristics of its wavefunction, even though its vibrational overlap with the ground state is actually quite small.

The sharp transition calculated at 7.728 eV could be characterized as a Rydberg species resulting from a $\pi \to (3py + 3py)$ excitation, which in turn has been suggested by Merer and Mulliken [11] as being responsible for the 7.45 eV peak in the electron impact spectrum of ethylene found by Ross and Lassettre [20]. On the other hand another transition which seems equally likely to be associated with this experimental peak is the $\pi \to (3s - 3s)$ species [11], which is also dipole forbidden but quadrupole allowed, and which has been calculated [4] to have very nearly the same vertical electronic excitation energy.

E) The $\pi \to \pi^*$ Triplet State

The complicating factors inherent in the description of the CH_2 twisting energy surface of the $\pi \to \pi^*$ singlet state of ethylene appear to have no counterpart in the case of the corresponding triplet T state; the angular potential curve obtained in the present treatment [5] is essentially equivalent to that predicted for this species earlier by Mulliken [1, 2]. Transitions to this state from the ^1A_g ground state are of course spin forbidden. Nevertheless it was decided to carry out oscillator strength calculations on the basis of the calculated T state potential curves (for CC stretch as well as CH_2 twist) under the assumption of a constant electronic transition moment in order to facilitate a comparison with the V_u and V_g state results. It is found that the vertical transition ($v'_2 = 4$ and $v'_4 = 8$) calculated at 4.04 eV is indeed most probable, as expected from the Franck-Condon Principle. This transition energy is somewhat lower than the vertical *electronic* transition energy (4.17 eV) obtained in the standard way: the small discrepancy is caused in large part by the differences in zero point energies for the N and T states.

Recent experimental studies [21] locate the maximum intensity in the $N - T$ bands at 4.22 eV, in quite good agreement with the present calculations[12]. The calculated O–O transition energy [5] (2.72 eV), however, is considerably lower than the T_0 value (3.6 eV) generally quoted on the basis of extrapolations of the CH_2 twisting frequency v'_4 of the T state. On the other hand, this experimental value seems to be in conflict with the established value of 2.83 eV (65 kcal/mole) for the barrier to internal rotation in the N state, since according to Hund's rules at $\theta = 90°$ the T state should be slightly more stable than the N state. The present calculation do in fact place the T state in antiplanar ethylene some 0.05 eV *below* the N state and furthermore represent the N-state barrier very well (2.764 eV). Merer and Mulliken [11] have recently estimated the actual T_0 value for this transition to be even smaller ($\sim$2.50 eV) than that presently calculated.

4. Vibrational Structure of the Rydberg Bands in Ethylene

A) The $\pi \rightarrow (3s + 3s)$ *Rydberg Bands*

In order to further investigate the reliability of the foregoing analysis of the $\pi \rightarrow \pi^*$ transition of ethylene an analogous study has been carried out for the allowed Rydberg transitions in this spectrum. The lowest of these energy bands is the $N - R$ species with a T_0 value of 7.11 eV. It has been assigned by Wilkinson and Mulliken [22] as the $\pi \rightarrow 4a_g(3s + 3s)$ transition, and earlier calculations by the authors [4, 5] are in complete agreement with this interpretation. The CH_2 twisting potential curve ($R = 1.35$ Å) for the upper state with associated calculated vibrational levels is shown in Fig. 8; the molecule is seen to be slightly non-planar in this state. Calculated equilibrium R_{CC} and θ values are 1.41 Å and 20° compared to the experimental data of 1.41 Å and 25° respectively. Although the calculated twisting barrier is comparatively small (0.0038 hartree) it still greatly overestimates the experimental value [23] of only 289 cm^{-1} or 0.0013 hartree; indeed the SCF treatment employed in these calculations finds a potential minimum for the planar geometry, i.e. no barrier *at all*.

The R state correlates with the degenerate ^1E species for the D_{2d} arrangement of CH_2 groups and as a consequence the twisting potential curve does not show a maximum with a horizontal tangent at odd multiples of $\theta = 90°$ but rather intersects at these points with the potential curve of the other component of the ^1E state. Merer and Schoonveld [23] have pointed out that this potential curve, with a period of 2π instead of π (as in the cases discussed above) requires in

---

[12] This experimental value is somewhat lower than the 4.4–4.6 eV range for this absorption maximum given previously [11].

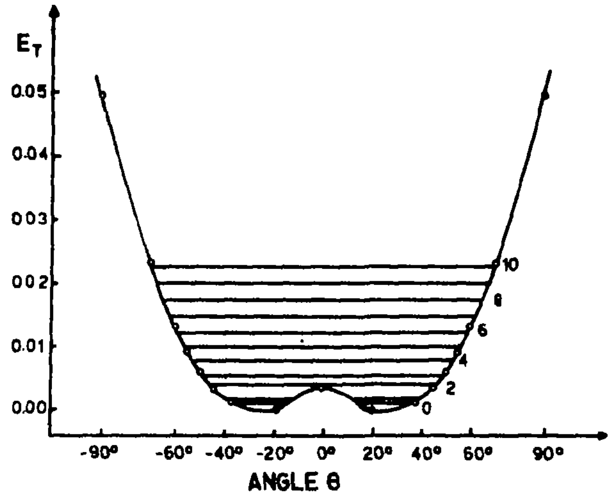

Fig. 8. CH_2 twisting potential curve for the $\pi \rightarrow (3s + 3s)$ or R state of ethylene obtained from the CI-1 treatment ($R_{CC} = 1.35$ Å). The lowest calculated vibrational levels are also indicated

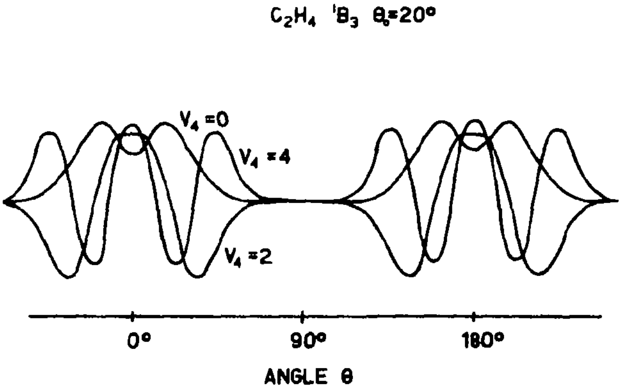

Fig. 9. Calculated important vibrational wavefunctions for the CH_2 twisting mode in the R state of ethylene obtained from the corresponding potential curve in Fig. 8

principle a more sophisticated treatment for obtaining the vibrational structure than has been outlined in Sect. 2. In practice, however, the more complicated treatment seems to have very little effect on the location of the *low-lying* twisting energy levels [23] and thus the results shown in Fig. 8 have been obtained in the same manner as the vibrational levels discussed previously (i.e. the potential is assumed to be periodic in π). The lowest energy vibrational wavefunctions of even quantum number obtained from this treatment are plotted in Fig. 9, from which it can be seen that a number of these species have appreciable overlap with the $v_4'' = 0$ ground state function (see Fig. 2).

The variation of electronic transition moment for the $R-N$ system with CH_2 twist is plotted in Fig. 10; there are two non-zero components for all angles

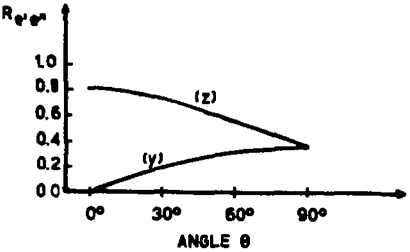

Fig. 10. Variation of the y- and z-components of the electronic transition moment $R_{e'e''}$ between the ground state of ethylene and the R state [obtained in the CI(GSMO) treatment] as a function of the CH_2 twisting angle θ

Tabelle 5. Tabulation of transition energies ΔE and oscillator strengths f for the $1\,^1B_3(R)$ state of C_2H_4. All results are obtained relative to the lowest vibrational level of the (^1A_g) ground state ($v_2'' = v_4'' = 0$). The corresponding calculated electronic vertical transition energy is 6.939 eV

v_4'	f	ΔE (eV)	f	ΔE (eV)	f	ΔE (eV)
	$v_2' = 0$		$v_2' = 1$		$v_2' = 2$	
0	0.0192	6.645	0.0138	6.781	0.0060	6.916
2	0.0196	6.719	0.0141	6.856	0.0062	6.991
4	0.0091	6.819	0.0065	6.956	0.0029	7.091
6	0.0026	6.941	0.0019	7.077	0.0008	7.212
8	0.0008	7.078	0.0005	7.214	0.0002	7.350
10	0.0002	7.225	0.0002	7.362	0.0001	7.497
12	0.0001	7.381	0.0001	7.517	0.0000	7.652
14	0.0000	7.545	0.0000	7.681	0.0000	7.816
16	0.0000	7.713	0.0000	7.850	0.0000	7.985
$\sum_{v_4'}$	0.0516	—	0.0371	—	0.0162	—
$\sum_{v_2'}\sum_{v_4'} f = 0.114$						

except $\theta = 0°$. The oscillator strengths for the various vibrational transitions present in this system (that is, those which involve either the CH_2 twisting or the CC stretch coordinates) calculated according to Eq. (8) on the basis of $R_{e'e''}$ data of Fig. 10 are listed in Table 5. Experimentally this transition appears as a progression of doublets [11, 24] in the stretching frequency v_2', with this doubling of levels believed to be caused by the nearly equal strengths of transitions to the first two even twisting vibrational species of the upper state. This behavior is mirrored in the calculated results, with transitions to $v_4' = 2$ being only slightly more probable than to the $v_4' = 0$ level. In addition it appears from these calculations that high overlap with the $v_2'' = 0$ ground state function is possible for the first two or three stretching levels of the R state, in contrast to what has been observed for the $\pi \rightarrow \pi^*$ states discussed previously; the doublet corresponding to the lowest v_2' level, however, is calculated to be the most intense, in agreement with what is observed experimentally [1, 22, 23].

The calculated T_0 value is only 6.645 eV, smaller by nearly 0.5 eV than the experimental result. Most of this discrepancy appears to come from the calculation of the vertical electronic energy difference, as evidenced by the fact that this quantity *increases* from 6.94 eV in the CI-1 treatment [5] (used for the present analysis) to 7.11 eV in the more extended CI-2 calculation also carried out by the authors. The fact that the potential curve in Fig. 8 overestimates the rotational barrier is undoubtedly also responsible for some (but certainly not all) of the remaining discrepancy (0.30 eV) between calculated and experimental T_0 values; the shallowness of the double minimum indicates that no more than 0.05 to 0.10 eV of this difference can be attributed to this effect. The total oscillator strength obtained from this transition (0.114) is also somewhat at odds with the experimentally observed value of approximately 0.03, but again uncertainties of this magnitude in absolute intensities are not unexpected. In summary, the assignment of this $N-R$ transition as being $\pi \rightarrow (3s+3s)$ is unambiguously supported by the present calculations.

B) The $\pi \rightarrow 3d\sigma(3pz+3pz)$ Rydberg Bands

The next allowed Rydberg transition found in the present calculations involves the $5a_u$ MO as the upper orbital. It has been shown earlier [4] that this MO is basically a $3d\sigma$ semi-united atom species, despite the fact that it is constructed in the present basis almost exclusively from the in-phase combination of $3pz$ AO's on the carbons. The CC stretching and CH_2 twisting potential curves obtained for this excited state are almost wholly similar to those discussed for the $\pi \rightarrow (3s+3s)$ R state (see Fig. 8) and the corresponding vibrational oscillator strength calculations (Tables 5–6) also have a strong resemblance to one another, complete with the pattern of doublets caused by corresponding transitions to $v_4' = 0$ and $v_4' = 2$ respectively.

There are two transitions found experimentally (T_0 values of 8.257 eV and 8.618 eV) in the appropriate region of the ethylene spectrum, characterized by

Table 6. Tabulation of the transition energies ΔE and oscillator strengths for the $2\,^1B_3$ state of C_2H_4. All results are obtained relative to the lowest vibrational level of the (^1A_g) ground state ($v_2'' = v_4'' = 0$). The corresponding calculated electronic vertical transition energy is 8.437 eV

v_4'	f	ΔE (eV)	f	ΔE (eV)	f	ΔE (eV)
	$v_2' = 0$		$v_2' = 1$		$v_2' = 2$	
0	0.0054	8.153	0.0038	8.287	0.0018	8.418
2	0.0054	8.223	0.0038	8.357	0.0018	8.488
4	0.0022	8.324	0.0015	8.458	0.0007	8.590
6	0.0006	8.446	0.0004	8.580	0.0002	8.712
8	0.0002	8.584	0.0001	8.718	0.0001	8.849
10	0.0001	8.732	0.0000	8.865	0.0000	8.997
12	0.0000	8.889	0.0000	9.022	0.0000	9.154
14	0.0000	9.054	0.0000	9.188	0.0000	9.320
16	0.0000	9.224	0.0000	9.358	0.0000	9.490
$\sum_{v_4'}$	0.0139		0.0096	-	0.0046	—
$\sum_{v_2}\sum_{v_4'} f = 0.031$						

Wilkinson [24] as $N-R'$ and $N-R''$ respectively, which appear likely to be associated with this $\pi\rightarrow 3d\sigma$ excitation. Betts and McKoy [25] have reported model potential calculations which indicate the correct assignment should be $N-R'$ and indeed the present calculated T_0 value of 8.153 eV is found to be in better agreement with the corresponding experimental value for this transition than with that of the $N-R''$ system. Nevertheless the great similarity between the $\pi\rightarrow(3pz+3pz)$ and $\pi\rightarrow(3s+3s)$ species found to exist in the present treatment still makes identification of $\pi\rightarrow(3pz+3pz)$ with $N-R''$ a definite possibility[13]. The total oscillator strength calculated for this transition is 0.031, some three or four times smaller than that calculated for the lower-energy $N-R$ band system.

C) Other Rydberg Transitions for Ethylene

The AO basis set employed in the present calculations [4, 5] includes 3*s* and 3*p* but no 3*d* or more diffuse functions associated with higher principal quantum numbers. The observed transitions at 8.92 eV and 9.05 eV, which are assigned as $\pi\rightarrow(4s+4s)$ or $N-4R$ and $\pi\rightarrow(4px-4px)$ or $N-R'''$ respectively, are thus not expected to have any counterparts in the present theoretical treatment. The same conclusion must be made relative to the study of all other higher energy Rydberg species thus far identified beyond 9.05 eV.

Basis set deficiency also appears to be responsible for the inability of the present calculations to find a second allowed Rydberg transition (other than $\pi\rightarrow 3d\sigma$) in the neighborhood of 8.5 eV; in this case the main difficulty seems to be the failure to employ semi-united atom $3d\sigma$ functions. The aforementioned model potential calculations [25] suggest an assignment of the $N-3R''$ bands as $\pi\rightarrow 3d_{x^2-y^2}$, for example, and also indicate that another possible Rydberg species ($N-3R''''$) may correspond to $\pi\rightarrow 3d_{xy}$ transitions of only slightly higher energy. An earlier assignment [5] for the $N-R'$ system, namely as a (diffuse) *vertical* $\pi\rightarrow\pi^*$ transition, now seems ruled out on the basis of the present oscillator strength calculations, discussed in Sect. 3 C. Additional SCF-CI calculations to investigate the $\pi\rightarrow 3d\delta$ transitions are planned in future work.

5. Conclusion

The main conclusion resulting from the present theoretical study of the ethylene electronic spectrum is that the energy of maximum absorption $\Delta E_{\max}$, indicated by explicit calculation of the oscillator strengths for the various vibrational transitions within a given electronic system, may well differ significantly from the vertical *electronic* energy difference ΔE_v usually equated with this quantity. These points are best illustrated by a comparison of specific values for ΔE_v and $\Delta E_{\max}$ for various electronic transitions in ethylene (Table 7); for simplicity differences between these two quantities are hereafter referred to as

---

[13] The vertical electronic energy to the $\pi\rightarrow(3pz+3pz)$ state increases by 0.17 eV from the CI-1 to the CI-2 treatment (the same change observed for the $\pi\rightarrow(3s+3s)$ excitation) and the depth of the associated double minimum in the upper state potential curve also appears to be overestimated by slightly less than 0.10 eV. Hence it might be concluded that the calculations underestimate the respective T_0 values for these two transitions by roughly equal amounts.

Table 7. Comparison of experimental and calculated transition energies to various excited states of C_2H_4. Vertical electronic transition energies are denoted by ΔE_v whereas excitation energies for the most probable transitions between the vibrational levels of ground and excited states are denoted by ΔE_{max}

Upper state (D_2 notation)	ΔE_v (eV)			Vibrational correction (eV)		ΔE_{max} (eV)		
	CI-1[a]	CI-2[a]	est. exact	CI-1[a]	est. exact	CI-1[a]	CI-2[a,b]	exptl.
$^3B_1$	4.17	4.19	4.35	−0.13	−0.13	4.04	4.06	4.22(*T*)[c]
$^1B_3$	6.94	7.10	7.31	−0.29	−0.20	6.65	6.81	7.11(*R*)[d]
$2\,^1B_1$	8.25	8.27	8.06	−0.36	−0.40	7.89	7.91	7.66(*V*)[e]
$2\,^1B_3$	8.44	8.61	8.46[f] 8.82[f]	−0.29	−0.20	8.16	8.32	8.26(*R'*)[d,f] 8.62(*R''*)[d,f]

[a] CI-1 and CI-2 refer to two different CI treatments, CI-2 being the more extensive, solving secular equations of the order of 500; details are given in Ref. [5].

[b] Entries in this column are obtained by adding the CI-1 vibrational corrections to the CI-2 values for ΔE_v.

[c] Ref. [21]

[d] The experimental number refers to T_0, Ref. [24].

[e] Ref [22].

[f] Two results are given because of the uncertainty in assignment in this case (see Sect. 4 B).

vibrational corrections, since the origin of the discrepancies is so intimately associated with the effects of vibrational motion in the initial and final states of a given transition.

In the case of the $V - N$ absorption bands the results of Table 7 indicate that the upper state involved (at least at the Franck-Condon maximum) is indeed the $\pi \rightarrow \pi^*$ singlet (V_u) suggested by Mulliken and others, but that transitions to this electronic state are distinctly *non-vertical* in nature, with a calculated vibrational correction of −0.36 eV. The calculations indicate that the main reason for this non-verticality is the existence of the lower energy V_g state and the resultant avoided crossing between the twisting potential curve of this species and that of the upper V_u state. On this basis it has been concluded that the observed system in reality corresponds to *two* distinct electronic transitions, heretofore unresolved as a consequence of the great similarity between their respective vibrational manifolds.

The remaining discrepancy between the calculated ΔE_{max} and the corresponding experimental value of 7.66 eV seems likely to be removed with improvements in the theoretical treatment since very elaborate calculations [6, 7] of more recent origin have found somewhat lower ΔE_v values and greater valence character for the $\pi \rightarrow \pi^*$ singlet of the planar molecule; the latter finding should lead to increased curvature for the CH_2 twisting potential curve of the upper state, thereby producing an even greater vibrational correction for this transition (see Table 7). At the same time it seems certain that the singlet $\pi \rightarrow \pi^*$ wavefunction (at least for planar ethylene) is still considerably more diffuse than that of the corresponding triplet. The most extensive calculation to date [7] yields a value for $\langle \pi^* | x^2 | \pi^* \rangle$ in the order of 27 bohr^2 (where π^* is the principal natural orbital)[14]; the corresponding value in the present CI-1 treatment is 32.0 bohr^2, while analogous results for the T state function fall consistently in the neighborhood of 10 bohr^2.

Transitions to the $T(^3B_1)$ state are found to be essentially vertical in character according to the present calculations, although the resultant vibrational correction is not negligible (Table 7). The calculated $\Delta E_{\max}$ is somewhat lower than the experimental value [21], thereby suggesting that the exact ΔE_e result is approximately 4.35 eV. The calculations of Ryan and Whitten [6] do in fact yield a larger ΔE_e value (4.98 eV) than that obtained in the present work and elsewhere [26] but this value appears quite high in view of the most recent experimental information and also because it leads to a difference of ΔE_e values between the $\pi \rightarrow \pi^*$ singlet and triplet respectively of only 3.04 eV, compared to the 3.9 eV obtained for this quantity by Bender *et al.* [7] and the value of 4.08 eV of the present calculations.

A fairly large vibrational correction is also indicated for the allowed Rydberg transitions $\pi \rightarrow (3s+3s)$ and $\pi \rightarrow (3pz+3pz)$ respectively (Table 7). Even though this result is propably overestimated by about 0.1 eV in the present treatment (because the depths of the double wells in the associated CH_2 twisting potential curves appear to be overestimated by this margin) it still remains a sizeable effect. In retrospect the reason that earlier results [4, 5] based solely on ΔE_e values appear to find far better agreement with the experimental transition energies for the Rydberg species than for the $\pi \rightarrow \pi^*$ singlet-singlet excitation turns out to be a cancellation of errors in the fortuitous case, coupled with a reinforcement in the other.

In summary the treatment of the vibrational characteristics of the electronic transitions of ethylene illustrates the need for employing a more appropriate value than the vertical *electronic* energy difference ΔE_e in order to predict the location of a given maximum in absorption ($\Delta E_{\max}$). Further theoretical studies of electronic spectra should therefore not only continue to pursue more accurate treatments for the calculation of ΔE_e values but should also include the calculation of oscillator strengths for associated vibrational transitions in order to obtain a more accurate estimate of the vibrational corrections which must be applied. In addition in the case of the $V-N$ bands of ethylene such investigations should not be restricted to the $\pi \rightarrow \pi^*$ singlet (V_u) state but rather should include the study of the $\pi \rightarrow (3py+3py)$ V_g species since there seems little question at this point that it is the interaction between these two states which ultimately holds the key to the understanding of this important absorption system.

Acknowledgements. The authors wish to thank Dr. H. L. Hsu for her assistance in carrying out the calculations reported in this paper. They are indebted to Profs. R. S. Mulliken, A. J. Merer and I Shavitt for several valuable discussions. They are also grateful to Profs. V. McKoy, J. H. Moore, H. F. Schaefer III and J. L. Whitten for communicating their results prior to publication. The services and computer time made available by the University of Nebraska and University of Mainz Computer Centers have been essential to this study. The financial support of the Deutsche Forschungsgemeinschaft is gratefully acknowledged.

---

[14] Ryan *et al.* [6] have obtained a $\pi \rightarrow \pi^*$ singlet wavefunction with more valence character, but the corresponding total energy is approximately 0.10 hartree higher than in the calculation of Bender *et al.* [7]. In addition the degree of diffuse character in their representation of this state appears to have been arbitrarily minimized by the omission of basis functions with exponents smaller than 0.06, whereas a value of 0.02 has been found to be *optimum* in the present calculations [4].

References

1. Mulliken, R.S.: Physic. Rev. **41**, 751 (1932).
2. Mulliken, R.S.: Physic Rev. **43**, 297 (1933).
3. Herzberg, G.: Molecular spectra and structure, Vol. I. Spectra of diatomic molecules, p. 200. Princeton, New Jersey: Van Nostrand 1966.
4. Buenker, R.J., Peyerimhoff, S.D., Kammer, W.E.: J. chem. Physics **55**, 814 (1971).
5. Buenker, R.J., Peyerimhoff, S.D., Hsu, H.L.: Chem. Physics Letters **11**, 65 (1971).
6. Ryan, J.A., Whitten, J.L.: A valence state description of the ethylene *V* state by configuration interaction theory; preprint communicated to the authors.
7. Bender, C.F., Dunning, T.H., Jr., Schaefer, H.F., III, Goddard, W.A., III: Multiconfiguration wavefunctions for the lowest ($\pi\pi^*$) excited states of ethylene; preprint communicated to the authors.
8. Rose, J., Tai-ichi Shibuya, McKoy, V.: Application of the equations-of-motion method to the excited states of N_2, CO and C_2H_4; preprint communicated to the authors.
9. Herzberg, G.: Molecular spectra and molecular structure II, Infrared and raman spectra of polyatomic molecules, p. 151 Princeton: D. Van Nostrand Company, Inc. 1966.
10. Buenker, R.J., Peyerimhoff, S.D.: J. chem. Physics **53**, 1368 (1970).
11. Merer, A.J., Mulliken, R.S.: Chem. Reviews **69**, 639 (1969).
12. Fletcher, W.H., Thompson, W.T.: J. molecular Spectroscopy **25**, 240 (1968).
13. Pulay, P., Meyer, W.: *Ab initio* calculation of the force field of ethylene, in Arbeitsbericht des Instituts für Theoretische Chemie der Universität Stuttgart, No. 18, p. 95.
14. Ref. [9], p. 107.
15. Huo, W.M.: J. chem. Physics **49**, 1482 (1968)
16. Popkie, H.E., Henneker, W.H.: J. chem. Physics **55**, 617 (1971); see also Schaefer, H.F., III: The electronic structure of atoms and molecules, p. 171. Addison-Wesley Publishing Company, Inc. 1972, for a discussion of this work.
17. Marchetti, M.A., La Paglia, S.R.: J. chem. Physics **55**, 1655 (1971).
18. Reid, C.: J. chem. Physics **18**, 1299 (1950).
19. McDiarmid, R.: J. chem. Physics **55**, 4669 (1971).
20. Ross, K.J., Lassettre, E.N.: J. chem. Physics **44**, 4633 (1966).
21. Moore, J.H., Jr.: An investigation of the low-energy singlet-triplet and singlet-singlet transitions in ethylene derivatives by ion-impact. Preprint communicated to the authors.
22. Wilkinson, P.G., Mulliken, R.S.: J. chem. Physics **23**, 1895 (1955).
23. Merer, A.J., Schoonveld, L.: Canad. J. Physics **47**, 1731 (1969).
24. Wilkinson, P.G.: Canad. J. Physics **34**, 643 (1956).
25. Betts, T., McKoy, V.: J. chem. Physics **54**, 113 (1971).
26. Dunning, T.H., Hunt, W.J., Goddard, W.A.: Chem. Physics Letters **4**, 147 (1969).

Prof. R. J. Buenker
Department of Chemistry
University of Nebraska
Lincoln, Nebraska 68508
USA

Prof. Dr. S. D. Peyerimhoff
Lehrstuhl für Theoretische Chemie
Universität Bonn
D-5300 Bonn
Federal Republic of Germany

Theoret. chim. Acta (Berl.) 27, 265--272 (1972)
© by Springer-Verlag 1972

Relatio

SCF LCAO MO Studies on the Hydration of Ions: The System $F^- \cdot 2H_2O$

Wolfgang P. Kraemer and Geerd H. F. Diercksen
Max-Planck-Institut für Physik und Astrophysik, 8000 München 40, Germany

Received July 4, 1972

The energy surface of the dihydrated fluoride anion $(F \cdot 2H_2O)^-$ is studied for a number of different geometry points near the equilibrium structure within the SCF LCAO MO framework, using an extended gaussian basis set to approximate the molecular wavefunctions. For the first and second hydration step of the fluoride anion the corresponding hydration energies are calculated to be $B_1^{SCF} = 24.1$ kcal/mole and $B_2^{SCF} = 20.8$ kcal/mole (experimental measurements: 23.3 kcal/mole and 16.6 kcal/mole, respectively). The hydration energies and equilibrium bond distances obtained for the dihydrated fluoride anion $(F \cdot 2H_2O)$ are compared with those found for the monohydrate (FHOH) and with corresponding results of the dihydrated lithium cation $(Li \cdot 2H_2O)^+$. The system $(F \cdot 2H_2O)$ is taken as a very simple model to discuss some basic features of the hydration process of small ions and to study the influence of a negative ion on an adjacent hydrogen bond.

In a series of previous investigations the monohydrates of the cations H^+, Li^+, Na^+ [1] and of the anions F^- [2], OH^- [3] as well as the dihydrated lithium cation [4] have been studied, expanding the molecular wavefunction of these systems into an extended basis set of gaussian functions to achieve a good approximation to the SCF-wavefunctions and a high accuracy in the total SCF-energies. It has been possible in these studies to obtain some detailed information about the minimum energy geometries and the single hydration energies. In the dihydrated system $(Li \cdot 2H_2O)^+$ the mutual interactions between all possible subparts have been studied: the interactions between the atomic Li^+-ion and two single water molecules or a dimeric water system, as well as between the monohydrated lithium cation and a single water molecule. To complete these investigations some results of SCF-calculations on the dihydrated fluoride anion $(F \cdot 2H_2O)^-$ will be presented here. The only theoretical work on this system published so far has been a quantum chemical CNDO calculation (CNDO = complete neglect of differential overlap) studying the mono-, di-, and tetrahydrates of a series of ions, including the (F^-)-anion [5].

The calculation of the wavefunctions and energies on the basis of Roothaan's SCF LCAO MO method has been carried out on an IBM 360/91 computer, using the program system IBMOL/VERSION IV [6], modified by one of the authors (G. D.) to avoid the explicit integral transformation [7], and using a test release of the program system Munich [8]. The molecular orbitals are expanded into a set of gaussian functions: $\eta = x^l y^m z^n \exp(-r^2)$ which are contracted to reduce the number of linear parameters. The basis sets used in these calculations have been described previously [2, 9] and consist of (11.7.1)-functions centred at the oxygen and fluorine nuclei, respectively, and of (6.1)-functions centred at the hydrogens (for a definition of the basis set notation used here, see [10]). In the actual SCF-calculations two different contractions of these basis functions are used: a contraction to [5.3.1]-functions at the oxygen and the fluorine centres and to [3.1]-functions at the hydrogen centres as well as a contraction to [5.4.1]-functions at the oxygens and the fluorine together with the same contracted set at the hydrogen centres as described above. An initial search for the equilibrium geometrical structure of the system $F^- \cdot 2H_2O$ is performed using the first, more contracted basis set, according to the experience that equilibrium geometrical parameters are somewhat less sensitive to small changes in the basis set than various other expectation values. Around the minimum obtained in this preliminary search some additional calculations using the slightly less contracted [5.4.1]-basis set are than performed, leading to the SCF-energies and hydration energy values discussed in this paper. For the systems F^-, H_2O, $(H_2O)_2$, and $(FHOH)^-$, previously studied, the calculated SCF-energies, using the contractions [5.4.1] at the oxygen and the fluorine centres, are found to be $E^{SCF}(F^-) = -99.45059$ a.u. [2]; $E^{SCF}(H_2O) = -76.05199$ a.u. [9] (for the experimental geometry); $E^{SCF}((H_2O)_2) = -152.11167$ a.u. [9]; $E^{SCF}(FHOH^-) = -175.54093$ a.u. [2]. The last two energy values are obtained for the theoretically calculated geometries which are close to the experimentally determined structures.

The accuracy of the computed hydration energies and bond distances can be proved by a comparison with mass spectroscopic measurements of the corresponding gas-phase hydration reactions, recently published by Kebarle and coworkers [11]. For all the hydrated systems studied in this series of investigations [1–4] the deviation of the calculated first hydration energies from the corresponding experimental data is only about 5%, while for the second hydration energies larger deviations are obtained (about 25%). The calculated equilibrium bond distances are in good agreement with experiments within an error of about 2–4%.

The molecular structures of the system $(F \cdot 2H_2O)$ investigated here may be described as follows:

A fluorine anion and two water molecules are able to form essentially three different geometrical configurations under the condition that the (F^-)-ion is bonded to the oxygen centres in the water molecules by a hydrogen bond. This hydrogen bond is in the following always assumed to be a linear one, in agreement with our previous studies on the monohydrate $(FHOH)^-$ [2]. In the first structure (denoted as (*S*) in Table 1), which has a highly symmetrical form, the two water molecules are attached to the fluoride anion F^- each by a linear hydrogen bond in such a way that the five centres O...H...F...H...O are positioned on a straight line and that the fluorine nucleus acts as a centre of inversion for the whole molecular system (F^- in position P in Fig. 1). In both of the two remaining structures (denoted as (*A*) and (*D*) in Table 1) the fluoride anion is attached to the dimeric water system as a whole, the geometrical configuration of which is taken from a previous study on this system [9]. In the structure (*A*), the (F^-)-anion is bonded by one of the hydrogens of the proton acceptor part of the water dimer (F^- in position P_1 in Fig. 2), while in the last possible structure (*D*) the (F^-)-anion is bonded by the outer hydrogen of the proton donor part of $(H_2O)_2$ (F^- in position P_2 in Fig. 2). For all the three

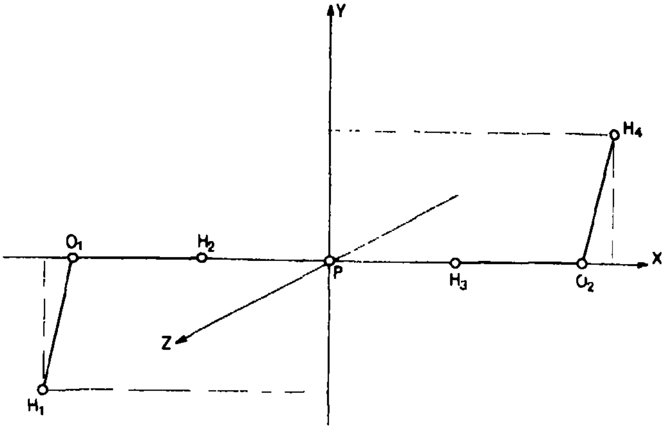

Fig. 1 Coordinate system for $F^- \cdot 2H_2O$ in the geometrical structure (*S*) (the fluoride anion is in position *P*)

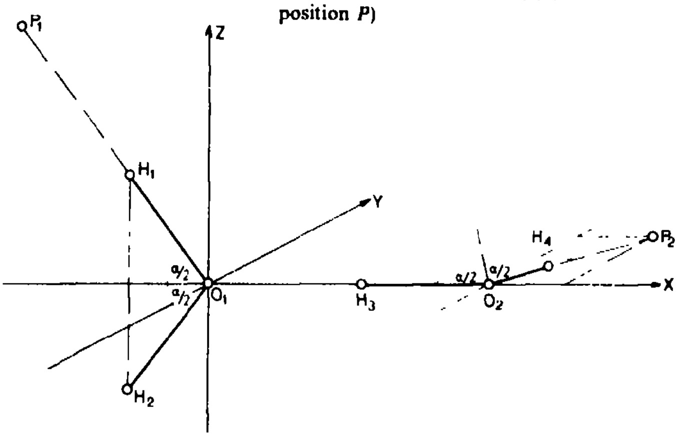

Fig. 2. Coordinate system for $F^- \cdot 2H_2O$ in the geometrical structures (*A*) and (*D*) (the fluoride anion is in position P_1 for structure (*A*) and in position P_2 for structure (*D*))

structures (*S*), (*A*), and (*D*) described here, the internuclear distances *d*(FO) between the fluorine and the corresponding oxygen centres have been varied around their equilibrium values. In addition, for the structures (*A*) and (*D*) a further variation of the oxygen/oxygen internuclear distance *d*(OO) has been performed, keeping the distance *d*(FO) fixed at its previously determined equilibrium value. During all the calculations referred here the water molecules were taken in their experimentally determined geometry ($d(OH) = 1.80887$ a.u., $\sphericalangle(HOH) = 104.52°$).

The computational SCF-results for the two different contractions, used in this investigation, are summarized in Table 1 and are displayed in Fig. 3. Some of the most interesting results, like the hydration energies and the bond distances, based on the less contracted, second basis set mentioned above, are collected in Table 2.

The symmetrical structure (*S*), which may be characterized by the formula $(HOHFHOH)^-$, is found in these studies to represent the most stable geometrical configuration of the dihydrated system $(F \cdot 2H_2O)^-$. From the variation of the

Table 1. Total SCF-energies of the system $(F \cdot 2H_2O)^-$ in different geometrical configuratio (structure (*S*): $(HOHFHOH)^-$; structure (*A*): $(HOHO(H)HF)^-$; structure (*D*): $(FHOHOH_2)^-$)

		d(FO) [a.u.]	*d*(OO) [a.u.]	*d*(OH) [a.u.]	∢ HOH	∢ $(P_1O_1O_2)$	E^{SCF} [a.u.]
(*S*)	1	4.00	8.00	1.80887	104.52		−251.5667
	2	4.50	9.00				−251.6154
	3	4.725	9.45				−251.6198
	4	4.82	9.64				−251.6201
	5	5.00	10.00				−251.6190
	6[a]	4.725	9.45	1.80887	104.52		−251.6256
	7[a]	4.82	9.64				−251.62614
	8[a]	5.00	10.00				−251.62537
(*A*)	1	4.00	5.66925	1.80887	104.52	127.74	−251.58738
	2	4.25					−251.60007
	3	4.50					−251.60437
	4	4.83					−251.60373
	5	5.00					−251.60202
	6	5.50					−251.59508
	7	4.50	5.06925	1.80887	104.52	127.74	−251.60527
	8		5.20000				−251.60557
	9		5.36925				−251.60546
	10[a]	4.62	5.12	1.80887	104.52	127.74	−251.61262
	11[a]		5.26				−251.61286
	12[a]		5.40				−251.61274
(*D*)	1	4.00	5.20	1.80887	104.52	104.52	−251.54902
	2	4.50					−251.57209
	3	5.00					−251.57438
	4	6.00					−251.56670
	5	8.00					−251.55579
	6	5.00	5.50	1.80887	104.52	104.52	−251.57715
	7		5.80				−251.57843
	8		6.40				−251.57908
	9		10.00				−251.57960

[a] These calculations have been performed using the [5.4.1] contraction at the oxygen and the fluorine centres.

hydrogen bond lengths between the fluorine centre and the two oxygen nuclei in the attached water molecules, an equilibrium FO-distance of *d*(FO) = 4.82 a.u. was obtained for both of the two different contractions (Fig. 3). From the minimum SCF-energy value of the less contracted basis set the binding energy, corresponding to a dissociation into: $(FHOH)^- + H_2O$ is calculated to be $B_2^{SCF} = 20.8$ kcal/mole. This energy is identified as the hypothetical second hydration energy of the fluoride anion. In previous studies on the monohydrated system $(FHOH)^-$ the first hydration energy was determined to be $B_1^{SCF} = 24.07$ kcal/mole [2]. The total binding energy of the system $(HOHFHOH)^-$ with respect to a complete decomposition into: $F^- + 2H_2O$, is obtained to be 44.9 kcal/mole, leading to an average hydration energy per water molecule in the dihydrated system of 22.45 kcal/mole. The corresponding experimental values, obtained from mass spectroscopy measurements of the gas-phase hydration reactions, were recently published by Kebarle and co-workers [11]: $-H_1 = 23.3$ kcal-Mole; $-H_2 = 16.6$ kcal/mole (from these two values an ex-

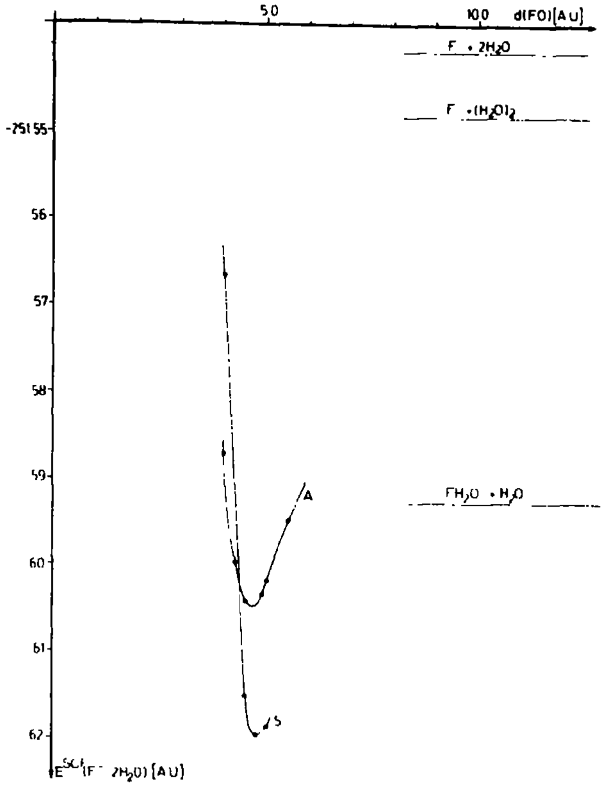

Fig. 3. Potential energy curves for the d(FO)-variation in the two different geometrical structures (*S*) and (*A*) of the system $F^- \cdot 2H_2O$

perimental average hydration energy for the dihydrate may be derived: 19.95 kcal/mole).

A comparison of these results for the dihydrated fluoride anion with previous studies on the hydration of the lithium cation [4] shows a general similarity of the hydration process for both types of ions. In both cases the bond lengths between the ionic centres and the oxygen nuclei of the water molecules are nearly unchanged if a second water molecule is added to the monohydrated system. The very small enlargements of the bond lengths of 0.05 a.u. for the two dihydrated systems, $(HOHFHOH)^-$ and $(H_2OLiOH_2)^+$, are beyond the accuracy of our calculations. As might be expected from chemical experience, there is further in both cases a remarkable change in bond strength comparing the mono- and the dihydrates. The differences between the single hydration energies of the monohydrates and the average hydration energies of the dihydrates are $\Delta B = 1.62$ kcal/mole for $(HOHFHOH)^-$ and $\Delta B = 2.05$ kcal/mole for $(H_2OLiOH_2)^+$ (in both cases the experimental measurements give a stronger decrease in the hydration energies: $\Delta B(HOHFHOH)^- = 3.35$ kcal/mole and $\Delta B(H_2OLiOH_2)^+ = 4.1$ kcal/mole).

Apart from these general similarities the absolute values of the hydration energies of the lithium – and the fluorine-ion are quite different. As would be

Table 2 Calculated binding energies and geometrical parameters for different structures of the systems $(F^- nH_2O)$, $n = 1, 2$[a]

System	B^{SCF} [kcal·mole]	Dissociation products	d(FO) [a.u.]	d(FH) [a.u.]	d(OO) [a.u.]	d(OH) [a.u.]	∢(HOH)
$(FHOH)^-$	24.1	$F^- + H_2O$	4.77	2.96	--	1.80887 (not varied)	104.52° (not varied)
$(HOHFHOH)^-$	44.9 40.1 20.8	$F^- + 2H_2O$ $F^- + (H_2O)_2$ $(FHOH)^- + H_2O$	4.82	3.01	9.66	1.80887 (not varied)	104.52° (not varied)
$(HOHO(H)HF)^-$	36.6 31.8 12.5	$F^- + 2H_2O$ $F^- + (H_2O)_2$ $(FHOH)^- + H_2O$	4.62	2.83	5.26	1.80887 (not varied)	104.52° (not varied)
$(FHOHOH_2)^-$	22.9 18.2 0	$F^- + 2H_2O$ $F^- + (H_2O)_2$ $(FHOH)^- + H_2O$	4.77	2.96	∞	1.80887 (not varied)	104.52° (not varied)

[a] All values, except those of the structure $(FHOHOH_2)^-$, are obtained from calculations using the [5.4.1] contraction at the oxygen and fluorine centres.

expected from the smaller size of the lithium cation its polarisation effect on the attached water molecules should be much stronger than that of any other ion discussed here, as it is the smallest known cation (except the proton). This explains the high bond energies calculated for the lithium hydrates [1, 4]. Our calculations show however that provided the ions are of comparable size, the sign of the ionic charge does not affect the hydration energies very much:

$$B^{SCF}(Na^+ \cdot H_2O) = 25.2\,\text{kcal/mole}\ [1],$$
$$B^{SCF}(F^- \cdot HOH) = 24.1\,\text{kcal/mole}\ [2],$$
$$B^{SCF}(HO^- \cdot HOH) = 24.3\,\text{kcal/mole}\ [3].$$

These results are in close agreement with experimental measurements performed by Kebarle and co-workers [11].

Considering the two unsymmetrical structures (*A*) and (*D*) of the system $(F \cdot 2H_2O)^-$, which appear to be less stable than the symmetrical one, the effect of a negative fluorine ion approaching the hydrogen bonded dimeric water system may be studied.

The potential curve, displayed in Fig. 3, indicates that the structure (*A*), characterized by the formula $(HOHO(H)HF)^-$, should be stable with respect to the three possible dissociations into: $(FHOH)^- + H_2O$, or into: $F^- + (H_2O)_2$, or into $F^- + 2H_2O$. Using the [5.3.1] contraction at the oxygen and the fluorine centres as basis set, the equilibrium bond length between the F^--ion and the oxygen nucleus of the water molecule acting as the proton acceptor part in the water dimer is calculated to be $d(FO) = 4.62$ a.u.; i.e. it is only very slightly different from the $d(FO)$-value found for the monohydrate (the change being about 2.7%). The effect of the fluoride anion on the length of the adjacent hydrogen bond between the two water molecules is more distinct: for the $d(FO)$-value given above a decrease of the oxygen/oxygen-bond length in the water dimer by approximately 8.3% (compared to the isolated dimer) is obtained. This remarkable change in the $d(OO)$-bond length due to the F^--ion was calculated with both of the two contracted basis sets. In accordance with these results the binding energy relative to the subsystems F^- and $2H_2O$ is larger than the sum of the binding energies of the subsystems FHOH and $(H_2O)_2$ by about 7.7 kcal/mole. This indicates a stabilisation of the hydrogen bond in the dimer perturbed by the F^--ion by about 7.7 kcal/mole compared to the isolated dimer. The value is estimated under the assumption that the (FHO)-hydrogen bond energy in the dihydrated fluorine anion $(HOHO(H)FH)^-$ is equal to the corresponding energy in the fluorine monohydrate $FHOH^-$, which is believed to be reasonable because of the nearly equal bond distances $d(FO)$ in both systems [4].

These results are in qualitative agreement with the stronger effects obtained for the dihydrated lithium cation, where the (Li^+)-ion is bonded to the proton donor part of the dimeric water molecule. In both cases the ions produce a charge shift in the region of the adjacent hydrogen bond in the dimeric water in such a way that the H-bond strength is increased compared to the isolated dimer [1]. The structure (*A*) of the dihydrated fluoride anion as well as the corresponding structure of the lithium dihydrate may therefore be considered as very simplified models to discuss the formation and the stabilisation of a second hydration shell for these ions in aqueous solutions. The stabilisation of the hydrogen bond between the two water molecules due to the (F^-)-ion was determined to be 7.7 kcal/mole. Similar values should be found for other ions of comparable size (like Na^+, OH^-). In our previous calculations on the corresponding model system in the case of the lithium cation, which may be characterized by the formula $(LiO(H)HOH_2)^+$, a stabilisation of the hydrogen bond between the two oxygen centres by about 11 kcal/mole was obtained [4]. While the hydration energies of the water molecules attached directly to the Li^+- or the F^--ion have been calculated to be quite different, there seems to be not such a strong difference in the influences of these two ions on an adjacent hydrogen bond, according to the fact that the polarisation effect of the lithium cation decreases rapidly with increasing distance from the ion. One has to expect that the absolute values of the stabilisation energies, which have been obtained for the very simplified models described above, become considerably smaller, if a complete first hydration shell around the ions is taken into account. Thus it might be concluded from these results, that in the case of the singly charged ions discussed in this series of investigations [1–4] a second hydration shell should be only weakly bonded and easily perturbed by other effects.

Considering finally the geometrical structure (*D*), in which the fluoride anion is attached to the proton donor part of the dimeric water system, and which may therefore be characterized by the formula $(FHOHOH_2)^-$, the computational results collected in Tables 1 and 2 (obtained with the [5.3.1]-contraction) indicate that this structure is unstable and leads to a dissociation into: $(FHOH) + H_2O$. The strong influence of the (F^-)-ion in the position P2 (Fig. 2) causes a stabilisation of the chemical bond between O2 and H3 (Fig. 2) and destroys the hydrogen bond between the two water molecules.

We would like to thank our technical staff for valuable help in carrying out these calculations.

References

1. Diercksen, G. H. F., Kraemer, W. P.: Theoret. chim. Acta (Berl.) **23**, 387 (1972).
2. Diercksen, G. H. F., Kraemer, W. P.: Chem. Physics Letters **5**, 570 (1970).
3. Kraemer, W. P., Diercksen, G. H. F.: Theoret. chim. Acta (Berl.) **23**, 398 (1972).
4. Kraemer, W. P., Diercksen, G. H. F.: Theoret. chim. Acta (Berl.) **23**, 393 (1972).
5. Lischka, H., Plesser, Th., Schuster, P.: Chem. Physics Letters **6**, 263 (1970).
6. Veillard, A.: IBMOL/VERSION IV Special IBM Technical Report, San Jose, California (1968).
7. Preuss, H., Diercksen, G.: Int. J. quant Chemistry **1**, 605 (1967).
8. Diercksen, G. H. F., Kraemer, W. P.: MUNICH, Molecular Program System Reference Manual, Special Technical Report, Max-Planck-Institut für Physik und Astrophysik (to be published).
9. Diercksen, G. H. F.: Chem. Physics Letters **4**, 373 (1969); Theoret. chim. Acta (Berl.) **21**, 335 (1971).
10. Moskowitz, J. W., Harrison, M. C.: J. chem. Physics **43**, 3550 (1965).
11. Dzidic, I., Kebarle, P.: J. physic. Chem. **74**, 1466 (1970).
    Arshadi, M., Yamdagni, R., Kebarle, P.: J. physic. Chem. **74**, 1475 (1970).
    Arshadi, M., Kebarle, P.: J. physic. Chem. **74**, 1483 (1970).

G. Diercksen
Max-Planck-Institut für Physik und Astrophysik
D-8000 München 40, Föhringer Ring 6
Federal Republic of Germany

Theoret. chim. Acta (Berl.) 27, 273—280 (1972)
© by Springer-Verlag 1972

Commentationes

Energy-Conformation Studies of Hydrogen Cyanide Tetramer: A Prebiotic Precursor

Gilda H. Loew

Department of Genetics, Stanford University Medical Center, Stanford, California, USA

Sherwood Chang

NASA Ames Research Center, Chemical Evolution Branch, Moffett Field, California, USA

Received February 23, 1972

Using the Iterative Extended Huckel Method (IEHT), we have made energy-conformation studies of the two isomers of hydrogen cyanide tetramer, a known purine precursor in prebiotic syntheses. Our results show that the *cis* isomer is more stable than the *trans* and that, for both, a totally planar conformation is most favorable, differing appreciably from the crystal structure determined by X-ray analysis. The ionization potential, dipole moment, π electron distribution and optical spectra for the tetramer have also been calculated. For all of these properties we find good agreement with experimental results Thus encouraged by the reliability of the description obtained, we plan to use these results for further studies of the chemical reactivity of the tetramer relevant to its postulated role in prebiotic syntheses.

Mit Hilfe der iterativen erweiterten Hückel Methode (IEHT) haben wir Energie-Konformations-Untersuchungen an den beiden Isomeren der HCN-Tetrameren, das als Purinvorläufer in vorbiotischen Synthesen bekannt ist, durchgeführt. Unsere Resultate zeigen, daß das *cis*-Isomere stabiler als das *trans*-Isomere und daß für beide die planere Konformation bevorzugt ist. Diese Ergebnisse weichen stark von der mit Hilfe der Röntgenstrukturanalyse bestimmten Kristallstruktur ab. Außerdem wurden Ionisationsenergie, Dipolmoment, π-Elektronenverteilung und optische Spektren des Tetrameren berechnet. Für alle wurde gute Übereinstimmung mit experimentellen Ergebnissen gefunden.

A. Introduction and Background

Hydrogen cyanide and its small polymers have long been proposed as key precursors in the prebiotic syntheses of purines, amino acids and polypeptides [1-4]. In particular, the tetramer has been shown to undergo efficient photorearrangement to a purine precursor which in a dark reaction with HCN forms adenine and by hydrolysis and condensation with other nitriles forms other purines, such as guanine, diaminopurine, and xanthine [5-8]. The photochemical step has been proposed as the only efficient pathway from hydrogen cyanide to the purines which is feasible in dilute aqueous solution. Because of its importance, the complicated photochemistry of the *cis* (I) and *trans* (II) isomers of HCN tetramer involving the purine precursor ACI (III) as well as other possible intermediates has been under extensive investigation [9-11].

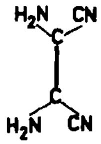

(I)

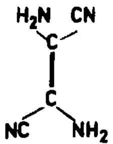

(II)

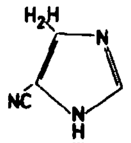

(III)

The tetramer has been suggested as a plausible, primordial, amino-acid condensing agent in aqueous solution [12]; and it is also thought to be an early intermediate in the formation of polymers from HCN under certain conditions [13]. These higher polymers have themselves been proposed as "foreproteins" leading by hydrolysis to polypeptides [14]. For these diverse reasons then the tetramer of HCN is considered a particularly key precursor molecule in chemical evolution.

In addition to studies exploring its role in chemical evolution, a number of other properties of the HCN tetramer have been investigated. For example, the X-ray crystal structure of the *cis* isomer (DAM I) [15] and the *trans* isomer (DAF II) [16] have been determined. While the *cis* isomer is thought to be experimentally more stable [10] both forms readily undergo photochemical interconversion [11]. The dipole moment [17] and the ionization potential [18] have both been measured for the lower energy form. Also simple Hückel, π-electron-only (SHT) molecular orbital calculations have been reported for the *cis* [15] and the *trans* [19] isomers.

Thus the HCN tetramer seemed an appropriate object of study for our continuing quantum chemical investigations of small molecules [20–23] which are considered important prebiotic precursors.

In the initial study presented here we have made a series of energy-conformation calculations to determine the most favorable isomer and conformer of the tetramer. In addition we have calculated such physical properties as dipole moment, ionization potential and electronic spectra, and compared our results with known experimental behavior.

To characterize the HCN tetramer we have used, as in the past [20, 22], the so-called Iterative Extended Hückel Theory (IEHT). The details of this approximate, all-valence-electron, semi-empirical method of solution of the molecular Schroedinger equation have been presented and discussed elsewhere [24–26]. Our method of calculation and values of input parameters are essentially those of Zerner and Gouterman [27]. Previous analysis have shown that, while this method does not pretend to give total molecular energies but rather just the valence-state-configuration energies, these latter appear to vary as the total energy with geometric variations of a given molecule [28, 29]. There are relatively few energy-conformation studies using IEHT reported in the literature [30]. Rather a simpler, less time-consuming but less reliable non-iterative EHT method has been extensively used. In our program, we automatically obtain the non-iterated energies and eigenfunction as our initial solution of the Schroedinger equation. We have uniformly found that using these zero-iteration results give much less reliable energy variations and eigenfunctions than do the charge-converged results.

B. Energy-Conformation Studies

The molecular geometries which resulted from the X-ray crystal structure determinations for the two isomers are given in Figs. 1a and 1b. Each has several interesting and unusual features. The *cis*-isomer, DAM, has no mirror plane and is twisted by 6° about the C=C bond. The bond angles of the two

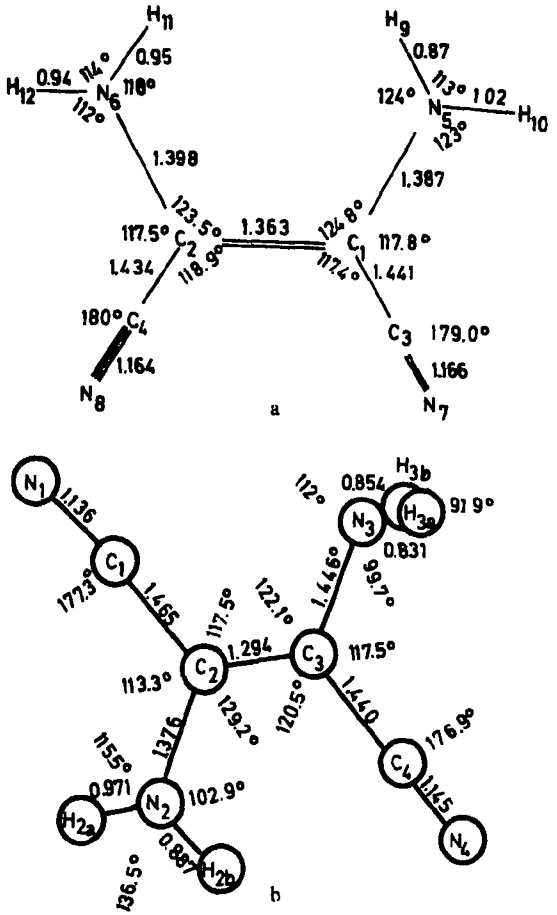

Fig. 1. a Molecular geometry of the *cis*-HCN tetramer as determined by the X-ray diffraction analysis of crystal structure (15). b Molecular geometry of the *trans*-HCN tetramer as determined by the X-ray diffraction analysis of crystal structure (16)

central ethylenic carbon atoms are highly anisotropic with two less than and one greater than 120°. The two amine groups have inequivalent geometry: one planar with anisotropic nitrogen bond angles and the other a distorted tetrahedron with the plane of the NH_2 group perpendicular to that of the remainder of the molecule and an abnormally large HNH bond angle of 114° compared to 107° in ammonia.

Interestingly, the same type of strained structure was obtained from the X-ray crystal analysis of the *trans*-isomer DAF by a different group of investigators [16]. Their results shown in Fig. 1b also yielded anisotropic ethylene carbon bond angles and one planar and one tetrahedral NH_2 group with highly anisotropic bond angles and a small HNH bond angle of 92°.

It seems highly unlikely that such distorted molecules are minimum energy conformers of the isolated molecules, i.e. the result of intramolecular interactions

Table 1. Molecular energy of HCN tetramer as a function of molecular geometry

Conformer	*cis*-isomer (I DAM) (eV)	*trans*-isomer (II DAF)
Planar	−707.83	−706.70
Exp.	−694.03	−693.50
Exp.′	−700.60	−701.90
Tetrahedral	−696.70	−697.70

alone. Since a great deal of the chemistry of the HCN tetramer relevant to prebiotic synthesis occurs either in the gas phase or dilute solution, we have made energy-conformation studies to determine the most energetically favored conformation in the isolated molecule. For each isomer the conformations chosen were: 1) the experimentally determined X-ray crystal structure (Exp); 2) an "idealized" experimental structure, (Exp′) with zero twist angle and isotropic bond angles of 120° for all trivalent planar bonds and 107° for tetrahedral amine bond angles. 3) Two rotational variations with the regular bond angles of the idealized crystal structure, a totally planar one and a totally tetrahedral one, obtained by a rotation of 90° about each C–N bond in turn.

The results of these calculations are given in Table 1. We see that for both isomers the experimentally determined structure is the least stable and the completely planar conformation is the most stable. The totally tetrahedral conformation appears also to be more stable than the experimental one but less stable than the idealized experimental conformer. Thus it appears that both the bond-angle-anisotropy and the inequivalence of the two amine groups are special features of the crystal structure of the *cis* and *trans* isomers which are not shared by the isolated molecule.

We also see from Table 1, that the *cis* isomer is energetically favored over the *trans* in agreement with experimental observations. However, there does not appear to be any definitive thermodynamic estimates of the energy difference between *cis* and *trans* isomers with which to compare our estimate of 1.1 eV (25 kcal/mole).

C. Ionization Potential

Values for the lowest ionization potential of the molecule obtained from the IEHT results as the energy of the highest filled molecular orbital, are given in Table 2 for each conformer studied. We see from this table that there is only a small variation in ionization potential with conformation and from *cis* to *trans* isomer. Recently, in order to check our results, colleagues at NASA Ames Research Center have obtained an estimate of the ionization potential of the tetramer from a mass spectroscopic study of the appearance potential of the molecular ion [18]. This value is also given in Table 2. We see that the calculated ionization potentials for all conformers are lower than the experimental one, but that, except for the X-ray structure value, all fall within the limits of experimental

Table 2. Dipole moment and ionization potential of conformers of *cis*- and *trans*-HCN tetramer

Conformation	*cis*-isomer (I DAM)		*trans*-isomer (II DAF)	
	DM (Debye)	IP (eV)	DM	IP
	Calc.	Calc.	Calc.	Calc.
Planar	−7.70	10.46	0.193	10.38
Exp	−9.47	10.14	0.956	9.74
Exp.′	−6.42	10.57	0.815	10.58
tetra	−5.04	10.62	0.122	10.61
	Exp.	Exp.		
Exp.	−7.78	11.2 ± 0.8		

error. In addition to providing verification of our calculation values this result might be regarded as further corroboration that the ground state in the isolated molecule is not the same as in the crystal.

D. Dipole Moments

From the molecular orbital functions resulting from the IEHT calculations, the dipole moment of each conformer was calculated. These values are also given in Table 2. We see that there is a marked distinction between the calculated values of dipole moments of the *cis* and *trans* isomer, the latter being quite small because of the symmetry of the molecule and the former having unusually large values which are quite sensitive to conformation changes.

The measured dipole moment of the tetramer in dioxane solution at 35° is −7.78 Debye. There is then excellent agreement between this measured value and our calculated value of dipole moment for the preferred planar *cis* conformer energy. The internal consistency and agreement with experiment is extremely heartening. Our results also suggest that the planar *cis*-isomer is the lowest energy form in dioxane solution with no large conformational changes in going from the isolated molecule to solution.

E. π-Electron Properties: Electron Distribution and Electronic Spectra

The HCN tetramer has 36 valence molecular orbitals and 40 valence electrons, so that in the totally paired ground state 20 molecular orbitals are filled and 16 empty. Of the 20 filled orbitals in the planar conformers, 5 are π orbitals, yielding 10 π and 30 σ electrons in the ground state tetramer with 3 empty π orbitals and 13 empty σ orbitals. The partitioning of electrons between π and σ orbitals is a result of the calculation and not an input restriction. The π electron density on each carbon and nitrogen, determined from the charge-iterated results of the IEHT calculation, is given in Table 3 for both DAM and DAF. These results may be compared to earlier, simple Hückel Theory (SHT) calculations reported for each isomer [15, 19], in which only the 8 π atomic orbitals were considered, and the number of π electrons were assumed for each molecule: 10 for DAM and 8 for DAF. The π electron distribution resulting from both of these calculations is also given in Table 3 under the heading SHT. We see that, for the *cis* isomer (DAM), the main difference is that the SHT results predict

Table 3 A comparison of π electron distribution in *cis*- and *trans*-planar HCN tetramer from SHT and IEHT calculation

Atom	SHT	IEHT	SHT	IEHT
Central C	0.976	1.107	0.490	1.106
Nitrile C	0.76	1.025	0.781	1.023
Nitrile N	1.37	1.085	1.176	1.077
Amine N	1.89	1.782	1.553	1.793
	4.99	4.999	4.000	4.999

Table 4 π electron distribution in the 5 filled and lowest empty π-orbitals of planar HCN-tetramer

Atom/π MO	1 (9)[a]	2 (13)	3 (16)	4 (19)	5 (20)	1[c] (21)
			cis-tetramer			
Central C	0.583[b]	0.087	0.172	0.123	0.142	0.250
Nitrile C	0.275	0.514	0.224	0.008	0.003	0.188
Nitrile N	0.071	0.370	0.438	0.094	0.111	0.418
Amine N	0.071	0.028	0.165	0.775	0.744	0.144
Type π MO	C–C–C–C	C≡N	Deloc.	N^{nb}_{amine}	N^{nb}_{amine}	Deloc.
			trans-isomer			
Central C	0.575	0.079	0.184	0.129	0.139	0.238
Nitrile C	0.277	0.528	0.208	0.005	0.004	0.190
Nitrile N	0.076	0.374	0.462	0.075	0.091	0.439
Amine N	0.071	0.018	0.147	0.791	0.766	0.133

[a] Position of π MO in energy-ordered list of 6 and π mos.

[b] Fraction of π electron on atom.

[c] Lowest empty molecular orbital

an electron-deficient π orbital for the nitrile carbon and an electron rich one for the nitrile nitrogen, i.e. a fairly polar CN π bond while the IEHT results predict almost equal π electron density on the nitrile carbon and nitrogen atoms. Since an accurate dipole moment is obtained for this molecule and since the method used includes all valence electrons, it may be assumed that our π electron distribution is more accurate than the earlier one. For the DAF isomer, the π electron distributions resulting from the two methods are very different. The main discrepancies are obviously caused by the assumption of 8 rather than 10 π electrons in the earlier calculation, i.e., the *a priori* assumption of 1 π electron per atom. This assumption in the SHT calculation particularly penalizes the ethylenic carbon atoms and illustrates the disadvantage of choosing the number of π electrons as an input quantity.

Tables 4a and b describe the nature of the 5 filled and lowest empty π molecular orbitals. The lowest energy π molecular orbital (MO 9) is delocalized over the four-carbon skeleton, the next (MO 13) is a fairly localized nitrile π bond, the 3rd (MO 16) is completely delocalized on all carbon and nitrogen atoms in the molecule and the 4th and 5th, which are the two highest filled orbitals [19, 20] are nearly non-bonding amine nitrogen orbitals. The lowest empty orbital [21], also a π orbital, is, like MO 16, delocalized on all the C and N atoms in the molecule, but primarily on the nitrile N atoms.

The π electron network appears to be relatively insensitive to *cis-trans* isomerism, with almost identical π electron distribution in each isomer.

The electronic spectra of both the *cis* and *trans* isomer have been measured in the region 2500–4500 Å at -196° K and room temperature [11]. The low temperature spectra exhibit broad absorptions with some structure and an absorption maximum of 3150 Å for the *cis* and 3350 for the *trans* isomer. There is some experimental evidence that these transitions involve charge transfer. While we can obtain transition energies only in the one electron approximation from our IEHT calculation, i.e. configuration energies uncorrected for total state formation, we can nevertheless obtain from our results some insight into the nature of the allowed transitions as well as an approximate estimate of transition energies. A series of 7 possible electronic transitions to the lowest empty orbital [21] is given in Table 5 in order of increasing energy. Included in this table are the $5\,\pi\rightarrow\pi^*$ transitions, 9, 13, 16, 19, 20→21, and the two lowest energy $\sigma\rightarrow\pi^*$ transitions 17, 18→21.

Looking at Table 5, we see that the 2 lowest energy transitions 19, 20→21 are $n(\pi)\rightarrow\pi^*$ between non-bonding and antibonding π orbitals involving about 80% charge transfer from an amine nitrogen to the other atoms of the molecule. While similar in character, these two non bonding π orbitals have somewhat different electron distributions resulting in rather different energies. We see from Table 5 that both transitions are predicted to fall within the broad range included in the experimental region, while the second corresponds very closely to the observed maxima for both *cis* and *trans* isomers. Our results also appear to confirm the suspected charge transfer nature of this transition. Also, in agreement with experiment, we calculate a small shift to higher energy of the $\lambda_{\max}$ from the *trans* to the *cis* isomer.

The next two, higher energy transitions 17, 18→21 are from two, essentially non-bonding, σ, nitrile-nitrogen orbitals. These are calculated by our IEHT program to have zero values of transition moments and oscillator strengths and hence are forbidden.

The 16→21 transition noted in Table 5, is a $\pi\rightarrow\pi^*$ transition, from a delocalized π bonding to an antibonding π orbital. It is allowed but has a calculated $\lambda_{\max}$ just on the high energy boundary of the experimental region. The

Table 5. Calculated $(\pi\rightarrow\pi^*)$ transitions for planar *cis* (DAM I) and *trans* (DAF II) HCN tetramer spectra

MO $(i\rightarrow j)$	Transition	$\Delta\varepsilon\,(\mathrm{eV})_{cis}$	$\Delta\varepsilon\,(\mathrm{eV})_{trans}$	$\lambda_{cis}^{\max}$	$\lambda_{trans}^{\max}$
20→21	$n(\pi)\rightarrow\pi^*$	3.16	2.97	3900 Å	4100 Å
19→21	$n(\pi)\rightarrow\pi^*$	3.74	3.72	3200^a	3400^a
18→21	$n(\sigma)\rightarrow\pi^*$	(4.03)^1	(3.81)	forbidden	
17→21	$n(\sigma)\rightarrow\pi^*$	(4.18)	(4.30)	forbidden	
16→21	$\pi\rightarrow\pi^*$	4.89	4.82	2500	2600
13→21	$l\pi\rightarrow\pi^*$	5.91	5.79	2000	2250
9→21	$\pi\rightarrow\pi^*$	7.31	7.15	1690	1730

[a] Observed $\lambda_{cis}^{\max} = 3150$ Å, $\lambda_{trans}^{\max} = 3350$ Å.

remaining two π electron transitions are of much higher energy than the experimental range.

It appears then that the π electron orbitals obtained and their calculated energy levels can account surprisingly well for the main features of the observed spectra for both isomers.

Encouraged by the success of our model in elucidating the more physical properties of the *cis* and *trans* isomers of the HCN tetramer we are proceeding to use it for an analysis of their chemical behavior and possible role in chemical evolution.

Acknowledgments. One of the authors, G. H. Loew, wishes to gratefully acknowledge partial support for this work from NASA grant NGR 05-020-405. She also wishes to thank her student, Miss Paula Elster, for help in obtaining these results.

Bibliography

1 Ponnamperuma,C., Gabel,N.W.: Space life sciences **1**, 64 (1968).
2 Abelson,P.H. Proc. nat. Acad. Sci. USA **55**, 1365 (1966).
3 Lowe,C.U., Rees,M.W., Markham,R.: Nature **199**, 219 (1963).
4 Oro,J., Kamat,S.S., Nature **190**, 442 (1961)
5 Sanchez,R., Ferris,J.P., Orgel,L.E.: Science **153**, 72 (1966).
6 Sanchez,R., Ferris,J.P., Orgel,L.E.. Science **154**, 784 (1966).
7. Ferris,J.P., Orgel,L.E.: J. Amer. chem. Soc. **88**, 1074 (1966).
8 Sanchez,R., Ferris,J.P., Orgel,L.E.: J. molecular Biol. **38**, 121 (1968).
9 Ferris,J.P., Kuder,J.E., Catalano,A.W.: Science **166**, 865 (1969).
10. Ferris,J.P., Kuder,J.E. J. Amer. chem. Soc. **92**, 2527 (1970).
11 Kolc,J., Becker,R.S.: University of Houston. Preprint.
12 Chang,S., Flores,J., Ponnamperuma,C. Proc. nat. Acad. Sci. USA **64**, No. 3, 1011 (1969).
13 Kliss,R.M., Mathews,C.N.: Proc. nat. Acad. Sci. USA **48**, 1300 (1962).
14a Mathews,C.N., Moser,R.E.: Proc. nat. Acad. Sci. USA **56**, 1087 (1967).
14b. Mathews,C.N., Moser,R.E.: Nature **215**, 1230 (1967).
15 Penfold,B.R., Lipscomb,W.N.: Acta Crystallogr. **14**, 589 (1961).
16. Yamada,Y., Nagashima,N., Iwashita,Y., Nakamura,A., Kumashiro,I.: Tetrahedron Letters **43**, 4529 (1968).
17. Webb,R.L., Frank,S., Schneider,W.C.: Org. and biol. Chem. **77**, 3491 (1955).
18. Romiez,M., Lawless,J.: NASA Ames Research Center, Unpublished (1971).
19. Ferris,J.P.: J. Amer. chem. Soc. **92**, 2527 (1970).
20 Loew,G.H.: Theoret. chim. Acta (Berl.) **20**, 203 (1971).
21 Loew,G.H., Chang,S.: Tetrahedron **27**, 3069 (1971).
22. Loew,G.H.: J. theoret. Biology **33**, 121 (1971).
23. Loew,G.H., Chang,S.: Tetrahedron **27**, 2989 (1971).
24a. Hoffman,R.: J. chem. Physics **39**, 1397 (1963)
24b. Hoffman,R.: J. chem. Physics **40**, 2480 (1964).
25. Rein,R., Fukuda,N., Win,H., Clarke,G.A., Harris,F.E.: J. chem. Physics **45**, 4743 (1966).
26. Pullman,A., Pullman,B.: Progress in nucleic acid research and molecular biology **9**, 327 (1969).
27a. Zerner,M., Gouterman,M.: Theoret. chim. Acta (Berl.) **14**, 44 (1966).
27b Zerner,M., Gouterman,M.: Theoret. chim. Acta (Berl.) **6**, 363 (1966).
28. Pan,D.C., Allen,L.C.: J. chem. Physics **46**, 1797 (1967).
29. Allen,L.C., Russell,J.D.: J. chem. Physics **46**, 1029 (1967).
30. Hoyland,J.R.: In: Molecular orbital studies in chemical pharmacology, pp. 31--81, ed. L. Kier. Berlin-Heidelberg-New York: Springer 1970.

Dr. G. H. Loew
Departments of Genetics
Stanford University Medical Center
Stanford, California 94305, USA

Theoret. chim. Acta (Berl.) 27, 281—287 (1972)
© by Springer-Verlag 1972

Ionization Potentials of Ferrocene and Koopmans' Theorem.
An *ab initio* LCAO-MO-SCF Calculation

Marie-Madeleine Coutière, Jean Demuynck and Alain Veillard
Institut de Chimie, Université Louis Pasteur
BP 296/R8, 67 – Strasbourg, France

Received July 31, 1972

The first ionization potentials of ferrocene have been computed in the LCAO–MO–SCF scheme as the difference of the total energy for the neutral molecule and the positive ion. The corresponding sequence of ionization potentials is found to be

$$\text{I.P.}(e_{2g}) < \text{I.P.}(a_{1g}) < \text{I.P.}(e_{1u}) < \text{I.P.}(e_{1g})$$

in good agreement with the experimental assignment. However, this is different from the sequence of orbital energies for the neutral molecule which is found to be

$$a_{1g}(3d) < e_{2g}(\sigma - \text{Cp}) \sim a_{2u}(\pi - \text{Cp}) \sim e_{2u}(\sigma - \text{Cp}) < e_{2g}(3d) < e_{1g}(\pi - \text{Cp}) \sim e_{1u}(\pi - \text{Cp}).$$

It is concluded that Koopmans' theorem is not valid for the ferrocene molecule. This is traced to the different extent of the electronic rearrangement which occurs upon ionization, depending on the nature (ligand or metal) of the orbital involved in the ionization process.

Das erste Ionisierungspotential von Ferrocen ist im Rahmen des LCAO–MO SCF-Verfahrens als Differenz der Gesamtenergie von Molekül zu Ion berechnet worden. Dabei ergibt sich in guter Übereinstimmung mit dem Experiment die Folge

$$\text{I.P.}(e_{2g}) < \text{I.P.}(a_{1g}) < \text{I.P.}(e_{1u}) < \text{I.P.}(e_{1g}).$$

Sie ist allerdings durchaus von der Orbitalreihenfolge des neutralen Moleküls, die

$$a_{1g}(3d) < e_{2g}(\sigma - \text{Cp}) \sim a_{2u}(\pi - \text{Cp}) \sim e_{2u}(\sigma - \text{Cp}) < e_{2g}(3d) < e_{1g}(\pi - \text{Cp}) \sim e_{1u}(\pi - \text{Cp})$$

ist, verschieden, woraus sich die Nichtgültigkeit des Koopmans-Theorems für Ferrocen ergibt, und zwar läßt sie sich auf den unterschiedlichen Umfang der Elektronenumordnung infolge Ionisation zurückverfolgen, je nachdem, aus welchem MO die Ionisierung stattfindet.

The nature of the bonding in ferrocene $Fe(C_5H_5)_2$ has attracted much interest among both theoreticians and experimentalists. Several semi-empirical calculations have been published [1–7]. Among the experimental techniques, the photoelectron, the electron spin resonance and the electronic absorption measurements have provided useful data for a comparison with theoretical calculations. The lowest two ionization potentials at 6.85 and 7.2 eV in the photoelectron spectrum of ferrocene [8] are due to removal of electrons from the e_{2g} and a_{1g} orbitals which are assumed to be for the greater part localized on the iron atom. One would thus expect from Koopmans' theorem that the sequence of orbitals in ferrocene is

$$a_{1g} < e_{2g}$$

(namely the energy associated with the a_{1g} orbital is larger). However Prins has noted that nothing definite may be said about the order of the a_{1g} and e_{2g} SCF orbitals due to the approximation inherent in Koopmans' theorem (neglect of the electronic relaxation associated with ionization) and to the neglect of correlation energy in the Hartree-Fock approximation [9]. The third and fourth ionization potentials at 8.8 and 9.3 eV in the photoelectron spectrum have been attributed to ionization from the e_{1u} and e_{1g} orbitals which, according to semi-empirical calculations, are essentially ligand π-orbitals. On the basis of ESR measurements for substituted ferricenium cations, it has been concluded that the ferricenium cation FeCp_2^+ has the ${}^2E_{2g}[a_{1g}^2 e_{2g}^3]$ ground state configuration and that the ${}^2A_{1g}[a_{1g}^1 e_{2g}^4]$ configuration belongs to an excited state [9]. From the above studies, Prins has concluded that the order of the highest filled and lowest empty orbitals in ferrocene is [9]

$$e_{1g}(\pi-\mathrm{Cp}) < e_{1u}(\pi-\mathrm{Cp}) < a_{1g}(3d) \sim e_{2g}(3d) < e_{1g}^*(3d)\,.$$

Semi-empirical MO calculations have not reproduced exactly this order [1–7]. Also they have not resolved the problem of the charge distribution in this molecule. Shustorovitch and Dyatkina obtained a positive charge of +0.69 e on the iron atom [1] whilst Dahl and Ballhausen obtained a negative charge of the same magnitude [2]. Simple theoretical arguments have suggested that the electronic structure of ferrocene involves some interaction between the $d_{\pm 1}$ orbitals of the metal and the e_1 orbitals of the cyclopentadienyl rings [10].

We report here some results from an *ab initio* SCF-LCAO-MO calculation including all the electrons. A basis set of 293 gaussian functions (basis sets $12s$, $7p$, $5d$ for the Fe atom [11], $8s$, $4p$ for the C atoms [12] and $3s$ for the H atoms [13]) has been reduced to 85 contracted functions (minimal basis set except for the $3d$ orbitals of Fe which are described by split functions). The bond lengths were taken as Fe–C = 2.106 Å, C–C = 1.43 Å and C–H = 1.12 Å [14]. The hydrogen atoms have been assumed lying in the plane of the carbon rings, although they may be slightly bent out of this plane [14]. The molecule has been assumed in an eclipsed (D_{5h}) equilibrium conformation in accordance with the results of an electron diffraction study in vapor phase [14]. However, all previous studies on the electronic structure of ferrocene have assumed a staggered (D_{5d}) configuration in accordance with the solid state structure. To conform with earlier usage, we adopt in the following discussion the notation of point group D_{5d}.

Orbital energies and LCAO coefficients for the highest occupied molecular orbitals are reported in Tables 1 and 2. The sequence of orbital energies for the ground state of the ferrocene molecule is found to be (Table 2, column 1)

$$\begin{aligned} &a_{1g}(3d) < e_{2g}(\sigma-\mathrm{Cp}) \sim a_{2u}(\pi-\mathrm{Cp}) \sim e_{2u}(\sigma-\mathrm{Cp}) \\ &< e_{2g}(3d) < e_{1g}(\pi-\mathrm{Cp}) \sim e_{1u}(\pi-\mathrm{Cp})\,. \end{aligned}$$

To investigate partially the effect of the basis set used on this sequence of energy levels, we have also performed a set of SCF calculations with different basis sets obtained from the above mentioned one by deleting one or several contracted functions. The corresponding values of the orbital energies are given in Table 2. Except for the interversion of the e_{1g} and e_{1u} levels which are very

Table 1. SCF orbitals for the ferrocene molecule and the ferricenium ion

Orbital	LCAO coefficients[a, b, d]
e_{1u} FeCp$_2$	$0.74\, z(C_1) - 0.26\, z(C_3) - 0.57\, z(C_4)$
FeCp$_2^+$ ($^2E_{1u}$)	$0.74\, z(C_1) - 0.26\, z(C_3) - 0.56\, z(C_4)$
e_{1g} FeCp$_2$	$0.34\, z(C_1) - 0.63\, z(C_3) + 0.30\, d^1_{yz} + 0.19\, d^2_{yz}$
FeCp$_2^+$ ($^2E_{1g}$)	$0.33\, z(C_1) - 0.62\, z(C_3) + 0.33\, d^1_{yz} + 0.20\, d^2_{yz}$
e_{2g} FeCp$_2$	$0.26\, y(C_1) - 0.89\, d^1_{x^2-y^2} - 0.13\, d^2_{x^2-y^2}$
FeCp$_2^+$ ($^2E_{2g}$)	$0.96\, d^1_{x^2\;\;y^2} + 0.07\, d^2_{x^2-y^2}$
a_{2u} FeCp$_2$	$0.52\, z(C_1) + 0.47\, z(C_3) + 0.32\, z(C_4)$
FeCp$_2^+$ ($^2A_{2u}$)	$0.51\, z(C_1) + 0.47\, z(C_3) + 0.32\, z(C_4)$
a_{1g} FeCp$_2$	$0.29\, z(C_1) + 0.27\, z(C_3) + 0.76\, d^1_{z^2} + 0.08\, d^2_{z^2}$
FeCp$_2^+$ ($^2A_{1g}$)	$0.99\, d^1_{z^2} + 0.05\, d^2_{z^2}$

[a] Only coefficients greater than 0.2 appear in this table, except for the coefficients of the 3*d* functions.

[b] The notations $y(C_1)$, $z(C_1)$, etc. refer to the appropriate symmetry adapted orbitals[c].

[c] The *z* axis is the five-fold axis of the molecule. Symmetry with respect to the plane *xOz* interchange the C_1 and C_2 atoms, the C_3 and C_5 atoms and leave the C_4 atom unchanged.

[d] The notation d^1 and d^2 refer to the split orbitals.

Table 2. Orbital energies (in a.u.) as a function of the basis set

	Basis set			
	I[a]	II[b]	III[c]	IV[d]
e_{1u}	−0.429	−0.435	−0.426	−0.429
e_{1g}	−0.437	−0.426	−0.446	−0.448
e_{2g}	−0.530	−0.507	−0.545	−0.542
e_{2u}	−0.585	−0.585	−0.586	−0.587
a_{2u}	−0.589	−0.592	−0.590	−0.593
e_{2g}	−0.594	−0.593	−0.597	−0.597
a_{1g}	−0.609	−0.599	−0.619	−0.617

[a] No function deleted.

[b] The 3*d* function of lowest exponent is deleted.

[c] The *p* function of lowest exponent (representative of the 4*p* atomic orbital) is deleted.

[d] The *s* and *p* functions of lowest exponent (4*s* and 4*p* atomic orbitals) are deleted.

close, the sequence appears as relatively independant of the basis set used. We may conclude that enlarging the basis set should not change appreciably the sequence of energy levels. It is dubious that the use of a larger basis set, leading to a better wavefunction, will be able to reconcile the computed sequence of orbital energy for the ground state of ferrocene with the "experimental" order of energy levels. The disagreement is emphasized when one realizes that the two highest occupied orbitals in our calculation are predominantly 2*pπ* ligand orbitals (Table 1) while the two highest orbitals e_{2g} and a_{1g} according to the photoelectron spectrum are predominantly metal orbitals.

We intend to show now that this disagreement regarding the sequence of orbitals is merely the result of a misplaced confidence in the validity of Koopmans' theorem. Experimentally, the sequence of energy levels given [9] for the ground state of the *neutral* ferrocene molecule has been assumed on the basis of the photoelectron spectrum which involves both the positive ion and the neutral parent, of the ESR spectrum of the ferricenium ion and of the absorption spectrum of the ferrocene molecule which involves an excited state besides the electronic ground state. This is based on a widespread conception that experimental information relating to excited states or to a positive ion may be used for the parent neutral molecule in its ground state, for instance that it is possible to equate orbital energies and experimental ionization potentials or to derive a sequence of orbital energies from the observed electronic transitions. Conversely SCF orbital energies are frequently used to predict ionization potentials and this is based on Koopmans' theorem. From the results presented below, it turns out that Koopmans' theorem is not valid for the ferrocene molecule, namely that the sequence of ionization potentials computed as the difference of the energy values for the molecule and the ion is different from the sequence of orbital energies computed for the neutral molecule in its ground state.

We have performed a series of SCF calculations for the ferricenium ion in various electronic configurations, keeping the geometry used for the parent molecule (although the iron-to-ring distance is estimated to be larger in $FeCp_2^+$ than in $FeCp_2$ [9]). The computed SCF energies in the restricted Hartree-Fock scheme [15] together with the corresponding ionization energies are given in Table 3. It turns out that the computed sequence of ionization potentials is now

$$\mathrm{I.P.}(e_{2g}) < \mathrm{I.P.}(a_{1g}) < \mathrm{I.P.}(e_{1u}) < \mathrm{I.P.}(e_{1g})$$

in good agreement with the experimental evidence. The computed ionization potential of 8.3 eV, corresponding to removal of one electron from the e_{2g} orbital, is in moderately good agreement with the experimental value of 6.8 eV [8]. There is only a moderate agreement between the computed energies of 23200 cm^{-1} and 23900 cm^{-1} for the charge-transfer transitions $^2E_{2g} \rightarrow {}^2E_{1u}$ and $^2E_{2g} \rightarrow {}^2E_{1g}$ of the ferricenium ion compared to the experimental estimates of 16200 cm^{-1} and 20000 cm^{-1} [9]. Nevertheless the agreement obtained with the experimental sequence of ionization potentials is gratifying when one considers the severe limitations of our calculation: use of a limited basis set which is slightly better than a minimal basis set of Slater functions, neglect of correlation energy and assumption of a similar geometry for the positive ions and the neutral molecule.

Table 3. Computed ionization energies

Molecule	Configuration	State	Energy (in a.u.)	Computed I.P. (in eV)	Experimental I.P. (in eV)
$FeCp_2$	$a_{2u}^2 a_{1g}^2 e_{2g}^4 e_{1g}^4 e_{1u}^4$	$^1A_{1g}$	−1643.125	–	–
$FeCp_2^+$	$a_{2u}^2 a_{1g}^2 e_{2g}^3 e_{1g}^4 e_{1u}^4$	$^2E_{2g}$	−1642.821	8.3[a] (14.4)[b]	6.8
	$a_{2u}^2 a_{1g}^1 e_{2g}^4 e_{1g}^4 e_{1u}^4$	$^2A_{1g}$	−1642.754	10.1 (16.6)	7.2
	$a_{2u}^2 a_{1g}^2 e_{2g}^4 e_{1g}^4 e_{1u}^3$	$^2E_{1u}$	−1642.715	11.1 (11.7)	8.8
	$a_{2u}^2 a_{1g}^2 e_{2g}^4 e_{1g}^3 e_{1u}^4$	$^2E_{1g}$	−1642.712	11.2 (11.9)	9.3
	$a_{2u}^1 a_{1g}^2 e_{2g}^4 e_{1g}^4 e_{1u}^4$	$^2A_{2u}$	−1642.556	15.5 (16.0)	–

[a] Ionization potential computed as the difference of the energy value for the molecule and the ion.
[b] Ionization potential computed according to Koopmans' theorem.

It is now clear that Koopmans' theorem is not valid for the ferrocene molecule. The reason is to be found in the different extent of the electronic rearrangement which occurs upon ionization, depending on the nature of the orbital involved in the ionization process. For a ligand orbital (e_{1u} or e_{1g} or a_{2u}) there is little electronic rearrangement upon ionization and the ionization potential computed as the difference of the energies for the molecule and the ion is close to the corresponding orbital energy (Table 3). For a metal orbital (a_{1g} or e_{2g}) there is a marked rearrangement upon ionization: while these orbitals include a small amount of ligand orbitals for the neutral molecule, they become nearly pure metal orbitals for the ion (Table 1) and the computed ionization energy may differ from the orbital energy by as much as 6 eV. This difference in the degree of electronic rearrangement is easily understood in terms of charge delocalization. Ionization from the a_{1g} or e_{2g} orbitals leaves a positive charge which is nearly localized on the iron atom, while the positive charge corresponding to ionization from the e_{1u} or e_{1g} orbitals is delocalized on the two cyclopentadienyl rings. The validity of Koopmans' theorem for metal complexes has been previously questionned on the basis of a disagreement between the experimental ionization potentials for tris (β-diketonate) metal complexes and semi-empirical orbital energies for the neutral molecule [16].

We have not considered ionization from the orbitals $e_{2g}(\sigma - \mathrm{Cp})$ and e_{2u}. This would lead to excited states of the ferricenium ion which are probably higher in energy since these orbitals are σ orbitals of the ligands.

The lowest bands in the electronic absorption spectrum of ferrocene have been analyzed as *d*–*d* transitions [17]. This does not conflict with our conclusion that the two "highest occupied" orbitals[1] in ferrocene are the predominantly ligand orbitals e_{1u} and e_{1g}. The highest occupied orbitals for the $\mathrm{Ni(CN)}_4^{2-}$ ion are ligand π-orbitals with the lowest virtual orbitals being either a π^* orbital of the ligand or a 4*s* or 4*p* orbital of the metal [18–19]. Nonetheless the lowest energy transitions are *d*–*d* transitions [18]. This may be traced to the fact that the transition energies are not given merely as a difference of orbital energies but include also a Coulomb and exchange term which may be significant enough to determine the sequence of electronic transitions [19–20]. We expect a similar situation in ferrocene and work is now in progress to compute some transition energies.

The following comments are intended to illustrate some details of the wavefunction and electron distribution. From the ESR spectrum, Prins has shown that the e_{2g} molecular orbital is essentially localized on the iron atom with an estimated value of $C_1 = 0.91 \pm 0.03$ for the coefficient of the atomic 3*d* orbital in this molecular orbital. This is in excellent agreement with the value of $C_1 = 0.89$ for the ferrocene molecule and $C_1 = 0.96$ for the ferricenium ion (Table 1). The relative sequence of some orbitals in the ferrocene molecule has been justified on the basis of metal-ligand interactions. According to Prins the bonding e_{1g} orbitals are probably more stabilized by interaction between the ligand π orbitals and the iron 3*d* orbitals than the bonding e_{1u} orbitals by interaction between the ligand π orbitals and the iron 4*p* orbitals [9]. The contribution of the 3*d* atomic

---

[1] It should be realized that the concept of highest occupied orbital looses any physical significance if the Koopmans' theorem is not valid.

Table 4. Gross atomic and orbital populations

	Fe	C	H
s	6.00	3.12 (3.04)[a]	0.81 (0.93)
$p_x + p_y$	8.24	2.13 (2.03)	
p_z	4.01	1.06 (1.20)	
d_{xz}, d_{yz}	0.43		
$d_{xy}, d_{x^2-y^2}$	1.86		
d_{z^2}	1.93		
Formal charge	+1.23	−0.31 (−0.27)	+0.19 (+0.07)

[a] The results in parentheses refer to the cyclopentadienyl ion.

orbital to the e_{1g} molecular orbital is indeed larger than the contribution of the 4*p* atomic orbital to the e_{1u} orbital. However this is probably balanced by the bonding character of the e_{1u} orbital with respect to the interaction of the two cyclopentadienyl rings compared to the antibonding character of the e_{1g} orbital (the overlap integral between the $2p\pi$ orbitals of opposite carbon atoms on the two rings amount to 0.067).

Two contracted gaussian functions have been used in this calculation to describe the iron 3*d* atomic orbitals. The first contracted function was taken as the atomic 3*d* orbital for the ion Fe^{2+} [11]. The second function is a gaussian function of exponent 0.15 which does not contribute at all to the atomic wavefunction of the ion Fe^{2+} but which is found to participate appreciably to the e_{1g} orbital of the ferrocene molecule. This is indicative of an orbital expansion upon formation of the complex, associated to a charge transfer from the cyclopentadienyl ring to the iron atom. The results of a population analysis reported in Table 4 for the cyclopentadienyl ion and the ferrocene molecule point to

– a transfer of 0.86 e from the $2p\pi$ orbitals of the rings to the d_{xz} and d_{yz} orbitals of the metal;

– a transfer of 0.24 e from the $2p\pi$ orbitals of the rings to the $4p_x$ and $4p_y$ orbitals of the metal;

– a back-bonding transfer of 0.35 e from the d_{z^2}, $d_{x^2-y^2}$ and d_{xy} orbitals of the metal to the orbitals of the rings.

The net balance is a shift of 0.39 e from each ring to the iron atom.

Acknowledgements. We are grateful to the CNRS for a grant of computer time at the Centres de Calcul d'Orsay (C.I.R.C.E.) and Strasbourg-Cronenbourg. We thank the staffs of the computation centers.

References

1. Shustorovich, E. M., Dyatkina, M. E.: Zh. Strukt. Khim 1, 98 (1960).
2. Dahl, J. P., Ballhausen, C. J.: Math.-fys. Meddr. 33, 5 (1961).
3. Fischer, R. D : Theoret. chim. Acta (Berl.) 1, 418 (1963).
4. Schachtschneider, J. H., Prins, R., Ros, P.: Inorg. chim. Acta 1, 462 (1967).
5. Armstrong, A. T., Carroll, D. G., McGlynn, S. P.: J. chem. Physics 47, 1104 (1967).
6. Rettig, M. F., Drago, R. S.: J. Amer. chem. Soc. 91, 3432 (1969).
7. Hillier, I. H., Canadine, R. M.: Discuss. Faraday Soc. 47, 27 (1969).

8. Turner, D. W.: In: Physical methods in advanced inorg. chem., ed. by Hill, H. A. O., Day, P. New York: Interscience Publishers 1968.
9. Prins, R.: Molecular Physics **19**, 603 (1970).
10. See for instance: Wilkinson, G., Cotton, F. A.: Progr. inorg. Chem. **1**, 1 (1959).
11. Roos, B., Veillard, A., Vinot, G.: Theoret. chim. Acta (Berl.) **20**, 1 (1971).
12. Whitman, D. R., Hornback, J. C.: J. chem. Physics **51**, 398 (1969).
13. Huzinaga, S.: J. chem. Physics **42**, 1293 (1965).
14. Böhn, R. K., Haaland, A.: J. Organometal. Chem. **5**, 470 (1966).
15. Roothaan, C. C. J.: Rev. mod. Physics **32**, 179 (1960).
16. Schildcrout, S. M., Pearson, R. G., Stafford, F. E.: J. Amer. chem. Soc. **90**, 4006 (1968).
17. Sohn, Y. S., Hendrickson, D. N., Gray, H. B.: J. Amer. chem. Soc. **93**, 3603 (1971).
18. Demuynck, J., Veillard, A., Vinot, G.: Chem. Physics Letters **10**, 522 (1971).
19. Demuynck, J., Veillard, A.: To be published.
20. Basch, H., Hollister, C., Moskowitz, J. W.: In: Sigma molecular orbital theory, Sinanoglu, O., Kenneth, W. (Ed.), p. 449. New Heaven: Yale University Press 1970.

Note Added in Proof. The electron spectrum of ferrocene has been analysed by Rabalais *et al.* (J. chem. Physics 57, 1185 (1972)). These authors invoke Koopmans' theorem in conjunction with a sequence of outer molecular orbitals from semi-empirical calculations. They point out that most calculations predict an ordering of $\ldots(e_{2g})^4(a_{1g})^2$ for the outer orbitals in contradiction with their experimental result that the $^2E_{2g}$ state of ferricenium is below the $^2A_{1g}$ state. Our calculation predicts the correct order of these two states.

Prof. Dr. Veillard
Institut de Chimie
Université Louis Pasteur
BP 296/R8
F-67 Strasbourg
France

Theoret. chim. Acta (Berl.) 27, 289—302 (1972)
© by Springer-Verlag 1972

A Semi-Empirical MO-Electron Correlation Method for Molecules and the Correlation Energies of π-System Linear and Polycyclic Hydrocarbons*

Oktay Sinanoğlu and H. Önder Pamuk

Sterling Chemistry Laboratory, Yale University, New Haven, Connecticut 06520, USA
and Teorik Kimya Bölümü, Orta-Doğu Teknik Üniversitesi, Ankara, Türkiye

Received June 16, 1972

A set of approximations referred to as the "EPCE-F2 Method" is presented starting from the MO-pair correlations theory by Sinanoğlu of ground state molecules. It yields estimates of the correlation energies using LCAO MO coefficients and one and two center pair correlation parameters. The method applied to π-systems yields explicit expressions for correlation energies in terms of the number of carbon atoms, π-bonds, and the number of rings. The π-correlation energies of polyenes and various types of polyacenes are given. Results are compared with available alternant MO (AMO) and π-CI calculations. Correlation energies per electron are also obtained as number of carbon atoms increase and approach the very large system limits like a layer of graphite.

Es wird ein als „EPCE-F2 Methode" bezeichneter Satz von Näherungen vorgeschlagen, der von der MO-Paarkorrelationstheorie für Moleküle im Grundzustand ausgeht. Die Methode liefert Näherungswerte der Korrelationsenergien, wobei die LCAO-MO-Koeffizienten und Ein- bzw. Zweizentren-Korrelationsparameter verwendet werden. Bei π-Elektronensystemen erhält man explizite Beziehungen für die Korrelationsenergien, die von der Anzahl der Kohlenstoffatome, der π-Bindungen und der Ringe ausgehen. Die π-Korrelationsenergien der Polyene und verschiedener Typen von Polyacenen werden angegeben und die Ergebnisse mit den zur Verfügung stehenden AMO-MO und π-CI Berechnungen verglichen. Auch die Korrelationsenergien pro Elektron werden in Abhängigkeit von der steigenden Anzahl der Kohlenstoffatome und für den Grenzfall sehr großer Systeme wie Graphitschichten mitgeteilt.

Introduction

The molecular orbital Hartree-Fock (MO HF) method gives the charge distribution related properties of singlet ground states well, but it does not account for dissociation energies, electron affinities and the like [1]. The F_2 molecule as an extreme case is predicted to be highly unstable with respect to 2F by rigorous Hartree-Fock MO results for example [2]. For energetics, the rest of the exact non-relativistic energy, i.e. electron correlation energy, E_{corr}, is needed.

MO-methods for large molecules, whether non-empirical or semi-empirical, formally start from the MO HF theory, but of necessity involve many approximations already at the HF MO level itself. The errors resulting from the difference between approximate MO-energies and actual HF energies are much larger than

---

* Work supported in part by a grant from the U.S. National Science Foundation.

quantities of interest. The calculations of rigorous HF for molecules beyond diatomics and the smallest of polyatomics, remain a technically formidable problem. In addition, by and large, approximate MO-methods do not deal with electron correlation.

Since 1959, a theory of electron correlation suitable for large atoms and molecules has been developed both for ground (MET) [3], and for excited states, i.e. general non-closed shell states (NCMET) [4]. This theory by Sinanoğlu has predicted and shown that, difficult to calculate, "dynamical" correlation effects can be obtained semi-empirically transferring them between atomic and molecular states, [5, 6]. Other, "non-dynamical" correlations however have to be calculated in detail based on the theory as it has been done for atomic excited states [7].

In this paper, we first discuss several previous semi-empirical schemes for the E_{corr} of molecules. We then use some of the rigorous expressions which has been derived recently by Sinanoğlu for molecular pair correlations in the LCAO MO description [8]. We make further approximations on these to extend an initial early suggestion by Sinanoğlu to treat π-electron correlation energies in terms of one- and two-center, E_{pp} and E_{pq}, pair correlations [9]. We apply the results, to linear and polycyclic hydrocarbons to obtain the π-system [10] E_{corr}'s of the doubly occupied ground states explicitly in terms of the numbers of carbon atoms and rings in the molecule. The results are compared with limited basis π-CI and AMO (alternant MO) calculations in the literature.

Semi-Empirical Methods

Except for the "Pair Population Method" (PPM) of Hollister and Sinanoğlu [11], present empirical or semi-empirical methods may be used only for diatomic molecules or polyatomic hydrides. Hartree-Fock calculations [12] and a previous argument given by McKoy have shown that the united atom approach [14] overestimates the correlation energy. In the separated ion (SI) approach [14, 15], the total correlation energy of diatomic molecule is obtained from the correlation energies of the two atoms and their ions. One can use this approach only for diatomic molecules and central hydrides. In the "Shrunk Core" model of Hollister and Sinanoğlu [11] outer MO electrons see a core which is quite like the cores of the constituent atoms. This model reduces to the united atom approach in the case of central hydrides, but it can predict the correlations energies of AH_nBH_m type molecules which the united atom cannot.

The "Pair Population Method", by contrast to the above, can be applied to any molecule as long as simple MO electron populations and atomic pair energies are known. The *correlation binding energy* is defined as the difference between the sum of the correlation energies of atoms in that molecule and the molecular correlation energy [6]. The correspondence between the correlation binding energies found by the PPM and the "experimental" ones [16] is excellent for small molecules. But the ratio of the estimated correlation binding energy to the experimental one decreases as the number of atoms in molecules increases [11].

It should be noted that PPM is based on the use of only the *gross atomic populations*. One converts these gross atomic populations into gross "pair populations" as defined in Ref. [11]. This allows one to express and obtain the E_{corr} (molecule) in terms of only the one-center, atomic pair correlations. The latter are given by MET [3]. In MO population analysis overlap populations are divided up and added onto *net populations* to get the *gross*. In the same way, implicit in PPM is the sub-division of the overlap region correlations among atoms and their addition to the purely one center ε_{pp} contributions. The study of this approximation requires more explicit expressions for the molecular E_{corr} suitable for a LCAO framework.

Sinanoğlu has derived rigorous LCAO-type expressions for molecular correlations and from these a number of different approximations applicable to both σ- and π-systems [8]. The use of zero differential overlap (ZDO)-like approximations on these expressions had led to his suggestion of a semi-empirical method in terms of one and two-center ε_{pp} and ε_{pq}-type pair correlations [9]. In the meanwhile, this suggestion has been developed to some extent with additional approximations and different contexts by Pamuk [17], by Brown and Roby [18], and by Labzowski [19]. We develop the ε_{pp}, ε_{pq}-method further here and apply it extensively to π-electron systems. The method is based on MET, i.e. only on the *ground state* correlation theory [3]. Thus it applies only to ground states. From it, one can also see what explicit approximations lead to PPM. For π-systems, even large polycyclics, the present one- and two-center method should yield better results.

The Ground State Molecular Correlation Energy in the LCAO Form for π-Systems

Theory of electron correlation in doubly occupied ground states shows that [3]

$$E_{\text{corr}} \cong \sum_{i>j\geq 1}^{N} \varepsilon_{ij}\,, \tag{1}$$

where $i, j \in \{1, 2, \ldots, N\}$ are occupied HF MO spin-orbitals and ε_{ij} are the MO-pair correlations of MET. These are in the spin-orbital form, further they are the "*total*" ε_{ij}'s of the MET-type [3], $\varepsilon_{ij}^{\text{T}}$. In the more detailed NCMET (applicable to excited states and which rigorously reduces to MET in the closed shell limit) one would have [1, 6]

$$\varepsilon_{ij}^{\text{T}} = \varepsilon_{ij}^{\text{INT}} + \varepsilon_{ij}^{\text{F}} + \varepsilon_{ij}^{\text{all-ext.}} \tag{2}$$

with the "internal" (INT), "semi-internal" (F), and "all-external" (all-ext) parts. For closed shells, one gets

$$\varepsilon_{ij} = \varepsilon_{ij}^{\text{T}} = \varepsilon_{ij}^{\text{all-ext.}}\,. \tag{3}$$

The ground states of π-systems are not closed, but "quasi-closed" shells (doubly occupied, single det HF). Thus the ε_{ij}'s pertinent to the present paper are in general of the $\varepsilon_{ij} = \varepsilon_{ij}^{\text{T}}$-type, Eq. (2).

From Eq. (1), Sinanoğlu has obtained [8] the spinless forms of E_{corr} and in the LCAO-form. Upon further making ZDO-type approximations for π-systems (invariant only for π-systems), he gets

$$\boxed{\begin{aligned} E_{\mathrm{corr}_{(\pi)}} \cong \tfrac{1}{4} &\sum_{\substack{\mu,\nu \\ (\mu\neq\nu)}} (P_{\mu\mu}P^*_{\nu\nu} + |P_{\mu\nu}|^2)\,\varepsilon(\mu^\alpha\nu^\beta) \\ &+ \tfrac{1}{4} \sum_{\substack{\mu,\nu \\ (\mu\neq\nu)}} (P_{\mu\mu}P^*_{\nu\nu} - 2|P_{\mu\nu}|^2)\,\varepsilon(\mu^\alpha\nu^\alpha) \\ &+ \tfrac{1}{4} \sum_{\mu} |P_{\mu\mu}|^2\,\varepsilon(\mu^\alpha\mu^\beta)\,. \end{aligned}} \tag{4}$$

The μ, ν are the spinless π-atomic orbitals (AO). $P_{\mu\nu}$ is the usual AO-density matrix

$$P_{\mu\nu} = 2\sum_{k}^{N/2} c^k_\mu c^{k*}_\nu \tag{5}$$

in terms of the π-spinless MO(k), LCAO coefficients c^k_μ.

The $\varepsilon(\mu^\sigma\nu^{\sigma'})$ are related to the ε_{ij} of Eq. (1) and are given by (cf. Ref. [6])

$$\varepsilon(\mu^\sigma\nu^{\sigma'}) = \langle B(\mu^\sigma\nu^{\sigma'})|g_{12}|\hat{u}(\mu^\sigma\nu^{\sigma'})\rangle \tag{6}$$

with $\hat{u}(\mu^\sigma\nu^{\sigma'})$, a AO-AO′ pair correlation function dependent on $\sigma\sigma'$ being $\alpha\beta$ or $\alpha\alpha$. The $\hat{u}$ are "orbital-orthogonal" rigorously, now to all the AO's, as in the original form of the theory [3, 6].

$$\langle \hat{u}(\mu^\sigma\nu^{\sigma'})|\lambda\rangle_{\vec{r}_1} = 0; \quad \lambda \in \{\text{all AO's}, \sigma \text{ and } \pi\}\,. \tag{7}$$

In Eq. (4) for π-systems, all multi-center cross-terms [6] have been neglected as for planar π-systems (excluding triple bonds) there are no one center cross terms anyway. However unlike in the MO-theory ZDO, here, two center exchange-terms which due to the difference of $\varepsilon(\mu^\alpha\nu^\beta)$ and $\varepsilon(\mu^\alpha\nu^\alpha)$, have been retained. In a correlation approximation strictly analogous to ZDO, one would have

$$\varepsilon(\mu^\alpha\nu^\beta) \underset{(\text{full ZDO-like})}{\cong} \varepsilon(\mu^\alpha\nu^\alpha)\,. \tag{8}$$

In that case Eq. (8) substituted in (4) would yield [8]

$$\boxed{\begin{aligned} E_{\mathrm{corr}} \underset{\substack{(\pi) \\ (\text{full ZDO-like})}}{\cong} &\sum_{\mu>\nu\geqq 1}^{(\text{all } \pi \text{ AO})} (P_{\mu\mu}P^*_{\nu\nu} - \tfrac{1}{2}|P_{\mu\nu}|^2)\,e^{\mu\nu} \\ &+ \tfrac{1}{4} \sum_{\mu\geqq 1}^{(\text{all } \pi \text{ AO})} |P_{\mu\mu}|^2\,e^{\mu\mu}\,. \end{aligned}} \tag{9}$$

where

$$e^{\mu\nu} \equiv \varepsilon^{\mu^\alpha\nu^\beta} \underset{(\text{full ZDO})}{\cong} \varepsilon^{\mu^\alpha\nu^\alpha}\,,$$

and

$$e^{\mu\mu} \equiv \varepsilon^{\mu^\alpha\mu^\beta}\,.$$

However, except for large internuclear distances where $e^{\mu\nu}$ reduces to the usual Van-der Waals dispersion attractions [20, 6], there is no reason to expect Eq. (8) to hold. In atoms the $\varepsilon(\alpha\alpha)$ and $\varepsilon(\beta\beta)$ differ appreciably [3, 6].

One can then either use different values [8] for $\varepsilon(\mu^\alpha\nu^\beta)$ and $\varepsilon(\mu^\alpha\nu^\alpha)$ in Eq. (4) in a semi-empirical method at the usual π-bond distances, or replace Eq. (8), by what may be a more reasonable approximation. Pamuk [17, 21], and independently but for a different purpose, i.e. to reparametrize σMO-theory itself, Brown and Roby [18] have implicitly used [22] such a different approximation which also simplifies Eq. (4) more than Eq. (9). This approximation which we shall refer to as the "Factor Two (F2)-Approximation" is

$$\varepsilon(\mu^\alpha\nu^\beta) \underset{(\mathrm{F2})}{\approxeq} 2\varepsilon(\mu^\alpha\nu^\alpha)\,. \tag{10}$$

Substitution of Eq. (10) in Sinanoğlu's Eq. (4) above yields

$$\boxed{\begin{aligned} E_{\mathrm{corr}} \overset{(\mathrm{F2})}{\underset{\pi}{\approxeq}} \tfrac{1}{4} \sum_{\substack{\mu,\nu \\ (\mu\neq\nu)}} P_{\mu\mu}P^{*}_{\nu\nu}\bar{\varepsilon}_{\mu\nu} \\ + \tfrac{1}{4}\sum_{\mu} |P_{\mu\mu}|^2\, \varepsilon(\mu^\alpha\mu^\beta) \end{aligned}}_{(\mathrm{F2})} \tag{11a}$$

where

$$\bar{\varepsilon}_{\mu\nu} \equiv \varepsilon(\mu^\alpha\nu^\beta) + \varepsilon(\mu^\alpha\nu^\alpha)\,. \tag{11b}$$

Thus $\bar{\varepsilon}_{\mu\nu}$ with the bar $(-)$ is the sum of $(\alpha\beta)$ and $(\alpha\alpha)$ pair correlations and was defined by Pamuk as an "effective pair energy" [17]. In the F2-approximation $\bar{\varepsilon}_{\mu\nu}$ strictly would become $(3/2)\,\varepsilon(\mu^\alpha\nu^\beta)$ due to Eq. (10). However, since neither $\varepsilon(\alpha\beta)$ nor $\varepsilon(\alpha\alpha)$ values are available as a function of internuclear distance *a priori*, $\bar{\varepsilon}_{\mu\nu}$ is derived semi-empirically and may be considered as a parameter in the (F2) context as such.

Eq. (11a) simplifies the two center terms eliminating P_{pq} $(p \neq q)$, while one center terms remain unchanged, as the π-systems considered in this paper have only one π-AO per center.

There are two primary input parameters in the "F2-method" which is the main concern of this paper, Eq. (11). These are 1) the two center πAO $-$ πAO$'$ effective $(\alpha\beta + \alpha\alpha)$ pair correlation value $(\bar{\varepsilon}_{\mu\nu})$, and the one-center $\varepsilon(2p_z^2)$ (cf. Ref. [23]).

Evaluation of the One- and Two-Center MET-Type "Effective Pair Correlation Parameters" for Planar π-Systems

The two-center correlation energies depend on the internuclear distance, R_{pq}, as well as the atomic orbitals to which they belong. The Hydrogen molecule is one system whose correlation energy has been studied extensively in a large internuclear distance-range [24]. The absolute value of the correlation energy of this system remains almost constant up to the equilibrium distance, then rapidly decreases with increasing distance. Let us assume that the π two-center "effective pair energies" behave similarly, and can be represented by an equation:

$$\bar{\varepsilon}_{pq} = \tfrac{1}{2}(\bar{\varepsilon}_{pp} + \bar{\varepsilon}_{qq})\, f(R_{pq}, p, q) \tag{12}$$

for the internuclear distances larger than the equilibrium distance. The function f can be fitted to the correlation energy values estimated from the empirical Pariser-Parr γ_{pq} parameters using the detailed analysis of these parameters given by Sinanoğlu and Orloff [9]. For this, in the present F2-method, Pamuk [17] interprets the empirical two-center Pariser-Parr parameter γ'_{pq} as

$$\gamma'_{pq} \underset{(F2)}{=} \gamma^{HF}_{pq} + \bar{\varepsilon}_{pq} . \tag{13}$$

This identification of γ'_{pq} (empirical) depends on which E^{π}_{corr} approximation is used along with the HF MO, ZDO approximation and how the semi-empirical E^{π}_{corr} expression is combined term by term with the E^{π}_{HF} (ZDO), i.e. the Pariser-Parr-Pople expression, [8], in

$$E^{\pi} = E^{\pi}_{HF}(ZDO) + E^{\pi}_{corr} . \tag{14}$$

Pamuk [17], and Brown and Roby [18, 25] have given forms which put some correlation also in the one-electron MO-matrix elements H'_{pq}. Sinanoğlu [8], in different approximations, adds the E^{π}_{corr} to the two-electron HF MO matrix elements only, this being closer to the rigorous formalism of electron correlation theory [3]. The F2-method here, nevertheless dictates the use of the form [17] given by Eq. (13).

Coming back to the evaluation of Eq. (12), we note that for $R_{pq} \to 0, f(R_{pq}) \to 1$, i.e. $\bar{\varepsilon}_{pq} \to \varepsilon(p^{\alpha} p^{\beta})$.

a) The One-Center Parameter

Empirically one-center Coulomb repulsion parameters are obtained from the Pariser formula [26]. Considering the valence state carbon charge transfer reaction

$$\dot{C} + \dot{C} \to C^{+} + \ddot{C}^{-} \tag{15}$$

Pariser used

$$\gamma'_{pp} = I_C - A_C , \tag{16}$$

where I_C and A_C are valence state ionization potential and valence state electron affinity, respectively.

The HF energy change, ΔE_{HF}, for the reaction in Eq. (15) and the energy change, $\Delta E^{orbital}_{HF}$, due to the changes in the σ and π orbitals have been calculated by Sinanoğlu and Orloff [9]. Then the HF Coulomb parameters were obtained from

$$\gamma^{HF}_{pp} = \Delta E_{HF} - \Delta E^{orbital}_{HF} . \tag{17}$$

Finally using Eq. (13) they found $\bar{\varepsilon}_{pp} = -1.09$ eV (for one center $\bar{\varepsilon}_{pp} = \varepsilon(p^{\alpha} p^{\beta})$).

b) The Two-Center Parameter

The semi-empirical π-electron theory has been fitted to the spectroscopic states of benzene to obtain empirical parameters for use in π-systems [27]. The resulting two-center empirical γ'_{pq} $(p \neq q)$ are $\gamma'_{00} = 11.35$ eV, $\gamma'_{01} = 7.19$ eV, $\gamma'_{02} = 5.77$ eV, and $\gamma'_{03} = 4.97$ eV. Assuming these parameters can be represented by a continuous function of the internuclear distance, R_{pq}, the following poly-

Table 1. Coulomb repulsion integrals for π-system carbon valence state-like Hartree-Fock orbitals and the two-center effective correlation parameter, $\bar{\varepsilon}_{pq}(=\varepsilon_{pq}(\alpha\beta)+\varepsilon_{pq}(\alpha\alpha))$

R_{pq}	$\gamma_{pq}^{\mathrm{HF}}$ (eV)	γ'_{pq} (eV)	$-\bar{\varepsilon}_{pq} \equiv (\gamma_{pq}^{\mathrm{HF}} - \gamma'_{pq})$ (eV)
0.0	11.69[a]	10.60[a]	1.09[a]
[0.0	12.889[b]	11.35[c]	1.539]
1.390	8.008	7.199	0.809
1.397	7.984	7.190	0.794
1.400	7.974	6.186	0.788
1.600	7.321	6.924	0.397

[a] From Ref. [9] in text.

[b] See section after Eq. (18) in text.

[c] Ref. [27] and Eq. (18).

nomial is fitted:

$$\gamma'_{pq} = -0.425_7 R_{pq}^3 + 2.281_1 R_{pq}^2 - 5.333_7 R_{pq} + 11.35 . \tag{18}$$

It has been pointed out by Sinanoğlu and Orloff [9] that the Roothaan open shell HF $2p_z$ atomic orbital of $(1s^2\, 2s\, 2p^4, {}^4P)$ of C^- is very close to the valence state average HF orbital occuring in the C^- valence state. We calculated the two-center Coulomb repulsion integrals using the diatomic integral program of Corbato and Switendick [29] for several internuclear distances around the experimental bond distances of benzene ($R_e = 1.397$ Å) with Hartree-Fock orbitals [28]. The results are given in the second column of Table 1. The empirical Coulomb repulsion parameters, given in the third column, are obtained from the polynomial in Eq. (18). The differences between the two calculations are listed in the last column. The Pamuk value [17] for the one-center $\gamma_{pp}^{\mathrm{HF}}$ indicates that both $\gamma_{pp}^{\mathrm{HF}} = 12.889$ eV and the present empirical γ'_{00} differ from the earlier results [9], probably because this $\gamma_{pp}^{\mathrm{HF}}$ does not include the energy change due to the change in the σ and π orbitals. We shall use the more accurate, older ε_{pp}. The trend of $(\gamma_{pp}^{\mathrm{HF}} - \gamma'_{pq})$ shows that the two-center correlation energy between non-neighboring atoms is very small and can be neglected. Identification of the $(\gamma'_{pq} - \gamma_{pq}^{\mathrm{HF}})$ according to the F2-approximations here, Eqs. (13) and (11b) yields the effective $\bar{\varepsilon}_{pq}$ values. In this paper the Pamuk [17] values for $\bar{\varepsilon}_{pq}$ in Table 1 will be used for $p \neq q$ although probably a better set of values can be derived from a more complete use of MET. The results in the next section for various molecules are given in such a way that even if a different $\bar{\varepsilon}_{pp}$ value were used in the future, the results would still be valid, only a proportionality factor changing.

π-System Correlation Energy as a Function of the Number of Atoms and of Rings in a Molecule

The smallness of the $\bar{\varepsilon}_{pq}$ values for non-nearest neighbor p, q's allows us to write E_{corr}^{π}, Eq. (11a) in the nearest neighbor (n.n.) approximations, as

$$E_{\mathrm{corr}}^{\pi}(\text{n.n.}) = \tfrac{1}{4} \sum_{p \geqq 1}^{N_\pi} P_{pp} \{ P_{pp} \bar{\varepsilon}_{pp} + P_{(p+1)(p+1)} \bar{\varepsilon}_{p(p+1)} + P_{(p-1)(p-1)} \bar{\varepsilon}_{p(p-1)} \} . \tag{19a}$$

This equation is for those planar π-systems in which every π-center has at most two π-center nearest neighbors. For linear systems, polyenes $P_{00} = P_{(N_\pi+1)(N_\pi+1)} = 0$. For monocyclics $P_{00} = 0$ and $P_{(N_\pi+1)(N_\pi+1)} = P_{11}$, i.e. the addition $(n_\pi + m)$ is modulo N_π.

For more general planar topologies with possibility of more than two nearest-neighbors, e.g. polycyclic aromatics we have

$$E^{\pi}_{\text{corr}}(\text{n.n.}) = \tfrac{1}{4} \sum_{p \geqq 1}^{N_\pi} P_{pp} \left\{ P_{pp}\bar{\varepsilon}_{pp} + \sum_{\substack{q \\ (q \neq p)}}^{m(p)} P_{qq}\bar{\varepsilon}_{pq} \right\}. \tag{19b}$$

For each p, the q runs over all nearest neighbors of which there are $m(p)$.

For planar hydrocarbons all one-center π effective pair energies are equal. Since the bond lengths do not vary much, we shall assume that $f(R_{pq})$, in Eq. (12), also does not change considerably for the distances around the equilibrium bond length and further that the two-center effective pair energies are proportional to values that may be taken for the one-center ones:

$$\bar{\varepsilon}_{p(p+1)} \cong \bar{\varepsilon}_{p(p-1)} \cong k\bar{\varepsilon}_{pp}\,. \tag{20}$$

In general, the charge order (or electron population) on atom p is very close to one. Since the sum of the electron populations is equal to the number of electrons, if we denote $P_{pp} = 1 - \delta_p$, the sum of the δ_p vanishes:

$$\sum_p \delta_p = 0\,. \tag{21}$$

With the help of Eqs. (20) and (21) and neglecting the terms like δ_p^2 or $\delta_p\delta_q$, Eq. (19) can be written as

$$E^{\pi}_{\text{corr}}(\text{n.n.}) \cong \tfrac{1}{4}\bar{\varepsilon}_{pp}(\nu + 2kB)\,, \tag{22}$$

where ν is the number of the π-electron contributing atoms in the molecule, (it is assumed that each atom contributes only one $2p$ electron); B is the number of the C–C bonds between C-atoms each contributing a π-electron, and $k = \bar{\varepsilon}_{pq}/\bar{\varepsilon}_{pp}$ (only for neighboring atoms).

B can be expressed in terms of the number of rings, ϖ, and the number of atoms, ν:

$$B = \nu + \bar{\omega} - 1\,. \tag{23}$$

Then the correlation energy expression becomes:

$$\boxed{E^{\pi}_{\text{corr}}(\text{n.n.}) \cong \tfrac{1}{4}\bar{\varepsilon}_{pp}[(1+2k)\nu + 2k\bar{\omega} - 2k]}_{\text{(F2)}} \tag{24}$$

Assuming $\bar{\varepsilon}_{pp} = -1.09$ eV and $\bar{\varepsilon}_{pq} = -0.79$ eV, we obtain $k = 0.7284$ and

$$E^{\pi}_{\text{corr}}(\text{n.n.}) \underset{\text{(in eV)}}{\cong} 0.397 - 0.669\nu - 0.397\bar{\omega}\,. \tag{25}$$

Rather than Eq. (25), the Eq. (24) is of course more significant since there could be different values of $\bar{\varepsilon}_{pp}$ and k used. On the other hand one could also extract the $\bar{\varepsilon}_{pp}$ and k values, if one had sufficiently complete non-empirical E^{π}_{corr} values for a set of molecules after testing their ν and $\bar{\omega}$-dependence.

In the following section we shall apply the above equations (especially Eq. (25)) to various types of planar π-molecules. In comparing the above equations with CI calculations on π-systems in the literature it needs to be kept in mind that our equations like Eq. (25) refer to the total E^{π}_{corr}, i.e. including the "internal", "semi-internal", and "all-external" correlations as in MET, Eq. (2). On the other hand, what is usually referred to as "full CI", e.g. for the benzene π-system in the literature, corresponds to CI with all the dets that can be formed from the $2p_{\pi}$-orbitals only. Thus "full CI" in that sense is only the "internal correlation" E_{int} of NCMET [30].

Also one may note that in the present semi-empirical E^{π}_{corr}, we have assumed that the "decoupled" or at least some type of transferable effective pair correlations suffice as predicted by MET [3, 20] and found to be true recently for many atoms and molecules by many workers [31, 3c]. However, MET also makes allowance for the calculation of three and more electron correlation remainders [3], R', which are in fact dominant in the other extreme of the uniform infinite electron gas [31]. Thus although still at benzene pair correlations seem quite adequate, it remains to be studied by non-empirical MET-CI procedures [3, 31] to what extent this is true in larger systems approaching a layer of graphite.

Applications

a) Linear Chains-Polyenes

Since $\bar{\omega} = 0$, Eq. (25) takes a simpler form:

$$E^{\pi}_{\mathrm{corr}}(\mathrm{n.n.}) \cong \tfrac{1}{4}\bar{\varepsilon}_{pp}[(1+2k)\nu - 2k]_{\mathrm{F2}}\,, \tag{26a}$$

or

$$E^{\pi}_{\mathrm{corr}}(\mathrm{n.n.}) \cong 0.397 - 0.669\nu \ \ (\text{in eV})\,. \tag{26b}$$

In Table 2 correlation energies obtained by the present effective pair correlation energy method (EPCE)-F2, are compared with the CI and best AMO results. For ethylene Eq. (26) gives only 84% of the correlation energy obtained by CI or AMO methods [32], but then this is subject to the lower $\bar{\varepsilon}_{pp}$ we used. In the case of butadiene, the correlation energy found by the EPCE-F2 method agrees very well with a CI treatment [33]. The AMO value for butadiene is smaller [34]. The slope of Eq. (26) gives the correlation energy per electron in the infinite chain.

Table 2. Correlation energies in electron volts of linear chains, E^{π}_{corr} of polyenes, as compared with CI and AMO

ν	CI[a]	AMO[a]	MET-EPCE-F2 (this work)
(Ethylene) 2	-1.127	-1.120	-0.941
(Butadiene) 4	-2.200	-1.746	-2.279
$\left[\lim_{\nu\to\infty}(E^{\pi}_{\mathrm{corr}}/\nu)\right.$	—	—	$\left.-0.669\ \mathrm{eV}\right]$

[a] See Refs. in Sect. Applications a) of text.

Table 3. π-System correlation energies (in eV) of quasi-linear cyclic hydrocarbons and comparison with CI and AMO

Number of atoms		$-E^{\pi}_{corr}$ (eV)				$-E^{\pi}_{corr}/\nu$ (eV)	
	ν	MET-EPCE-F2	AMO[a]	(in text Eq. (30))	CI[a]	MET-EPCE-F2	AMO[a]
(Benzene)	6	4.014	3.696	3.78	3.054	0.669	0.616
((Naphthalene)	10	7.088	6.732	6.73	–	0.709	0.673
(Anthracene)	14	10.161	9.653	9.62	–	0.726	0.690
	18	13.234	12.465	12.54	–	0.735	0.693
(Infinitely long)	∞			-	–	0.768	0.7

[a] See Refs. in Sect. Applications b) of text.

b) Quasi-Linear Polycyclics

In these polyacenes, except the extreme ones, every ring has two neighboring rings. There is a simple relation between the number of atoms, ν, and the number of rings, $\bar{\omega}$:

$$\bar{\omega} = \tfrac{1}{4}(\nu - 2)\,. \tag{27}$$

Substituting Eq. (27) into Eq. (24) yields an equation:

$$E^{k}_{corr}(\text{n.n.}) \cong \tfrac{1}{4}\bar{\varepsilon}_{pp}[(\tfrac{5}{2}k + 1)\nu - 3k]_{k=2} \tag{28}$$

or using again $\bar{\varepsilon}_{pp} = -1.09$ eV and $k = 0.728$,

$$E^{\pi}_{corr}(\text{n.n.}) \cong 0.5955 - 0.768\,\nu \ \ (\text{eV}) \tag{29}$$

which is again a linear function of the number of π-electrons or atoms, ν. The total correlation energies and the correlation energies per electron obtained from Eq. (29), and the many parameter AMO results [35] are tabulated in Table 3. Unfortunately, CI calculations for larger systems are very difficult. $E^{\pi}_{corr} = -3.05$ eV obtained by a 22×22 CI treatment is only a portion of the total correlation energy of the π-electrons in benzene [36]. The EPCE-F2 results are constantly larger in absolute magnitudes than the AMO values. This is reasonable because these non-empirical calculations are approximations only to some of the correlation effects. The AMO results are approximately reproduced (see Table 3) if Eq. (29) is rewritten as:

$$E^{\pi}_{corr}(\text{AMO}) = 0.6 - 0.733\,\nu \quad (\text{eV})\,. \tag{30}$$

c) Correlation Energy Per Electron in Very Large Systems

Let us assume there exists a very large molecule as in Fig. 1, in which every ring has three neighboring rings. From Eq. (25) we expect that the limit value of the correlation energy per electron will be larger in magnitude than the one found for quasi-linear cyclic systems. Indeed the number of the rings in this system can be expressed in terms of the number of atoms as (cf. Fig. 1)

$$\bar{\omega} = \tfrac{1}{3}(\nu - 4)\,. \tag{31}$$

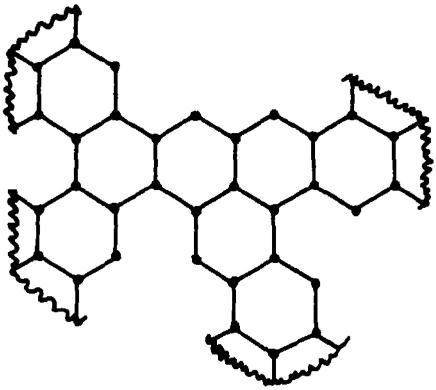

Fig. 1. A large molecule in which every ring has three neighboring rings

Then the total correlation energy is approximately

$$E^{\pi}_{\text{corr}} \cong 1.730 - 1.002\,\nu \quad (\text{eV}) \tag{32}$$

and

$$\lim_{\nu \to \infty}\left(\frac{E^{\pi}_{\text{corr}}}{\nu}\right) = -1.002 \quad (\text{eV})\,. \tag{33}$$

An estimation of the correlation energy per electron in a graphite-like layer is also possible. Let us pick a ring as the center, and draw circles as shown in Fig. 2. If we take n as the number of the circles, B, ν, and $\bar{\omega}$ can be written as follows:

$$B = 6\left[4 \sum_{i \geq 1} (i) + 1\right] \tag{34a}$$

$$\nu = 6\left[\sum_{i \geq 1} (2i + 1) + 1\right] \tag{34b}$$

$$\bar{\omega} = 6\left[\sum_{i \geq 1} (i) + \tfrac{1}{6}\right]. \tag{34c}$$

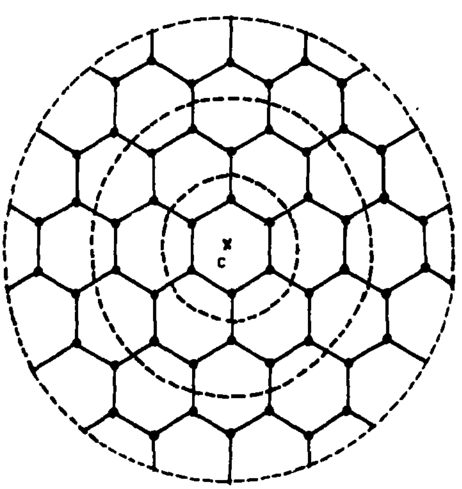

Fig. 2. A layer of graphite

The number of the bonds, B, can also be expressed as

$$B = 2\nu - 12n - 6\,. \tag{35}$$

From Eqs. (22) and (35) or Eqs. (25) and (34), we obtain

$$E^{\pi}_{\mathrm{corr}}(\mathrm{n.n.}) = 2.382 - 4.764n - 1.066\nu \quad (\mathrm{eV}) \tag{36}$$

which yields

$$\lim_{\nu \to \infty}\left(\frac{E^{\pi}_{\mathrm{corr}}}{\nu}\right) = -1.066 \quad (\mathrm{eV})\,. \tag{37}$$

Since the interactions between the layers are not included, the absolute value of the correlation energy per electron in graphite must be larger than 1.066 eV.

d) Cyclic H_6 *Molecule*

Although this molecule does not have π-electrons, theoretically, it can be treated like benzene. Its correlation energy, for $R = 2$ a.u. separation, is calculated by a 9×9 CI and found to be $E_{\mathrm{corr}} = -2.058$ eV [37]. The AMO calculation has been rather unsuccessful for this molecule, giving only a small portion of the correlation energy [38]: $E_{\mathrm{corr}} = -1.272$ eV. In the united atom approach, the correlation energy of this system would be an average of $E_{\mathrm{corr}}(^1S, \text{carbon}) = -5.415$ eV and $E_{\mathrm{corr}}(^1D, \text{carbon}) = -4.6$ eV. Therefore, we expect a higher absolute value of the correlation energy for the H_6 ring to be about 4.5 eV. Neglecting the interactions between molecules, we assume that a lower absolute value of E_{corr} should be about three times the absolute value of the correlation energy for the Hydrogen molecule, i.e. 3.18 eV. At the 2 a.u. internuclear distance the two-center correlation energy for the H_2 molecule is -0.82 eV [24]. Using $\bar{\varepsilon}_{pp}(\mathrm{H}^-) = -1.08$ eV, we find $k = 0.7593$ and from Eq. (26) we obtain $E_{\mathrm{corr}} = -4.08$ eV. This value is inbetween the two limiting estimates which we just stated. It appears to be a good value.

Conclusion

The comparison of the present results with those given by other methods shows that a simple semi-empirical model based on Sinanoğlu's many electron theory for singlet ground states (MET) is adequate to approximately predict the correlation energies of the π-electron systems. The present form of the effective pair correlation energy method (F2-Approximation) can be applied to any singlet, single determinantal system in which every atom contributes only one electron to the molecular orbitals. The extension of the method to all systems including σ electrons requires further and quite different approximations which can be made on the LCAO form of the MET pair correlations derived recently [8]. A number of semi-empirical methods for E_{corr} of σ molecules are derived in subsequent papers by Sinanoğlu and by Pamuk.

References

1. See e.g. Sinanoğlu, O., Tuan, D. F.: Annu. Rev. physic. Chem. **15**, 251 (1964); and Sinanoğlu, O.: Atomic physics, Vol. I, p. 131. New York: Plenum Press 1969.
2. Das, G., Wahl, A. C.: J. chem. Physics **44**, 87 (1966).

3a. Sinanoğlu, O.: J. chem. Physics **33**, 1212 (1960).

3b. Advances chem. Physics VI, 315 (1964); See also 3c) Sinanoğlu, O., Brueckner, K. A.: Three approaches to electron correlation in atoms. New Haven and London: Yale Press 1970.

4a. Sinanoğlu, O.: Advances chem. Physics **14**, 237 (1968).

4b. Sinanoğlu, O., Silverstone, H. J.: In: Modern quantum chemistry, Vol. II, (O.S. Ed.). New York: Academic Press. 1965.

5. A rigorous theoretical basis for atomic semi-empirical correlations was given in Ref. [3]. The suggestion was applied by a) Allen, L. C., Clementi, E., Gladney, H. M.: Rev. mod. Physics **35**, 465 (1963) who however omitted the MET (Ref. [3]) "exclusion effects" thereby arriving at incorrect pair values. The actual ground state pair correlations for B, C, N, O, F, Ne were first obtained by b) McKoy, V., Sinanoğlu, O.: J. chem. Physics **41**, 2683 (1964).

6. For semi-empirical molecular correlation energies and their theoretical aspects cf. Ref. [4a].

7. Theory of electron correlation for general non-closed shell and excited states has been applied quantitatively to several hundred excited and ground states of atoms and ions (B, C, N, O, F, Ne, Na); Sinanoğlu, O., Öksüz, I.: Physic. Rev. Letters **21**, 507 (1968), and (Mg, Al, Si, P, S, Cl); Beck, D., Sinanoğlu, O.: Physic Rev. Letters **28**, 945 (1972). The wave-functions obtained which contain all of the non-closed shell-type correlation effects yield e.g. the optical transition probabilities to a few percent accuracy in contrast to the Hartree-Fock method's factors of 2–10 discrepancies with experiments (cf. Beck and Sinanoğlu, O. (1972) Ref. above and Westhaus, P., Sinanoğlu, O.: Physic. Rev. **183**, 56 (1969).

8. Sinanoğlu, O.: To be published.

9. Sinanoğlu, O., Orloff, M. K.: Modern quantum chemistry, Vol. I (Ed. O. Sinanoğlu). New York: Academic Press 1965.

0. The MET [3, 9] showed some time ago that E_{corr} rigorously separates into

$$E_{\text{corr}} = E^{\pi}_{\text{corr}} + E^{\sigma}_{\text{corr}} + E^{\sigma\pi}_{\text{corr}}\,.$$

Further $\sigma - \pi$ interactions are predicted to be appreciable [5b, 9]. The theory also shows that -correlations change with the occupation of π-MO's (MET-"exclusion effect"). For σ, π-electron spectra, the non-closed shell theory (NCMET) [4] provides a rigorous and practicable theoretical framework. Progress along these lines has been made recently by K. Freed (to be published) and W. Rienhardt (to be published).

1. Hollister, C., Sinanoğlu, O.: J. Amer. chem. Soc. **88**, 13 (1966).

2. Ritchie, C. D., King, H. F.: J. chem. Physics **47**, 564 (1967).

3. McKoy, V.: J. chem. Physics **42**, 2232 (1965).

4. Stanton, R. E.: J. chem. Physics **36**, 1928 (1962).

5. Neshet, R. K.: J. chem. Physics **36**, 1518 (1962).

6. By "experimental E_{corr}" we mean $(E_{\text{exp}} - E_{\text{HF}} - E_{\text{REL}})$. This can in general involve errors if the HF calculations taken from the literature had not reached the HF limit, if E_{REL} is estimated poorly, and further, if E_{exp} has used some high inner ionization potentials which are experimentally poorly known.

7. Pamuk, H. Ö.: Ph.D. Thesis, Chem. Dept., Yale University (1968).

8. Brown, R. D., Roby, K. R.: Theoret. chim. Acta (Berl.) **16**, 291 (1970).

9. Labzowski (Leningrad, ca. 1970; Ref. could not be located).

0. c.f. Refs. [3a, b], [4a], and Sinanoğlu, O.: Potential energy surfaces and reactive scattering. Comm. Ato., Molec. Phys. III, 53 (1971).

1. Pamuk [17] has obtained similar approximations also by retaining overlap in MO's and using the Mulliken approximations (MULAP) instead of ZDO. The approximations that have to be made in the lengthy MULAP forms however, are not as clear as in the ZDO forms. Pamuk [17] has also compared such one and two center approximations with PPM [11]. The PPM also had MO's with overlap retained and used overlap containing gross populations.

2. Pamuk [17] initially arrived at Eq. (11) in somewhat more *ad hoc* ways than presented in this paper. That, Eq. (10) yields Eq. (11) when substituted in Sinanoğlu's equation (4) has been noticed more recently by the present authors.

3. Prior to the appearance of the first theoretically reasonable value of $E(2p_z^2)$ in the literature given by McKoy and O. Sinanoğlu (Ref. [5b]; "MET V") based on MET, it had been customary to neglect, e.g. in the L-shell of Neon atom, all $2s2p$ and other correlations except $(2p_i^2)$ $(i = x, y, z)$. This neglect led to very large (3 eV) values of $E(2p_z^2)$.

24. Fischer-Hjalmars, I.: In: Modern quantum chemistry, Vol. I (Ed. O. Sinanoğlu). New York: Academic Press 1965.
25 Brown and Roby [18] found different corrections for $\gamma_{\mu\mu}^{HF}$ in the diagonal and non-diagonal matrix elements of HF operator F_0. This does not agree with the semi-empirical calculations in which the same parameter is used in diagonal and nondiagonal matrix elements of F_0.
26. Pariser, R.: J. chem. Physics **21**, 568 (1953).
27 Parr, R. G.: Quantum theory of molecular electronic structure. New York: W. Benjamin, Inc. 1964.
28. See also: Pamuk, Ö., Sinanoğlu, O.: Hacettepe Fen ve Muhendislik Dergisi 1, 41 (1971).
29. The integral program, QCPE 29 DIAT, was written by Corbato and Switendick, and modified for IBM 7090 computer system by E. B. Moore. For details see Corbato, F. J., Switendick, A. C. in Methods in computational physics, Vol. 2. New York and London: Acad. Press Inc. 1963.
30. Sinanoğlu, O., Cizek, J.: Chem. Physics Letters **1**, 337 (1967); (Full internal correlation of benzene π-system and its components).
31 E.g. Davidson, E. R.: In: Sigma molecular orbital theory (O. Sinanoğlu and K. B. Wiberg, Eds.). New Haven and London. Yale Press 1970.
32 Lowe, J. P.. J. chem. Physics **41**, 502 (1964)
33 Pulman, A.: J. chem. Physics **51**, 188 (1954).
34 Paunez, R.: In: Molecular orbitals in chemistry, physics, and biology. A tribute to R. S. Mulliken (1964).
35 Swalen, J. D., de Heer, J.: J. chem. Physics **40**, 378 (1964).
36. Moskowitz, J. W., *et al.* Quart. Perog. Rep. **47**, Solid State and Molecular Theory Group MIT (1963).
37 Mattheiss, L.: Physic. Rev. **123**, 1209 (1961).
38 Moskowitz, J. W.: J. chem. Physics **38**, 677 (1963).

Prof. Dr. Sinanoğlu
Sterling Chemistry Laboratory
Yale University
New Haven, Connecticut 06520, USA

Theoret. chim. Acta (Berl.) 27, 303—313 (1972)
© by Springer-Verlag 1972

Semiempirical Molecular Orbital Studies of Phthalocyanines

II. The Electronic Structure and Excited States of Copper Phthalocyanine, CuPc

A. Henriksson, B. Roos, and M. Sundbom

Institute of Theoretical Physics, University of Stockholm, Vanadisvägen 9,
S-113 46 Stockholm, Sweden

Received May 23, 1972

A semi-empirical MO method, the PEEL method, has been applied in an investigation of the electronic structure and excited states of copper phthalocyanine. The absorption spectrum of CuPc is discussed and assignments are made. New bands of $n-\pi^*$, $d-d$ and CT types are predicted. The calculated values of ESR parameters accord very well with experimental values, indicating that the method gives a correct electronic distribution.

Eine semiempirische MO-Methode, die PEEL-Methode, wurde bei der Untersuchung der Elektronenstruktur und der angeregten Zustände von Kupferphthalocyaninen angewendet. Das Absorptionsspektrum des CuPc wird interpretiert. Neue Banden vom $n-\pi^*$-, $d-d$- und CT-Typ werden vorhergesagt. Die berechneten Werte der ESR-Parameter stimmen gut mit den experimentellen Werten überein, wodurch gezeigt wird, daß die Methode eine korrekte Elektronenverteilung ergibt.

Une méthode d'OM semi-empirique, la méthode PEEL, est appliquée à l'étude de la structure électronique et des états excités de la phtalocyanine du cuivre. Le spectre d'absorption de CuPc est discuté et des attributions sont effectuées. De nouvelles bandes de type $n-\pi^*$, $d-d$ et CT sont prédites. Les valeurs calculées des paramètres ESR sont en bon accord avec les valeurs expérimentales, indiquant que la méthode donne une distribution électronique correcte.

1. Introduction

In a previous investigation we have studied the electronic structure and the excited states of copper porphin, CuP, [1]. We have now applied the same semiempirical SCF MO method (in the following denoted the Peel method [2-4]) to study copper phthalocyanine, CuPc. A Pariser-Parr-Pople CI study of free base phthalocyanine, H_2Pc, has also recently been performed [5].

In the Peel method the metal ion is explicitly taken into account. This method permits a study of the metal ligand bond and an analysis of the different types of electronic transitions ($d-d$, CT, and $\pi-\pi^*$), found in the electronic spectrum.

Taube [6] used the simple Wolfsberg-Helmholz (W-H) method on a whole series of metal phthalocyanines, but he presented no detailed results for CuPc. Chen, Abkowitz, and Sharp [7] have published W-H calculation results together with their ESR study of CuPc. Recently Schaffer performed extended Hückel calculations on several metal phthalocyanines [8].

The extended Hückel method allows for a discussion of the magnetic properties and the geometry of the complexes. It can however only be used for a qualitative description of the excited states, since electron repulsion is not explicitly included. The present study predicts new bands (*d*−*d* and CT). ESR parameters have been calculated and accord very well with experimental values.

2. Details of the Calculation

Method. The Peci method, which is used in the present investigation, has been thoroughly presented elsewhere [1–4]. It includes the valence electrons of the metal atom, the ligand lone-pair electrons and the π electrons of the ligands. Excited states are calculated by means of the method of superposition of configurations, where all types of singly excited configurations are included. The fixed parameters used in the present calculation are determined from experimental data from a chosen set of small standard molecules, and they are the same parameters used in the previous calculations on porphin [9], phthalocyanine [5] and copper porphin [1].

Geometry. Crystalline H_2Pc and CuPc exist in at least two polymorphic modifications: the stable β-form and the unstable α-form. The molecular geometry used in the present calculations is based on X-ray data for the β-form [10]. The molecule is considered to be planar with D_{4h} symmetry. The assumed geometry together with the numbering of the atoms are shown in Fig. 1.

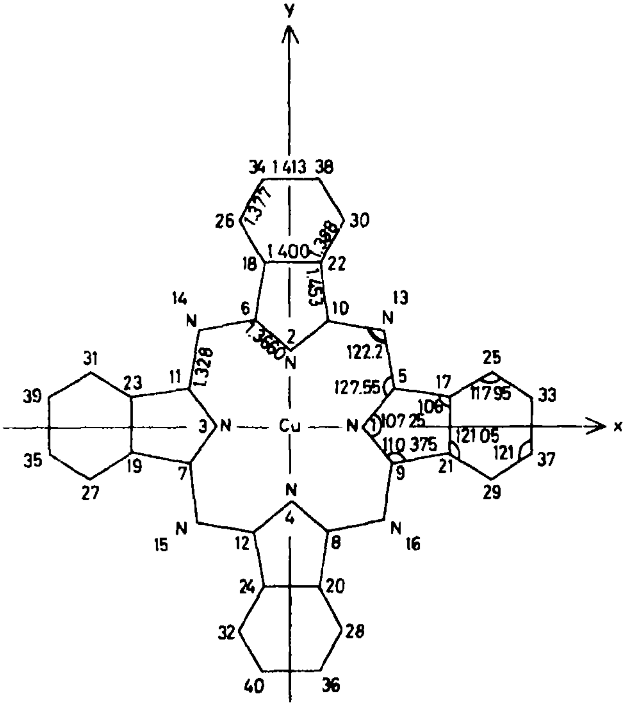

Fig. 1. The numbering system and the geometry of CuPc used in the present investigation. The geometry is based on X-ray data [10] (the arithmetic means of the published values)

Calculations. The atomic orbitals that constitute the basis for the calculation are 57: 40π orbitals in the phthalocyanine ring, $8sp^2$-hybridized nitrogen lone-pair orbitals, the $3d$, $4s$, and $4p$ orbitals of the copper atom. The number of electrons taken into account is 67: 9 from the copper ion and 58 from the ring.

The self-consistent field molecular orbitals have been calculated by means of a computer program, SCF-OPSZDO, written by Roos and Sundbom. This program calculates the energy levels of excited states by mixing configurations obtained from single excitations. An IBM 360/75 computer was used.

3. Molecular Orbitals and Ground State Properties

The SCF molecular orbitals of CuPc are presented in Table 1, where the orbital energies, ε_i, and the electronic populations are given. The orbital pattern is very similar to the one found in CuP [1]. The orbital $1b_{2g}$ is purely metallic ($3d_{xy}$). The singly occupied orbital $2b_{1g}$ is mainly metallic with 71% $3d$ character. $2a_{1g}$ is also mainly metallic $3d$ (78%). The occupied e_g orbitals show the same general structure as was obtained by Chen *et al.* [7] from their Hückel calculations. The orbital $4a_{2u}$ is stabilized by mixing with the $4p_z$ orbital of the copper ion.

The total electron population of the atomic orbitals is given in Table 2. The configuration of the copper atom is found to be $(3d)^{9.143}(4s)^{0.536}(4p)^{0.474}$. The net charge on copper is thus +0.848. For copper porphin the calculations gave $(3d)^{9.168}(4s)^{0.543}(4p)^{0.483}$ with a net charge on copper of +0.801. The interaction between the phthalocyanine π system and the copper results in a transfer of electrons (0.14) from the ring to $4p_z$ orbitals of Cu in the molecular orbitals of symmetry a_{2u}. An electron transfer in the opposite direction (0.09) takes place from the $3d_{xz}$ and $3d_{yz}$ orbitals of Cu in the molecular orbitals of symmetry e_g.

4. Excited States

The transition energies were calculated by superposition of singly excited configurations. The program and the computer limit the number of configurations of each symmetry to 140. Thus only a reduced number (~50%) of single excitations could be considered. Transitions between orbitals with the largest energy difference were omitted. This reduction leads to an error in the transition energies, which we estimate to be of the order +1 kK. We have, however, reduced the number of configurations in each symmetry by about the same amount. Thus the transition energies can be expected to come out in the correct order.

There are three types of singly excited configurations arising from excitations of an electron from.

1. A doubly occupied orbital to the half filled orbital $2b_{1g}$.
2. $2b_{1g}$ to an empty orbital.
3. A doubly occupied orbital to an empty orbital.

Table 1. Molecular orbitals of CuPc. Orbital energies ε_i in a.u. The electronic population. The numbering system as in Fig. 1

No	MO[b] φ_i		The electronic population[a,c]											
	Symmetry[c]	ε_i	N_1[d]	C_5	N_{13}[d]	C_{17}	C_{25}	C_{33}	z^2	xy	x^2-y^2	$xz+yz$	s	$x+y$
1	$1a_{1g}$	−0.6493	0.164*n*						0.193				0.1520	
2	$1b_{1g}$	−0.5845	0.178*n*								0.288			
3, 4	$1e_g$	0.5604	0.176	0.054	0.028	0.011	0.002	0.001				0.647		
5	$1a_{2u}$	−0.5494	0.084	0.047	0.037	0.012	0.003	0.001						
6	$1b_{2g}$	−0.5148								1.000				
7	$1b_{2u}$	−0.4981	0.087	0.037		0.028	0.011	0.005						
8, 9	$1e_u$	−0.4958	0.458*n*											0.167
10, 11	$2e_g$	−0.4731	0.002	0.029	0.043	0.055	0.036	0.025				0.658		
12	$1b_{1u}$	−0.4523		0.058	0.113	0.007	0.003	0.000						
13	$2a_{2u}$	−0.4469	0.020	0.001	0.002	0.025	0.041	0.047						
14	$2b_{2u}$	−0.4368	0.056	0.008		0.011	0.033	0.046						
15, 16	$3e_g$	−0.4353	0.003	0.042	0.093	0.018	0.050	0.069				0.190		
17	$2a_{1g}$	−0.4115	0.025*n*						0.784				0.116	
18	$3a_{1g}$	0.3857			0.250*n*									
19, 20	$2e_u$	−0.3857			0.500*n*									
21	$2b_{2g}$	0.3857			0.250*n*									
22, 23	$4e_g$	0.3775	0.048	0.065	0.030	0.034	0.049	0.035				0.233		
24	$1a_{1u}$	−0.3595		0.014		0.024	0.070	0.017						
25	$3a_{2u}$	0.3458	0.073	0.003	0.027	0.033	0.000	0.035						
26	$2b_{1u}$	−0.3410		0.001	0.013	0.013	0.082	0.022						
27, 28	$5e_g$	0.3319	0.009	0.018	0.058	0.032	0.111	0.052				0.020		
29	$3b_{2u}$	0.3282	0.032			0.059	0.000	0.050						
30, 31	$6e_g$	−0.3156	0.105	0.007	0.003	0.089	0.008	0.066				0.202		
32	$4a_{2u}$	−0.2926	0.031	0.004	0.105	0.030	0.001	0.019						
33	$2a_{1u}$	−0.2309		0.094		0.005	0.017	0.009						
34	$2b_{1g}$	−0.1199	0.072*n*								0.7122			
35, 36	$7e_g$	−0.0372	0.076	0.095	0.103	0.030	0.012	0.019				0.034		
37	$3b_{1u}$	0.0383		0.016	0.065	0.045	0.001	0.031						
38	$4b_{2u}$	0.0397	0.035	0.029		0.004	0.056	0.019						
39; 40	$8e_g$	0.0602	0.010	0.010	0.024	0.039	0.133	0.051				0.002		
41	$5a_{2u}$	0.0618	0.002	0.004	0.012	0.016	0.076	0.022						
42	$3a_{1u}$	0.0956		0.010		0.036	0.005	0.074						
43; 44	$9e_g$	0.1005	0.011	0.035	0.003	0.058	0.024	0.125				0.003		
45	$5b_{2u}$	0.1159	0.039	0.051		0.024	0.025	0.006						
46	$4b_{1u}$	0.1285		0.029	0.044	0.002	0.016	0.056						
47; 48	$10e_g$	0.1657	0.057	0.103	0.085	0.025	0.025	0.025				0.010		
49	$6a_{2u}$	0.1673	0.010	0.059	0.063	0.009	0.004	0.001						
50	$4a_{1u}$	0.2014		0.008		0.060	0.033	0.025						
51	$4a_{1g}$	0.2052	0.061*n*						0.023				0.732	
52; 53	$11e_g$	0.2096	0.005	0.042	0.030	0.110	0.050	0.033						
54	$5b_{1u}$	0.2130		0.021	0.015	0.057	0.024	0.015					0.001	
55; 56	$3e_u$	0.2828	0.042*n*											1.833
57	$7a_{2u}$	0.3079	0.030	0.007	0.003	0.001								

[a] Formal population of the virtual orbitals. N_i and C_i denotes π orbitals on nitrogen and carbon. z^2 stands for $3d_{z^2}$, *s* for 4*s* and *x* for $4p_x$.

[b] The 33 lowest orbitals are doubly occupied. Orbital no. 34 contains the odd electron.

[c] For orbitals of *e* symmetry the sum of the populations for e_x and e_y is given.

[d] The letter *n* after the number indicates a nitrogen σ lone pair orbital. Otherwise the orbital is a nitrogen π orbital.

Table 2. The electronic population of the atomic orbitals in CuPc and H_2Pc

AO[a]	CuPc	H_2Pc	
n_1	1.722	2.000	
n_2	1.722	—	
n_{13}	2.000	2.000	
N_1	1.454	1.232	1.453
N_2	1.454	1.675	
N_{13}	1.107	1.146	
C_5	0.963	0.925	0.939
C_6	0.963	0.952	
C_{17}	0.968	0.959	0.981
C_{18}	0.968	1.003	
C_{25}	1.035	1.030	1.020
C_{26}	1.035	1.010	
C_{33}	0.998	1.019	1.012
C_{34}	0.998	1.003	
d_{z^2}	1.954		
d_{xy}	2.000		
$d_{x^2-y^2}$	1.288		
$d_{xz,yz}$	1.951		
4s	0.536		
p_x, p_y	0.167		
p_z	0.141		

[a] n denotes a nitrogen σ lone pair orbital. N and C denote π orbitals on nitrogen and carbon.

The first two types of excitations gives rise only to doublet states, while the third results in two doublet states (singdoublets and tripdoublets) and one quartet state. The singdoublets correspond to the singlets in phthalocyanine, whereas the tripdoublets correspond to the triplets. The triplets are forbidden but the tripdoublets are slightly allowed because of the interaction between the phthalocyanine triplet and the unpaired metal electron.

The results of the present CI treatment are given in Tables 3–5. In Table 3 the allowed doublets (< 55 kK) are given together with the two lowest quartets and those forbidden doublets with a considerable $d-d$ or CT character. In column one of Table 3 the exited states are roughly classified as:

1. Transitions within the phthalocyanine ring: P denotes $\pi-\pi^*$ transitions. n_b denotes $n-\pi^*$ transitions from the bridge nitrogen lone pairs. n_i denotes $n-\pi^*$ transitions from inner nitrogens.
2. Charge transfer transitions to the phthalocyanine orbitals from the metal orbital $2b_{1g}$ (labelled CT).
3. $d-d$ transitions on Cu.

A detailed presentation of the configuration mixing for some of the excited states is found in Table 4. Only those configurations which contribute to the wave function with coefficients larger than 0.2 are given in the table.

Table 3. Electronic transitions below 55 kK in CuPc. Calculated allowed transitions. The two lowest quartets and some forbidden singdoublets

Calculated				Observed[a] (vapour)		
Type[b]	Symmetry[c]	ν (kK)	f[d]	Notation	ν (kK)	Range (kK)
P	${}^4E_u$	9.8	-			
P	${}^2E_u(T)$	10.1	0.0002			
P	${}^2E_u(S)$	18.4	0.44	Q	15.2	14-17
n_i + CT	${}^2E_g$	20.6	-			
P	${}^4E_u$	21.0	—			
P	${}^2E_u(T)$	21.6	0.00000			
n_b	${}^2B_{2u}(T)$	22.0	z-pol.			
$d-d$	${}^2A_{1g}$	23.1				
$d-d$	${}^2E_g$	23.3	—			
P	${}^2E_u(T)$	26.6	0.00006			
$d-d$	${}^2B_{2g}$	26.8				
P	${}^2E_u(T)$	30.3	0.0001			
P	${}^2E_u(T)$	31.2	0.0006			
n_b	${}^2B_{2u}(S)$	31.4	z-pol.			
P	${}^2E_u(T)$	34.4	0.001			
P	${}^2E_u(S)$	34.5	2.1	B	30.8	26-36
P	${}^2E_u(S)$	35.3	1.4			
P	${}^2E_u(S)$	36.6	0.01			
n_i + CT	${}^2B_{2u}$	38.3	z-pol.			
P	${}^2E_u(T)$	39.6	0.00002			
P	${}^2E_u(T)$	39.7	0.00003			
P	${}^2E_u(S)$	40.1	0.00003	N	36.2	shoulder
n_b	${}^2A_{2u}$	41.7				
CT	${}^2A_{1u}$	41.7	-			
P	${}^2E_u(T)$	41.8	0.001			
n_b	${}^2B_{2u}$	42.3	z-pol.			
P	${}^2E_u(T)$	42.6	0.0003			
P	${}^2E_u(S)$	42.9	0.002	L	41.6	38-42
P	${}^2E_u(S)$	45.1	0.0001			
P	${}^2E_u(T)$	46.2	0.00003			
P	${}^2E_u(S)$	47.7	0.11			
CT	${}^2A_{2u}$	48.8				
P	${}^2E_u(T)$	48.9	0.002			
P	${}^2E_u(S)$	50.0	0.79	C	45.8	43-50
P	${}^2E_u(T)$	50.8	0.005			
P	${}^2E_u(S)$	52.6	0.08			
P	${}^2E_u(T)$	53.3	0.06			
P	${}^2E_u(S)$	53.9	0.05			
P	${}^2E_u(T)$	54.0	0.003			
P	${}^2E_u(S)$	55.1	0.38			

[a] See Ref. [11].

[b] P: $\pi-\pi^*$ transitions in the phthalocyanine ring.
n_b: $n-\pi^*$ transitions from bridge nitrogens,
n_i: $n-\pi^*$ transitions from inner nitrogens,
CT: Charge transfer transitions.

[c] T stands for tripdoublet and S for singdoublet, cf. Table 4.

[d] For each E_u doublet, the theoretical f value is given for one transition of the degenerate pair.

Table 4. Configuration mixing[a] for some of the excited states of CuPc

Symmetry[b]	ν (kK)	Wave function[b]
^4E_u	9.8	$0.97(2a_{1u}-7e_g)^Q+\cdots$
$^2E_u(T)$	10.1	$0.97(2a_{1u}-7e_g)^T+\cdots$
$^2E_u(S)$	18.4	$0.89(2a_{1u}-7e_g)^S-0.40(4a_{2u}-7e_g)^S+\cdots$
^2E_g	20.6	$0.90(2b_{1g}-7e_g)+0.14(1b_{1g}-7e_g)^S+0.26(1b_{1g}-7e_g)^T+\cdots$
^4E_u	21.0	$0.88(4a_{2u}-7e_g)^Q+0.25(3a_{2u}-7e_g)^Q+\cdots$
$^2E_u(T)$	21.6	$0.88(4a_{2u}-7e_g)^T+0.21(3a_{2u}-7e_g)^T+\cdots$
$^2B_{2u}(T)$	22.0	$0.69(2e_u-7e_g)^T-0.43(2b_{2g}-3b_{1u})^T+0.30(2e_u-10e_g)^T+0.25(3a_{1g}-6a_{2u})^T+\cdots$
$^2A_{1g}$	23.1	$0.98(2a_{1g}-2b_{1g})+\cdots$
^2E_g	23.3	$-0.53(6e_g-2b_{1g})+0.48(2e_g-2b_{1g})-0.45(4e_g-2b_{1g})+0.34(1e_g-2b_{1g})$ $-0.24(2b_{1g}-7e_g)+\cdots$
$^2E_u(T)$	26.6	$0.36(3a_{2u}-7e_g)^T-0.33(3b_{2u}-7e_g)^T+0.31(6e_g-3b_{1u})^T+0.30(2a_{1u}-8e_g)^T$ $+0.26(5e_g-5a_{2u})^T-0.26(2b_{1u}-8e_g)^T+0.24(1a_{1u}-8e_g)^T-0.24(5e_g-4b_{2u})^T+\cdots$
$^2B_{2g}$	26.8	$1.00(1b_{2g}-2b_{1g})$
$^2B_{2u}(S)$	31.4	$0.75(2e_u-7e_g)^S-0.43(2b_{2g}-3b_{1u})^S+0.22(2b_{2g}-4b_{1u})^S+0.21(3a_{1g}-6a_{2u})^S+\cdots$
$^2E_u(S)$	34.5	$0.57(4a_{2u}-7e_g)^S-0.55(3b_{2u}-7e_g)^S+0.31(2a_{1u}-7e_g)^S-0.20(3a_{2u}-7e_g)^S+\cdots$
$^2E_u(S)$	35.3	$0.61(4a_{2u}-7e_g)^S+0.50(3b_{2u}-7e_g)^S-0.28(6e_g-3b_{1u})^S-0.25(3a_{2u}-7e_g)^S$ $+0.23(2a_{1u}-7e_g)^S-0.21(2b_{1u}-7e_g)^S+\cdots$
$^2E_u(S)$	36.6	$-0.50(3a_{2u}-7e_g)^S+0.37(2b_{1u}-7e_g)^S-0.28(1a_{1u}-7e_g)^S+0.27(6e_g-4b_{2u})^S$ $+0.26(5e_g-3b_{1u})^S-0.25(3b_{2u}-8e_g)^S+\cdots$
$^2B_{2u}$	38.3	$0.78(2b_{1g}-4b_{2u})+0.48(2b_{1g}-5b_{2u})+0.13(1b_{1g}-4b_{2u})^S+0.24(1b_{1g}-4b_{2u})^T+\cdots$
$^2A_{1u}$	41.7	$0.99(2a_{1u}-2b_{1g})+\cdots$
$^2B_{2u}$	42.3	$0.45(2e_u-7e_g)^S+0.78(2e_u-7e_g)^T+\cdots$
$^2E_u(S)$	47.7	$0.60(1a_{1u}-7e_g)^S+0.41(2b_{1u}-7e_g)^S+0.20(2a_{1u}-8e_g)^S+\cdots$
$^2E_u(S)$	50.0	$0.64(2a_{1u}-8e_g)^S+0.27(5e_g-5a_{2u})^S+0.25(2a_{1u}-9e_g)^S-0.22(6e_g-4b_{2u})^S$ $-0.22(2b_{1u}-8e_g)^S+0.21(4a_{2u}-8e_g)^S+\cdots$
$^2E_u(S)$	55.1	$0.39(6e_g-3b_{1u})^S+0.34(6e_g-4b_{2u})^S+0.32(5e_g-3b_{1u})^S+0.28(1a_{1u}-7e_g)^S$ $-0.27(2a_{1u}-9e_g)^S-0.21(3a_{2u}-7e_g)^S+\cdots$

[a] The configurations are those appropriate to the state.

$(k-v)^T=\frac{1}{\sqrt{6}}[2(kv\bar{o})-(k\bar{v}o)-(\bar{k}vo)]$ and $(k-v)^S=\frac{1}{\sqrt{2}}[(k\bar{v}o)-(\bar{k}vo)]$, where o stands for $2b_{1g}$.

[b] Q stands for quartet, T for tripdoublet and S for singdoublet.

Table 5. Populations for some excited states in CuPc. Population for the ground state. Change from the ground state population for the excited states

te	$3d_{z^2}$	$3d_{xy}$	$3d_{x^2-y^2}$	$3d_{xz}+3d_{yz}$	$4s$	$4p_x+4p_y$	$4p_z$	$\sum_{i=1}^{4} n_i$[a]	$\sum_{i=13}^{16} n_i$[a]	π[b]
ound state	1.954	2.000	1.288	3.902	0.536	0.334	0.141	6.888	8.000	41.95
$_g$: 20.6	0.000	0.000	−0.236	−0.038	0.000	0.000	0.000	−0.630	0.000	+0.90
$_{g}$: 23.1	−0.888	0.000	+0.707	0.000	−0.076	0.000	0.000	+0.256	0.000	0.00
$_g$: 23.3	0.000	0.000	+0.675	−0.821	0.000	0.000	0.000	+0.250	0.000	−0.10
$_{g}$: 26.8	0.000	−1.000	+0.712	0.000	0.000	0.000	0.000	+0.288	0.000	0.00
$_{u}$: 38.3	0.000	0.000	−0.253	0.000	0.000	0.000	0.000	−0.732	0.000	+0.98
$_{u}$: 41.7	0.000	0.000	0.000	+0.018	0.000	0.000	0.000	0.000	−1.000	+0.98
$_{u}$: 41.7	0.000	0.000	+0.712	0.000	0.000	0.000	0.000	+0.292	0.000	−1.00
$_{u}$: 42.3	0.000	0.000	0.000	+0.018	0.000	0.000	0.000	0.000	−1.000	+0.98
$_{u}$: 48.8	0.000	0.000	+0.709	0.000	0.000	0.000	−0.055	+0.288	0.000	−0.94

[a] n_i denotes a nitrogen σ lone pair orbital.

[b] The π system of the phthalocyanine ring.

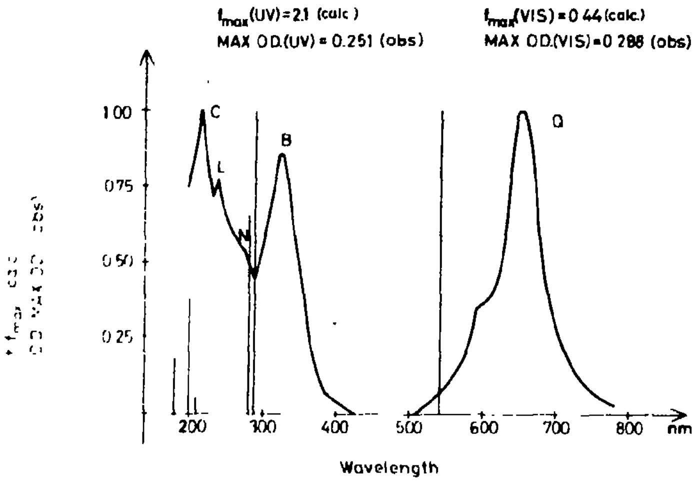

Fig. 2. Observed vapor-phase absorption spectra of CuPc from [11]. Calculated $\pi-\pi^*$ singlets with f 0.2. Cf. Table 3. The calculated transitions are found to be around 3 kK too high in energy in comparison with observations. For further discussion, see text

For some of the excited states, Table 5 shows the change in electronic population in comparison with the ground state population. Edwards and Gouterman [11] recently published vapour absorption spectra of several metal phthalocyanines. They found five bands (*Q*, *B*, *N*, *L*, and *C*) characteristic for the ring for all the phthalocyanines studied. Their data for CuPc is quoted in Table 3 and Fig. 2.

Transitions within the Phthalocyanine Ring

The observed *Q*, *B*, *N*, *L*, and *C* bands all can be attributed to allowed $\pi-\pi^*$ singdoublets. The calculated strong ^2E_u transition at 18.4 kK is assigned as the *Q* band. The blue of the *Q* band is predicted to contain two weakly allowed tripdoublets: the $\pi-\pi^*$ transition ^2E_u (21.6 kK) and the $n-\pi^*$ transition $^2B_{2u}$ (22.0 kK; z-polarized, from the bridge nitrogen lone pairs). These two transitions may be responsible for the observed shoulder on the high energy side of the *Q* band. It has, however, been suggested that this shoulder should be due to the $Q(1-0)$ vibronic band [11].

Two calculated, close intense $\pi-\pi^*$ transitions at 34.5 and 35.3 kK are assigned to the *B* (Soret) band. Previous calculations on H_2Pc [5] gave three $\pi-\pi^*$ transitions in the *B* band region. These results indicate that the *B* band has a more complicated structure than the *Q* band for both copper phthalocyanine and the free base. Three weakly allowed transitions are further predicted to be found in the *B* band: an $n-\pi^*$ singdoublet at the low energy side (31.4 kK, z-polarized, from the nitrogen bridge lone pairs), one $\pi-\pi^*$ tripdoublet at 34.4 kK, and one $\pi-\pi^*$ singdoublet at 36.6 kK.

The calculations give three weak $\pi-\pi^*$ tripdoublets (39.6, 39.7, 41.8 kK) and one weak $\pi-\pi^*$ singdoublet (40.1 kK), all of which are to be found in the observed *N* band region. The calculation also gives several weak $\pi-\pi^*$ transitions in the L band. The calculated $n-\pi^*$ transition at 42.3 kK is expected to be located in the N, L region. A strong calculated $\pi-\pi^*$ transition at 50.0 kK is assigned as the C band. The calculations further show that the C band also contains several weaker $\pi-\pi^*$ transitions.

Previous calculations of the excited states of H_2Pc [5] gave a spectral pattern in good agreement with experimental findings. In the present investigation the calculated transitions are consistently found to be around 3 kK too high in energy in comparison with observations. The discrepancy between calculated and experimental values may partly be ascribed to our not taking into account all singly excited configurations as we did for H_2Pc. As mentioned previously this will cause an error of around +1 kK. The main reason for the discrepancy is probably due to an overemphasized bonding between the copper ion and the phthalocyanine ring in our model. The $4a_{2u}$ and $3a_{2u}$ orbitals may have been somewhat exessively stabilized, which would lead to a too large shift of the bands in comparison with the free base. The same effect was found in the calculations for copper porphin [1]. The choice of geometry can also influence the calculated spectrum. A geometry with a somewhat larger hole size would weaken the metal-ligand bonding and cause a smaller shift.

It should, however, be stressed that the method is not expected to give an exact detailed description of the electronic spectra. But we think that it does give a reasonable pattern of the electronic energy levels, which can be used as a basis for spectral assignments and for searching for new bands.

As pointed out previously [1], calculations with the present parameters will give too low values for tripdoublets and quartets. In copper porphin the calculated gap (6.2 kK) between the lowest tripdoublet and the Q band was found to be 3 kK too high in comparison with experiment. For CuPc the corresponding gap is calculated to be 8.3 kK, considerably larger than in copper porphin. The energy gap between the lowest tripdoublet and quartet levels is calculated to be 300 cm^{-1}. It is of the same size as found in copper porphin. The fact that CuPc has a larger gap between Q and the lowest tripdoublet and quartet may explain why CuPc has a much weaker luminescence [12] than CuP [13].

Ligand Field and Charge Transfer States

Excited states of organic transition metal compounds are conventionally classified as: $d-d$ transitions, charge transfer transitions, and ligand $\pi-\pi^*$ transitions. As pointed out in previous works on copper complexes [1–4] it is not always possible to make this simple classification. In the present CI treatment there will be a mixing of configurations of different types for some of the transitions.

In the preceeding section we discussed transitions with mainly ligand character. They give rise to the five band pattern (Q, B, N, L, and C) also observed in free base phthalocyanine [5, 13]. Some of the transitions can also be classified as almost pure CT or $d-d$ transitions, as can be seen in Tables 3–5.

The lowest forbidden doublet is a ${}^2E_g$ transition at 20.6 kK. According to Tables 4 and 5 it can be classified as mainly a $n-\pi^*$ transition from the inner nitrogens. But it has also some CT character. This state is at 2.2 kK higher energy than the strong ^2E_u state, assigned as the Q band. It can thus not contribute to radiationless decay.

The calculation predicts three forbidden $d-d$ transitions between the Q and the B bands: $^2A_{1g}$(23.1 kK), ^2E_g(23.3 kK), and $^2B_{2g}$(26.8 kK). They should thus appear in the phthalocyanine window (18–25 kK), where a weak absorption has been observed for some metal phthalocyanines, but not yet for copper [13].

An allowed $^2B_{2u}$ transition at 38.3 kK (z-polarized), is predicted to be found at high energy side of the B band. It is mainly a $n-\pi^*$ transition (from the inner nitrogens) with some CT character.

5. Electronic Paramagnetic Resonance

A calculation of paramagnetic resonance parameters was performed by means of second order perturbation theory [2, 14] using calculated values for the excitation energies. The hyperfine structure parameters were obtained with the constant $\varkappa$ in the Fermi contact term equal to 0.30 [15]. For the spin-orbit coupling constant the free atom value -828 cm^{-1} was used [16].

Quite many experimental studies of the ESR spectrum of CuPc have been reported in the literature (see Refs. [17, 7] for a review of experimental data). The experimental values of the ESR parameters reported in [17] and [7] are given in Table 6 together with our calculated values. The good agreement with the most recent measurements indicates that the calculated electronic distribution is correct, as the g-values and the hyperfine structure constants are very sensitive to the electronic distribution in normal and excited states.

Table 6. Electronic paramagnetic resonance parameters for CuPc[a]

	Calculated	Observed	
		Ref. [17]	Ref. [7]
$g_{\parallel}$	2.18	2.160	2.158 ± 0.001
$g_{\perp}$	2.04	2.045	2.041 ± 0.001
$A_{\parallel}$	201	217	212 ± 5
$A_{\perp}$	27	31.5	29 ± 2
A_N^{iso}	17	17	17 ± 1

[a] A values in units of 10^{-4} cm^{-1}.

Acknowledgement. This investigation has been supported by grants from the Swedish Natural Science Research Council. The authors wish to express their gratitude to Professor Inga Fischer-Hjalmars for her encouraging interest throughout the work. One of us (A.H.) wish to express her gratitude for grants from Ella and Georg Ehrnrooths stiftelse, Helsingfors.

References

1. Roos, B., Sundbom, M.: J. Mol. Spectry **36**, 8 (1970).
2. Roos, B.: Acta chem. scand. **20**, 1673 (1966).
3. Roos, B.: Acta chem. scand. **21**, 1855 (1967).
4. Roos, B.: Svensk Kem. Tidskr. **80**, 204 (1968).

5. Henriksson, A., Sundbom, M.: Theoret. chim. Acta (Berl.), (in press).
6. Taube, R.: Z. Chem. **6**, 8 (1966).
7. Chen, I., Abkowitz, M., Sharp, H.: J. chem. Physics **50**, 2237 (1969).
8. Schaffer, A. M.: Ph. D. Thesis in preparation.
9. Sundbom, M.: Acta chem. scand. **22**, 1317 (1968).
10. Brown, C. J.: J. chem. Soc. A **1968**, 2488.
11. Edwards, L., Gouterman, M.: J. Mol. Spectry **33**, 292 (1970).
12. Rieckhoff, K. E., Voigt, E. M.: In: Molecular luminescence, ed. Lim, E. C. New York: Benjamin 1969.
13. Eastwood, D., Gouterman, M.: J. Mol. Spectry **30**, 437 (1969).
14. Abragam, A., Pryce, M. H. L.: Proc. Roy. Soc (London) A **205**, 135 (1951).
15. Falk, K.-E., Ivanova, E., Roos, B., Vänngård, T.: Inorg. Chemistry **9**, 566 (1970).
16. Maki, A. H., McGarvey, B. R.: J. chem. Physics **29**, 31 (1958).
17. Guzy, C. M., Raynor, J. B., Symons, M. C. R.: J. chem. Soc. A **1969**, 2299.

A. Henriksson
Department of Physical Chemistry
University of Helsinki
Meritullink 1
Helsinki 17, Finland

Dr. M. Sundbom
Institute of Theoretical Physics
University of Stockholm
Vanadisvägen 9
113 46 Stockholm, Sweden

Theoret. chim. Acta (Berl.) 27, 315—324 (1972)
© by Springer-Verlag 1972

Effect of Atomic Dipole in Semi-Empirical Calculation of π-Electron Energy Levels

Jiro Higuchi

Department of Chemistry, Yokohama National University, Minami-ku, Yokohama, Japan

Received June 26, 1972

The importance of the effect of atomic dipole is emphasized and clarified in semi-empirical calculations for π-electron energy levels of molecules with lone pair electrons. The actual examples taken up here are the excitation energies in CO_2 molecule and NCN radical. The calculation was carried out by improving the treatment used for oxygen molecule by Fumi and Parr [1]. It is shown that the experimental results cannot satisfactorily be explained by disregarding the terms of charge-dipole interaction except in some limited cases.

Die Bedeutung des Effekts von Atomdipolen wird hervorgehoben und in semiempirischen Rechnungen für π-Elektronen Energieniveaus von Molekülen mit einsamen Elektronenpaaren näher erläutert. Als Beispiel werden die Anregungsenergien des CO_2 Moleküls und des NCN Radikals berechnet. Diese Berechnung wurde mit der von Fumi und Parr [1] für das Sauerstoffmolekül benutzten Methode, die verbessert wurde, durchgeführt. Es wird gezeigt, daß die experimentellen Ergebnisse nur in Ausnahmefällen ohne Berücksichtigung der Ladungs-Dipol-Wechselwirkung zufriedenstellend erklärt werden können.

Introduction

On the multipole expansion of charge distribution in molecules, the second important part is the charge (monopole)-dipole interaction. However, in usual semi-empirical calculation of π-electron energy levels such as Pariser-Parr-Pople method [2], such terms are not *explicitly* included. In the present work, the importance of the effect of charge-dipole interaction will be emphasized and clarified by a semi-empirical calculation for π-electron energy levels of some symmetric linear molecules in which such a contribution is predominant. The examples taken up here are ACA-type molecules, which A is an atom with lone pair electrons and C is a central carbon atom bonded to the two A atoms. In this case, the σ bonding electrons of the C atom may simply be assumed as the *sp* hybridized orbitals:

$$\chi_{\substack{1C\\2C}} = 2^{-1/2}[\chi_{sC} \pm \chi_{\sigma C}]\,. \tag{1}$$

where χ_{sX} and $\chi_{\sigma X}$ are, respectively, the 2*s* and the 2*pσ* orbitals of atom X. If the 2*s*-character of A atom with N_A valence electrons is taken as n_A, the bonding and the lone pair σ orbitals of A atom may be expressed as

$$\chi_{bA} = (1+\lambda_A^2)^{-1/2}[\chi_{sA} + \lambda_A \chi_{\sigma A}] \tag{2}$$

and

$$\chi_{lA} = (1+\lambda_A^2)^{-1/2}[\lambda_A \chi_{sA} - \chi_{\sigma A}]\,, \tag{3}$$

respectively, where

$$\lambda_A = [(n_A - 1)/(2 - n_A)]^{1/2}\,. \tag{4}$$

Including the effect of atomic dipoles, the Coulomb integrals of atoms C and A are described as follows:

$$\begin{aligned}\alpha_C = W_{\pi C} - F_{\pi C} - 2N_A(A:\pi_C\pi_C) + 2n_A(\pi_C\pi_C : s_A s_A)\\ + 2(N_A - n_A)(\pi_C\pi_C : \sigma_A\sigma_A) - 4\lambda_A(1+\lambda_A^2)^{-1}(\pi_C\pi_C : s_A\sigma_A)\end{aligned} \tag{5}$$

and

$$\begin{aligned}\alpha_A = W_{\pi A} - F_{\pi A} - 4(C:\pi_A\pi_A) + (\pi_A\pi_A : s_C s_C) + (\pi_A\pi_A : \sigma_C\sigma_C)\\ - N_A(A':\pi_A\pi_A) + n_A(\pi_A\pi_A : s_{A'} s_{A'}) + (N_A - n_A)(\pi_A\pi_A : \sigma_{A'}\sigma_{A'})\\ - 2\lambda_A(1+\lambda_A^2)^{-1}(\pi_A\pi_A : s_{A'}\sigma_{A'}),\end{aligned} \tag{6}$$

where $W_{\pi X}$ is average π-electron energy of the corresponding valence state of the X atom, $F_{\pi X}$ is an average interaction energy of the π-electron in question with the other π-electrons in the same atom,

$$(X:pq) = \int \chi_p^*(1)(1/r_{X1})\chi_q(1)\,d\tau_1 \tag{7}$$

and

$$(pq:rs) = \iint \chi_p^*(1)\chi_r^*(2)(1/r_{12})\chi_q(1)\chi_s(2)\,d\tau_1\,d\tau_2\,. \tag{8}$$

The last term of Eqs. (5) and (6) is evidently due to the charge-dipole interaction. The other procedures adopted are similar with those of oxygen molecule by Fumi and Parr [1] in which the assumption of zero overlap and zero differential overlap was made except that in a same atom. The $W_{\pi A}$'s for various values of n_A are linearly interpolated as a function of n_A from the ionization energy of the corresponding valence state with $s^2p^{N_A-2}$ configuration and that with sp^{N_A-1} configuration. The $F_{\pi A}$'s and the other one-center integrals were estimated from the experimental data [3] using the method of least-squares. The two-center integrals of CO_2 molecule are taken from the paper by Mulligan [4], and those of NCN and HCCCH radicals are obtained by using the simple Slater orbitals with orbital exponent of $\delta_C = 1.625$ and $\delta_N = 1.950$. The internuclear distances are taken as $R_{CO} = 1.162\,A$, $R_{CN} = 1.232\,A$ and $R_{CC} = 1.277\,A$[1] and $1.3084\,A$[2]. The LCAO-MO's used are the solutions of the restricted Hartree-Fock equations.

CO_2 Molecule

In the CO_2 molecule, the three lowest excited states observed [7] are due to the excitation of one of the π-electrons from the ground state ${}^1\Sigma_g^+$ into the other π-orbitals. They are the ${}^1B_2$, ${}^1A_1$, and ${}^1B_1$ states with symmetry of C_{2v} corresponding to the ${}^1\Delta_u$, ${}^1\Delta_g$, and ${}^1\Sigma_g^-$ states with symmetry $D_{\infty h}$, respectively. This may show the fact that the CO_2 molecule is a fairly suitable example for knowing the contribution of the charge-dipole interaction, although the definite values of the vertical excitation energies may be rather difficult to estimate because of lack of the experimental data. In the present work, these energies from the ground state ${}^1\Sigma_g^+$ to the lower electronic states were calculated by varying the ratio of $2s-2p$ hybridization of the oxygen orbitals, (2) and (3), and also the value of resonance integral $\beta_{CO}(CO_2)$ between the π-orbitals of carbon and oxygen. The ${}^1\Delta_g$ state obtained is always close to locate the ${}^1\Sigma_g^-$ state in good agreement with the experiment [7].

---

[1] The internuclear distance of C_3 radical [5].

[2] The internuclear distance of allene molecule [6].

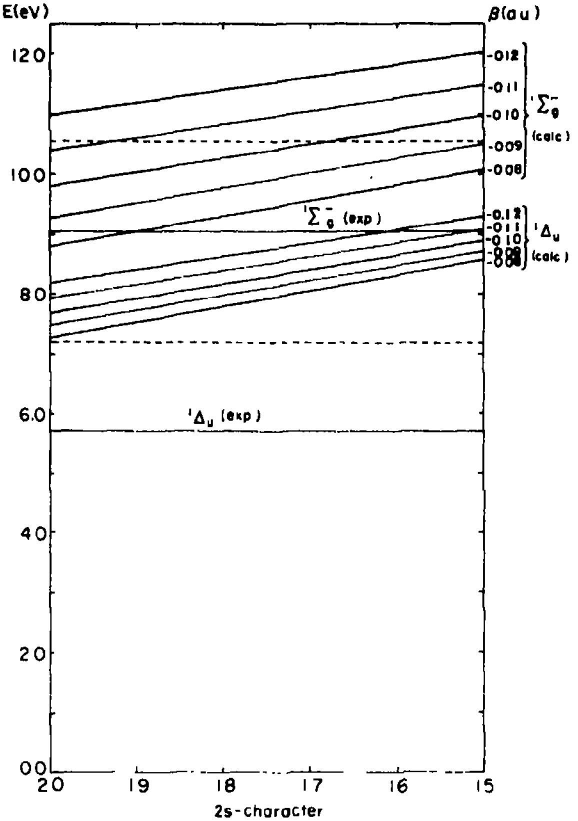

Fig. 1. Vertical π-electron excitation energies without charge-dipole interaction in CO_2 molecule as a function of 2s-character of oxygen and of resonance integral between π-orbitals of carbon and oxygen (β). The horizontal full lines are the experimental excitation energies to the $^1B_2(^1\Delta_u)$ and the $^1B_1(^1\Sigma_g^-)$ states with equilibrium structure, while the dotted lines are the roughly estimated ones to these states with linear structure, i.e. 1.5 eV above the experimental values

The vertical excitation energies from the ground state $^1\Sigma_g^+$ to the $^1\Delta_u$ and the $^1\Sigma_g^-$ states calculated for various conditions are shown in Figs. 1 and 2 corresponding to the cases without and with the terms of charge-dipole interaction, respectively. In these cases, the restricted configuration interaction (CI) was included among $(1\pi_u)^4(1\pi_g)^4$, $(1\pi_u)^4(1\pi_g)^2(2\pi_u)^2$, $(1\pi_u)^3(1\pi_g)^4(2\pi_u)$ and $(1\pi_u)^4(1\pi_g)^3(2\pi_u)$. Because of lack of experimental data, the vertical excitation energies to these states may roughly be estimated to be 1.5 ± 0.3 eV above the values between the most stable structures of the states concerned. It should be noted here that the results without CI and those without charge-dipole interaction are completely unsatisfactory in elucidating both the excitation energies, even if the change of the molecular structure in the excited states is taken into consideration. As can be seen in Fig. 2, however, the results with such interactions are fairly good under some restricted conditions: for example, $n_O = 1.90 \sim 1.96$ for $\beta_{CO}(CO_2) = -0.13$ a.u., and $n_O = 1.80 \sim 1.83$ for $\beta_{CO}(CO_2) = -0.14$ a.u. Evidently, this does show the

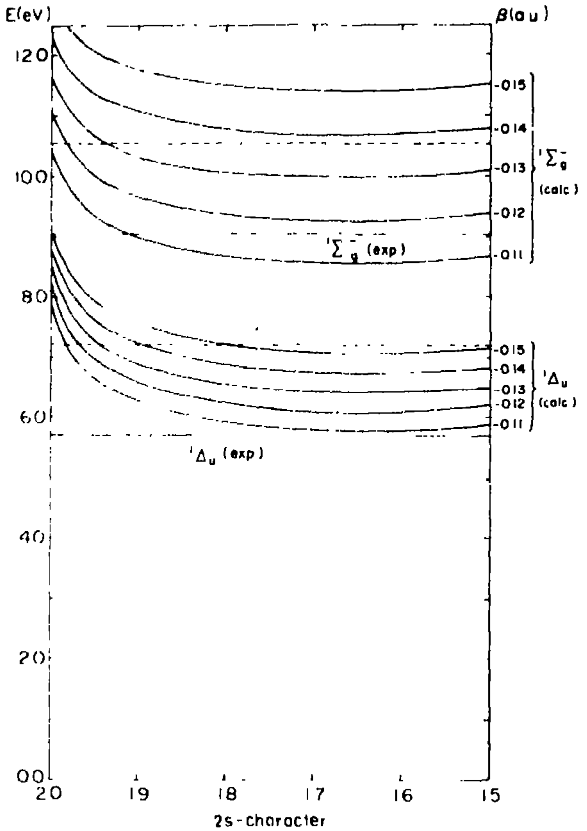

Fig. 2. Vertical π-electron excitation energies with charge-dipole interaction in CO_2 molecule as function of 2s-character of oxygen and of resonance integral between π-orbitals of carbon an oxygen (β). The horizontal full lines are the experimental excitation energies to the $^1B_2(^1\Delta_u)$ and t $^1B_1(^1\Sigma_u^-)$ states with equilibrium structure, while the dotted lines are the roughly estimated ones these states with linear structure, i.e. 1.5 eV above the experimental values

importance of inclusion of the electron-atomic dipole interaction. Table 1 give the two examples for the calculated vertical excitation energies of the low electronic states with $n_O = 1.90$ and $\beta_{CO}(CO_2) = -0.13$ a.u. and those wit $n_O = 1.80$ and $\beta_{CO}(CO_2) = -0.14$ a.u. Although these results should not be fina the probable values of the 2s-character of oxygen n_O do not essentially contradic to the σ-electron populations of $(2s)^{1.84}(2p\sigma)^{1.16}$ obtained from the SCF-LCAO MO's by Mulligan [4].

NCN Radical

Although the electronic structure of the NCN radical is rather similar t that of the oxygen molecule, the observed lower electronic states due to th $\pi_u - \pi_g$ type excitation have hardly been known, except for the $^3\Sigma_u^-$ state [8 Therefore, the estimation of excitation energies from the ground state $^3\Sigma_g^-$ t

Table 1. Vertical π-electron excitation energies in CO_2 molecule (eV)

State	$n_O = 1.90$ $\beta = -0.130$ a.u.				$n_O = 1.80$ $\beta = -0.140$ a.u.			
	With charge-dipole interaction		Without charge-dipole interaction		With charge-dipole interaction		Without charge-dipole interaction	
	With CI	Without CI	With CI	Without CI	With CI	Without CI	With CI	Without CI
$^1\Sigma_g$	10.36	11.60	11.81	12.58	10.79	12.21	12.63	13.37
$^3\Sigma_g^-$	10.26	11.54	11.74	15.85	10.66	11.19	12.56	16.76
$^1\Delta_g$	10.19	11.73	11.67	12.63	10.60	12.36	12.49	13.44
$^3\Delta_g$	9.96	10.92	11.37	11.97	10.34	11.51	12.18	12.75
$^3\Sigma_g^+$	9.67	10.24	10.97	11.36	10.17	10.80	11.77	12.13
$^1\Sigma_g^+$	8.47	9.62	9.70	10.84	8.96	10.07	10.44	11.54
$^1\Delta_u$	6.90	6.27	8.65	8.36	6.88	6.13	9.13	8.85
$^1\Sigma_u$	6.75	6.11	8.61	8.33	6.67	5.92	9.08	8.81
$^3\Sigma_u$	6.75	6.11	8.61	8.33	6.67	5.92	9.08	8.81
$^3\Delta_u$	6.22	5.58	8.16	7.87	6.11	5.36	8.62	8.34
$^3\Sigma_u^+$	5.70	5.05	7.70	7.42	5.55	4.80	8.15	7.88
$^1\Sigma_g^+$	0.00	0.00	0.00	0.00	0.00	0.00	0.00	0.00

these states is of interest from both the experimental and the theoretical viewpoints.

In order to determine the value of resonance integral $\beta_{CN}(NCN)$ between the π-orbitals of carbon and nitrogen for the NCN radical, the values of $\beta_{CN}(HCN)$ of the HCN molecule corresponding to the various values of n_N (2s-character of nitrogen) were chosen so as the calculated excitation energy of $^1\Sigma^+(^1A'') \leftarrow {}^1\Sigma^+$ to give the experimental value of 7.434 eV. The procedure used here is quite the same as in the previous CO_2 molecule. Then, the values of $\beta_{CN}(NCN)$ were determined adopting the relation of

$$[\beta_{CN}(NCN)/\beta_{CN}(HCN)] \cong [S_{CN}(NCN)/S_{CN}(HCN)], \tag{9}$$

where the S_{CN} is the overlap integral between π-orbitals of carbon and nitrogen. Using the $\beta_{CN}(NCN)$ so obtained, the restricted SCF-LCAO-MO's were determined and the $\pi - \pi$ excitation energies were calculated for various values of n_N. In these calculations, the vertical excitation energy of the HCN molecule was estimated from the experimental data [9] by assuming that the vibrations of the HC and the CN fragments are harmonic and that the potential energy curve of the HCN bending vibration is quartic parabolic. The electronic configurations included in the restricted CI calculations are as follows: $(1\pi)^4$, $(1\pi)^3(2\pi)$ and $(1\pi)^2(2\pi)^2$ for the HCN molecule, and $(1\pi_u)^4(1\pi_g)^2$, $(1\pi_u)^2(1\pi_g)^4$, $(1\pi_u)^4(2\pi_u)^2$, $(1\pi_u)^3(1\pi_g)^2(2\pi_u)$, $(1\pi_u)^3(1\pi_g)^3$, and $(1\pi_u)^4(1\pi_g)(2\pi_u)$ for the NCN radical. The calculated excitation energies of the NCN radical from the ground state $^3\Sigma_g^-$ are shown as a function of n_N in Figs. 3 and 4, corresponding to the cases without and with charge-dipole interaction, respectively.

Comparing these two figures, the excitation energies to the $^1\Sigma_u^-$, $^3\Delta_u$, and $^3\Sigma_u^+$ states are significantly different near $n_N = 1.98$. This is apparently due to the fact that in the case with charge-dipole interaction the electron configuration with

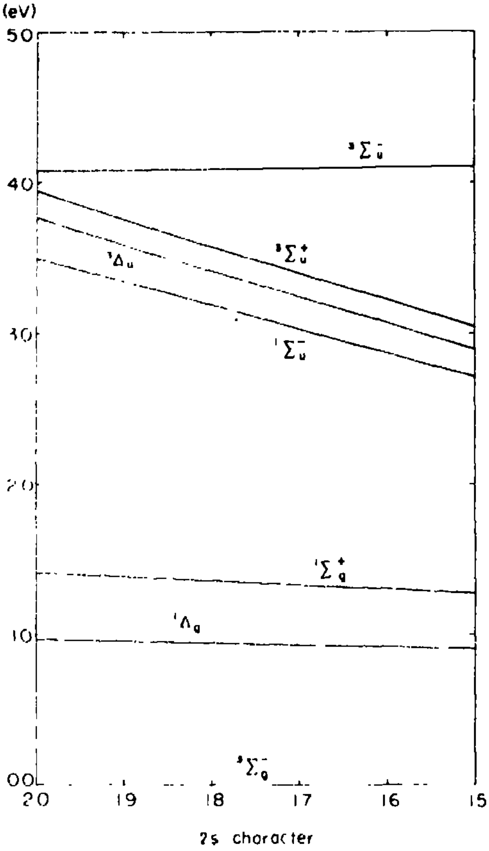

Fig. 3 Vertical π-electron excitation energies without charge-dipole interaction in NCN radical as a function of 2s-character of nitrogen

the greatest contribution changes from $(1\pi_u)^3(1\pi_g)^3$ to $(1\pi_u)^4(1\pi_g)(2\pi_u)$ at this proximity when the n_N decreases, while the main configuration does not change in the case without such an interaction.

Since the calculated excitation energy of the observed state $^3\Sigma_u^-$ $(\Delta E_{obs} \cong 4.1$ eV) is relatively insensitive to the n_N, it may be difficult to determine the most preferable value of n_N from only the present results, although the n_N of NCN may slightly be smaller than the n_O of CO_2. As an example, the calculated vertical excitation energies of the NCN radical from the ground state $^3\Sigma_g^-$ to the lower electronic states at $n_N = 1.80$ are given in Table 2. It may be noted here that the change of these excitation energies with charge-dipole interaction is not large in the range of $1.80 \geqq n_N \geqq 1.50$ as compared with the case without such terms. The reason why the values of β_{CN}(NCN) are slightly different according to the cases with and without CI is due to the fact that these values used in the calculations with and without CI were determined from the excitation energy of $^1\Sigma^+(^1A'') \leftarrow {}^1\Sigma^+$ in the calculation of HCN with and without CI, respectively. Of course,

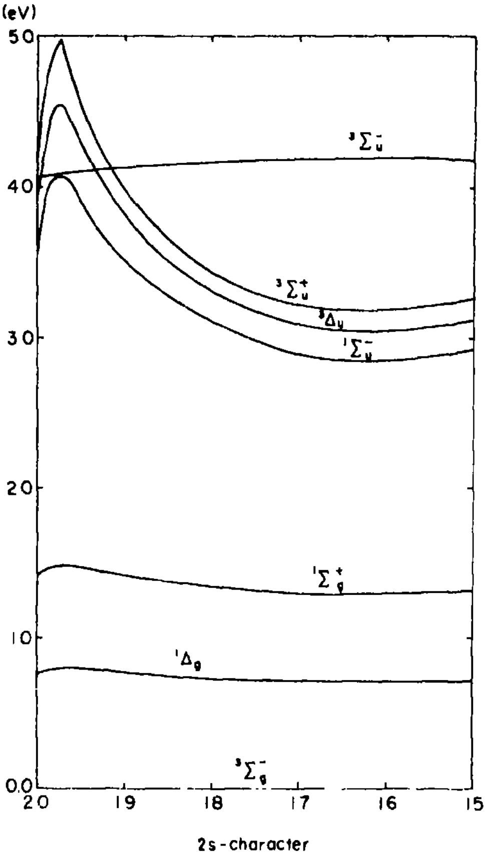

Fig. 4. Vertical π-electron excitation energies with charge-dipole interaction in NCN radical as a function of 2s-character of nitrogen

Table 2. Vertical π-electron excitation energies in NCN radical (eV) [$n_N = 1.80$]

State	With charge-dipole interaction		Without charge-dipole interaction	
	With CI	Without CI	With CI	Without CI
$^1\Delta_u$	5.37	6.54	5.28	6.50
$^3\Sigma_u^-$	4.17	5.56	4.08	5.54
$^3\Sigma_u^+$	3.45	2.49	3.57	2.55
$^3\Delta_u$	3.30	2.38	3.41	2.43
$^1\Sigma_u^-$	3.09	2.27	3.19	2.32
$^1\Sigma_g^+$	1.34	1.41	1.37	1.41
$^1\Delta_g$	0.73	0.70	0.75	0.70
$^3\Sigma_g^-$	0.00	0.00	0.00	0.00
β_{CN}(NCN) (a. u.)	−0.10503	−0.10661	−0.10308	−0.10346

the results with charge-dipole and configuration interactions in Table 2 should not be conclusive but possibly may fairly be useful in estimating the π-electron excitation energies to the unobserved states.

Some Remarks

Although the present CI calculations included only the first and the second lowest excited configurations, the results obtained are of some importance and cannot essentially be changed by performing any semi-empirical improvement. It may be of special interest to see that there is a significant difference between the calculated excitation energy with the charge-dipole interaction and that without such terms. Actually, the influence of the atomic dipole is absolutely necessary for elucidating some electronic energy levels as has been shown in a result of the CO_2 molecule. Also, the π-electron density of nitrogen atom in the NCN radical generally decreases with decreasing the $2s$-character n_N (except near $n_N = 1.50$) if the charge-dipole interaction is included, while this relation is not satisfied if such terms are disregarded. These facts show the importance of the inclusion of the charge-dipole interaction.

On the other hand, semi-empirical calculations of aromatic molecules have not usually been carried out by including the effect of atomic dipole in formulation, but the obtained values are generally in good agreement with experiment. The reason of this may partly due to the fact that the integrals of charge-dipole interaction are semi-empirically not very easy to estimate separately but such terms can implicitly be included in the Coulomb integrals α_X's in the form of some empirical adjustments. Furthermore, the effect of atomic dipole is almost perfectly cancelled out for π-electrons of aromatic hydrocarbons and also not very large in usual nitrogen-containing heterocyclic aromatic molecules, since the direction of the lone pair orbital makes an angle of about 120° from that of the bonding orbitals directed to the neighboring atoms. As a result, this influence is not as great as in the linear molecules with lone pair electrons discussed here. On the other hand, some calculation of a homonuclear diatomic molecule showed that the results obtained are not sensitive to the hybridization parameter [10]. This may possibly due to the fact that the change of Coulomb integrals α_X's are the same in both atoms and may approximately regard as only an additive constant. These facts may sometimes make possible to treat lightly the influence of dependence on the $s-p$ hybridization in semi-empirical calculations.

For references, a similar calculation with the present work was carried out for the HCCCH linear radical which is isoelectronic with the NCN radical but has no lone pair electron. The C–C internuclear distance has not yet been determined experimentally and was assumed to be that of the C_3 radical [5] and that of the allene molecule [6]. In advance, the resonance integral of acetylene molecule β_{CC}(HCCH) was chosen so as the calculated excitation energy of ${}^1\Sigma_u^+({}^1A_u) \leftarrow {}^1\Sigma_g^+$ to give the value of 6.85 eV which is estimated from the experimental data [11] by assuming that the vibrations of the HC and the CC fragments are harmonic and the potential energy curve of the HCC bending vibration is quartic parabolic. Then, the β_{CC}(HCCCH) was determined assuming the proportionality of β_{XY} to S_{XY} as in Eq. (9). In spite of no lone pair electrons

Table 3. Vertical π-electron excitation energies in HCCCH radical (eV)

State	$R = 1.277$ Å		$R = 1.3084$ Å	
	With CI	Without CI	With CI	Without CI
$^1\Delta_u$	5.20	6.22	5.02	6.12
$^3\Sigma_u^+$	4.11	3.46	4.03	3.33
$^3\Sigma_u$	4.03	5.31	3.87	5.24
$^3\Delta_u$	3.91	3.32	3.83	3.19
$^1\Sigma_u^-$	3.62	3.18	3.52	3.06
$^1\Sigma_g^+$	1.39	1.37	1.40	1.36
$^1\Delta_g$	0.75	0.68	0.76	0.68
$^3\Sigma_g^-$	0.00	0.00	0.00	0.00
$\beta_{CC'}$(HCCCH) (a. u.)	−0.10730	−0.10836	−0.10200	−0.10300

in the HCCCH radical, the form of SCF-LCAO-MO's obtained is rather close to that of the NCN radical with charge-dipole interaction than that without such terms. The vertical excitation energies calculated are summarized in Table 3, while the corresponding observed values have scarcely been known [12].

In an improvement of the present work, it may be possible to use a different hybridization parameter for each excited state from that of the ground state. However, this may correspond to increase the number of adjustable parameters to the experiment in a sense of semi-empirical calculation and is essentially outside the present discussion. At any rate, it should be emphasized that the inclusion of terms with charge-dipole interaction in Coulomb integrals α_X's is desirable for calculations of π-electron energy levels of molecules with lone pair electrons even in a semi-empirical form.

Acknowledgement. The author wishes to thank Dr. T. Nogami and H. Shimizu for their help in the preliminary calculation of NCN radical.

References

1. Fumi, F. G., Parr, R. G.: J. chem. Physics **21**, 1864 (1953).
2. Pariser, R., Parr, R. G.: J. chem. Physics **21**, 466, 767 (1953). — Pople, J. A.: Trans. Faraday Soc. **49**, 1375 (1953).
3. Hurley, A. C.: Proc. Roy. Soc. (London) A **249**, 402 (1959). — Moore, C. E.: Atomic energy levels, Natl. Bur. Standards (U.S.), Cir. No. 467 (1949).
4. Mulligan, J. F.: J. chem. Physics **19**, 347 (1951).
5. Herzberg, G.: Electronic spectra of polyatomic molecules, p. 591. Princeton: D. Van Nostrand Co. 1966.
6. Herzberg, G.: Electronic spectra of polyatomic molecules, p. 640. Princeton: D. Van Nostrand Co. 1966.
7. Herzberg, G.: Electronic spectra of polyatomic molecules, p. 597. Princeton: D. Van Nostrand Co. 1966, and references therein.
8. Herzberg, G.: Electronic spectra of polyatomic molecules, p. 592. Princeton: D. Van Nostrand Co. 1966. — Herzberg, G., Travis, D. N.: Canad. J. Physics **42**, 1658 (1964). — Milligan, D. E., Jacox, M. E., Bass, A. M.: J. chem. Physics **43**, 3149 (1965). — Kroto, H. W.: J. chem. Physics **44**, 831 (1966). — Kroto, H. W.: Canad. J. Physics **45**, 1439 (1967).

9. Herzberg, G.: Electronic spectra of polyatomic molecules, p. 588. Princeton: D. Van Nostrand Co. 1966
10 Öpik, U., Thomas, T. H.: Molecular Physics **10**, 289 (1965).
11 Herzberg, G.: Electronic spectra of polyatomic molecules, p. 611. Princeton: D. Van Nostrand Co. 1966
12. Herzberg, G.: Electronic spectra of polyatomic molecules, p. 622. Princeton: D. Van Nostrand Co 1966.

Professor Jiro Higuchi
Department of Chemistry
Yokohama National University
Minami-ku, Yokohama 233
Japan

Theoret. chim. Acta (Berl.) 27, 325—338 (1972)
© by Springer-Verlag 1972

CNDO/2 Calculations and Configuration Analyses for Some Hydrogen-Bonded Systems

H. Morita and S. Nagakura

The Institute for Solid State Physics, The University of Tokyo, Roppongi, Minato, Tokyo, Japan

Received August 14, 1972

The potential energy curves of hydrogen-bonded systems were calculated for the water, methanol, and formic acid dimers and for the hydrogen maleate ion by a modified CNDO/2 method, the core resonance integrals between σ-electrons being distinguished from those between π-electrons, the different bonding parameters being used for $-O$ and $=O$, and the core potential integrals V_{AB}^c for O–H, C=O, and O···O being determined semi-empirically. Consequently, the following results were obtained: 1) a potential energy curve with a single minimum at $r(O \cdot H) = 0.95$ Å and with a concavity near 1.70 Å for the linear chain dimers of water and methanol; 2) a symmetrical potential energy curve with two minima at $r(O-H) = 0.95$ and 1.78 Å for the cyclic dimer of formic acid; 3) a flat-bottomed symmetrical potential energy curve for the hydrogen maleate ion. The configuration analysis method was applied to the hydrogen-bonded systems; the contributions of the covalent $((O\text{–}H\ \ O)^{-1})$ and ionic $(O^- H^+ O^-)$ structures being 54% and 39%, respectively, for the symmetrical hydrogen bonding of the hydrogen maleate ion.

Die Kurven potentieller Energie von Systemen mit H-Brücken wurden im Fall von H_2O-, CH_3OH- und HCOOH-Dimeren und für das Hydrogen-Maleatanion mittels eines modifizierten CNDO-Verfahrens berechnet, wo für Rumpf-σ- und -π-Elektronen jeweils verschiedene Resonanzintegrale und verschiedene Bindungsparameter für $=O$ und $-O$ verwendet und wo die Rumpfpotential-Integrale für O H, C=O und O···O semiempirisch bestimmt werden.
Die Resultate sind 1) eine Potentialkurve mit einem einfachen Minimum für lineare Ketten von H_2O und CH_3OH, 2) eine symmetrische Potentialkurve mit zwei Minima für das cyclische Dimere von HCOOH und 3) eine Potentialkurve mit einem flachen Minimum für das Maleatanion. Konfigurationsanalyse ergab einen Beitrag von 39% für die ionischen Strukturen.

1. Introduction

The potential energy curves of hydrogen-bonded systems are important to understand their physico-chemical and biological properties. From the theoretical point of view, the determination of their potential energy curves has hitherto been performed by many authors semi-empirically [1–5] and non-empirically [6, 7] for the water, alcohol, and formic acid dimers, and also for the guanine-cytosine and adenine-thymine base pairs. On the other hand, the experimental determination of the potential energy curves has scarcely been made. In a previous paper [8], we determined the double minimum potential energy curves for the formic acid and acetic acid dimers from the analysis of their overtone bands which appear in $5000 \sim 12000 \text{ cm}^{-1}$.

For the purpose to compare the experimentally determined potential energy curve with the theoretical one, we have undertaken to study the electronic structure of the hydrogen-bonded formic acid dimer by a semi-empirical method in which the CNDO/2 method [9–13] is modified by taking bonding parameters consistent with the core resonance integrals used in the Pariser-Parr-Pople method [14, 15] for π-electron systems and semi-empirically determined core potential integrals. The same theoretical method has been extensively applied to the hydrogen-bonded water and methanol dimers, and also to the hydrogen maleate ion. The structures of hydrogen-bonded alcohols have been discussed by several authors from the experimental view-point [16–20], but, concerning them, there are still problems to be solved. The hydrogen maleate ion is an interesting research subject, because its hydrogen bond is extraordinary strong as revealed from its short oxygen-oxygen distance of 2.437 Å and may be expected to have the large covalent character.

Baba, Suzuki, and Takemura [21] presented the configuration analysis method in which the wave functions of such substituted aromatic hydrocarbons as aniline, phenol, and aminonaphthol are expanded with regard to ground, locally(within a parent hydrocarbon and a substituent group)-excited, and charge-transfer (between a parent hydrocarbon and a substituent group) configurations. This method was found to be useful for understanding the natures of the ground and excited states of the substituted aromatic hydrocarbons. We have undertaken to apply this method to inter- and intra-molecular hydrogen-bonding systems, expecting that vivid interpretation can be obtained for the natures of hydrogen bonds, in particular for their covalent or charge-transfer characters.

2. Methods of Calculation

Modified CNDO/2 Method. The calculation procedure is essentially the same as the original CNDO/2 method presented by Pople, Santry, and Segal [9, 10], but some modifications have been made concerning the evaluation of two-center integrals, bonding parameters, and core potential integrals.

(a) The one-center Coulomb integrals γ_{AA} concerning the valence electron orbitals of the hydrogen, carbon, and oxygen atoms are taken to be 12.845, 11.144, and 13.707 eV, respectively [11].

The two-center Coulomb integral γ_{AB} between the two valence ($2s$ or $2p$) orbitals on the A and B atoms was determined by Klopman's semi-empirical equation [11], γ_{AB} between σ and π electrons being taken to be equal:

$$\gamma_{AB} = e^2 \Bigg/ \left[R_{AB}^2 + \frac{1}{4}\left(\frac{e^2}{\gamma_{AA}} + \frac{e^2}{\gamma_{BB}}\right)^2\right]^{\frac{1}{2}}, \tag{1}$$

where R_{AB} is the distance between the A and B atoms.

(b) The core resonance integrals β_{pq} between σ electron orbitals were distinguished from those between π electron orbitals by the equation presented by Bene and Jaffé [12].

Furthermore, the oxygen atoms of the carbonyl and hydroxyl groups were treated differently from each other, by adopting different bonding parameters, $\beta^0(=\mathrm{O}) = -26.5$ eV and $\beta^0(-\mathrm{O}-) = -50.3$ eV. The bonding parameters for the hydrogen and carbon atoms, $\beta^0(\mathrm{H})$ and $\beta^0(\mathrm{C})$, are taken to be equal to -12.0 and -16.7 eV, respectively. These bonding parameters were determined in such a way that the calculated β_{pq} between π orbitals coincides with the core resonance integral used in the Pariser-Parr-Pople method [14, 15].

(c) The core potential integral, V^c_{AB}, necessary for the calculation of the total energy was represented by the following equation in the present study:

$$V^c_{AB} = Z_B \gamma^c_{AB} = Z_B\left[\gamma_{AB} + c\left(\frac{e^2}{R_{AB}} - \gamma_{AB}\right)\right]. \tag{2}$$

Here, Z_B is the core nuclear charge of atom B, and a parameter, c, was determined for each valence bond in such a way that the calculated equilibrium bond length coincides with the observed one. The ordinary CNDO/2 calculation corresponds to the case of $c = 0$. The present procedure for determining the core potential integral is a practical method for considering the shielding effect upon the core Coulomb repulsion and is particularly useful when we use smaller γ_{AB}'s estimated semi-empirically [11–13] than those obtained by Pople and Segal [10].

Configuration Analysis Method. The ground state wave functions of inter- and intra-molecular hydrogen-bonding systems calculated by the modified CNDO/2 method mentioned above, were analysed by the configuration analysis method presented by Baba, Suzuki, and Takemura [21]. As the reference wave functions in these analyses, the ground and singly excited configurations constructed from the monomer MO's were adopted for the intermolecular dimers, and the ground configuration and the singly and doubly excited configurations constructed from the MO's of the maleate dinegative ion and from the 1s orbital of the hydrogen-bonded hydrogen, were adopted for the hydrogen maleate ion.

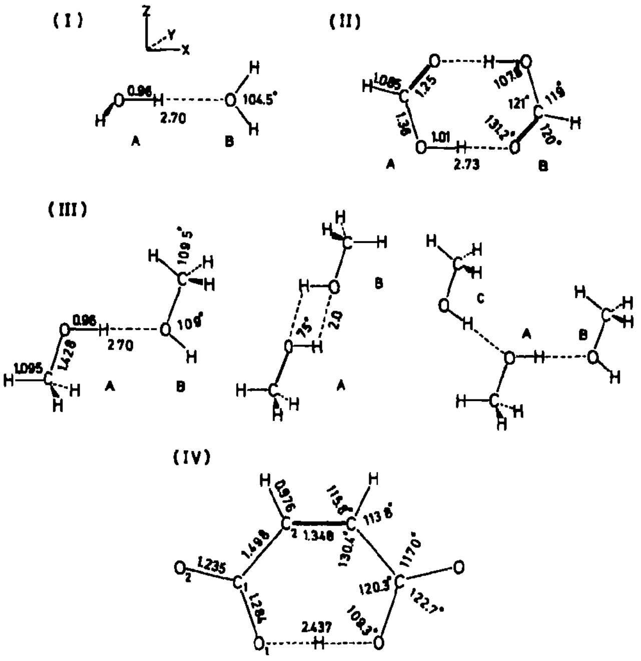

Fig. 1. The geometrical structures of the hydrogen-bonded systems: (*I*) the water dimer, (*II*) the formic acid dimer, (*III*) the methanol dimers and trimer, and (*IV*) the hydrogen maleate ion

Molecular Parameters. The geometries and the molecular parameters of hydrogen-bonded water, methanol, formic acid and hydrogen maelate ion are shown in Fig. 1. These molecular parameters were taken from the electron [22, 23] and X-ray [24, 25] diffraction studies and also from other works [7, 26]. In the water dimer, the left hand side (A-site) molecule lies in the $x-y$ plane, while the other (B-site) molecule in the $x-z$ plane. The molecular geometries of the cyclic dimers were assumed to have the C_{2h} symmetry, and for the cyclic dimer of methanol, the O···H distance and the H–O···H angle were taken to be 2.0 Å and 75°, respectively, by referring to the results calculated by the CNDO/2 method [3, 4].

3. Results and Discussion

The total energies of the water and formic acid monomers and the water dimer were calculated by the modified CNDO/2 method, the c (in Eq. (2)) value and the O–H, C=O, or O···O interatomic distance being changed. The values of c in the core potential integrals, V^c_{AB}, were determined to be $c_{OH}=0.21$, $c_{CO}=0.38$, and $c_{OO}=0.77$ for the O–H, C=O, and O···O, respectively, in such a way as the calculated bond lengths are coincident with the observed ones [27–30] as well as possible: the γ^c_{AB} values calculated by the use of the above c values are shown in Fig. 2, together with the values of the two-center Coulomb integrals, γ_{AB}, obtained by Eq. (1).

The total energies of the monomer and dimer of water calculated with the above-mentioned c values are -383.91 and -768.20 eV, respectively, and the monomer and dimer of formic acid are -871.54 and -1744.57 eV, respectively. According to the present calculation, hydrogen bonding energies are obtained to be 0.38 and 1.49 eV for water and formic acid, respectively.

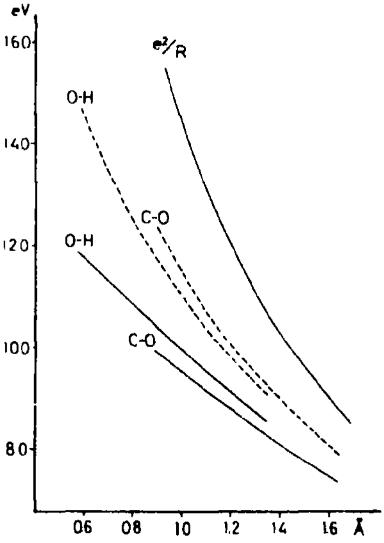

Fig. 2. The core potential integrals (γ^c_{AB}) and the two center Coulomb integrals (γ_{AB}) for O–H and C=O bonds. ——— γ_{AB}, - - - - - γ^c_{AB}

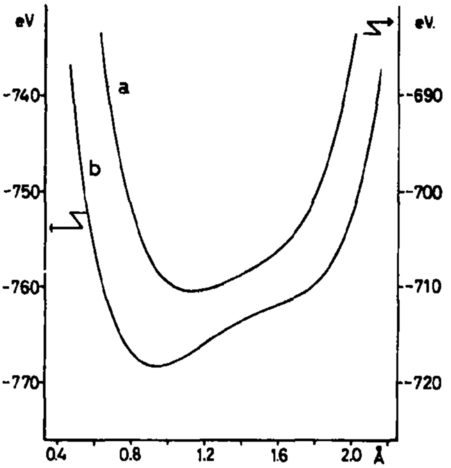

Fig. 3. The total energy (eV) calculated for the water dimer as a function of the hydrogen-bonded O···H distance (Å), the O···O distance being fixed at 2.70 Å. The c values in Eq. (2) are taken as follows: $c_{OH} = c_{OO} = 0$ for (a); $c_{OH} = 0.21$ and $c_{OO} = 0.77$ for (b)

Potential Energy Curves for Hydrogen-Bonded Systems. The potential energy curve for the water dimer was calculated by the modified CNDO/2 method; the result is shown in Fig. 3. The shape of the potential energy curve calculated for the linear dimer of methanol is entirely the same as that of the water dimer. The potential energy curve (b) calculated with $c_{OH} = 0.21$ and $c_{OO} = 0.77$ has a minimum at r(O–H) = 0.95 Å and a concavity near 1.70 Å and is qualitatively in good agreement with the curve calculated by Murthy, Davis, and Rao for methanol [3]. The value of r(O–H) calculated with the c values is in better agreement with the observed value [31] than the value calculated with $c = 0$ (r(O–H) = 1.12 Å). From curve (b), the fundamental frequency, ν_{OH}, was obtained to be $\sim 5900\,\text{cm}^{-1}$[1]; this is 1.8 times larger than the observed frequency [16]. Our result for the methanol or water dimer shows a concavity in addition to the potential minimum. Experimentally, a double minimum potential energy curve was obtained for the linear chain hydrogen bond of formic acid in pure liquid from the analysis of the overtone bands [8]. From an analogy with this case, the linear dimer of methanol or water may be expected to show a double minimum potential energy curve.

Potential energy curves calculated for the formic acid dimer are shown in Fig. 4. The solid lines in this figure indicate the total energy calculated by varing the two hydrogen-bonded O–H distances simultaneously from 0.7 ~ 1.3 Å on the assumption that the other atoms are fixed on the experimentally determined molecular geometry [23] and by using the core potential integrals with $c_{OH} = 0.21$, $c_{CO} = 0.38$, and $c_{OO} = 0.77$. The broken line in Fig. 4 indicates the total energy calculated for the system with the four equivalent C–O bonds of 1.27 Å [30].

---

[1] This frequency was calculated by the aid of the analytical potential curve, $v(q) = \frac{1}{2}[15q + 4q^2 + 100q^3 + 128q^4]$, which was determined to coincide with the potential energy curve (b) in Fig. 3 as well as possible.

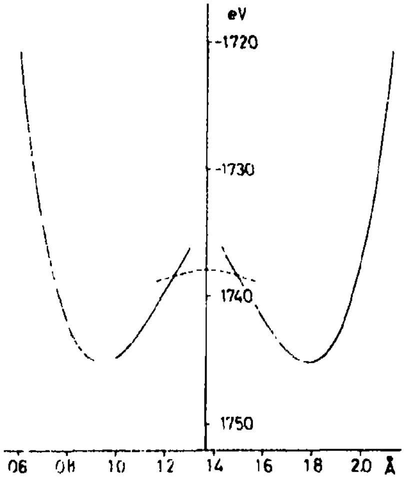

Fig. 4

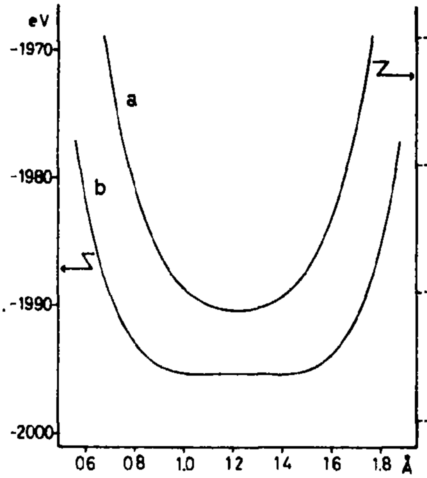

Fig. 5

Fig. 4 The total energy (eV) calculated for the coupled O H stretching vibration of the formic acid dimer, the O···O distance being fixed at 2.73 Å

Fig. 5 The total energy (eV) calculated for the hydrogen maleate ion as a function of the hydrogen-bonded O H distance (Å), the O···O distance being fixed at 2.437 Å. The c values in Eq. (2) are taken as follows: $c_{OH} = c_{CO} = c_{OO} = 0$ for (a); $c_{OH} = 0.21$, $c_{CO} = 0.38$, and $c_{OO} = 0.77$ for (b)

The potential energy curve in Fig. 4 gives the equilibrium O–H bond length of 0.95 Å and the barrier height of 7.3 eV. The calculated bond length agrees well with the spectroscopically determined one (1.01 Å) [26], but the calculated barrier height and the calculated fundamental frequency (~15100 cm^{-1})[2] are too large compared to the experimentally determined values (0.80 ~ 0.86 eV, ~3110 cm^{-1}) [8, 32]. This discrepancy may be due to a little lower (~0.16 eV) estimation of the γ'_{AB} value for the O–H bond at comparatively large distances (~1.365 Å). According to the total energy calculated for the formic acid dimer at r(O H) = 1.365 Å by the use of the γ'_{AB} values of $c = 0.29$ (which is 0.16 eV larger than the one of $c = 0.21$) the barrier height is reduced to 0.8 eV. This value is nearly equal to the experimentally determined one [8]. This fact suggests that better theoretical potential energy curves can be obtained by taking into account the O–H bond length dependency of c.

Now let us turn to the hydrogen maleate ion. The potential energy curve calculated for this ion is shown in Fig. 5. Curve (b) calculated with $c_{OH} = 0.21$, $c_{CO} = 0.38$, and $c_{OO} = 0.77$ shows a flat-bottomed symmetrical potential energy curve with a negligibly small barrier. This coincides well with the expectation from the experimental point of view for this strong hydrogen bond [33]. The calculated fundamental frequency for curve (b) is about 1660 cm^{-1}[3], in good agreement with the observed one [33].

---

[2] This frequency was calculated by the aid of the analytical potential curve, $v(q) = \frac{1}{2} \times 193q^2 + 48.0 \exp(-4.0q^2)$, with the barrier height of 7.3 eV and with the energy minimum at r(O–H) = 0.95 Å, which was simulated for the potential energy curve of Fig. 4.

[3] This frequency was calculated by the aid of the analytical potential curve, $v(q) = \frac{1}{2}[q^2 + 180q^4]$, which was determined in such a way to fit as well as possible into curve (b) in Fig. 5.

Configuration Analyses for Hydrogen-Bonded Systems. The results of the configuration analyses obtained for the linear dimers of water and methanol and for the cyclic dimers of methanol and formic acid are given in Tables 1–3. In these tables, G denotes the ground configuration, and $i-j$ represents a singly excited configuration of the monomer in which one electron on the i-th occupied orbital is excited to the j-th vacant orbital. In the present calculation, the monomer MO's were calculated by the modified CNDO/2 method for each monomer component of the dimer, and the orbitals are numbered in such a way that MO's belonging to the A- and B-components are denoted by odd and even numbers in the order of increasing orbital energies, respectively. Singly excited configurations in which i and j are both even numbers or both odd numbers correspond to locally-excited configurations, while those in which i is even and j is odd or vice versa, correspond to intermolecular charge-transfer configurations.

The configuration analyses were performed by taking all the singly excited configurations. For the cyclic methanol and formic acid dimers, owing to their C_{2h} symmetry, the singly excited configurations having the indices of $2m-2n$

Table 1. The result of the configuration analysis obtained for the ground state of the water dimer at $R(\mathrm{O}\cdots\mathrm{O}) = 2.50$, 2.70, and 2.90 Å

Group	Configuration	Weights		
		2.50 Å	2.70 Å	2.90 Å
A	*G*	0.9271	0.9596 (0.9632)[a]	0.9788
B	6–9	0.0267	0.0151	0.0079
	6–11	0.0313	0.0176	0.0092
	2–9	0.0022	0.0012	0.0006
	2–11	0.0029	0.0015	0.0008
	Total for group *B*	0.0631	0.0354 (0.0352)	0.0185
C	5–12	0.0002	0.0001	0.0001
	3–12	0.0007	0.0004	0.0002
	1–12	0.0004	0.0002	0.0001
	Total for group *C*	0.0013	0.0007 (0.0007)	0.0004
D(*A*)	5–11	0.0007	0.0003	0.0002
	3–9	0.0016	0.0008	0.0004
	1–11	0.0005	0.0002	0.0001
	Total for group *D*(*A*)	0.0028	0.0013 (0.0003)	0.0007
D(*B*)	6–12	0.0005	0.0004	0.0003
	4–10	0.0027	0.0017	0.0010
	2–12	0.0007	0.0004	0.0003
	Total for group *D*(*B*)	0.0039	0.0025 (0.0005)	0.0016
Total		0.9982	0.9995 (0.9998)	1.0000

[a] The values in the parentheses are calculated by taking all the c values to be zero.

Table 2. The result of the configuration analysis obtained for the ground states of the linear and cyclic dimers of methanol

Group	Configuration	Weights	
		Linear dimer	Cyclic dimer
A	G	0.9576 (0.9639)[a]	0.9747 (0.9826)[a]
B	12 23	0.0181	0.0036
	10 23	0.0052	0.0023
	6 23	0.0059	0.0001
	4 23	–	0.0006
	2 23	0.0026	0.0006
	Total for group B	0.0313 (0.0296)	0.0072 (0.0073)
B'	12 21	0.0007	0.0003
	10 21	0.0001	0.0001
	6 21	0.0002	0.0003
	4 21	–	0.0003
	2 21	0.0001	0.0001
	Total for group B'	0.0011 (0.0029)	0.0011 (0.0009)
B''	12 17	0.0011	0.0003
	10 17	0.0003	0.0001
	6 17	0.0003	–
	2 17	0.0001	–
	Total for group B''	0.0018 (0.0023)	0.0004 (0.0005)
C'	11 24	0.0002	
	9 24	0.0001	
	5 24	0.0002	
	3 24	0.0002	
	1 24	0.0002	
	Total for group C'	0.0009 (0.0008)	
$D(A)$	11 23	0.0001	0.0002
	5 23	0.0001	0.0001
	3 23	0.0001	0.0002
	1 23	0.0001	0.0002
	Total for group $D(A)$	0.0004 (0.0007)	0.0007 (0.00005)
$D(B)$	12 24 etc.	0.0012	
$D'(A)$	9 21	0.0002	0.0006
	5 21	0.0001	0.0004
	3 21	–	0.0001
	Total for group $D'(A)$	0.0003	0.0011
$D'(B)$	10–22 etc.	0.0009	
$D''(A)$	1 21	–	0.0002

[a] The values in the parentheses are calculated, by taking all the c values to be zero.

Table 2 (continued)

Group	Configuration	Weights	
		Linear dimer	Cyclic dimer
$E(A)$	13–19	0.0006	0.0013
	11–17	0.0003	0.0004
	9–15	0.0001	0.0001
	9–17	0.0001	–
	5–15	–	0.0001
	Total for group $E(A)$	0.0011	0.0019
$E(B)$	14–20 etc.	0.0026	
$E'(B)$	12–16	0.0001	
Total		0.9998 (1.0002)	0.9999[b] (1.0001)[b]

[b] The other counterpart of each configuration (B, B', B'', D, D', D'', and E) is involved.

are equivalent to those of $(2m-1)-(2n-1)$, and $2m-(2n-1)$ to $(2m-1)-2n$, where m and n are integers. For these cyclic dimers only one of the equivalent two configurations is listed in Tables 2 and 3.

By considering the characteristics of the monomer MO's and the signs of the expansion coefficients, configurations belonging to Group (A), (B), ..., and (F) can be classified into the two types of configurations; namely, the intermolecular charge-transfer and locally-excited configurations as shown in Fig. 6.

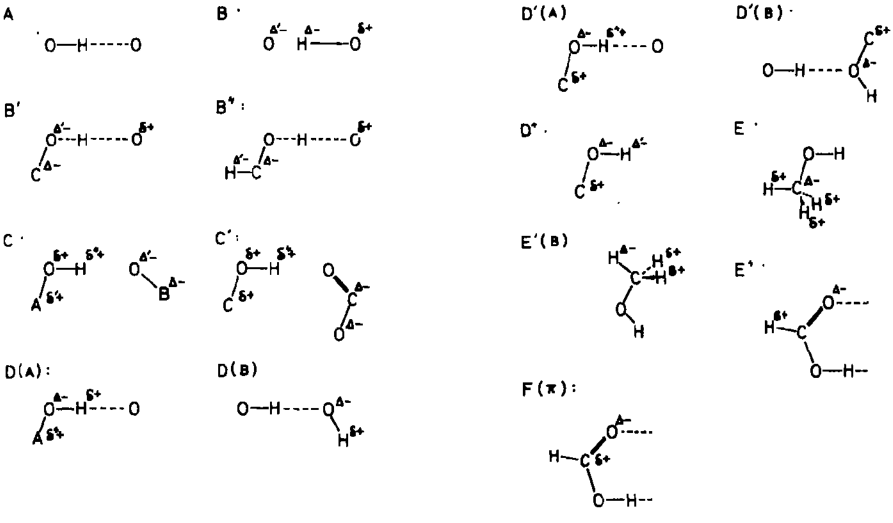

Fig. 6. Configurations of Groups (A), (B), ..., and (F). In configuration (C), B atom represents the hydrogen atom for the water and methanol dimers, and the carbon atom for the formic acid dimer. $\sigma \gtrsim \sigma' \gg \sigma''$ and $\Delta \gtrsim \Delta' \gg \Delta''$ generally hold

Table 3. The result of the configuration analysis obtained for the ground state of the formic acid dimer

(*A*) The contribution of each configuration to the ground state at R(O···O) = 2.73 Å

Group	Configuration	Weight	Group	Configuration	Weight
A	*G*	0.9014	*D*	13–27	0.0003
B	15 26	0.0014		5–27	0.0001
	15 28	0.0050		1-27	0.0001
	9 26	0.0005	*D*′	7-25	0.0002
	9 28	0.0023		5 25	0.0002
	3 26	0.0003	*E*	15–23	0.0001
	3 28	0.0013		7–21	0.0003
B″	15 24	0.0005		5–23	0.0001
	9 24	0.0006		5–21	0.0001
	9 22	0.0001	*E*″	15 21	0.0007
	3 24	0.0002		13–21	0.0003
C	13 22	0.0002	*F*	17-19(π)	0.0215
	7 24	0.0004		11–19(π)	0.0064
	7 22	0.0001			
	5 22	0.0001			
	1 22	0.0001			
C″	13 26	0.0004			
	13 28	0.0010			
	7 26	0.0001			
	7 28	0.0009			
	5 26	0.0003			
	5 28	0.0005			
	1 26	0.0001			
	1 28	0.0004			

(*B*) The contribution of each group to the ground state at *R*(O···O) = 2.53, 2.73, and 2.93 Å

Group	Weights 2.53 Å	2.73 Å	2.93 Å
A	0.8338	0.9014	0.9413
B	0.0190	0.0108	0.0058
B″	0.0026	0.0014	0.0007
C	0.0019	0.0009	0.0005
C″	0.0063	0.0037	0.0020
D	0.0010	0.0005	0.0003
D′	0.0006	0.0004	0.0002
E	0.0008	0.0006	0.0005
E″	0.0011	0.0010	0.0007
F(π)	0.0437	0.0279	0.0182
Total[a]	0.9880	0.9960	0.9991

[a] The other counterpart of each configuration (*B*, *B*″, ..., and *F*) is involved.

As is clearly seen in Tables 1 and 2, the natures of hydrogen bonds are similar to each other for the linear dimers of water and methanol[4], except for the fact that the latter has a small contribution of configuration (*E*) which comes from the polarization of the methyl group. For these linear dimers, the intermolecular charge-transfer configuration (*B*) contributes significantly to the ground state. The contributions of configurations (*B*′), (*B*″), (*C*), (*D*(*B*)), (*D*′), and (*E*) show that the effect of hydrogen-bonding can not be simply expressed by the effect within the fictitious three atom model, O–H···O. This conclusion is consistent with that of Morokuma and Pedersen [7]. According to the present calculation the water dimer has only a negligibly small contribution of the $O^+H^-\cdots O$ configuration although a valence bond treatment [34] predicted a fairly large contribution of the configuration.

---

[4] The same result was obtained for the neighboring two component molecules of the linear trimer of methanol.

As is clearly seen in Table 2, the contributions of the configurations (*B*) and (*B*″) are much smaller for the cyclic dimer of methanol than for the linear dimer[5]. These facts suggest that the former is mainly stabilized by the electrostatic interaction and is less stabilized by the delocalization energy (charge-transfer energy) than the latter.

Because of the delocalization of the monomer MO's, the nature of the formic acid dimer is a little complicated. As is seen in Table 3, beside the configuration (*B*), the configurations (*B*″), (*C*′), (*E*″), and (*F*)[6] contribute to the ground state of the formic acid dimer. Of these, configuration (*F*) is a locally-excited π-electron configuration.

For the water and formic acid dimers, the configuration analyses were performed taking various O···O distances; the results are tabulated in Tables 1 and 3. When the O···O distances are shortened by 0.2 Å, the contributions of the excited configurations increase about two times.

The core potential integrals used in our modified CNDO/2 calculations are different from those used by other authors [3–5, 9–13]. We made also the calculation taking $c=0$ for all bonds. The obtained wave functions were analysed by the configuration analysis method. The results of the configuration analysis listed in Tables 1 and 2 are found to be rather insensitive to the choice of the core potential integrals.

Now let us turn to the hydrogen maleate ion. The configuration analysis was performed, the MO's of the maleate dinegative ion calculated by the modified CNDO/2 method and the 1*s* orbital[7] of the hydrogen-bonded hydrogen being employed as reference orbitals; the result is tabulated in Table 4. The configurations of groups (*A*), (*B*), ..., and (*F*) are shown in Fig. 7. In order to obtain the satisfactory convergence for this case, it is necessary to take doubly excited configurations in addition to singly excited ones. The doubly excited configurations of the $V_{ik,ik}$ and $V_{ik,jk}$ types (*i* and *j* represent occupied MO's, and *k*, vacant MO's) significantly contribute mainly to the configurations (*F*) and (*A*), respectively. The doubly excited configurations of the $V_{ik,jl}$ type (*i* and *j* represent σ and π occupied MO's, respectively, and *k* and *l*, σ and π vacant MO's, respectively) contribute to the configuration, (*A*) + (*C*′), and the doubly excited configuration

---

[5] Owing to the C_{2h} symmetry of the cyclic dimer, configuration (*C*) is equivalent to configuration (*B*).

[6] More strictly, each of the (*D*), (*E*), (*E*″), and (*F*) groups for the formic acid dimer can be divided into two or more subgroups.

[7] This orbital is treated as a vacant orbital in the present analysis.

Table 4. The result of the configuration analysis obtained for the ground state of the hydrogen maleate ion

Group	Weights	
	Singly excited configurations	Doubly excited configurations
A	0.3558	0.0827^{a}
$A + C''$ (or C')		0.0002^{b} 0.0942^{c}
$A + E''$		0.0002^{b} 0.0064^{c}
B	0.2945	
C	0.0019	
C''	0.0771	0.0007^{b} 0.0052^{c} 0.0019^{d}
D	0.0001	
D'	0.0003	
E	0.0004	
E'	0.0004	
E''	0.0053	
$C'' + E''$		0.0012^{c}
F		0.0246^{d}
Total	0.9531	

[a] From doubly excited configurations, $V_{ik,jk}$.
[b] From doubly excited configurations, $V_{ik,il}$.
[c] From doubly excited configurations, $V_{ik,jl}$.
[d] From doubly excited configurations, $V_{ik,ik}$.

of the $V_{ik,jl}$ type ($i \neq j$, $k \neq l$, and all indeces represent σ MO's), to the $(A)+(E'')$ configuration.

Table 4 shows that configurations corresponding to the covalent structure of hydrogen bond (namely, singly excited configuration (A) and doubly excited configurations (A), $(A)+(C')$ and $(A)+(E'')$), contributes to the ground state of the hydrogen maleate ion by 54%, while the contribution of configurations corresponding to the ionic structure (namely, singly excited configurations (B), (C), (C'), (E), (E'), (E'') and doubly excited configuration (C')) is 39%. It is worth noticing that the covalent character is more predominant for the hydrogen bond of the hydrogen maleate ion than the ionic character.

Charge Shift due to Hydrogen-Bond Formation. The charge shift due to hydrogen-bond formation of water, methanol, formic acid, and hydrogen maleate ion are shown in Fig. 8. For the linear dimers of water and methanol, the hydrogen-bond formation causes the electron migration from the hydrogen atom and the methyl group of B-component molecule to the proton accepting oxygen atom, and further from both the proton accepting oxygen atom and the hydrogen-bonded hydrogen atom to the proton-donating oxygen atom. The electron migration corresponds to the large contribution of configurations (B) and (D) to the ground state of the dimers. This result is in agreement with that obtained by others [3, 4]. The calculated dipole moments of the monomer and

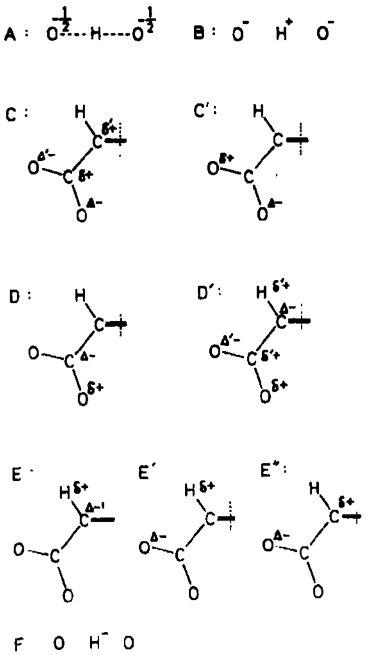

Fig. 7. Configurations of Groups (*A*), (*B*), ..., and (*F*) for the hydrogen maleate ion

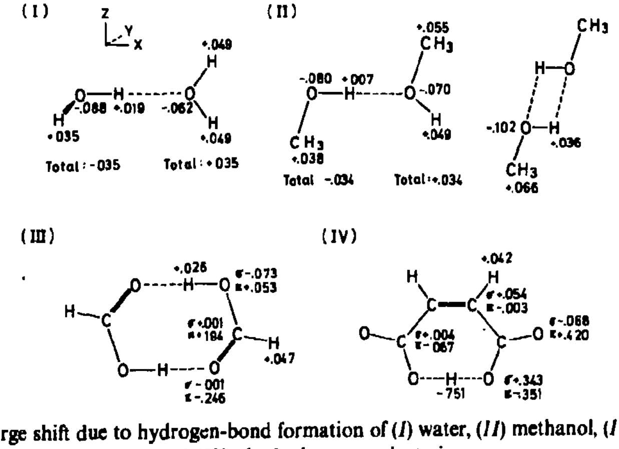

Fig. 8. The charge shift due to hydrogen-bond formation of (*I*) water, (*II*) methanol, (*III*) formic acid, and (*IV*) the hydrogen maleate ion

the linear dimer of water are 1.73 (exp. 1.82 [35]) and 3.70 *D*, respectively, and those of methanol are 1.51 (exp. 1.71 [35]) and 3.20 *D*, respectively. Compared to the linear dimers, O–H bonds are more polarized in the cyclic dimer of methanol in hydrogen-bond formation.

For the hydrogen-bonded formic acid, σ electrons move from the hydrogen-bonded hydrogen atom to the oxygen atom (–O–), while π electrons move from the oxygen atom (–O–) and the carbon atom to the oxygen atom (=O). Therefore, the excess σ electrons on the oxygen atom (–O–) are compensated by π electrons. The dipole moment of monomeric formic acid was calculated to be 0.65 (exp. 1.7 [35]) D.

In hydrogen-bond formation (i.e., when the proton is attached to the maleate dinegative ion), σ electron density on the hydrogen-bonded oxygen atom, O_1 decreases greatly, while π electrons move from the oxygen atom, O_2 to O_1.

The calculated dipole moment of the hydrogen maleate ion is 1.94 D.

References

1. Rein, R., Harris, F. E: J. chem. Physics **43**, 4415 (1965).
2. Lunell, S., Sperber, G.: J. chem. Physics **46**, 2119 (1967).
3. Murthy, A. S. N., Davis, R. E., Rao, C. N. R.: Theoret. chim. Acta (Berl.) **13**, 81 (1969).
4. Hoyland, J. R., Kier, L. B.: Theoret. chim. Acta (Berl.) **15**, 1 (1969).
5. Schuster, P.: Int. J. quant. Chemistry **3**, 851 (1969).
6. Clementi, E., Mehl, J., Niessen, W.: J. chem. Physics **54**, 508 (1971).
7. Morokuma, K., Pedersen, L.: J. chem. Physics **48**, 3275 (1968).
8. Morita, H., Nagakura, S.: J. molecular Spectroscopy **42**, 536 (1972).
9. Pople, J. A., Santry, D. P., Segal, G. A.: J. chem. Physics **43**, S129 (1965).
10. Pople, J. A., Segal, G. A.: J. chem. Physics **43**, S136 (1965); **44**, 3289 (1966).
11. Klopman, G.: J. Amer. chem. Soc. **86**, 4550 (1964); **87**, 3300 (1965).
12. Del Bene, J., Jaffé, H. H.: J. chem. Physics **48**, 1807, 4050 (1968).
13. Tinland, B.: Molecular Physics **16**, 413 (1969).
14. Pariser, R., Parr, R. G.: J. chem. Physics **21**, 466 (1953); **21**, 767 (1953).
15. Pople, J. A.: Proc. physic. Soc. **A68**, 81 (1955).
16. Liddel, U., Becker, E. D.: Spectrochim. Acta **10**, 70 (1957); Becker, E. D.: In: Hydrogen bonding, ed. by Hadži, D., P. 155 162. New York: Pergamon Press 1959.
17. Becker, E. D., Liddel, U., Shoolery, J. N.: J. molecular Spectroscopy **2**, 1 (1958).
18. Smith, F. A., Creitz, E. C.: J. Res. Nat. Bur. Stand. **46**, 145 (1951).
19. van Thiel, M., Becker, E. D., Pimentel, G. C.: J. chem. Physics **27**, 95 (1957).
20. Weltner, W., Jr., Pitzer, K. S.: J. Amer. chem. Soc. **73**, 2606 (1951).
21. Baba, H., Suzuki, S., Takemura, T.: J. chem. Physics **50**, 2078 (1969).
22. Kimura, K., Kubo, M.: J. chem. Physics **30**, 151 (1959).
23. Karle, J., Brockway, L. O.: J. Amer. chem. Soc. **66**, 574 (1944).
24. Harvey, G. G.: J. chem. Physics **6**, 111 (1938).
25. Darlow, S. F., Cochran, W.: Acta crystallogr. **14**, 1250 (1961); Darlow, S. F.: Acta crystallogr. **14**, 1257 (1961).
26. Kishida, S., Nakamoto, K.: J. chem. Physics **41**, 1558 (1964); Nakamoto, K., Kishida, S.: J. chem. Physics **41**, 1554 (1964).
27. Benedict, W. S., Gallar, N., Plyler, E. K.: J. chem. Physics **24**, 1139 (1956).
28. Kwei, G. H., Curl, R. F., Jr.: J. chem. Physics **32**, 1592 (1960).
29. Lerner, R. G., Dailey, B. P., Friend, J. P.: J. chem. Physics **26**, 680 (1957).
30. Zachariasen, W. H.: J. Amer. chem. Soc. **62**, 1011 (1940).
31. Peterson, S. W., Levy, H. A.: Physic. Review **92**, 1082 (1953).
32. Millikan, R. C., Pitzer, K. S.: J. Amer. chem. Soc. **80**, 3515 (1958); Bratož, S., Hadži, D., Sheppard, N.: Spectrochim. Acta **8**, 249 (1956).
33. Cardwell, H. M. E., Dunitz, J. D., Orgel, L. E.: J. chem. Soc. 1953, 3740; Blinc, R., Hadži, D., Novak, A.: Z. Electrochem. **64**, 566 (1960); Nakamoto, K., Sarma, Y. A., Behnke, G. T.: J. chem. Physics **42**, 1662 (1965).
34. Tsubomura, H.: Bull. chem. Soc. Japan **27**, 445 (1954).
35. McClellan, A. L.: Tables of experimental dipole moments. San Francisco, California: Freeman, W. H. and Company 1963.

Prof. Dr. S. Nagakura, The Institute for Solid State Physics, The University of Tokyo
Roppongi, Minato, Tokyo, Japan

Theoret. chim. Acta (Berl.) 27, 339—354 (1972)
© by Springer-Verlag 1972

A Theoretical Study of the Interaction of Ethylene with Transition Metal Complexes

E. J. Baerends, D. E. Ellis*, and P. Ros

Scheikundig Laboratorium, Vrije Universiteit, Amsterdam, The Netherlands

Received July 3, 1972

In order to be able to describe the ethylene molecule bonded to an active site of a Titanium- or Nickel fluoride crystal, we have used the Hartree-Fock-Slater model, implemented by a Discrete Variational Method, as introduced by Ellis and Painter. The study of the ethylene molecule at a crystal surface then gives a clear, easily interpreted picture of the electronic structure. The π-back donation from metal to olefin is found to be extremely important, both in the Ti- and in the Ni-complex. This back donation is caused by a strong interaction of a d orbital of the central ion with a σ^* as well as the π^* molecular orbital of ethylene. As a result of these interactions, the C–C bond of ethylene is weakened considerably.

A comparison is made between the Ti-ethylene and the Ni-ethylene systems.

Die Elektronenstruktur von Äthylen, das an ein aktives Zentrum eines Titan- bzw. Nickelfluoridkristalls gebunden ist, ist mittels der Hartree-Fock-Slater-Theorie kombiniert mit der sog. Discrete Variational Method theoretisch behandelt worden. Es zeigt sich, daß die π-Backdonation sowohl im Nickel- als auch im Titankomplex außerordentlich wichtig ist; sie entsteht durch eine starke Wechselwirkung eines Metall-d-Orbitals sowohl mit einem σ^*- als auch einem π^*-Orbital des Äthylens. Dies führt zu einer erheblichen Schwächung der Doppelbindung.

Außerdem werden die beiden Systeme (Titan und Nickel) miteinander verglichen.

1. Introduction

The metal olefin bond in transition-metal π-complexes is very interesting, both because of its wide occurrence in organometallic chemistry and because of the special character of this type of chemical bond. The bonding in these π-complexes can be explained in terms of a σ-bond, which is formed through electron donation from the olefin to the metal, and a π-bond which is formed through back donation of electrons from the metal to the olefin. Although this model, due originally to Dewar [1] and Chatt *et al.* [2], has been generally accepted, there is still quite some uncertainty as to the extent to which each of these bonding mechanisms, σ-donation and π-back donation, is operative. Recently, this problem has been extensively discussed in the literature [3–6].

Not only can quantum chemical calculations shed some light on the intricacies of the metal olefin bond, they should also aim at a better understanding of the extremely important role of transition metals in olefin chemistry. In particular, catalysis of many reactions of olefins by transition metals is very intriguing.

---

* Alfred P. Sloan Research Fellow, permanent address: Department of Physics, Northwestern University, Illinois, USA.

In order to study the catalytic activity of transition metals in reactions of olefins, the participants in these reactions, viz. the catalytic site and the reacting molecules, have to be known in detail. Such a detailed description can only be given for a limited number of catalytic reactions. The heterogeneous catalysis of the polymerization of α-olefins at the surface of an α-$TiCl_3$ crystal (Ziegler-Natta) forms an example of this category. Here the reaction can be described in some detail due to the fact that a well-crystallized compound can be employed as a catalyst, and due to the high stereoregularity of the product [7].

The main obstacle to the use of quantum chemical calculations as an aid in clarifying the problems indicated above, is the complexity of the systems involved. Thus, only a few calculations on transition-metal olefin π-complexes have been reported, most of them taking Pt for the transition metal. Two calculations on Zeise's salt, $K^+[PtCl_3(C_2H_4)]$, have been published, the first using the iterative Extended Hückel method [8], the other a CNDO-type method [9]. Although the absolute accuracy of these calculations is rather poor, both of them indicate σ-bonding as well as π-back bonding to be important. Recently an *ab initio* calculation on the $Ag^+ - C_2H_4$ complex, employing a limited basis set of Gaussian orbitals has appeared [10]. For this complex the σ-donation was found to be significantly larger than the π-back donation. We should also mention here the extension of the Dewar-Chatt scheme to acetylene, which has been based on non-iterative Extended Hückel calculations [11]. To obtain some insight in the Ziegler-Natta catalysis mentioned above, Extended Hückel calculations have been used [12].

In order to study both the bonding model and the role of transition metal ions in catalytic reactions, we have performed a number of quantum chemical calculations on two model systems. These model systems consisted of a TiF_5 or NiF_5 cluster and an ethylene molecule at various distances. We have used a method which we believe to be more reliable than the semi-empirical schemes, being at the same time practicable even for large systems. The method used essentially is based on the Hartree-Fock-Slater model, which has been widely applied in solid state calculations. The method, which contains a number of new features, is described in Section 2. Section 3 contains a detailed description of the model systems we have used. The results are discussed in Section 4 and the conclusions are summarized in Section 5.

2. The Quantum Chemical Method

The quantum chemical approach used in this work can be described in three steps:

a) Replacement of the conventional Hartree-Fock equations for the one-electron spinorbitals by those of the simpler Hartree-Fock-Slater (HFS) model.

b) Solution of the HFS equations by efficient numerical discrete variational methods (DVM).

c) Definition of a minimal effort self-consistent iterative scheme based on the main quantities of interest, viz., the molecular charge matrix.

We discuss each of these steps and their implications in the following section.

A. One Electron Model

We begin by reviewing the familiar Hartree-Fock equations for the one-electron spinorbital which for a closed shell system can be written as

$$f(1)\varphi_i(1)=\varepsilon_i\varphi_i(1)\,, \tag{1}$$

or

$$\{V_k(1)+V_N(1)+V_c(1)+V_x(1)\}\,\varphi_i(1)=\varepsilon_i\varphi_i(1)\,,$$

where $V_k(1)=-\frac{1}{2}\nabla^2(1)$, (kinetic energy)

$$V_N(1)=-\sum_\alpha \frac{Z_\alpha}{r_{1\alpha}} \quad \text{(electron-nucleus interaction)}$$

$$V_c(1)=\int\frac{\sum_k n_k\varphi_k^*(2)\varphi_k(2)}{r_{12}}\,d\tau_2=\int\frac{\varrho(2)}{r_{12}}\,d\tau_2 \quad \text{(coulomb repulsion)}$$

$$V_x(1)=-\int\frac{\sum_k n_k\varphi_k^*(2)P_{12}\varphi_k(2)}{r_{12}}\,d\tau_2 \quad \text{(exchange interaction)}$$

(n_k is the occupation number of spin-orbital φ_k). Usually these equations are solved in the expansion scheme (LCAO-MO), formulated by Roothaan [13]. For large systems however, solving these equations straightforwardly, that is, using a non-empirical all-electron all integral scheme, becomes intractable.

Moreover, uncertainties in a calculation due to limitations in the basis set can be quite large, [14], and the necessity of using limited basis sets in calculations of this type on large systems (if possible at all), remains a serious drawback of these methods. The semi-empirical methods one has to resort to, then, (iterative [8, 12], or even non-iterative Extended Hückel [11] or CNDO-type [9]) are known to be somewhat unreliable as far as quantitative results are concerned.

In an attempt to overcome the difficulties presented both by the non-empirical and semi-empirical methods mentioned, we have used a method which leans heavily on techniques from solid-state calculations (as suggested by the crystalline part of our systems). In solving the HF-equations (1), the largest difficulties are due to the HF exchange potential V_x because of its non-local character. Slater suggested replacing the non-local exchange terms in the original equations by an averaged local exchange potential. He approximated this average by the exchange potential of a free electron gas with the same local density [23]:

$$V_{xs}(1)=-3\left(\frac{3}{8\pi}\varrho(1)\right)^{1/3}. \tag{2}$$

This exchange approximation has been used extensively in energy-band calculations and in calculations on heavy atoms. We refer to [24] for a recent discussion and a comprehensive bibliography. We have adopted the Slater exchange approximation throughout. Then, we only need the density in each sample point, which is determined as mentioned under C, to generate the Hamiltonian. We have, in the present calculations, not yet treated the spin-up and spin-down densities separately, which is necessary if we want to carry through our calculations in an Unrestricted Hartree-Fock formalism (different orbitals for different spins). In fact, in our calculations we neglect the spin polarization due to the presence of one unpaired spin in the Ti-complexes. It is not expected that this will lead to serious errors, since only the gross features of the charge distribution and bonding in these complexes are being studied.

B. Numerical Integration and the Discrete Variational Method

The Discrete Variational Method (DVM) and some of its previous applications have been described elsewhere [15–19]. We give a brief survey of the method here, treating successively the most important features.

Using the atomic orbital χ_i, we have to calculate the matrix elements $\langle\chi_i|f|\chi_j\rangle$. We evaluate these integrals directly by numerical integration, i.e. we approximate the integral $\langle\chi_i|f|\chi_j\rangle$ with the sum:

$$\sum_{k=1}^{N} \chi_i^*(\boldsymbol{r}_k)\,(f\,\chi_j(\boldsymbol{r}_k))\,w(\boldsymbol{r}_k)\,.$$

For the generation of the integration points $\boldsymbol{r}_k$ we have used the Diophantine procedure. This is a method for the numerical evaluation of multidimensional integrals, developed by Haselgrove [20], and applied to the molecular integral problem by Conroy [21] and Ellis [15]. A number of integration points is distributed around each nucleus of the system, the distribution in the periodic ϑ- and φ-domains following immediately from the Diophantine procedure. In the r-domain a fermi-distribution appears to be most useful [15]. Convergence is rather rapid: an accuracy of roughly 1% in energy can be obtained with two to three hundred points for first row elements, while six to eight hundred points may suffice for third row transition elements. It should be stressed that, even if the absolute accuracy in the matrix elements may not be high, due to the necessarily limited number of sample points, it is an over-all accuracy we are dealing with. The error is *not*, as in most methods, propagated in an uncontrollable way through some n^4 operations (where n is the number of basis functions). This means that we need not fear an imbalance caused by the fact that some matrix elements deviate much more from their exact value than others. The latter situation is quite common in semi-empirical calculations, where some integrals are calculated exactly, others approximated more or less severely, and many neglected completely.

The evaluation of the one-electron matrix elements for the kinetic energy and potential energy with respect to the nuclei doesn't present any special difficulty. Further approximations which have been made to simplify the electron potentials (Coulomb and exchange) are considered next.

C. Approximations in Coulomb Potential

In the numerical evaluation of $\langle\chi_i|V_c|\chi_j\rangle$ we need to know the value of the Coulomb potential $\int \varrho(\boldsymbol{r}_2)/(|\boldsymbol{r}_k-\boldsymbol{r}_2|)\,d\boldsymbol{r}_2$ at each sample point $\boldsymbol{r}_k$. In principle we can again determine this integral numerically, which, however, raises the total computational effort considerably. So we have approximated the density $\varrho(\boldsymbol{r})$ with a sum over spherically symmetric densities around each center, $\varrho(\boldsymbol{r}) \approx \sum_{A} \varrho_{A}(\boldsymbol{r})$. This reduces the determination of the Coulomb potential at each sample point to the calculation of a number of one-center integrals, which can be done analytically. A Mulliken population analysis is used to decide in which way the total density must be broken up into atomic parts. We simply use the total gross orbital populations of the atomic sub-shells to calculate the spherically symmetric densities around each nucleus. It should be noted that we do not further approximate the densities around the atoms in the molecule by their "muffin tin" average, as is often done in energyband calculations (APW and KKR methods) and sometimes in molecular calculations (cf. the scattered wave method [22]). This point is of some importance when considering the origins of molecular bond formation.

D. Iterative Procedure

As a self-consistency criterion we have used the requirement that the gross orbital populations of the 1*s*-, 2*s*-, 2*p*-, etc. subshells of the atoms, which follow from a Mulliken population analysis, should be the same as those which are used in calculating the spherically symmetric atomic densities. This procedure can be criticized as well as the Mulliken population analysis on which it is based. Since, however, in our calculations the majority of the overlap populations are very small (ionic bonds), the conventional equipartitioning of the overlap charges hardly affects the results. The resulting SCF procedure is easier to implement, and converges more rapidly than the conventional scheme. This form of self-consistent constraints on the input potentials is admittedly an ad hoc construction; nevertheless, it seems well suited to the problem at hand.

E. Possible Extensions of the Method

We may make a few remarks concerning the advantages offered by this combination of approximations. In the first place, we can handle arbitrary basis functions, STO's taking no more time, for instance, than GTO's. Secondly, the number of matrix elements to be calculated increases only as the square of the number of orbitals (not as the fourth power!). Furthermore, we have gained so much in speed of computation and in storage requirements, that large systems can be dealt with in an all-electron treatment. An additional advantage lies in the nature of the approximations involved, which makes it possible to get a very direct physical picture of the interactions, and what may be sources of errors.

As is immediately apparent, the relative position of metal *d* orbital and hydrocarbon π-orbital energies is crucial to any discussion of d-π interactions in the systems studied here. In addition to depending upon the molecular environment, we must expect these level spacings to be somewhat model dependent. This model dependence can be anticipated because of the relatively different response of (somewhat tightly bound) *d* orbitals and (rather diffuse) hydrocarbon π orbitals under *exchange scaling*. Very briefly, one can put forward arguments for choosing slightly different numerical parameters in Eq. (2); the so-called X_{α}

method is one prescription for choosing the exchange scaling parameter, which has been widely exploited [24]. For the present we have only used the unscaled full Slater exchange, as in Eq. (2), but recognize that in future calculations it may be important to consider modified potentials.

To obtain a more detailed understanding of reaction mechanisms, one would like to study variations of *total energy* of the molecular systems for various geometries. Several obstacles have to be overcome before the present methods can be extended in this direction. First, "tighter", more rigorous self-consistency conditions must be imposed, since we are then interested in small changes in total energy which are rather sensitive to molecular charge re-arrangement. Good progress is being made in this direction; however, the computational load is greatly increased. Second, we must consider whether approximate total energy expressions (derived in the spirit of the HFS model) are sufficiently accurate for our purpose, and devise more effective ways of obtaining numerical values to the required accuracy. We consider that, at present, the values for the total energy obtained by our methods are not accurate enough to perform a meaningful geometry optimization.

F. Ethylene, A Comparison with Other Methods

That the present method can be used to obtain an adequate description for the crystalline part of our systems, may be inferred from experience with applications to crystals [15 18]. To test the validity of this method in molecular calculations, we performed calculations on some small molecules. The results for ethylene, which are most interesting in the context of this paper, will be discussed briefly. In Table 1 we present the orbital energies calculated by the present (DVM)-method in a double ζ basis of STO's (exponents from Clementi [25]). For comparison purposes we also give the orbital energies from an all-integral Hartree-Fock calculation in a Gaussian basis [26]. The latter basis consists of 10*s*, and 5*p* functions on C and 5*s* functions on H, contracted to a (4,2|1) basis. We may consider this basis to have double ζ quality. The geometry is the same in both calculations. We see that the agreement between the orbital energies calculated by the two methods is satisfying. The largest deviations occur for the highest orbitals, but always they remain less than 0.1 a.u.

A more sensitive test for the quality of a wavefunction is a population analysis. It is rather difficult to compare population analyses which have been performed in different bases. Therefore we compared a Hartree-Fock calculation by Palke and Lipscomb [27] on ethylene, in a minimal Slater basis, with a DVM calculation using exactly the same geometry and basis set. The agreement for the orbital energies was even better than in the previous Gaussian case. The population analyses for the two calculations are given in Table 2. The agreement in overlap populations is striking. The gross orbital populations also compare favourably, although for the 2*s* and $2p_y$ orbitals we observe slight deviations. These deviations, being all of the same sign, add up to significant differences in atom charges. We may conclude from these test calculations that the method employed gives a rather correct picture (i.e., agrees with HF) of one electron energies and charge densities, not only for crystals but also for covalent molecules.

Table 1. Comparison between orbital energies of C_2H_4 from the present approximate Hartree-Fock-Slater method, and from an *ab initio* all-electron, all-integral calculation [26]

Symm.	HFS	*Ab initio*
A_g	−11.2136	−11.2358
	− 0.9904	− 1.0344
	− 0.6553	− 0.5863
B_{2u}	−11.2133	−11.2343
	− 0.8278	− 0.8002
B_{3u}	− 0.6956	− 0.6481
B_{1g}	− 0.5890	− 0.5085
$B_{1u}(\pi)$	− 0.4560	− 0.3691

Table 2. Comparison between population analyses from the present approximate Hartree-Fock-Slater method, and from an *ab initio*, all-electron, all-integral calculation [27]. Exactly the same, minimal Slater, basis has been used in both calculations

	HFS	*Ab initio*
Atom-atom		
Overlap populations		
C-C	0.58	0.61
$(C\text{-}C)_\pi$	0.21	0.21
$(C\text{-}C)_\sigma$	0.37	0.40
C-H	0.39	0.41
Orbital populations		
C 1*s*	2.00	2.00
2*s*	1.31	1.20
$2p_x$	1.04	1.01
$2p_y$	1.14	1.07
$2p_z$	1.00	1.00
H 1*s*	0.76	0.86
Atom charges		
C	−0.49	−0.28
H	+0.24	+0.14

When we compare the results of the present method with those of semi-empirical methods, it appears that our method is certainly in better agreement with all-integral all-electron Hartree-Fock calculations. It is our own experience that the *orbital energies* calculated with a CNDO or INDO scheme deviate considerably from the *ab initio* values. This fact has already been noted by Pople *et al.* [28], and must be considered a most unfortunate feature of the semi-empirical schemes if we want to study the interaction between such different systems as a hydrocarbon like C_2H_4 and a transition metal ion in a crystal environment. It is an additional advantage of the present method that the electronic bonding structure, as determined from a population analysis, is much closer to the all-integral Hartree-Fock results than the bond structure calculated by a semi-empirical method.

3. Model Systems

As model systems we have chosen the $[(C_2H_4)TiF_5]^{2-}$ and $[(C_2H_4)NiF_5]^{3-}$ complexes (see Fig. 1), with Ti formally trivalent and Ni divalent. The metal-fluorine distances have been taken from the respective crystals; the ethylene geometry has been kept constant in all calculations. The metal-ethylene distance has been varied to get an idea of the changes which occur when an ethylene molecule approaches the vacant coordination position. Details of the geometry are given in Fig. 1. The Ti-complex bears a close resemblance to the Ziegler-Natta catalyst; however, we have replaced the Cl^- ligands by F^-, because of the smaller number of basis functions required. It is plausible to assume that substituting F^- for Cl^- has little effect on the Ti-ethylene interaction. This is substantiated by our results which indicate that the purely electrostatic effect of the negative charges on these ligands is by far the dominating factor.

We have neglected in all our calculations the influence of the rest of the crystal, and confined ourselves to the first coordination sphere of Ti (or Ni). The Madelung part of the potential energy, due to the second and following coordination spheres, can be considered to be constant over a sphere with a radius of approximately 7 a.u., centered at the position of the metal. Only our calculations with ethylene at a distance of 10 a.u. from the metal fall outside this range, and we have merely used these calculations as a reference, since there is virtually no interaction between ethylene and the crystal at this distance. Thus the only effect of the Madelung potential would be an equal shift of all one-electron energies. We have neglected the influence of the non-spherical terms occurring in the lattice sum, which makes up the potential due to the rest of the crystal. Their contribution is difficult to calculate for all the points of interest and, anyhow, small. For comparison purposes we have performed analogous calculations on the interaction between an ethylene molecule and a Ni^{2+} ion in a nickel fluoride crystal, where one finds a d^8 system instead of the d^1 system of Ti^{3+}.

The metal-orbitals which are important with respect to the σ-donation from ethylene to the metal are the $3d_{z^2}$ and perhaps the $4s$ orbital. These orbitals belong

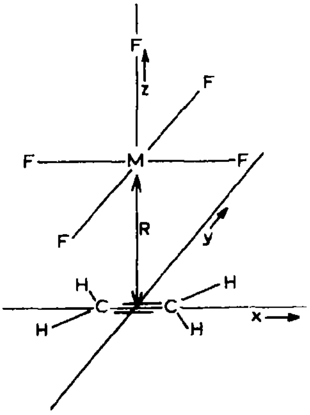

Fig. 1. Geometry of the model system. M is Ti^{3+} or Ni^{2+}. The $M-C_2H_4$ distance, R, has been varied (10, 6, 4 and 3 a.u.). The following distances have been used (in a.u.): C-C, 2.534; C-H, 2.003; Ti-F 3.61; Ni F, 3.79. The HCH angle was 120°

to the A_1 representation of the C_{2v} symmetry group of our complexes. The orbital with the proper symmetry for π-back donation is the $3d_{xz}$ orbital, having B_1 symmetry. The ethylene orbitals which play a dominant role in σ-donation and π-back donation are supposed to be the π and π* MO's respectively. We continue to use the conventional symbols π and π* for the ethylene MO's, although these MO's have, with respect to the metal ethylene bond, σ and π type symmetry respectively. It is to be noted, moreover, that it is no longer forbidden by symmetry for the carbon 2*s* AO's, to mix with the carbon 2*p*π AO's. We have used, in all calculations reported, a complete double-ζ basis of Slater-type orbitals. The exponents have been taken from Clementi [25], and Clementi *et al.* [29]. Although we did not optimize the basis set, we believe this basis to be sufficiently flexible to describe bonding and hybridization effects adequately.

It is satisfying, indeed, that our method allows the use of such an extensive basis for systems which are quite large.

4. Results

We will now consider the results of the calculations in detail.

A. Atom Charges

The atom charges, resulting from a Mulliken population analysis, have been collected in Table 3. We should not attach too much significance to the absolute quantities, but they are useful for a comparison between the different metal-ethylene distances. Looking first at the trends in the Ti complex, we see a sharp increase in the negative charge on ethylene if we go from 6–4 a.u., which is followed by a decrease if we go further to 3 a.u. The positive charge on Ti exhibits the same trend. As the π-back donation and σ-donation have an opposite effect upon the charges, it is clear that we have to be careful in interpreting these changes in the charges. However, from the net negative charge on C_2H_4 we can safely conclude that the π-back donation is stronger than the σ-donation at all distances, although in going from 4–3 a.u. the σ-donation must become relatively more important. We furthermore see that the F^- ions act as a buffer: the building up of a large positive charge on Ti is opposed by an electron shift from the negative ligands towards the central metal ion.

Table 3. Charges resulting from a Mulliken population analysis for the systems TiF_5–C_2H_4 and $NiF_5C_2H_4$. *R* is the distance from the metal atom to center of the CC bond

R(a.u.)	3	4	6	10
Ti	+2.30	+2.32	+2.21	+2.16
F_5	−4.16	−4.115	−4.18	−4.16
C_2H_4	−0.13	−0.20	−0.02	0.00
Ni	+1.72	+1.685	+1.66	+1.60
F_5	−4.48	−4.52	−4.55	−4.59
C_2H_4	−0.24	−0.16	−0.11	−0.005

The situation in the Ni-complexes is slightly different. The positive charge on Ni and the negative charge on C_2H_4 now increase monotonically. We shall see in a following paragraph, that the large negative charge found on ethylene even when this molecule is still at a distance of 6 a.u. from Ni, is caused by the fact that at this distance only π-back donation is operative; σ-donation, which could lower the charge, becomes important only at smaller distances.

B. Orbital Energies

In Fig. 2 we show the orbital energies in the Ti-complex at different values of *R*, the Ti–C=C bond distance.

The shifts in orbital energies of the ethylene MO's can (apart from binding effects, which influence mainly the π and π^* orbitals), be explained in detail as

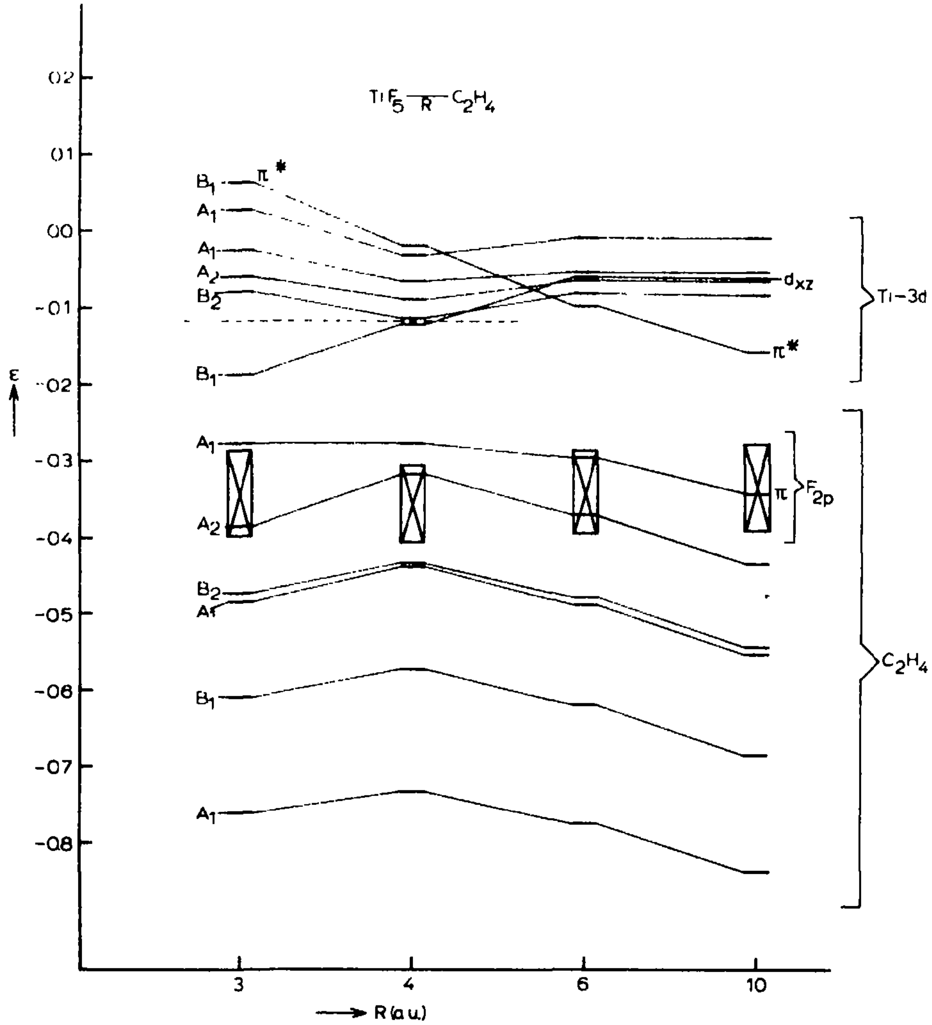

Fig. 2. Orbital energy diagram for the TiF_5 C_2H_4 complex. *R* and ε in a.u.

arising from two effects: a) the purely electrostatic potential due to the ions of the cluster; b) the negative charge on ethylene.The relatively high orbital energies at 4 a.u. reflect, for instance, the high negative charge on ethylene at that distance, whereas the low orbital energies of the Ti–3d orbitals arise from the high positive charge on Ti. The most striking feature of this energy diagram is the strong interaction between the Ti–3d_{xz} and the ethylene π^* MO. There is one d-electron in Ti^{3+}. If we use an Aufbau principle we should place it in the π^* MO of ethylene, at $R=6$ or 10 a.u. However, if we occupy the π^* MO, we deal with a negative ethylene ion, and a Ti^{4+} ion. Of course, the π^* MO then rises, the Ti- 3d orbitals descend and become much lower than the ethylene π^* MO. The situation that we have a negative ethylene molecule at these large distances, is totally unrealistic, so we avoided this oscillation by simply putting the d-electron in one of the Ti-3d orbitals, the π^* MO thus being empty, as it should be. In fact, at these distances there is not yet any binding between ethylene and the cluster, and we merely use the calculations at these distances as a reference point for comparison with the shorter distances. For this reason, we took the Ti-3d_{xz} orbital as the one to be filled, providing a continuous transition to the situation which occurs also at $R=3$ and 4 a.u. We are able, then, to follow the mixing of the Ti-3d_{xz} and ethylene π^* MO's through the decrease of the Ti-3d_{xz} population and increase of the π^* population. The latter effect is exactly what is commonly denoted as π-back bonding.

The orbital energy diagram for the Ni-complex is quite analogous to that given for the Ti-complex, so we do not show it here. The most remarkable feature is again the interaction between the Ni-3d_{xz} and ethylene π^* orbitals.

The σ-donation doesn't show up as clearly as the π-back donation in the orbital energy diagrams. Only the very slight deviation of the shift in the ethylene π MO as compared with the general pattern of the other ethylene MO's indicates this orbital to be involved in bonding.

C. *Orbital Populations*

To obtain a more quantitative description of the σ-donation, we may use the gross orbital population of the 3d_{z^2} orbital, which appears, together with 3$d_{x^2-y^2}$ in the A_1 symmetry. The σ-donation effect will result in an increase of this orbital population. We have collected in the Tables 4 and 5 the total s and total p gross orbital populations, and the d populations for each symmetry separately (3d_{xz} has B_1-symmetry, 3d_{xy} A_2- and 3d_{yz} B_2-symmetry). The total s and p populations remain constant, so we may conclude that these orbitals are not involved in σ-donation or π-back donation. The only significant changes in orbital populations occur in the 3d_{xz} and 3$d(A_1)$ orbitals. This very simple picture allows the following scheme to be set up: we assume the π-back donation to be equal to the decrease in 3d_{xz} population, and infer from the charge on C_2H_4 how large the σ-donation must be. Internal consistency of this very simple scheme follows from the increase in 3$d(A_1)$ population, which should be roughly equal to the σ-donation as determined in this way. The agreement is rather good indeed. The deviations find a natural explanation in two effects, first the influence of the F^- ions, secondly slight redistributions of the electrons in the metal ion. As far as the

Table 4. Gross orbital populations of Ti-orbitals in TiF_5–C_2H_4, charges on C_2H_4 and amounts of π-back donation and σ-donation derived from these quantities

R(a.u.)	10	6	4	3
Ti $3d(xz)$	1.04	1.02	0.74	0.58
$3d(xy)$	0.09	0.09	0.10	0.11
$3d(yz)$	0.09	0.08	0.10	0.13
$3d(A_1)$	0.50	0.49	0.63	0.77
s	6.11	6.10	6.11	6.10
p	12.01	12.01	12.01	12.01
$Q(C_2H_4)$	0.00	− 0.02	− 0.20	− 0.13
π-back donation	0.00	0.02	0.30	0.46
σ-donation	0.00	0.00	0.10	0.33

Table 5. Gross orbital populations of Ni-orbitals in NiF_5 C_2H_4, charges on C_2H_4 and amounts of π-back donation and σ-donation derived from these quantities

R(a.u.)	10	6	4	3
Ni $3d(xz)$	2.00	1.90	1.82	1.52
$3d(xy)$	2.00	2.00	2.00	2.00
$3d(yz)$	2.00	2.00	2.00	1.99
$3d(A_1)$	2.24	2.28	2.34	2.60
s	6.16	6.16	6.16	6.16
p	12.00	12.00	12.00	12.00
$Q(C_2H_4)$	− 0.01	− 0.11	− 0.16	− 0.24
π-back donation	0.00	0.10	0.18	0.47
σ-donation	0.00	0.00	0.03	0.24

first point is concerned, we have already seen from the atom charges that the electron flow from the negative ligands towards the central metal ion is always small. Moreover, these electrons go mainly into $3d_{x^2-y^2}$ (and $3d_{z^2}$), and do not enhance the $3d_{yz}$ and $3d_{xy}$ populations, a result which also gives us good grounds to neglect their influence on the $3d_{xz}$ population. By way of illustration we take the Ni complex, at $R = 3$ a.u., where the increase of the $3d(A_1)$ population exceeds the σ-donation by 0.12 electrons. This is due almost entirely to electrons from the F^- ions (0.11 e).

Turning now to the second point, we find an example of internal rearrangement in the metal in the Ti-complex at $R = 3$ a.u. The 0.33 electrons, donated by C_2H_4, through the σ-donation, go largely (0.27 e) into $3d(A_1)$, but also contribute noticebly to the $3d_{xy}$ and $3d_{yz}$ populations (0.02 and 0.04 e respectively).

The estimates for the π-back donation and σ-donation obtained in this way, show some remarkable features. The π-back donation is larger than the σ-donation at all distances, but the latter effect becomes relatively more important at shorter distances. It should be pointed out however, that the calculation at $R = 3$ a.u. describes a rather unrealistic situation. From Van der Waals radii one can infer [12] that a distance of approximately 4 a.u. between the center of the ethylene double bond and the central metal ion is to be expected. So our results indicate that σ-donation will be quite small in the Ni case, which is not unexpected since Ni^{2+} is a much more electron-rich ion than Ti^{3+}. For the same reason it is not surprising that we find a considerable π-back donation in the Ni-complex, which is, at $R = 6$ a.u., even larger than in the Ti-complex.

When $R = 4$ a.u. however, which is probably closest to the actual bond distance, we see a much larger interaction with ethylene in the Ti complex, both with respect to π-back donation and to σ-donation.

Although one should be careful not to attach too much significance to these quantities, this might be considered to reflect the experimentally found strong interaction in the Ti-complex. That we have found throughout a larger π-back donation than σ-donation is rather unexpected, because of the high formal charge of the central metal ions. It has been generally assumed that σ-donation will prevail in these cases, while π-back donation might be important in complexes with electron-rich metals, like zero valent group VIII elements. Direct information about the balance between the two effects is of course difficult to obtain, but calculations on the Ag^+–C_2H_4 complex [10] showed σ-donation to be already dominant in that case. The crucial point her is probably the relative position of the metal d orbitals, with respect to the π and π^* orbitals of ethylene. Metals with d orbitals close to or below the ethylene π orbital will be predominantly acceptors; metals with valence-shell electrons in the energy range of the π^* orbital will form strong π-bonds [3, 30]. It is precisely here that the role of the crystal environment of the central metal ions becomes manifest. Due to this crystal environment the position of the metal d orbitals is favourable for π-back donation to occur. The π-back donation heavily influences the electronic structure of the ethylene molecule, as we shall see next.

D. The Ethylene Double Bond

It is clear that both σ-donation and π-back donation tend to weaken the ethylene double bond. The strength of this bond can be related to the C–C overlap population. We give, in Table 6, these overlap populations. The $(C–C)_\pi$ overlap population is that part of the total which is due to the p-π orbitals of the

Table 6. C–C Overlap populations in TiF_5–C_2H_4 and NiF_5–C_2H_4

R(a.u.)	10	6	4	3
		F_5Ti–C_2H_4		
$(C–C)_\sigma$	0.29	0.29	0.16	−0.17
$(C–C)_\pi$	0.21	0.20	0.14	0.10
$(C–C)_{total}$	0.49	0.50	0.31	−0.07
		F_5Ni–C_2H_4		
$(C–C)_\sigma$	0.29	0.27	0.16	−0.18
$(C–C)_\pi$	0.20	0.19	0.17	0.09
$(C–C)_{total}$	0.49	0.46	0.33	−0.09

carbon atoms (the p orbitals perpendicular to the plane of the C_2H_4 molecule), whereas $(C-C)_\sigma$ is due to the σ-frame. We see comparable trends in the Ni- and Ti-complexes, viz., a large decrease in the total overlap population, which is mainly due to the $(C-C)_\pi$ part, particularly at short distances. These overlap populations reveal the unrealistic character of the situation where we have pushed the ethylene molecule as close as 3 a.u to the central metal ion. There is virtually no bonding between the C-atoms any more. If we compare the situation at larger distance, with $R=6$ and 4 a.u., we see that at $R=6$ a.u. the overlap population in the Ni-complex is lower than in the Ti-complex. The reason for this is the π-back donation, which is already considerable in the former complex at this distance. At $R=4$ a.u. however, we see that the overlap population in the Ti-complex has become the smaller of the two, as we expect because of the stronger interaction already noted in this complex.

A detailed analysis of the factors which cause the large decrease in the $(C-C)_\pi$ term, reveals that this must be ascribed to the mixing of carbon $2s$ orbitals into the π^* MO. As a consequence of the larger overlap between the $2s$ AO's than between the $2p$-π AO's, there is a pronounced effect upon the overlap population. Although it is evident that the σ-π separation in the ethylene molecule cannot be carried through in these complexes, one still might be inclined to do so in qualitative considerations of this type of bond. Our calculations indicate this to be a simplification that is not allowed.

E. The Geometry of the Ethylene Molecule

In the π-complexes studied here, (and similar examples) the protons of C_2H_4 are known to be bent away from the central metal ion in a symmetrical way [11c, and references therein]. Also, the C–C distance is often longer than in free ethylene. Although we were not able to perform a geometry optimization, we may conclude from the lowering of the C C overlap population, that we should expect a lengthening of the C C bond in our complexes. The *cis*-bending of the protons away from the central metal ion has been explained by Blizzard and Santry [31] as a purely electronic effect for the analogous case of acetylene bonded to a transition metal. They were able to relate this bending to the populations of the π^* and π MO's. Although they could only perform simplified model calculations, without explicity including the central metal ion, we may point out an interesting parallelism between their calculations and ours, as far as the bonding in these π-complexes of olefins is concerned. From their model calculations and symmetry considerations, Blizzard and Santry concluded that *cis*-bending indicates that π-back bonding is very important, a result which is confirmed by our calculations on the complete complexes. Moreover, they found the contribution of the σ^* MO $(2s_{C1}-2s_{C2})$ to the π-bond to be nearly as important as that of the π^* MO, a result which is also confirmed by our calculations. In view of this correspondence, we may, arguing along the same lines as they did, expect that a proper geometry variation would lead to a *cis*-bent structure. Of course we cannot give a definite answer about the magnitude of the angle of deviation from planarity of the ethylene molecule.

5. Conclusions

We may conclude that the method presented here lends itself very well to the description of a system which consists of such diverse subsystems as a hydrocarbon and a transition-metal crystal. We recall that this is achieved without any need for reparametrization or special adaptations in the theoretical model.

Although we must classify the central metal ions, in particular Ti^{3+}, as electron acceptors ("hard"), we find the π-back donation to be extremely important in both the Ti- and the Ni-complex. This is probably due to the crystal environment of the ions. Especially important is the back bonding because of its great influence upon the electronic structure of the ethylene molecule. The large decrease in C–C overlap population (from 0.50–0.31 at 4 a.u.), which is due mainly to the π-back bonding, reflects the weakening of the C–C double bond. This weakening will lead to a considerable lengthening of this bond. It appears that the decrease of the C–C overlap population must be attributed to the strong interaction of the central metal ion with a σ^* as well as the π^* MO of ethylene. These findings are contrary to habitual thinking in chemistry, although the considerations of Blizzard and Santry, based on simple model calculations and symmetry arguments, already pointed in the same direction. Comparing the Ni^{2+} and Ti^{3+} complexes, we find at $R=4$ a.u., a considerably stronger interaction between ethylene and the central metal ion for Titanium than for Nickel. This can be related to the experimentally found catalytic activity of the Ziegler-Natta catalyst but we should not lose sight of the model character of our systems. We mention in this respect, not only the replacement of a chloride by a fluoride crystal, but also the fact that the influence of steric factors fell outside the scope of this investigation. The latter, however, may play an important role in the actual catalytic reaction [7].

Acknowledgement. The calculations reported here were performed on the IBM 360/65 computer, Rekencentrum, Technische Hogeschool, Delft. The cooperation of the staff of the centre is gratefully acknowledged. We thank Dr. T. Parameswaran for advice and assistance in the early stages of this work.

References

1. Dewar, M.J.S.: Bull. Soc. chim. France **18**, C 79 (1951).
2. Chatt, J., Duncanson, L. A.: J. chem. Soc. **1953**, 2939.
3. Pettit, L. D.: Quart. Rev. **25**, 1 (1971).
4. Bonding in Metallo-organic Compounds. Discus. Faraday Soc. **47**, (1969).
5. Heimbach, P., Traunmüller, R.: Chemie der Metall-Olefin Komplexe. Weinheim: Verlag Chemie 1968.
6. Mulliken, R.S., Person, W.B.: Molecular complexes. New York: Wiley 1969.
7. Cossee, P.: Stereoregular polymers, ed. G. Natta, F. Danusso. Vol. I, Ch. 9. Oxford: Pergamon Press 1967.
8. Moore, J.W.: Acta chem. scand. **20**, 1154 (1966).
9. Kato, H.: Bull. chem. Soc. Japan **44**, 348 (1971).
10. Basch, H.: J. chem. Physics **56**, 441 (1972).
11. Nelson, J. H., Wheelock, K.S., Cusachs, L.C., Jonassen, H.B.:
11a. J. Amer. chem. Soc. **92**, 5110 (1970).
11b. J. Amer. chem. Soc. **91**, 7005 (1969).
11c. Inorg. Chemistry **11**, 422 (1972).

12. Cossee, P., Ros, P., Schachtschneider, J. H.: Proceedings of the fourth International Congress on Catalysis, Moscow, 1968. Akadémiai Kiado, Boedapest, 1971.
13. Roothaan, C. C. J.: Rev. mod. Physics **23**, 69 (1951).
14. Jansen, H. B., Ros, P.: Theoret. chim. Acta (Berl.), in press.
15. *Ellis, D. E.: Int. J. quant. Chemistry* **2S**, *35 (1968).*
16. Ellis, D. E., Painter, G. S.: Physic Rev. **B2**, 2887 (1970).
17. Painter, G. S., Ellis, D. E.: Physic Rev. **B1**, 4747 (1970).
18. Painter, G. S.: Int. J. quant. Chemistry **5S**, 501 (1971).
19. *Ellis, D. E., Parameswaran, T.: Int. J. quant. Chemistry* **5S**, 443 (1971).
20. Haselgrove, C B.: Math. Comp. **15**, 323 (1961).
21 Conroy, H.: J. chem. Physics **47**, 5307 (1967).
22. Johnson, K. H., Smith, F. C.: Chem. Physics Letters **7**, 541 (1970); Chem. Physics Letters **10**, 219 (1971).
23 Slater, J. C.: Physic. Rev. **81**, 385 (1951).
24. Slater, J. C., Wood, J. H.: Int. J. quant. Chemistry **4S**, 3 (1971).
25 Clementi, E.: Tables of atomic functions, Suppl. to IBM J. Research Developm. **9** (2), (1965).
26. Buenker, R. J., Peyerimhoff, S. D., Kammer, W. E.: J. chem. Physics **55**, 814 (1971).
27. Palke, W. E., Lipscomb, W. N.: J. Amer. chem. Soc. **88**, 2384 (1966).
28. Pople, J. A., Segal, G. A.: J. chem. Physics **43**, S 136 (1965).
29. Clementi, E., Matcha, R., Veillard, A.: J. chem. Physics **47**, 1865, (1967).
30 Greaves, F. O., Lock, C. J. L., Maitlis, P. M.: Canad. J. Chem. **46**, 3879 (1968).
31. Blizzard, A. C., Santry, D. P.: J. Amer. chem. Soc. **90**, 5749 (1968).

Prof. Dr. P. Ros
Scheikundig Laboratorium
Vrije Universiteit
Amsterdam
Holland

Theoret. chim. Acta (Berl.) 27, 355—366 (1972)
© by Springer-Verlag 1972

First Order Pair Functions for the Beryllium Isoelectronic Sequence

B. C. Webster and R. F. Stewart

Department of Chemistry, The University of Glasgow, Scotland

Received June 12, 1972

The first order pair equations have been solved for the four electron sequence Li^- to Ne^{6+}. A variational perturbation procedure is blended with numerical methods to generate a method for computing pair functions which is both accurate and efficient with respect to time of computation.

The variation in the pair correlation energies as a function of atomic number is discussed and the asymptotic behaviour of $E^2(l)$ as l^{-4} and l^{-6} for singlet and triplet states respectively is corroborated. An estimate is made for the electron affinity of lithium.

Die Paargleichungen 1. Ordnung wurden für die Reihe der Ionen mit 4 Elektronen von Li^- bis Ne^{6+} gelöst. Ein Variations-Störungsverfahren wird mit numerischen Methoden verknüpft, um eine Methode zur Berechnung von Paarfunktionen zu erhalten, die genau ist und möglichst geringe Rechenzeiten benötigt. Die Variation der Paarkorrelationsenergien als Funktion der Atomnummer wird diskutiert und das asymptotische Verhalten von $E^2(l)$ wie l^{-4} und l^{-6} für Singulet- und Tripletzustände wird bestätigt. Für Lithium wird die Elektronenaffinität abgeschätzt.

Résolution des équations de paires au premier ordre pour la série à 4 électrons: Li^- à Ne^{6+}. Un procédé de perturbation variationnel est lié à des méthodes numériques pour engendrer une méthode de calcul des fonctions de paires simultanément précise et économique. La variation des énergies de corrélation de paires en fonction du nombre atomique est discutée ainsi que le comportement asymptotique de $E^2(l)$ par rapport à l^{-4} et l^{-6} pour les états singlet et triplet respectivement.

Introduction

There have been numerous attempts to obtain atomic wave functions in which correlation of electron motion is permitted. Amongst review articles concerning the problem, those of Nesbet [1], Sinanoğlu [2], Kelly [3], and Silverman and Bridgman [4] are very informative. Unlike one electron functions, compilations of two electron wave functions for atoms have as yet to appear.

An exact solution of the N electron wave equation for an atom may be expressed in the form

$$\psi = \psi_0 + \sum_{ij} \alpha(ij) + \sum_{ijk} \beta(ijk) + \cdots$$

where the leading term is a Slater determinant composed of one electron functions. This is complemented by successive summations which allow for all two electron, three electron, and higher order interactions respectively. The two electron component is defined by

$$\alpha(ij) = \det|\varphi_1(r_1)\,\varphi_2(r_2)\dots\varphi_{i-1}(r_{i-1})\,\varphi_{j-1}(r_{j-1}) \cdot \varphi_{i+1}(r_{i+1})\,\varphi_{j+1}(r_{j+1})\,\chi(r_i r_j)| \,.$$

In this expression $\chi(r_i r_j)$ is an antisymmetrised pair function whilst normalisation and antisymmetrisation of $\alpha(ij)$ is implied by the symbol det.

Termination of the series at the opening term ψ_0 and invocation of the variation principle, as is well known, leads to the Hartree-Fock equations for the one electron functions $\varphi_k(r_k)$. On truncation at the second term, there is a choice in the manner in which the equations for the two electron functions may be derived.

If ψ_0 is held to be a determinant of Hartree-Fock one electron functions then the two electron functions are given by the equations derived originally by Sinanoğlu [5] though links to an early study of Fock, Veselov, and Petrashen [6] have been traced. Such equations are also known as the Bethe-Goldstone equations. As Nesbet has succinctly written, "An nth order Bethe-Goldstone equation can be defined as the exact solution of an n-particle Schrödinger equation with the wave function constrained to be orthogonal to the remaining $N-n$ orbitals of an N particle Fermi Sea" [1]. When the one electron functions are determined variationally together with the two electron functions then the one electron functions no longer satisfy the Hartree-Fock equations. Rather they comply to the equations developed by Nesbet following the studies of Brueckner [7] and independently by Szasz [8].

Cogent arguments have been presented for the retention of a Hartree-Fock basis. In the Hartree-Fock model as applied to an atom, each electron is regarded as moving in the field of the nucleus and the spherically averaged charge distribution of the remaining electrons. A natural extension of this model is to permit each pair of electrons to interact directly whilst moving in the nuclear field and the averaged charge distribution of the remaining electrons as described by their Hartree-Fock functions.

Often in the calculation of such pair functions, the Hylleraas inequality is used within a variational perturbation approach. Less frequently numerical methods have been employed. In this study, the central theme of which is a four electron atomic sequence, a blend of the two approaches has been attempted to obtain the first order pair functions.

The Pair Equations

The theory of Sinanoğlu has been delineated several times by a variety of authors and does not require repetition. In the particular example of Beryllium, Byron, and Joachain [9] show that commencing from the functional

$$F(\Phi') = \langle \Phi' | H_0 - E_0 | \Phi' \rangle + 2 \langle \Phi' | H_1 - E_1 | \Phi_0 \rangle$$

the pair function from which Φ' is constituted are given as solutions to the equation of type

$$\begin{aligned} &[H^{\mathrm{HF}}(r) + H^{\mathrm{HF}}(r') - \varepsilon_i - \varepsilon_j]\, \chi_{ij}(r, r') \\ &\qquad = -[1/|r-r'| - V_i(r) - V_j(r) - V_i(r') - V_j(r') - \varepsilon^1(ij)] \qquad (1) \\ &\qquad \cdot \frac{1}{\sqrt{2}} [\varphi_i(r)\, \varphi_j(r') - \varphi_i(r')\, \varphi_j(r)]\,. \end{aligned}$$

The zeroth order function Φ_0 satisfies the Hartree-Fock equation

$$H_0\Phi_0 = E_0\Phi_0$$

with

$$E_0 = \sum_i \varepsilon_i$$

ε_i being the one electron orbital energy. The Hartree-Fock coulomb and exchange energies are expressed within $V_i(r)$

$$\begin{aligned} V_i(r)f(r) &= \int \varphi_i(r')\,1/|r-r'|\,\varphi_i(r')\,dr'\,f(r) \\ &\quad -\int \varphi_i(r')\,1/|r-r'|\,f(r')\,dr'\,\varphi_i(r) \end{aligned}$$

$E_1 = \sum_{ij} \varepsilon^1(ij)$ is compounded from such coulomb and exchange terms.

A perturbation arises from the difference between the exact electron interaction and that provided by the Hartree-Fock potential. Corrections to the total energy to third order may then be evaluated in the usual manner. For example with the function Φ' held orthogonal to Φ_0, the second order energy is given by

$$E_2 = \langle\Phi_0|H_1|\Phi'\rangle\,.$$

Partitioned as a sum of pair energies

$$E_2 = \sum_{ij} \varepsilon^2(ij)$$

where

$$\begin{aligned} \varepsilon^2(ij) = \Big\langle \chi_{ij}(rr')\Big|\, & 1/|r-r'| - V_i(r) - V_j(r) \\ & - V_i(r') - V_j(r') - \varepsilon^1(ij)\Big|\, \frac{1}{\sqrt{2}}\,[\varphi_i(r)\,\varphi_j(r') \\ & - \varphi_i(r')\,\varphi_j(r)]\Big\rangle\,. \end{aligned}$$

Byron and Joachain discuss further the relative merits of various functional forms to represent the trial function. Adoption of a Legendre expansion for $\chi(r_1 r_2)$ in the manner first suggested by Luke, Meyerott, and Clendenin [10] permits the pair Eq. (1) to be uncoupled.

$$\chi^{ij}(r_1 r_2 \cos\theta_{12}) = 1/4\pi \sum_l U_l^{ij}(r_1 r_2)/r_1 r_2 \cdot P_l(\cos\theta_{12})\,.$$

The expansion coefficients may be obtained as solutions to the set of equations of type

$$\begin{aligned} \left[\frac{\partial^2}{\partial r_1^2} + \frac{\partial^2}{\partial r_2^2} + \frac{2Y(r_1)}{r_1} + \frac{2Y(r_2)}{r_2} - \frac{l(l+1)}{r_1^2} - \frac{l(l+1)}{r_2^2} - \varepsilon_i - \varepsilon_j\right] U_l(r_1 r_2) \\ = r_1 r_2 G_l(r_1 r_2)\,. \qquad (2) \end{aligned}$$

In these equations $Y(r_i)$ is a potential function containing the nuclear and Hartree-Fock potentials, whilst $G_l(r_1 r_2)$ consists of terms arising from the expansion of $1/|r-r'|$, together with the use of Hartree-Fock one electron functions to represent $\varphi_k(r_k)$.

Alternatively the coefficients might be expressed in an analytical form, for example a configuration mixing function could be adopted.

$$U_{l\pm}^{ij}(r_1 r_2) = \Sigma C_{lmn}(r_1^m r_2^n + r_1^n r_2^m) \cdot [(\exp(-\alpha/2 \cdot r_1)\exp(--\beta/2 \cdot r_2) \pm \exp(-\beta/2 r_1)\exp(-\alpha/2 \cdot r_2))]$$

in which the sign indicates the symmetry with respect to the space co-ordinates. The advantages of this type of function are marred by the slow convergence of the series. Accuracy in the calculation of the higher partial waves is inhibited. In an early study of the problem Schwartz remarks "For high l values the most important part of this function is concentrated very sharply about the point $r_1 = r_2$ and a direct attack on the associated two dimensional partial differential equations might be the best way to solve for these highly correlated functions" [11].

It is this suggestion which is pursued further here. The $l = 0$ component is determined using the above type of function in which the number of terms included in the expansion is taken to yield the desired accuracy for the pair under consideration. Higher partial waves are determined by direct solution of the associated differential equations. By proceeding in this manner a further difficulty is obviated. "The 120 strip s wave calculation required the solution of 14000 linear equations which took about 1h on the IBM 360/75. The s wave cut off was taken at 24 a.u. which was still not far enough from the nucleus. Clearly it was not practical to resolve the equations with a larger cut off. The functions for $l > 0$ were much less difficult and could be obtained easily in only a few minutes." Such is the comment of Winter and McKoy in seeking a numerical solution of the hydrogenic pair equation for a three electron atom [12]. This viewpoint is corroborated by the present authors' experience with the helium atom. Numerical calculation of the s wave to an accuracy comparable with the higher waves is the major part of a total numerical calculation. In sharp contrast, the s wave for the (1s 1s) pair of beryllium as obtained here required ~12 secs upon a UNIVAC 1108, the total calculation of all higher waves and energies being completed in the order of four minutes.

The use of finite difference methods in obtaining pair functions for helium has been elaborated in a series of papers by McKoy and Winter which are notable for their clarity [13]. Similar techniques are deployed in this study. The kernel of the approach is to transform the partial differential equations (2) into a set of linear equations by means of a difference approximation. A fourth order difference has been adopted.

$$\frac{\partial^2 f}{\partial r^2} \sim \frac{1}{h^2}\left[-\frac{1}{12}f(r-2h) + \frac{4}{3}f(r-h) - \frac{5}{2}f(r) + \frac{4}{3}f(r+h) - \frac{1}{12}f(r+2h)\right].$$

At the boundary a switch to a second difference is effected. The calculations are performed over a range of grid sizes, defined by h, the equations being solved by the method of successive over-relaxation. By use of the Bolton-Scoins relation linking the energy at $h = 0$ to the energies evaluated at other choices for h, accurate values for the energy may be obtained [14].

$$E(h) = E(0) + C_2 h^2 + C_4 h^4 + C_6 h^6 + \cdots .$$

The ($1s$ $1s$), ($2s$ $2s$) and ($1s$ $2s$) pairs of the four electron sequence $\mathrm{Li}^-(1s^2\, 2s^2)$ to Ne^{6+} $(1s^2\, 2s^2)$ now will be discussed in detail against a comparative background provided by earlier studies.

The ($1s$ $1s$) Pair

Collated in Tables 1, 2 and 3 are the pair correlation energies for the four electron sequence. Beryllium is highlighted in the opening tables.

For the ($1s$ $1s$) pair the results are obtained in the manner which has been discussed. A configuration function is employed of the form

$$\psi(r_1 r_2) = \sum_i C_i (r_1^m r_2^n + r_1^n r_2^m) \exp(-\alpha r_1) \exp(-\alpha r_2) .$$

That functions of this type simulate very well the behaviour of the s wave is indicated by a comparison of the analytical studies of Byron and Joachain on the helium sequence with the numerical functions obtained by McKoy and Winter [12, 15]. A 65 term expansion is taken with the parameter α assigned a value equal to the atomic number, and m, n ranging over 0, 1 to 10, 10 respectively. It is from the compilation of Clementi that the Hartree-Fock functions required have been obtained [16].

In the calculation of the higher partial waves "square root" grids of size 20, 25, 30, 35 and 40 are adopted with the cut-off for the ($1s$ $1s$) pairs being determined as $15/Z$. The cut-off requirement has been gauged from studies upon two electron systems, and investigations in which a variety of choices for the cut off were employed.

Table 1. Partial wave components of $E_2(l)$ for the electron pairs of beryllium, and the third order energies ε^3 (atomic units)

l	Pair $1s\uparrow 1s\downarrow$ $-\varepsilon^2$	Pair $2s\uparrow 2s\downarrow$ $-\varepsilon^2$	Pair $1s\uparrow 2s\downarrow$ $-\varepsilon^2$	Pair $1s\uparrow 2s\uparrow$ $-\varepsilon^2$
0	0.01247	0.00226	0.000522	0.000014
1	0.02248	0.02214	0.001241	0.000663
2	0.00355	0.00382	0.000148	0.000050
3	0.00101	0.00119	0.000041	0.000008
4	0.00039	0.00048	0.000015	0.000002
5	0.00018	0.00023	0.000007	0.6×10^{-6}
6	0.00009	0.00012	0.000003	0.2×10^{-6}
7	0.00005	0.00007	0.000002	0.1×10^{-6}
8	0.00003	0.00004	0.000001	0.5×10^{-7}
9	0.00002	0.00003	0.000001	0.3×10^{-7}
$\geqq 10$	0.00005	0.00007	0.000002	0.4×10^{-7}
Totals	0.04031	0.03044	0.001993	0.000738
$-\varepsilon^3$	0.00205	0.00745	0.000200	0.000100

Table 2. A comparison of the pair correlation energies for beryllium (a.u.)

Source	$-\varepsilon(1s\,1s)$	$-\varepsilon(2s\,2s)$	$-\varepsilon(1s\,2s)$	(Expt. −0.0944)	% $E^{\mathrm{cal}}/E^{\mathrm{obs}}$
Watson[a]	0.03759	0.04178	0.00505	0.08442	89.4
Nesbet[b]	0.04183	0.04535	0.00586	0.09304	98.6
Geller, Taylor, and Levine[c]	0.04208	0.04438	--	0.09143	96.9
Kelly[d]	0.04242	0.04488	0.00497	0.09099	96.4
Szasz and Byrne[e]	0.04235	0.04450	-	0.09182	97.3
Present calculation	0.04236	0.03789	0.00606	0.08631	91.4
Byron and Joachain [9]	0.04247	0.0448	0.00524	0.09253	98.0
Bunge[f]	0.04261	0.04550	0.00530	0.09341	99.0
Tuan and Sinanoğlu[g]	0.04395	0.04392	0.00648	0.09435	99.9

[a] Watson, R. E.: Physic Rev. **119**, 170 (1960).

[b] Nesbet, R. K.: Physic. Rev. **155**, 51 (1967).

[c] Geller, M., Taylor, H.S., Levine, H. B.: J. chem. Physics **43**, 1727 (1965).

[d] Kelly, H. P.: Physic Rev. **131**, 684 (1963); **136**, 3896 (1964)

[e] Szasz, I., Byrne, W.: Physic. Rev. **158**, 34 (1967).

[f] Bunge, C. F.: Physic Rev. **168**, 92 (1968)

[g] Tuan, D. F., Sinanoğlu, O.: J. chem. Physics **41**, 2677 (1964).

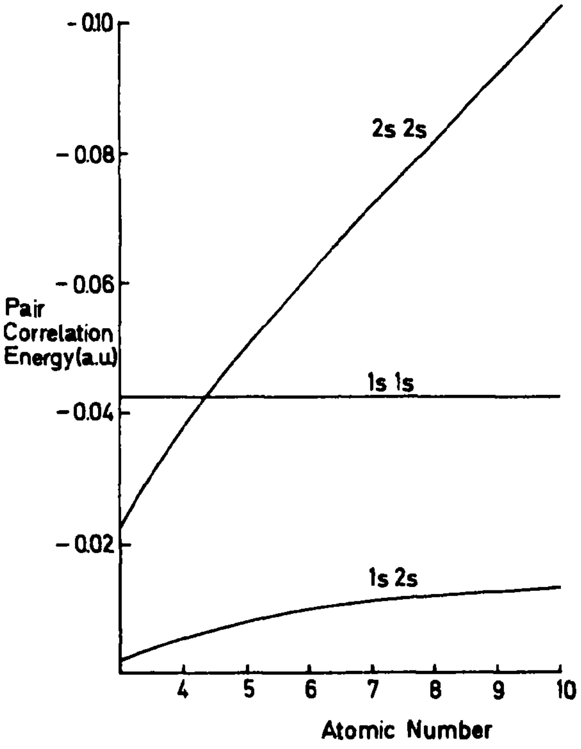

Fig. 1. The variation of the (1s 1s) (2s 2s) and (1s 2s) pair correlation energies (a.u.) with atomic number

Table 3. The pair and total correlation energies of the beryllium sequence (a.u.)

Pair \ Z	3	4	5	6	7	8	9	10
$-\varepsilon(1s\,1s)$	0.04234	0.04236	0.04233	0.04230	0.04229	0.04228	0.04228	0.04228
$-\varepsilon(2s\,2s)$	0.02232	0.03789	0.05005	0.06118	0.07159	0.08178	0.09164	0.10135
$-\varepsilon(1s\,2s)$	0.00247	0.00606	0.00840	0.00995	0.01102	0.01187	0.01250	0.01299
$-E^{\text{corr}}$	0.06713	0.08631	0.10078	0.11343	0.12491	0.13593	0.14642	0.15662
Expt.[a]	—	0.0944	0.1123	0.1268	0.1412	0.1551	0.1684	0.1814
% $E^{\text{calc}}/E^{\text{obs}}$	—	91.4	89.7	89.5	88.5	87.6	86.9	86.3

[a] Clementi, E.: I.B.M. Journal of Research and Development 9, 2 (1965).

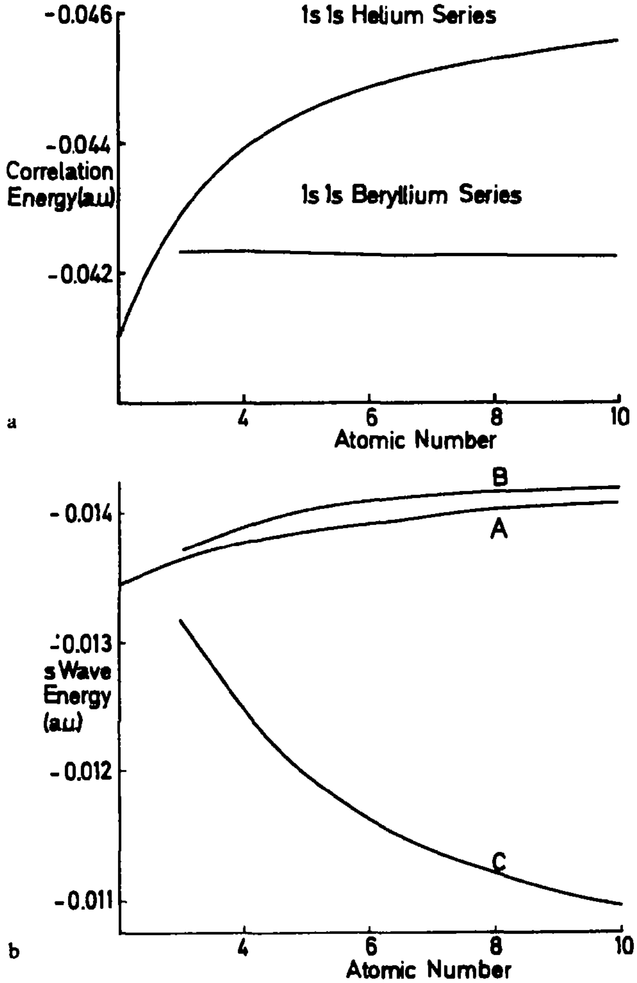

Fig. 2. a The variation of the (1s 1s) pair correlation energy for the helium isoelectronic sequence as compared with the beryllium sequence (a.u.). b The energy of the s wave for the helium sequence and for the beryllium sequence (a.u.). Curve *A*: He sequence. Curve *B*: Be sequence without projection of 2s functions. Curve *C*: Be sequence with projection of 2s functions

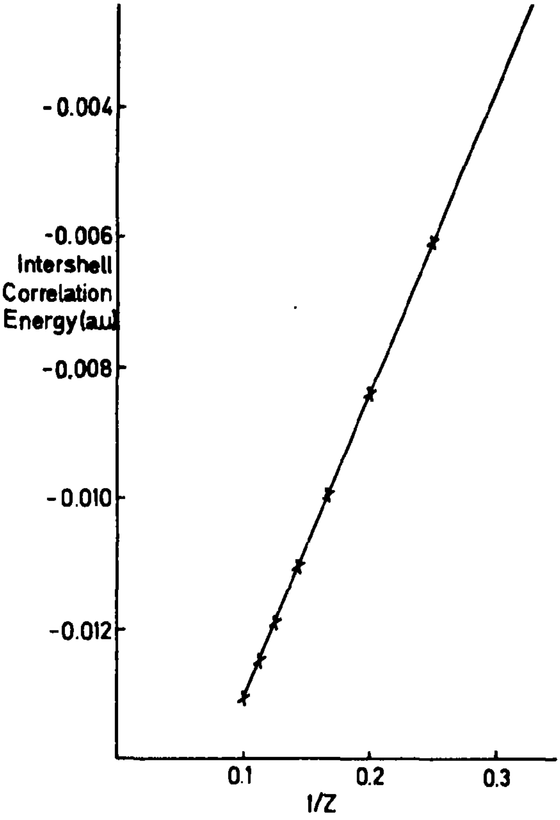

Fig. 3. The intershell correlation energy for the beryllium sequence as a function of 1/Z (a.u.)

larger in magnitude than those of Byron and Joachain, in accord with the viewpoint propagated here.

As the atomic number varies from lithium to neon, the intershell correlation energy follows the behaviour depicted in Fig. 1. In Fig. 3 it is shown that this variation is near to linear in $1/Z$. Miller and Ruedenberg have observed this relationship within an augmented separated pair calculation [20].

It was Schwartz who pointed out that the energy $E(l)$ for singlet states should vary with l as l^{-4} and a guess was made that for the triplet states "the asymptotic rate of decrease would be l^{-6}" [10]. In Fig. 4 the function $\log|\varepsilon^2(l)|$ is plotted against $\log l$. The behaviour for the triplet portion of the $(1s\,2s)$ pair is indeed seen to converge on the line of slope 6 whilst the singlet states of the $(1s\,1s)$, $(1s\,2s)$ and $(1s\,2s)$ pairs follow the line of slope 4. The contribution of partial waves for $l \geq 10$ has been estimated on the basis of this behaviour.

Concluding Discussion

One of the purposes of this study has been to find an efficient technique with respect to time of computation and accuracy in calculation for obtaining pair functions for atoms. An ultimate objective is to be able to compute two

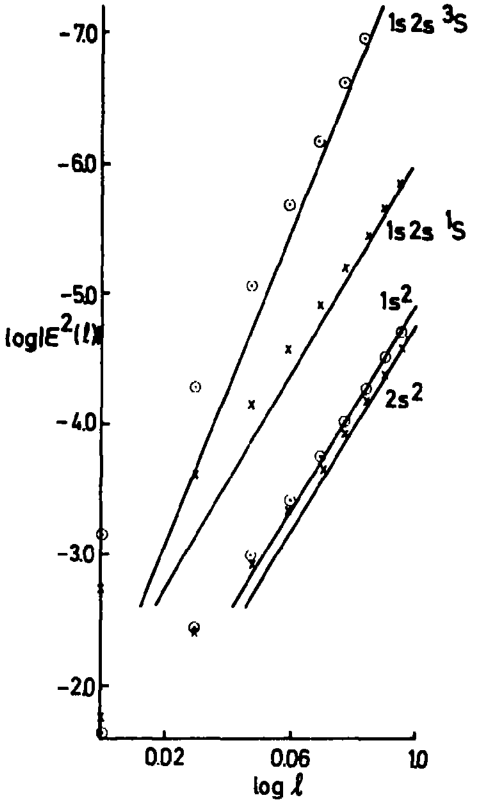

Fig. 4. The asymptotic behaviour of the second order energy

electron functions for atoms of any atomic number. In 1962 Szasz wrote "we shall be able to apply the theory of correlated wave functions to the calculation of wave functions for atoms with any number of electrons". That this is possible in principle may be correct, yet in the ensuing ten years no solutions for other than light atoms have appeared.

A combination of the variational perturbation approach and a numerical approach when the trial functions are represented by a Legendre expansion would seem to offer a tractable route to the evaluation of pair functions. In the four electron sequence studied the first order pair equations have been solved to quite a high order of accuracy without excessive computation time. The central deficiency, as has been remarked, lies in the need for including higher order effects for the (2*s* 2*s*) pair. The calculations have not been extended in this fashion, since it is not felt that for chemical purposes there is a vital need to seek the remaining 10% of the correlation energy. It may be seen from Table 3 that 86–91% of the correlation energy has been accounted for by the present calculations in a situation where a $2p^2$ configuration lies in close proximity to the ground state.

To support such a viewpoint one might consider the calculation of the electron affinity of lithium. On the basis of a Hartree-Fock calculation this is evaluated to be −0.12 eV [16]. With the energy of Li taken to be −7.47807 a.u. which is the result of Weiss, a value of +0.47 eV is found for the electron affinity [20]. The experimental value is cited to be 0.6 eV or alternatively lies between the limits 0.65 eV and 1.05 eV [22, 23]. Should one estimate that the error in the (2s 2s) pair energy is of the order ~0.1 eV, the former value observed is matched, when one allows ~0.03 eV for additional terms which pass neglected. A recent study by Victor and Laughlin yields 0.591 eV for the electron affinity of lithium, strengthening the view that the experimental result of Ya'Akobi is to be preferred [24].

In the early calculations of Hartree upon atomic wave functions numerical techniques played a dominant role. For a period of time now they have passed out of fashion. This is a pity for they are indeed a powerful device in computing atomic properties. The manner in which the computation of single centre molecular expansions, and of atomic polarisabilities is facilitated with numerical techniques will be the subject of subsequent papers. Calculations upon other atomic systems also are in progress.

Acknowledgements One of us (R.F.S.) would like to thank the Carnegie Trust for Universities of Scotland for the award of a scholarship

References

1 Nesbet, R. K. Advances in chemical physics **XIV**, 1 (1969) Int. J. quant. Chemistry, Symposium No 4, 117 (1971)
2 Sinanoğlu, O.: Advances in chemical physics **XIV**, 237 (1969).
3 Kelly, H. P.: Advances in theoretical physics **2**, 75 (1968).
4. Silverman, J. N., Bridgman, G. H.: Rev. mod. Physics **39**, 228 (1967).
5 Sinanoğlu, O.: Proc. Roy. Soc. (London) A **250**, 379 (1961). J. chem. Physics **86**, 706, 3198 (1962). - J. physic. Chem. **1962**, 2283.
6 Fock, V., Vesselov, M., Petrashen, M.: J. expt. theoretical Physics (U.S.S.R.) **10**, 723 (1940).
7 Nesbet, R. K.: Physic. Rev. **109**, 1632 (1958).
8 Szasz, L.: J. math. Physics **3**, 1147 (1962).
9 Byron, F. W., Joachain, C. J.: Physic. Rev. **157**, 7 (1967).
10. Luke, P. J., Meyerott, R. E., Clendenin, W. W.: Physic. Rev. **85**, 401 (1952).
11 Schwartz, C.: Physic. Rev. **126**, 1015 (1962).
12. Winter, N. W., McKoy, M.: Physic. Rev. A **2**, 2219 (1970).
13 McKoy, V., Winter, N. W.: J. chem. Physics **48**, 5514 (1968). - Winter, N., Laferriere, A., McKoy, V.: Physic. Rev. A **2**, 49 (1970). - Winter, N., McKoy, V., Laferriere, A.: Chem. Physics Letters **6**, 175 (1970).
14 Bolton, H. C., Scoins, H. J.: Proc. Cambridge philos. Soc. **53**, 150 (1956).
15. Byron, F. W., Joachain, C. J.: Physic. Rev. **157**, 1 (1967).
16. Clementi, E.: Tables of atomic functions. Supp. to IBM Journal of Research and Development **9**, 2 (1965)
17. Linderberg, J., Shull, H.: J. molecular Spectroscopy **5**, 1 (1960).
18. Alper, J. S.: Physic. Rev. **177**, 86 (1969)
19. Pan, K. C., King, H. F.: J. chem. Physics **56**, 4667 (1972).
20. Miller, K. J., Ruedenberg, K.: J. chem. Physics **48**, 3450 (1968).
21. Weiss, A. W.: Physic. Rev. **122**, 1826 (1961).
22. Ya'Akobi, B.: Physic. Letters **23**, 655 (1966).
23. Scheer, M., Fine, J.: J. chem. Physics **50**, 4343 (1969).
24. Victor, G. A., Laughlin, C.: Chem. Physics Letters **14**, 74 (1972).

Dr. B. C. Webster
Department of Chemistry
The University of Glasgow
Glasgow, Scotland

Theoret. chim. Acta (Berl.) 27, 367—372 (1972)
© by Springer-Verlag 1972

Relationes

Approximate Radial Functions

I. First-Row Transition-Metal 4s and 3d Atomic Orbitals

DAVID A. COPELAND

Department of Chemistry, The University of Tennessee at Martin, Martin, Tennessee 38327, USA

Received February 24, 1972

The approximate 4*s* and 3*d* radial wavefunctions of Richardson *et al.* [J. chem. Physics **36**, 1057 (1962)] for first-row transition-metal atoms and ions have been extended to additional electronic configurations. The results suggest several improvements in the 4*s* wavefunction parameters. Formulas are reported for extending the "double-ζ" 3*d* wavefunctions over the range of atomic orbitals d^1 through d^{10}. The results are intended for use in calculations of chemical bonding.

1. Introduction

The extensive use of the approximate Hartree-Fock wavefunctions for first-row transition metals of Richardson *et al.* [1, 2] and a need [3–6] for more consistent wavefunctions of the same type indicate that additional 4*s* and 3*d* wavefunctions are needed for completeness. A common procedure in LCAO-MO calculations is to vary the AO's for the atoms involved in forming the molecule. By using the wavefunctions of the atoms and ions of the species involved some insight is gained about the bonding of the molecule. Although it has been claimed that the one-electron LCAO-MO model is relatively insensitive to the effect of choice of wavefunctions [7], this has not been the case for orbital energies in several MO calculations [5, 6, 8].

The 4*p* wavefunctions of the first-row transition metals are varied extensively in the reports of Richardson and his co-workers [1, 2] as are the 3*d* and 4*s* wavefunctions which are varied over several common oxidation states. Reported in the present article are approximate 4*s* wavefunctions for several additional atomic electronic configuration and formulas for obtaining approximate 3*d* wavefunctions over the entire range of atomic orbitals d^1 through d^{10}.

2. Procedure

By using the procedure similar to that described by Richardson *et al.* [1], we have taken the approximate radial *s* symmetry wavefunctions to have the form

$$R_{ns} = \sum_{k=1}^{n} \chi_{ks} C_{ks,n} \tag{1}$$

where

$$\chi_{kl} = [(2\zeta_{kl})^{2k+1}/(2k)!]^{\frac{1}{2}} r^{k-1} \exp(-\zeta_{kl} r) \tag{2}$$

and

$$\int R_{ns} R_{n's} r^2 dr = \delta_{n,n'} . \tag{3}$$

Thus we have a linear combination of STO's (Slater type orbitals) which form an orthonormal set over the s symmetry atomic orbitals. We have taken the ground state wavefunction for the $1s$, $2s$, and $3s$ orbitals for each metal to be adequately [9] represented by the Schmidt orthogonal sets given by Richardson *et al.* [1]. The four term $4s$ wavefunctions have been constructed to be Schmidt orthogonal to these orbitals. Consequently the ζ_{4s} parameter is the only variable remaining to be determined. Unlike Richardson *et al.* [1] we have varied the ζ_{4s} extensively until a maximum overlap is obtained between the approximate $4s$ wavefunction and its corresponding Hartree-Fock wavefunction which is taken from Clementi [10] tables.

By utilizing the maximization of overlap as the criterion for the choice of ζ_{4s} for all calculated $4s$ wavefunctions of neutral atoms and ions, the resulting orbitals should be more representative of atomic electronic configuration in MO calculations [11] than those reported by Richardson *et al.* [1, 2] who estimated ζ_{4s} values for the ions.

The radial $3d$ wavefunctions obtained by Richardson *et al.* are of the "double-ζ" type with the formula:

$$R_{3d} = C_1\chi_{3d,1}(\zeta_1) + C_2\chi_{3d,2}(\zeta_2) \tag{4}$$

with

$$\zeta_1 = 0.20Z + 0.15\,, \tag{5}$$

$$\zeta_2 = 0.30Z - 0.20n - 4.40\,, \tag{6}$$

where Z is the nuclear charge, and n is the number of $3d$ electrons. The values of the coefficients in Eq. (4) were obtained by maximizing the overlap with Hartree-Fock wavefunctions (as were the ζ_1 and ζ_2 initially). Since Eqs. (5) and (6) are compact formulas for obtaining the ζ_1 and ζ_2 values, it would be advantageous to have a compact formula to obtain the coefficients. With this in mind we have in Fig. 1 the C_2 values plotted against their respective ζ_2 values for several of the first-row transition metals. In Fig. 1 we have that C_2 is almost linear with ζ_2. Consequently we have assumed that we can express C_2 for each metal in the following form as a function of ζ_2 for its respective metal:

$$C_2(\mathrm{M}) = \alpha_1 + \alpha_2\zeta_2 + \alpha_3\zeta_2^2\,. \tag{7}$$

The values for α_1, α_2 and α_3 for each metal were obtained by a quadratic least square fit of the C_2 and ζ_2 values given by Richardson *et al.* [1]. The remaining C_1 coefficients can be obtained through normalization. With Eqs. (4) thru (7) we now have a systematic procedure for obtaining "double-ζ" $3d$ wavefunctions over the entire range of orbitals from d^1 to d^{10}.

3. Results

Overlaps, S, with Hartree-Fock wave functions and parameters for $4s$ radial functions are presented in Table 1. From the values of S in this table we see that the best approximate wavefunctions are obtained for the $+1$ metal ions for each of the metals with a decrease in accuracy with increasing atomic number. The least accurate representations are obtained with the -1 metal ions, although these are

Table 1. Parameters and overlaps with Hartree-Fock wavefunctions for 4s radial functions

Metal	Ti	V	Cr	Mn	Fe	Co	Ni	Cu
[a] ζ_{1s}	21.40	22.395	23.39	24.385	25.38	26.375	27.37	28.365
ζ_{2s}	8.05	8.475	8.90	9.325	9.75	10.175	10.60	11.025
ζ_{3s}	3.64	3.85	4.06	4.27	4.48	4.69	4.90	5.11

System		ζ_{4s}	C_1	C_2	C_3	C_4	S[b]
Ti	s^2d^1	1.4779	−0.03614	0.12603	−0.33192	1.04515	0.998
	s^2d^2	1.2077	−0.02266	0.07875	−0.20184	1.01691	0.993
	s^2d^3	0.8133	−0.00774	0.02679	−0.06655	1.00185	0.96
V	s^2d^2	1.5364	−0.03541	0.12267	−0.31947	1.04177	0.998
	s^2d^3	1.2582	−0.02222	0.07671	−0.19462	1.01569	0.993
	s^2d^4	0.8390	−0.00731	0.02514	−0.06183	1.00159	0.96
Cr	s^2d^3	1.5918	−0.03459	0.11910	−0.30702	1.03852	0.997
	s^2d^4	1.3061	−0.02172	0.07451	−0.18731	1.01450	0.992
	s^2d^5	0.8608	−0.00684	0.02337	−0.05695	1.00135	0.96
Mn	s^2d^4	1.6456	−0.03379	0.11564	−0.29526	1.03558	0.997
	s^2d^6	1.3486	−0.02105	0.07182	−0.17894	1.01320	0.991
	s^2d^7	0.8998	−0.00682	0.02316	−0.05602	1.00130	0.95
Fe	s^2d^5	1.6954	−0.03286	0.11191	−0.28317	1.03269	0.996
	s^2d^6	1.3997	−0.02076	0.07049	−0.17429	1.01250	0.990
	s^2d^7	0.9290	−0.00658	0.02224	−0.05340	1.00118	0.95
Co	s^2d^6	1.7504	−0.03224	0.10927	−0.27432	1.03063	0.996
	s^2d^7	1.4466	−0.02035	0.06877	−0.16881	1.01170	0.99
	s^2d^8	0.9605	−0.00641	0.02158	−0.05147	1.00109	0.95
Ni	s^2d^7	1.8013	−0.03148	0.10625	−0.26483	1.02852	0.996
	s^2d^8	1.4913	−0.01989	0.06691	−0.16320	1.01092	0.99
	s^2d^{10}	0.9881	−0.00618	0.02072	−0.04912	1.00099	0.96
Cu	s^2d^9	1.5343	−0.01940	0.06504	−0.15766	1.01017	0.99
	s^2d^{10}	1.3505	−0.01380	0.04620	−0.11079	1.00503	0.98
	s^2d^{10}	1.0085	−0.00584	0.01951	−0.04597	1.00087	0.95

[a] ζ_{1s}, ζ_{2s} and ζ_{3s} values were taken from Richardson *et al.* J. chem. Physics 36, 1057 (1962).

[b] S is the overlap between the approximate and the Hartree-Fock wavefunctions.

probably adequate for most purposes. The accuracy obtained for the neutral ground state wavefunctions is intermediate to that of the +1 and −1 ions. A close look at the Hartree-Fock wavefunctions [10] gives some indication as to the inaccuracy of the −1 ion wavefunctions. Since the +1 ion and neutral atom wavefunctions have only one or two dominant terms to be represented by the approximate wavefunction, they can be represented fairly accurately. The −1 ion Hartree-Fock wavefunctions have three dominant terms which contain a greater range of zeta values and thus can only be poorly represented by one dominant term containing ζ_{4s}.

In Table 2 we have tabulated the calculated ζ_{4s} values and several estimated values. The many trends within the calculated values lend considerable confidence to the estimated values. An average value for the differences between successive calculated ζ_{4s} values, $\Delta\zeta_{4s}$, for each horizontal series reveals that each sequence is uniform and has an almost linear increase. This trend is found in the ground state $\zeta_{4s}(3d^n4s^2)$ values reported by Richardson *et al.* [1], but is not found in their

Table 2. Calculated and estimated ζ_{4s} values[a]

Metal System	Ti $n = 2$	V 3	Cr 4	Mn 5	Fe 6	Co 7	Ni 8	Cu 9	$\Delta\zeta_{4s}$
$3d^{n+1}4s^2$	0.8133	0.8390	0.8608	0.8998	0.9290	0.9605	(0.986)	1.0085	0.029
$4s^1$	(1.08)	(1.12)	(1.16)	(1.20)	(1.24)	(1.28)	(1.32)	1.3505	(0.04)
$3d^n\ 4s^2$	1.2077	1.2582	1.3061	1.3486	1.3997	1.4466	1.4913	1.5343	0.046
$4s^1$	(1.39)	(1.44)	(1.49)	(1.55)	(1.59)	(1.65)	(1.70)	(1.75)	(0.05)
$3d^{n-1}4s^2$	1.4779	1.5364	1.5918	1.6456	1.6954	1.7504	1.8013	(1.85)	0.054
$4s^1$	(1.60)	(1.66)	(1.72)	(1.78)	(1.83)	(1.94)	(1.94)	(1.99)	(0.06)
$3d^{n-2}4s^2$	(1.66)	(1.72)	(1.78)	(1.85)	(1.90)	(1.95)	(2.01)	(2.06)	(0.06)

[a] Values in parentheses are estimated values.

estimated values of ζ_{4s} for ions. On comparison, the values reported in Table 4 of Ref. [1] are consistently lower on the Ti end of a horizontal sequence and high on the Ni end of the sequence (*e.g.*, $3d^{n-1}4s^2$, Ti $\zeta_{4s} = 1.45$ as compared with 1.48 reported here; and Ni $\zeta_{4s} = 1.90$ as compared with 1.80). By combining the above mentioned trends with changes in vertical sequences we have made several estimates for additional ζ_{4s} values. Some of the values estimated (and also calculated) are similar to those reported by Richardson *et al.*, but several are markedly different.

The coefficients obtained for Eq. (7) for each of the metals considered are given in Table 3. A standard estimate of error, σ, is also given for each curve and indicates an accuracy of about three significant figures. By comparing graphically the values reported by Richardson *et al.* in Fig. 1 with those obtained by extrapolating with Eq. (7), there seems to be reasonable accuracy except for the case of Ti. Since there are only four reported [1] values for the C_2 coefficients for Ti, it should be expected that a fairly good quadratic least square fit would be obtained. But we should not place much confidence in the result as shown by curve 1 in

Table 3. Coefficients obtained from quadratic least square fits of 3*d* wavefunction C_2 coefficients as a function of ζ_2 for the first-row transition metals. Coefficients obtained from a linear least square fit for Ti are also given[a]

Metal	α_1	α_2	α_3	$\sigma \times 10^4$	N
Ti	0.90085	0.03268	−0.08312	9.6	4
	1.13693	−0.24994		47.5	6
V	1.09163	−0.21257	−0.00892	14.3	5
Cr	1.14006	−0.28382	0.01383	17.0	6
Mn	1.10747	−0.26185	0.01071	6.0	6
Fe	1.04582	−0.21241	0.00133	8.3	6
Co	1.03985	−0.21358	0.00312	9.5	6
Ni	1.03482	−0.21017	0.00352	17.0	6
Cu	1.13194	−0.28572	0.01895	10.7	5
Average[b]	1.0845	−0.2400	0.0075		

[a] σ is the standard estimate of error (standard deviation) and N is the number of data points used for the least square fit.

[b] The average α_i coefficients do not include Ti results.

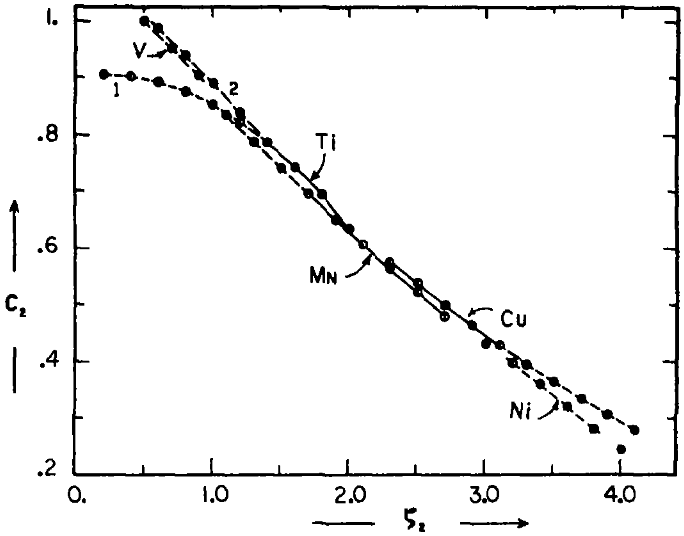

Fig. 1. Typical C_2 versus ζ_2 relations for "double-ζ" 3*d* wavefunctions. Solid curves for the metals shown are from those reported by Richardson *et al.* [J. chem. Physics 36, 1057 (1962)]. Dashed curves are obtained by using Eq. (7) with the α_i coefficients given in Table 3. Curve 1 is the quadratic extension of C_2 (Ti) and curve 2 is the linear extension of C_2 (Ti). The solid black points, ●, are obtained by using the general relation given in Eq. (8)

Fig. 1. A more acceptable curve is obtained with a linear least square fit for C_2 (Ti) as illustrated by curve 2 in Fig. 1. This is borne out by considering the trends of the other metals. Although the C_2 (Ti) results are probably the poorest, the remaining curves indicate at least an internal consistency.

By taking an average value for each α_i (excluding Ti), we have obtained an equation that has general validity over the entire range of metals except for Ti and Cu which are at the ends of the series. The equation is as follows:

$$C_2 = 1.0845 - 0.2400\zeta_2 + 0.0075\zeta_2^2 . \tag{8}$$

On combining Eq. (8) with Eqs. (4), (5), and (6) we complete the set of equations for obtaining "double-ζ" 3*d* wavefunctions that are fairly accurate from vanadium through nickel. The solid black points, ●, in Fig. 1 are obtained from Eq. (8) and illustrate the validity of this equation.

4. Conclusions

Although many of the results obtained by this study are similar to those of Richardson *et al.* [1, 2] a more reasonable set of ζ_{4s} values is reported for a larger range of electronic configurations. By reasonable we mean that the wavefunctions give a fairly good representation of atomic electronic configurations in MO calculations for approximate 4*s* wavefunctions. The internal consistency of estimated ζ_{4s} values indicate several improvements over previously reported values.

With Eqs. (4), (5), (6), and (8) we are now able to obtain "double-ζ" $3d$ wavefunctions for the sequence of metals from vanadium through nickel with reasonable accuracy for the entire range of electronic configurations from d^1 through d^{10}. A more accurate representation of the wavefunction can be obtained for each metal in the sequence from Ti through Cu by using Eq. (7) instead of Eq. (8). Only the $3d$ wavefunctions of Ti seem to be questionable on being extended to additional oxidation states.

References

1. Richardson, J. W., Nieuwpoort, W. C., Powell, R. R., Edgell, W. F.: J. chem. Physics **36**, 1057 (1962).
2. Powell, R. R., Nieuwpoort, W. C.: J. chem. Physics **38**, 796 (1963).
3. Brown, R. D., James, B. H., O'Dwyer, M. F.: Theoret. chim. Acta (Berl.) **17**, 264 (1970).
4. Fenske, R. F., Caulton, K. G., Radtke, D. D., Sweeney, C. C.: Inorg. Chemistry **5**, 951 (1966).
5. Dahl, J. P., Johansen, H.: Theoret. chim. Acta (Berl.) **11**, 8 (1968).
6. Becker, C. A. L., Dahl, J. P.: Theoret. chim. Acta (Berl.) **14**, 26 (1969).
7. Shulman, R. G.: Bell Telephone Laboratories, Memorandum for File, Case 38140-13.
8. Copeland, D. A., Ballhausen, C. J.: Theoret. chim. Acta (Berl.) **20**, 317 (1971).
9. Watson, R. E.: Physic. Rev. **118**, 1036 (1960); **119**, 1934 (1960).
10. Clementi, E.: IBM J. Res. Devel. **9**, 2 (1965) and the supplement to this paper.
11. Burns, G.: J. chem. Physics **41**, 1521 (1964).

Dr. D. A. Copeland
Department of Chemistry
The University of Tennessee at Martin
Martin, Tennessee 38327, USA

Theoret. chim. Acta (Berl.) 27, 373—375 (1972)
© by Springer-Verlag 1972

Ground States of Molecules

XXIII.* MINDO/2 Calculations for Naphthalene**

MICHAEL J. S. DEWAR and PAUL WEINER
Department of Chemistry, The University of Texas at Austin, Austin, Texas 78712, USA

Received June 21, 1972

Detailed MINDO/2 calculations of naphthalene using the SIMPLEX minimization algorithm are reported. Comparison of results with experiment and various π approximations is made. The results are in good agreement with experiment.

The geometry of naphthalene has been of considerable interest to theoreticians both because it has been determined with unusual precision by X-ray crystallography [1] and electron diffraction [2] and because the majority of theoretical treatments have failed to account for the length of the 9, 10 bond. We have now studied this problem in detail, using MINDO/2 [3].

Recent work in these laboratories has led to the development of a semiempirical SCF MO procedure (MINDO/2 [3]) which seems to give good estimates of ground state properties. We have also developed a procedure [4], based on the SIMPLEX algorithm [5] for calculating molecular geometries. Application of these techniques to naphthalene seemed of interest for two reasons. First, we have recently modified [6] the parameters in MINDO/2 to overcome two of its shortcomings, i. e. the systematic overestimation of dipole moments (by ca. 50%) and of lengths of bonds involving hydrogen (by 0.1 Å); calculations for naphthalene seemed to provide a good test of its ability to still deal adequately with CC bonds. And secondly, such a calculation seemed to provide a good test of our SIMPLEX program in a molecule whose geometry involves a rather large number of independent coordinates.

Since the number of coordinates was so large, the calculation was carried out in stages. We first assumed all the CH bonds to have the same length (1.09 Å) and to bisect the adjacent CCC bond angle; the CC bond lengths and CCC bond angles were calculated on this basis by a standard SIMPLEX minimization. Assuming these CC bond lengths and CC bond angles, we then calculated the CH bond lengths and HCC bond angles by a second SIMPLEX minimization. As a check, the cycle was repeated; the bond lengths, bond angles, and energy from the second cycle were identical within the limits of accuracy of the SCF treatment, with those from the first. Since the number of SCF calculations for SIMPLEX minimization of a system with n independent coordinates is approximately n^2, this type of iterative procedure should prove helpful for large molecules since it evidently can converge quite rapidly.

---

* Part XXII: Bingham, R. C., Dewar, M. J. S.: J. Amer. chem. Soc. (in press).

** This work was supported by the Air Force Office of Scientific Research through Contract F44620-70-C-0121, and the Robert A. Welch Foundation through Grant F-126.

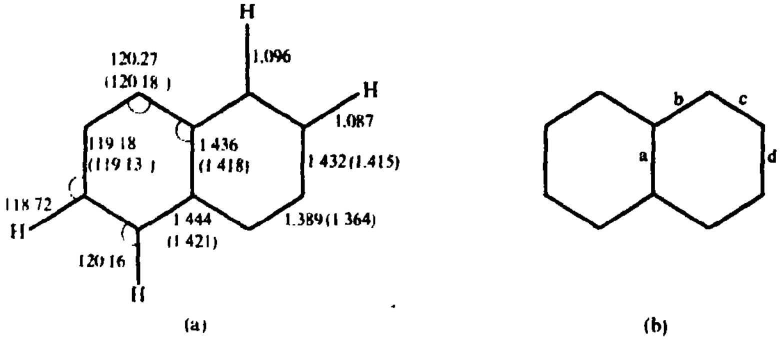

Fig. 1 (a) Calculated (observed [1]) bond lengths (Å) and bond angles in naphthalene; (b) key to Table 1

The final geometry is indicated in Fig. 1, together with Cruickshank's experimental values [1]. The calculated heat of formation (18.6 kcal/mole) was less than that observed (36.2 kcal/mole).

The agreement between the calculated and observed bond angles is almost perfect. The calculated CC bond lengths are systematically too long; if a corre-

Table 1. Bond lengths for naphthalene, calculated by various methods and observed

Method[a]	*a*[b]	*b*[b]	*c*[b]	*d*[b]	*Ref.*
This paper	1.436	1.444	1.389	1.432	
SCF-π	1.420	1.426	1.382	1.419	c
SC-π	1.396	1.424	1.364	1.418	d
SCF-CI	1.415	1.423	1.380	1.416	e
MO-SC	1.419	1.420	1.382	1.414	f
HMO	1.409	1.439	1.363	1.432	g
SCP	1.412	1.425	1.378	1.418	h
PED	1.408	1.424	1.369	1.417	i
VB	1.407	1.434	1.377	1.428	j
SMO	1.424	1.416	1.384	1.406	k
X-ray	1.418	1.421	1.364	1.415	l
ED	1.420	1.422	1.371	1.412	l, m

[a] SCF-π, semiempirical SCF MO π approximation with parameters chosen to reproduce ground state properties; SCF-CI, Pople π approximation with configuration interaction; MO-SC, self-consistent HMO; HMO, refined Hückel MO; SCF, self-consistent perturbation theory; PED, projected electron density; VB, valence bond; ED, electron diffration.

[b] For key, see Fig. 1(b).

[c] Lo, D. H., Whitehead, M. A.: Canad. J. Chemistry **46**, 2027 (1968).

[d] Pritchard, H. O., Sumner, F. H.: Proc. Roy. Soc. (London) A **226**, 128 (1954).

[e] Kichisuke, Nishimoto: Theoret. chim. Acta (Berl.) **7**, 207 (1967).

[f] Boyd, G. V., Singer, N.: Tetrahedron **22**, 3383 (1966).

[g] Goodwin, T. H.: J. chem. Soc. **1960**, 4851.

[h] Amos, A. T.: Theoret. chim. Acta (Berl.) **8**, 91 (1967).

[i] Fosterling, H. D., Huber, W., Kuhn, H.: Int. J. quant. Chemistry **1**, 225 (1967).

[j] Goodwin, T. H.: Theoret. chim. Acta (Berl.) **2**, 315 (1964).

[k] Coulson, C. A., Daudel, R., Robertson, J. M.: Proc. Roy. Soc. (London) A **207**, 306 (1951).

[l] Cruickshank, D. W. J., Sparks, R. A.: Proc. Roy. Soc. (London) A **258**, 270 (1960).

[m] Almenningen, A., Bastiansen, O., Dyvik, F.: Acta crystallogr. **14**, 1056 (1961).

sponding correction (0.021 Å) is made, the errors are then all less than ±0.005 Å, within the limits of error of the X-ray crystallographic analysis [1]. The calculated CH bond lengths agree with the electron diffraction [2] value (1.09 Å).

Table 1 compares bond lengths for naphthalene calculated by various π approximations with the values in Fig. 1 and with experiment. It will be seen that MINDO/2 reproduces the relative lengths more accurately than any of the π approximations, suggesting that reasonable reliance can be placed in its predictions for molecules even as large as this.

References

1. Cruickshank, D. W. J., Sparks, R. A.: Proc. Roy. Soc. (London) A **258**, 270 (1960).
2. Almenningen, A., Bastiansen, O., Dyvik, F.: Acta crystallogr. **14**, 1056 (1961).
3. (a) Dewar, M. J. S., Haselbach, E.: J. Amer. chem. Soc. **92**, 590 (1970). – (b) Bodor, N., Dewar, M. J. S., Harget, A., Haselbach, E.: J. Amer. chem. Soc. **92**, 3854 (1970). – (c) Dewar, M. J. S.: Fortschritte der Chem. Forschung (1971) in press.
4. Brown, A., Dewar, M. J. S., Schoeller, W. W.: J. Amer. chem. Soc. **92**, 5516 (1970).
5. Nelder, J. A., Mead, R.: Computer J. 7, 308 (1964).
6. Bodor, N., Dewar, M. J. S., Lo, D. H.: J. Amer. chem. Soc., in press.

Dr. M. J. S. Dewar
Department of Chemistry
The University of Texas at Austin
Austin, Texas 78712
USA